NASA CR 114757
AVAILABLE TO THE PUBLIC
Contractor Report No.
LG74ER0096

SMALL SCALE MODEL STATIC ACOUSTIC INVESTIGATION OF HYBRID HIGH LIFT SYSTEMS COMBINING UPPER SURFACE BLOWING WITH THE INTERNALLY BLOWN FLAP

By T. W. Cole and E. A. Rathbun

July, 1974

Prepared under Contract NAS2-7812 (Task I) by
LOCKHEED GEORGIA COMPANY

86 South Cobb Drive
Marietta, Georgia

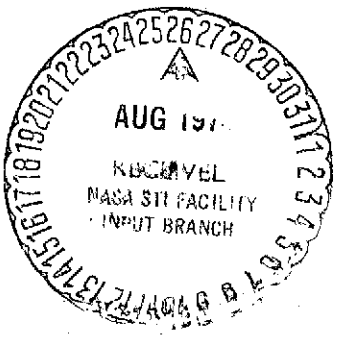

for

Ames Research Center

NATIONAL AERONAUTICS AND SPACE ADMINISTRATION

TABLE OF CONTENTS

	Page
TABLE OF CONTENTS	i
SUMMARY OF FIGURES	ii - iii
SUMMARY	1
INTRODUCTION	2
SYMBOLS	3 - 5
TEST APPARATUS	6 - 10
PROPULSION DATA ACQUISITION AND REDUCTION	11 - 12
ACOUSTIC DATA ACQUISITION AND REDUCTION	13 - 15
PROPULSION RESULTS	16 - 18
ACOUSTIC RESULTS	19 - 25
CONCLUSIONS	25 - 26
REFERENCES	27
FIGURES	28 - 220
ADDENDUM	A-1 - A-56

SUMMARY OF FIGURES

Figure	Description	Page
1 - 19	Description of test site, model, instrumentation, data reduction and data analysis.	28 - 57
20	Summary of test program.	58
	Aerodynamic and Propulsion Data	
21 - 24	Nozzle performance.	59 - 66
25 - 26	Flap performance.	67 - 72
27	Flap trailing edge wake survey.	73 - 82
	Basic Acoustic Data	
28 - 35	Nozzle only.	83 - 90
36 - 39	Comparison of flap. Slot configuration: JH and Flex Flap.	91 - 94
40 - 57	Baseline; NR4D nozzle, JH flap, landing and takeoff.	95 - 112
58 - 65	Baseline; NR8 nozzle, JH flap, landing and takeoff.	113 - 120
66 - 73	Baseline; NR4 nozzle, JH flap, landing and takeoff.	121 - 128
74 - 77	Baseline; NSE nozzle, JH flap, takeoff.	129 - 132
78 - 93	Baseline; NR4D nozzle, Flex Flap, landing and takeoff.	133 - 148
94 - 101	Baseline; NR8 nozzle, Flex Flap, landing and takeoff.	149 - 156
102 - 109	Baseline; NR4 nozzle, Flex Flap, landing and takeoff.	157 - 164

Figure	Description	Page
110 - 117	Baseline; NSE nozzle, Flex Flap, landing and takeoff.	165 - 172
118 - 125	Baseline; USB only, NR4D nozzle, JH flap, landing and takeoff.	173 - 180
126 - 133	Baseline; USB only, NR4D nozzle, Flex Flap, landing and takeoff.	181 - 188
134 - 141	Baseline; USB only, NR8 nozzle, Flex Flap, landing and takeoff.	189 - 196
	Parametric Acoustic Data	
142 - 143	Nozzle longitudinal position; NR4D nozzle, JH flap, landing and takeoff.	197 - 198
144 - 145	Nozzle impingement angle; NR4D nozzle, JH flap, landing and takeoff.	199 - 200
146 - 147	Auxiliary flap angle; NR4D nozzle, JH flap, landing and takeoff.	201 - 202
148 - 153	Flap pressure ratio; NR4D nozzle, JH flap, landing and takeoff.	203 - 208
154 - 155	Nozzle spanwise position; NR4D nozzle, JH flap, landing and takeoff.	209 - 210
156 - 157	Nozzle longitudinal position; NR4D nozzle, Flex Flap, landing and takeoff.	211 - 212
158 - 159	Nozzle impingement angle; NR4D nozzle, Flex Flap, landing and takeoff.	213 - 214
160 - 161	Auxiliary flap angle; NR4D nozzle, Flex Flap, landing and takeoff.	215 - 216
162 - 164	Flap pressure ratio; NR4D nozzle, Flex Flap, landing.	217 - 219
165	Nozzle spanwise position; NR4D nozzle, Flex Flap, landing.	220

SUMMARY

A static acoustic and propulsion test of a small radius Jacobs-Hurkamp and a large radius "Flex Flap" combined with four upper surface blowing (USB) nozzles was performed at the Lockheed-Georgia Company during early and mid-1974. The early test results are included in the body of this report, and the later test results are in the Addendum.

Nozzle force and flow data, flap trailing edge total pressure survey data, and acoustic data were obtained in both series of tests. Jacobs-Hurkamp flap surface pressure data, flow visualization photographs, and spoiler acoustic data from the limited mid-year tests are reported in the Addendum. A pressure ratio range of 1.2 to 1.5 was investigated for the USB nozzles and for the auxiliary blowing slots. The acoustic data were scaled to a four-engine STOL airplane of roughly 110,000 kilograms or 50,000 pounds gross weight, corresponding to a model scale of approximately 0.2 for the nozzles without deflector. The model nozzle scale is actually reduced to about .17 with deflector although all results in this report assume 0.2 scale factor.

Trailing edge pressure surveys indicated that poor flow attachment was obtained even at large flow impingement angles unless a nozzle deflector plate was used. Good attachment was obtained with the aspect ratio four nozzle with deflector, confirming the small scale wind tunnel tests of Reference 1. Good attachment was also obtained with the aspect ratio eight nozzle, but the aspect ratio four nozzle is a more practical design for an aircraft. The JH flap model incorporated both knee and trailing edge slot nozzles. Most of the testing was done without trailing edge blowing, since the relatively small gains in aerodynamic performance did not justify the large noise penalty of 5 to 7 PNdB. Most of the penalty can be attributed to blowing from the lower surface, however.

The JH flap at the landing setting produced higher than expected noise levels aft of the flap, and the increase in noise level with nozzle exit velocity is more rapid than would be anticipated. The Flex Flap did not exhibit these peculiarities.

INTRODUCTION

The work reported in this document was performed under Task I of Contract NAS2-7812, "Hybrid Propulsive Lift Noise Study and Aerodynamic Investigation". Complementary low speed wind tunnel testing was performed under Task II of the same contract, and results are reported in Reference 1. The low speed wind tunnel tests reported in Reference 1 were completed about one month prior to initiation of the Task I tests.

The Task I tests were initially planned to include three nozzle configurations and two basic flap configurations. The two flaps differed in concept in that the first, a large-radius design, utilized internal blowing over an aft flap element on both upper and lower surfaces, but depended solely on the Coanda effect to turn the USB flow. This flap would utilize a flexible upper skin on an actual airplane, and is called the "Flex Flap" in this report. The second concept, a small radius design, also utilized internal blowing over an aft flap element as well as blowing over the main flap knee. This flap is called the "Jacobs-Hurkamp" (JH) flap, after its inventors of the scheme which increases the internal flap cross-sectional area as it is deflected. The Task II tests disclosed that the JH flap possessed better aerodynamic performance than the Flex Flap, and that a deflector was needed on the engine exhaust nozzle. A nozzle deflector was therefore added to the Task I tests, and the program was conducted using the JH flap and the nozzle with deflector as the primary configuration.

SYMBOLS

Aero-Propulsion

AK	flap knee slot nozzle area, sq. in.
ANT	total internally blown flap and upper surface blowing nozzle area, sq. in.
ATE	flap trailing edge total slot nozzle area, sq. in.
B	flap span, in.
C	wing chord length, in.
CNPR	core nozzle effective pressure ratio = PTCN/PAM
C_V	nozzle velocity coefficient
C_D	nozzle flow coefficient
D	nozzle axial thrust component, lb.
ETA	a distance parallel to the wing chord plane from the flap slot inboard edge to the nozzle centerline, in.
FCCOR	corrected core nozzle thrust, lb.
FD	flap deflection angle from wing chord plane, deg.
FF	Flex-flap
FFCOR	corrected fan nozzle thrust, lb.
FNPR	fan nozzle effective pressure ratio = PTFN/PAM
FSCOR	corrected total flap slot nozzle thrust, lb.
JH	Jacobs-Hurkamp flap
L	nozzle side load thrust component, lb.
NR4	rectangular nozzle with width to height ratio of 4
NR4D	NR4 nozzle with exit deflector and bottom plate
NR8	rectangular nozzle with width to height ratio of 8
NSE	simulated engine nozzle with core nozzle
PAM	local ambient pressure, psia.
PPR	rake probe pressure ratio = PTP/PAM
PSCD	core duct static pressure, psia.
PSTD	transition duct static pressure, psia.
PSTR	trapeze duct static pressure, psia.

PTCD	core duct total pressure, psia.
PTCN	core nozzle effective total pressure, psia.
PTFN	fan nozzle effective total pressure, psia.
PTP	rake probe total pressure, psia.
PTSN	flap slot nozzle total pressure, psia.
PTTD	transition duct total pressure, psia.
P4ORI	4 inch orifice upstream pressure, psia.
P6ORI	6 inch orifice upstream pressure, psia.
ΔP4ORI	4 inch orifice differential pressure, psi.
ΔP6ORI	6 inch orifice differential pressure, psi.
q_s	local compressible dynamic pressure at distance s, psi.
q_n	compressible dynamic pressure at USB nozzle exit, psi.
s	distance along flap upper surface measured from knee slot, in.
SK	slot nozzle height at knee of flap, in.
SNPR	flap slot nozzle pressure ratio = PTSN/PAM
STE	slot nozzle height at trailing edge of flap (total of upper and lower slots), in.
TAM	local ambient temperature, ^{o}R
TFRE	flap supply duct total temperature, ^{o}R
THETA	angle between nozzle centerline and wing chord plane, deg.
TTTD	transition duct airflow total temperature, ^{o}R
T4ORI	4 inch orifice pipe temperature, ^{o}R
T6ORI	6 inch orifice pipe temperature, ^{o}R
USB	upper surface blowing
WCCOR	corrected core nozzle airflow rate, lb/sec.
WFCOR	corrected fan nozzle airflow rate, lb/sec.
X	distance parallel to the wing chord plane from wing leading edge to the nozzle exit plane, in.
Y	perpendicular distance above or below flap trailing edge ((+) sign above), in.

Acoustics

$S_{K/TE}$	Knee/trailing edge slot height, JH flap (TE is total of upper and lower slots), in.
S_{TE}	Slot nozzle height at trailing edge of Flex Flap (total of upper and lower slots), in.
θ_N	Angle between nozzle centerline and wing chord plane, deg.
Ψ	Auxiliary flap angle relative to flap, deg.
NPR, NPR_N	Nozzle pressure ratio
NPR_F	Flap nozzle pressure ratio
θ	Microphone or observer angle relative to nozzle centerline
ϕ	arch elevation angle
PNL	perceived noise level

TEST APPARATUS

General

The test apparatus consists of the upper surface blowing (USB) nozzles, wing, flaps, air supply system, test stand, and instrumentation. A photographic overall view of the test site is shown in Figure 1. A closeup view of one nozzle-flap configuration installed on the test stand is shown in Figure 2.

Nozzles

Four USB nozzle configurations were tested. Nozzle configuration NSE was intended to be representative of an aircraft configuration having a rectangular fan nozzle of aspect ratio $\simeq$ 4 and a circular core nozzle discharging near the mid-upper surface of the fan nozzle. Photographs and a drawing showing the pertinent dimensions for this nozzle are shown in Figure 3.

The NR8 nozzle is a rectangular nozzle having an aspect ratio of eight. Photographs and a drawing of this nozzle are shown in Figure 4.

The NR4 nozzle is a rectangular nozzle having an aspect ratio of four. Photographs and drawings of this nozzle are shown in Figure 5.

The NR4D nozzle consists of the NR4 nozzle with a deflector extension on the top of the nozzle spanning the major axis. A bottom plate is also attached. These additions increase the nozzle aspect ratio at the trailing edge to 6.5. Figure 5d gives the pertinent details of these attachments. The side plates shown in this figure are not a part of the NR4D configuration but were used in a limited number of tests for obtaining basic data.

Wing/Flap

A sketch of the wing test section is shown in Figure 6, and coordinates are given for the basic wing section. End views are shown of the various flap configurations. Two basic

flap configurations were tested, both being internally blown. The Flex-Flap utilized a large leading edge radius and blowing at the trailing edge over both upper and lower surfaces of the aft flap. The Jacobs-Hurkamp flap utilized a small leading edge radius with knee and trailing edge blowing.

Both flap designs could be set up in either a takeoff or landing configuration, and an auxiliary trailing edge flap is provided for both designs. Trailing edge and knee slots were adjustable to provide various thrust splits between the trailing edge and knee slots and/or between the wing surface blowing and internally blown flap.

The wing tip was removable so that the shielding effect of the outer wing could be investigated.

Air Supply System

Air flow rates up to 18 pounds/second at 75 psig and essentially ambient temperature were delivered to the test site by a 6-inch pipe system. The 6-inch pipe system then branches into 6 and 4-inch orifice pipes followed by flow and pressure control valves. The supply pipe on the downstream side of the 6-inch valve was connected to a 6-inch trapeze. The trapeze had flexible rubber tubing in each vertical leg of the trapeze to permit nozzle axial and vertical thrust to be measured with little resistance from the air supply system. The 6-inch pipe system downstream of the trapeze consisted of a conical diffuser, two mufflers, and a transition duct, and was supported six feet above a concrete pad in the test stand "A" frame by vertical and horizontal rods equipped with self-alignment rod-end fittings. The conical diffuser increases the 6-inch pipe to 12 inches which is the inlet and exit diameter of the mufflers. The mufflers are AMF Beaird, Inc., Model FPS, and each muffler is approximately 24 inches in diameter and 48 inches long. These mufflers are recommended for silencing of high frequency noise and the design incorporates a "stuffer" to eliminate any line of sight noise. The transition duct is a conical converging section with inlet and exit diameters of 12.0 and 10.6 inches, respectively, having a length of 27 inches. The test nozzles were attached to the downstream end of the transition duct.

The 4-inch pipe system downstream of the pressure control valve consisted of a 4-inch-to-6 inch conical transition piece, a section of 6-inch pipe, two mufflers, a manifold section, and three flexible 3 1/2-inch hoses. The 3 1/2-inch hoses connect directly to the internally blown flap air supply pipes as shown in Figure 7. The mufflers are similar to those in the nozzle air supply line, but are only about half as large.

The entire air supply system from the upstream end of the orifice pipes to the mid-section of the transition duct preceding the test nozzle and to the upstream side of the flexible hoses on the flap air supply system was wrapped with acoustic material.

Test Stand

The test stand consists of two structural frame-works: one supports the air supply system and the other supports the wing/flap assembly. The air supply support is made up of two "A" frames with an overhead beam extending across the top of these frames as shown in Figure 8.

The air supply system is suspended in this frame-work by vertical and horizontal rods equipped with self-alignment rod-end fittings.

Mounting provisions for the wing/flap assembly consisted of a moveable carriage assembly mounted on tracks. Movement along the tracks allows positioning of the wing/flap assembly relative to the USB nozzle in the longitudinal and lateral directions. These movements are accomplished by lead screw and hand crank arrangements. Vertical and angular positioning of the wing/flap assembly was accomplished by movement of the wing support shaft within its support column on the carriage. Vertical movement was obtained with a scissor jack positioned under the wing support shaft. Angular movement was easily made by hand. Methods for rigidly clamping the model in a fixed position were provided for each mode of adjustment.

Instrumentation

A schematic of the propulsion instrumentation is shown in Figure 9.

Airflow Rates

Airflow rates supplied to the USB nozzle were measured using a sharp-edged orifice plate and pressure taps in a 6-inch diameter pipe. Airflow rates supplied to the flap were measured with a sharp-edged orifice plate and pressure taps in a 4-inch diameter pipe. Pressure transducers were connected to the upstream orifice pressure and orifice plate differential pressures. Orifice pipe airflow temperature was measured with a nickel resistance grid.

Nozzle Thrust, Temperature and Pressure

Nozzle axial and vertical thrust were measured with TOROID Model 36-233 type load cells. The axial load cell was installed along the air supply system as shown in Figure 10. The vertical load cell was installed normal to the air supply transition duct centerline in a horizontal plane just upstream of the nozzle attachment flange as shown in Figure 11. The test nozzle was rotated 90 degrees about its centerline relative to a horizontal plane since the wing was mounted vertically. Pressure and temperature instrumentation were installed in the transition duct just upstream of the nozzle attachment flange as shown in Figure 12. Four total pressure probes, four wall static pressure ports and one temperature sensor were installed in the transition duct. The four total and static pressures were manifolded to provide a single average pressure for each, and were connected to pressure transducers. The temperature sensor was the same type as that used in the orifice pipe. The separate core nozzle duct of the NSE nozzle had one total pressure probe and one wall static port installed just upstream of the nozzle exit plane. Figure 3 shows this instrumentation.

Flap Pressures and Temperature

Four Kiel pressure probes were mounted in the flap assembly just upstream of the auxiliary trailing edge flap. Figure 13 shows the pertinent details of this installation. Each of these probes was connected to a pressure transducer. A temperature sensor was installed

in the flap air supply line downstream of the mufflers.

Flap Trailing Edge Survey

A 31-tube pressure rake was used for flap trailing edge surveys to determine if the wing upper surface blowing was attached to the flap. Figure 14 shows this installation. The 31 tubes were connected to a Scanivalve which in turn was connected to a pressure transducer.

Ambient Conditions

Local wind velocity and direction was determined by a cup-type anemometer/wind direction unit mounted on the roof of the test control center building. Ambient pressure was measured with a diaphragm type barometric gage. Ambient temperature was measured with a mercury-in-glass thermometer.

Calibrations

All load cells, pressure transducers, temperature probes and the barometric pressure gage were laboratory calibrated prior to testing. During the test period, inplace calibrations were conducted on all load cells, pressure transducers, and temperature probes utilizing the entire data acquisition system to establish units for data reduction.

The axial and vertical nozzle measuring system including the trapeze was also calibrated to determine tares for the system. The tares were determined as a function of static pressure in the trapeze and were incorporated into the data reduction program.

PROPULSION DATA ACQUISITION AND REDUCTION

Data Acquisition

All temperature, pressure, and load cell instrumentation were connected to a pulse code modulation data acquisition system whose output was recorded on analog magnetic tape. A view of this equipment can be seen in Figure 15 on the right hand side of the operator. Each channel of instrumentation bridge input was supplied to a signal conditioning module which provided a balance and span adjustment for the bridge. These modules have a series resistance calibration circuit to provide a known millivolt output for calibration purposes. All amplification, multiplexing, analog to digital conversion, and encoding of conditioned signals were done by a Pulse Code Modulation Unit (PCM). This unit corrected the 0 to 10 millivolt signals from each module and digital scanivalve channel identification from each scanivalve into a serial digital pulse train containing the necessary channel and amplitude or value information. The PCM unit output was recorded on one channel of a Honeywell 7600 analog magnetic tape recorder using direct record mode.

Data Reduction

A computerized data reduction program was developed to provide three basic types of data from the recorded test parameters: (1) nozzle performance data, (2) flap performance data, and (3) flap trailing edge survey data. The recorded analog, magnetic tapes were processed by converting the analog recordings to digital engineering units, thus making the data compatible for input into the final data reduction program.

Nozzle Performance Data - Airflow rate, thrust, nozzle pressure ratio, and velocity and flow coefficients are computed from measured pressures, temperatures, areas and load cell reactions. The airflow rate is determined from equations and coefficients presented in Reference 2 for a square-edged orifice with flange taps. Nozzle resultant thrust is obtained from axial and normal load cell reactions with appropriate test

rig trapeze tares applied. The nozzle pressure ratio is computed as an effective pressure ratio from the continuity equation based on measured airflow rate, and static pressure, temperature and area just upstream of the test nozzle entry plane. The velocity coefficient is the ratio of measured velocity based on thrust and airflow rate to isentropic velocity based on effective nozzle pressure ratio. The flow coefficient is the ratio of measured airflow rate to the ideal airflow rate based on geometric nozzle area and effective nozzle pressure ratio.

The simulated engine nozzle (NSE) has a separate fan and core nozzle but both nozzles receive air from a common air supply and the total load is reacted by the load cells. Therefore, the fan flow circuit was blocked off and the core calibrated. The data identified in the preceding paragraph is computed for the core flow only case. The thrust and airflow rate data are curve fitted to polynomial equations in terms of effective nozzle pressure ratio so that the airflow rate and thrust for the fan nozzle can be extracted from the total measured airflow rate and thrust with both nozzles open.

Flap Performance Data - Airflow rate, slot nozzle pressure ratio and thrust are computed from measured pressures, temperatures, and areas. The airflow rate is determined from equations and coefficients presented in Reference 2 for a square-edged orifice with flange taps. The slot nozzle pressure ratio is the flap manifold mean total pressure to ambient pressure ratio. The slot nozzle thrust is based on measured airflow rate, isentropic velocity (based on slot nozzle pressure ratio) and slot area.

Flap Trailing Edge Survey Data - The flap trailing edge total pressure ratios are the measured total pressures divided by ambient pressure.

ACOUSTIC DATA ACQUISITION AND REDUCTION

Acoustic Instrumentation

Noise measurements were obtained with eleven microphones mounted on a variable-position arch which can traverse the elevation angles within the hemisphere shown in Figure 16. B & K Model 4136 one-quarter inch condenser microphones were used with protective grids that connect to B & K model 2615 preamplifiers. This combination provided a frequency sensitivity range of 250 Hz to 50,000 Hz, which was required for compatibility with the one-fifth scale model. From the preamplifiers, 200 ft. of cable was necessary to reach from the test rig to the test control facility. A line driver amplifier was utilized to maintain a flat frequency response ($\pm$ 0.5 dB through 80,000 Hz) through this cable.

Foam windscreens, B & K Model UA 2037, were used to reduce wind effects on the microphone diaphrams and a foam lined ring clamp was used to provide a soft mount for the microphones. The microphone mount consisted of a phenolic slab, cantilevered from the arch and wrapped with damping tape to minimize vibratory effects and repel moisture.

Data Acquisition

The acoustic data acquisition system is shown on the lower half of Figure 17. The end product in this system was the digital tape obtained with the Kennedy 1600H tape recorder. Monitoring of the acoustic data was performed with the storage display unit and digital printer.

Prior to the start of the program a spectral calibration was performed on the elements of the acoustic data recording system from 100 Hz through 50,000 Hz. Corrections obtained were applied to measured data along with the free field microphone corrections related to the protecting grid and wind screen. A Photo-con microphone calibrator, with a 1000 Hz signal, was used daily to provide a system correction level relative to the pre-test calibration.

Data Reduction

Digital tape data were processed in the sequence shown on Figure 18. The digitized data were directly read by the EMR 6040 computer tape drives and were combined with the punch card input that includes run identification, daily calibration delta dB, temperature, and relative humidity. Model acoustic data were then corrected with the calibration and standard day factors. Thus, the initial program output consisted of the standard day model 1/3 octave band sound pressure levels and the associated overall sound pressure levels at the twenty foot radius microphone location.

Next, the model acoustic levels were projected to the source, scaled to a four engine configuration, and then projected to 500 ft. sideline, or flyover, and 500 ft. radial position using standard day absorption factors. The two final program outputs therefore, were: (1) 500 ft. (152.4M) radial 1/3 octave band sound pressure levels, overall sound pressure levels and PNL, and (2) 500 ft. (152.4M) sideline (or flyover) 1/3 octave band sound pressure levels, overall sound pressure levels and PNL. This process is illustrated on Figure 19a, and the full-scale observer distances associated with all arch and microphone positions are listed on Figure 19b. Note that the calculated full-scale noise levels derive from geometric scaling of the flap and nozzle noise only. Forward speed effects, differing shielding, and other corrections necessary to simulate the total noise level produced by the flying aircraft are not included.

The model scale is approximately 0.2 for engines rated at about 7000 pounds total thrust at a fan pressure ratio of 1.5 without a nozzle deflector. Since the deflector used on the NR4D nozzle configuration reduced the simulated fan airflow, the model scale for that configuration is reduced to about .17, but all calculations in this report assume a scale of 0.2.

Acoustic Test Outline

The original test plan was designed as a parametric program encompassing three nozzles, the NR4, NR8 and NSE, and two flap configurations, the Jacobs-Hurkamp and Flex-Flap.

The earlier low speed wind tunnel tests indicated that a deflector was needed. The trailing edge surveys of the static test program confirmed this finding in that poor flow attachment with the aspect ratio four and simulated engine nozzles restricted their usefulness in providing a baseline for parametric variations. Good flow attachment to the flap was obtained with the aspect ratio four nozzle with a flow deflector plate. Thus, the test scope was reduced for the NR4 and NSE nozzles, and the major portion of the testing was devoted to the NR4D nozzle. A summary of the test program is shown on Figure 20.

PROPULSION RESULTS

Nozzle Performance

Nozzle performance data without the wing/flap are presented in Figures 21 through 24 for the four nozzle configurations investigated. The nozzle configurations are: 1) NR4 - a rectangular nozzle having an exit aspect ratio of four, 2) NR4D - same as NR4 nozzle except deflector plates are attached to top and bottom (along the major axis) changing the NR4 nozzle internal flow surfaces by 15 and 12 degrees respectively (deflector trailing edge aspect ratio 6.5), 3) NR8 - a rectangular nozzle having an aspect ratio of eight, and 4) NSE - a simulated engine nozzle co-planar with a rectangular fan nozzle exit (same area and height as the NR4 nozzle.). Nozzle velocity coefficients (C_V) are shown in Figure 21 as a function of nozzle pressure ratio. This velocity coefficient is the ratio of measured thrust to ideal thrust, where ideal thrust is based on measured airflow rate and isentropic velocity. Figure 22 presents nozzle airflow coefficients (C_D) as a function of nozzle pressure ratio. Two flow coefficients for the NR4D nozzle are shown: one for the nozzle area at the deflector trailing edge and the second for the open side area at the edges of the deflector. These flow coefficients are the ratio of measured airflow rate to ideal airflow rate based on geometric nozzle area and isentropic velocity.

Corrected measured nozzle airflow rates and thrust are presented in Figures 23 and 24 as a function of nozzle pressure ratio. Data are presented for the NR8 nozzle, the NR4 nozzle, the NR4D nozzle, the NR4D nozzle with side plates, the NSE nozzle core only, the NSE nozzle fan only, and the NSE nozzle core and fan.

Flap Performance

Calculated corrected flap slot thrust (FSCOR) based on measured airflow rates and nozzle pressure ratio are presented in Figures 25 and 26.

Figure 25 is applicable to the Jacobs-Hurkamp flap and presents data for the various knee and trailing edge slot heights tested for both the 70° (landing) and 30° (takeoff) flap configurations. The slot thrust shown is the total of the knee and trailing edge slot thrusts. Either can be calculated individually from the total by simply multiplying by the ratio of slot height to total slot height. Figure 26 presents similar slot thrust data for the Flex-Flap.

Those trailing edge slot heights (STE) which are denoted by: (number)/0 (example STE = 0.126/0 in.) indicate that the upper trailing edge slot gap was set at the indicated number and the lower slot was sealed. Where a single number (example STE = 0.316 in.) is noted, both upper and lower slots are set equally (for the example: 0.158 in.) for a total gap height of the number indicated. Both slots are sealed when STE = 0 is noted.

Flap Trailing Edge Total Pressure Surveys

Comparisons of flap trailing edge pressure distribution are shown in Figures 27a through 27j, for both flaps, four nozzle configurations, for USB jet impingement angle (THETA) on wing upper surface, for nozzle exit locations relative to wing chord (X/C), for the effect of a simulated upper surface duct installation, and for the effect of nozzle pressure ratio. The effect of flap blowing on and off, as indicated by the flap slot nozzle pressure ratio (SNPR), is also shown in Figure 27a. The JH flap had blowing at the knee and trailing edge. The trailing edge slots were sealed for some of the pressure surveys as indicated by a flap trailing edge total slot area ratio (ATE/ANT) of zero. All pressure data presented are for a flap deflection of 70 degrees and USB and flap blowing nozzle pressure ratio of 1.5, except Figures 27a and 27j which include two cases of USB only at 1.5 (no flap blowing).

Early in the test program, trailing edge surveys revealed that the NR4 and NSE nozzles did not produce adequate flow attachment with the Jacobs-Hurkamp flaps in the landing position. A deflector and bottom plate were added to the basic aspect ratio four nozzle. This combination achieved good flow attachment and became the baseline for the test

program. These findings are illustrated by the flap trailing edge pressures shown on Figure 27b. These surveys supported the companion, earlier low speed wind tunnel results of Reference 1, where deflectors were found to improve model aerodynamic performance significantly. Other investigations (References 3 and 4) have also found deflectors necessary for good attachment.

ACOUSTIC RESULTS

General

Acoustic data in this report are presented on three basic plotting formats that attempt to summarize the acoustic performance while allowing enough flexibility to cope with the configuration and parametric changes. They are:

- Full Scale PNL vs Azimuth - This format displays the full scale PNL for the eleven observer positions on the 500 ft. (152.4M) sideline plane, or flyover, as indicated by the selected elevation angle. The distances to the eleven 500 ft. azimuth positions at each elevation angle are shown in Figure 19. Two general types of data are shown: (1) Noise for a single configuration at various pressure ratios, and (2) Noise for two or more configurations at a single test pressure ratio. The nozzle pressure ratios used on all plots are calculated from measured data.

- Full Scale OASPL vs Nozzle (Flap) Exhaust Velocity - These figures illustrate the velocity dependence for a particular configuration at selected microphone (azimuth) and sideline, or flyover, positions. Velocities are isentropic values based on measured propulsion data. A reference line for the V^8 and V^6 noise-velocity dependence is included for the nozzle alone and nozzle-wing, respectively.

- Full Scale 1/3 Octave Band Sound Pressure Level vs Frequency - The spectrum is plotted for a configuration at various pressure ratios and a selected microphone (azimuth) and sideline, or flyover position(s). As described previously, nozzle pressure ratios are calculated from measured data.

In general, the data are organized in the following sequence: (1) baseline model configurations with their associated PNL, OASPL, and 1/3 octave band data, in that order, and (2) parametric variations as illustrated by PNL vs azimuth plots.

Summary Of Test Data

Nozzle Calibrations - Nozzle acoustic properties, with no wing, were measured at the beginning of the test program. This data also provided a checkout of the testing and instrumentation system. Figures 28 and 29 provide a comparison of full scale PNL sideline and flyover levels for the four nozzles. Overall sound pressure levels at the test nozzle velocities are shown on Figures 30 and 31 for the 90° azimuth position and for the 150° azimuth position. Figures 32 through 35 show the 1/3 OB sound pressure levels for each nozzle at the same two azimuth positions.

The NR4 nozzle displays the most desirable noise characteristics of the four units tested; however, as discussed elsewhere it does not produce the required flow attachment when married to the wing-flap lift system. The selected baseline nozzle, NR4D, produces more acoustic energy relative to the other nozzles at the higher frequencies which may be due to the deflector and bottom plate edges. All nozzles exhibit a typical V^8 dependence on flow velocity.

Selection of Baseline Configurations

Jacobs-Hurkamp Flap - The initial testing effort with the assembled model was to determine those flap-nozzle combinations which provided flow attachment at the landing flap angle of 70°. In this respect, the JH flap was considered the most critical because of the small knee radius. As outlined in the propulsion performance discussion, attached flow was obtained with the aspect ratio eight (NR8) nozzle and aspect ratio four nozzle with deflector (NR4D). The aspect ratio four (NR4) and simulated engine (NSE) nozzles did not produce attached flow when combined with the JH landing flap at reasonable impingement angles, and was unsatisfactory even at 21°.

Consequently, the test was organized to emphasize the NR8 and NR4D nozzles, with primary consideration given to the latter because of its more reasonable geometry.

Measurements for five knee/trailing edge combinations with the NR4D nozzle were made with the JH landing flap. Figure 36 is a comparative plot of sideline PNL for these five configurations and it shows that trailing-edge-blowing creates a significant noise penalty. A quieter trailing-edge-blowing configuration results from sealing the lower trailing edge slot and allowing flow through the knee and upper trailing edge slots. Figure 37 shows a comparison of this configuration and three other trailing edge slot configurations. It is apparent from this figure that the lower slot is the stronger noise source.

The noise contribution of these slot configurations can be assessed by referring to Figure 38, which summarizes the radial PNL produced by the slots with no upper surface blowing.

Flex Flap - The NR4D and NR8 nozzles, with primary emphasis on the NR4D, were used for the Flex Flap acoustic measurements. As with the JH flap, a slot evaluation was performed to select a test baseline configuration. Figure 39 summarizes these test runs and demonstrates that the best acoustic configuration tested is with the lower slot sealed and with an upper slot height of 0.158 inches.

Acoustic Data Baseline Configurations

Jacobs-Hurkamp Flap; 70° Flap Angle, NR4D Nozzle - Sideline and flyover PNL values are shown for the four elevation angles on Figures 40 through 43. The effect of

wing shielding, a "bucket" that forms in the 105° - 135° azimuth arc, can be observed by comparing these four figures in sequence from 0 through 90° elevation angle. This accentuates the upper surface and trailing edge noise sources that are apparent at the 90° and 150° azimuth positions.

Sideline and flyover velocity dependence and spectra are shown on Figures 44 through 49 at the 90° and 150° azimuth positions. The OASPL displays a velocity dependence that is closer to V^8 than the reference V^6. In addition, at the 150° azimuth, the exponential increases with velocity, particularly in the sideline case. The spectra, Figure 47, confirms the increase with a sharp buildup with increasing pressure ratio in the 315 Hz and 400 Hz frequency bands.

Jacobs-Hurkamp Flap; 30° Flap Angle, NR4D Nozzle - Sideline and flyover PNL, as shown in Figures 50 through 53 for the takeoff configuration are generally lower than those measured for landing at equivalent flow conditions. Wing shielding is more effective at the aft azimuth positions from 120° through 150° and the reduced flap angle has shifted the upper surface noise sources away from these observer positions. Figures 54 and 55 show the velocity dependence at a mid and aft azimuth position and Figures 56 and 57 show typical spectra.

Jacobs-Hurkamp Flap; NR8, NR4, and NSE Nozzles - Acoustic noise levels for the JH flap combined with the aspect ratio eight, aspect ratio four, and simulated engine nozzles are presented on Figures 58 through 77.

Flex Flap - NR4D Nozzle - Acoustic data are presented for the baseline Flex Flap configuration with the NR4D nozzle in Figures 78 through 93. Basic noise characteristics are similar to those produced by the JH Flap except that the landing configuration noise levels at the aft azimuth locations are greatly reduced. Consequently, the aft spectra does not exhibit the narrow band growth characteristics of the JH Flap.

Flex Flap; NR8, NR4, and NSE Nozzles - Acoustic noise levels for the Flex Flap combined with the aspect ratio eight, aspect ratio 4, and simulated engine nozzles are presented in Figures 94 through 117.

Flex Flap and Jacobs-Hurkamp Flap, Upper Surface Blowing Only - Figures 118 through 141 summarize the noise levels associated with the wing-flap model without flap blowing, i.e., with only upper surface blowing. Figures 118 through 133 illustrate these noise levels for the aspect ratio four nozzle with deflector for both the JH and the Flex Flap. Figures 134 through 141 illustrate similar data for the aspect ratio eight nozzle combined with the Flex Flap.

Parametric Data

Jacobs-Hurkamp Flap, Nozzle Chordwise Position - Full scale sideline PNL's for nozzle chord positions of 20, 35, and 50 percent are shown on Figure 142 for the landing flap configuration. At the aft azimuth positions, the 35 percent location is loudest, i.e., the noise level reduces if the nozzle is moved either forward or aft of this position. The comparable takeoff flap data are shown on Figure 143 for nozzle positions of 35 and 50 percent chord. In this case, the 35 percent chord noise levels are approximately 2 dB lower than those for 50 percent chord at all azimuth locations.

Jacobs-Hurkamp Flap, Nozzle Impingement Angle - Figures 144 and 145 show the sideline PNL for landing and takeoff flap angles and nozzle impingement angles of 12° and 19°. No significant differences are noted except at the aft azimuth positions for the landing flap where the noise levels for the 12° configuration are higher by approximately 1 to 1.5 dB.

Jacobs-Hurkamp Flap, Auxiliary Flap Angle - Sideline PNL's for landing and takeoff flap angles and auxiliary (trailing edge) flap angles of 0, $+30^{\circ}$, and -30° relative to the primary flap angle are shown on Figures 146 and 147. The directivity varies

somewhat with auxiliary flap position; however, the +30° (flap trailing edge down) position may produce the highest levels.

Jacobs-Hurkamp Flap, Variation of Flap Pressure Ratio With Constant Nozzle Pressure Ratio - Figures 148 through 153 summarize the sideline PNL's for the takeoff and landing flap angles. No strong differences between various flap pressure ratios are noted, but the PNL's increase slightly with increasing pressure ratio. This reflects the relatively small influence of knee blowing on noise level.

Jacobs-Hurkamp Flap, Nozzle Spanwise Location - Figures 154 and 155 provide a comparison of sideline PNL's for the nozzle locations at 50, 75, and 85 percent flap span. For both the takeoff and landing flap configurations, the 50 percent span location produces the lowest noise levels, the single exception being the 150° azimuth position with the landing flap.

Flex Flap, Nozzle Chordwise Position - Sideline PNL's for 20, 35, and 50 percent chord position are shown on Figures 156 and 157. With the landing flap configuration, the noise levels increase when moving the nozzle either forward or aft of the 35 percent chord position. However, no significant noise level changes are noted among the three chord positions with the takeoff flap.

Flex Flap, Nozzle Impingement Angle - Figures 158 and 159 compare the sideline PNL's for 12° and 19° nozzle impingement angles. For the landing configuration, the noise levels increase at the higher angle and show a similar but less pronounced characteristic for the takeoff flap.

Flex Flap, Auxiliary Flap Angle - Sideline PNL's for auxiliary flap angles of -30°, -15°, 0, and +30° are summarized on Figures 160 and 161. Significant changes in directivity occur when traversing from the forward to aft observer positions; however, the predominant noise levels occur with the TE flap at the +30° position.

Flex Flap, Variation of Flap Pressure Ratio with Constant Nozzle Pressure Ratio - Figures 162, 163 and 164 summarize the variation of flap blowing pressure ratio at three nozzle pressure ratios. The change in noise levels with increasing flap pressure ratio is greater than the comparable JH flap case, as the trailing edge slot contributes more to the overall noise than the knee slot.

Flex Flap, Nozzle Spanwise Location - Sideline PNL's for the 50, 75, and 85 percent nozzle spanwise positions are shown on Figure 165. As with the JH flap, the levels produced at the 50 percent position are significantly less than those outboard.

CONCLUSIONS

1. The aspect ratio eight nozzle produced good attachment without a deflector. Attempts to achieve comparable attachment with the aspect ratio four and simulated engine nozzles by increasing the nozzle-to-wing impingement angle were not successful, even at a relatively high 21° impingement angle. A deflector was added to the aspect ratio four nozzle which achieved satisfactory attachment at the maximum flap angle of 70°.

2. Addition of the deflector to the aspect ratio four nozzle increased the basic nozzle noise levels approximately 3-4 PNdB. The noise levels produced by this nozzle, with and without deflector, when combined with the JH Flap, are approximately equal, however.

3. The JH Flap at the landing angle of 70° displays an aft directivity generated by an upper surface noise source that has not been as yet fully defined.

4. Using the PNL's produced by the JH Flap with upper surface blowing as a base:

   (a) Knee blowing increases the base PNL's approximately 1 PNdB, (b) Knee plus upper trailing edge slot blowing increases the base PNL's 3 PNdB, and (c) Knee plus upper and lower trailing edge slot blowing increases the base PNL's 6-7 PNdB.

   Hence, trailing edge blowing was found to be a very powerful noise source.

5. At the landing flap angle, the JH Flap produces approximately 1-2 PNdB higher noise levels than the Flex-Flap; at the takeoff flap angle, the Flex Flap produces approximately 3 PNdB higher noise levels than the JH Flap.

6. Noise levels for the JH Flap at the landing angle of 70° are approximately 3 PNdB higher than equivalent levels at the takeoff flap angle.

7. With the JH Flap and knee blowing, angular changes in auxiliary flap position of $\pm 30^{\circ}$, relative to the primary flap position, affect the maximum PNL's less than 1 PNdB. Conversely, significant changes in directivity and magnitude occur with the Flex Flap over the same auxiliary flap deflection range; the highest noise levels occuring at the $+30^{\circ}$ position. Apparently the trailing edge slot noise source, associated with the Flex Flap only, is affected by the angular change.

REFERENCES

1. Waites, W. L., and Chin, Y. T.: "Small Scale Wind Tunnel Model Investigation of Hybrid High Lift Systems Combining Upper Surface Blowing with the Internally Blown Flap." NASA CR 114758, June 1974.

2. Supplement ASME Power Test Codes: PTC 19.5; 4 Flow Measurement, The American Society of Mechanical Engineers, 29 West 39th Street, New York, N.Y. 1959.

3. Aoyagi, Kiyoski; Falarski, Michael D.; and Koenig, David G.: "Wind Tunnel Investigation of a Large-Scale Upper Surface Blown-Flap Transport Model Having Two Engines." NASA TM X-62,296, August 1973.

4. Dorsch, R. G.; Reshotko, M.; and Olsen, W. A.: "Flap Noise Measurements for STOL Configurations Using External Upper Surface Blowing". Paper 72-1203, November 1972, AIAA, New York, N.Y.

Figure 1 Test site overall view.

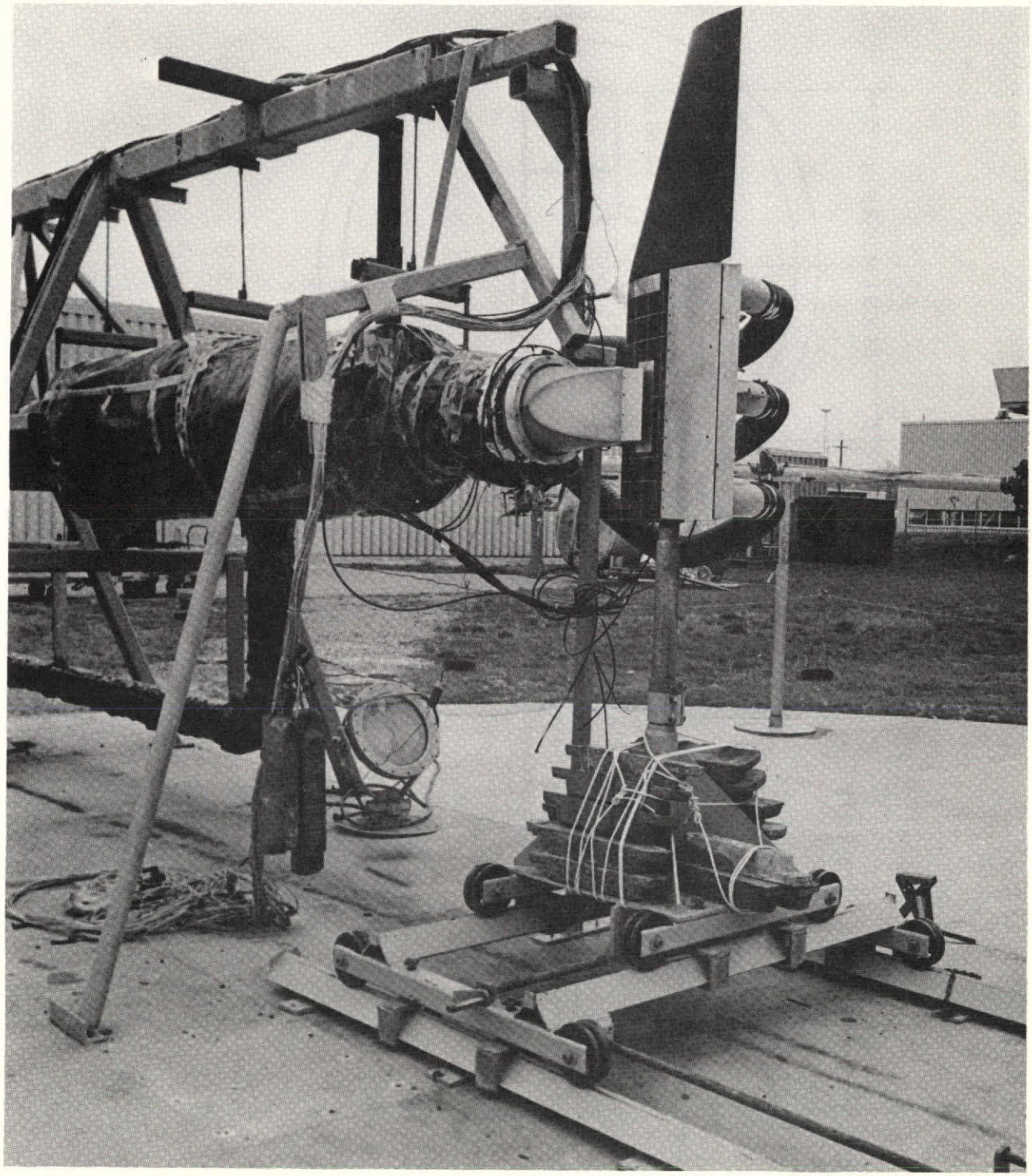

Figure 2 Typical test model installation.

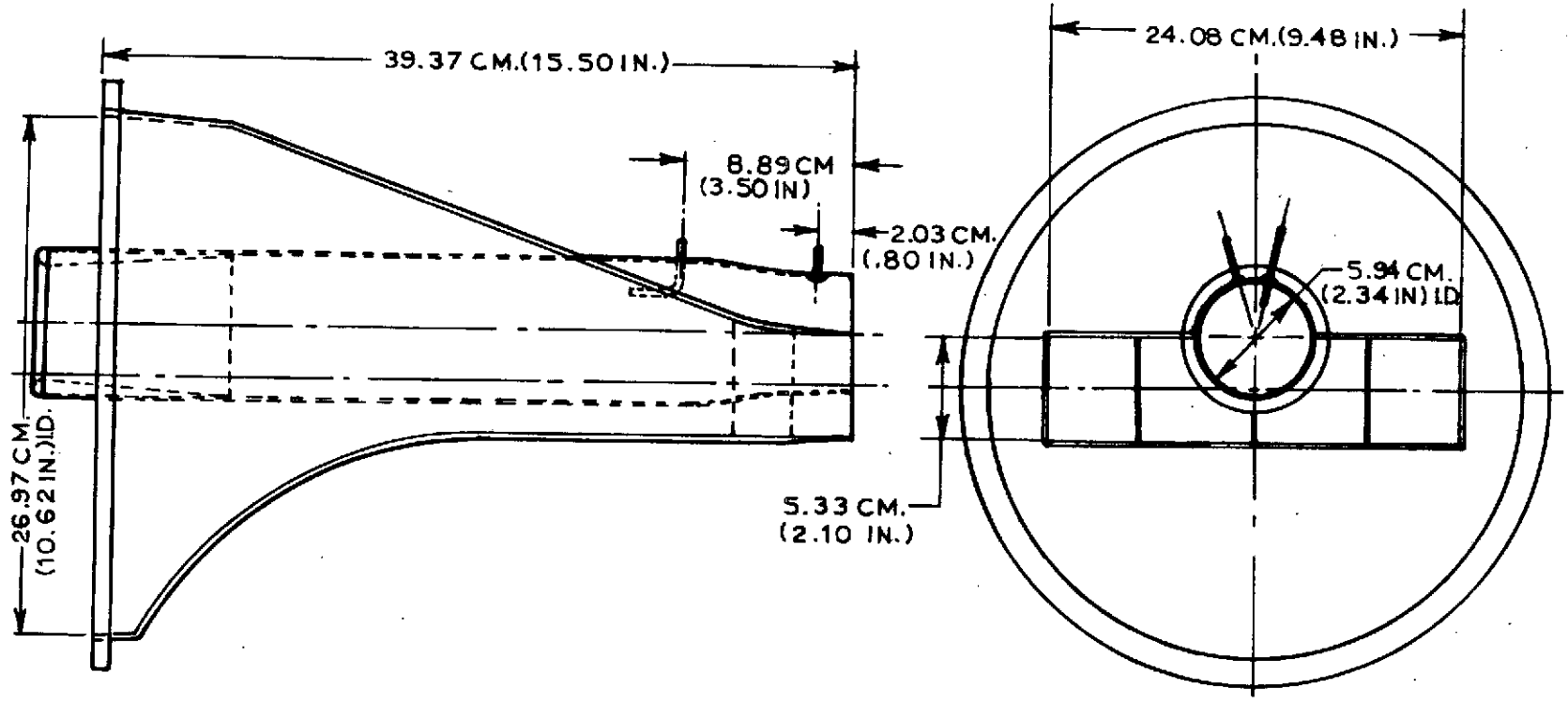

(a) Geometry of NSE nozzle.

Figure 3 NSE nozzle.

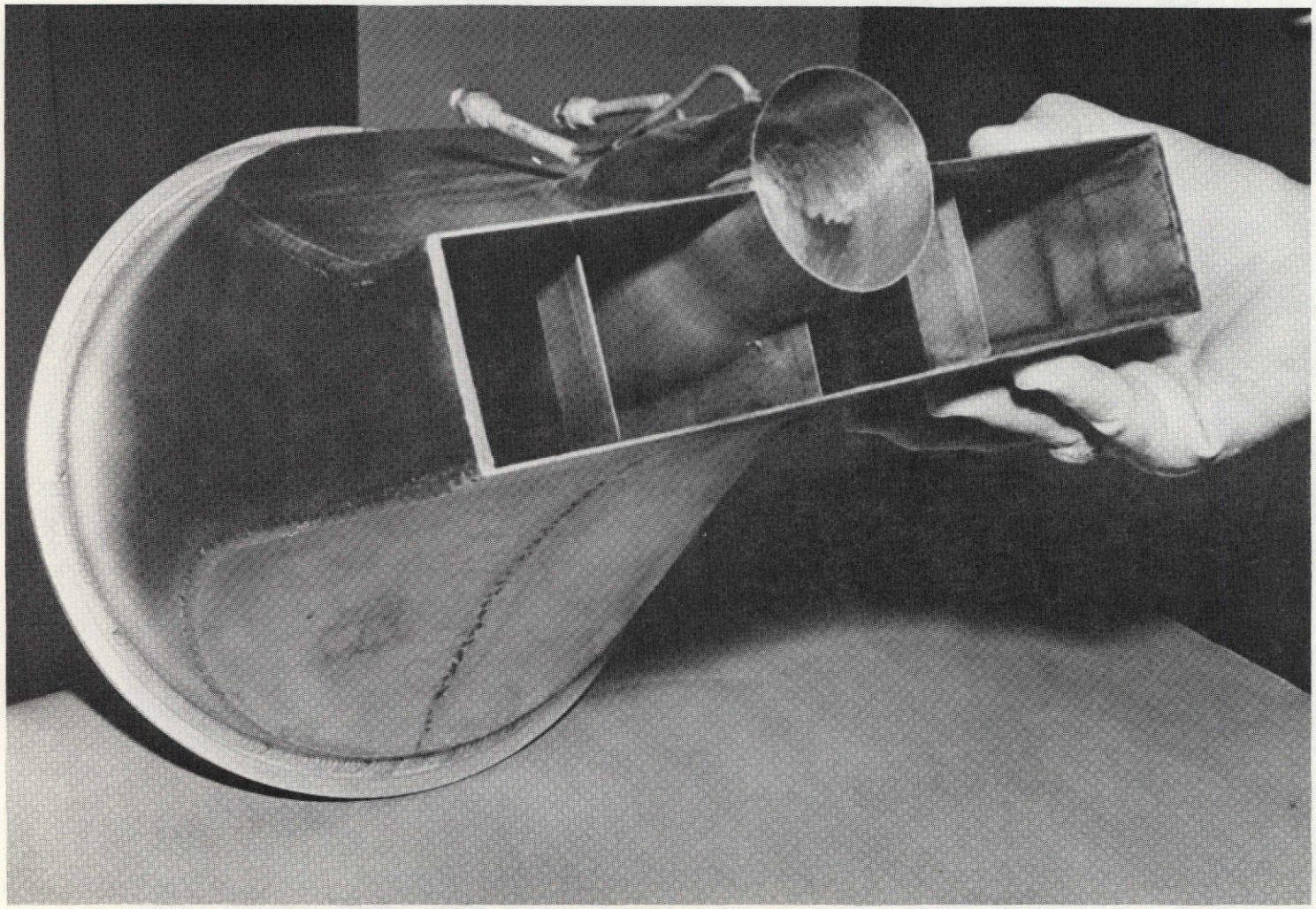

(b) NSE nozzle exit view.

Figure 3 Continued.

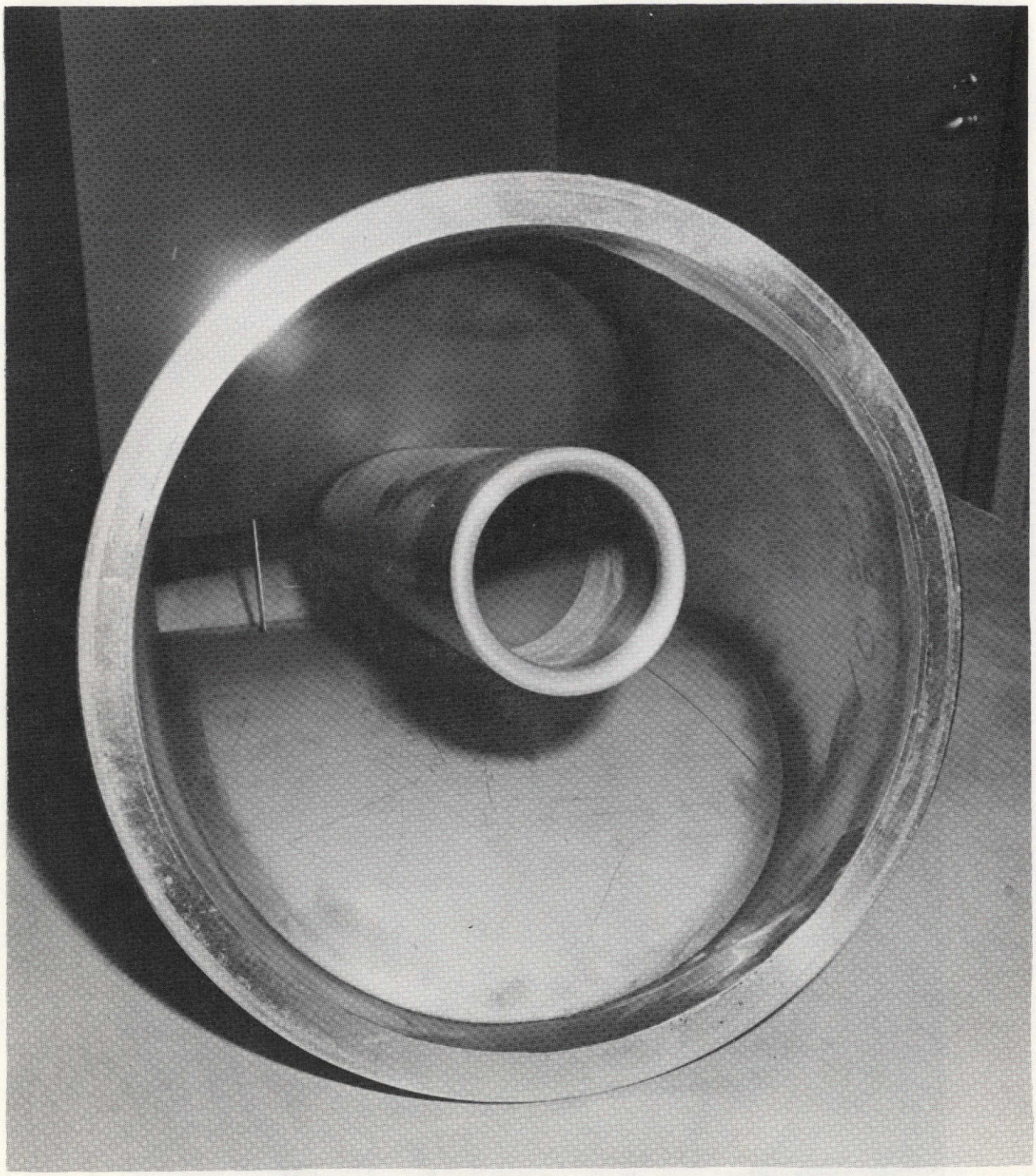

(c) NSE nozzle entrance view.

Figure 3 Concluded.

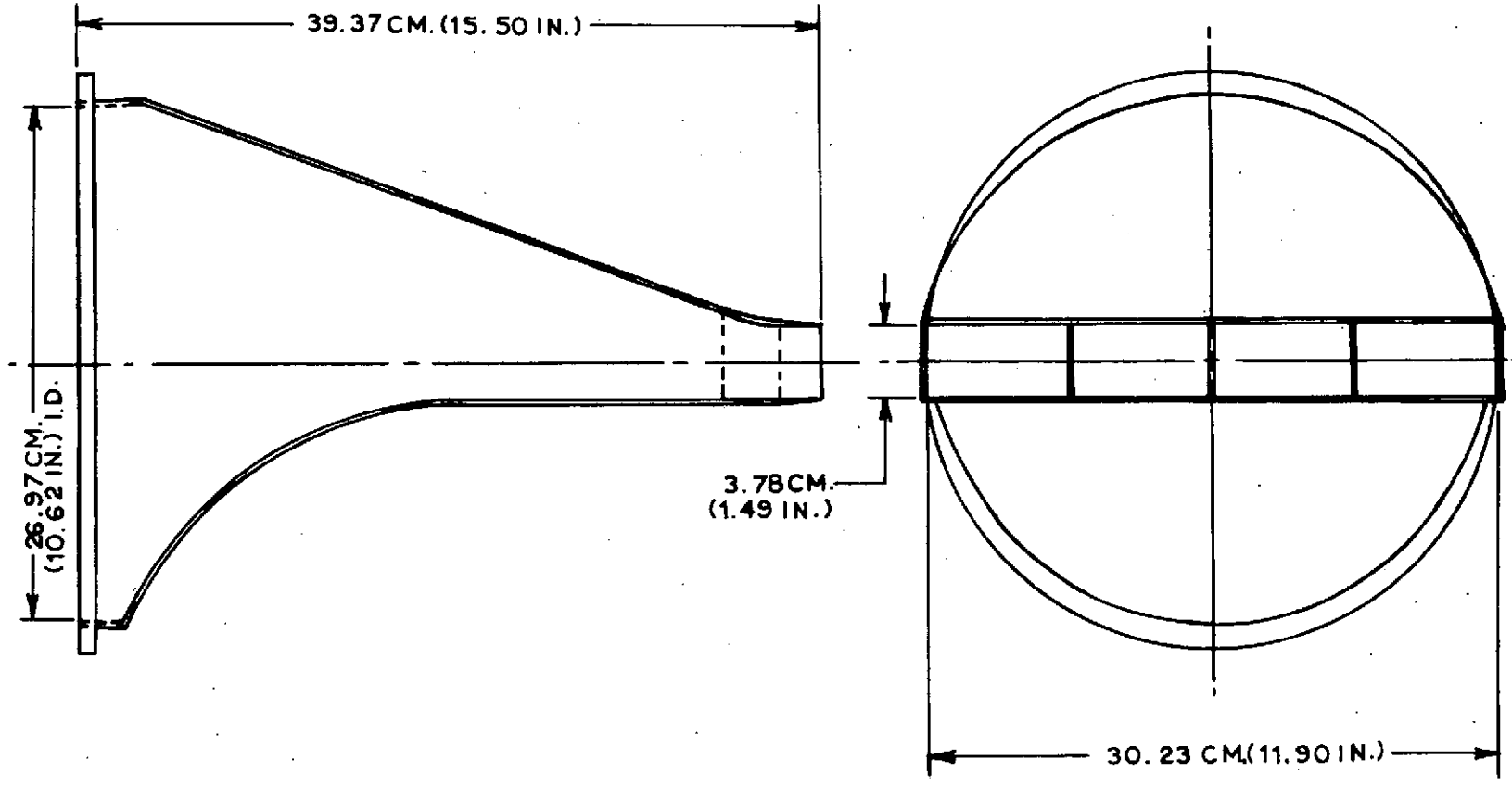

(a) Geometry of NR8 nozzle.

Figure 4 NR8 nozzle.

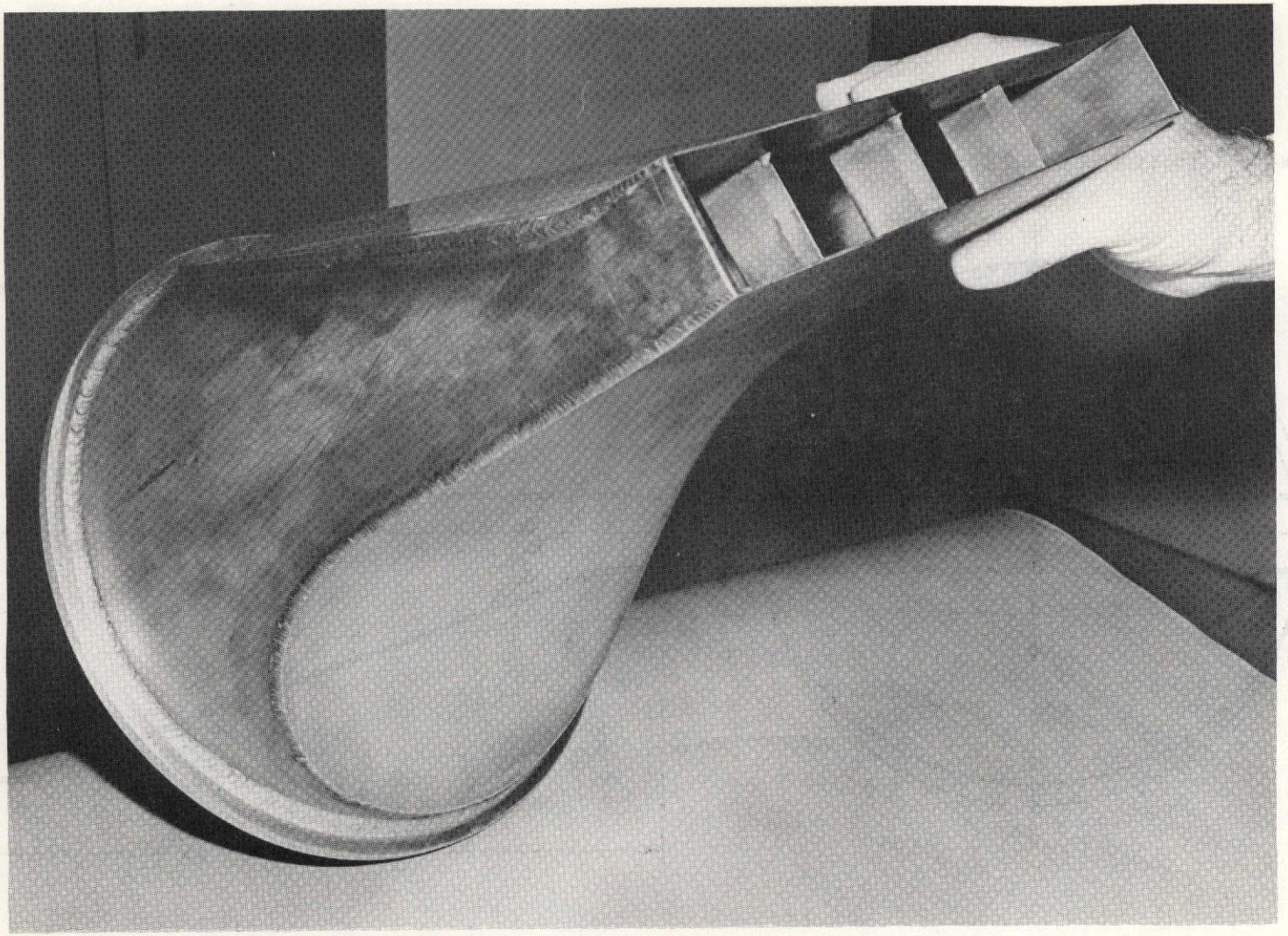

(b) NR8 nozzle exit view.

Figure 4 Continued.

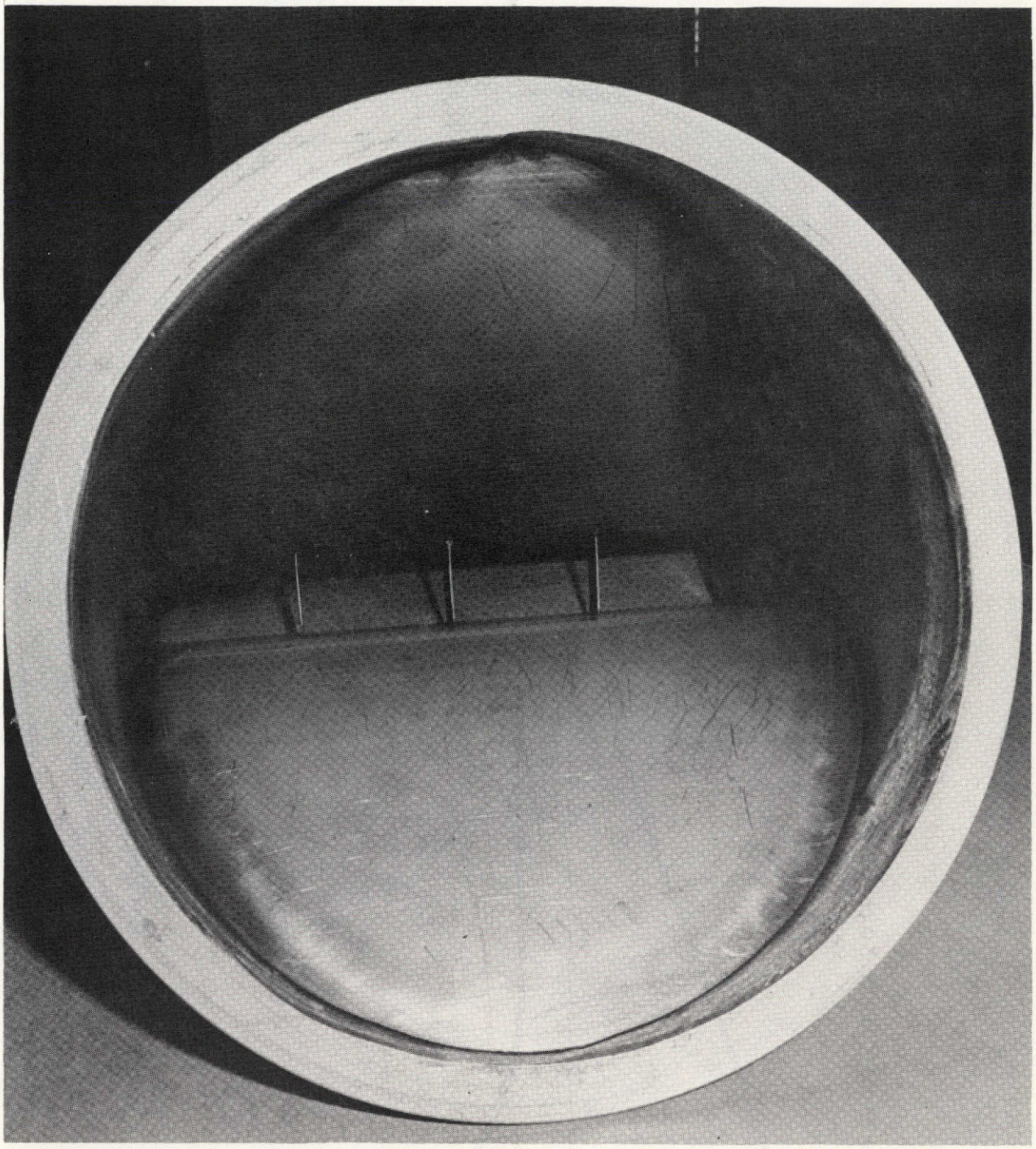

(c) NR8 nozzle entrance view.

Figure 4 Concluded.

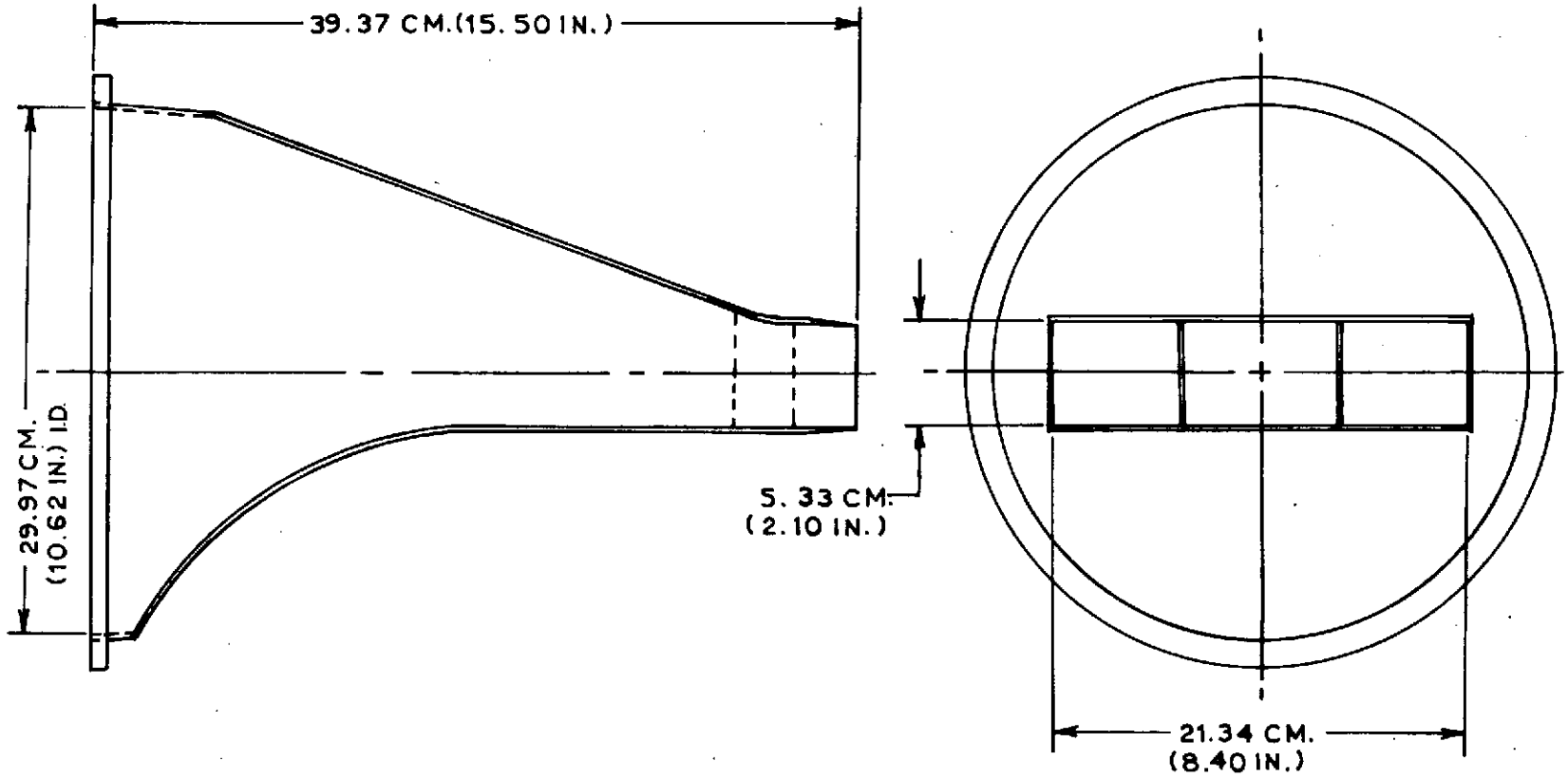

(a) Geometry of basic NR4 nozzle.

Figure 5 NR4 and NR4D nozzles.

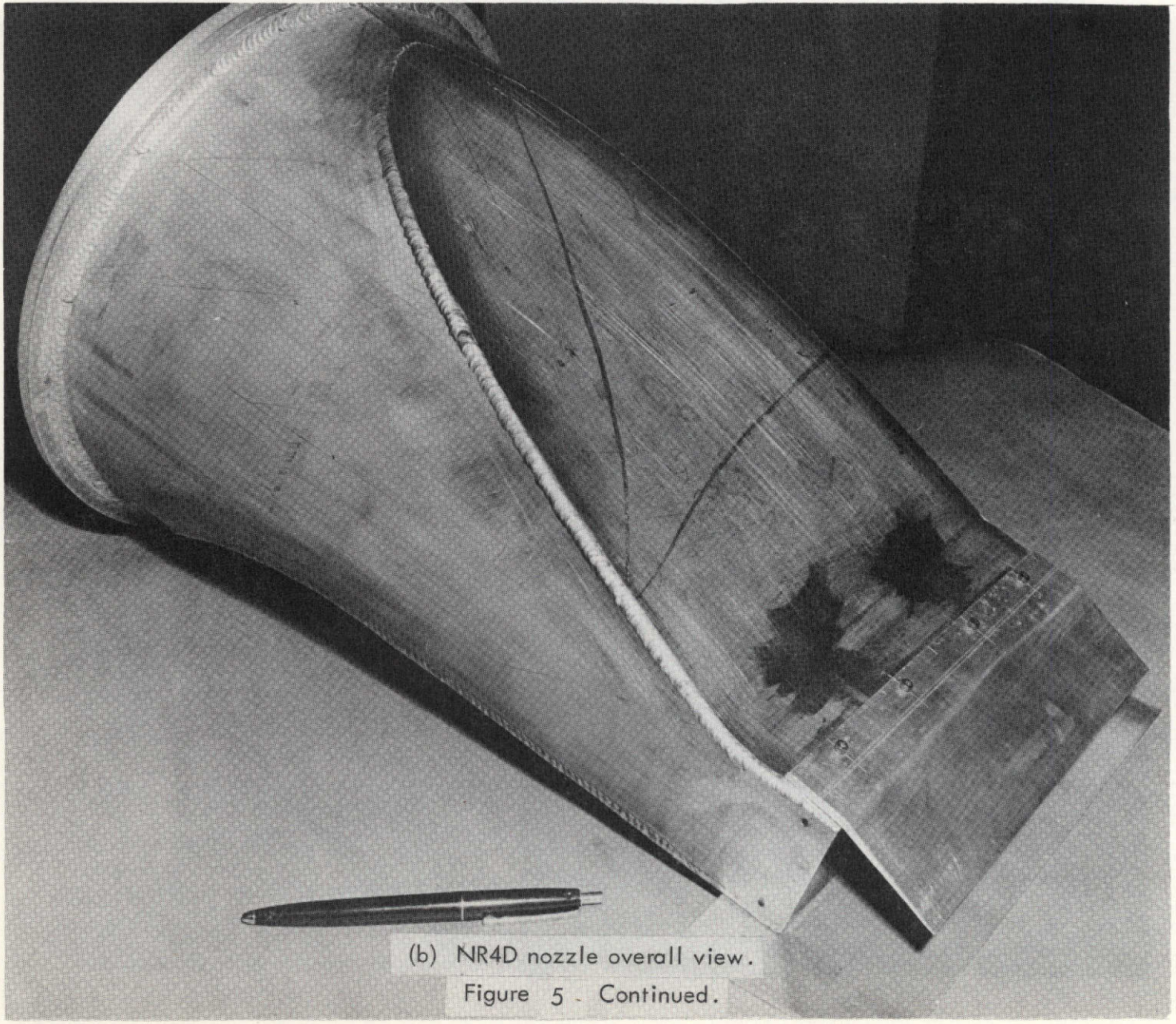

(b) NR4D nozzle overall view.

Figure 5 - Continued.

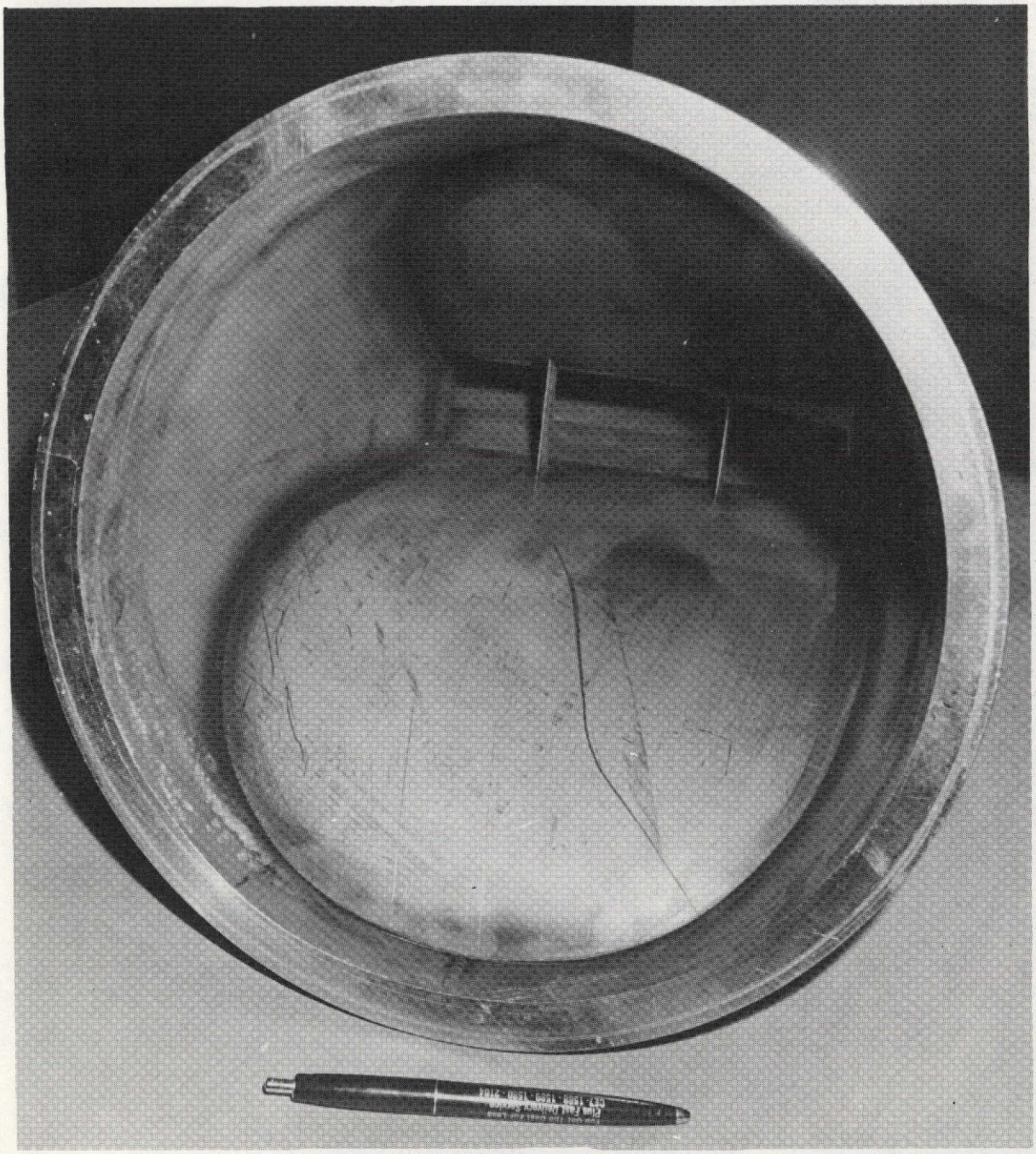

(c) NR4 nozzle entrance view.

Figure 5 Continued.

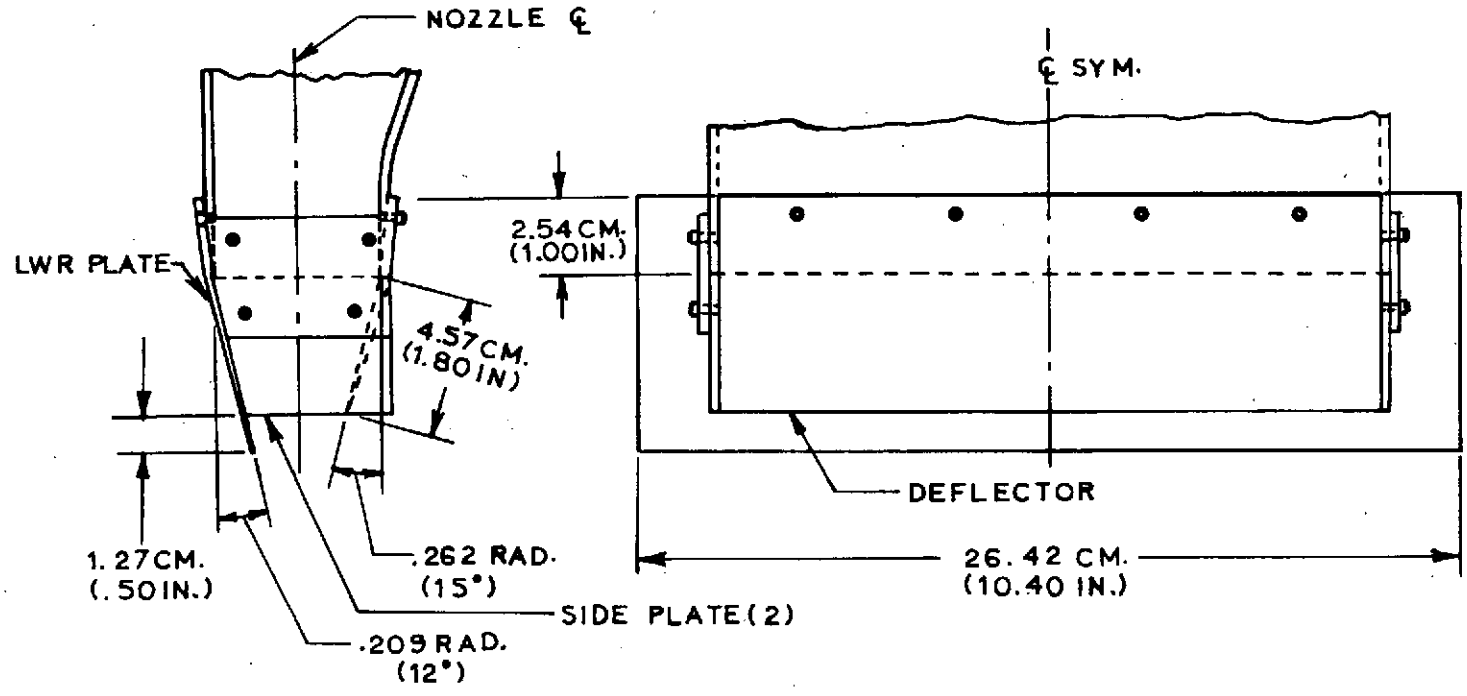

(d) NR4D nozzle deflector details.

Figure 5 Concluded.

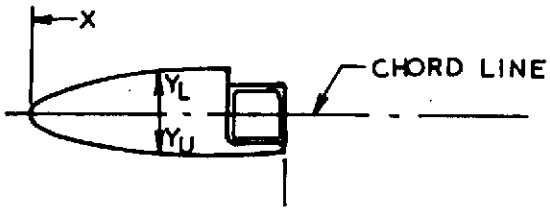

SECTION B-B (SEE FOLLOWING PAGES FOR END VIEWS OF FLAPS)

SECTION A-A

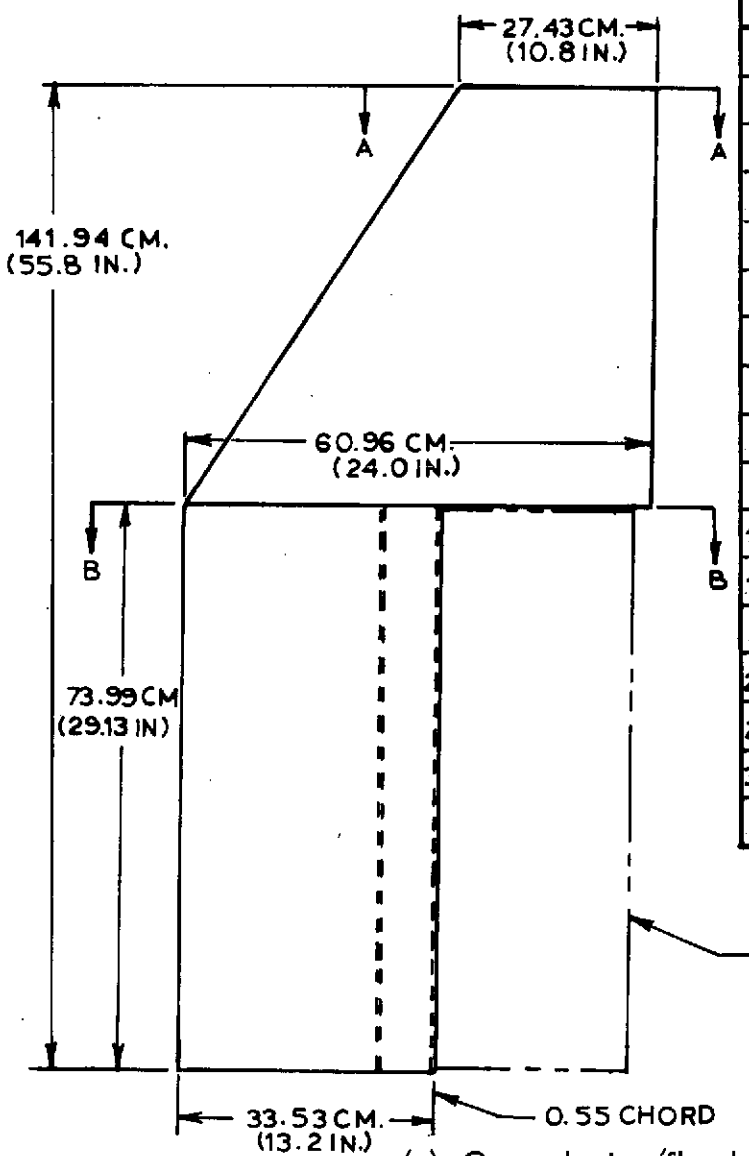

WING COORDINATES

X, CM.(IN.)	Y_U, CM.(IN.)	Y_L, CM.(IN.)
0.0 (0.0)	0.0 (0.0)	0.0 (0.0)
0.30 (0.12)	0.81 (0.32)	-1.04(-0.41)
0.61 (0.24)	1.12 (0.44)	-1.43 (-0.56)
1.22 (0.48)	1.50 (0.59)	-1.93 (-0.76)
1.83 (0.72)	1.78 (0.70)	-2.31 (-0.91)
2.44 (0.96)	2.03 (0.80)	-2.62 (-1.03)
3.05 (1.20)	2.24 (0.88)	-2.87(-1.13)
6.10 (2.40)	2.97 (1.17)	-3.78 (-1.49)
9.14 (3.60)	3.53 (1.39)	-4.37(-1.72)
12.19 (4.80)	3.94 (1.55)	-4.62(-1.82)
15.24 (6.00)	4.27 (1.68)	-4.98 (-1.96)
18.29 (7.20)	4.47 (1.76)	-5.13 (-2.02)
21.34 (8.40)	4.60 (1.81)	-5.13 (-2.02)
24.38 (9.60)	4.67 (1.84)	-5.08 (-2.00)
27.43 (10.80)	4.67 (1.84)	-4.93 (-1.94)
30.48 (12.00)	4.57 (1.80)	-4.75 (-1.87)
33.53 (13.20)	4.42 (1.74)	-4.55 (-1.79)

(a) General wing/flap layout.

Figure 6 Wing/Flap geometry.

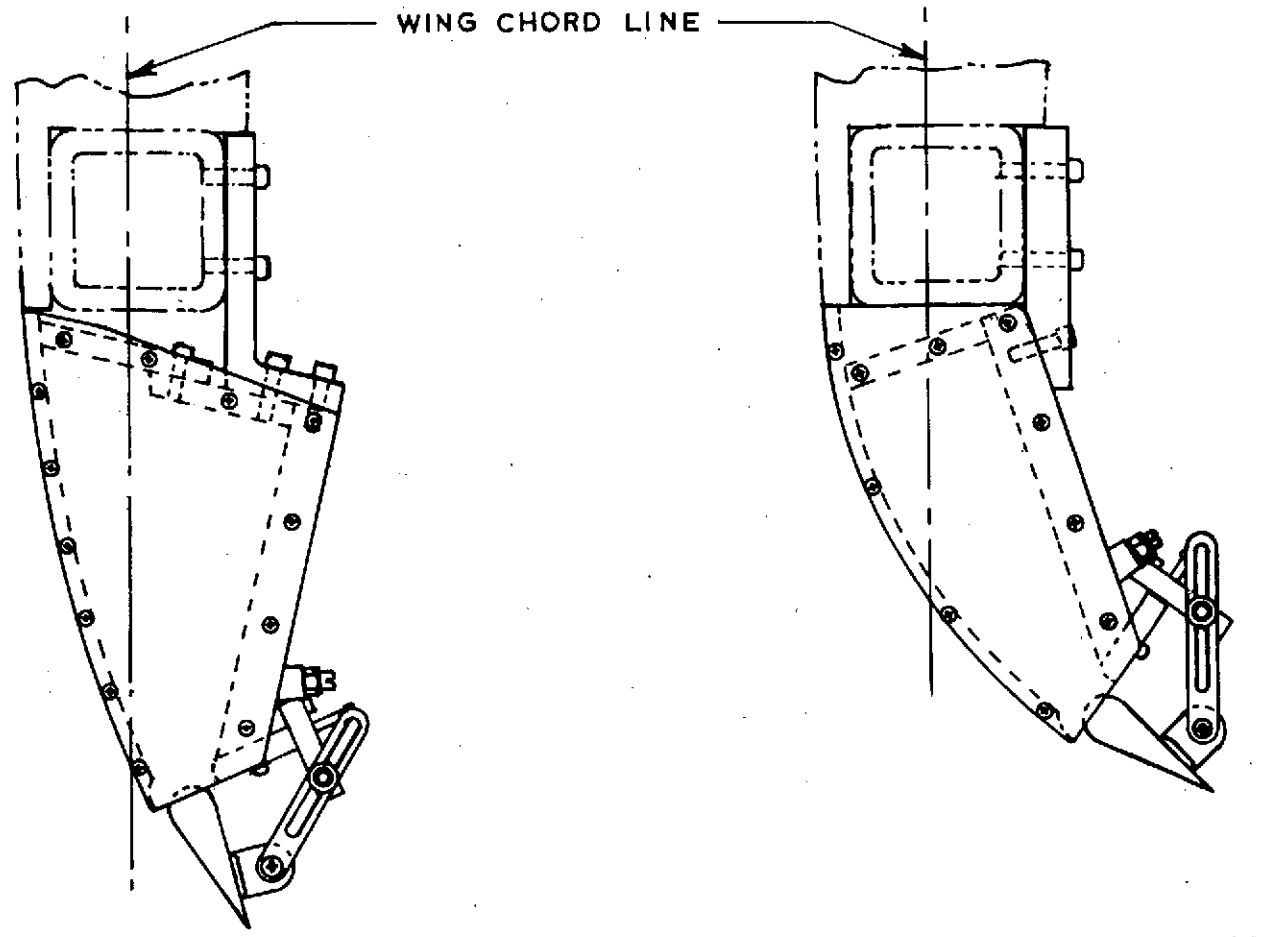

(b) Flex-Flap end view.

Figure 6 Continued.

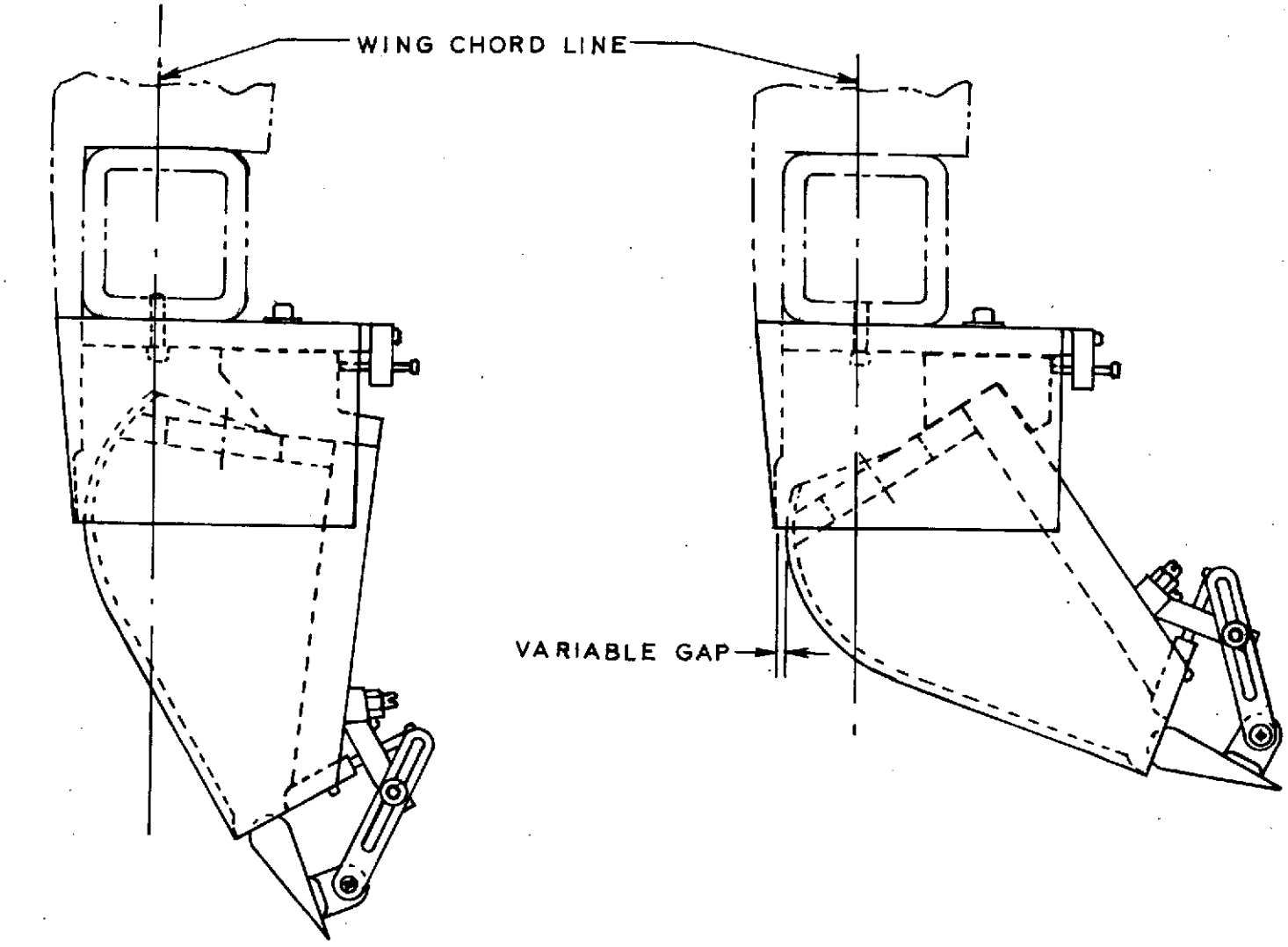

(c) Jacobs-Hurkamp flap end view.

Figure 6 Concluded.

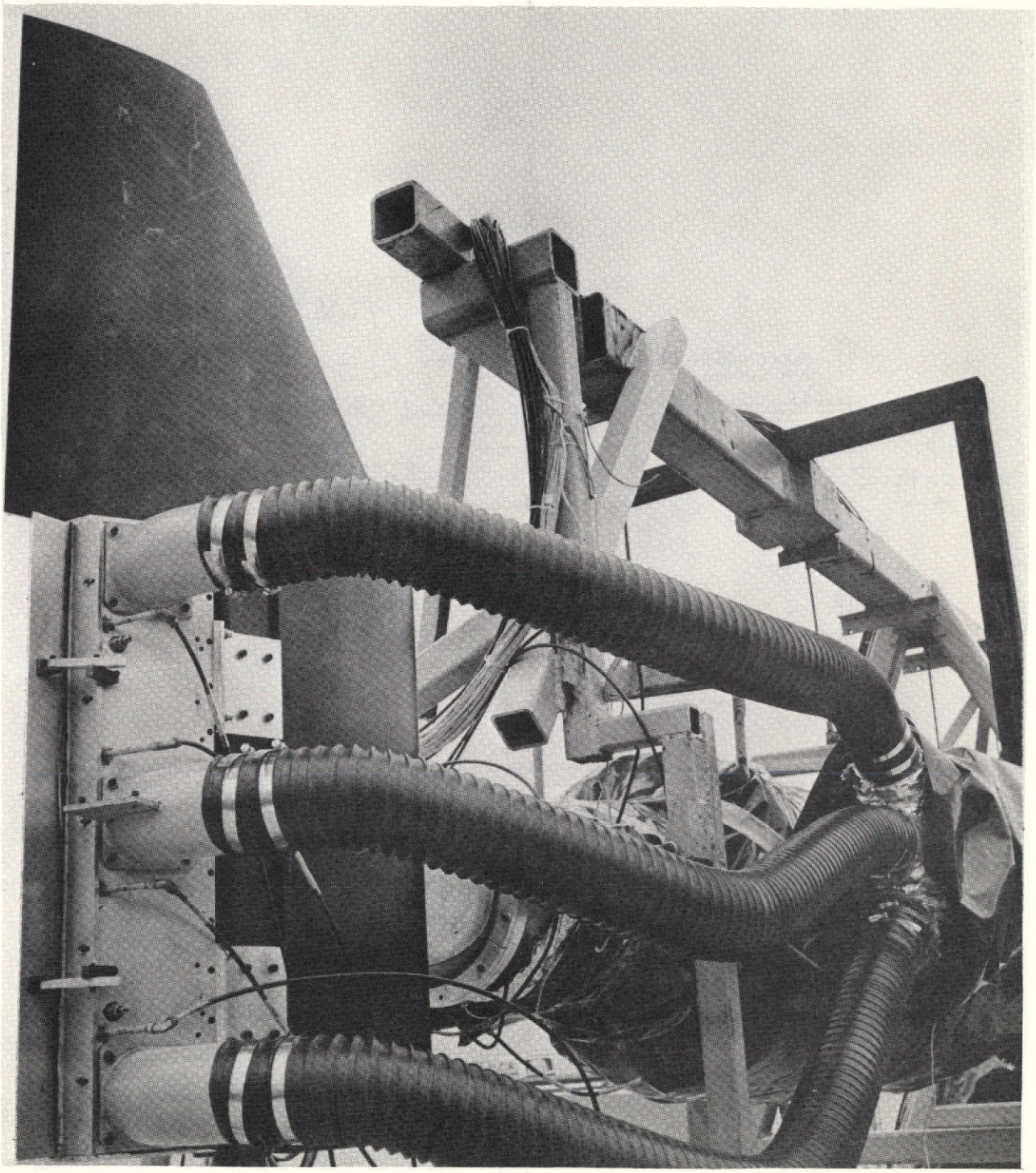

Figure 7 Flap air supply.

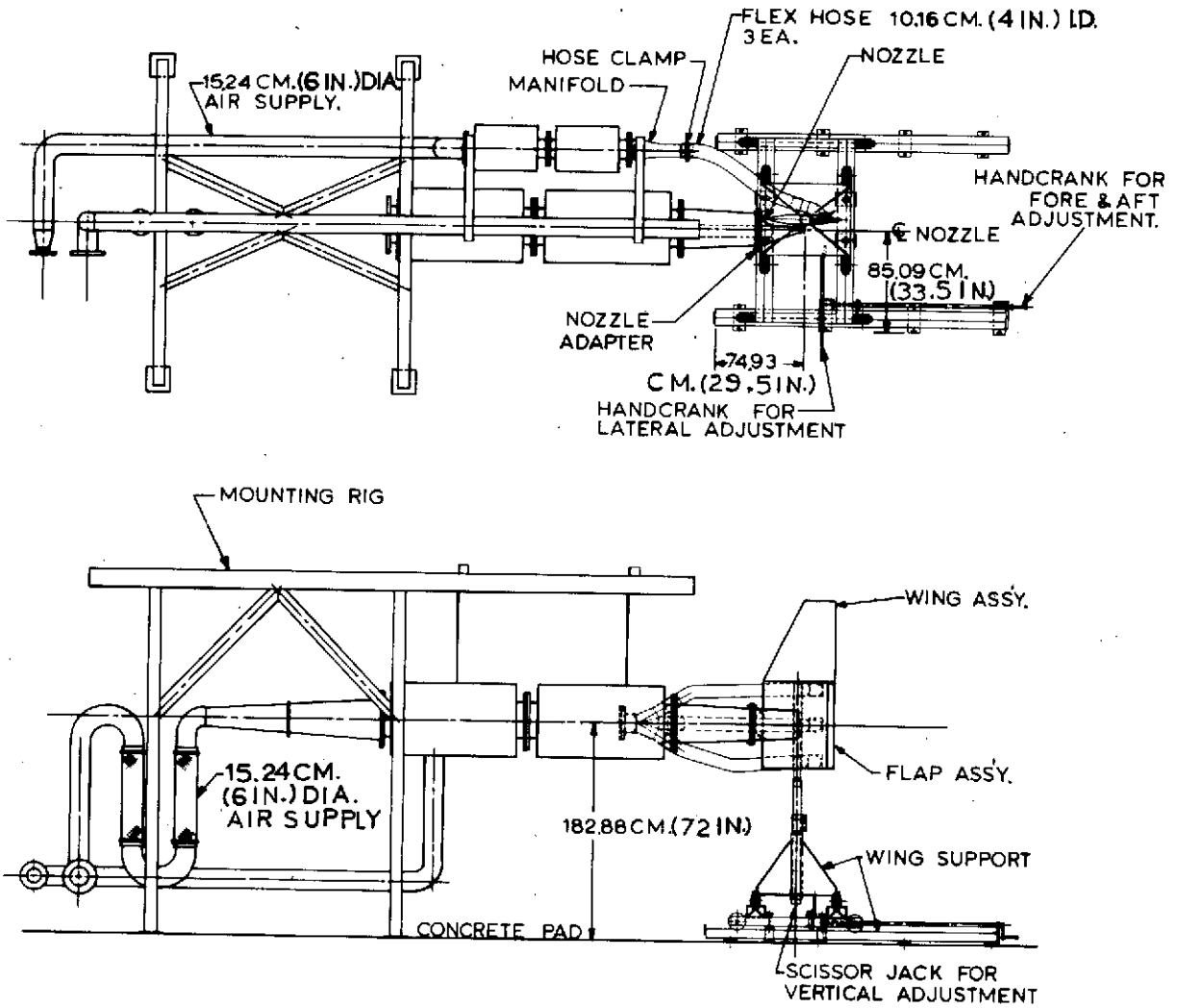

Figure 8 Test stand details.

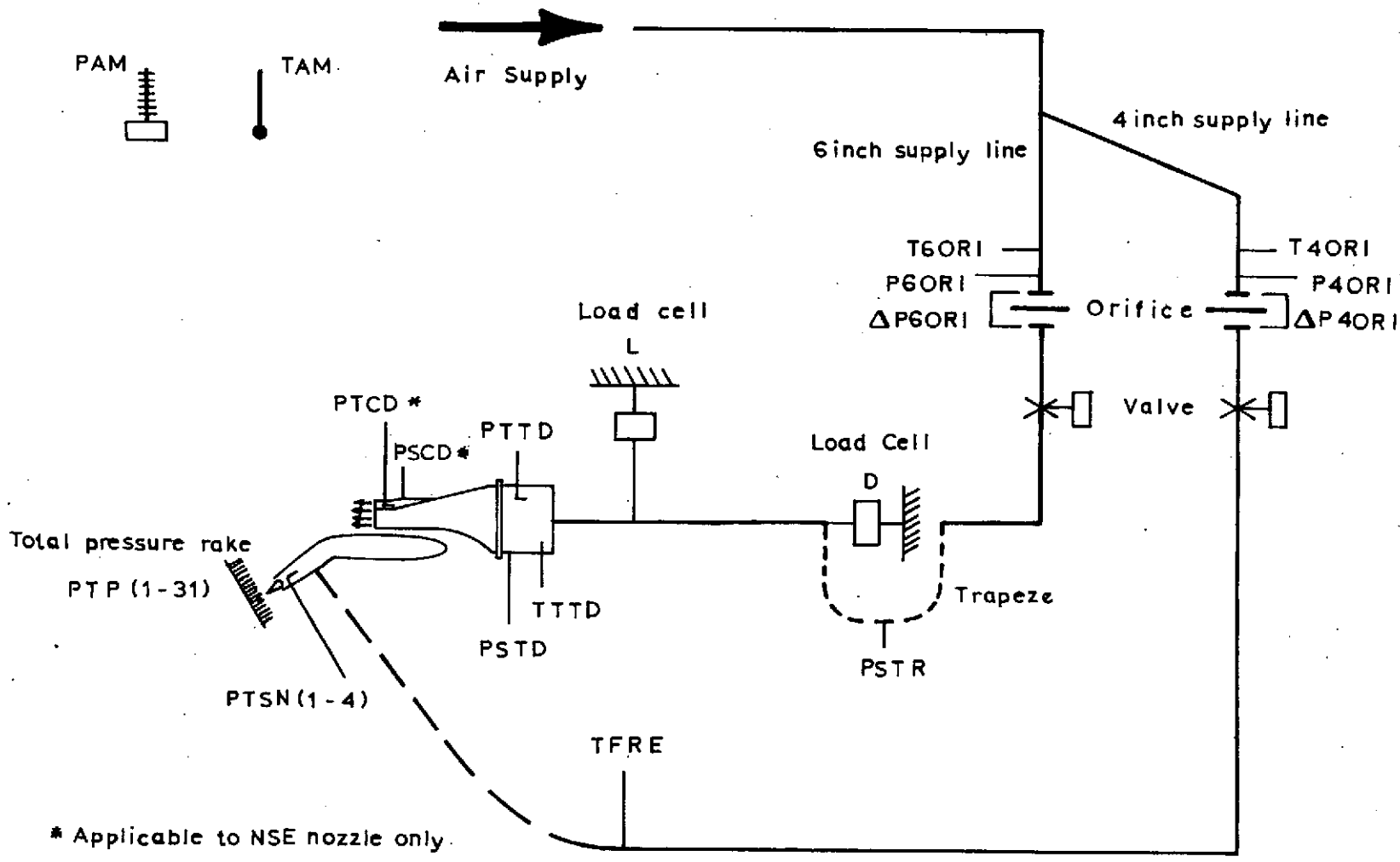

Figure 9 Instrumentation schematic.

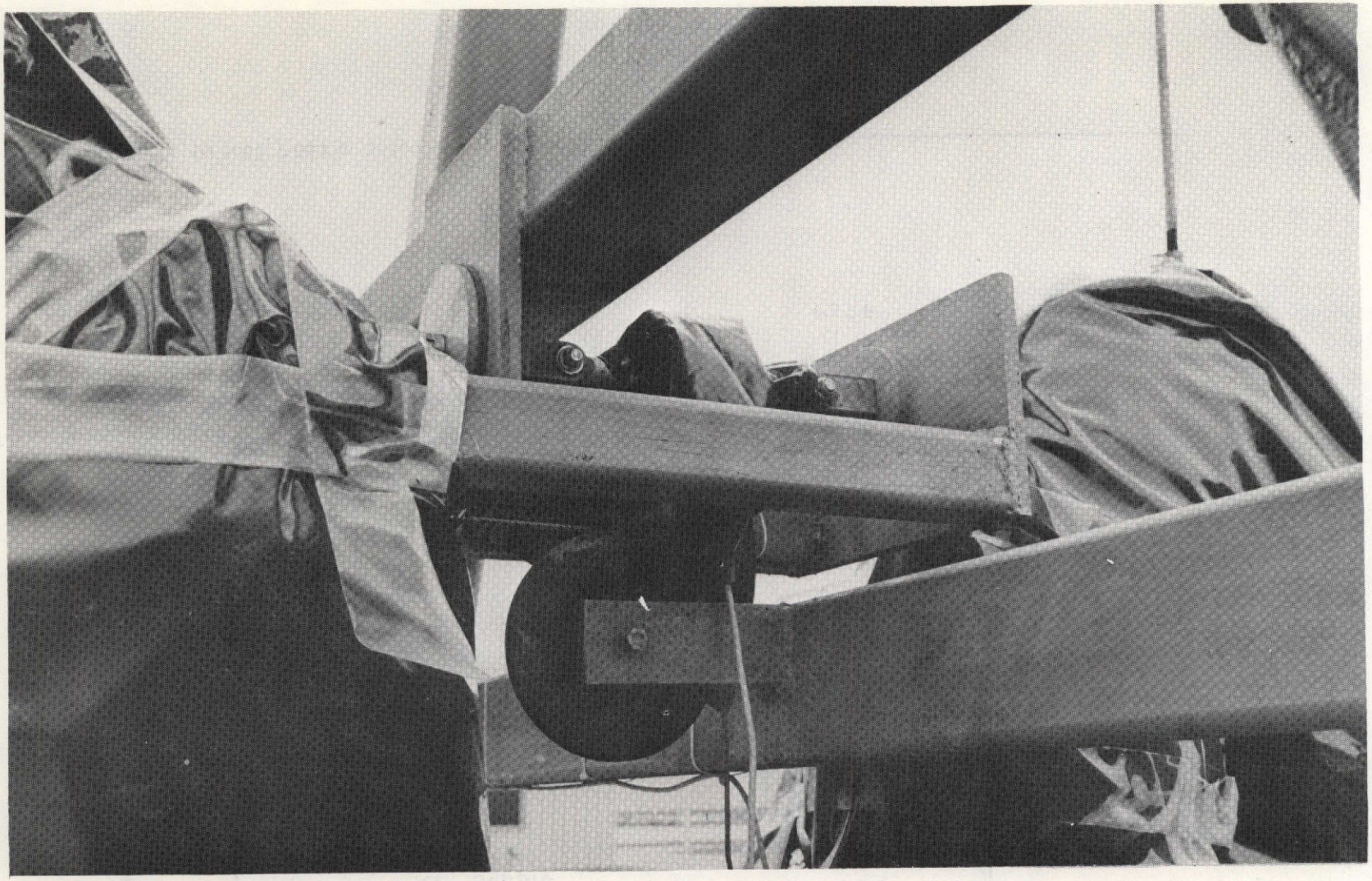

Figure 10 View of axial load cell installation.

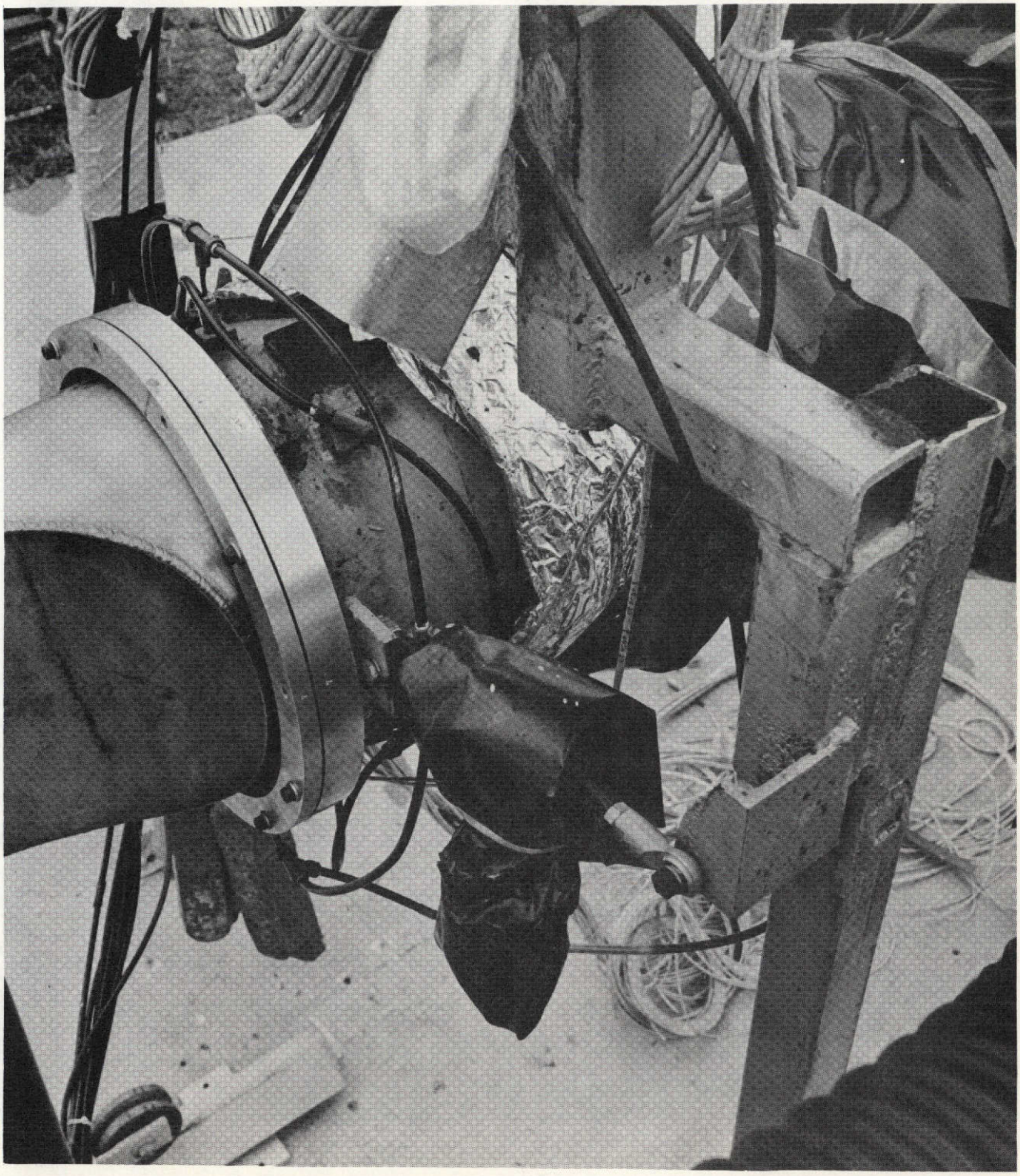

Figure 11 View of vertical load cell installation.

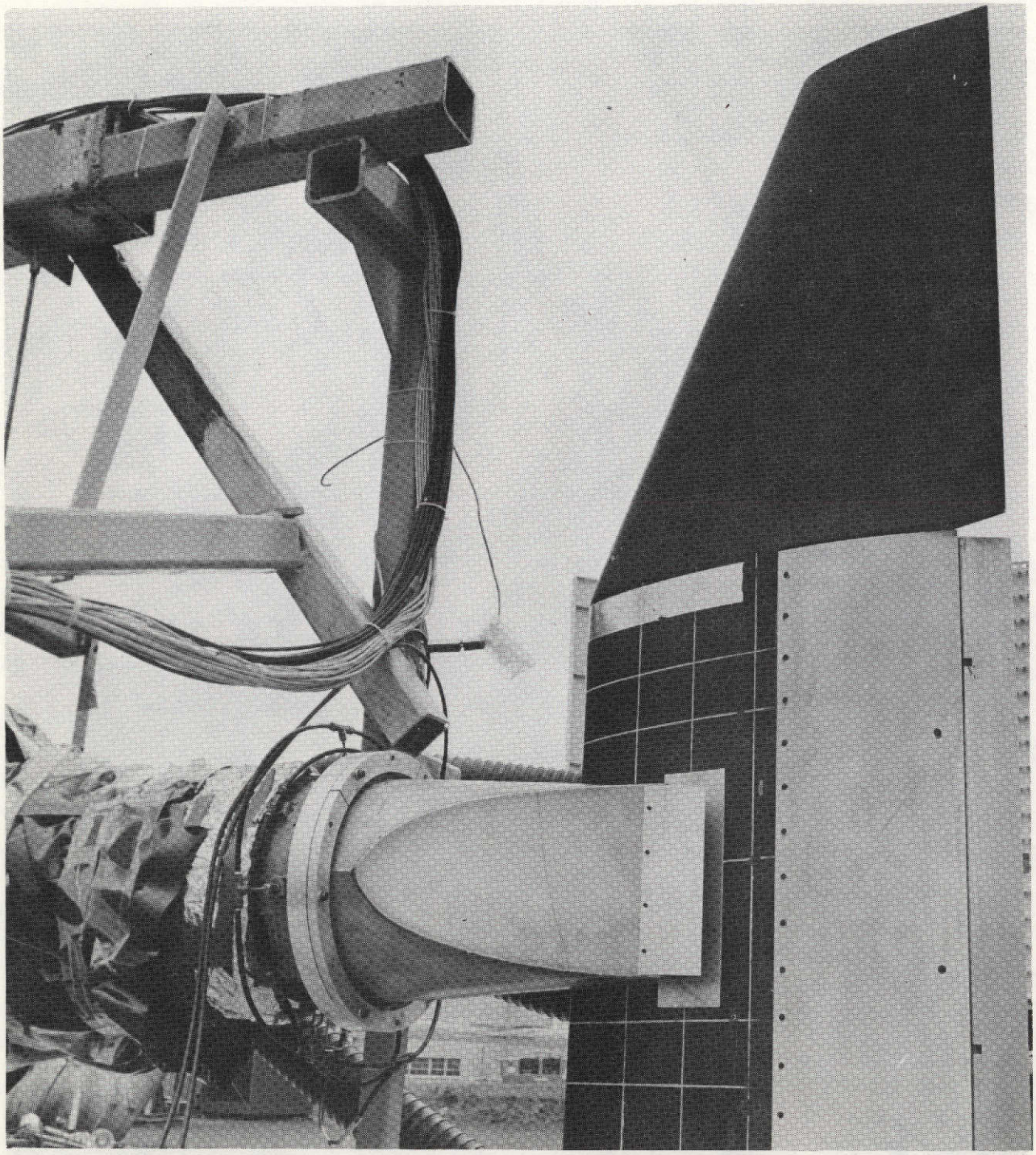

Figure 12 Nozzle pressure and temperature instrumentation.

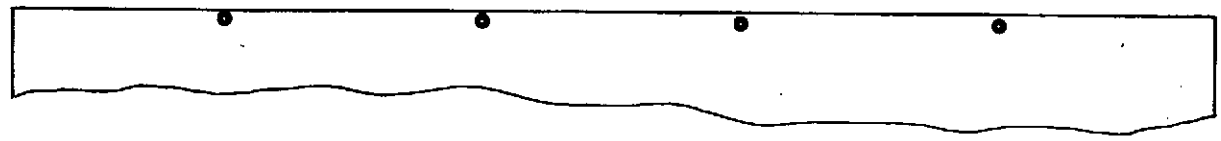

VIEW A-A (ROTATED)

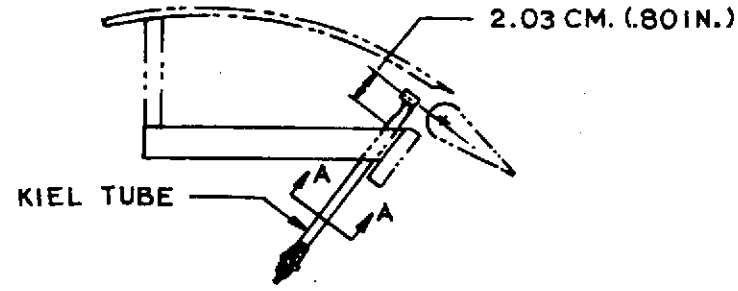

Figure 13 Detail of flap pressure probe installation.

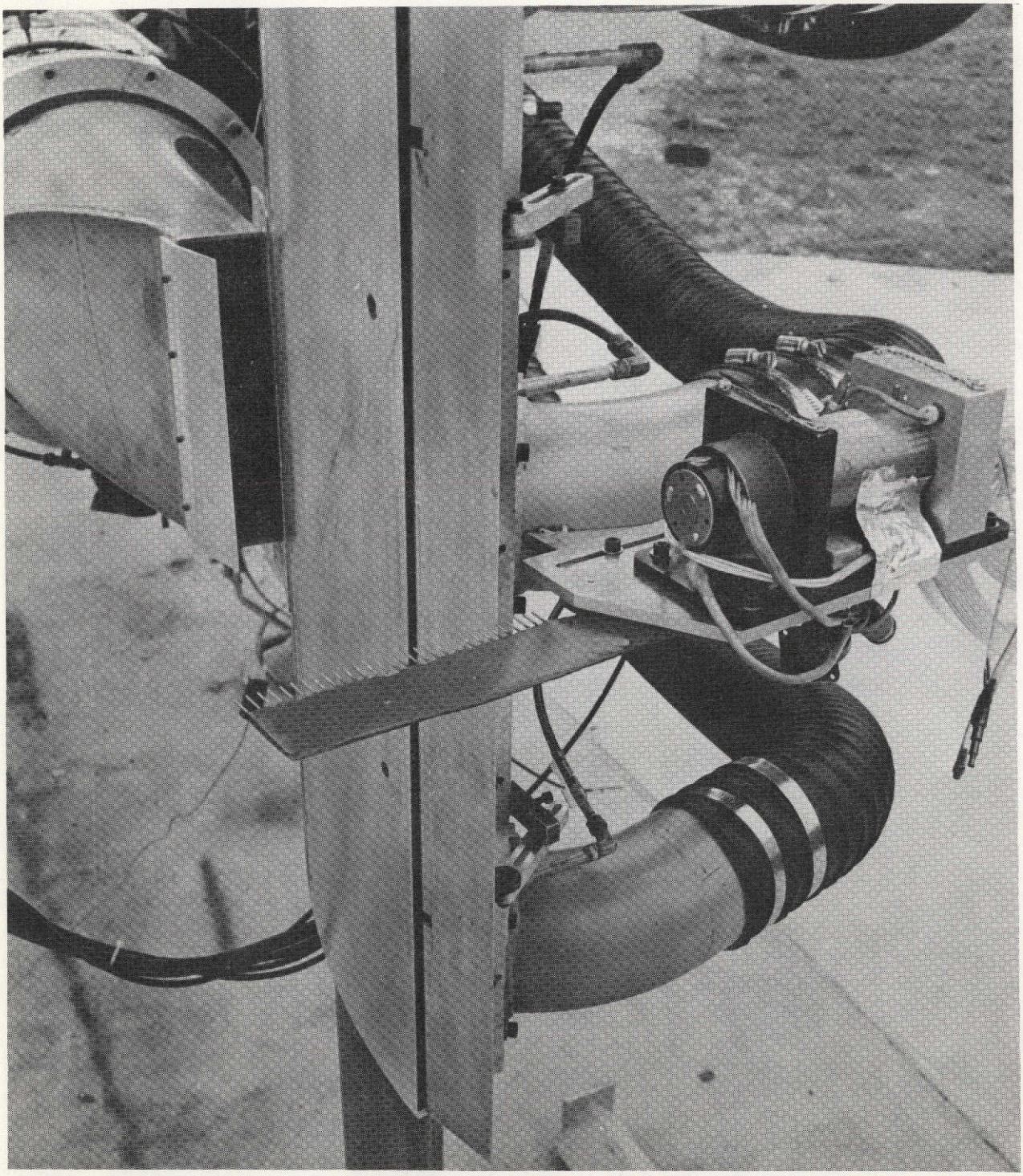

(a) Overall view.

Figure 14 Flap trailing edge pressure survey rake installation.

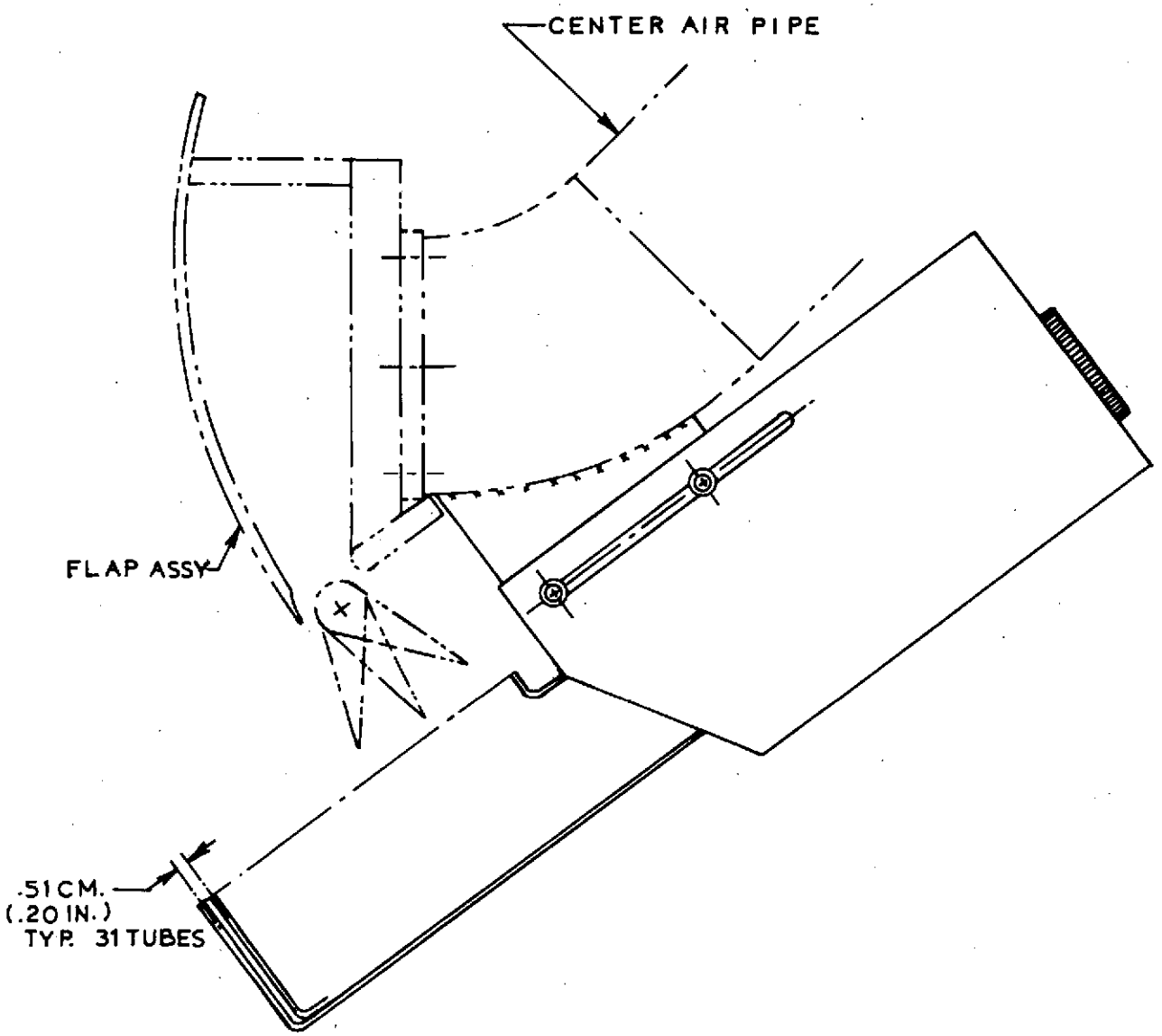

(b) Rake detail.

Figure 14 Concluded.

Figure 15 View of data acquisition system.

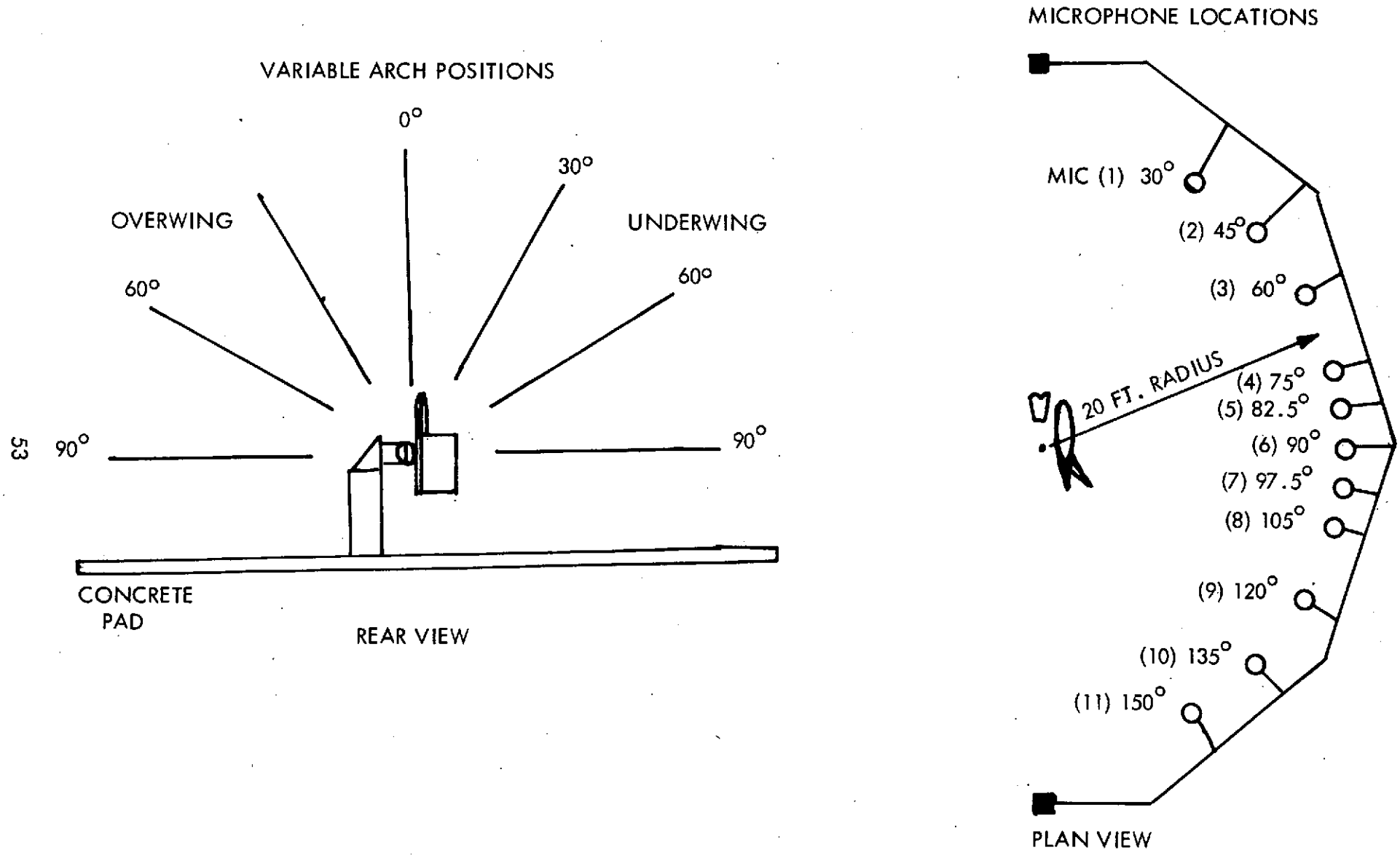

TEST FACILITY MICROPHONE LOCATIONS

FIGURE 16

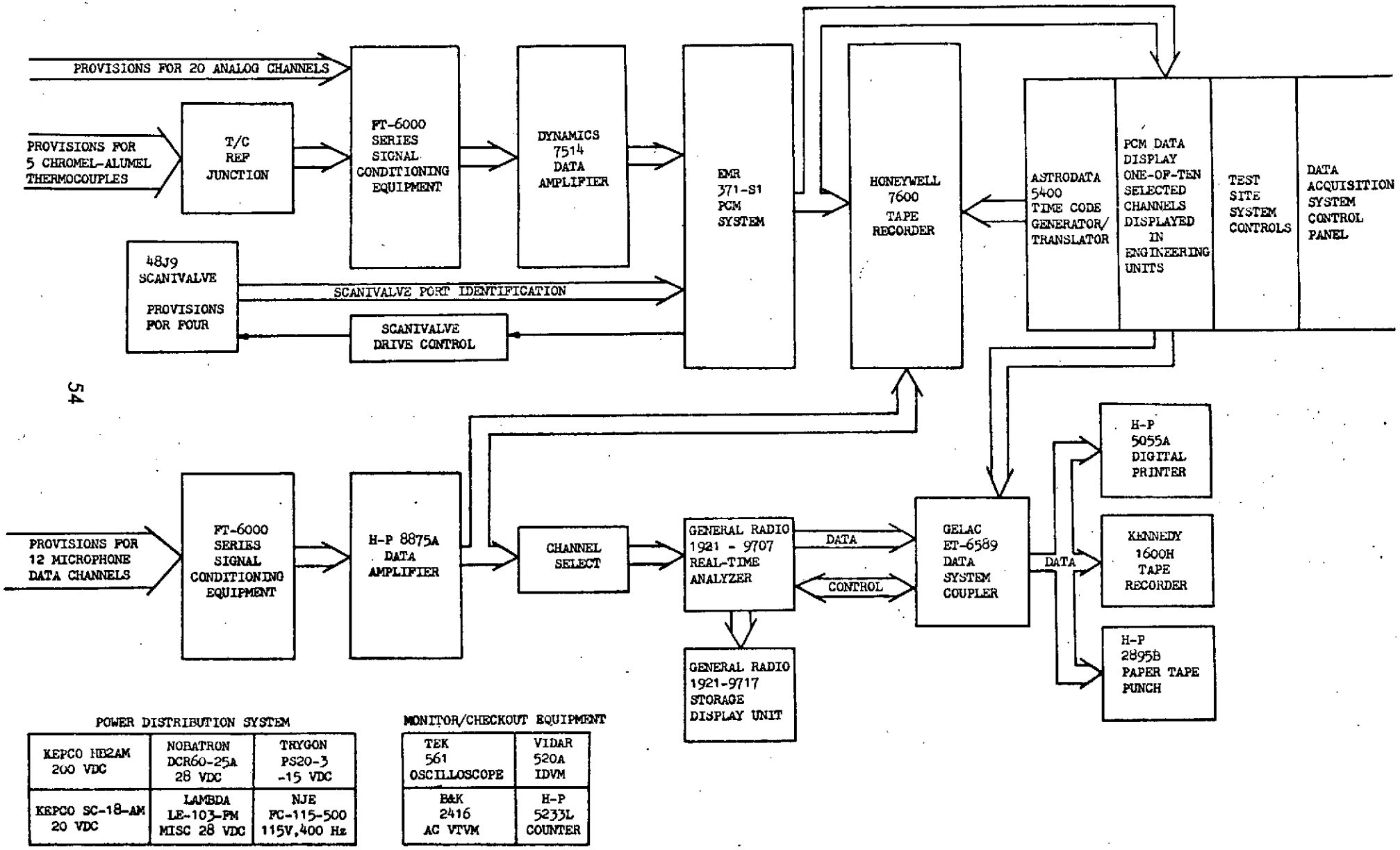

POWER DISTRIBUTION SYSTEM

KEPCO HB2AM 200 VDC	NOBATRON DCR60-25A 28 VDC	TRYGON PS20-3 -15 VDC
KEPCO SC-18-AM 20 VDC	LAMBDA LE-103-FM MISC 28 VDC	NJE FC-115-500 115V,400 Hz

MONITOR/CHECKOUT EQUIPMENT

TEK 561 OSCILLOSCOPE	VIDAR 520A IDVM
B&K 2416 AC VTVM	H-P 5233L COUNTER

ACOUSTIC AND PERFORMANCE DATA ACQUISITION SYSTEM BLOCK DIAGRAM

FIGURE 17

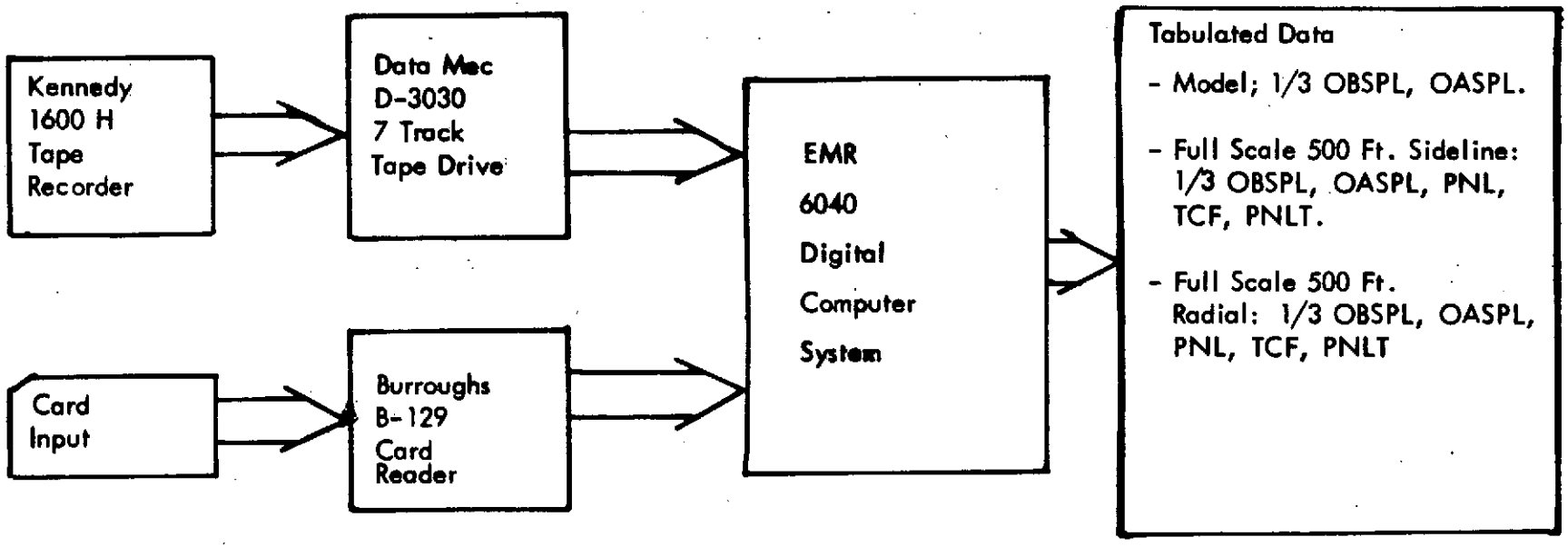

Figure 18 Acoustic Data Reduction System

DATA REDUCTION AND SCALING

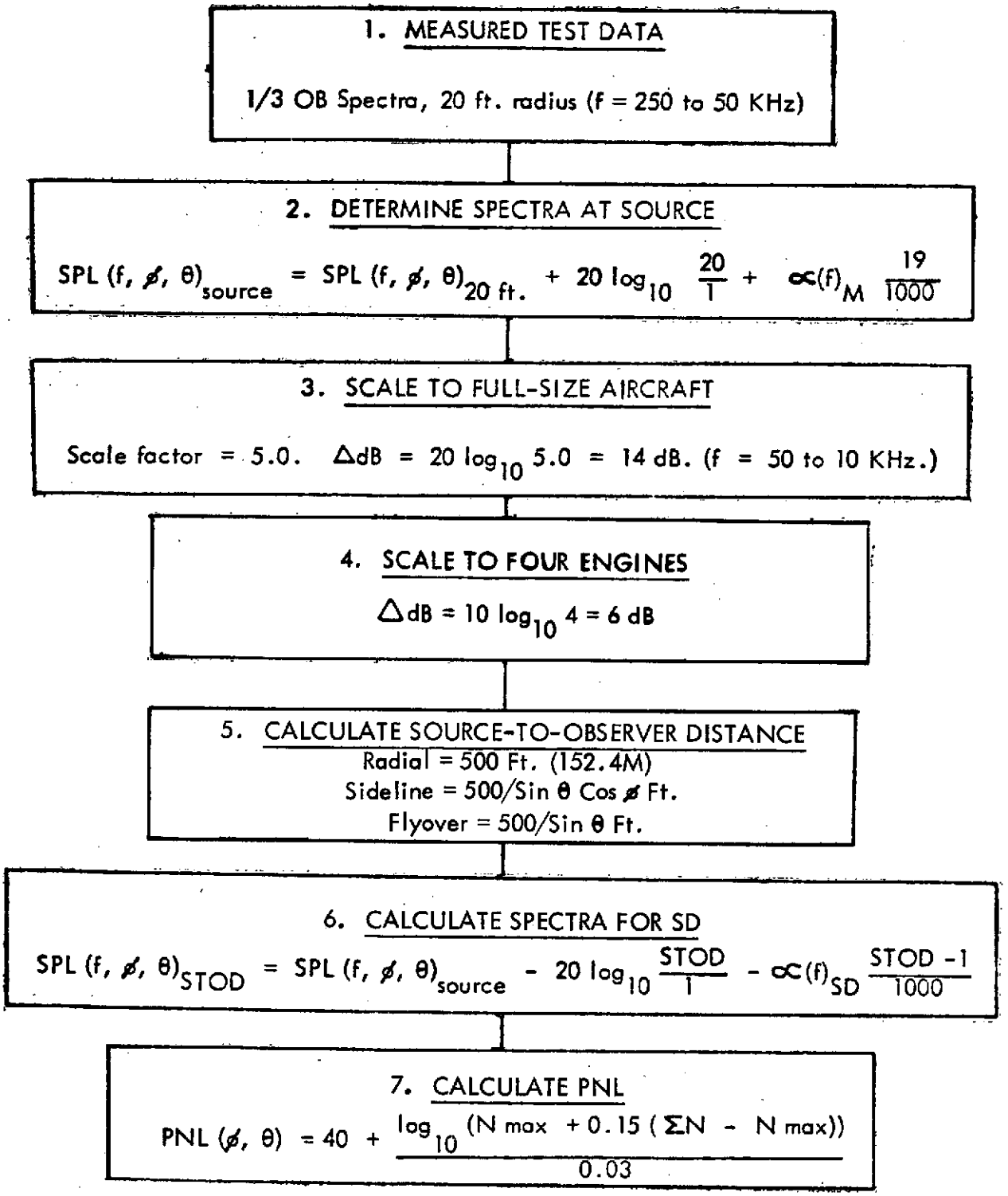

Figure 19a

MIC Pos. No.	Angular Position 0		Microphone Distance		500 Ft. Radial		500 Ft. Sideline						500 Ft. Flyover	
							0° Arch		30° Arch		60° Arch		90° Arch	
	Deg.	Rad.	Ft.	M.	Ft.	M.	Ft.	M.	Ft.	M.	Ft.	M.	Ft.	M.
1	30.0	.524	20.0	6.1	500.0	152.4	1000.0	304.8	1154.7	352.0	2000.0	609.6	1000.0	304.8
2	45.0	.785					707.1	215.5	816.5	248.9	1414.2	431.1	707.1	215.5
3	60.0	1.047					577.4	176.0	666.7	203.2	1154.7	352.0	577.4	176.0
4	75.0	1.309					517.6	157.8	597.7	182.2	1035.3	315.6	517.6	157.8
5	82.5	1.440					504.3	153.7	582.3	177.5	1008.6	307.4	504.3	153.7
6	90.0	1.571					500.0	504.3	577.3	176.0	1000.0	304.8	500.0	152.4
7	97.5	1.702					504.3	153.7	582.3	177.5	1008.6	307.4	504.3	153.7
8	105.0	1.833					517.6	157.8	597.7	182.2	1035.3	315.5	517.6	157.8
9	120.0	2.094					577.3	176.0	666.7	203.2	1157.7	351.9	577.3	176.0
10	135.0	2.356					707.1	215.5	816.5	248.9	1414.2	431.0	707.1	215.5
11	150.0	2.618					1000.0	304.8	1154.7	351.9	2000.0	609.7	1000.0	304.8
5'	165.0	2.880	19.83	6.03			1931.9	588.8	2230.7	679.9	3863.7	1177.7	1931.9	588.8
7'	172.5	3.011	19.42	5.90			3830.7	1167.6	4423.3	1348.2	7661.3	2335.2	3830.7	1176.7

Figure 19b Description of Microphone and Full Scale Locations

Parametric Variations or Test Condition / Model Configurations	Baseline	Nozzle Chord Position	Noz. Impingement Angle	Auxiliary Flap Deflection	Nozzle/Flap Area	TE/Knee Flow Split	Flap Flow with no USB	Flap Flow relative to Noz.	USB only	Nozzle Span Location	Wing Tip Removed	Overwing Noise	Flap-Wing Tip Gap Closed	NR4D Bottom Plate Off	Effect of Attachment
JH Flap - Landing															
NR4D	X	X	X	X	X	X	X	X	X	X	X	X	X	X	
NR8	X	X	X												
NR4	X														X
NSE															
JH Flap - Takeoff															
NR4D	X	X	X	X	X	X		X	X	X	X	X			
NR8	X	X	X	X	X	X									
NR4	X														
NSE	X														
Flex Flap - Landing															
NR4D	X	X	X	X	X		X	X	X	X		X			
NR8	X	X	X	X	X			X	X			X			
NR4	X		X						X						X
NSE	X		X						X						X
Flex Flap - Takeoff															
NR4D	X	X	X	X	X				X			X			
NR8	X	X	X	X	X				X			X			
NR4	X		X						X						X
NSE	X		X						X						X
Nozzle Calibration															
NR4D	X														
NR8	X														
NR4	X														
NSE	X														

Figure 20 Summary of Test Program

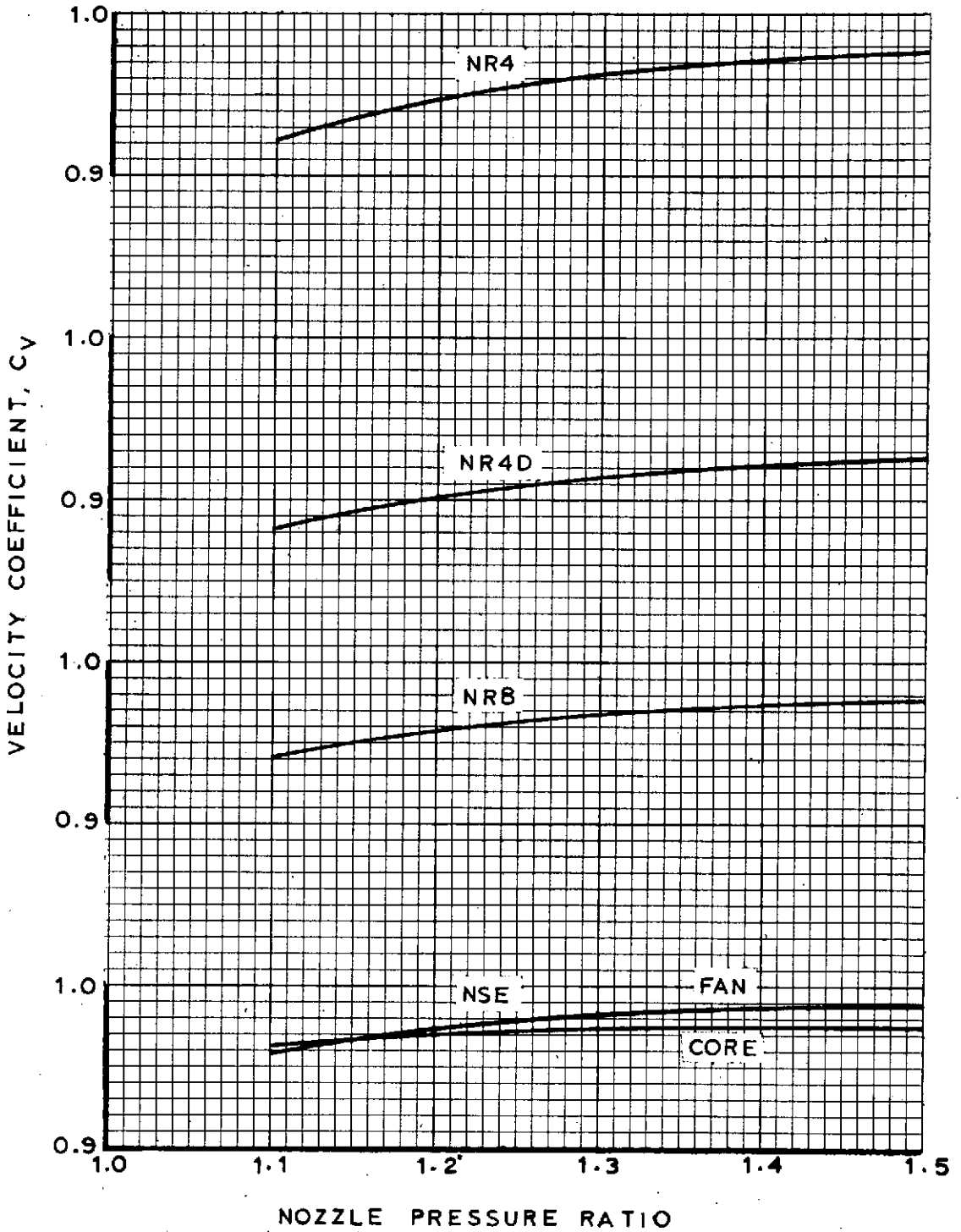

Figure 21 Nozzle velocity coefficients.

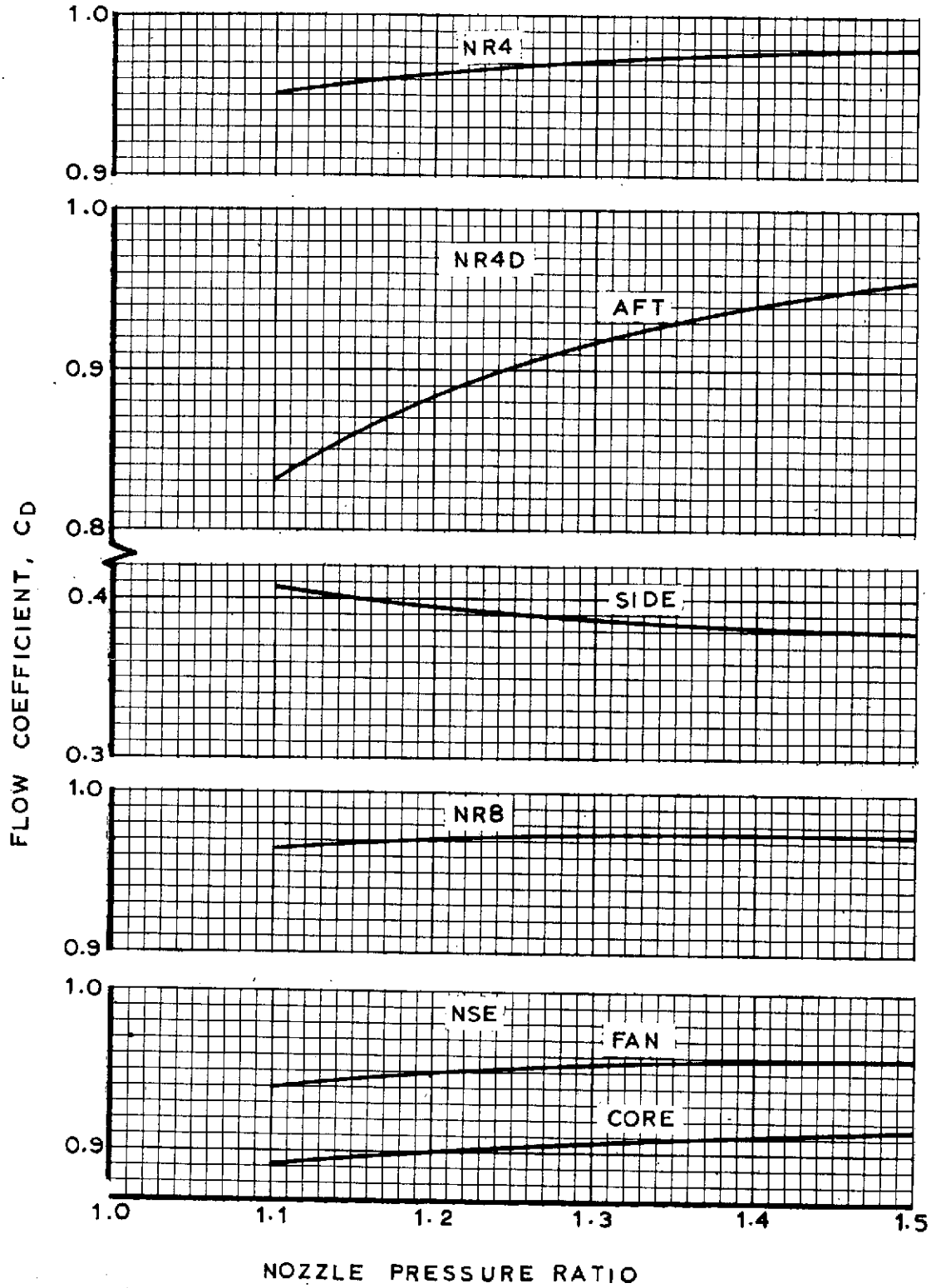

Figure 22 Nozzle flow coefficients.

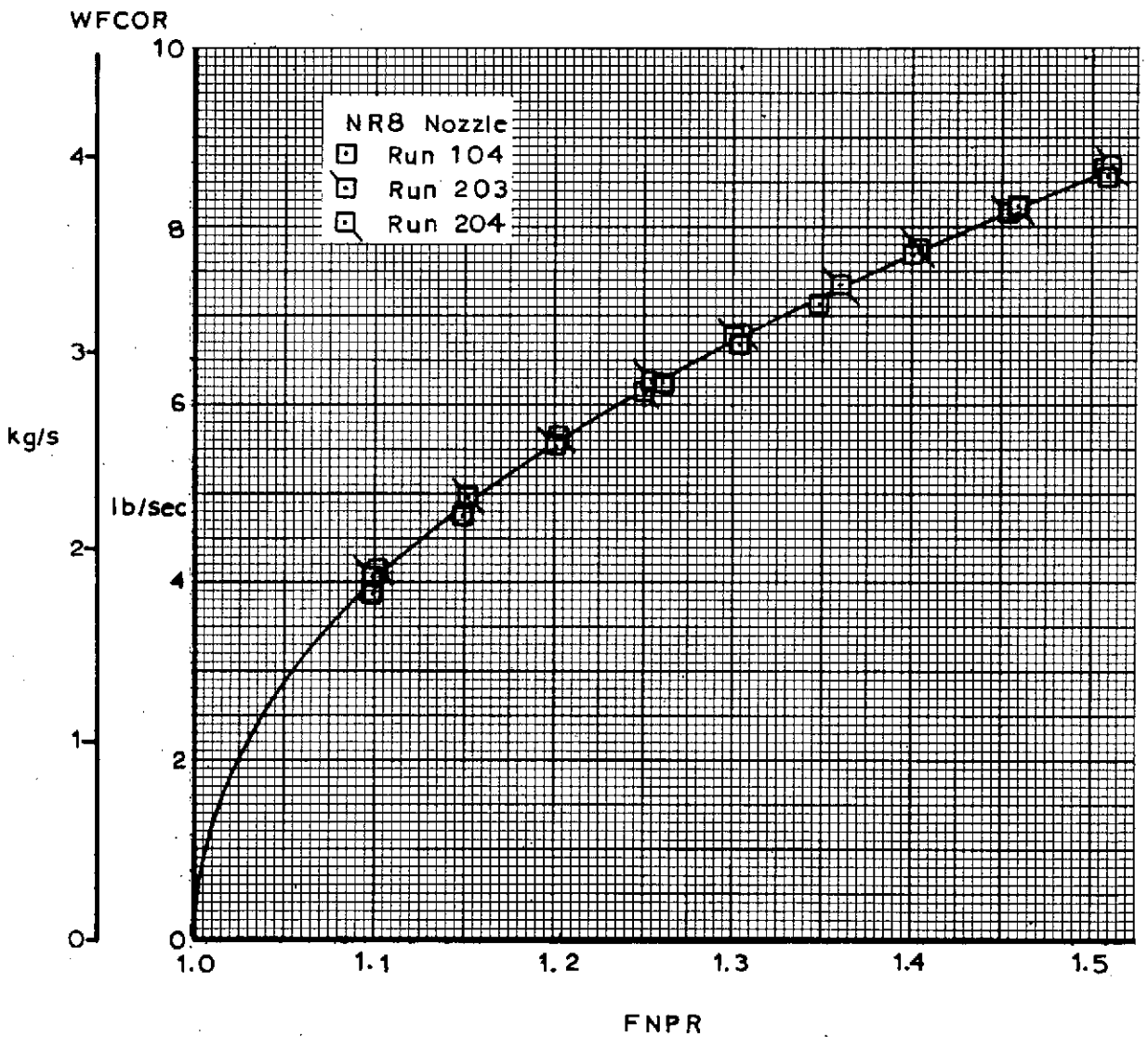

(a) NR8 nozzle.

Figure 23 Measured nozzle airflow rate.

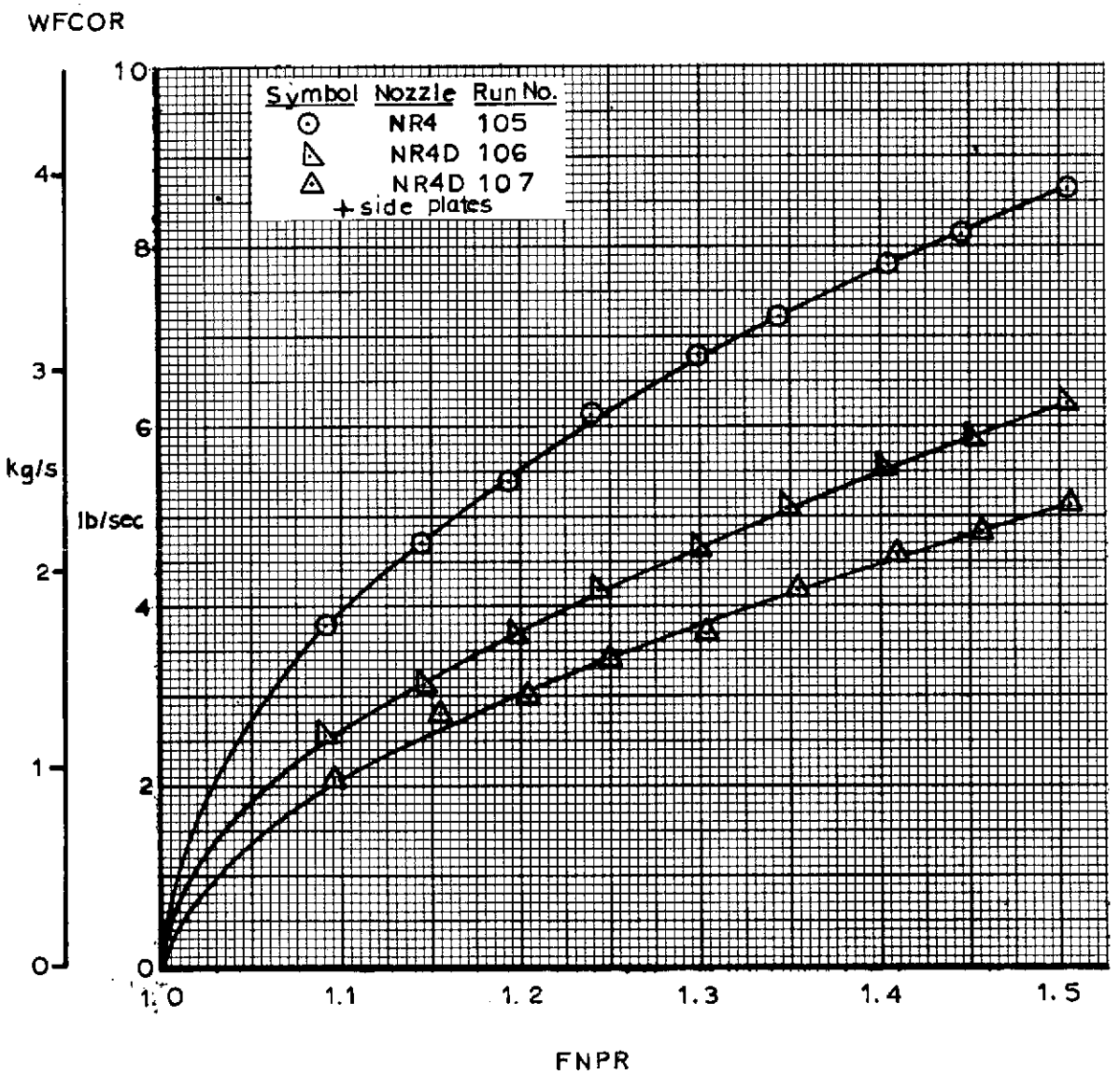

(b) NR4 and NR4D nozzle.

Figure 23 Continued.

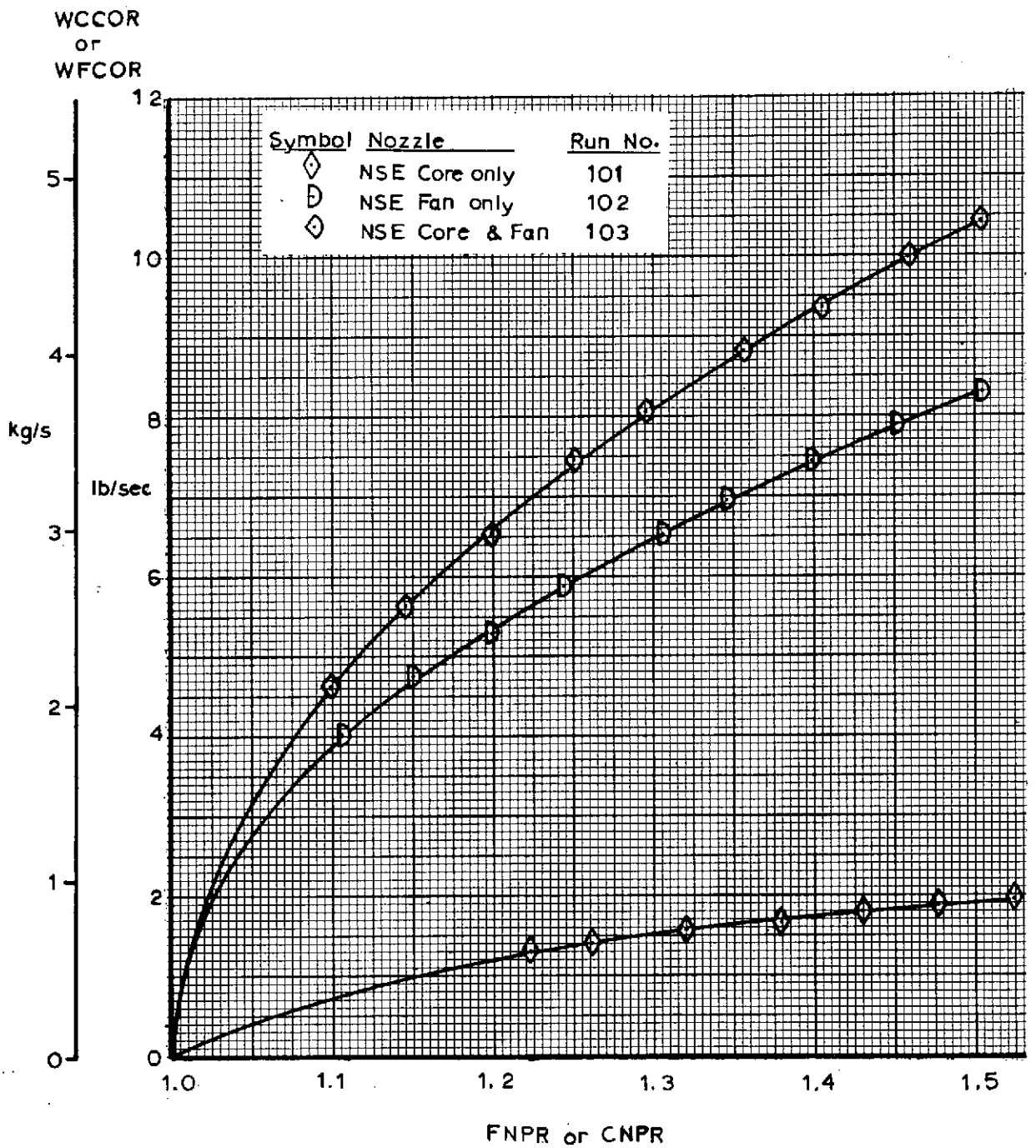

(c) NSE nozzle.

Figure 23 Concluded.

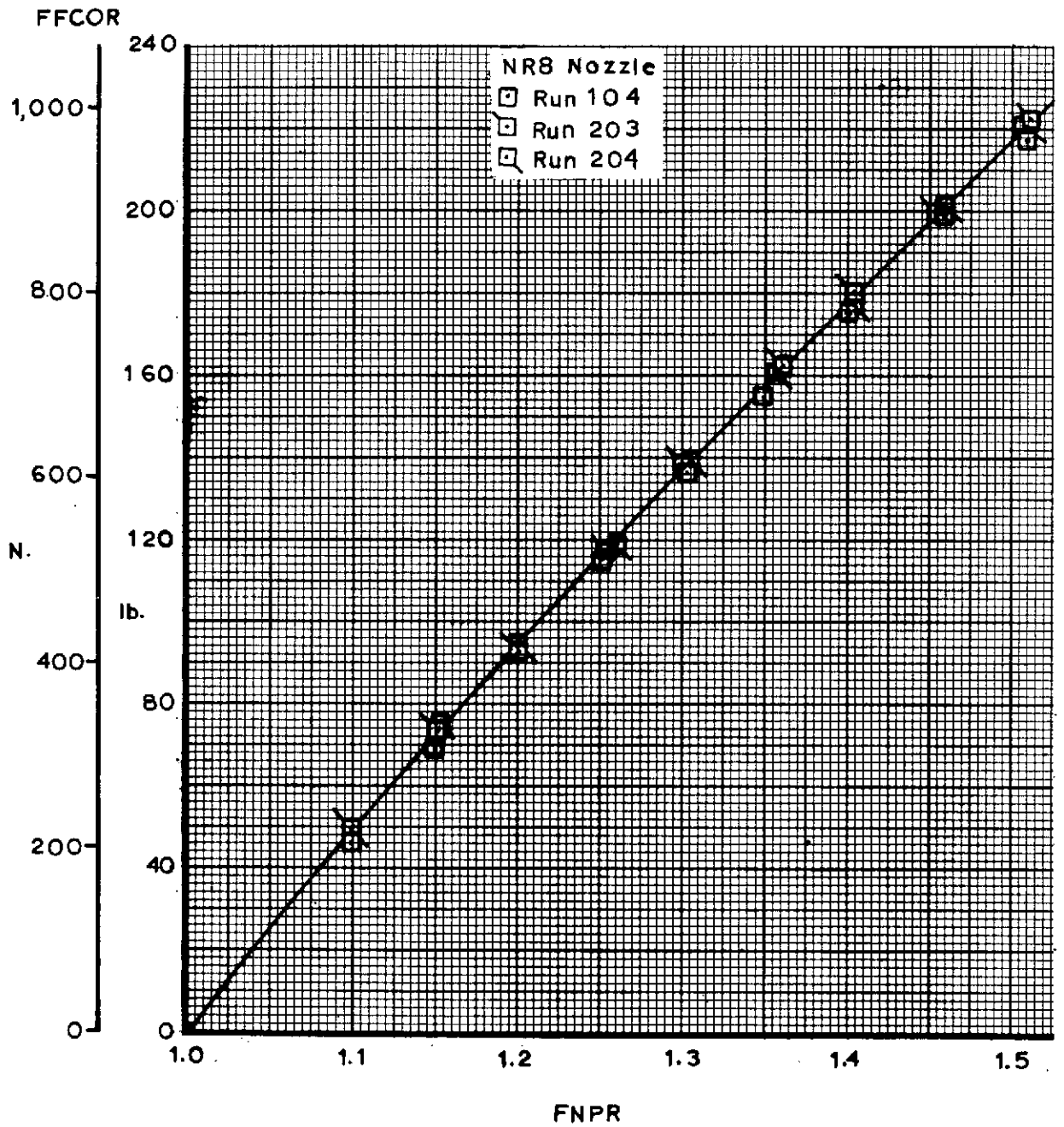

(a) NR8 nozzle.

Figure 24 Measured nozzle thrust.

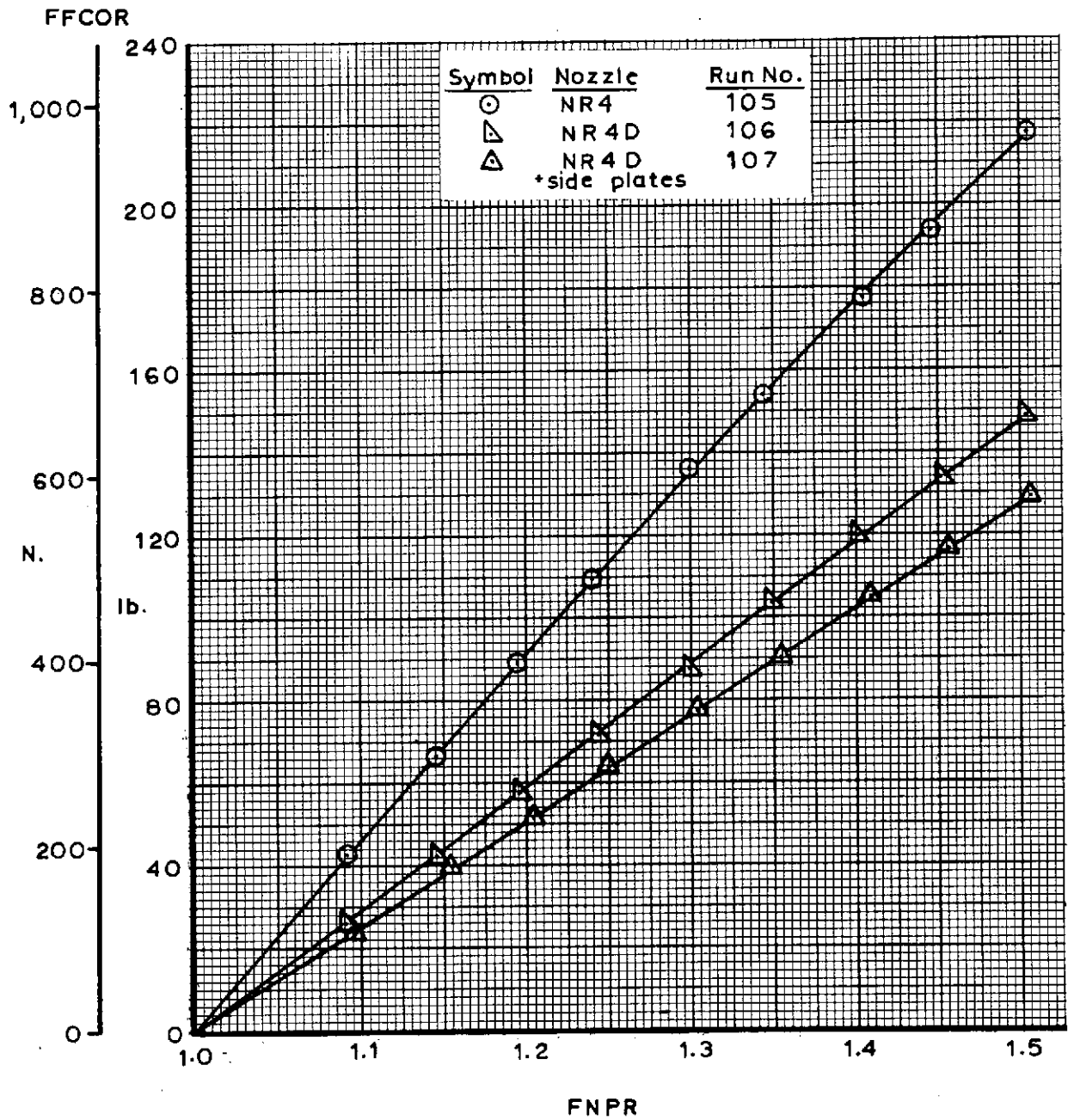

(b) NR4 and NR4D nozzle.

Figure 24 Continued.

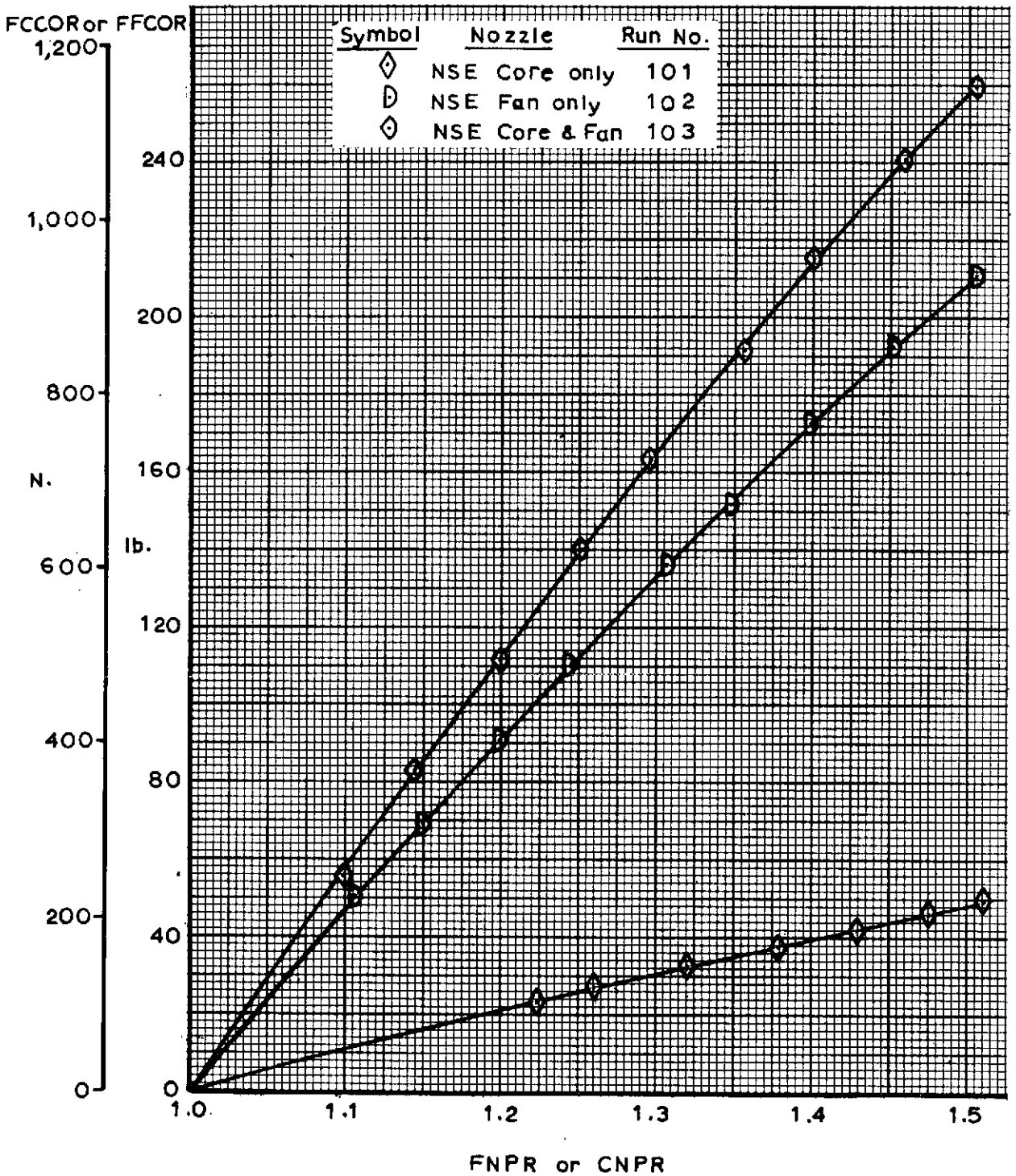

(c) NSE nozzle.

Figure 24 Concluded.

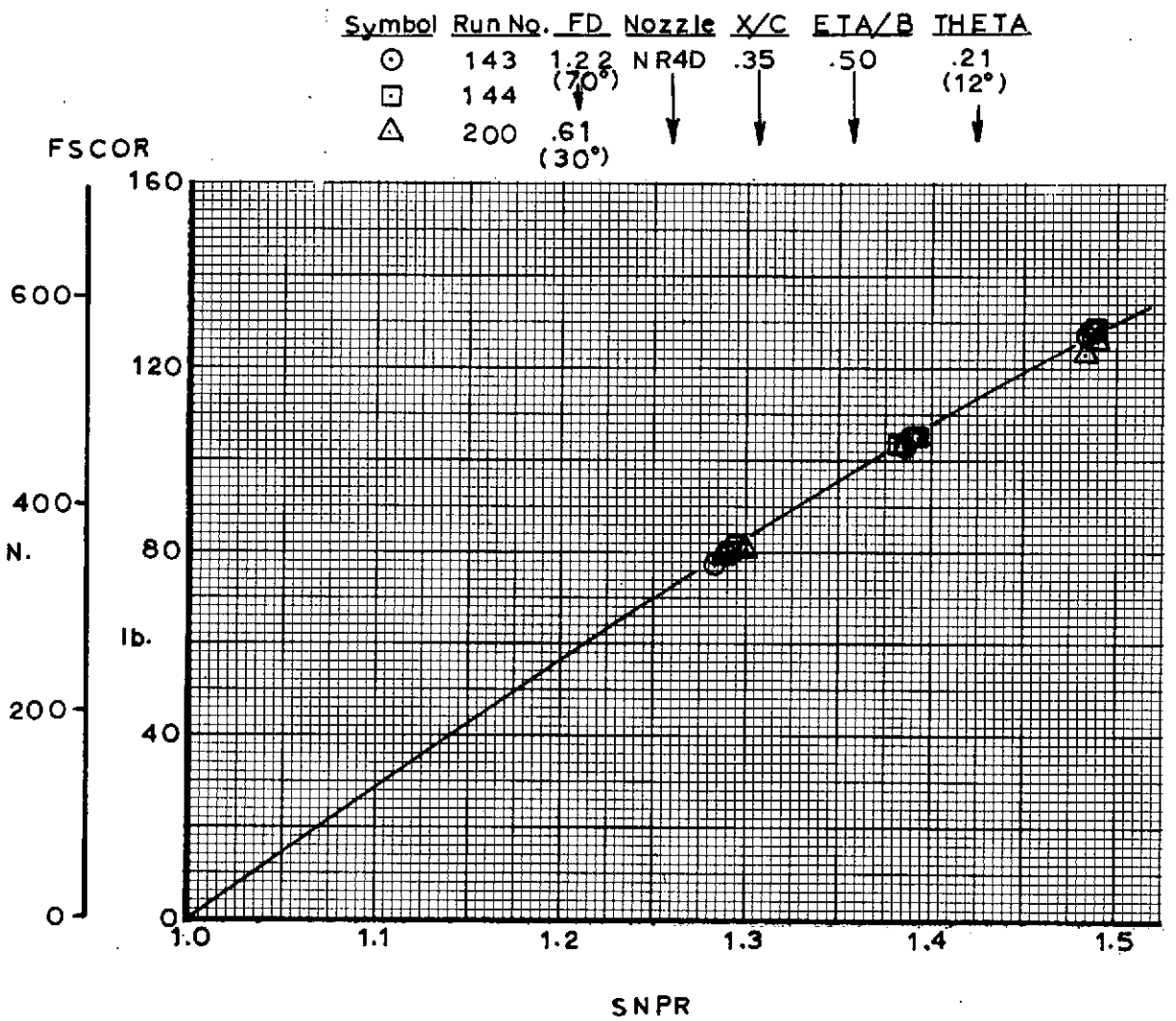

(a) Knee slot height, SK = 0.032 in. (0.081 cm.). Trailing edge slot height, STE = 0.284 in. (0.721 cm.).

Figure 25 Calculated flap slot thrust based on measured airflow rates and nozzle pressure ratio. Jacobs-Hurkamp flap.

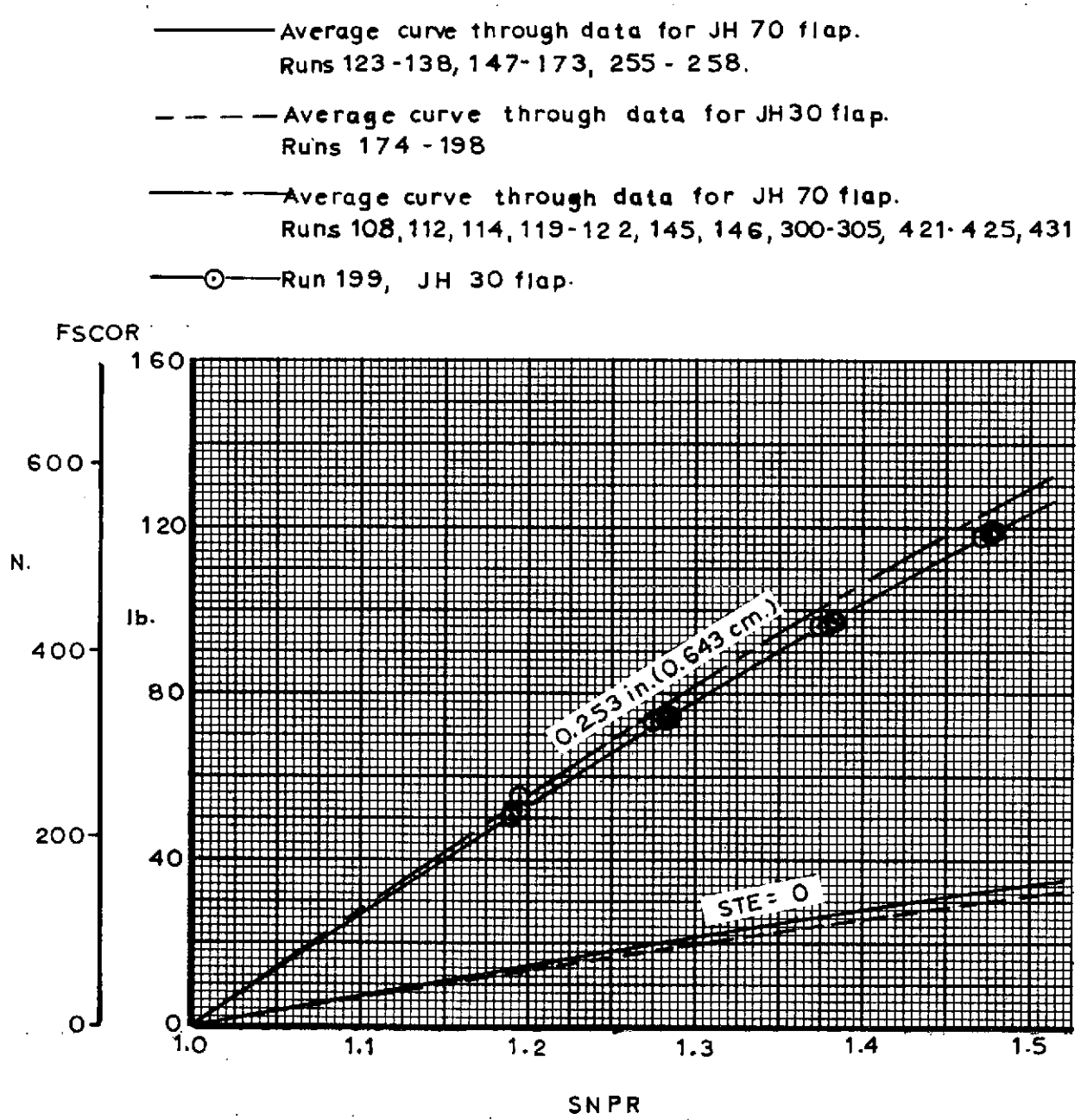

(b) Knee slot height, SK = 0.063 in. (0.160 cm.). Trailing edge slot height, STE = 0 and 0.253 in. (0.643 cm.).

Figure 25 Continued.

Symbol	Run No.	FD	Nozzle	X/C	ETA/B	THETA
○	253	1.22 (70°)	NR4D	.35	.50	.21 (12°)
□	254					
△	259					
◇	260					
▽	261					
D	262		NR4D1			

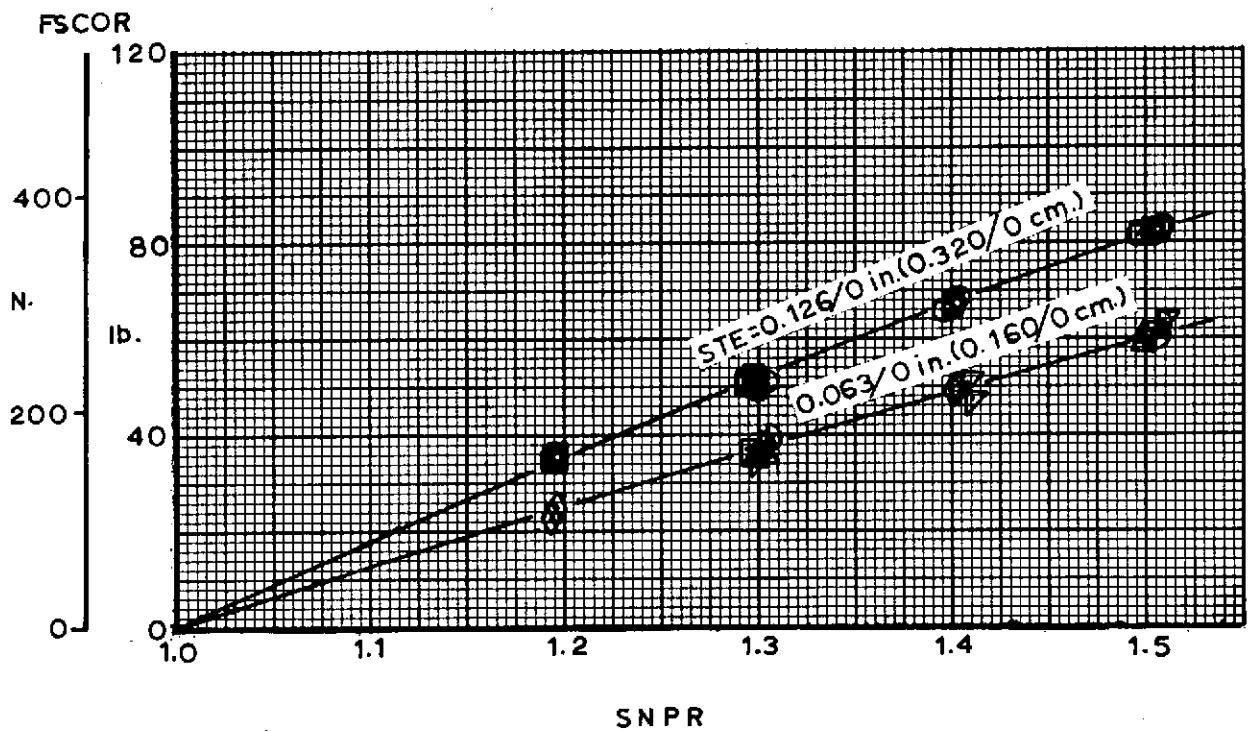

(c) Knee slot height, SK = 0.063 in. (0.160 cm.). Trailing edge slot height, STE = 0.063/0 in. (0.160/0 cm.) and 0.126/0 in. (0.320/0 cm.).

Figure 25 Continued.

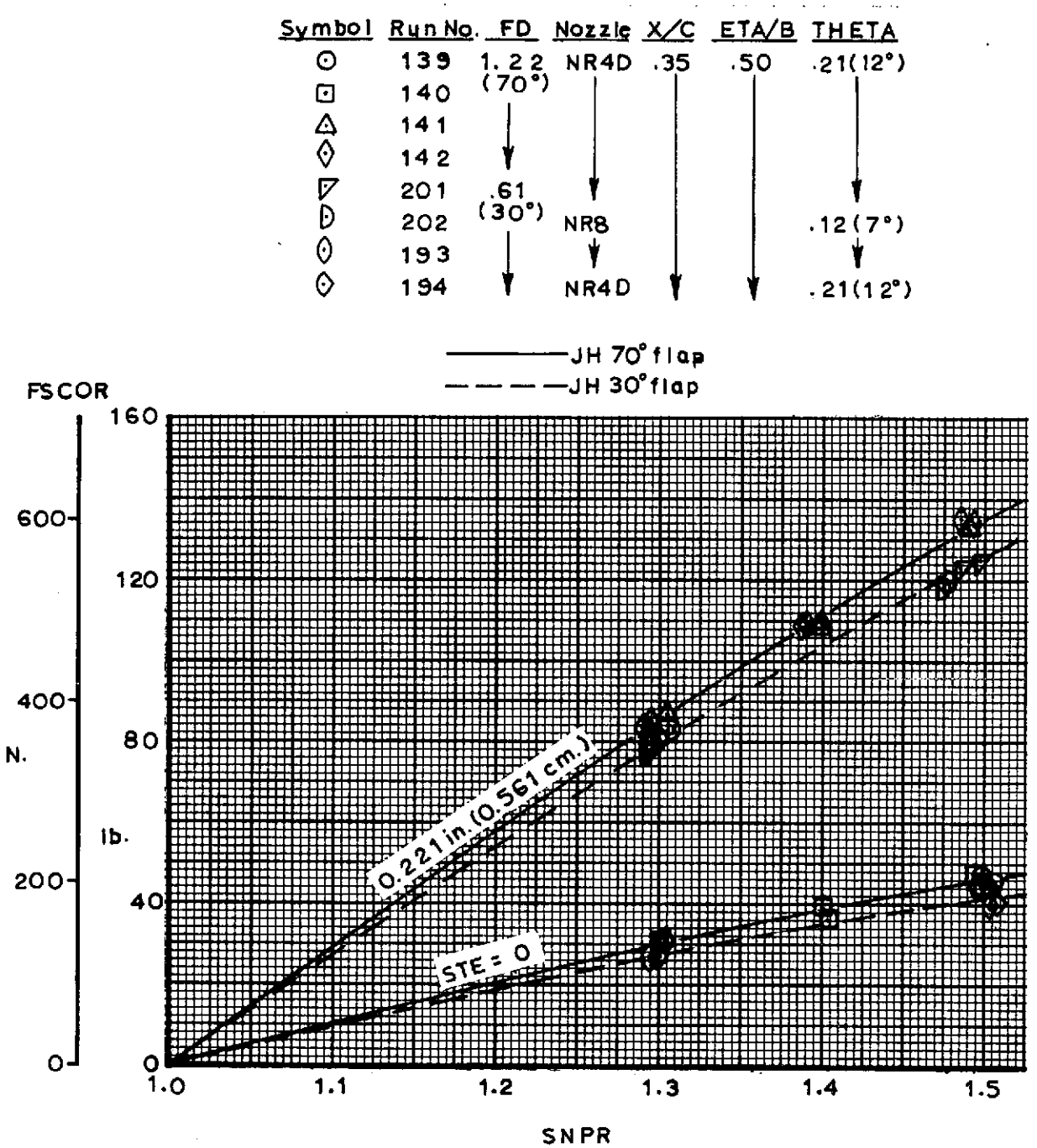

(d) Knee slot height, SK = 0.095 in. (0.241 cm.). Trailing edge slot height, STE = 0 and 0.221 in. (0.561 cm.).

Figure 25 Concluded.

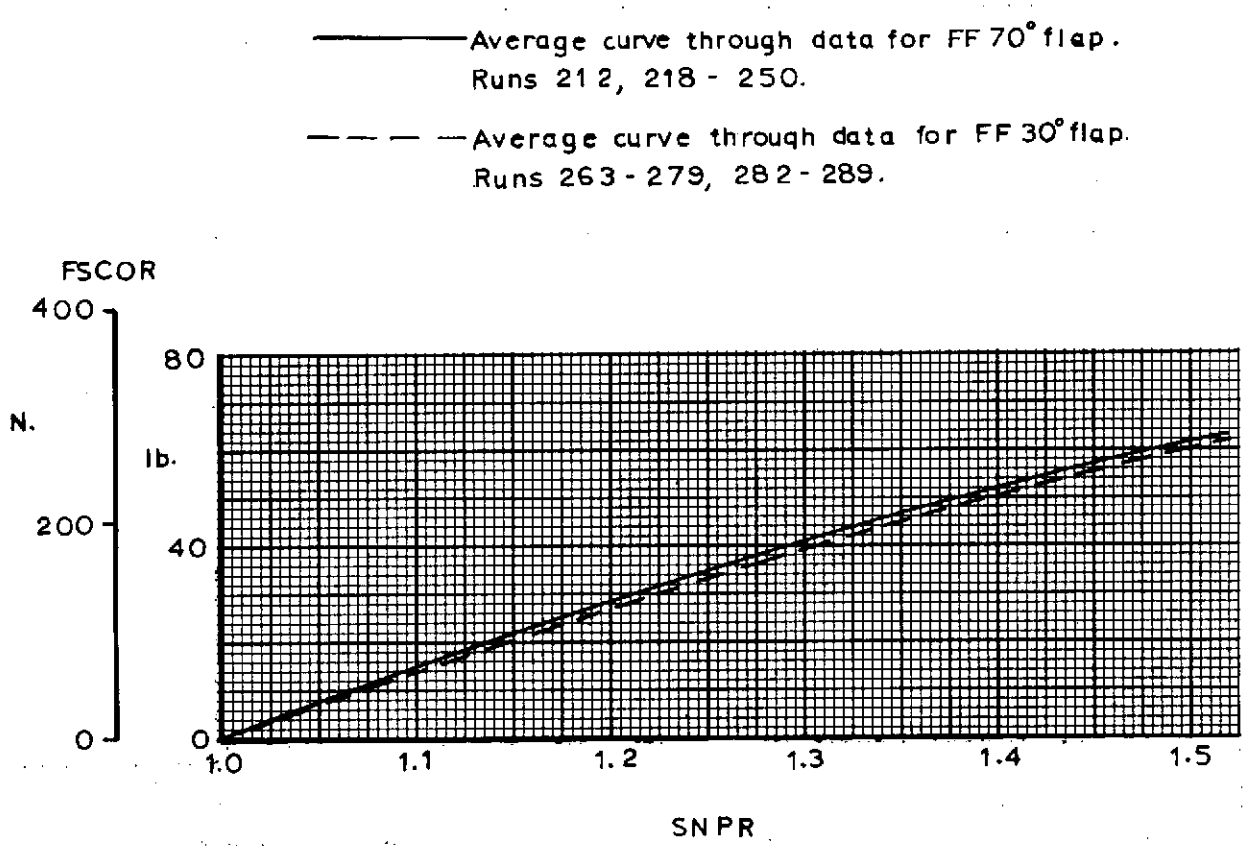

(a) Trailing edge slot height, STE = 0.158/0 in. (0.401/0 cm.).

Figure 26 Calculated flap slot thrust based on measured airflow rates and nozzle pressure ratio. Flex-Flap.

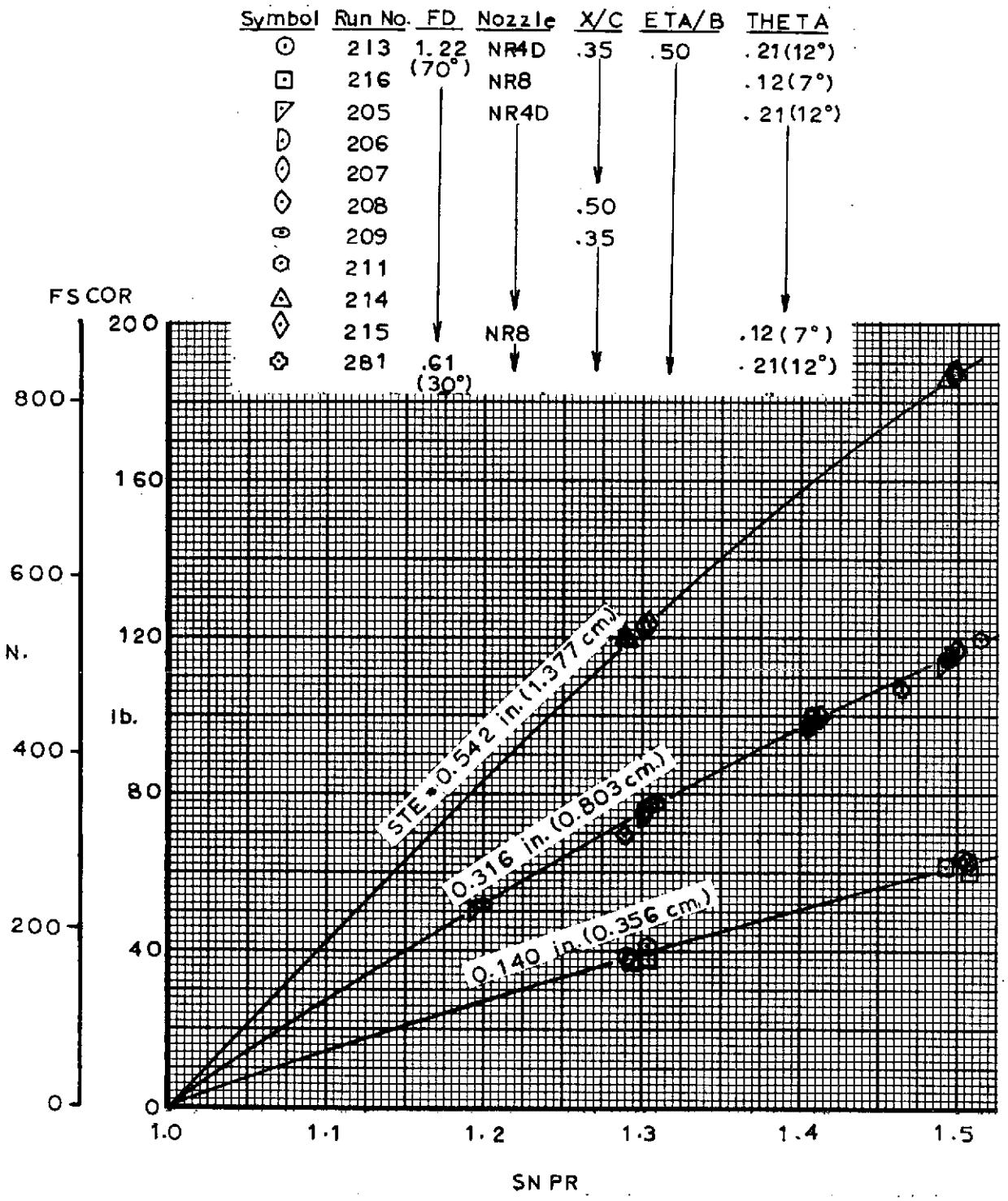

(b) Trailing edge slot height, STE = 0.542 in. (1.377 cm.), 0.316 in. (0.803 cm.), and 0.140 in. (0.356 cm.).

Figure 26 Concluded.

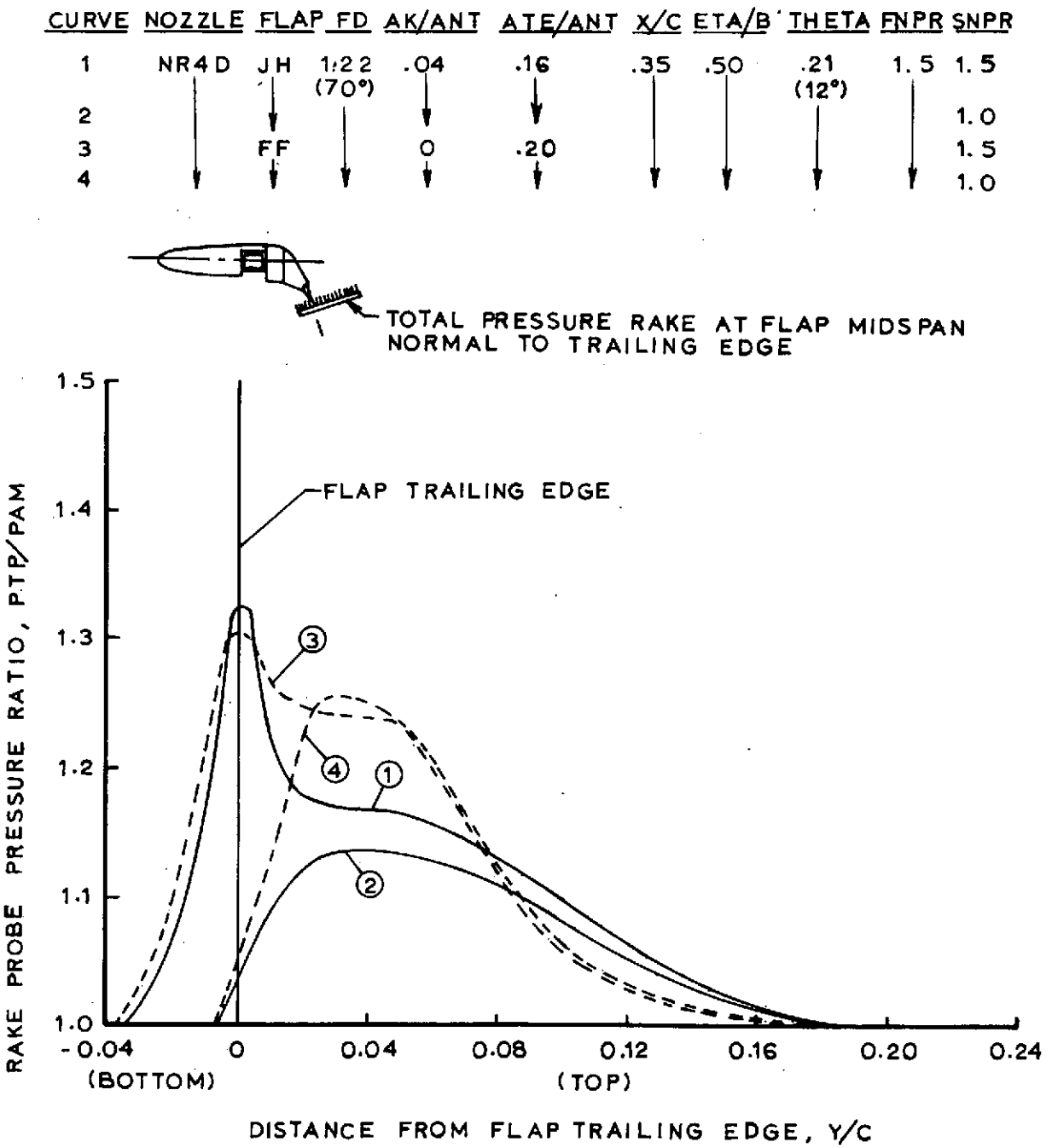

(a) Comparison of Jacobs-Hurkamp and Flex-Flap pressure distributions at the flap trailing edge.

Figure 27 Flap trailing edge wake survey.

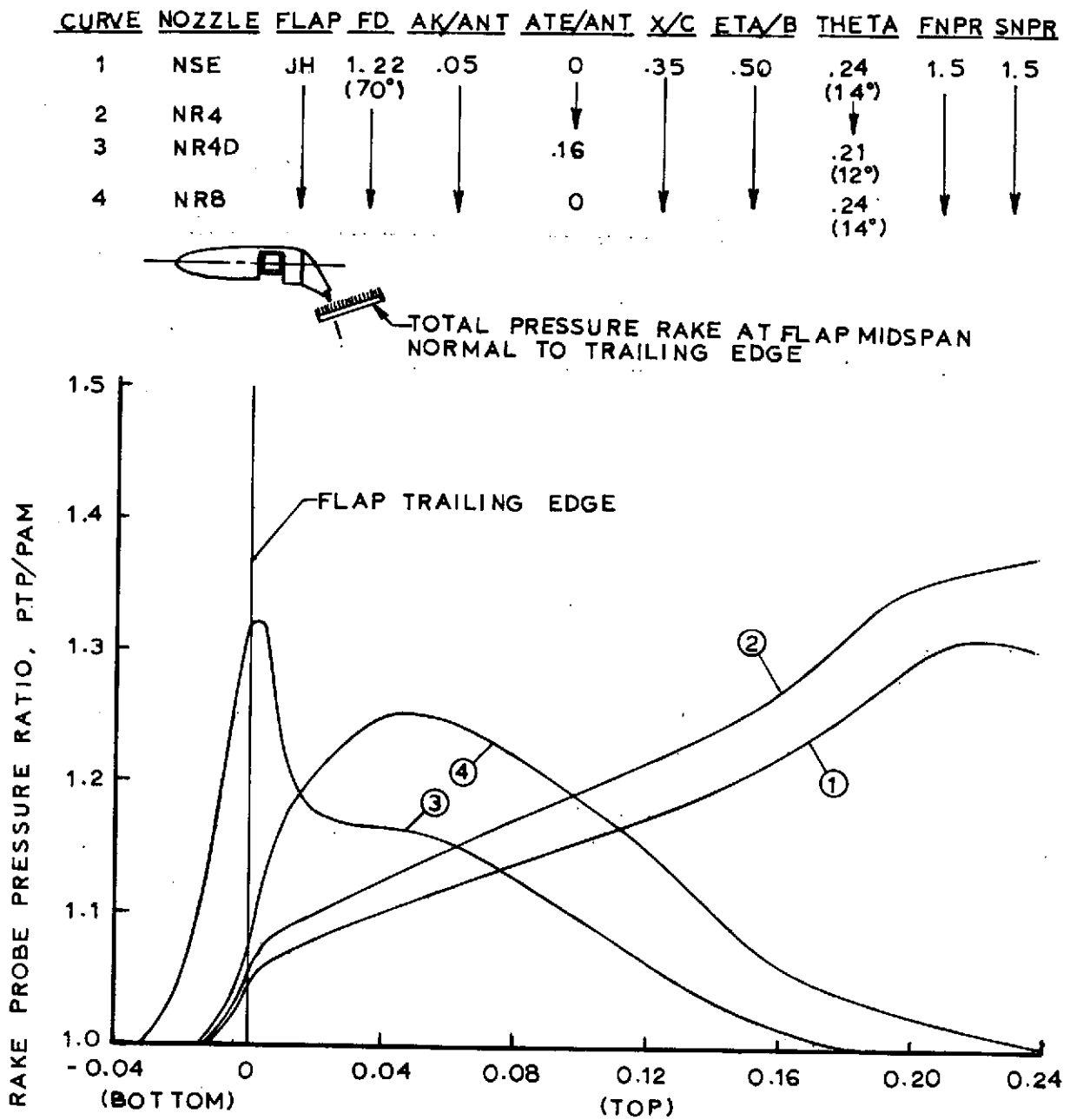

(b) Comparison of USB nozzle configurations on pressure distributions at the flap trailing edge.

Figure 27 Continued.

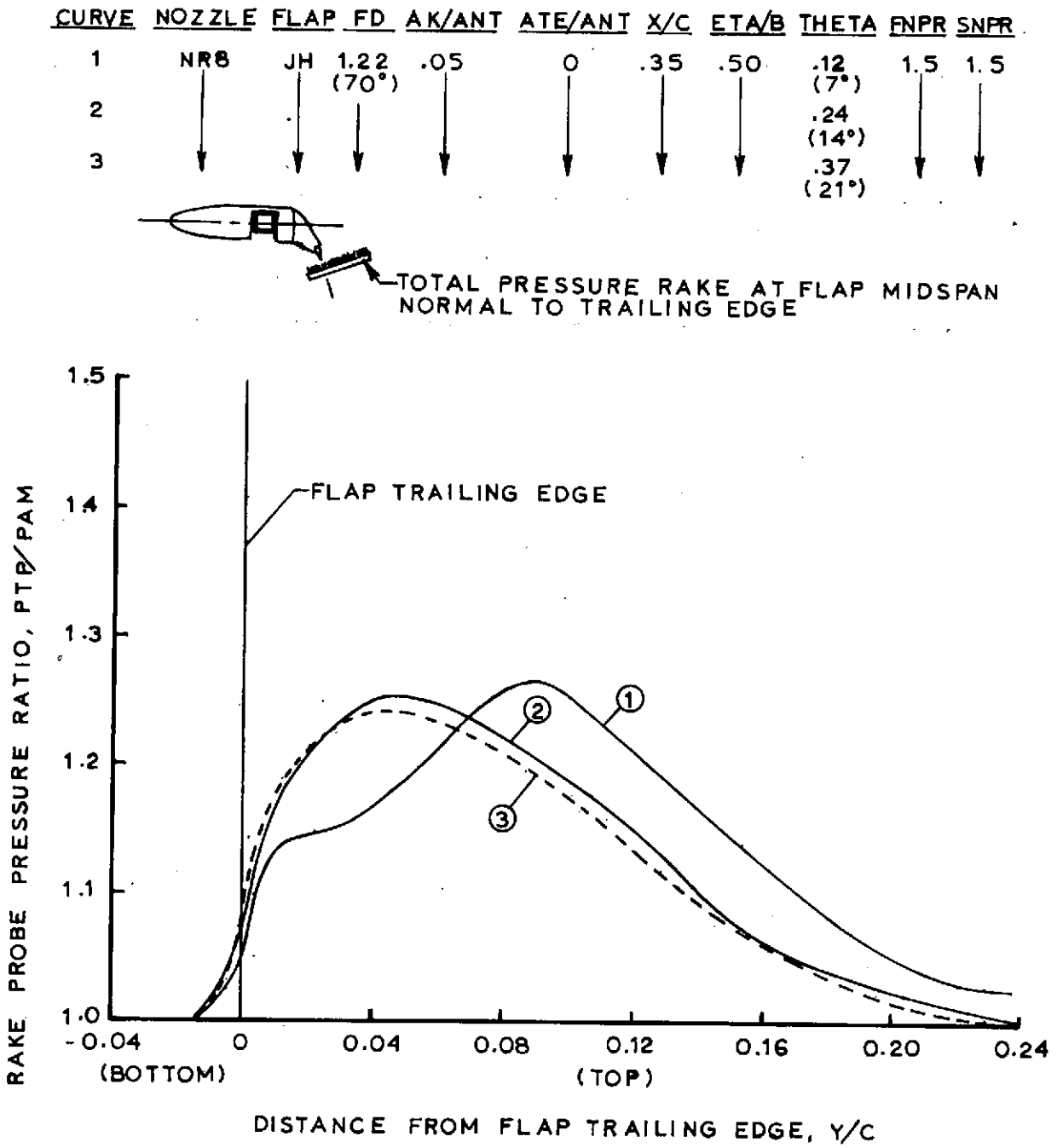

(c) Comparison of nozzle flow impingement angle on pressure distributions at the flap trailing edge. NR8 nozzle.

Figure 27 Continued.

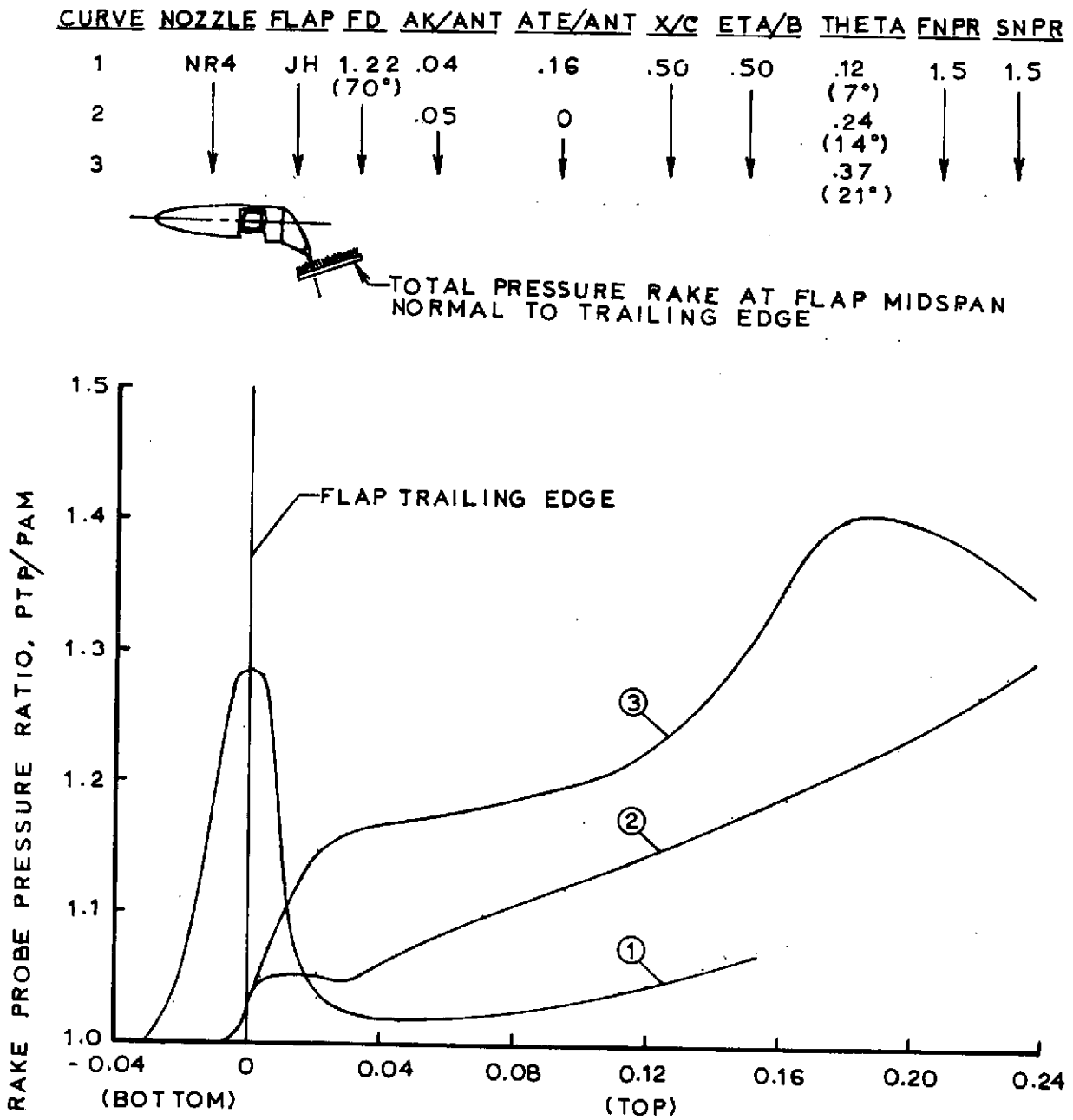

(d) Comparison of nozzle flow impingement angle on pressure distributions at the flap trailing edge. NR4 nozzle.

Figure 27 Continued.

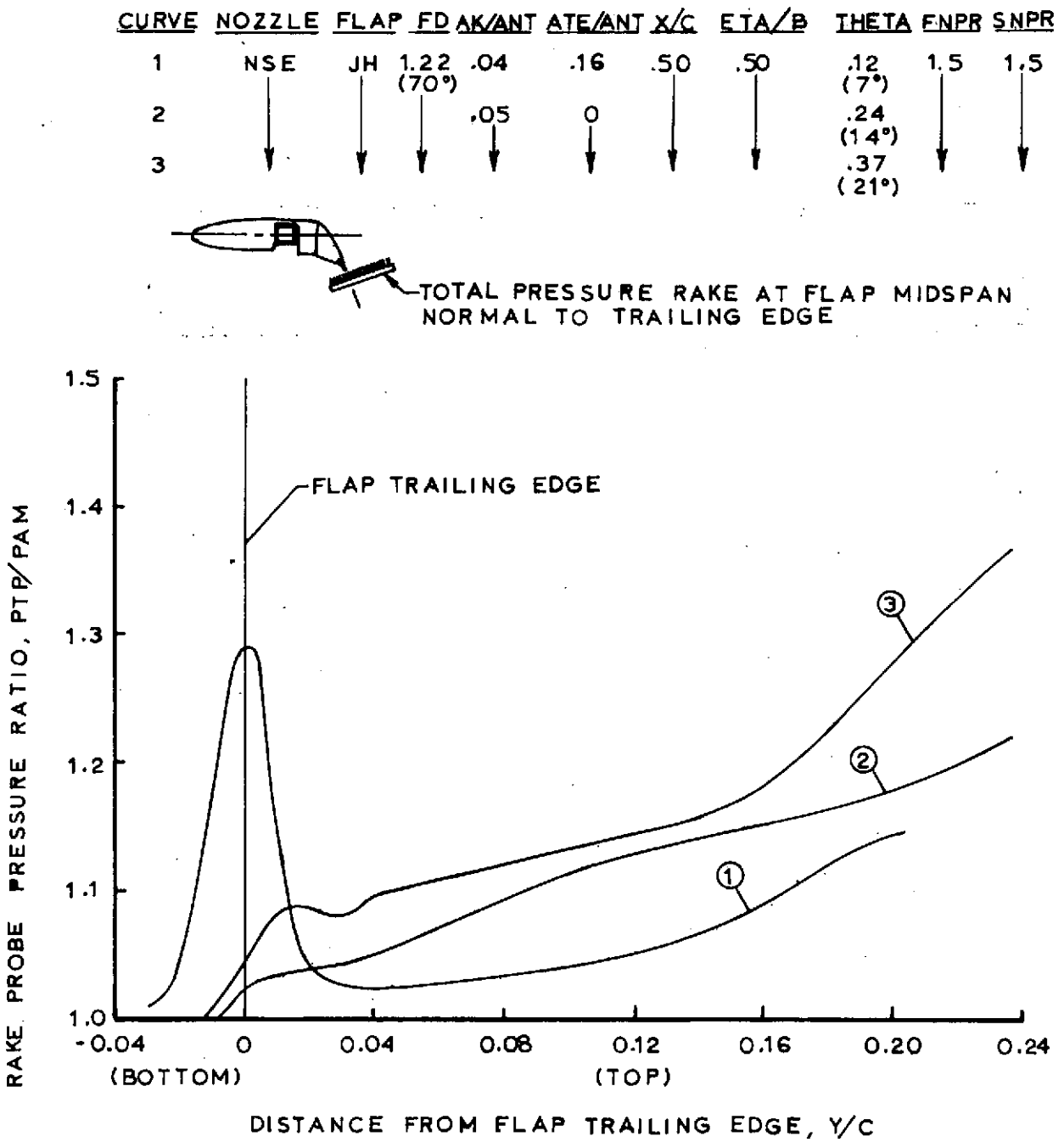

(e) Comparison of nozzle flow impingement angle on pressure distributions at the flap trailing edge. NSE nozzle.

Figure 27 Continued.

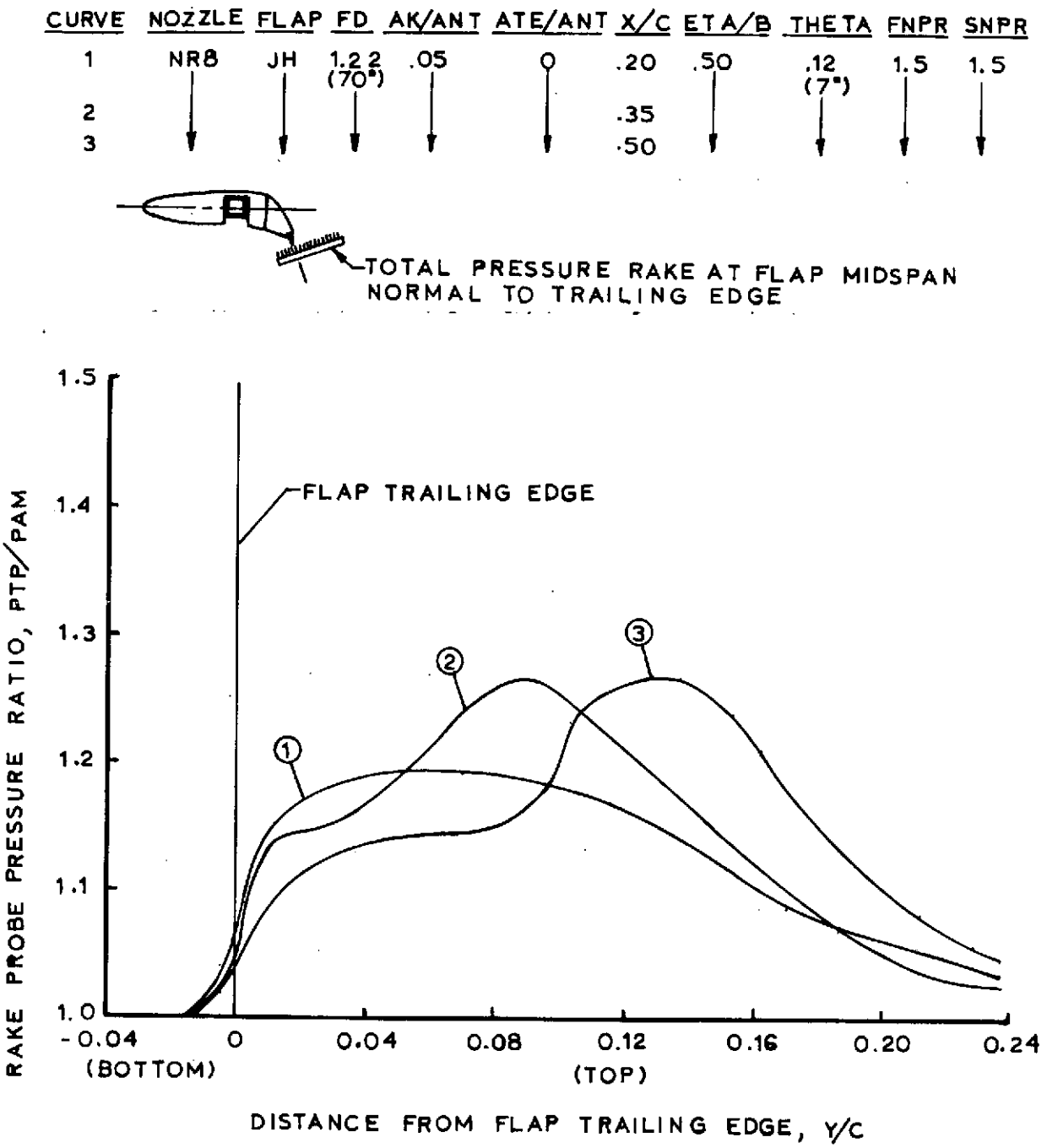

(f) Comparison of nozzle exit location on pressure distributions at the flap trailing edge. NR8 nozzle.

Figure 27 Continued.

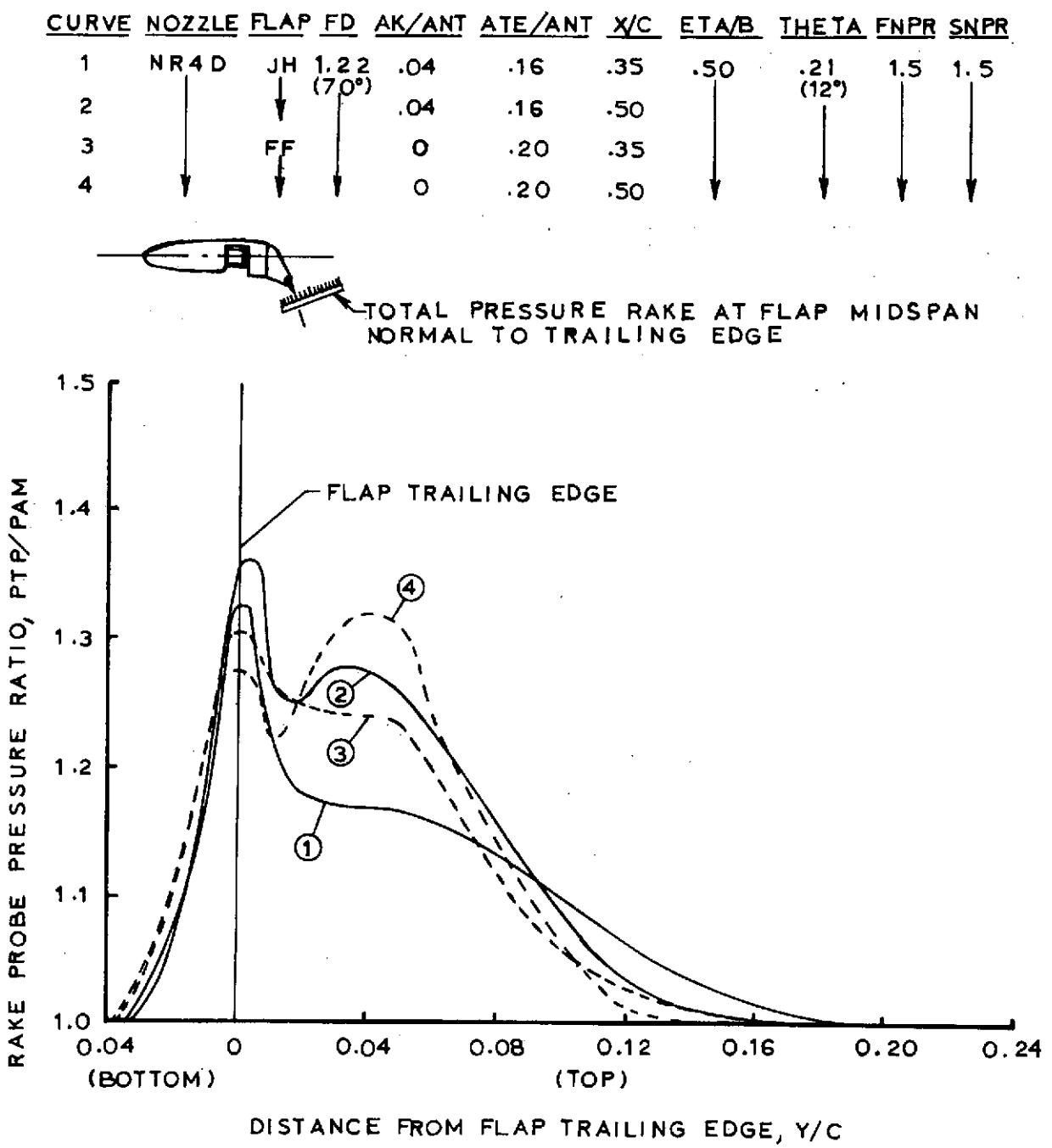

(g) Comparison of nozzle exit location on pressure distributions at the flap trailing edge. NR4D nozzle.

Figure 27 Continued.

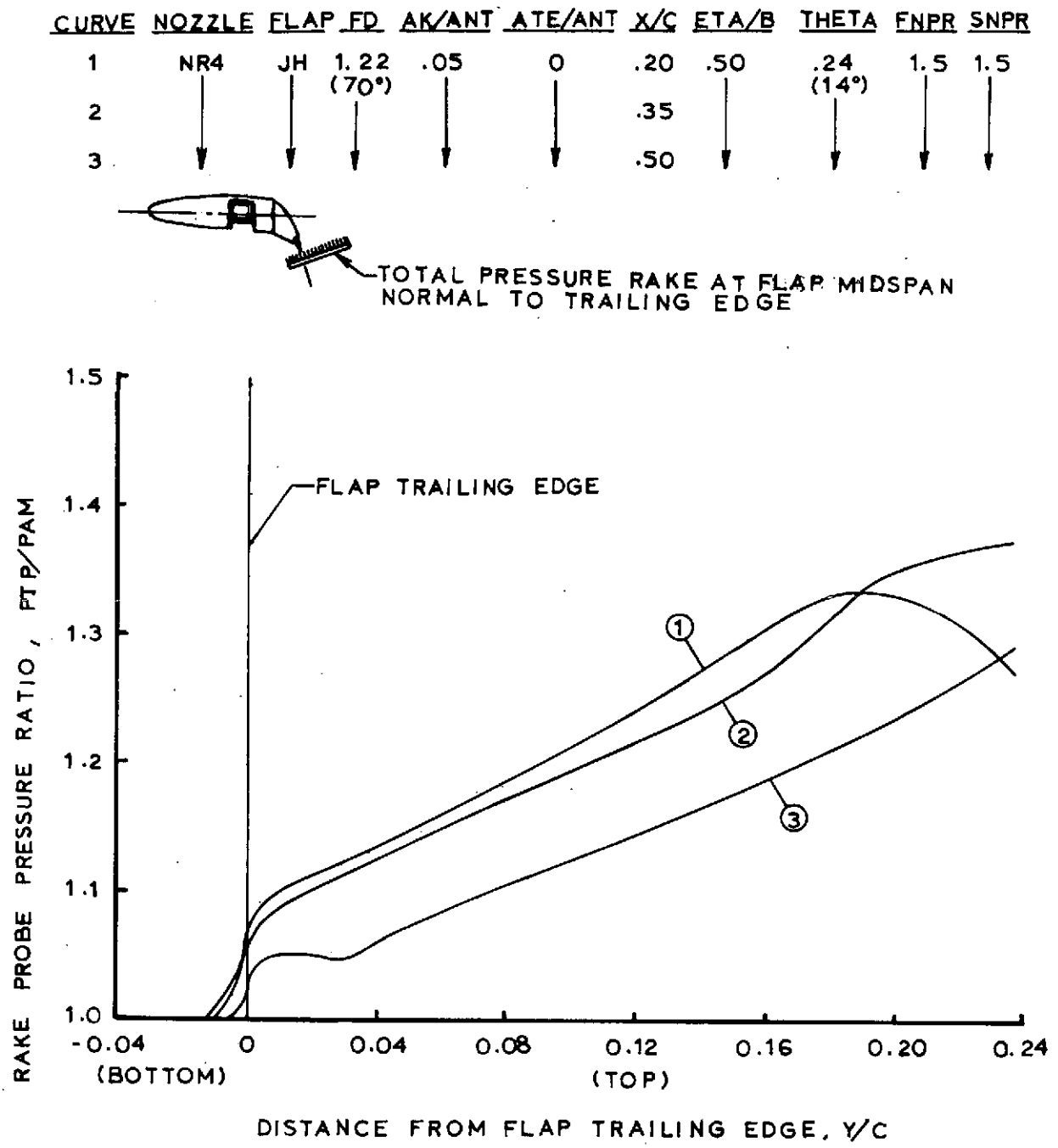

(h) Comparison of nozzle exit location on pressure distributions at the flap trailing edge. NR4 nozzle.

Figure 27 Continued.

NOZZLE	FLAP	FD	AK/ANT	ATE/ANT	X/C	ETA/B	THETA	FNPR	SNPR
NR4D	JH	1.22 (70°)	.04	.16	.35	.50	.21 (12°)	1.5	1.5

TOTAL PRESSURE RAKE AT FLAP MIDSPAN NORMAL TO TRAILING EDGE

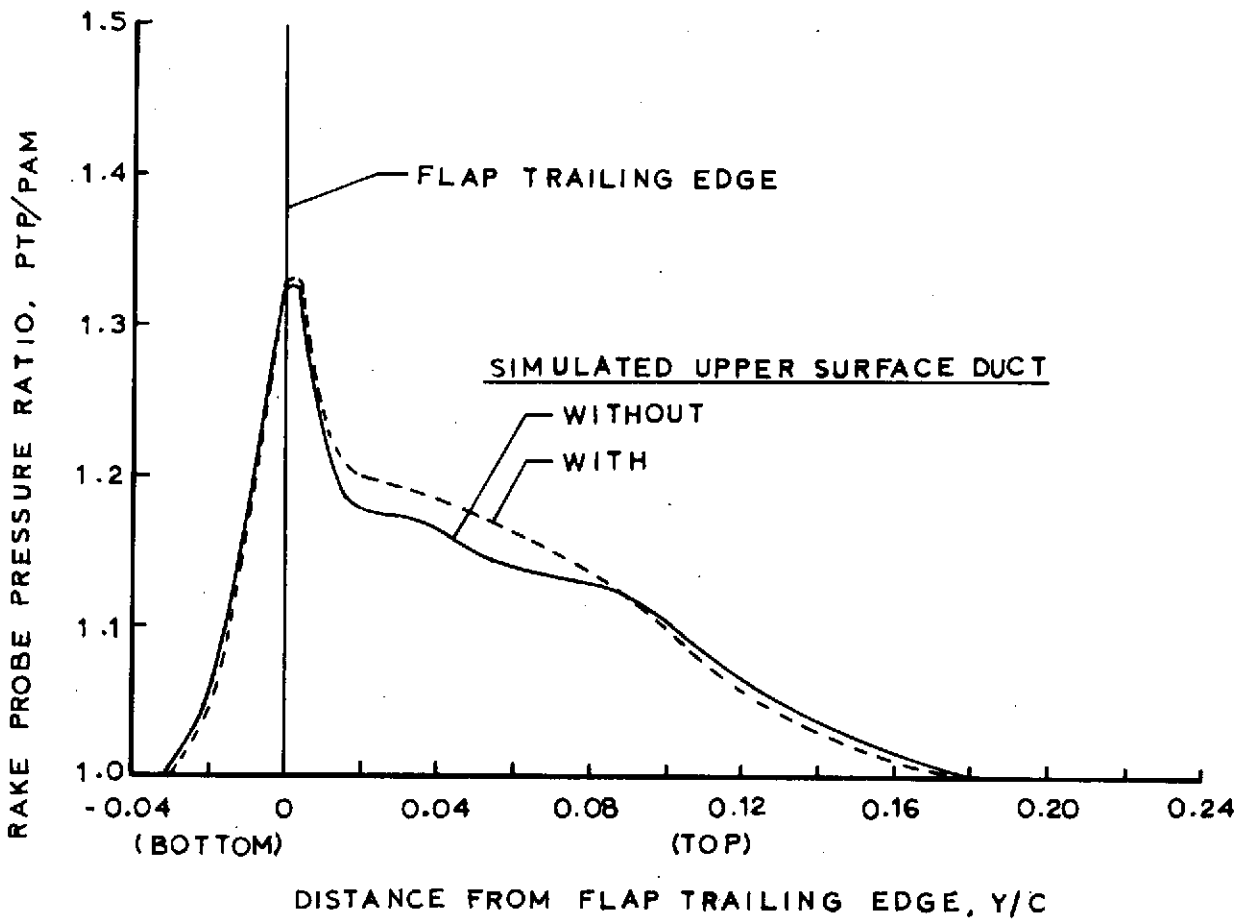

(i) Comparison of simulated upper surface duct installation on pressure distributions at the flap trailing edge.

Figure 27 Continued.

NOZZLE	FLAP	FD	AK/ANT	ATE/ANT	X/C	ETA/B	THETA
NR4D	JH	1.22 (70°)	.04	.16	.35	.50	.21 (12°)

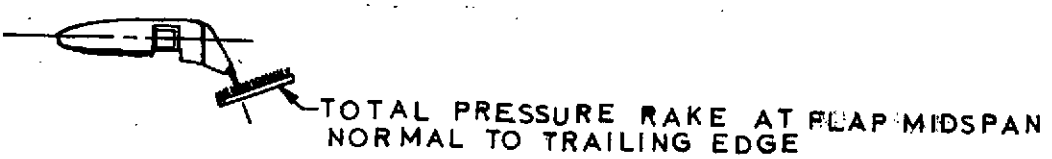

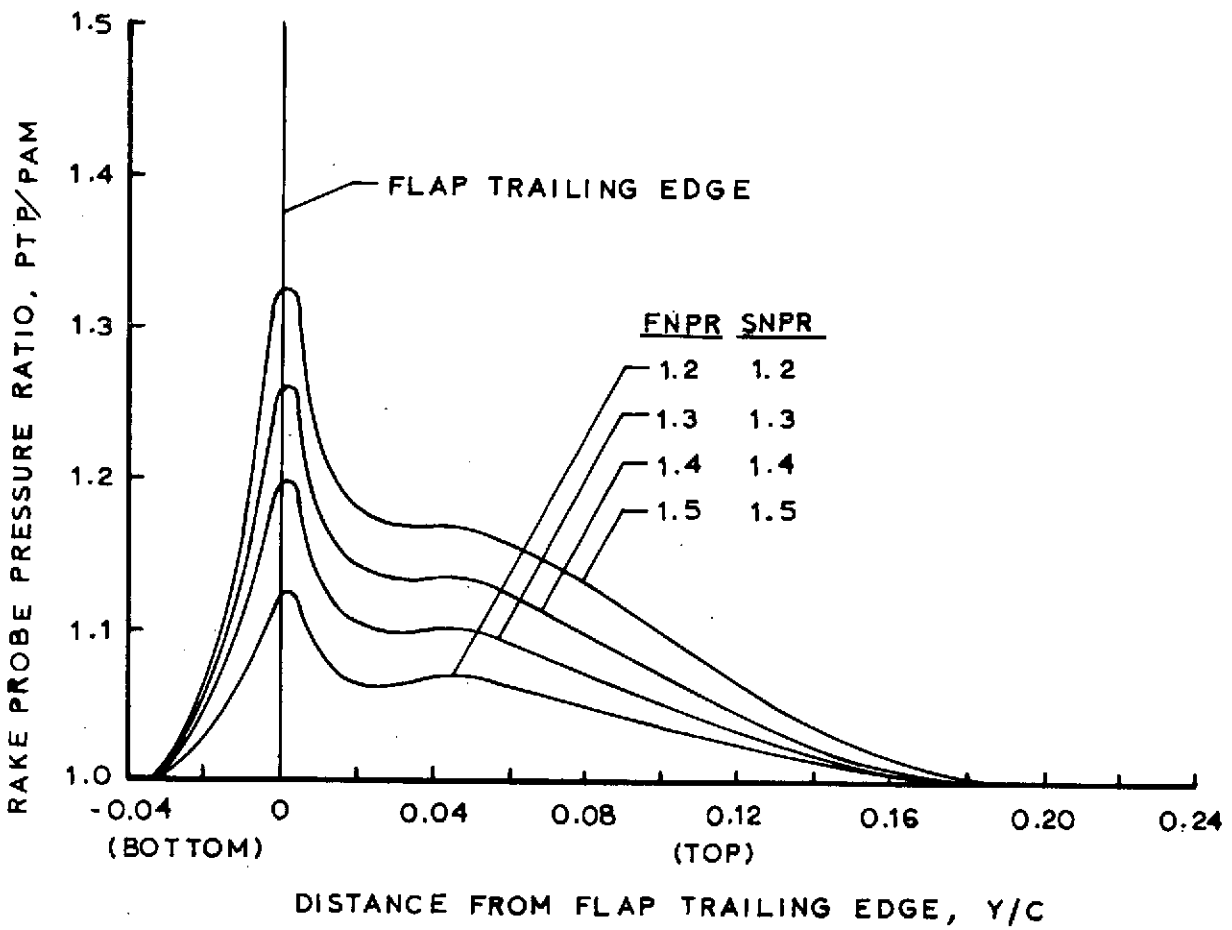

(j) Comparison of nozzle pressure ratio on pressure distribution of the flap trailing edge.

Figure 27 Concluded.

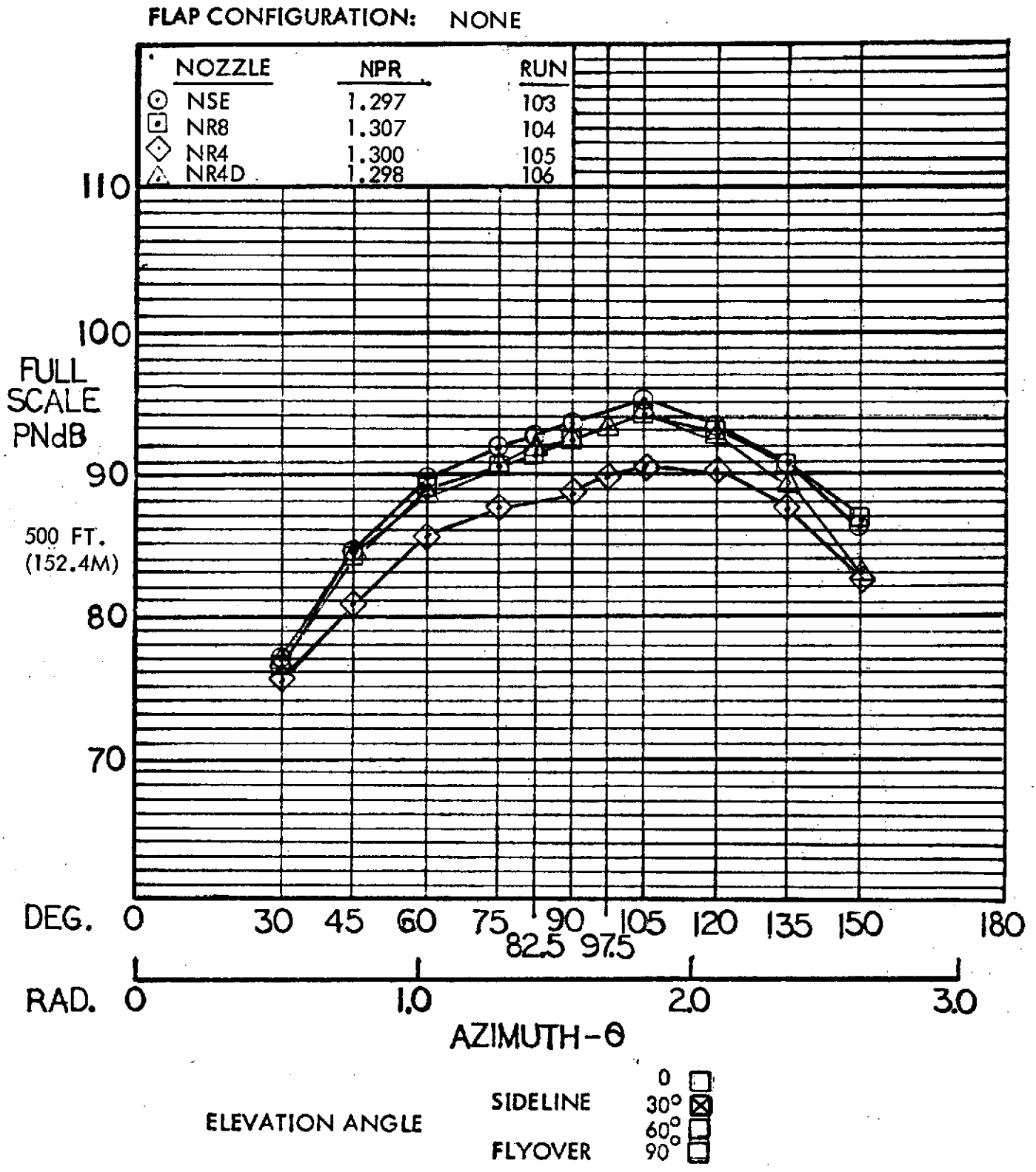

Figure 28 Full scale sideline PNL of four slot nozzles.

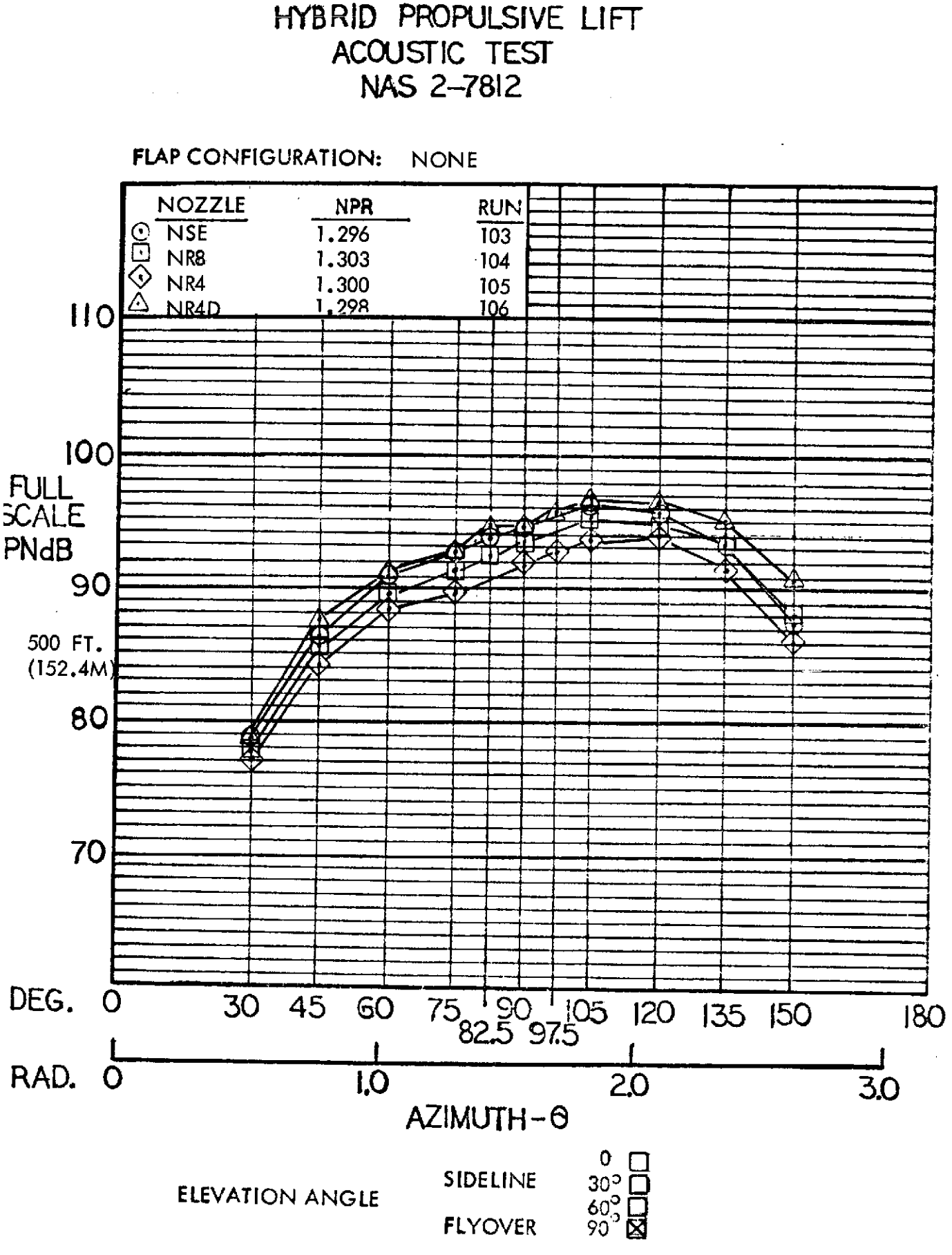

Figure 29 Full scale flyover PNL of four slot nozzles.

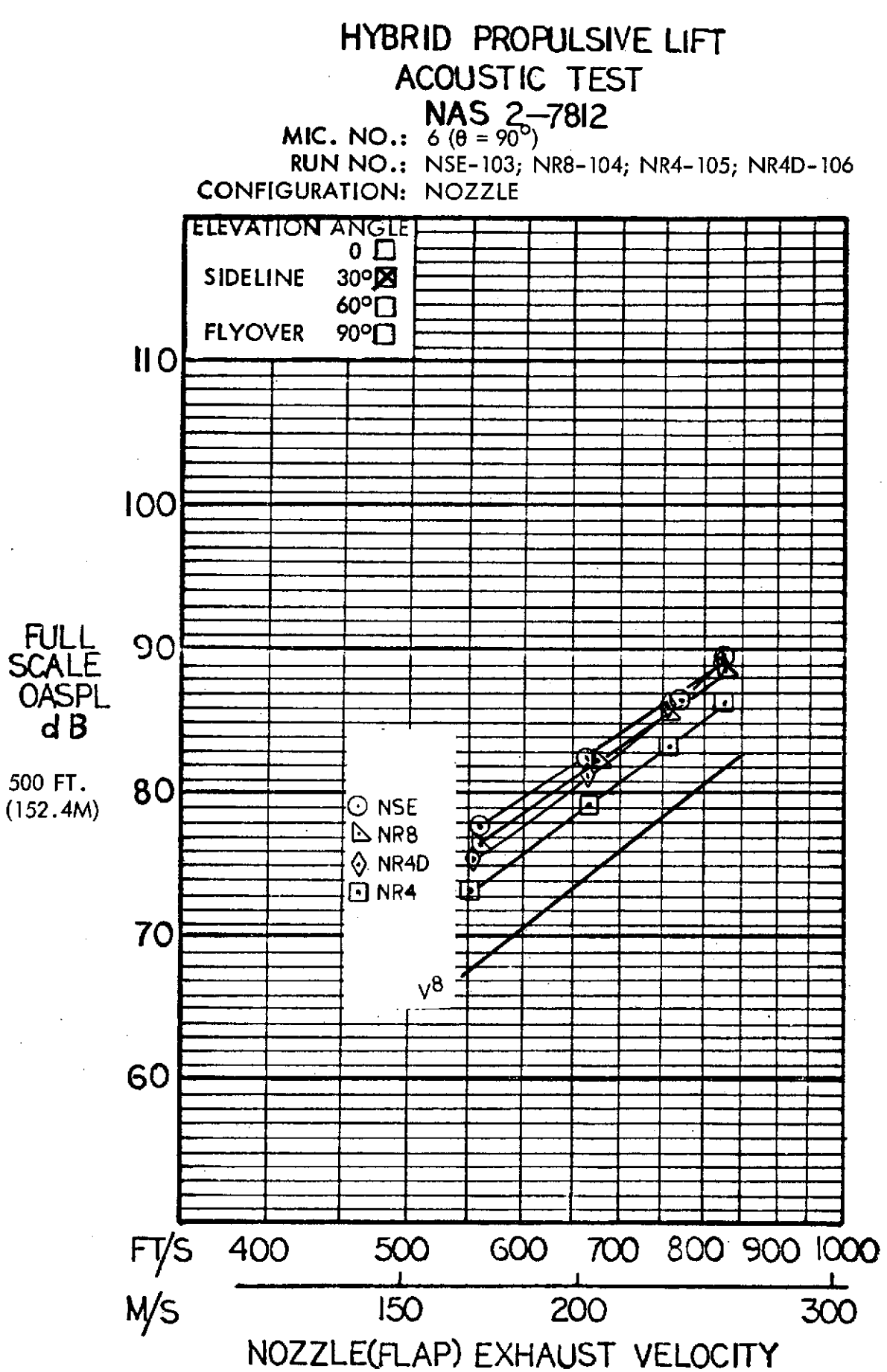

Figure 30 Full scale OASPL of four slot nozzles as a function of nozzle exhaust velocity; 90° azimuth.

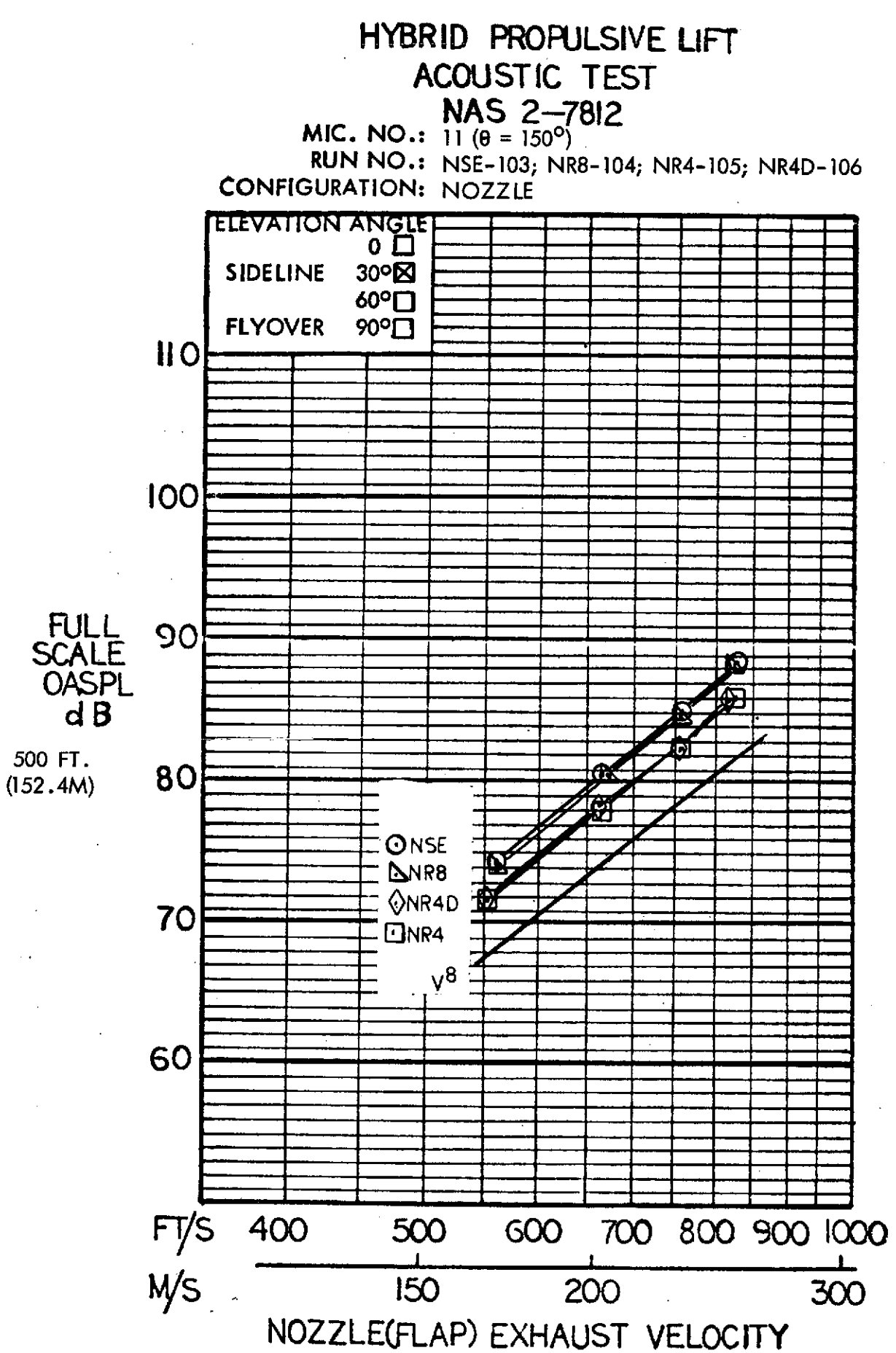

Figure 31 Full scale OASPL of four slot nozzles as a function of nozzle exhaust velocity; 150° azimuth

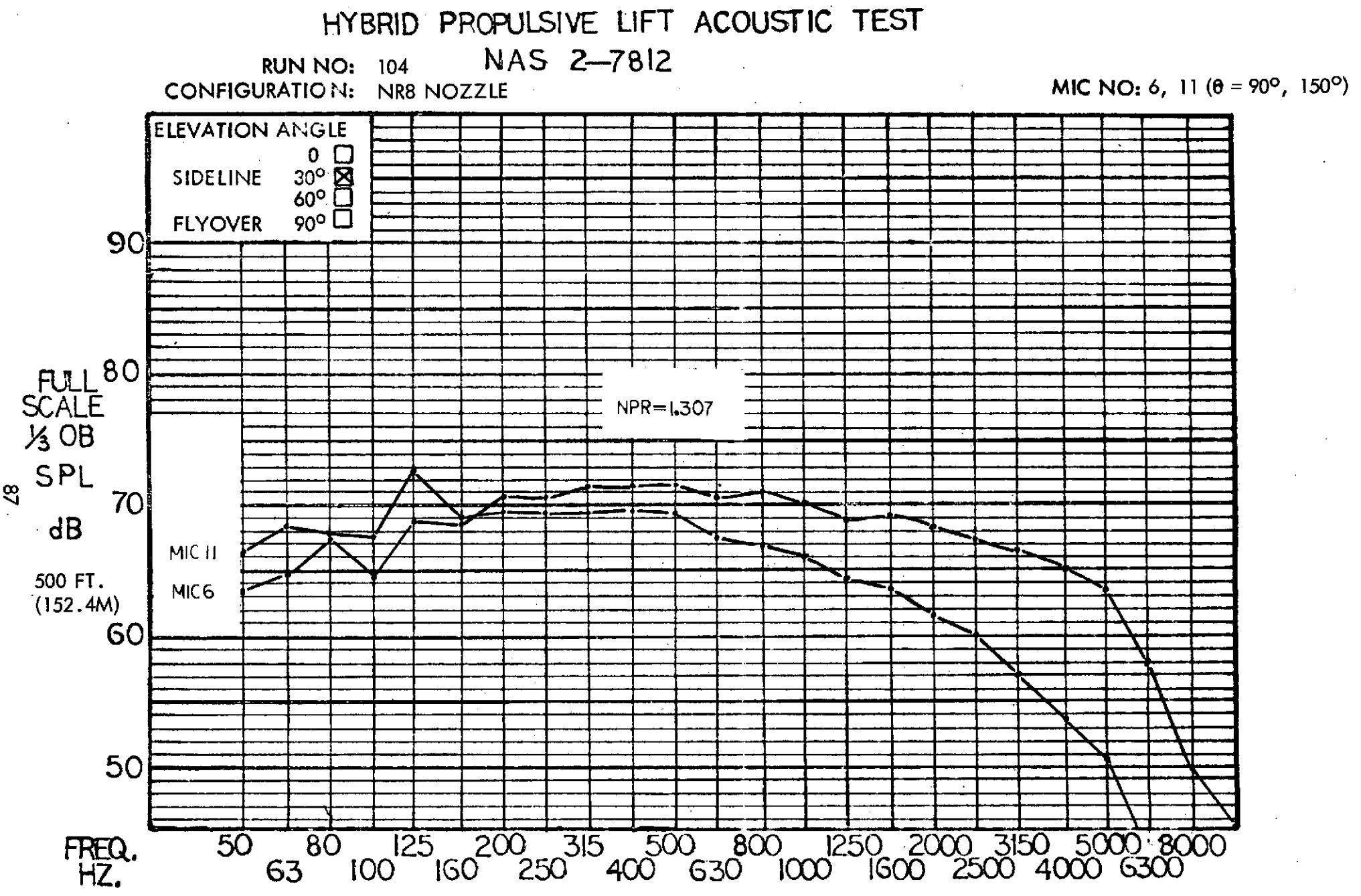

Figure 32 Full scale sideline 1/3 OBSPL for aspect ratio 8 nozzle at 90° and 150° azimuth.

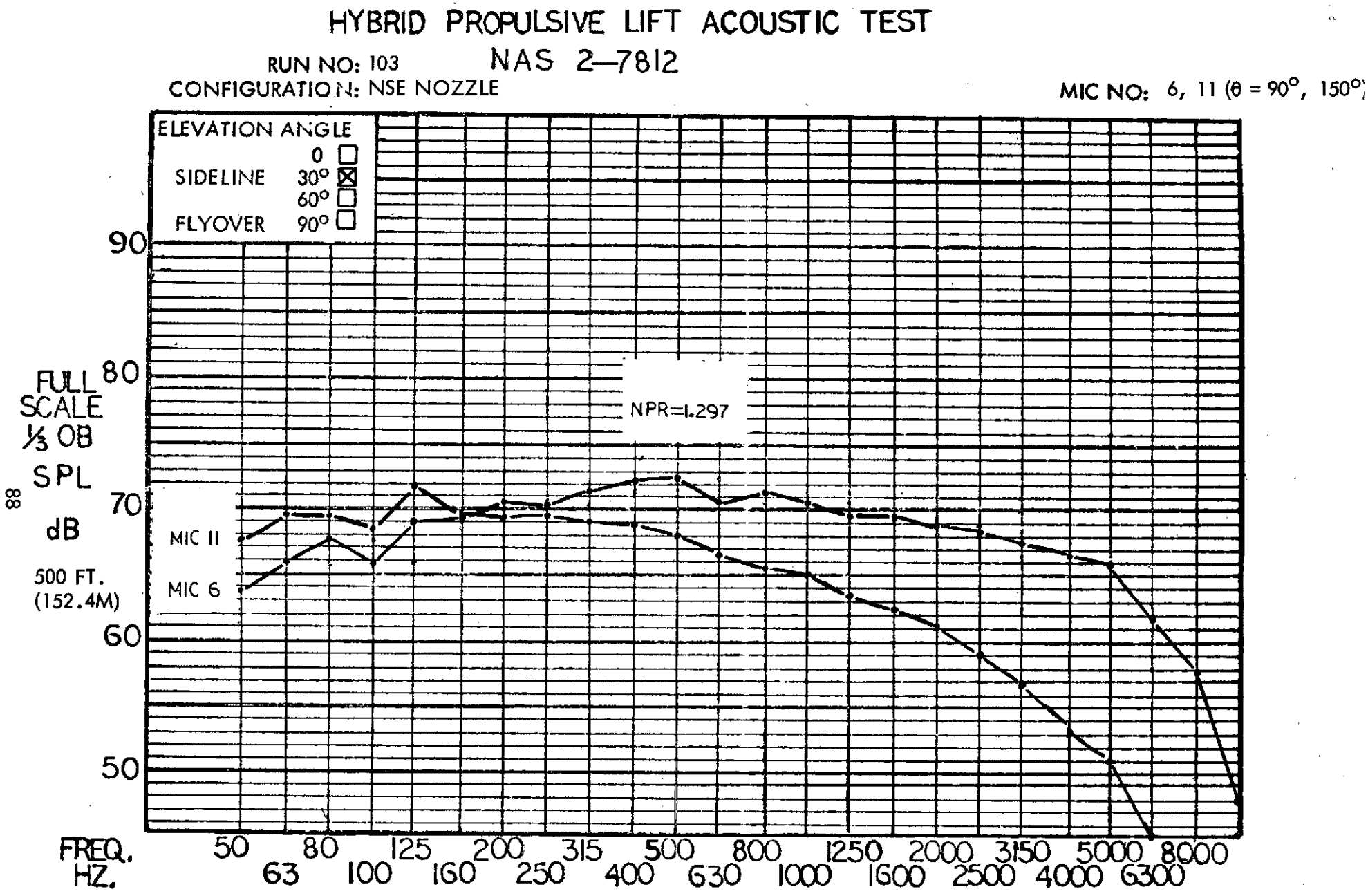

Figure 33 Full scale sideline 1/3 OBSPL for a simulated engine nozzle at 90° and 150° azimuth.

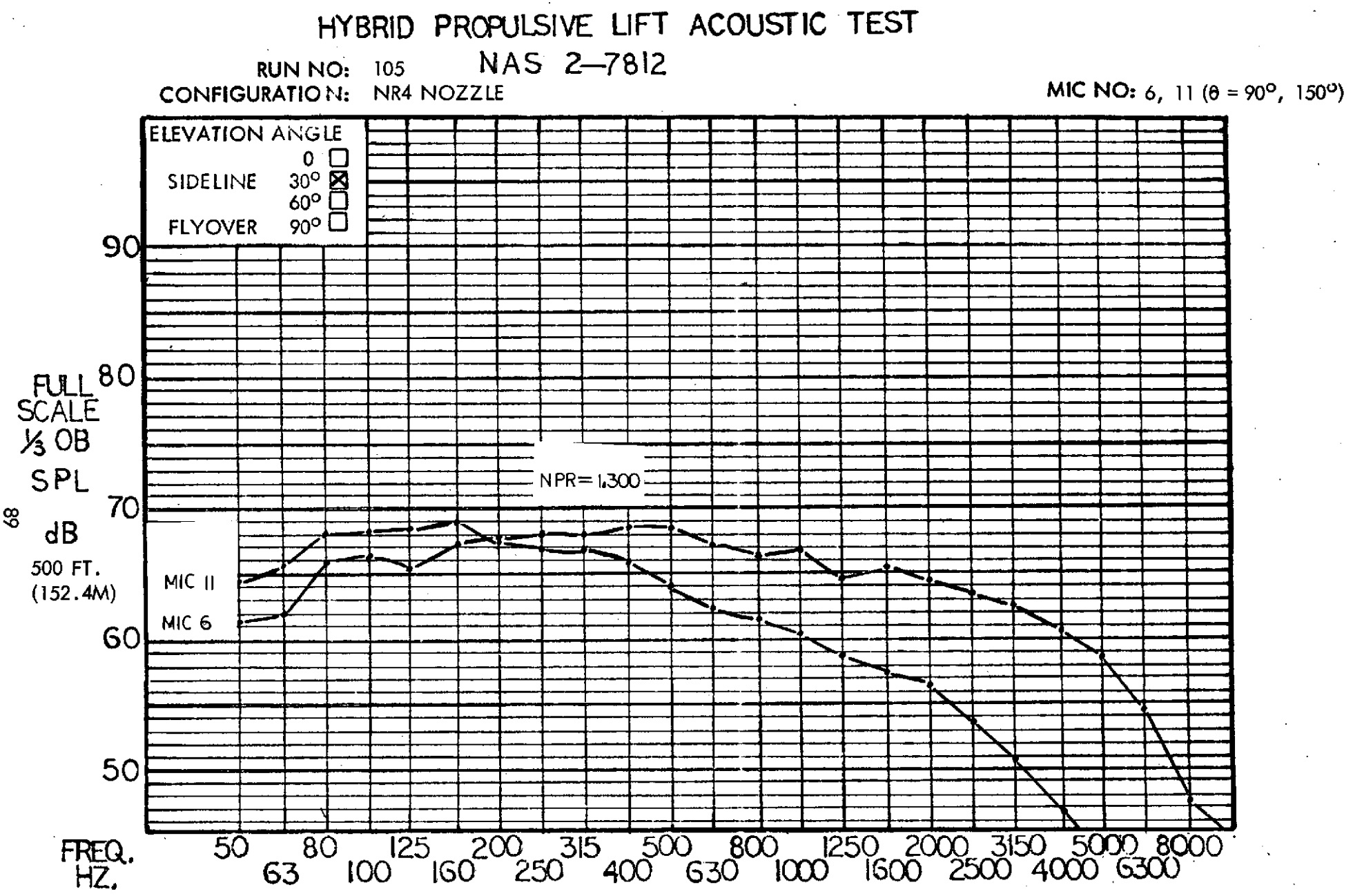

Figure 34 Full scale sideline 1/3 OBSPL for aspect ratio 4 nozzle at 90° and 150° azimuth.

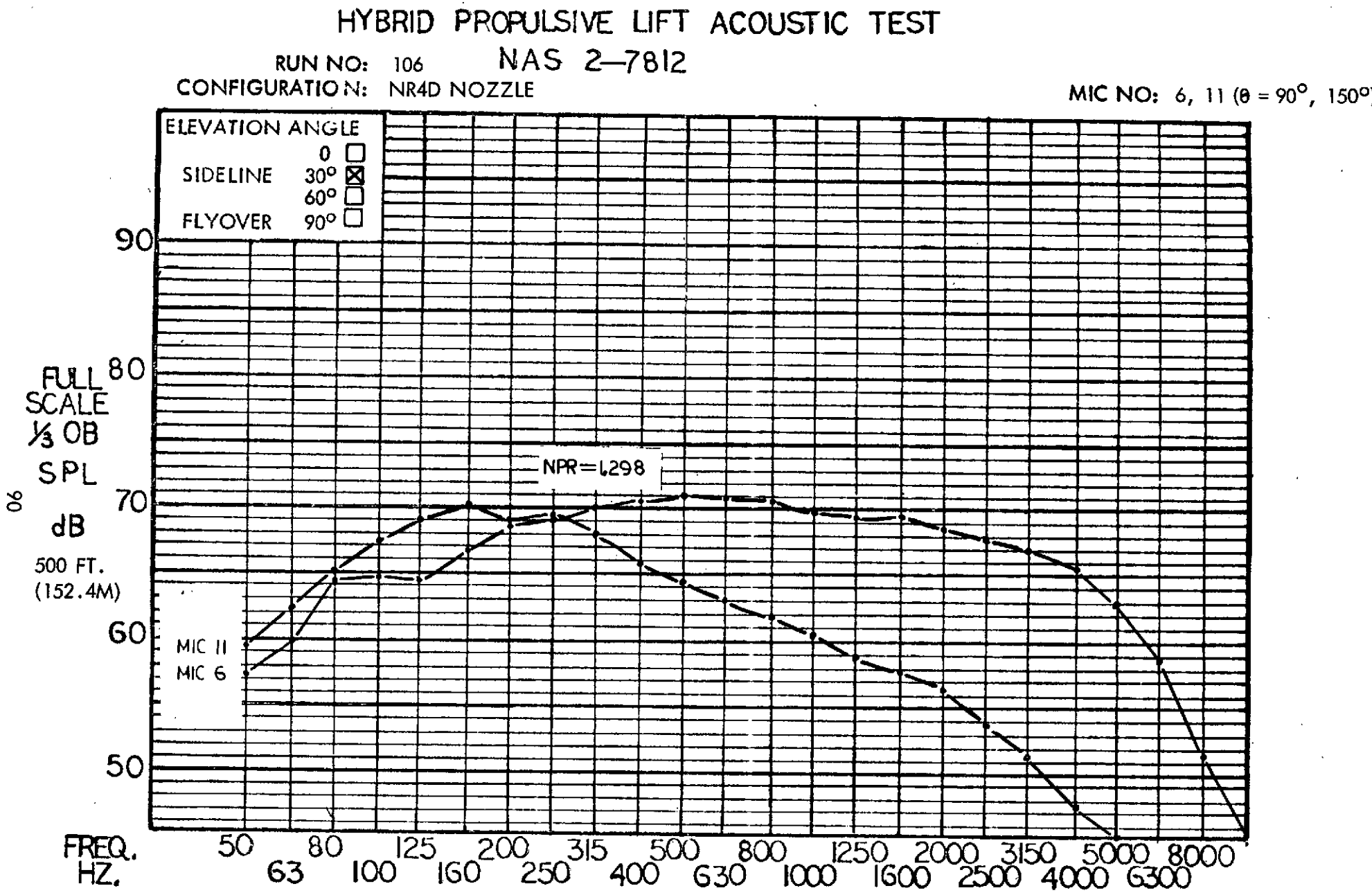

Figure 35 Full scale sideline 1/3 OBSPL for aspect ratio 4 nozzle with deflector at 90° and 150° azimuth.

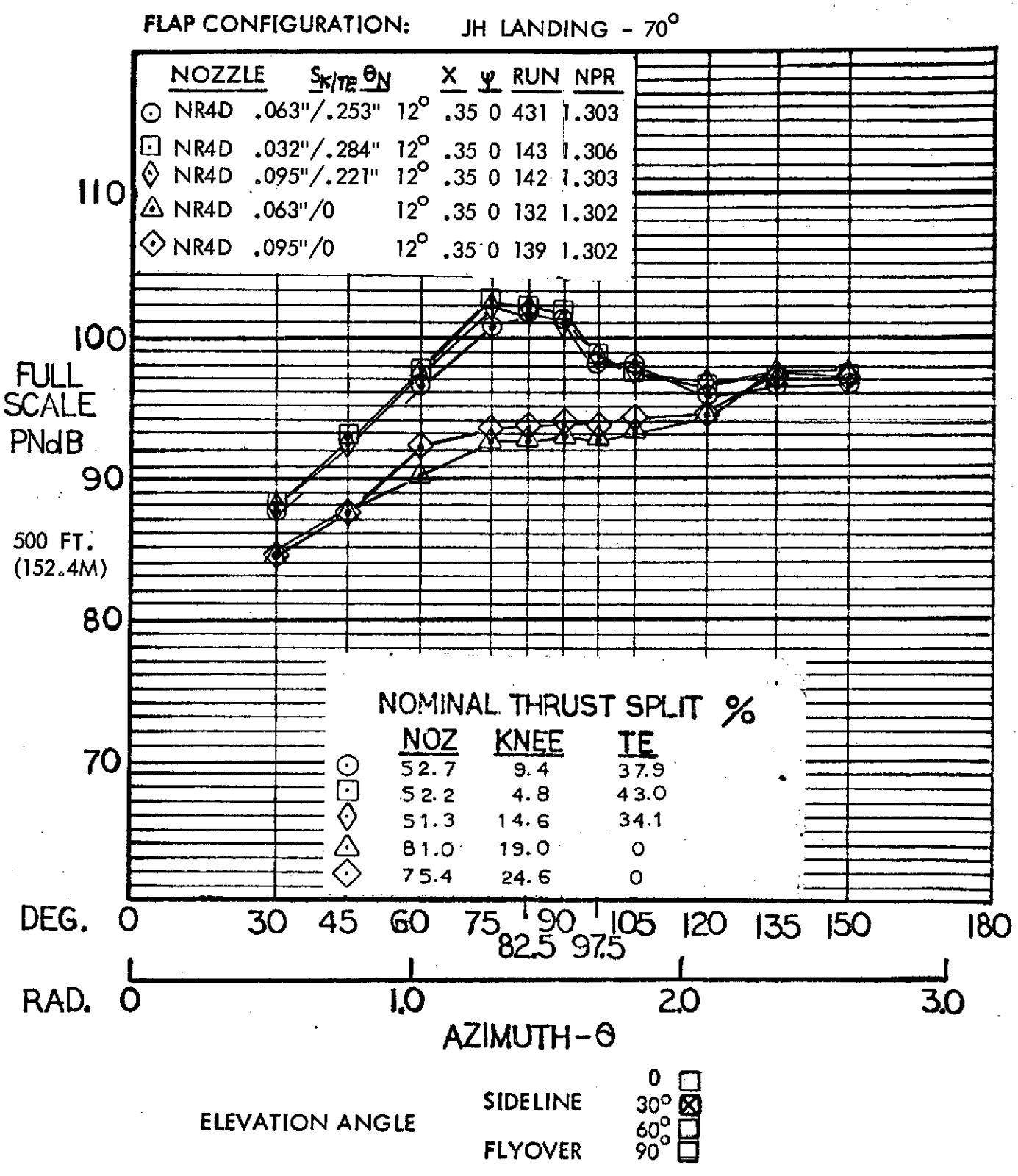

Figure 36 Full scale sideline PNL; comparison of five JH flap knee-TE slot configurations, aspect ratio 4 nozzle with deflector, 70° flap angle.

HYBRID PROPULSIVE LIFT
ACOUSTIC TEST
NAS 2-7812

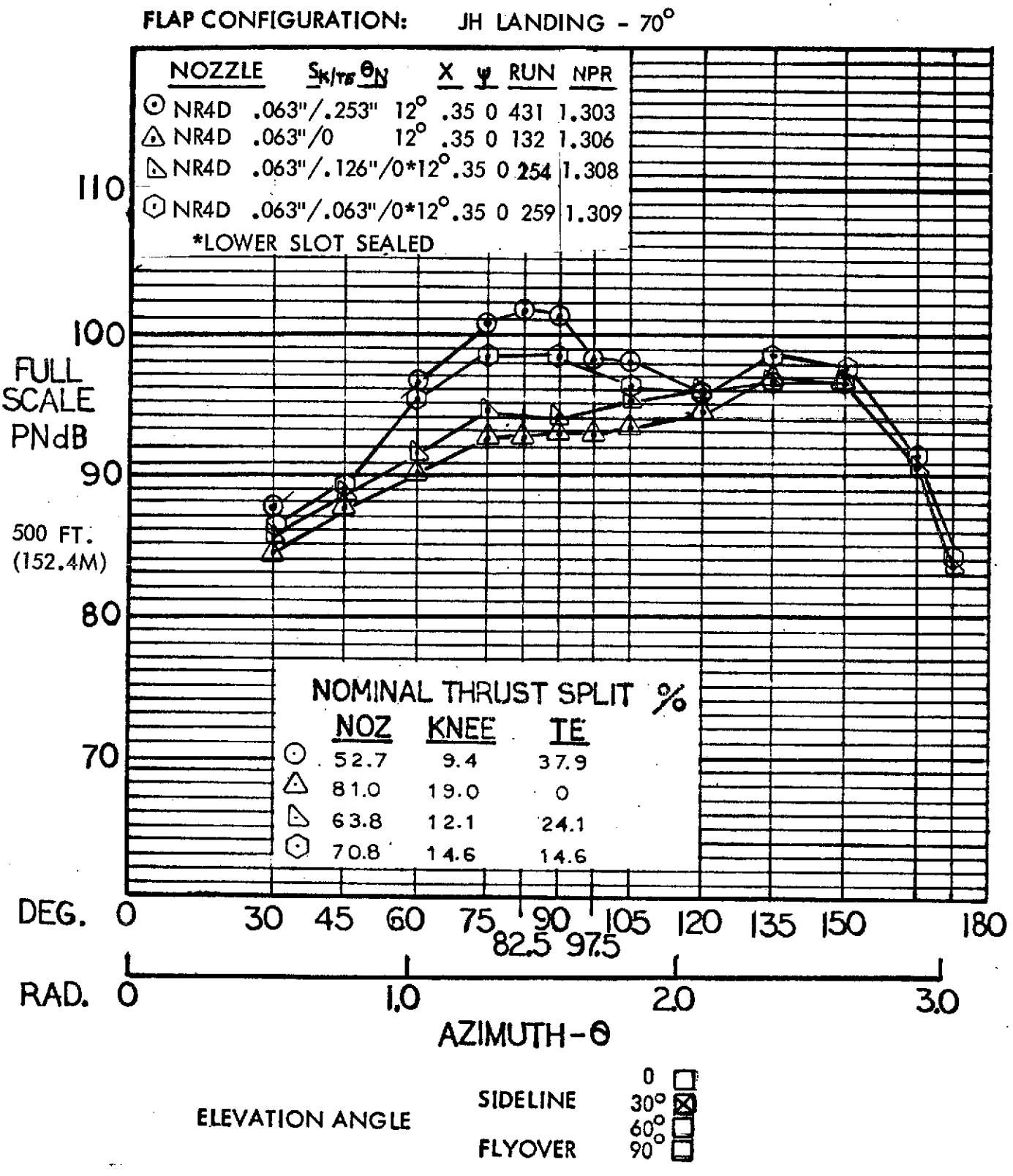

Figure 37 Full scale sideline PNL; comparison of four JH flap TE slot configurations with constant knee slot, aspect ratio 4 nozzle with deflector, 70° flap angle.

HYBRID PROPULSIVE LIFT
ACOUSTIC TEST
NAS 2-7812

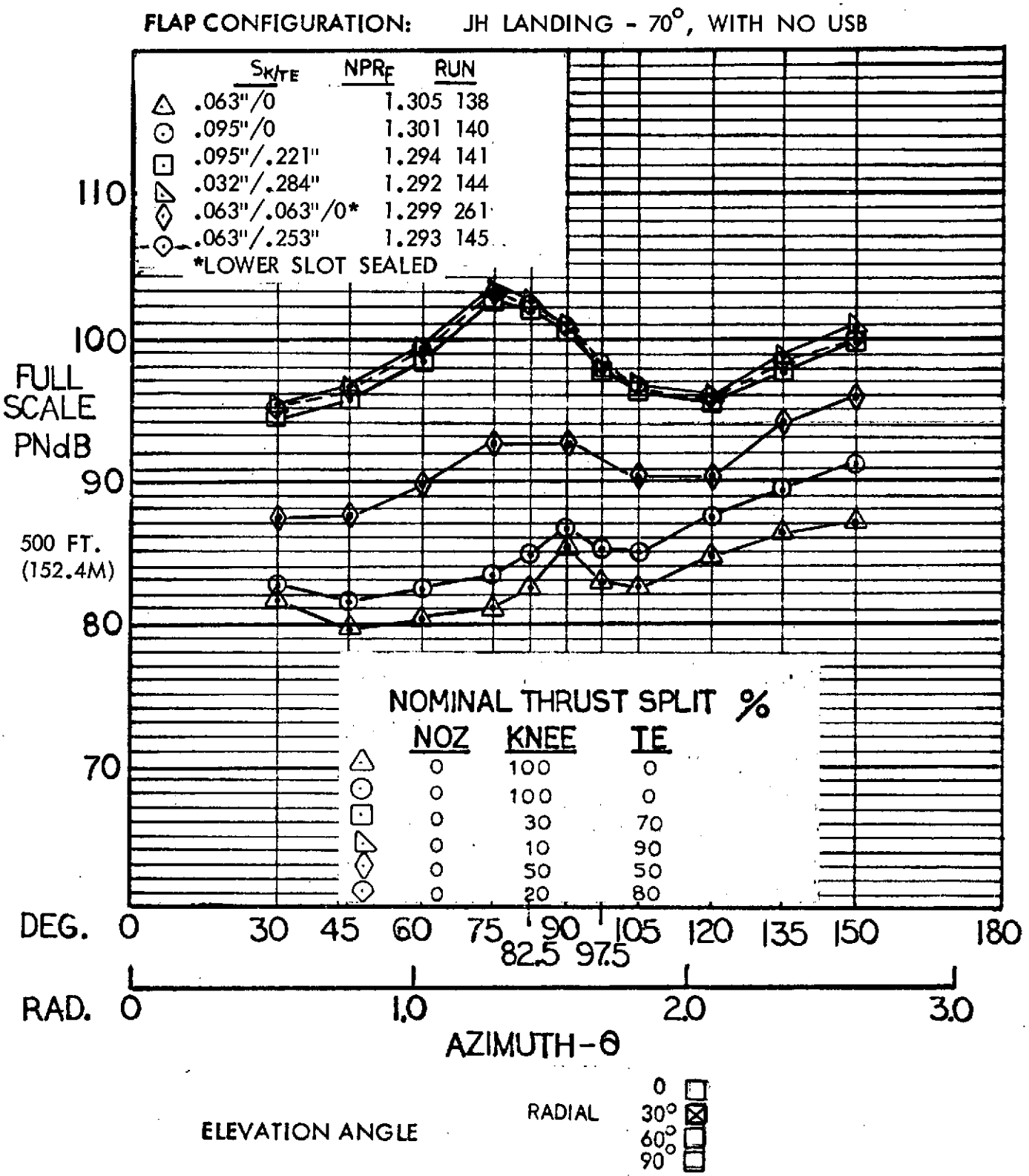

Figure 38 Full scale radial PNL; comparison of six JH flap knee - TE slot configurations, no upper surface blowing, 70° flap angle.

HYBRID PROPULSIVE LIFT
ACOUSTIC TEST
NAS 2-7812

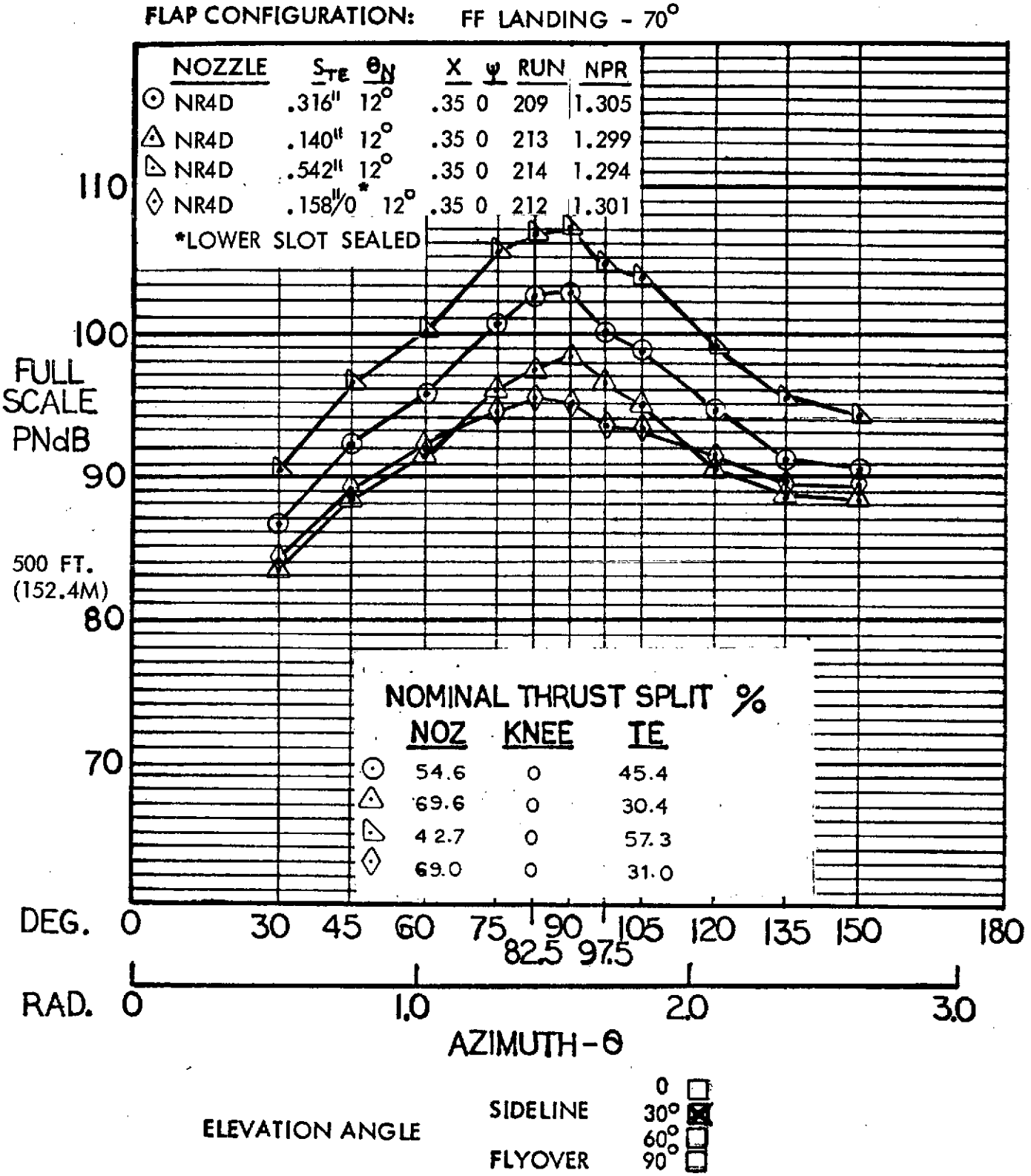

Figure 39 Full scale sideline PNL; comparison of five Flex Flap TE slot configurations, aspect ratio 4 nozzle with deflector, 70° flap angle.

HYBRID PROPULSIVE LIFT
ACOUSTIC TEST
NAS 2-7812

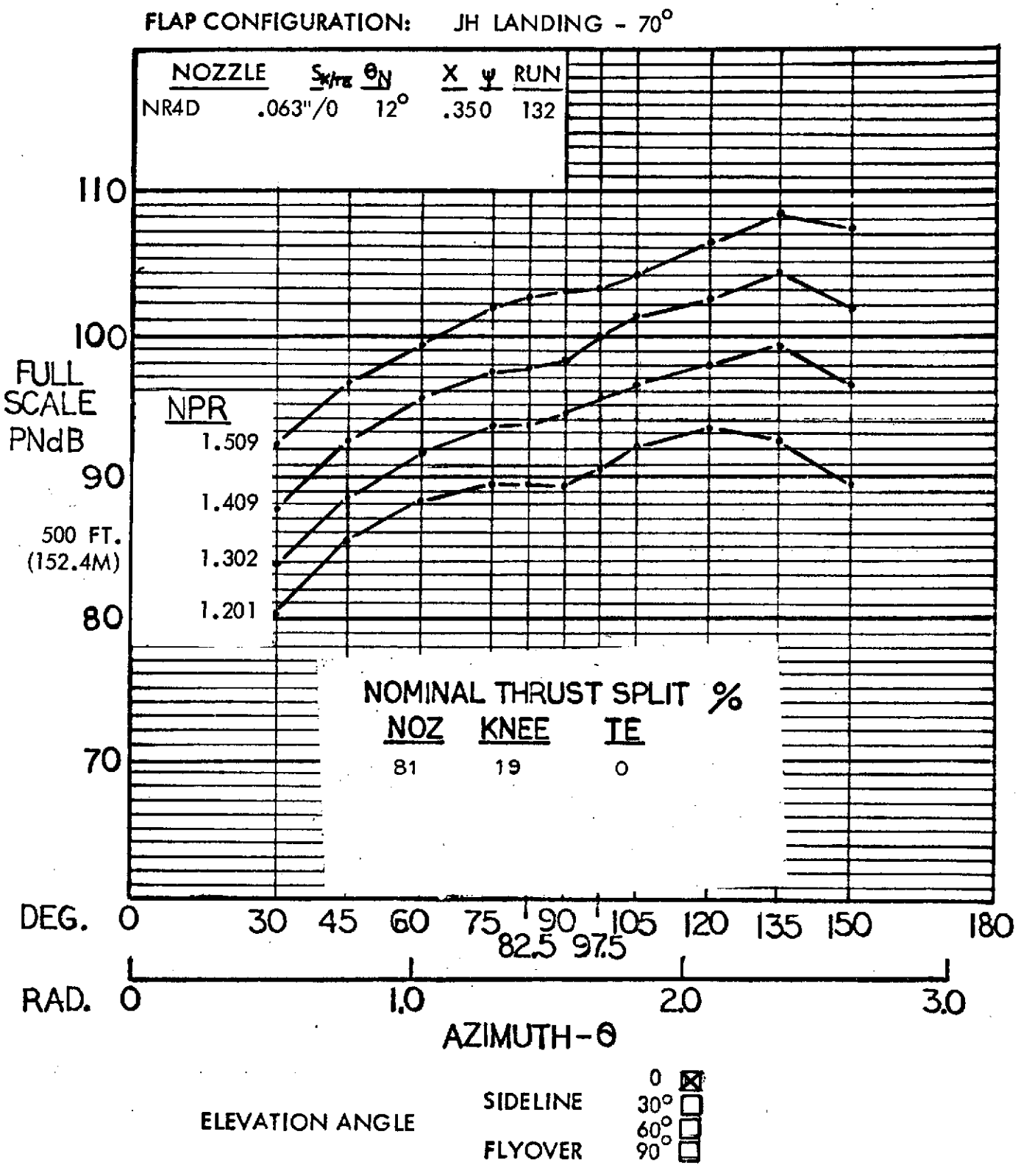

Figure 40 Full scale sideline PNL for the aspect ratio 4 nozzle with deflector and JH flap with knee blowing; 70° flap angle.

HYBRID PROPULSIVE LIFT
ACOUSTIC TEST
NAS 2-7812

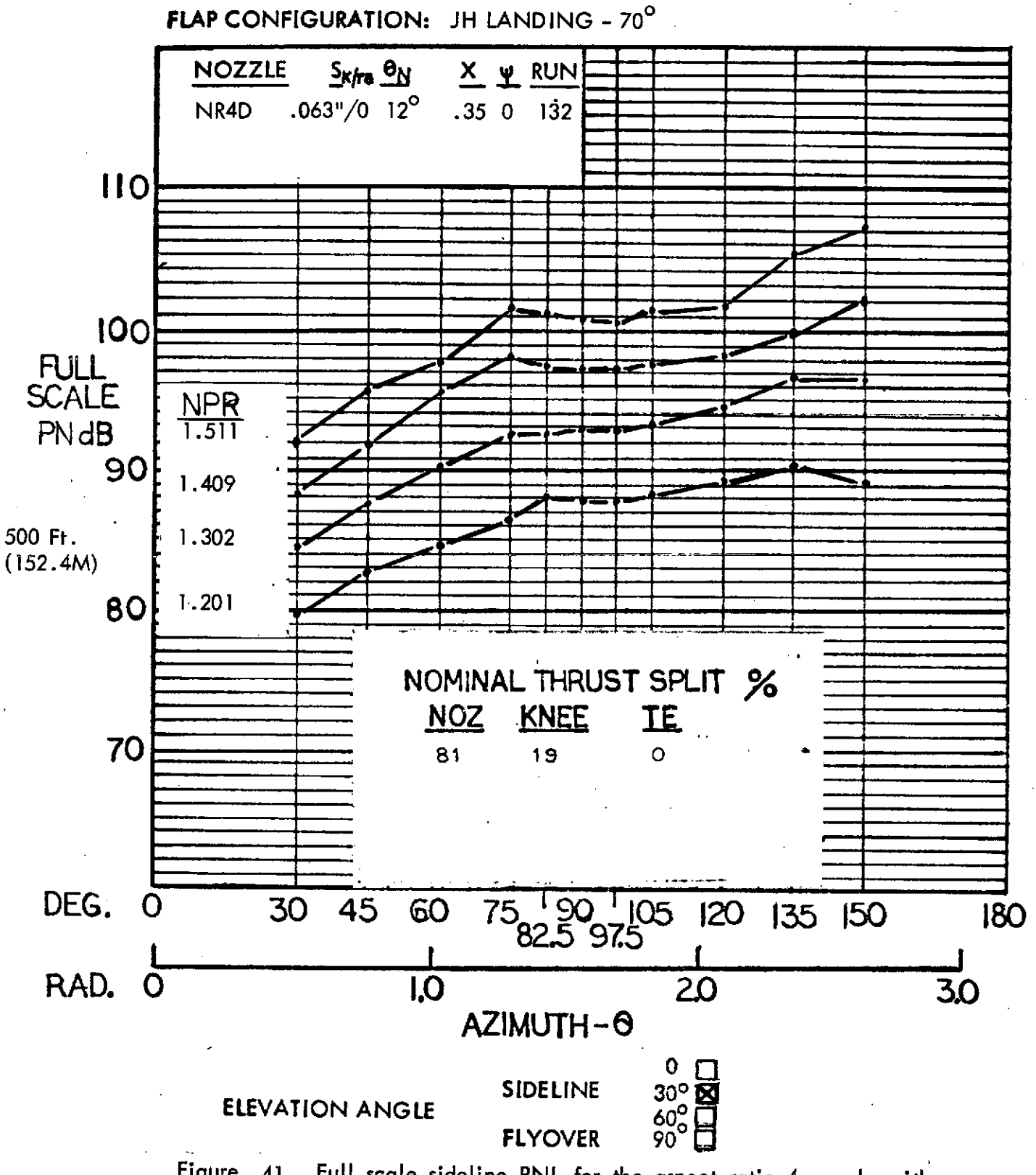

Figure 41 Full scale sideline PNL for the aspect ratio 4 nozzle with deflector and JH flap with knee blowing; 70° flap angle.

HYBRID PROPULSIVE LIFT
ACOUSTIC TEST
NAS 2-7812

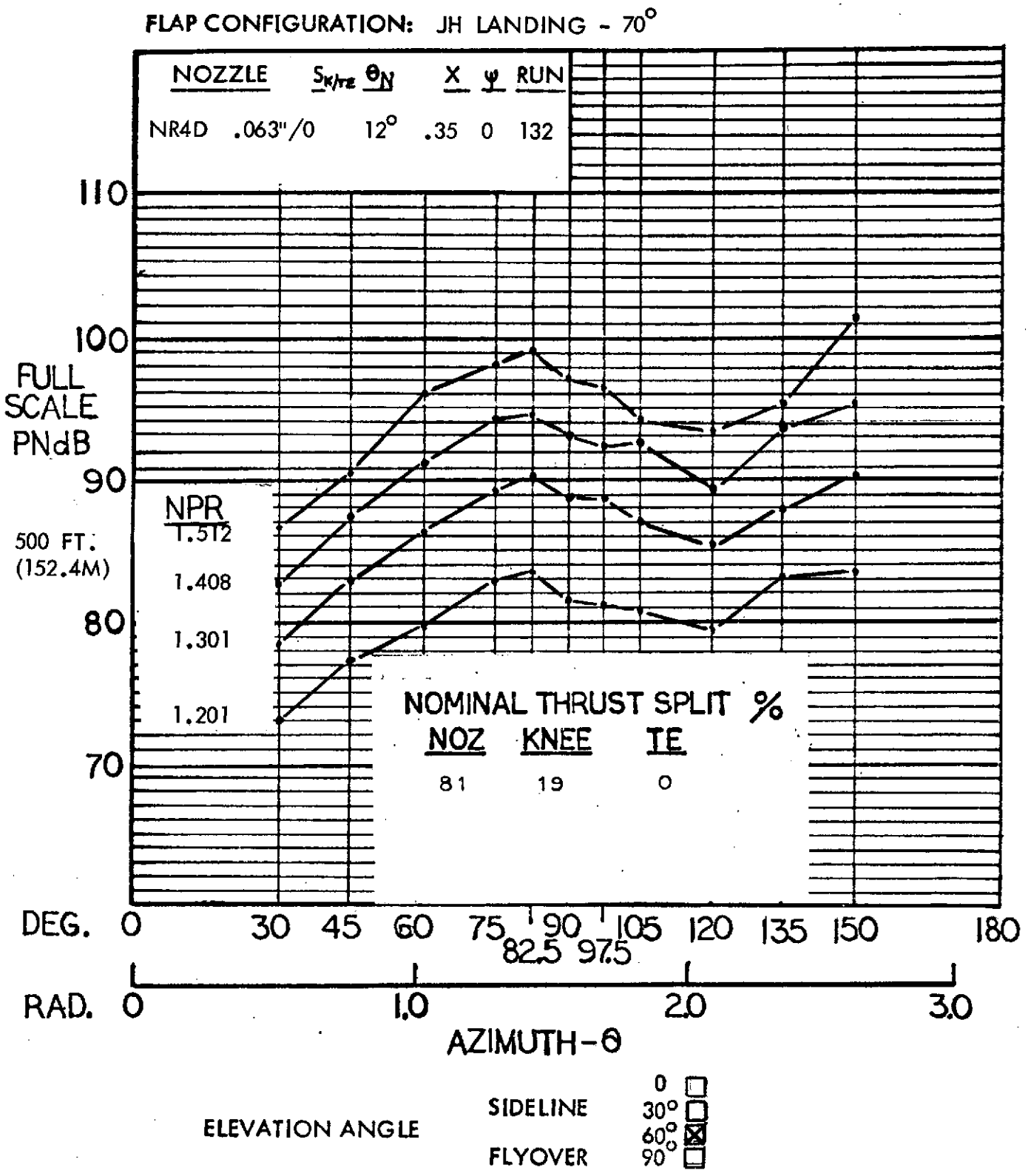

Figure 42 Full scale sideline PNL for the aspect ratio 4 nozzle with deflector and JH flap with knee blowing; 70° flap angle.

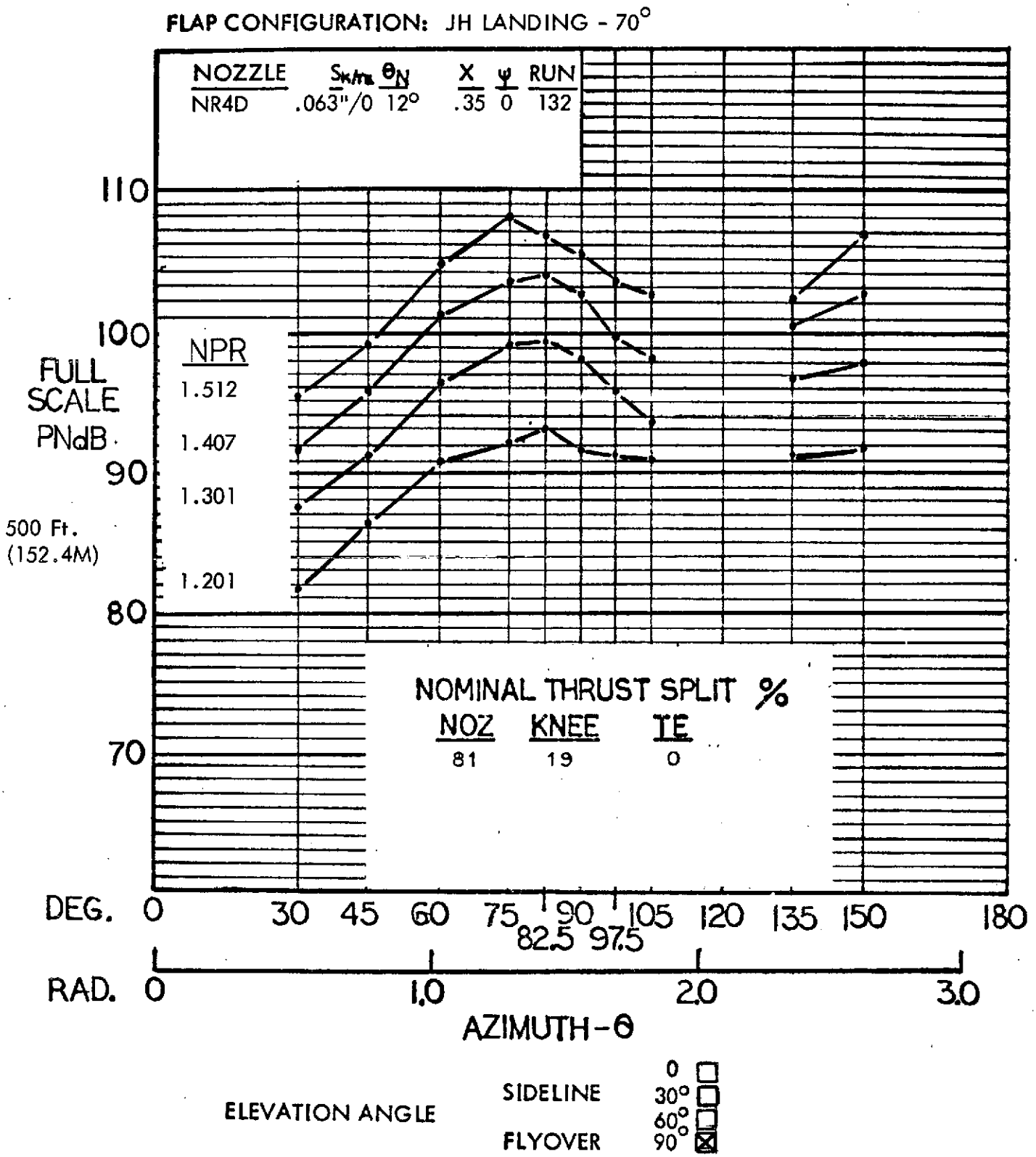

Figure 43 Full scale flyover PNL for the aspect ratio 4 nozzle with deflector and JH flap with knee blowing; 70° flap angle.

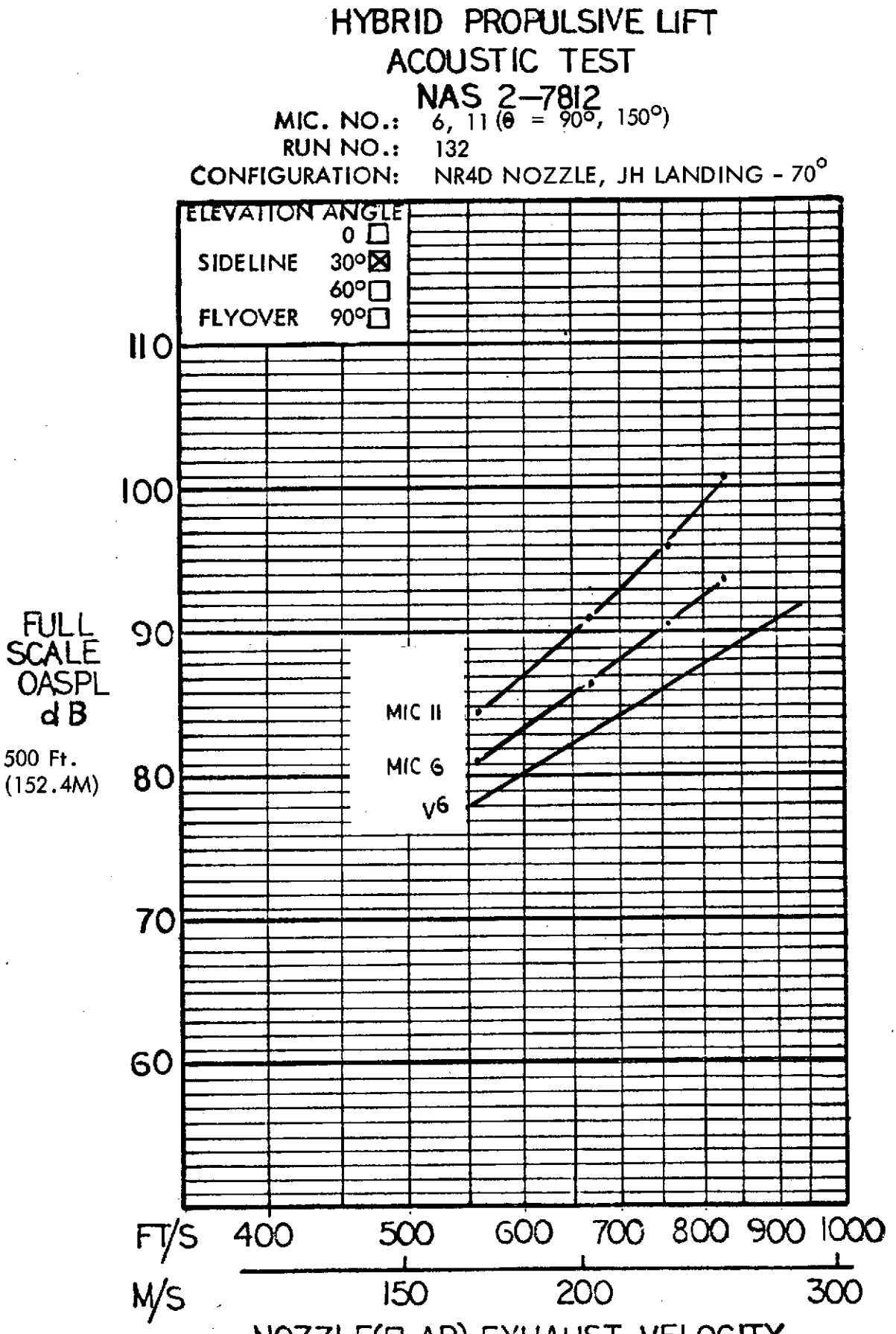

Figure 44 Full scale sideline OASPL at 90° and 150° azimuth for the aspect ratio 4 nozzle with deflector and JH flap with knee blowing; 70° flap angle

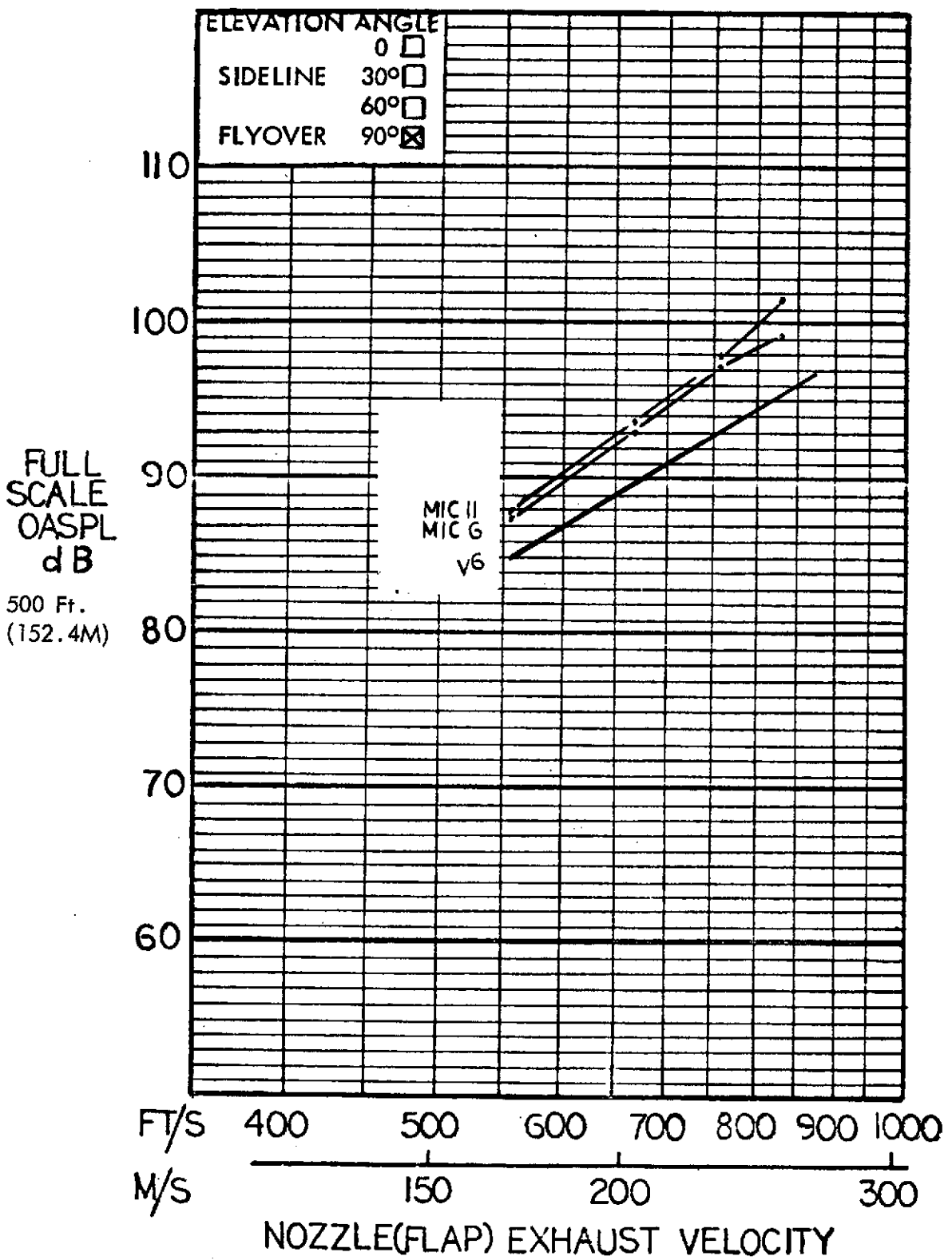

Figure 45 Full scale flyover OASPL at 90° and 150° azimuth for the aspect ratio 4 nozzle with deflector and JH flap with knee blowing; 70° flap angle.

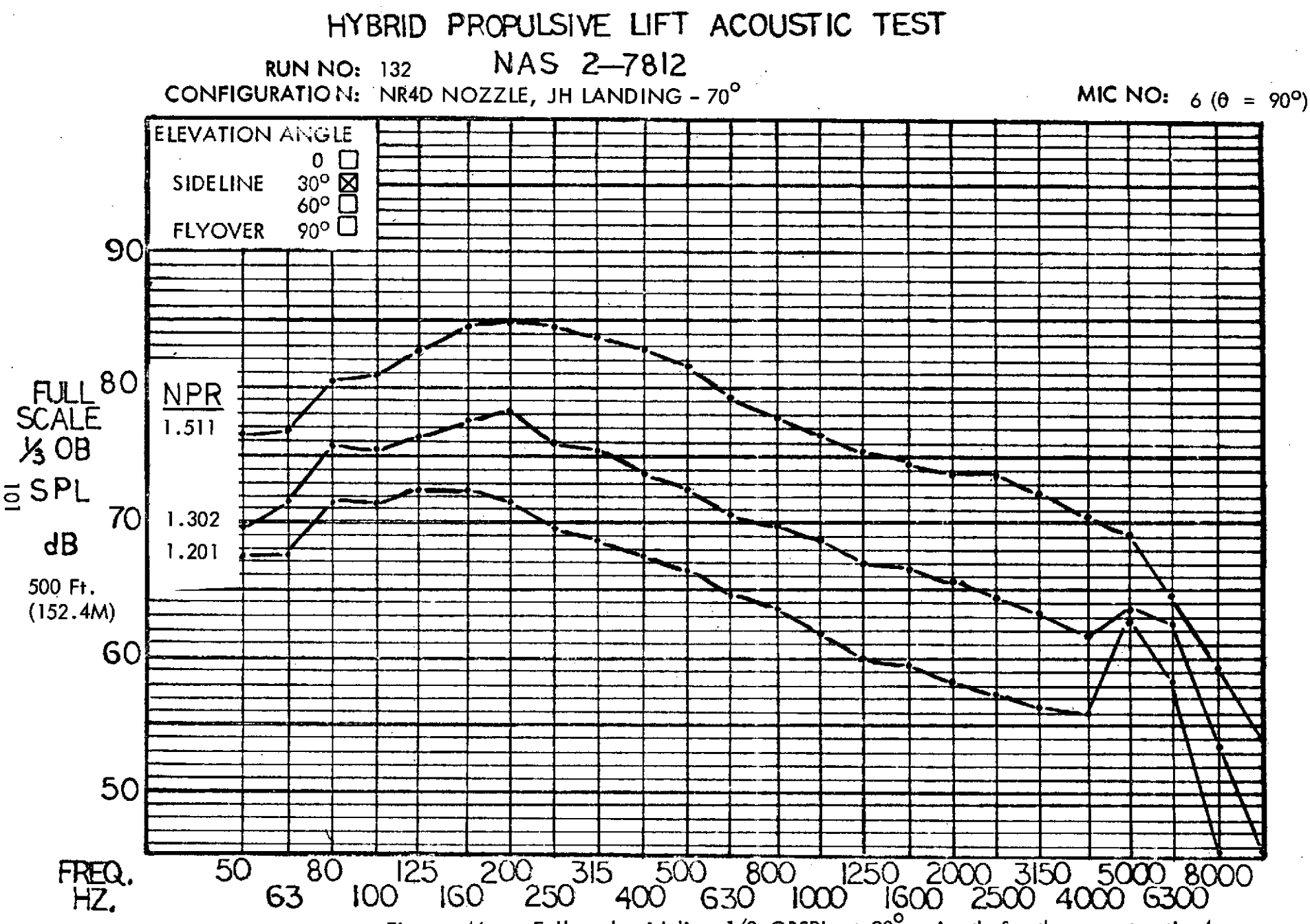

Figure 46 Full scale sideline 1/3 OBSPL at 90° azimuth for the aspect ratio 4 nozzle with deflector and JH flap with knee blowing; 70° flap angle.

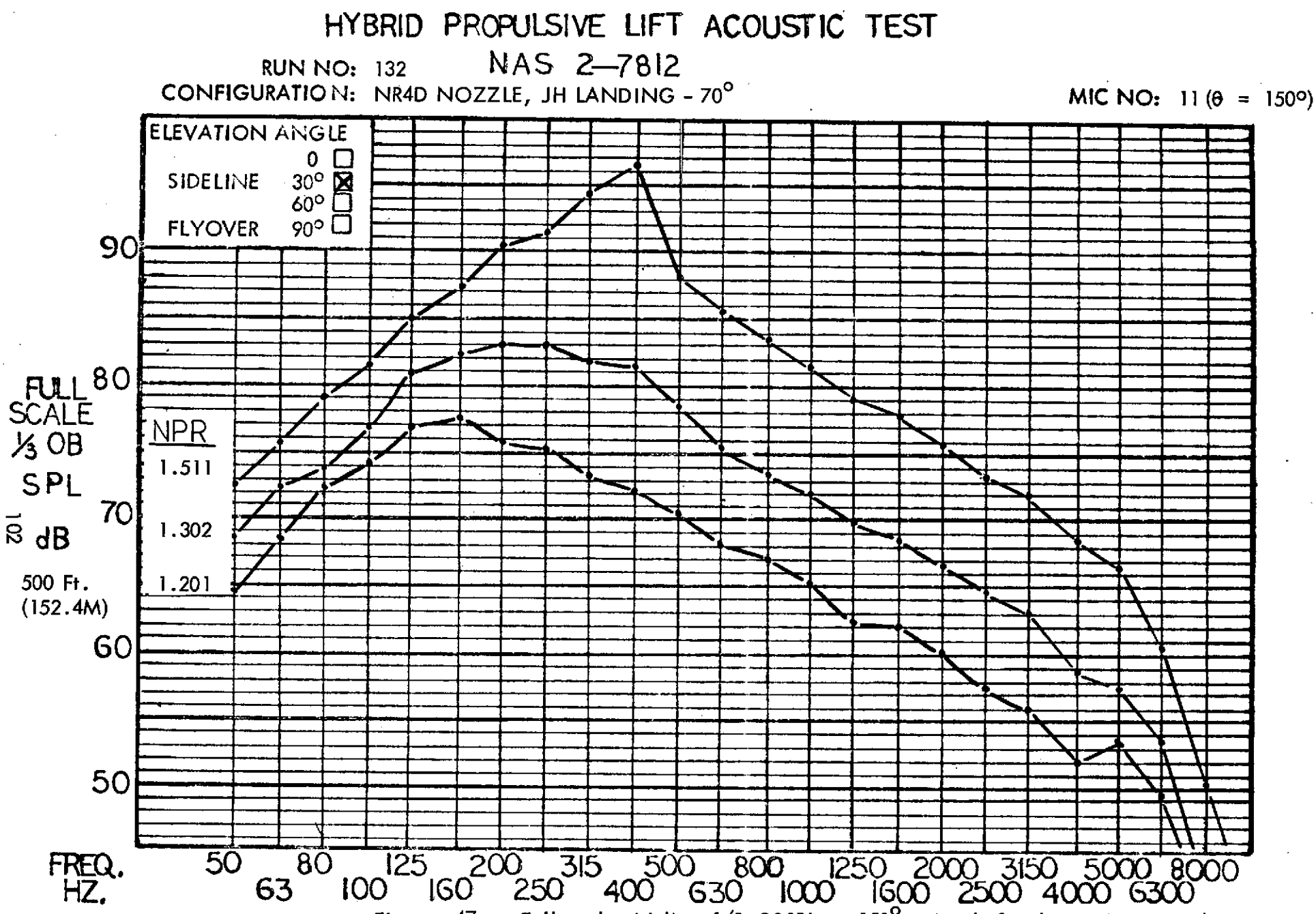

Figure 47 Full scale sideline 1/3 OBSPL at 150° azimuth for the aspect ratio 4 nozzle with deflector and JH flap with knee blowing; 70° flap angle.

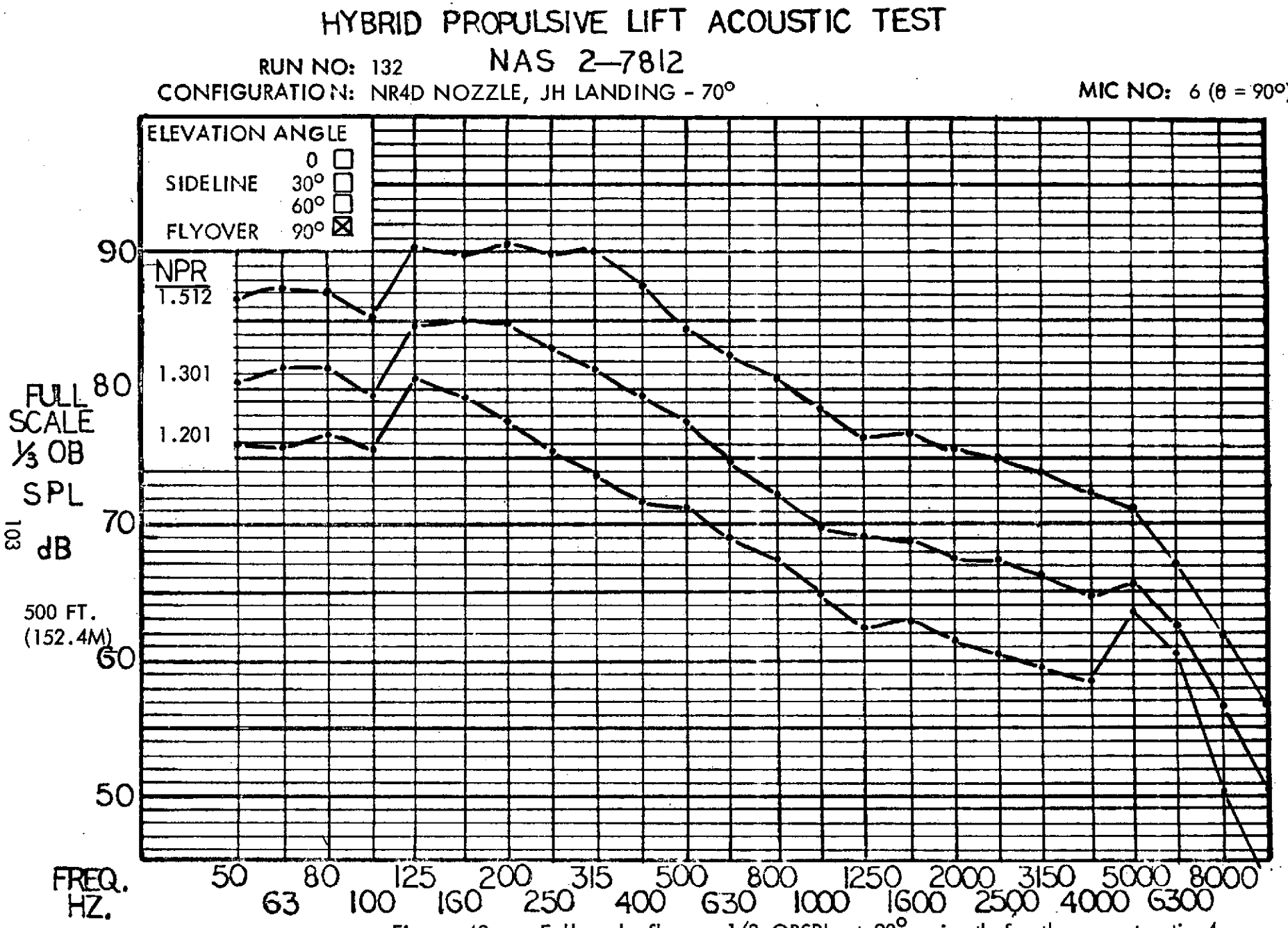

Figure 48 Full scale flyover 1/3 OBSPL at 90° azimuth for the aspect ratio 4 nozzle with deflector and JH flap with knee blowing; 70° flap angle.

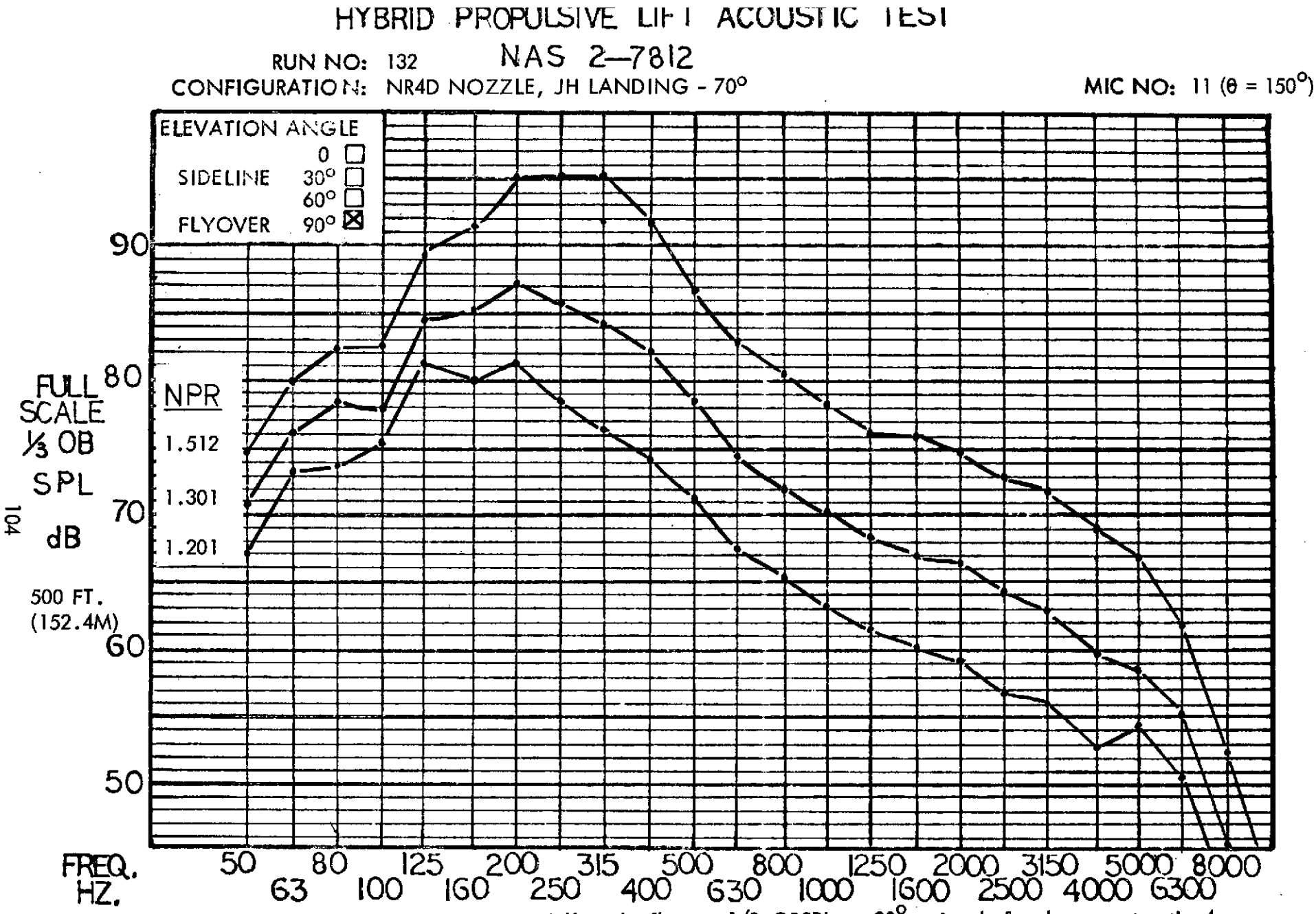

Figure 49 Full scale flyover 1/3 OBSPL at 90° azimuth for the aspect ratio 4 nozzle with deflector and JH flap with knee blowing; 70° flap angle.

HYBRID PROPULSIVE LIFT
ACOUSTIC TEST
NAS 2-7812

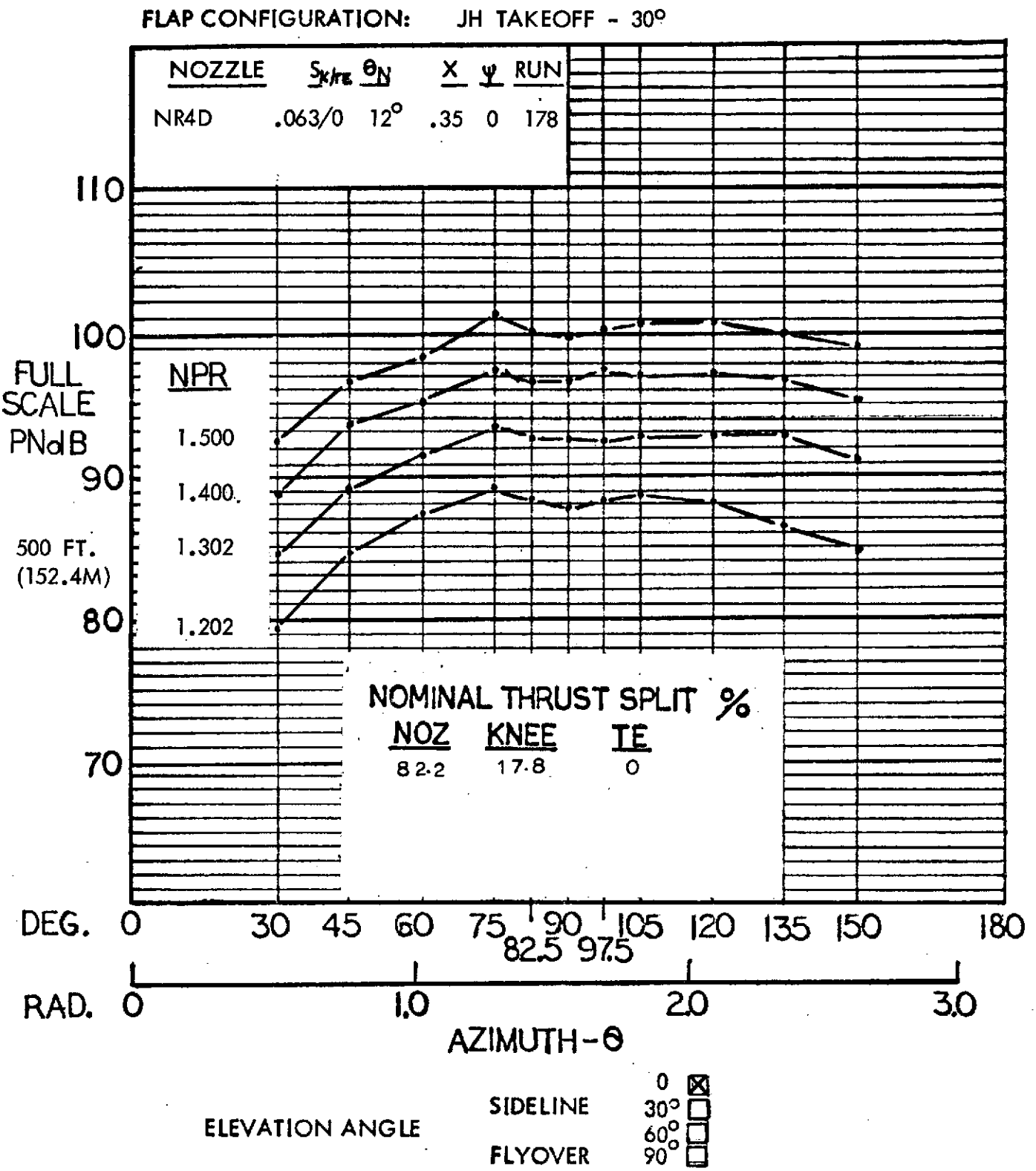

Figure 50 Full scale sideline PNL for the aspect ratio 4 nozzle with deflector and JH flap with knee blowing; 30° flap angle.

HYBRID PROPULSIVE LIFT
ACOUSTIC TEST
NAS 2-7812

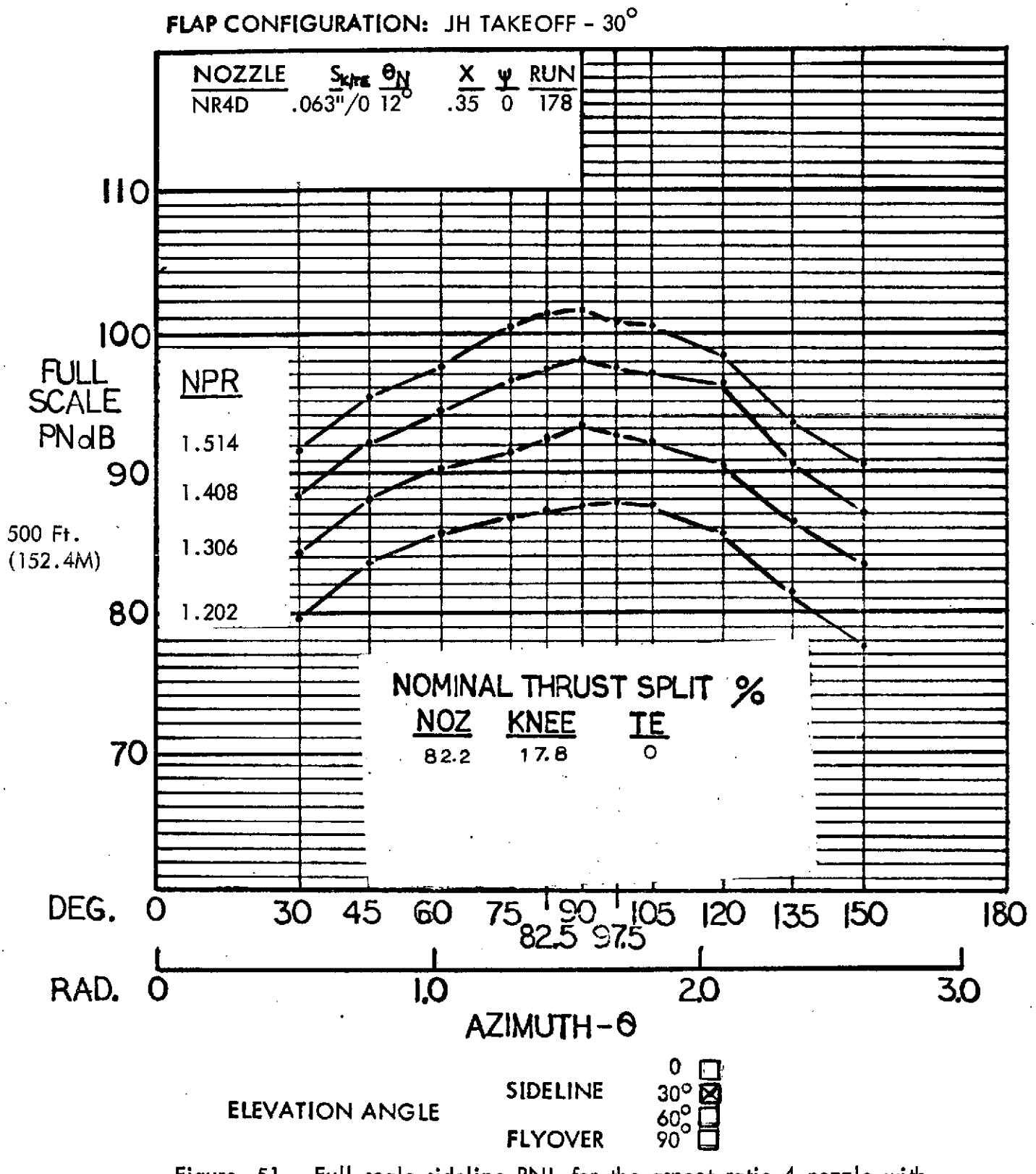

Figure 51 Full scale sideline PNL for the aspect ratio 4 nozzle with deflector and JH flap with knee blowing; 30° flap angle.

HYBRID PROPULSIVE LIFT
ACOUSTIC TEST
NAS 2-7812

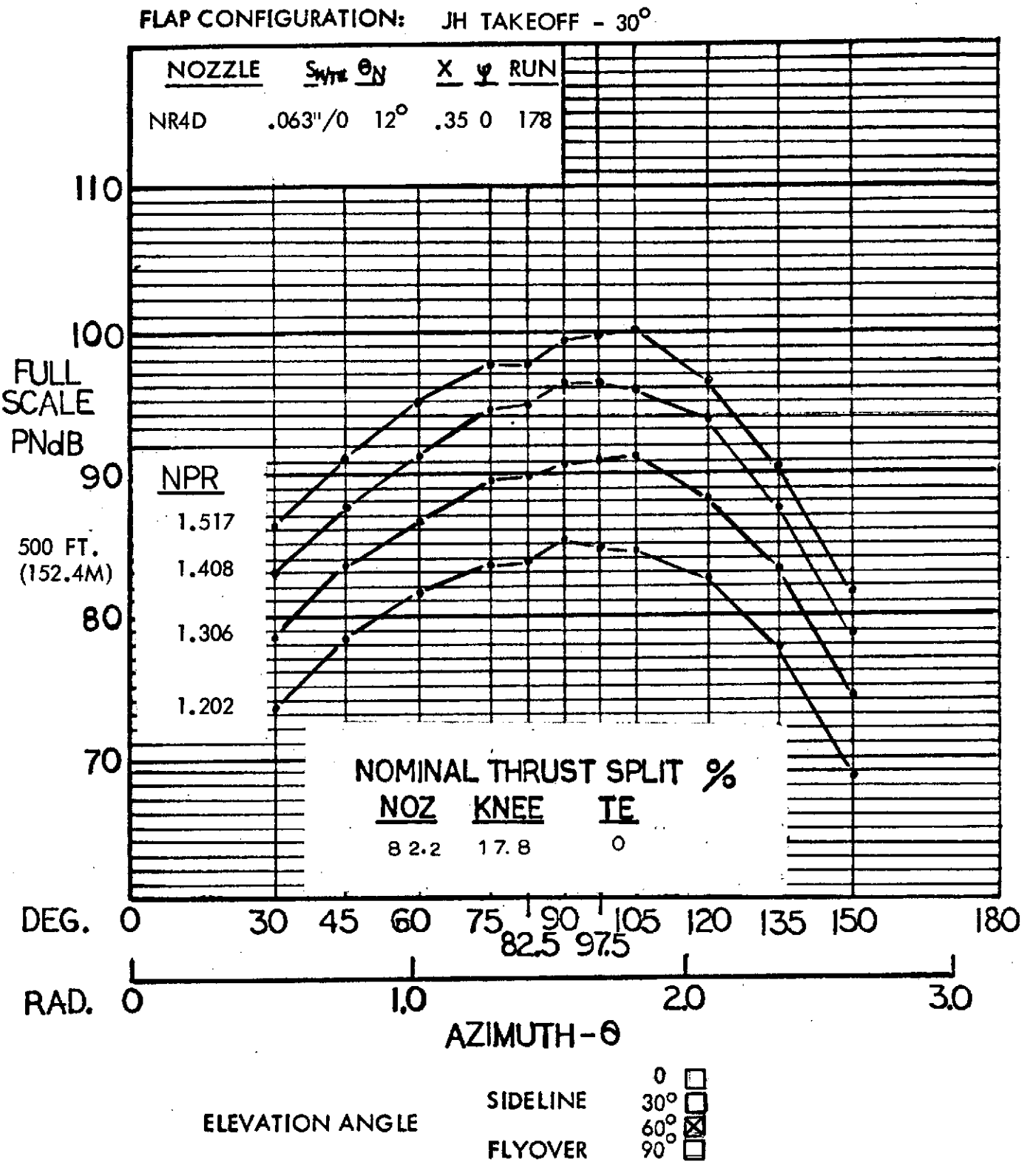

Figure 52 Full scale sideline PNL for the aspect ratio 4 nozzle with deflector and JH flap with knee blowing; 30° flap angle.

HYBRID PROPULSIVE LIFT
ACOUSTIC TEST
NAS 2-7812

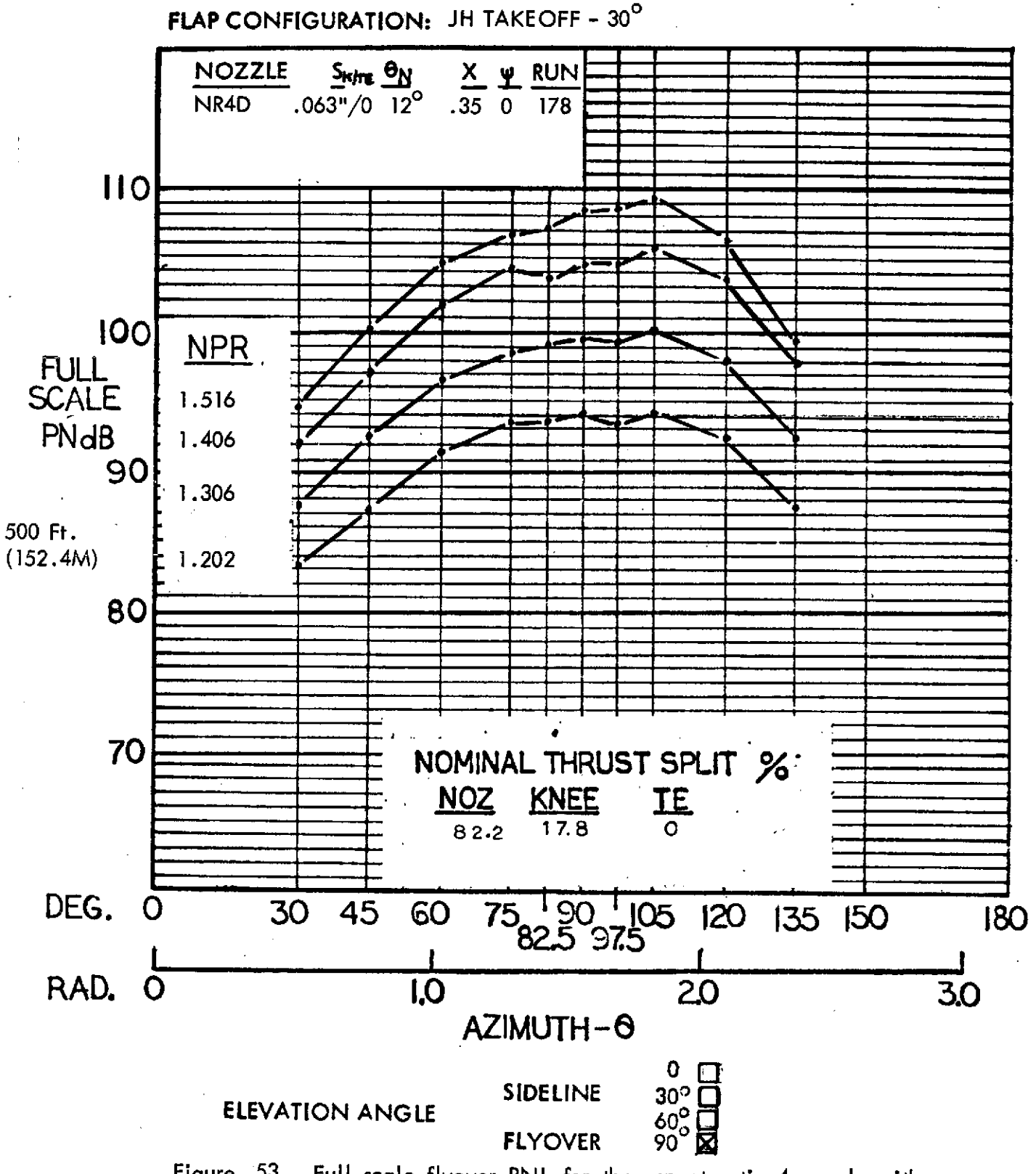

Figure 53 Full scale flyover PNL for the aspect ratio 4 nozzle with deflector and JH flap with knee blowing; 30° flap angle.

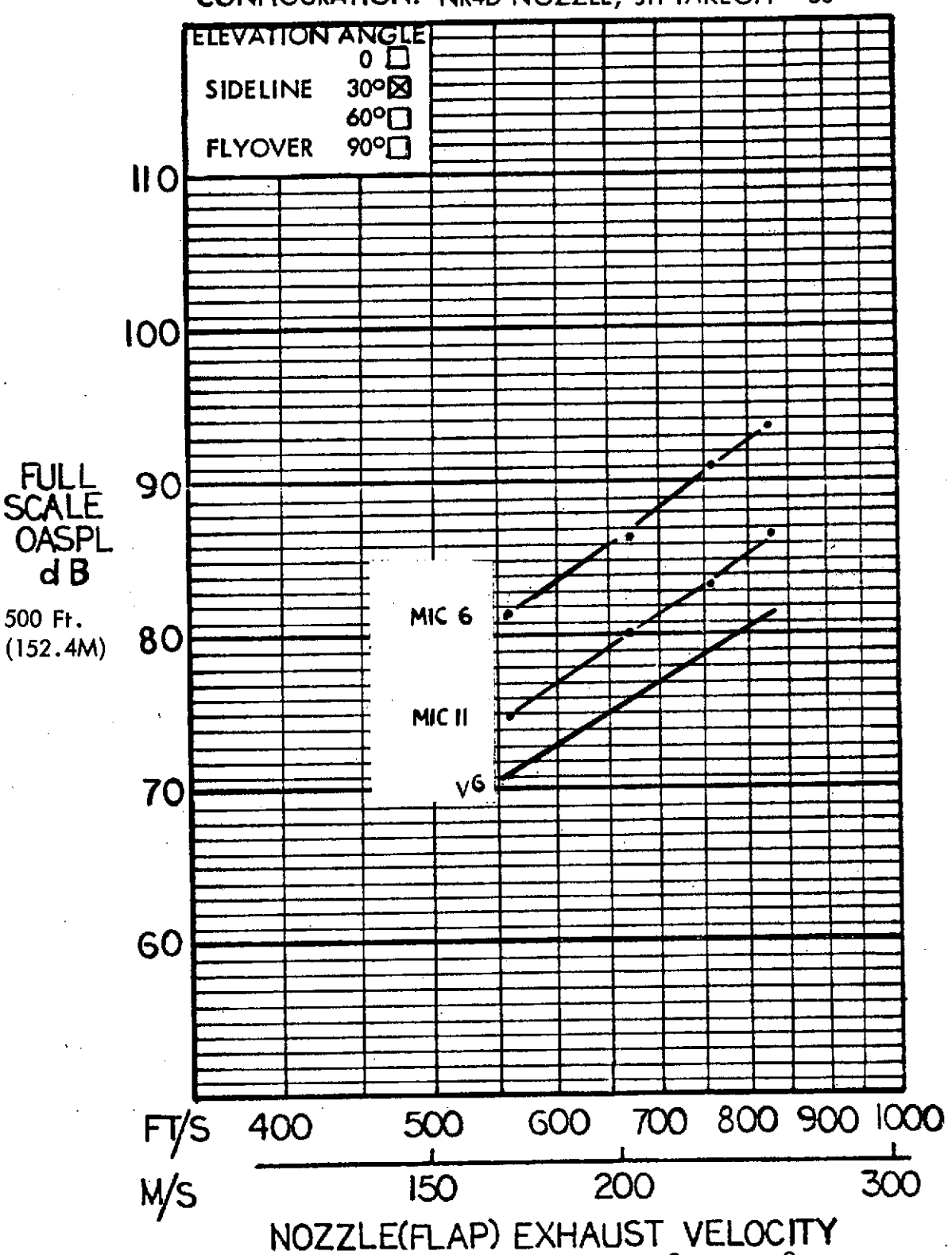

Figure 54 Full scale sideline OASPL at 90° and 150° azimuth for the aspect ratio 4 nozzle with deflector and JH flap with knee blowing; 30° flap angle.

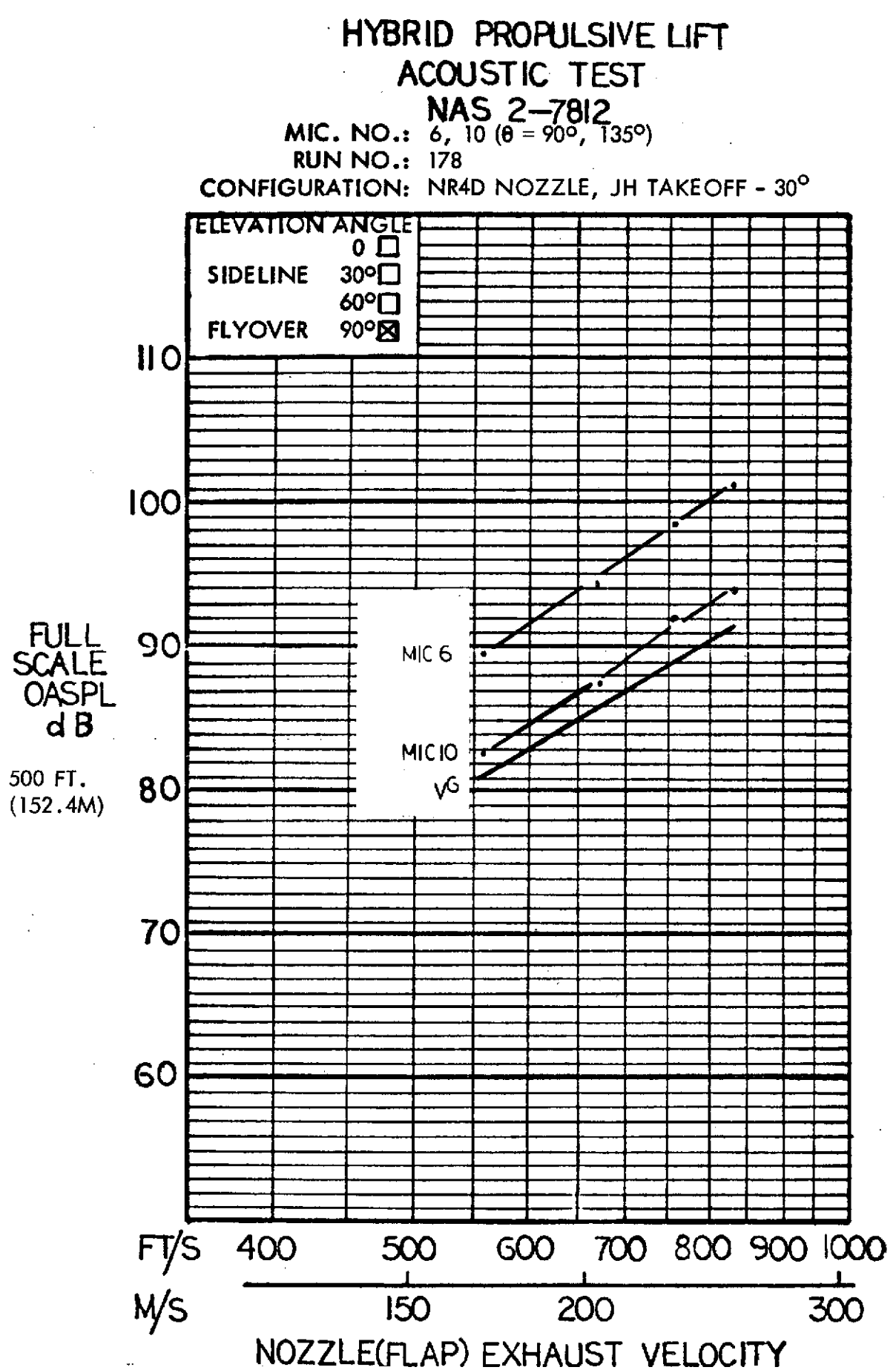

Figure 55 Full scale flyover OASPL at 90° and 135° azimuth for the aspect ratio 4 nozzle with deflector and JH flap with knee blowing; 30° flap angle.

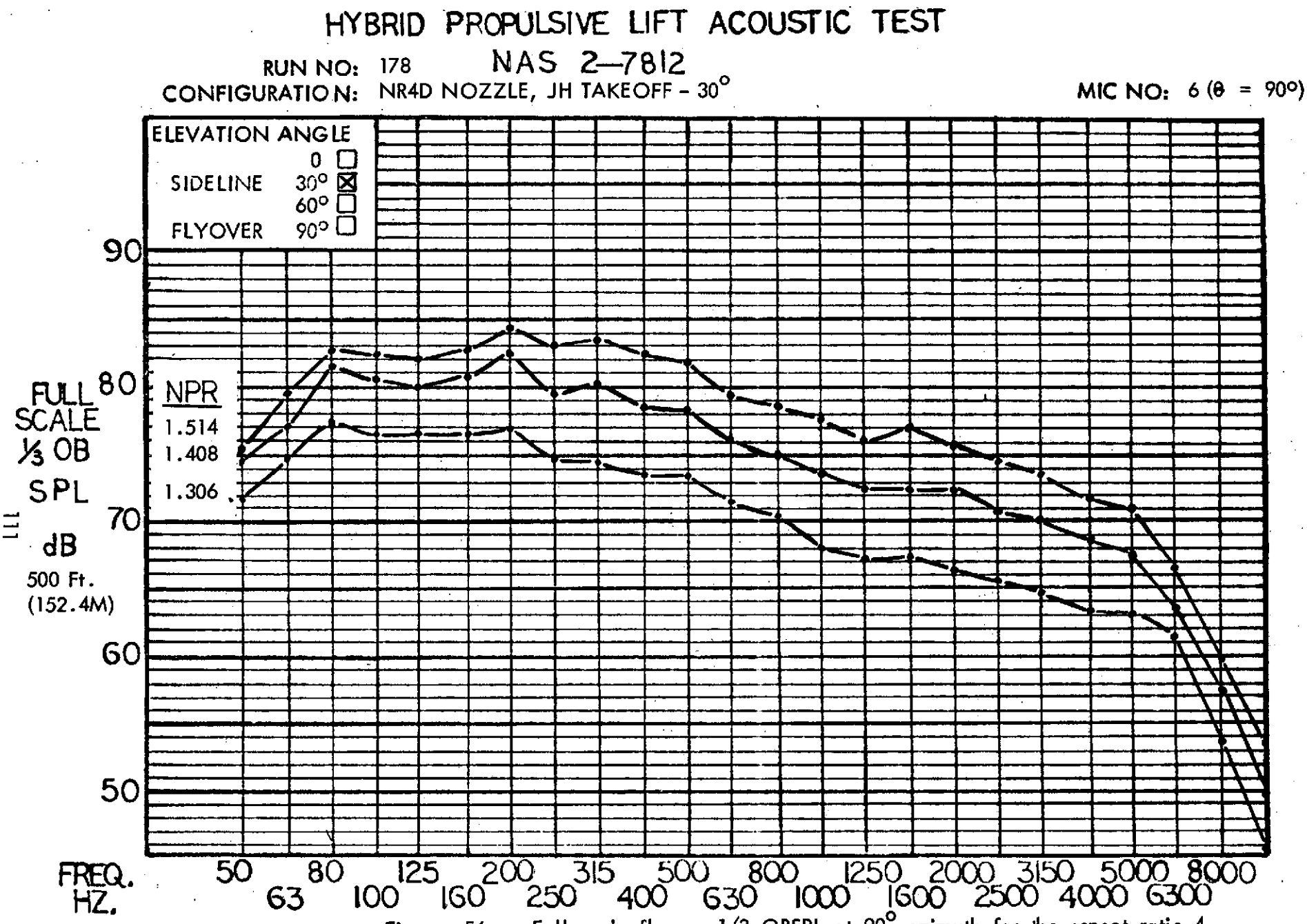

Figure 56 Full scale flyover 1/3 OBSPL at 90° azimuth for the aspect ratio 4 nozzle with deflector and JH flap with knee blowing; 30° flap angle

HYBRID PROPULSIVE LIFT ACOUSTIC TEST

RUN NO: 178 NAS 2—7812

CONFIGURATION: NR4D NOZZLE, JH TAKEOFF - 30°

MIC NO: 8 (θ = 105°)

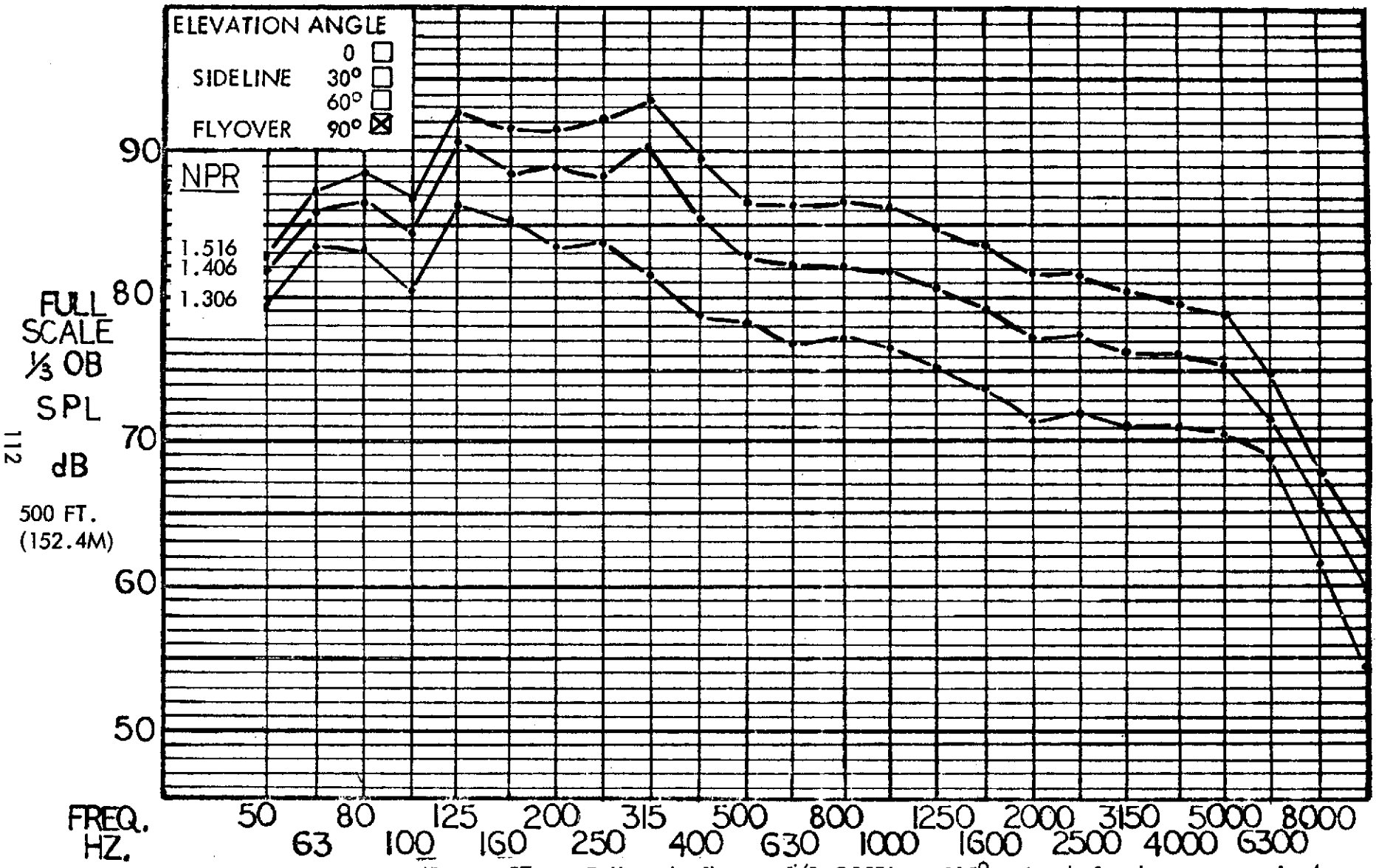

Figure 57 Full scale flyover 1/3 OBSPL at 105° azimuth for the aspect ratio 4 nozzle with deflector and JH flap with knee blowing; 30° flap angle.

HYBRID PROPULSIVE LIFT
ACOUSTIC TEST
NAS 2-7812

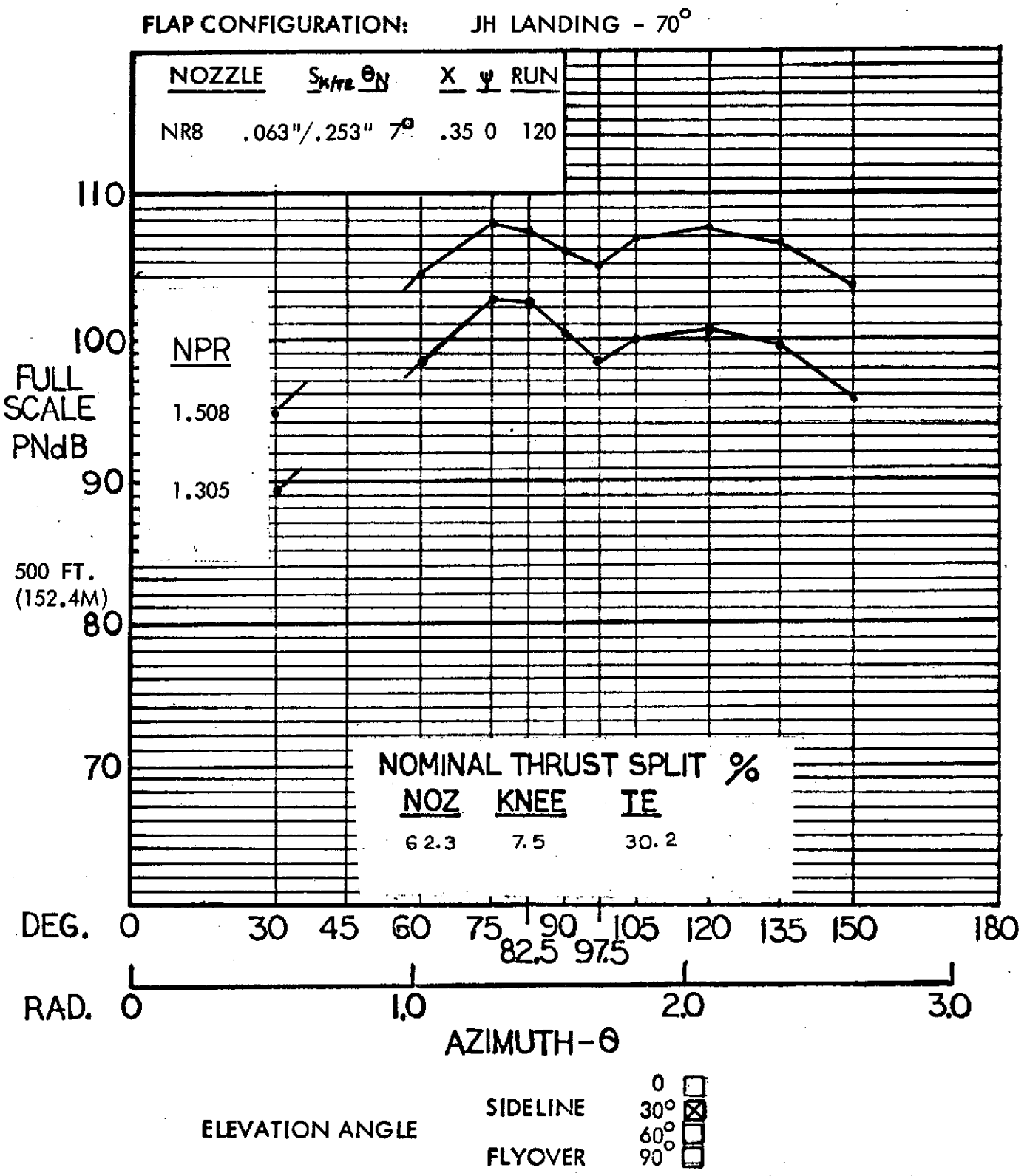

Figure 58 Full scale sideline PNL for the aspect ratio 8 nozzle and JH flap with knee and TE blowing; 70° flap angle.

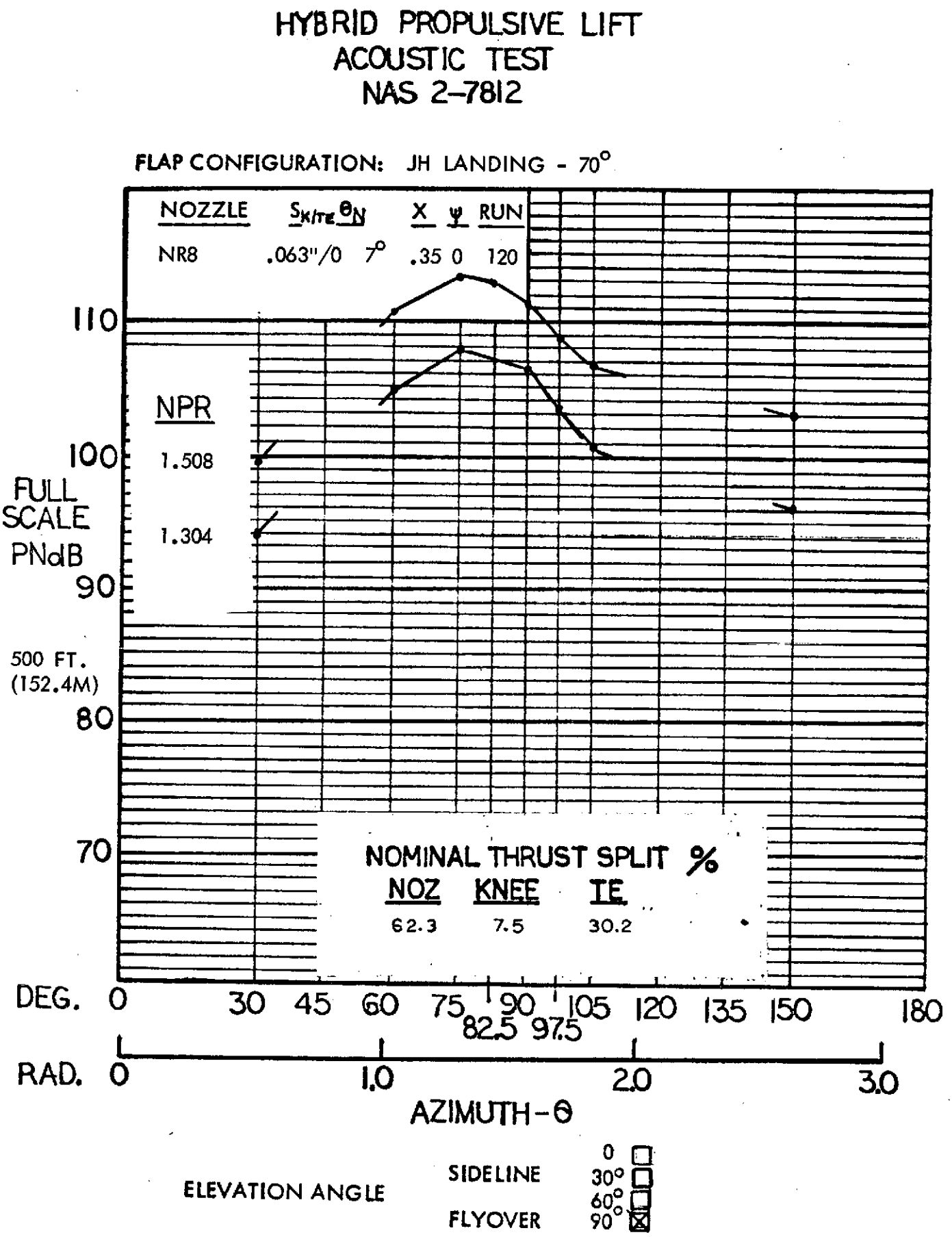

Figure 59 Full scale flyover PNL for the aspect ratio 8 nozzle and JH flap with knee and TE blowing; 70° flap angle.

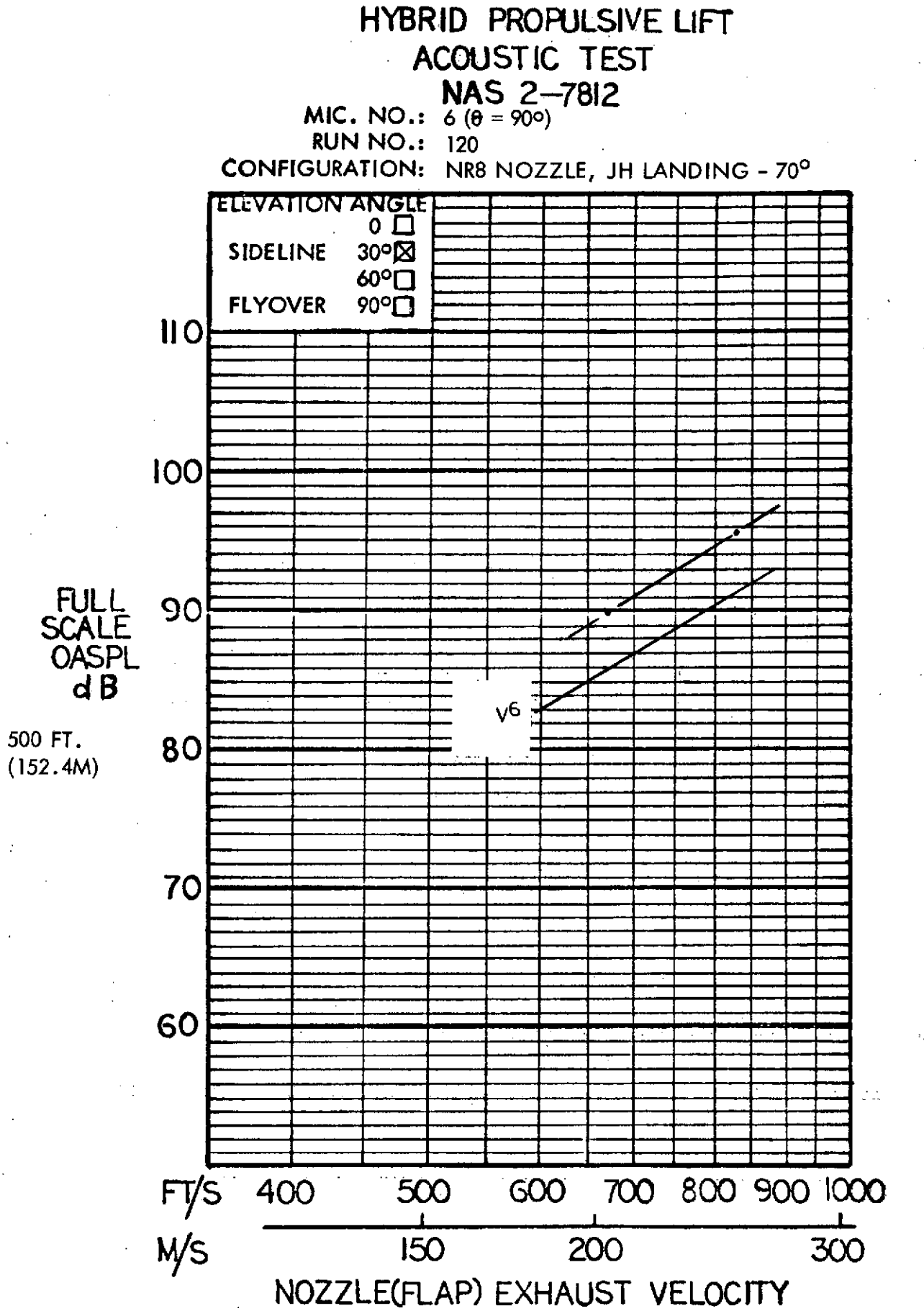

Figure 60 Full scale sideline OASPL at 90° azimuth for the aspect ratio 8 nozzle and JH flap with knee and TE blowing; 70° flap angle.

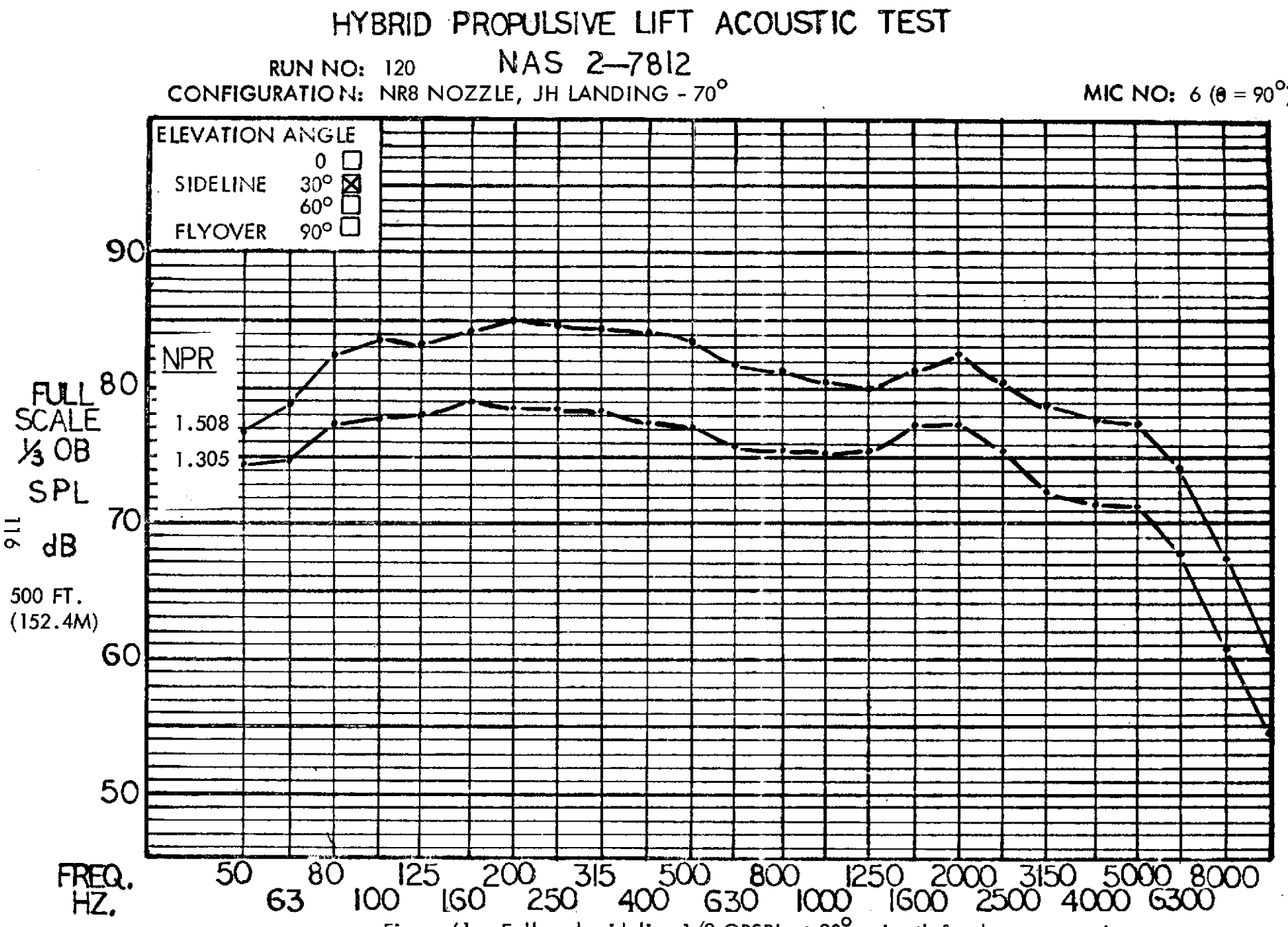

Figure 61 Full scale sideline 1/3 OBSPL at 90° azimuth for the aspect ratio 8 nozzle and JH flap with knee and TE blowing; 70° flap angle.

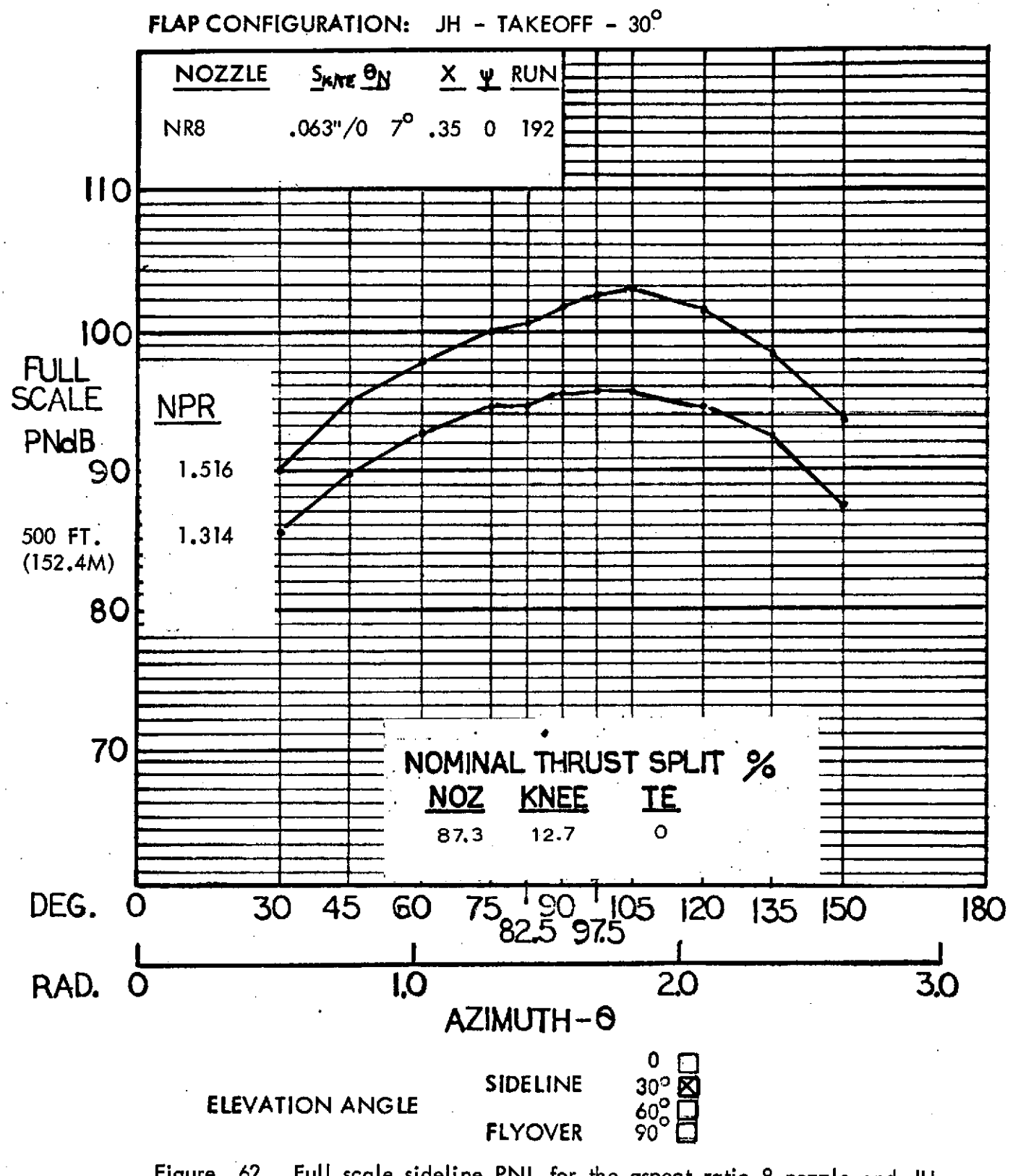

Figure 62 Full scale sideline PNL for the aspect ratio 8 nozzle and JH flap with knee blowing; 30° flap angle.

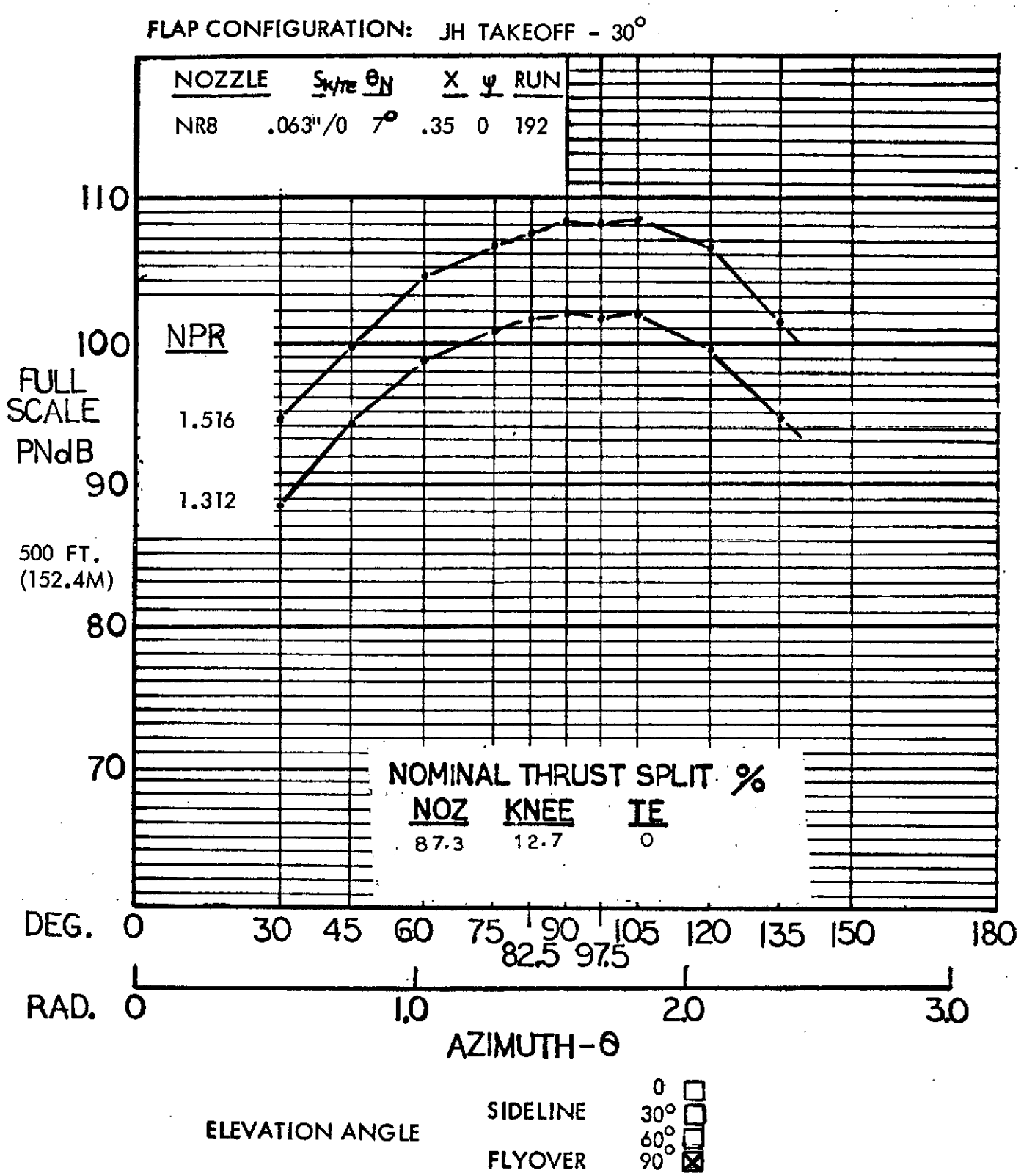

Figure 63 Full scale flyover PNL for the aspect ratio 8 nozzle and JH flap with knee blowing; 30° flap angle.

HYBRID PROPULSIVE LIFT
ACOUSTIC TEST
NAS 2-7812

MIC. NO.: 6 ($\theta = 90^\circ$)
RUN NO.: 192
CONFIGURATION: NR8 NOZZLE, JH TAKEOFF - 30°

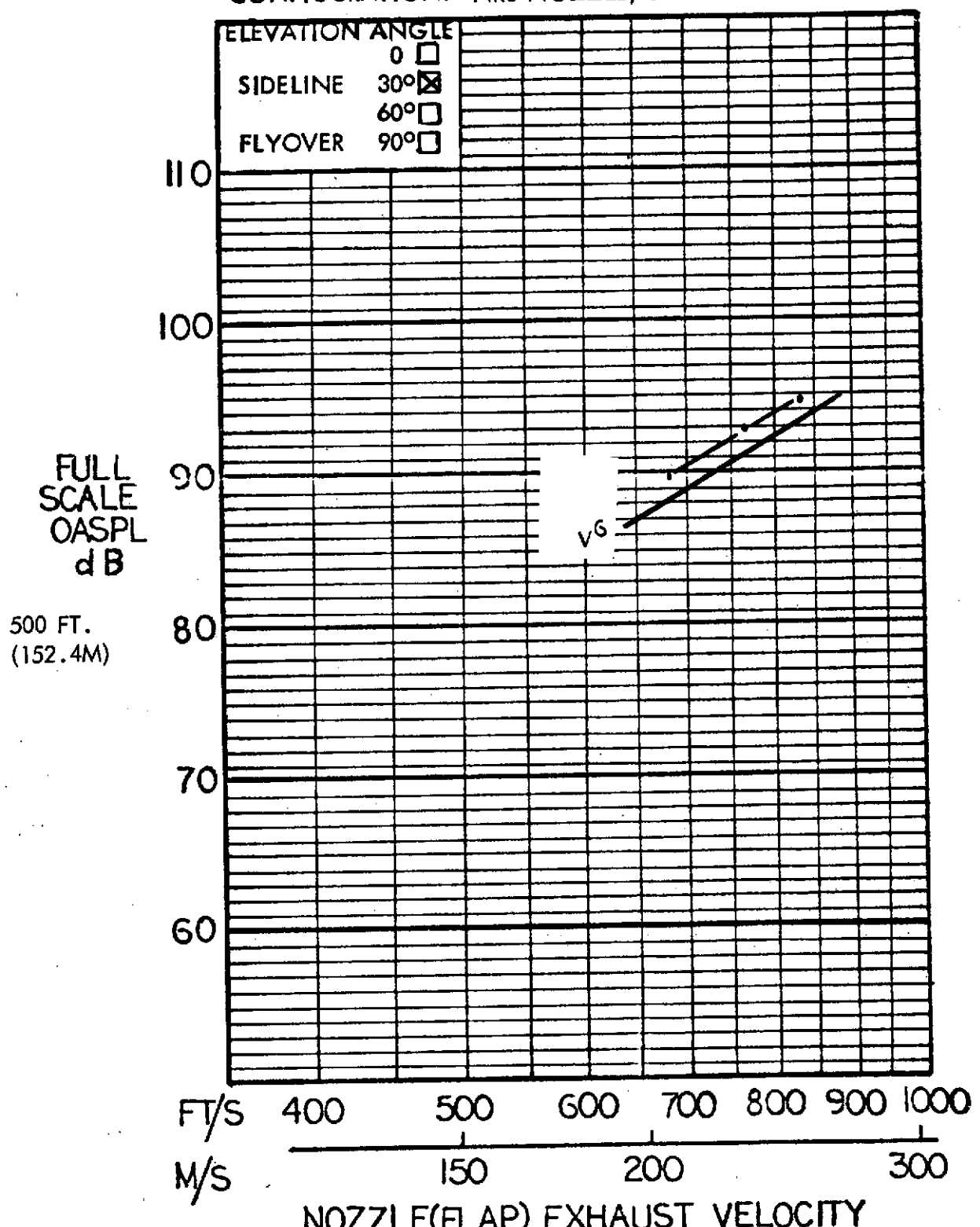

Figure 64 Full scale sideline OASPL at 90° azimuth for the aspect ratio 8 nozzle and JH flap with knee blowing; 30° flap angle.

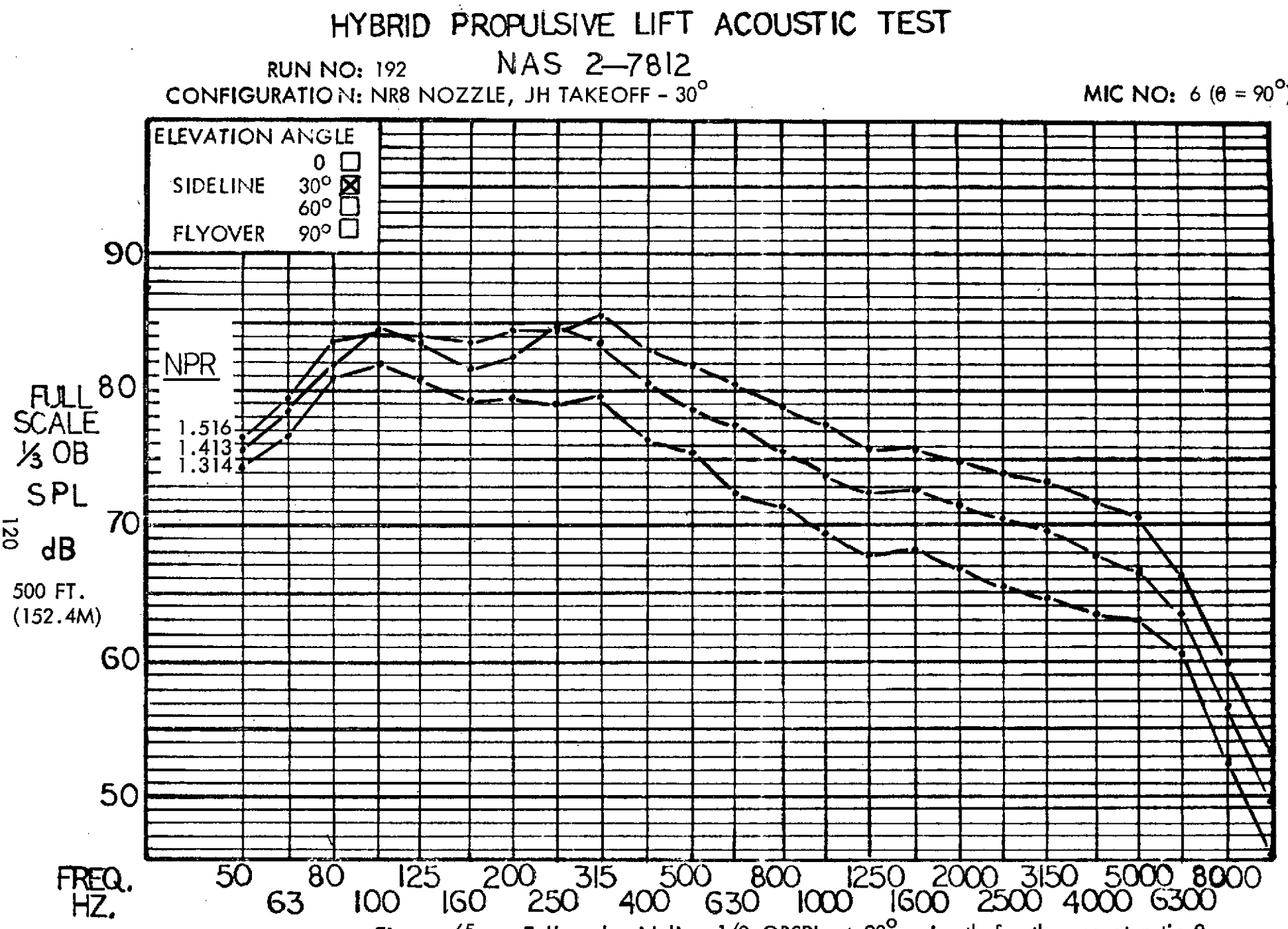

Figure 65 Full scale sideline 1/3 OBSPL at 90° azimuth for the aspect ratio 8 nozzle with deflector and JH flap with knee blowing; 30° flap angle.

HYBRID PROPULSIVE LIFT
ACOUSTIC TEST
NAS 2-7812

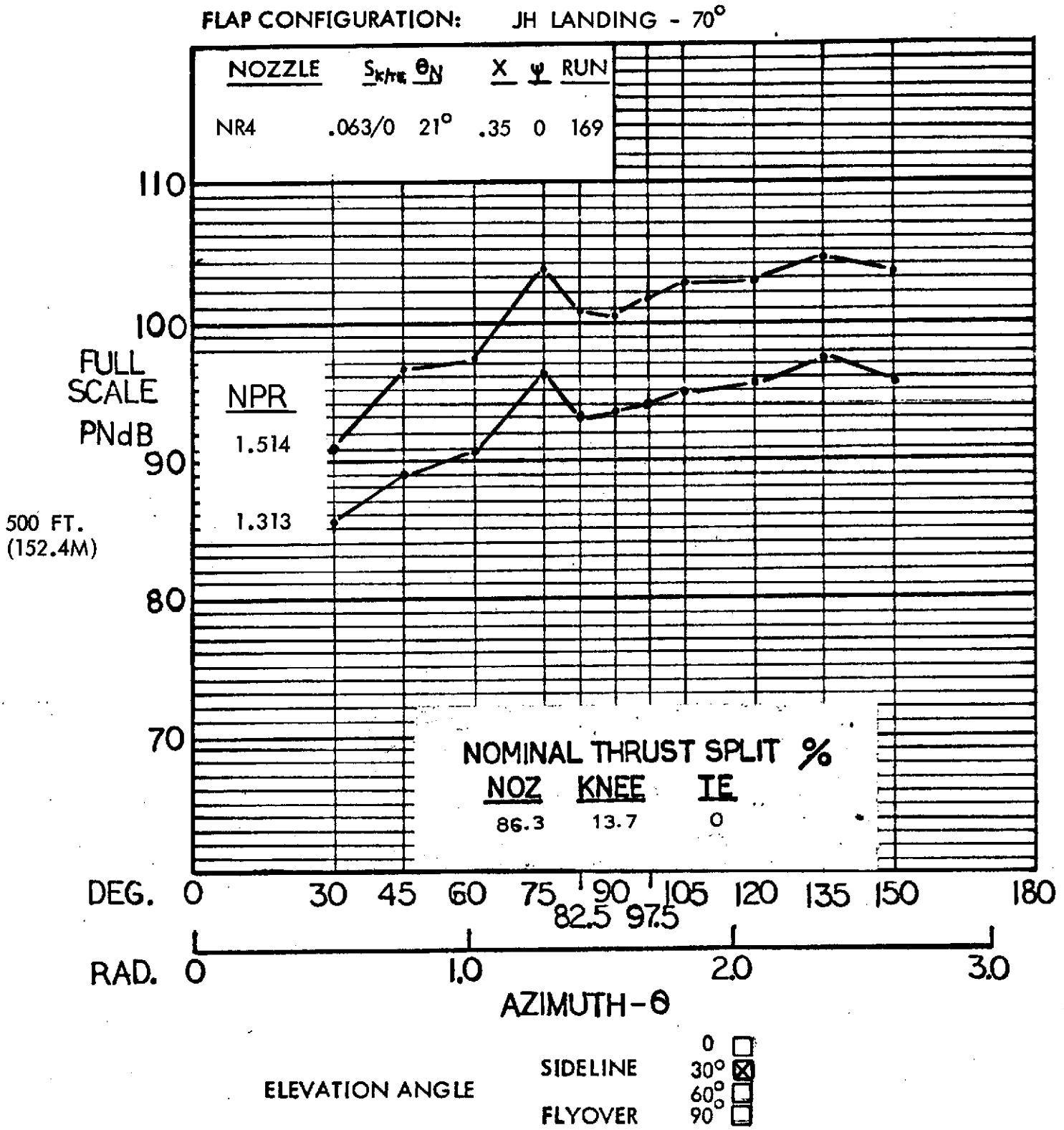

Figure 66 Full scale sideline PNL for the aspect ratio 4 nozzle and JH flap with knee blowing; 70° flap angle.

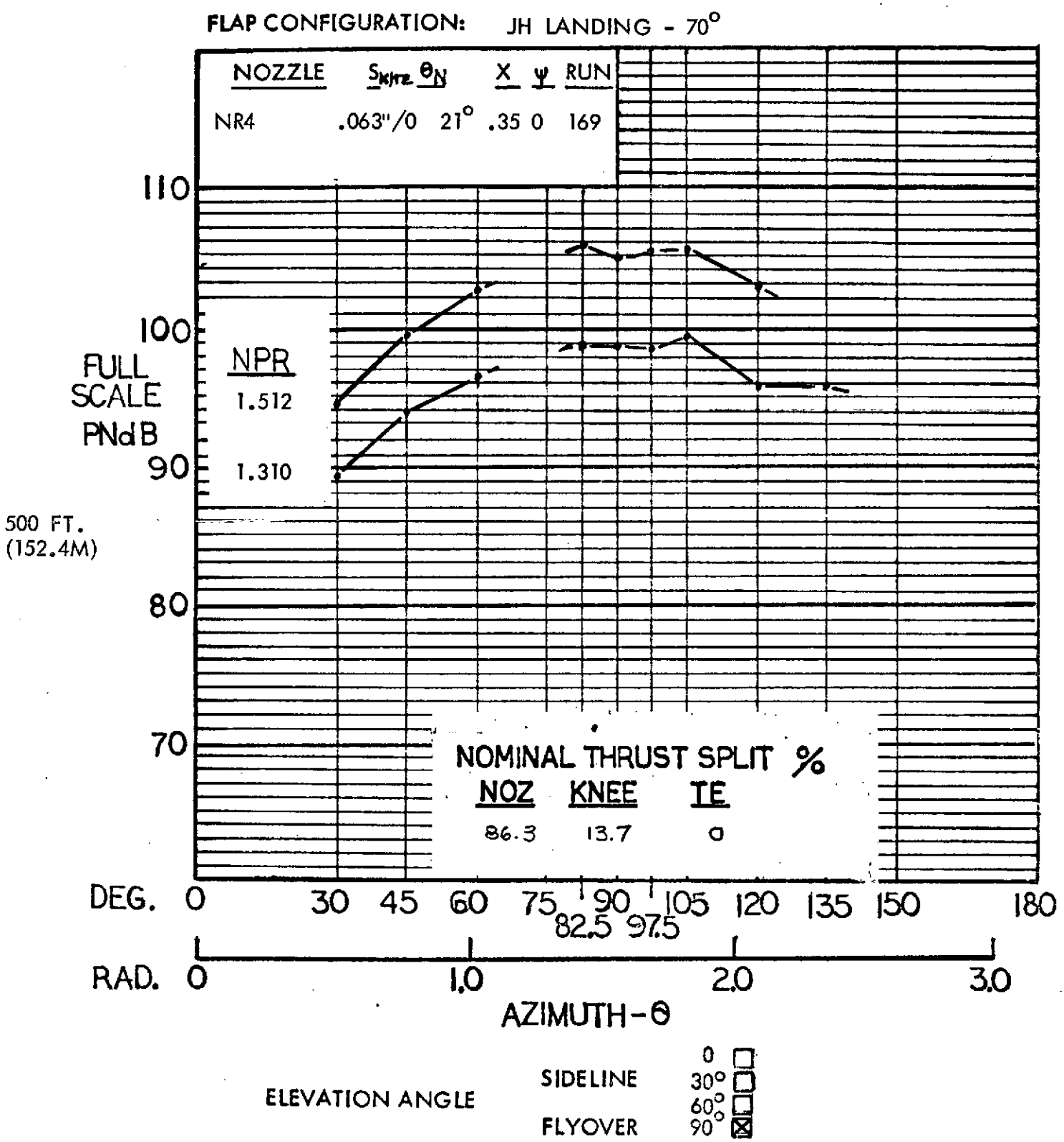

Figure 67 Full scale flyover PNL for the aspect ratio 4 nozzle and JH flap with knee blowing; 70° flap angle.

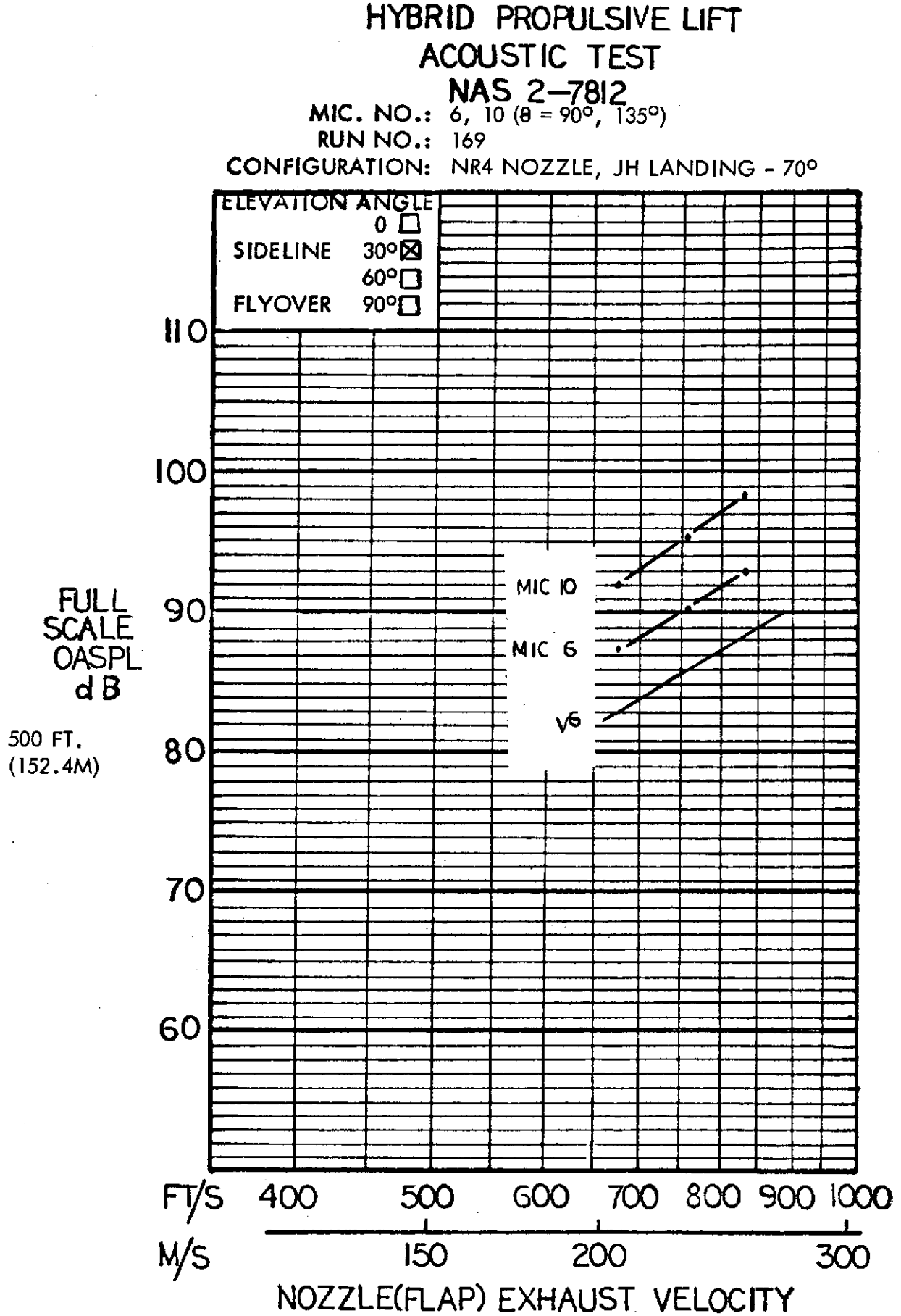

Figure 68 Full scale sideline OASPL at 90° and 135° azimuth for the aspect ratio 4 nozzle and JH flap with knee blowing; 70° flap angle.

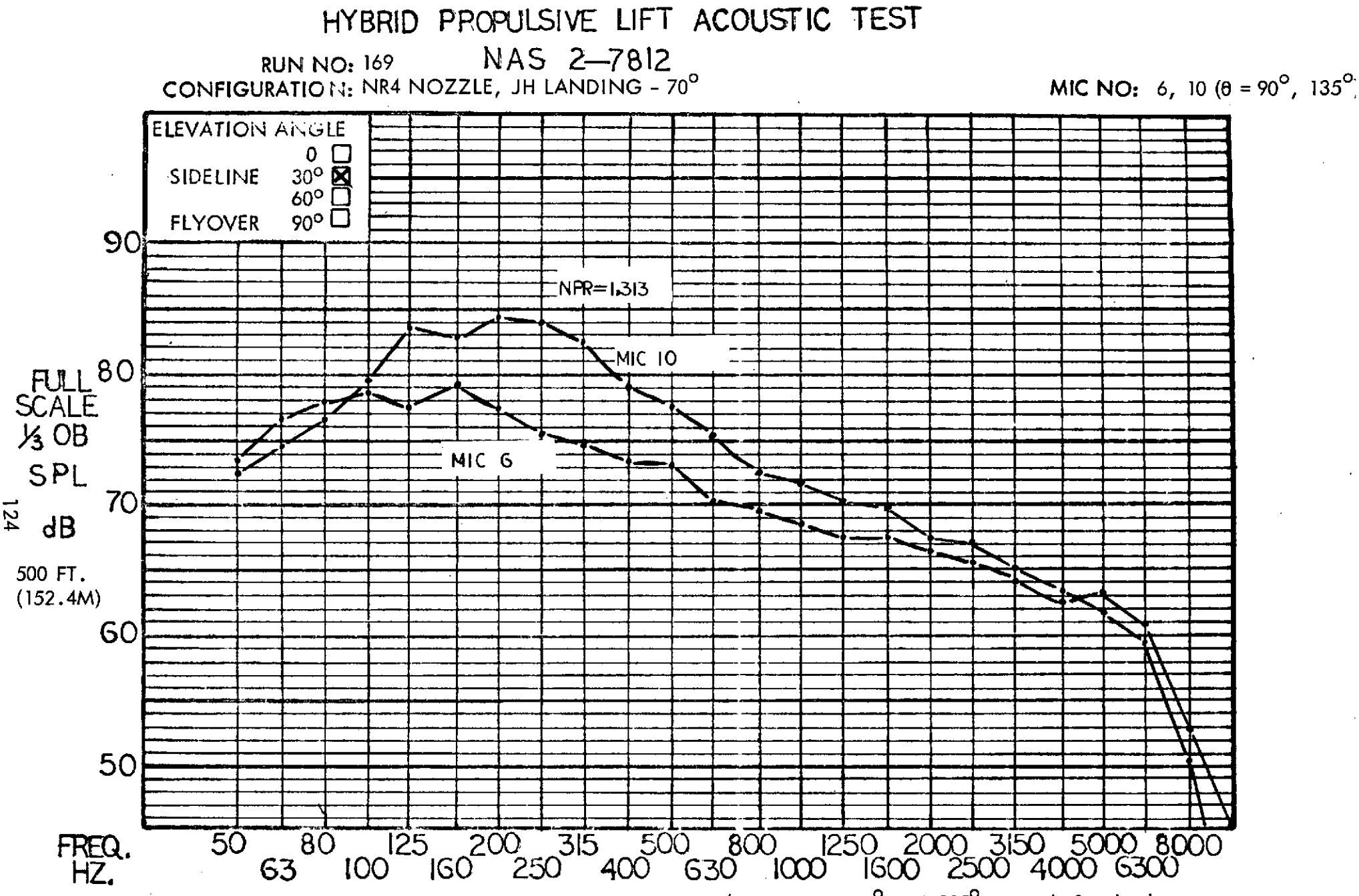

Figure 69 Full scale sideline 1/3 OBSPL at 90° and 135° azimuth for the aspect ratio 4 nozzle and JH flap with knee blowing; 70° flap angle.

HYBRID PROPULSIVE LIFT
ACOUSTIC TEST
NAS 2-7812

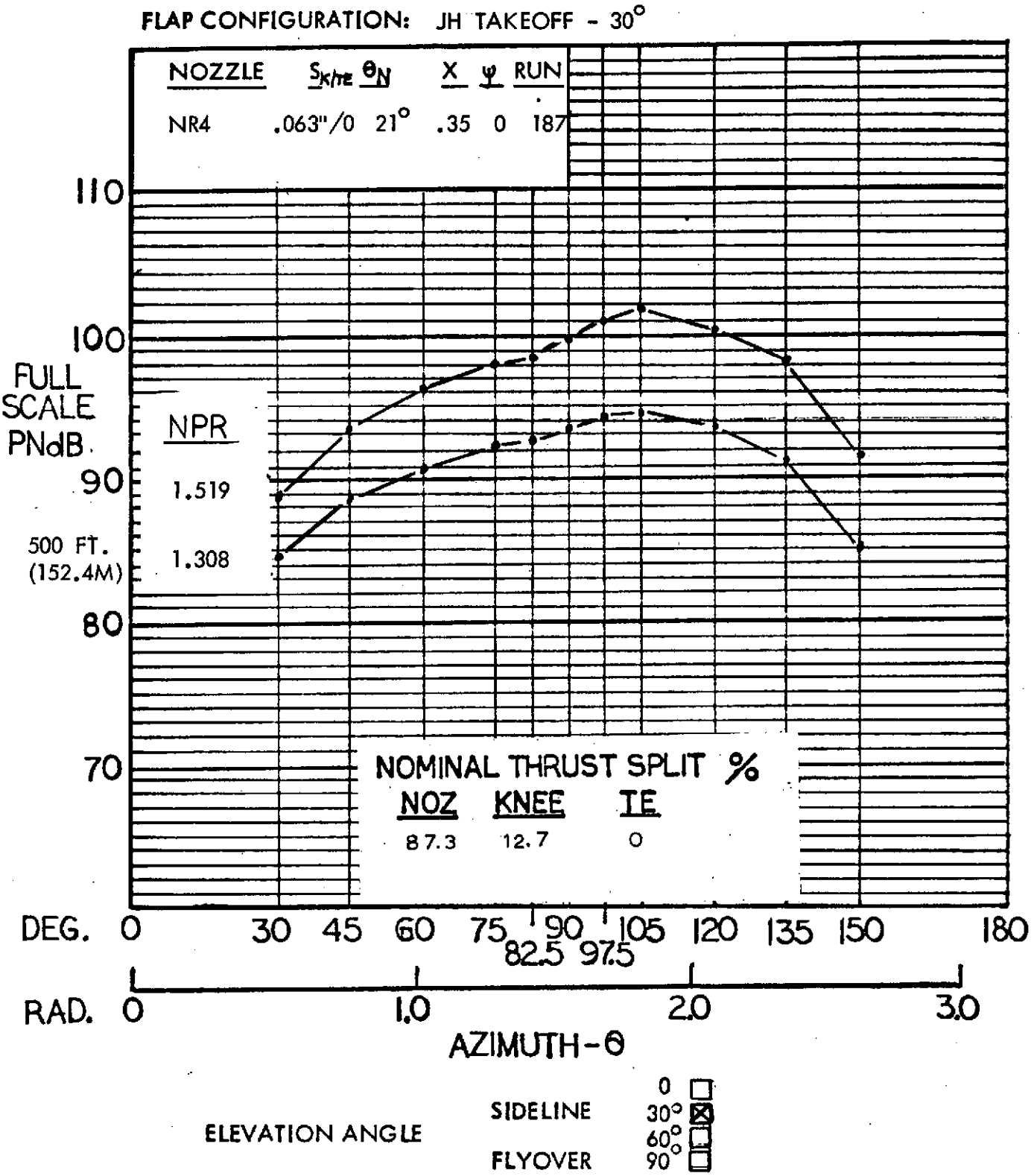

Figure 70 Full scale sideline PNL for the aspect ratio 4 nozzle and JH flap with knee blowing; 30° flap angle.

HYBRID PROPULSIVE LIFT
ACOUSTIC TEST
NAS 2-7812

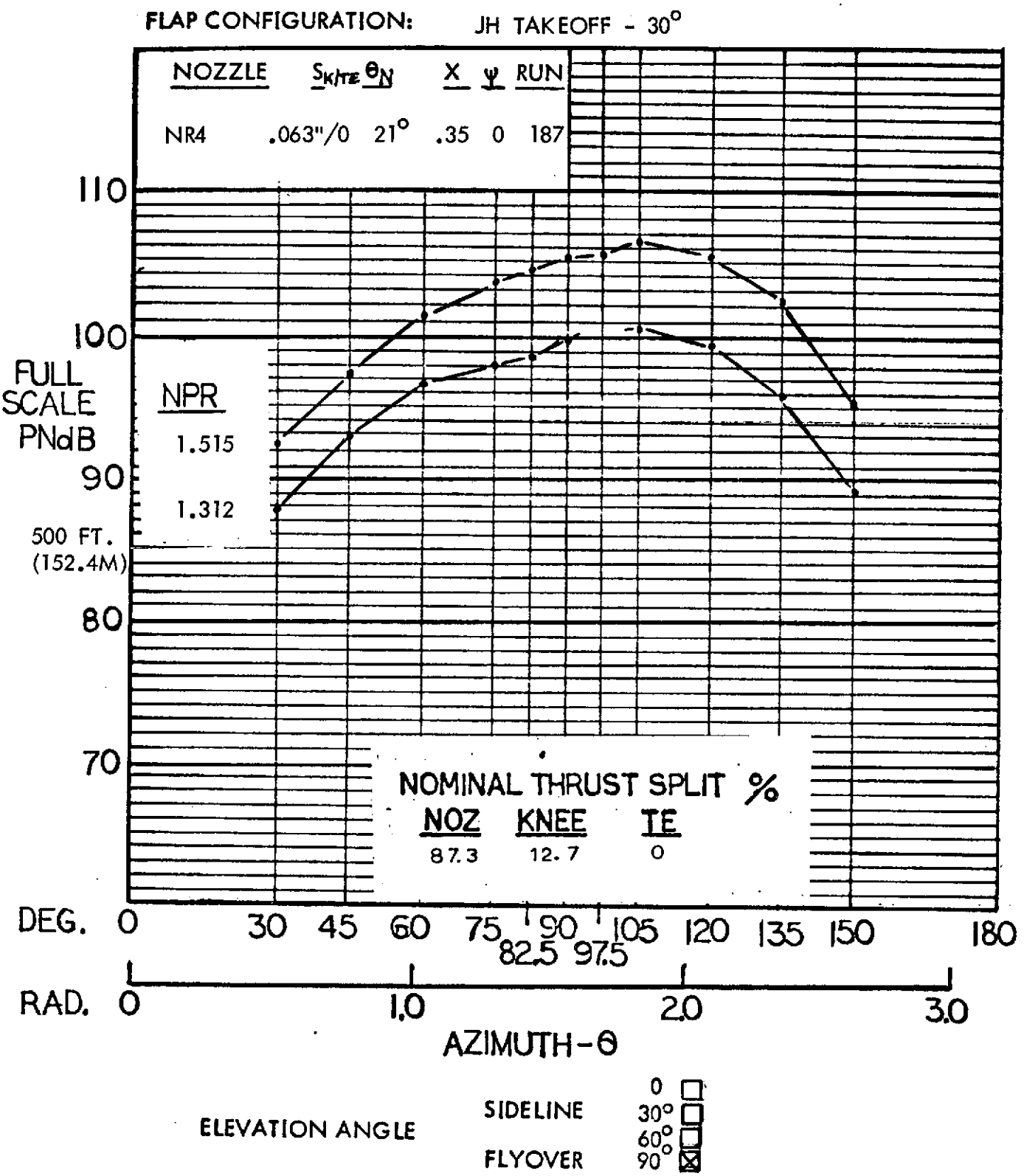

Figure 71 Full scale flyover PNL for the aspect ratio 4 nozzle and JH flap with knee blowing; 30° flap angle.

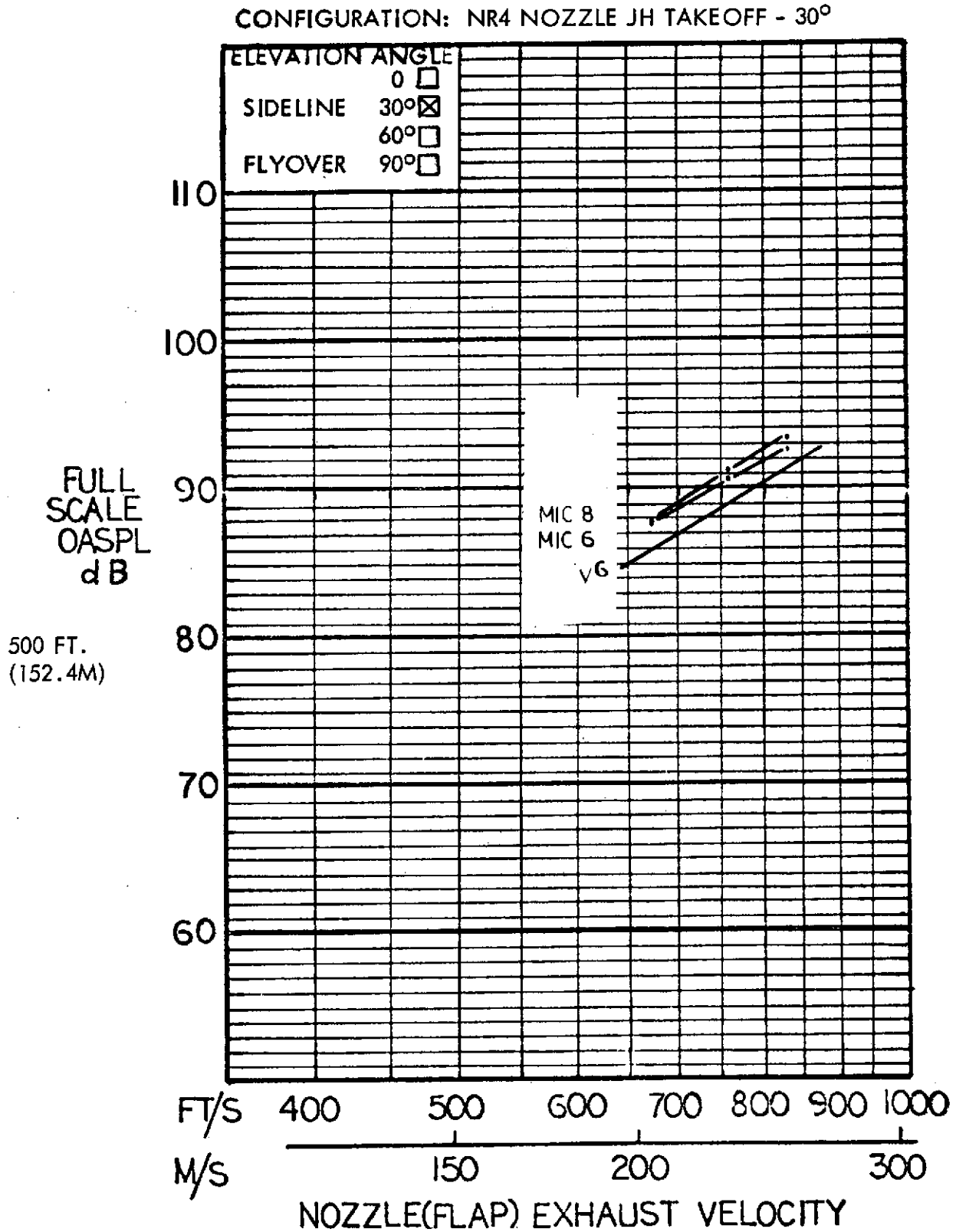

Figure 72 Full scale sideline OASPL at 90° and 105° azimuth for the aspect ratio 4 nozzle and JH flap with knee blowing; 30° flap angle.

HYBRID PROPULSIVE LIFT ACOUSTIC TEST

NAS 2-7812

RUN NO: 187

CONFIGURATION: NR4 NOZZLE, JH TAKEOFF - 30°

MIC NO: 6, 8 ($\theta = 90°, 105°$)

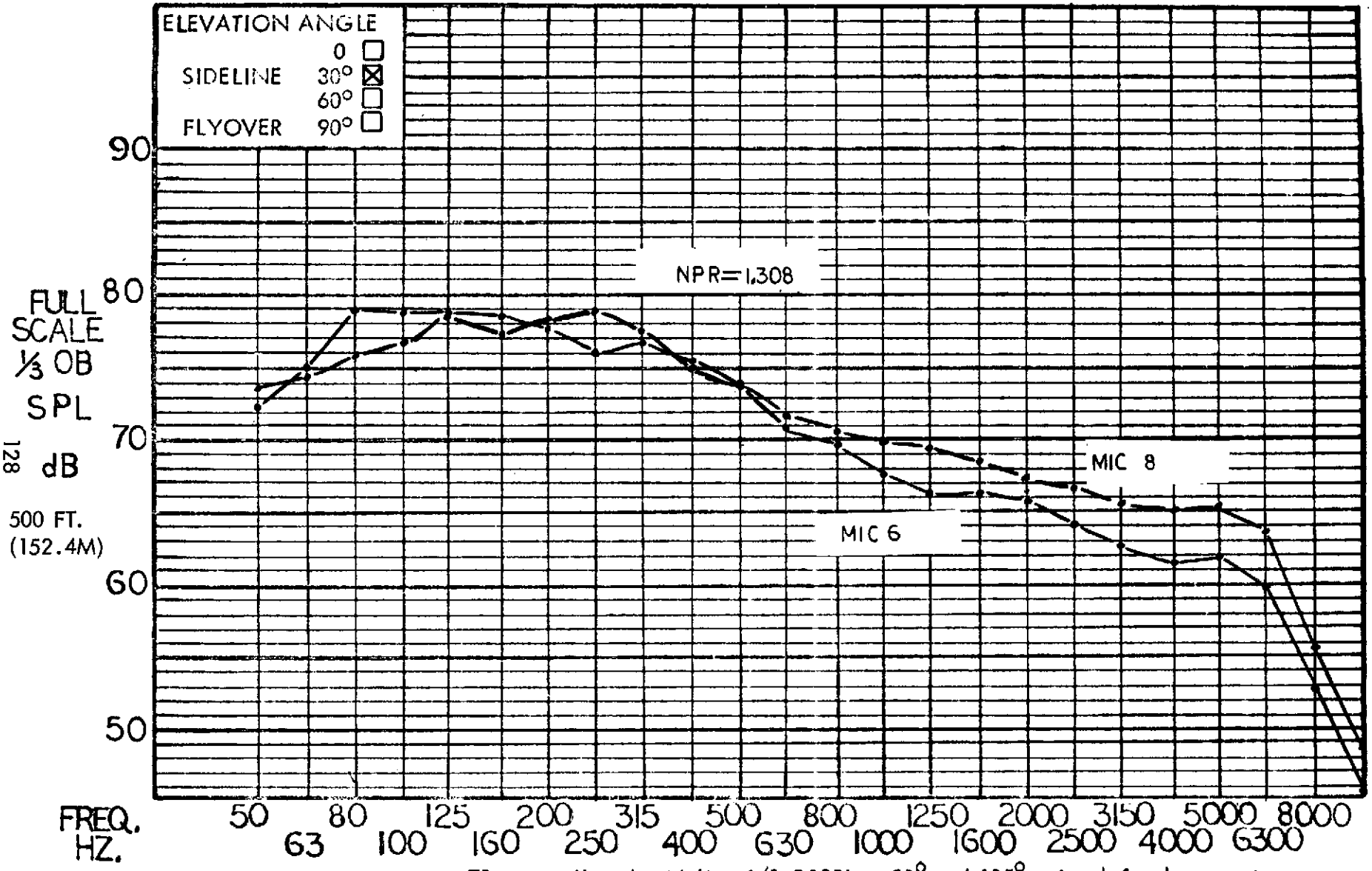

Figure 73 Full scale sideline 1/3 OBSPL at 90° and 105° azimuth for the aspect ratio 4 nozzle and JH flap with knee blowing; 30° flap angle.

HYBRID PROPULSIVE LIFT
ACOUSTIC TEST
NAS 2-7812

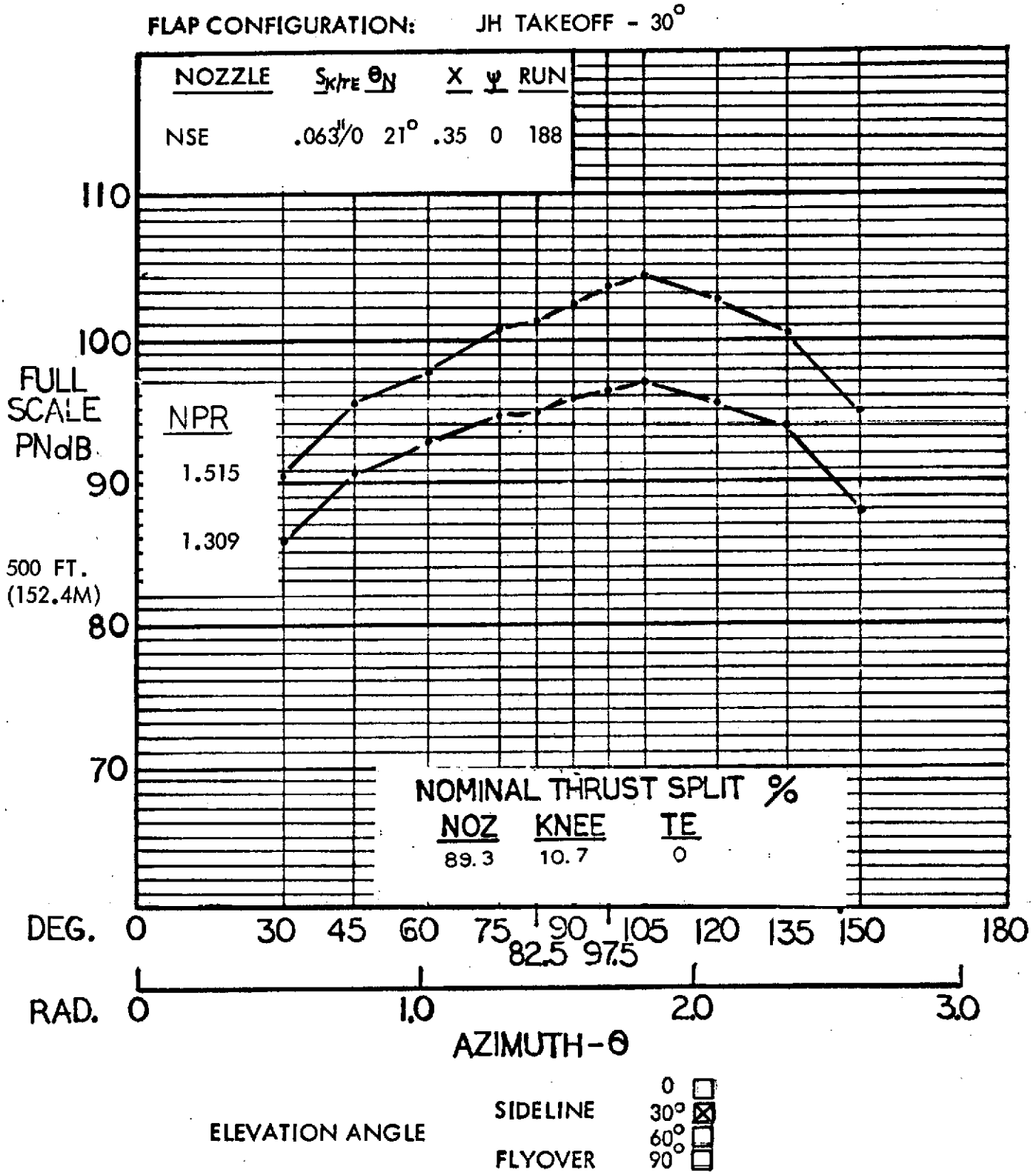

Figure 74 Full scale sideline PNL for the simulated engine nozzle and JH flap with knee blowing; 30° flap angle.

HYBRID PROPULSIVE LIFT
ACOUSTIC TEST
NAS 2-7812

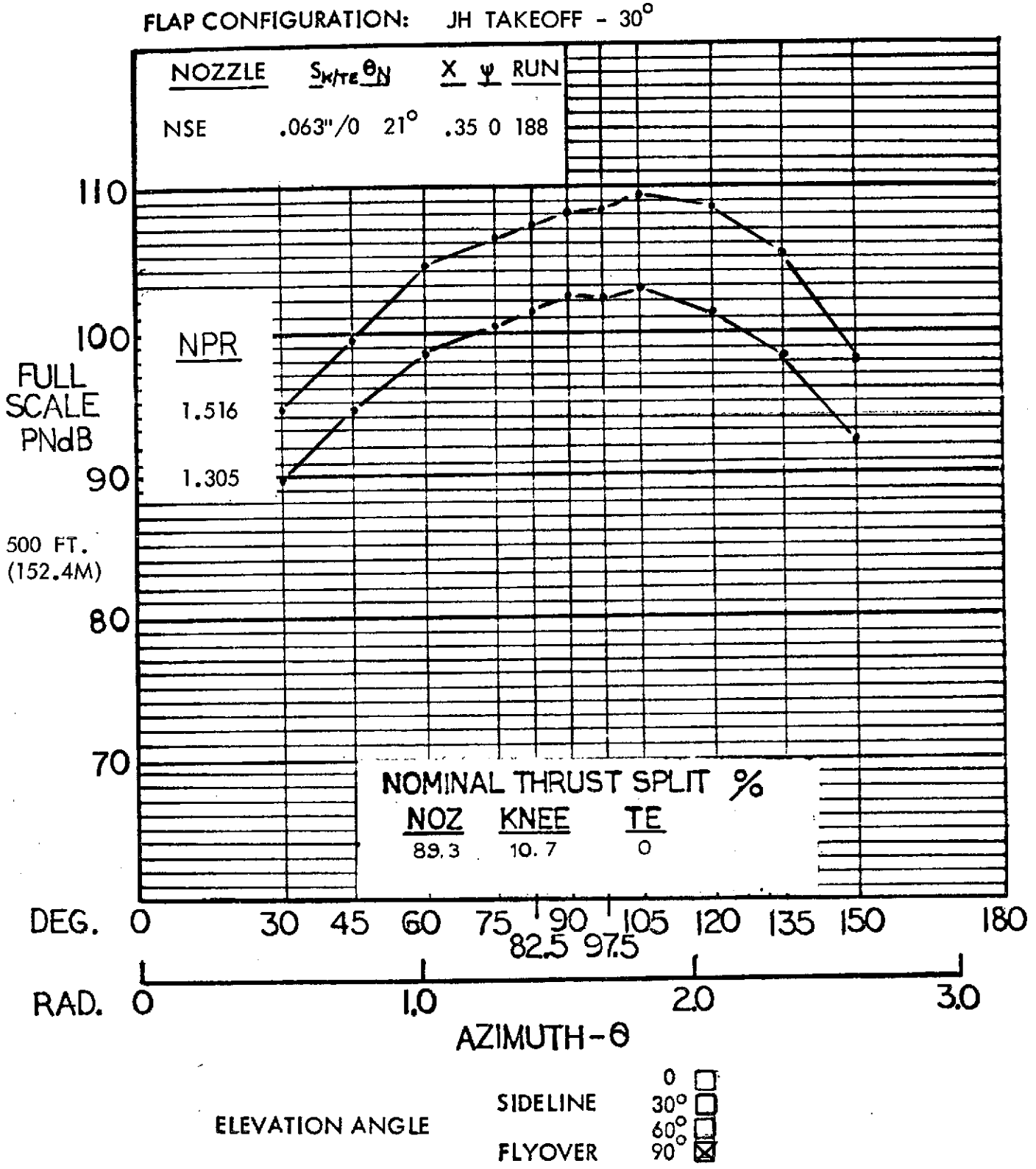

Figure 75 Full scale flyover PNL for the simulated engine nozzle and JH flap with knee blowing; 30° flap angle.

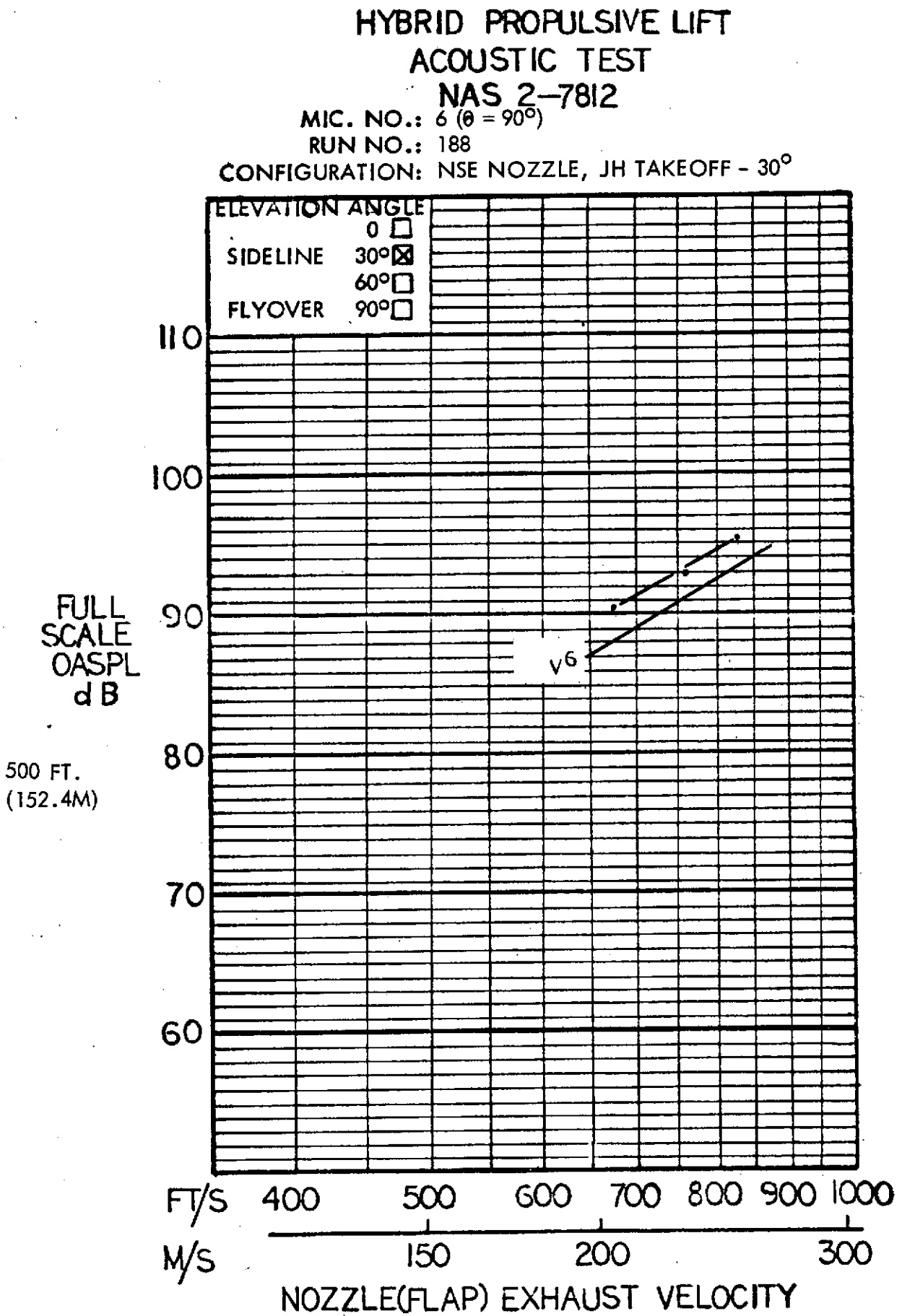

Figure 76 Full scale sideline OASPL at 90° azimuth for the simulated engine nozzle and JH flap with knee blowing; 30° flap angle.

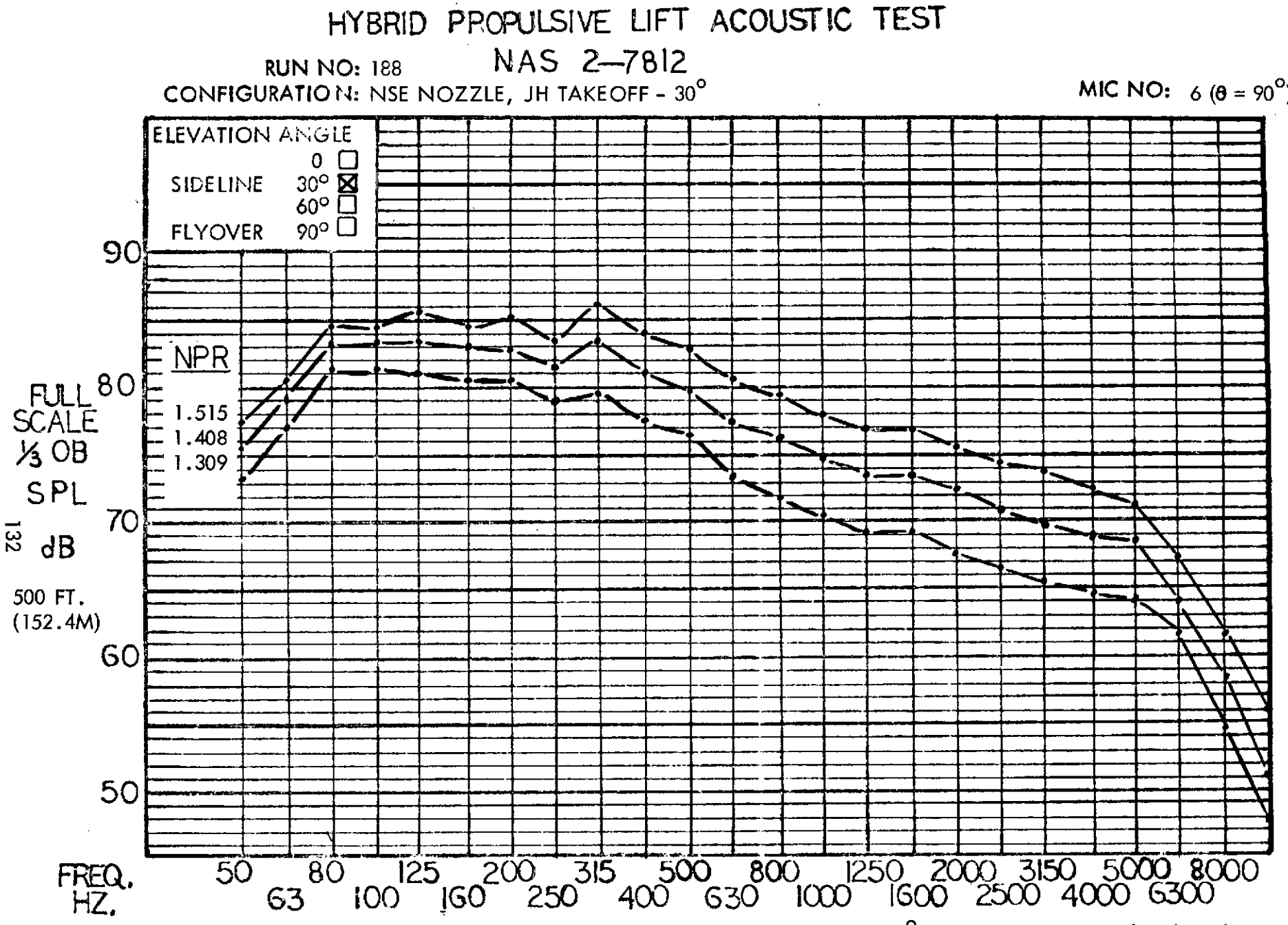

Figure 77 Full scale sideline 1/3 OBSPL at 90° azimuth for the simulated engine nozzle and JH flap with knee blowing; 30° flap angle.

HYBRID PROPULSIVE LIFT
ACOUSTIC TEST
NAS 2-7812

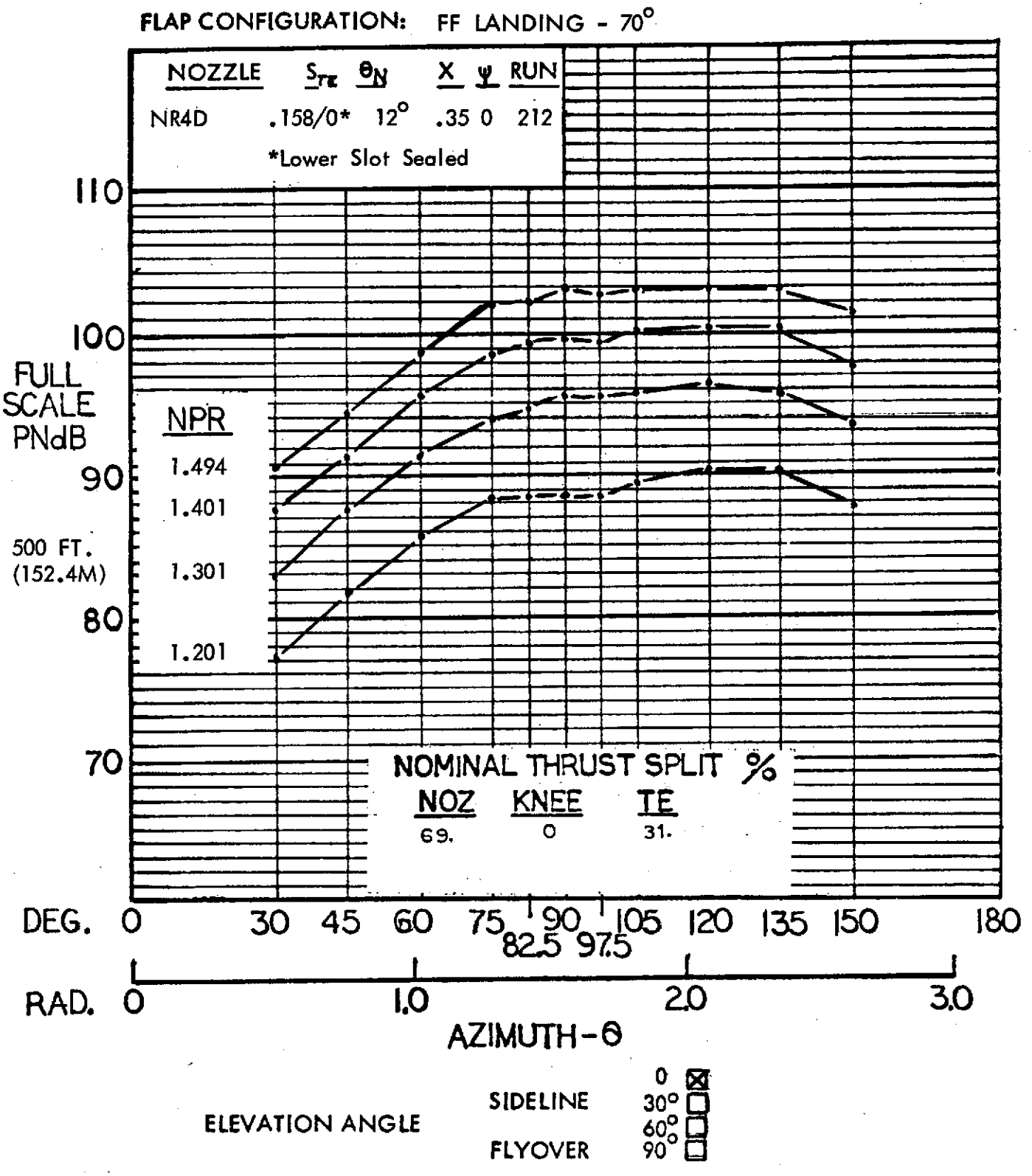

Figure 78 Full scale sideline PNL for the aspect ratio 4 nozzle with deflector and Flex Flap with upper TE blowing; 70° flap angle.

HYBRID PROPULSIVE LIFT
ACOUSTIC TEST
NAS 2-7812

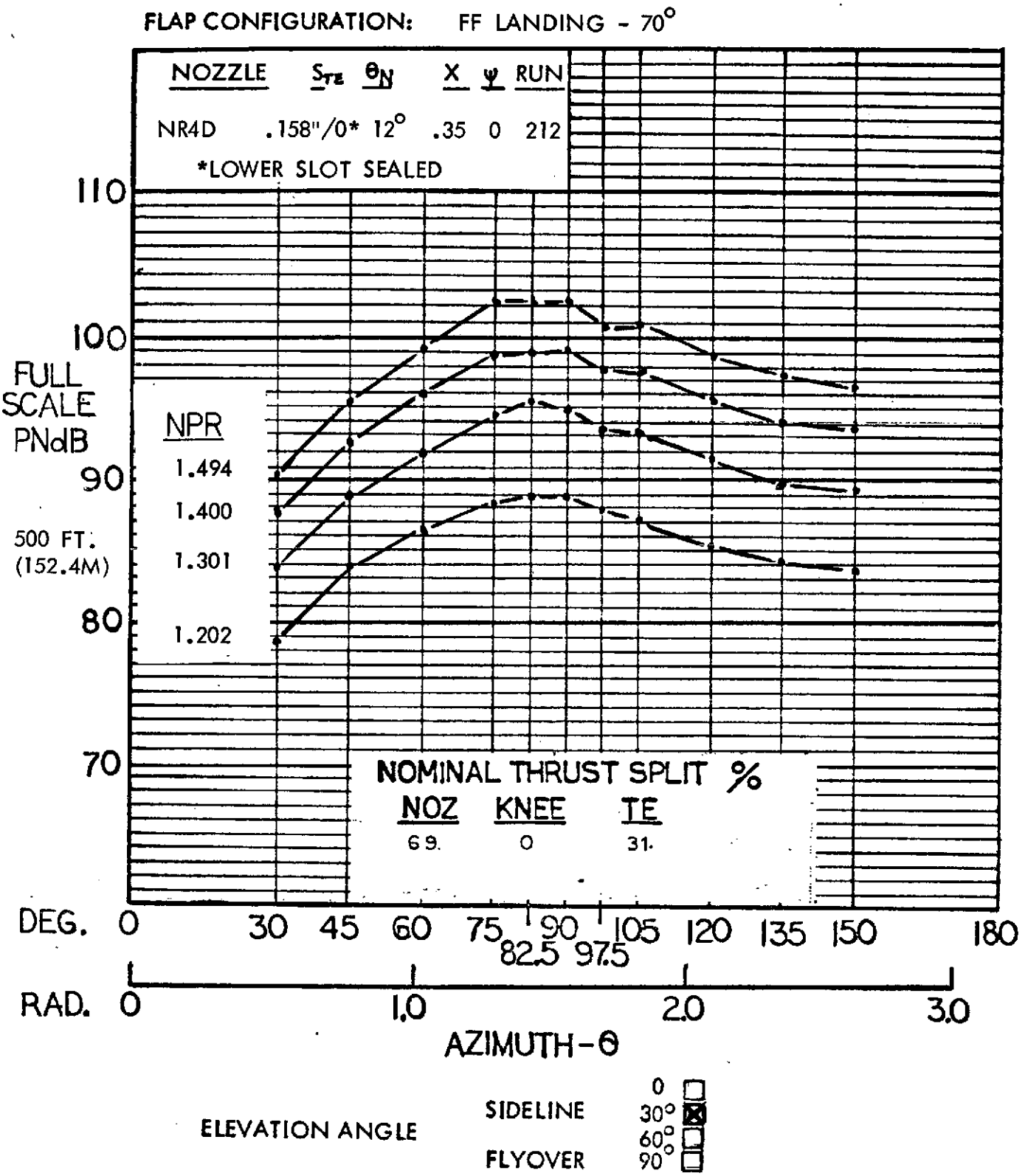

Figure 79 Full scale sideline PNL for the aspect ratio 4 nozzle with deflector and Flex Flap with upper TE blowing; 70° flap nozzle.

HYBRID PROPULSIVE LIFT
ACOUSTIC TEST
NAS 2-7812

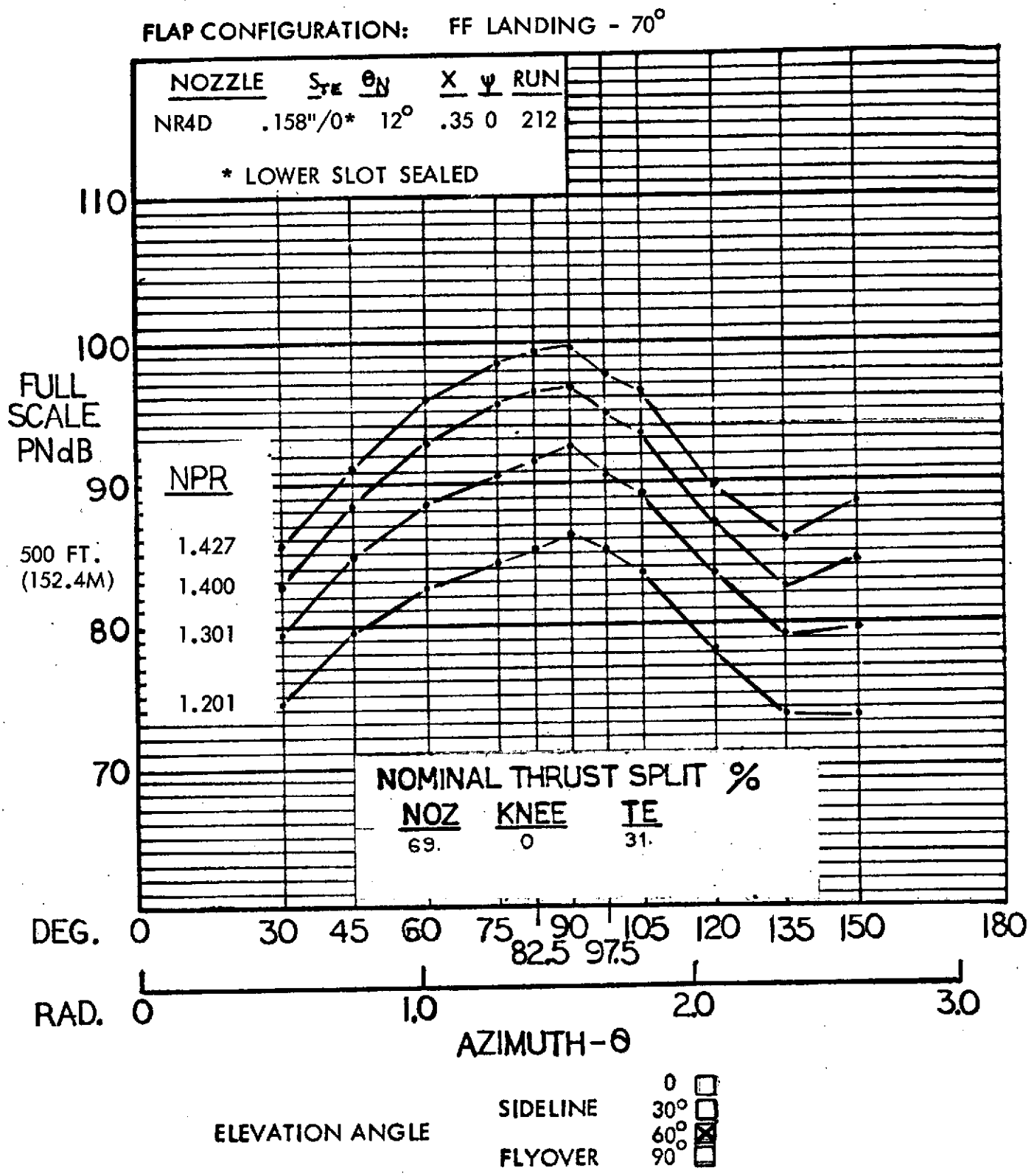

Figure 80 Full scale sideline PNL for the aspect ratio 4 nozzle with deflector and Flex Flap with upper TE blowing; 70° flap angle.

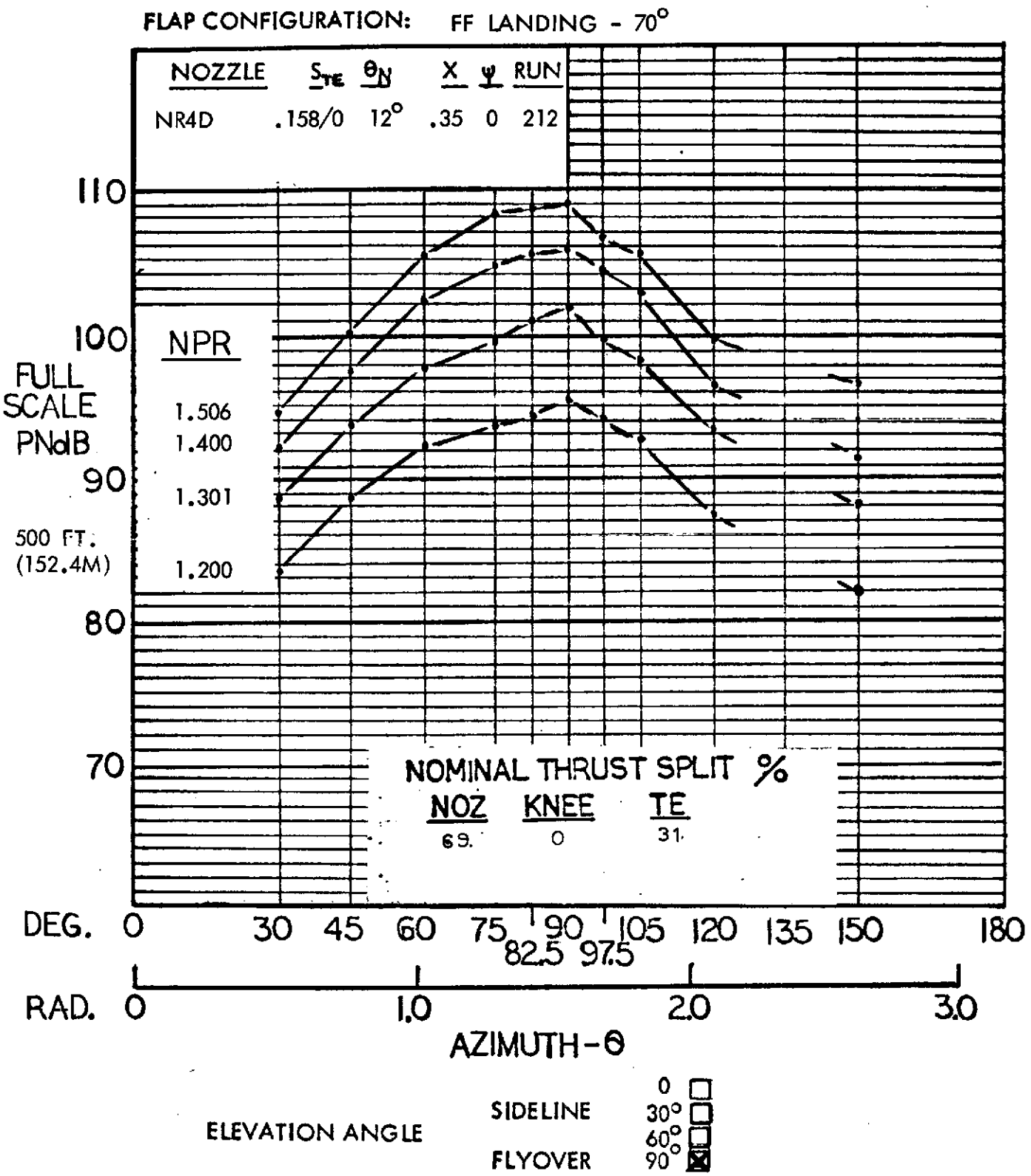

Figure 81 Full scale flyover PNL for the aspect ratio 4 nozzle with deflector and Flex Flap with upper TE blowing; 70° flap angle.

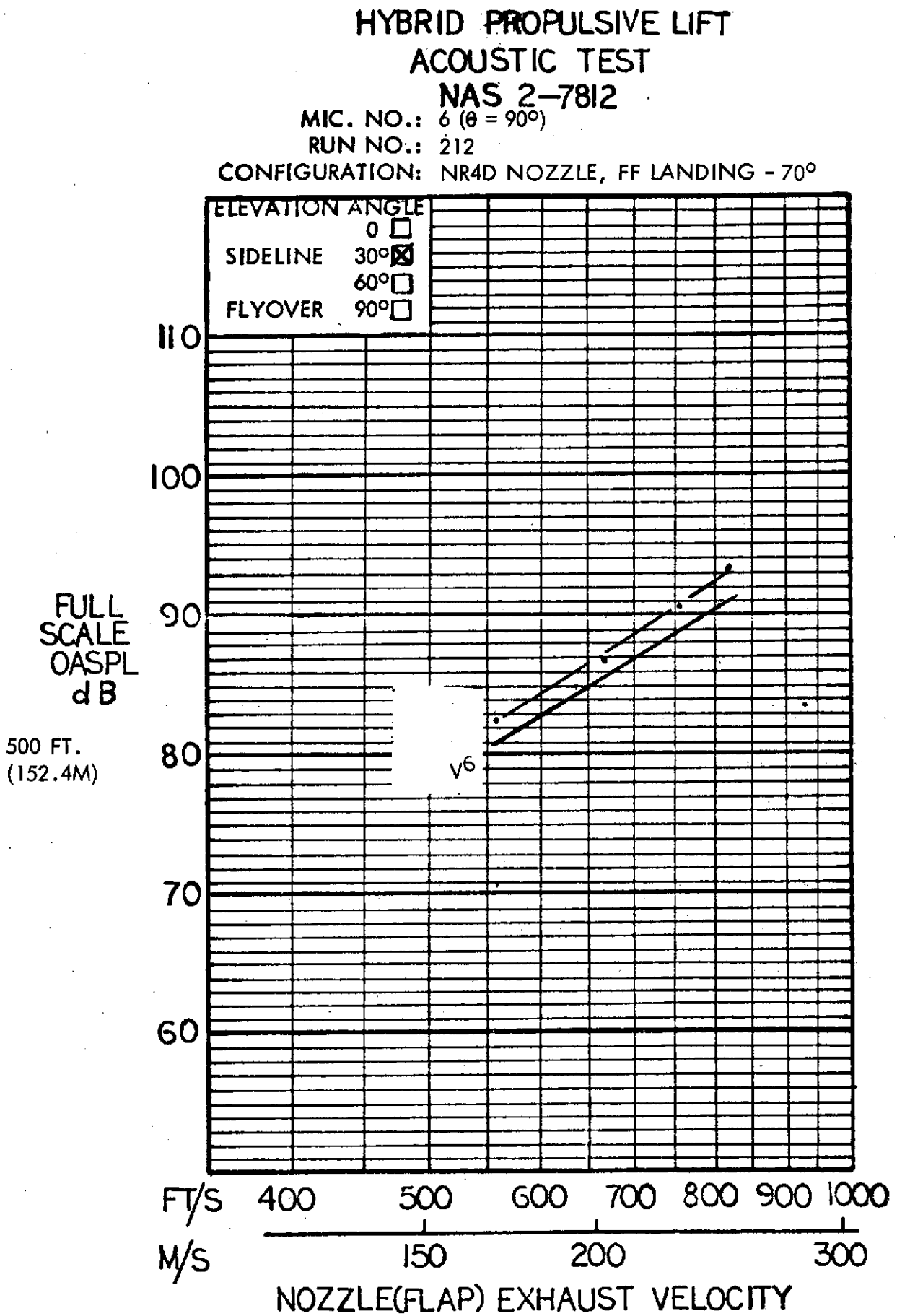

Figure 82 Full scale sideline OASPL at 90° azimuth for the aspect ratio 4 nozzle with deflector and Flex Flap with upper TE blowing; 70° flap angle.

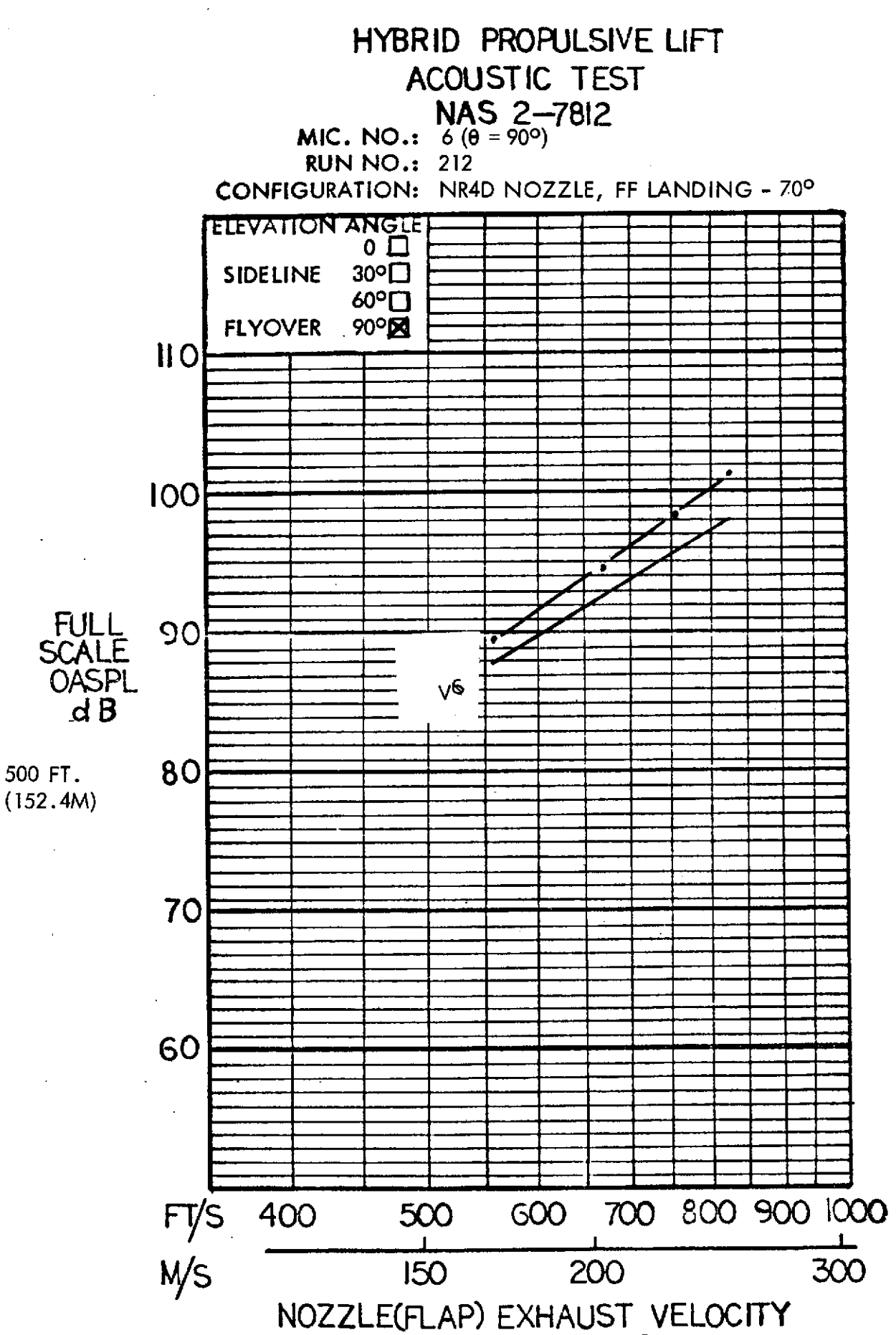

Figure 83 Full scale flyover OASPL at 90° azimuth for the aspect ratio 4 nozzle with deflector and Flex Flap with upper TE blowing; 70° flap angle.

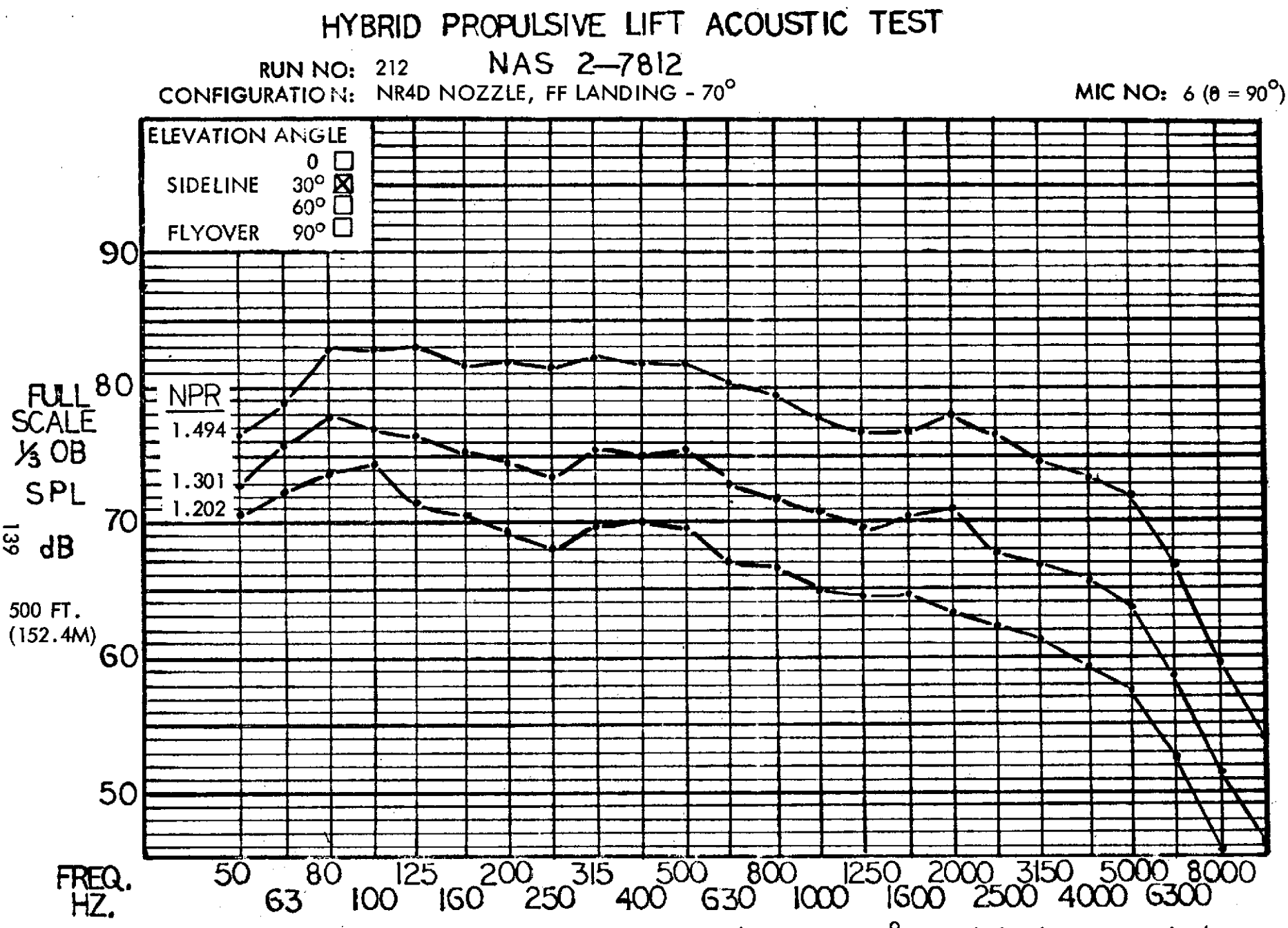

Figure 84 Full scale sideline 1/3 OBSPL at 90° azimuth for the aspect ratio 4 nozzle with deflector and Flex Flap with upper TE blowing; 70° flap angle.

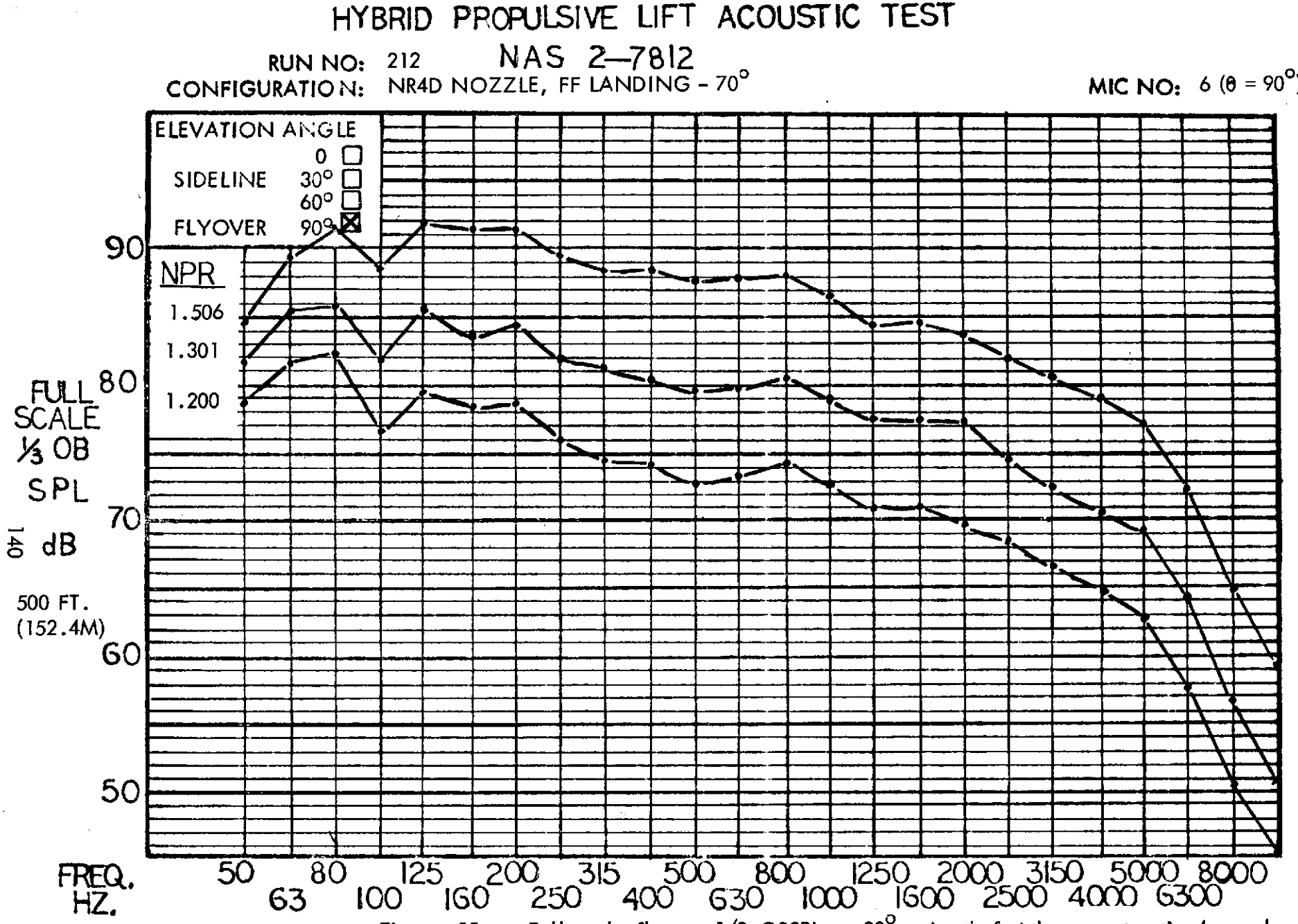

Figure 85 Full scale flyover 1/3 OBSPL at 90° azimuth for the aspect ratio 4 nozzle with deflector and Flex Flap with upper TE blowing; 70° flap angle

HYBRID PROPULSIVE LIFT
ACOUSTIC TEST
NAS 2-7812

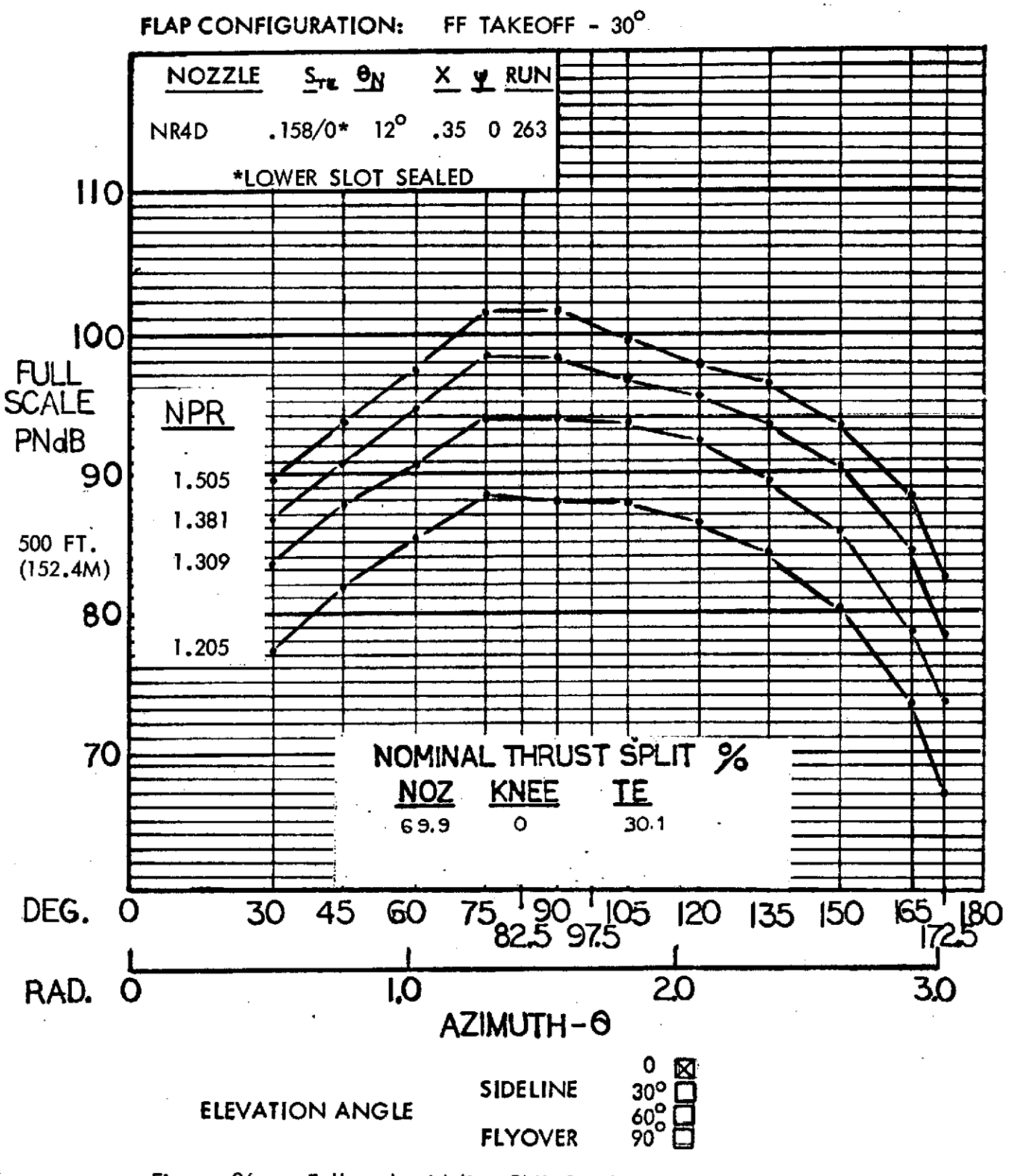

Figure 86 Full scale sideline PNL for the aspect ratio 4 nozzle with deflector and Flex Flap with upper TE blowing; 30° flap angle.

HYBRID PROPULSIVE LIFT
ACOUSTIC TEST
NAS 2-7812

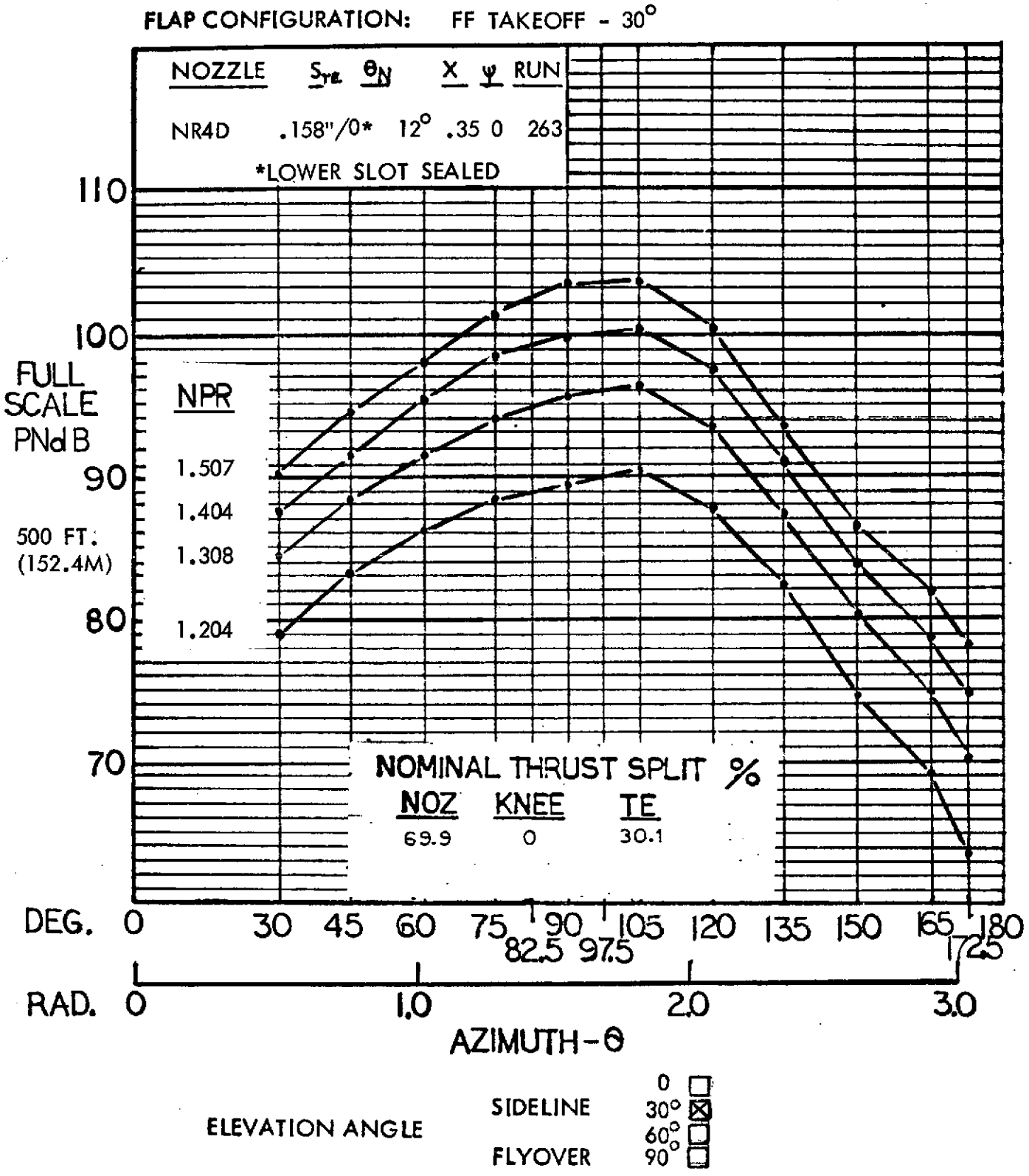

Figure 87 Full scale sideline PNL for the aspect ratio 4 nozzle with deflector and Flex Flap with upper TE blowing; 30° flap angle.

HYBRID PROPULSIVE LIFT
ACOUSTIC TEST
NAS 2-7812

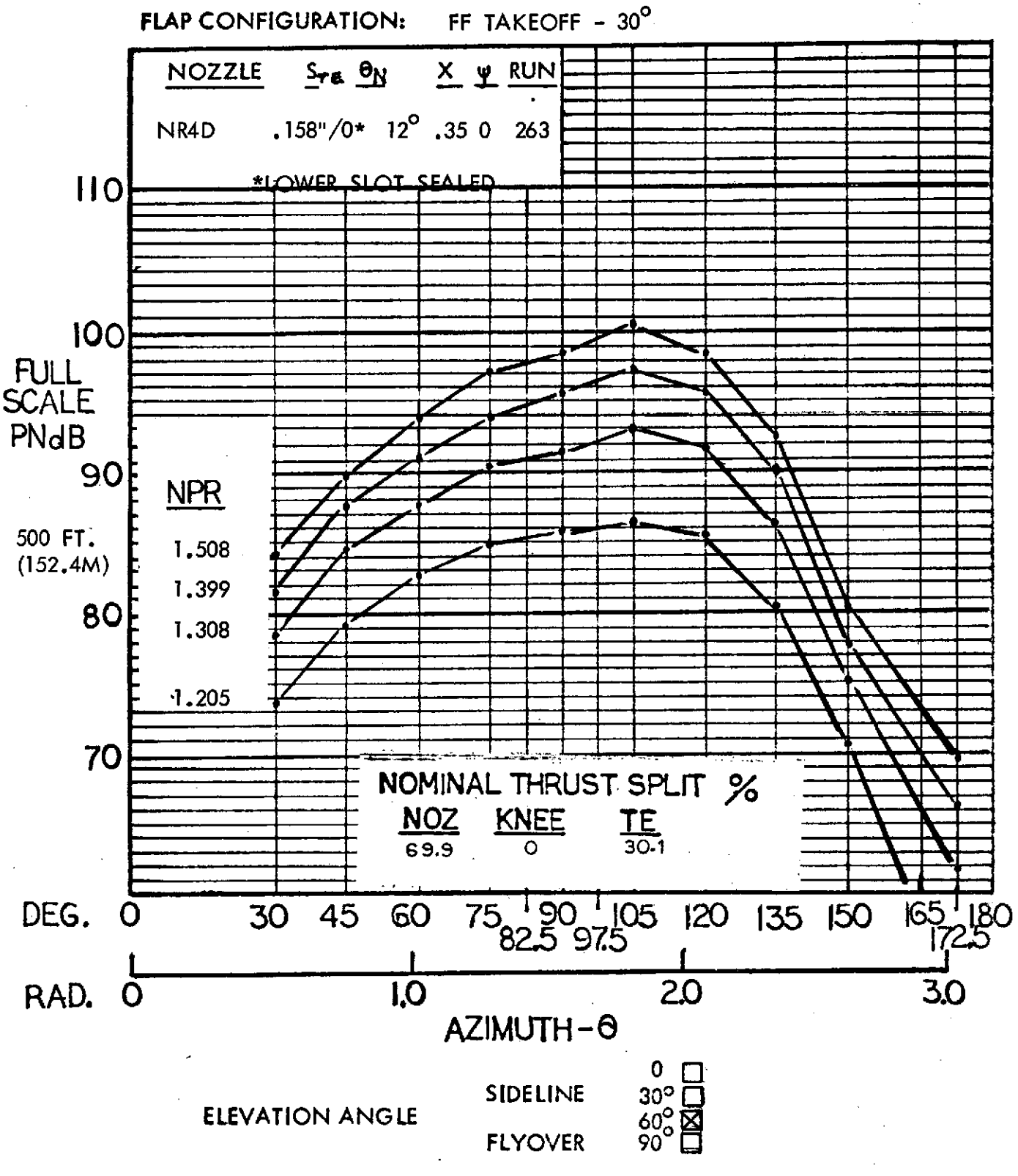

Figure 88 Full scale sideline PNL for the aspect ratio 4 nozzle with deflector and Flex Flap with upper TE blowing; 30° flap angle.

HYBRID PROPULSIVE LIFT
ACOUSTIC TEST
NAS 2-7812

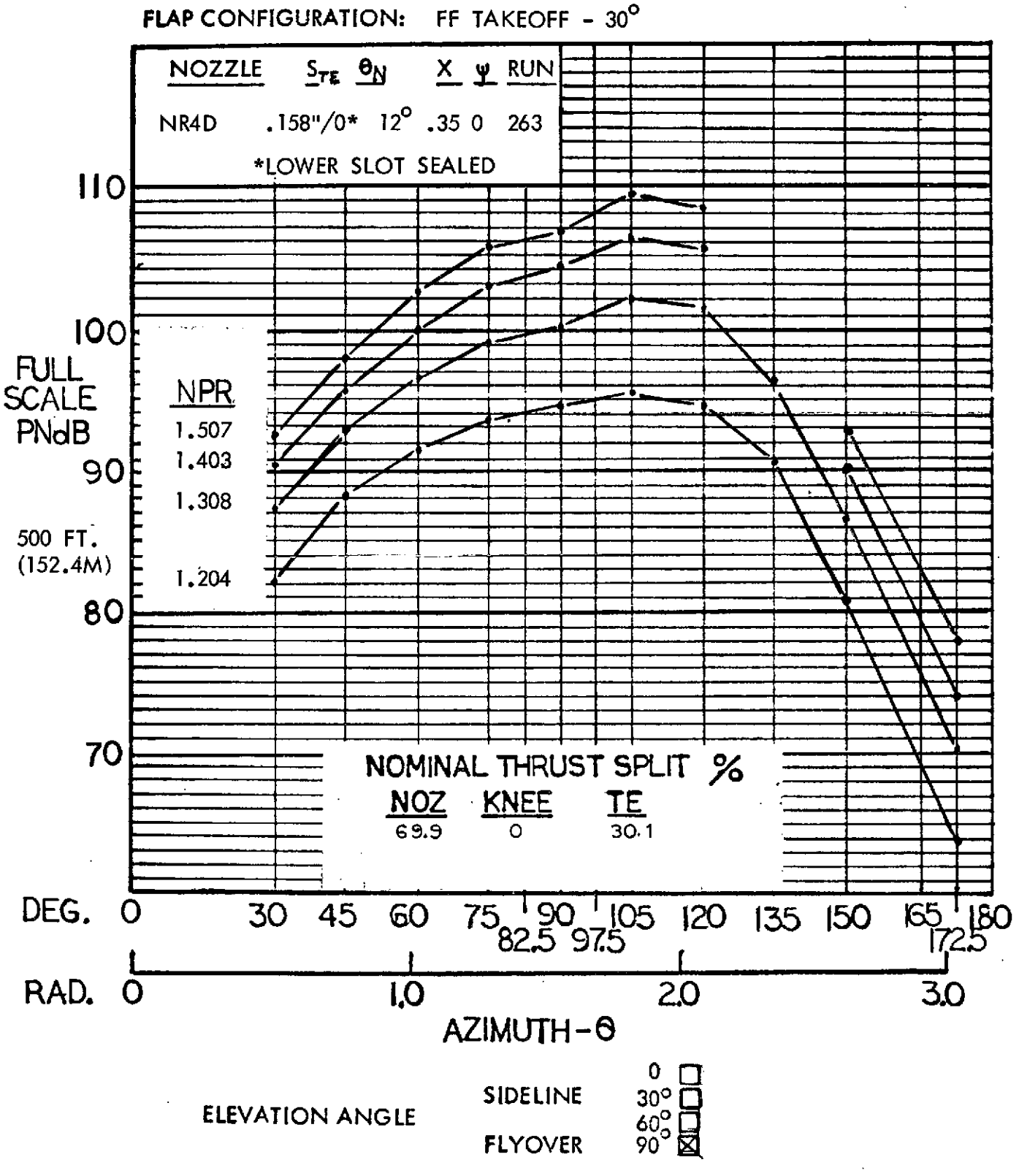

Figure 89 Full scale flyover PNL for the aspect ratio 4 nozzle with deflector and Flex Flap with upper TE blowing; 30° flap angle

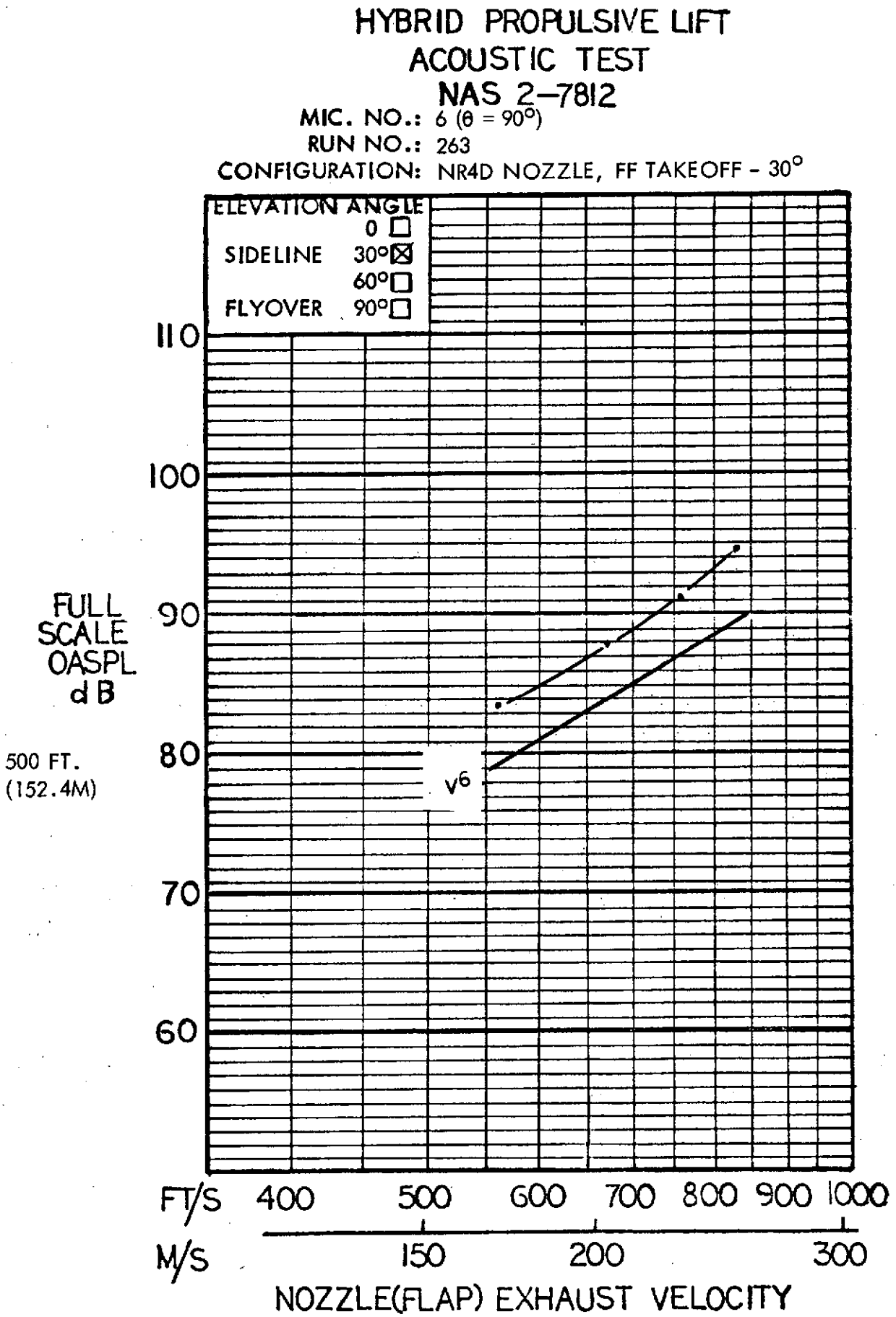

Figure 90 Full scale sideline OASPL at 90° azimuth for the aspect ratio 4 nozzle with deflector and Flex Flap with upper TE blowing; 30° flap angle.

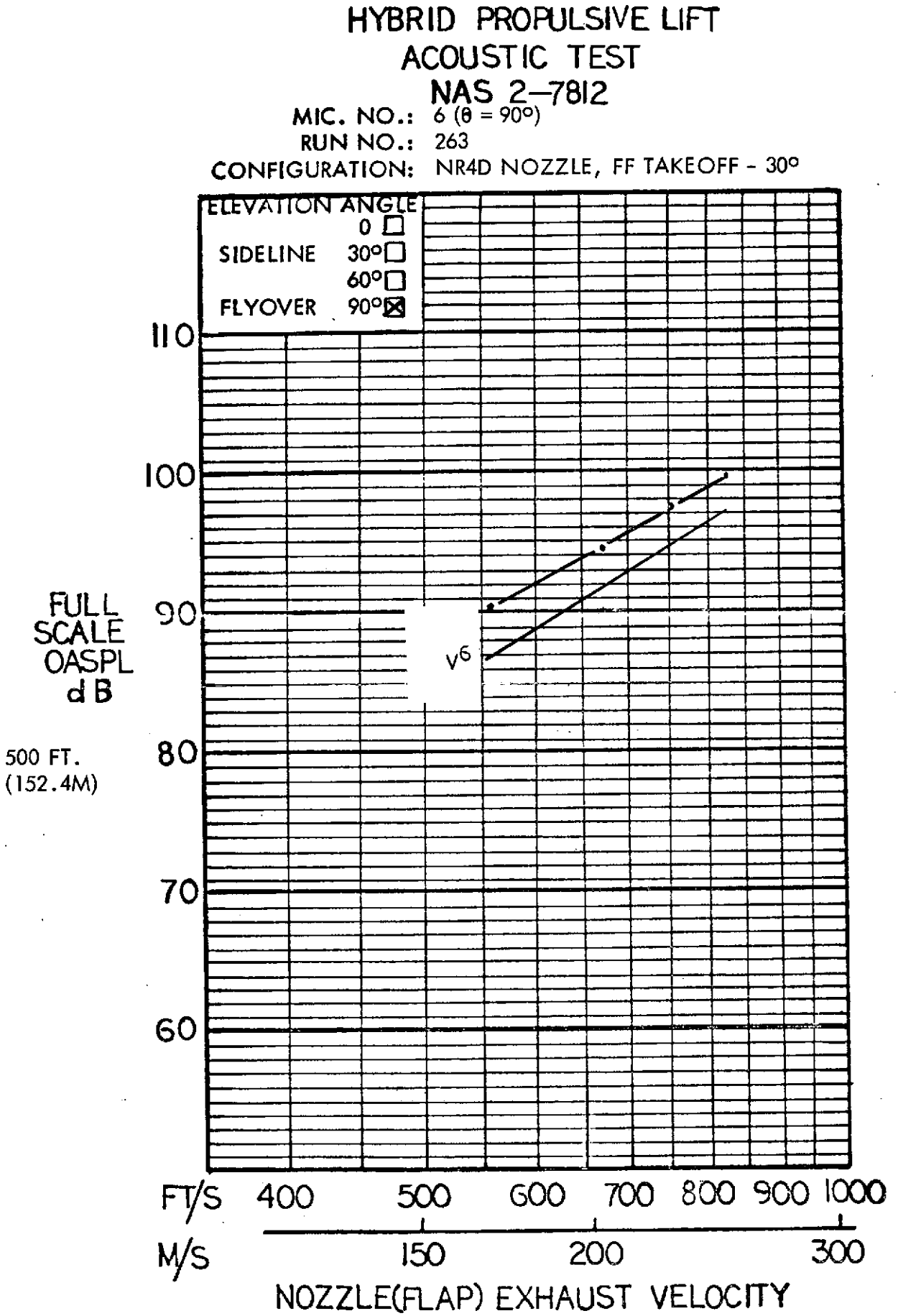

Figure 91 Full scale flyover OASPL at 90° azimuth for the aspect ratio 4 nozzle with deflector and Flex Flap with upper TE blowing; 30° flap angle.

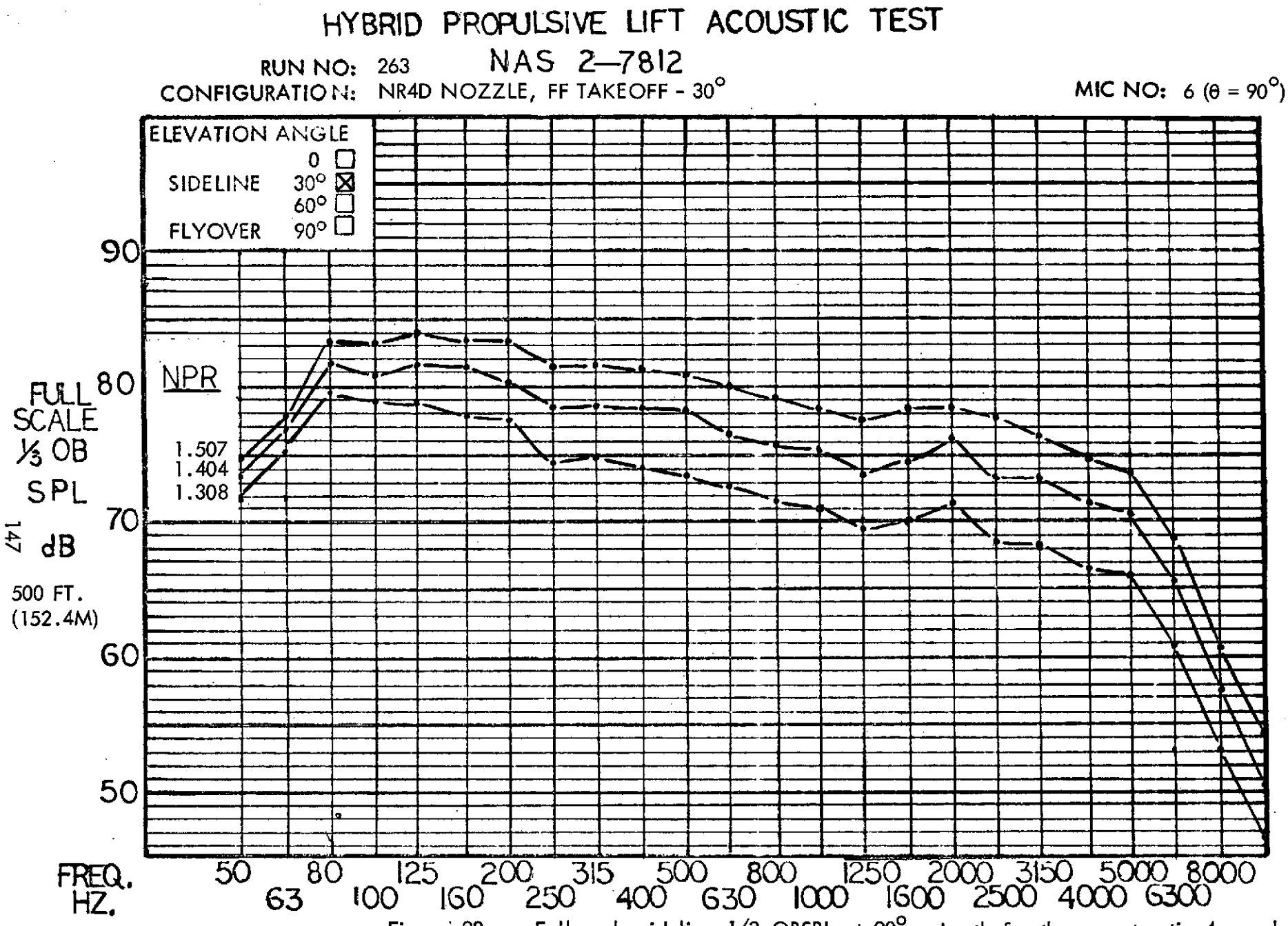

Figure 92 Full scale sideline 1/3 OBSPL at 90° azimuth for the aspect ratio 4 nozzle with deflector and Flex Flap with upper TE blowing; 30° flap angle.

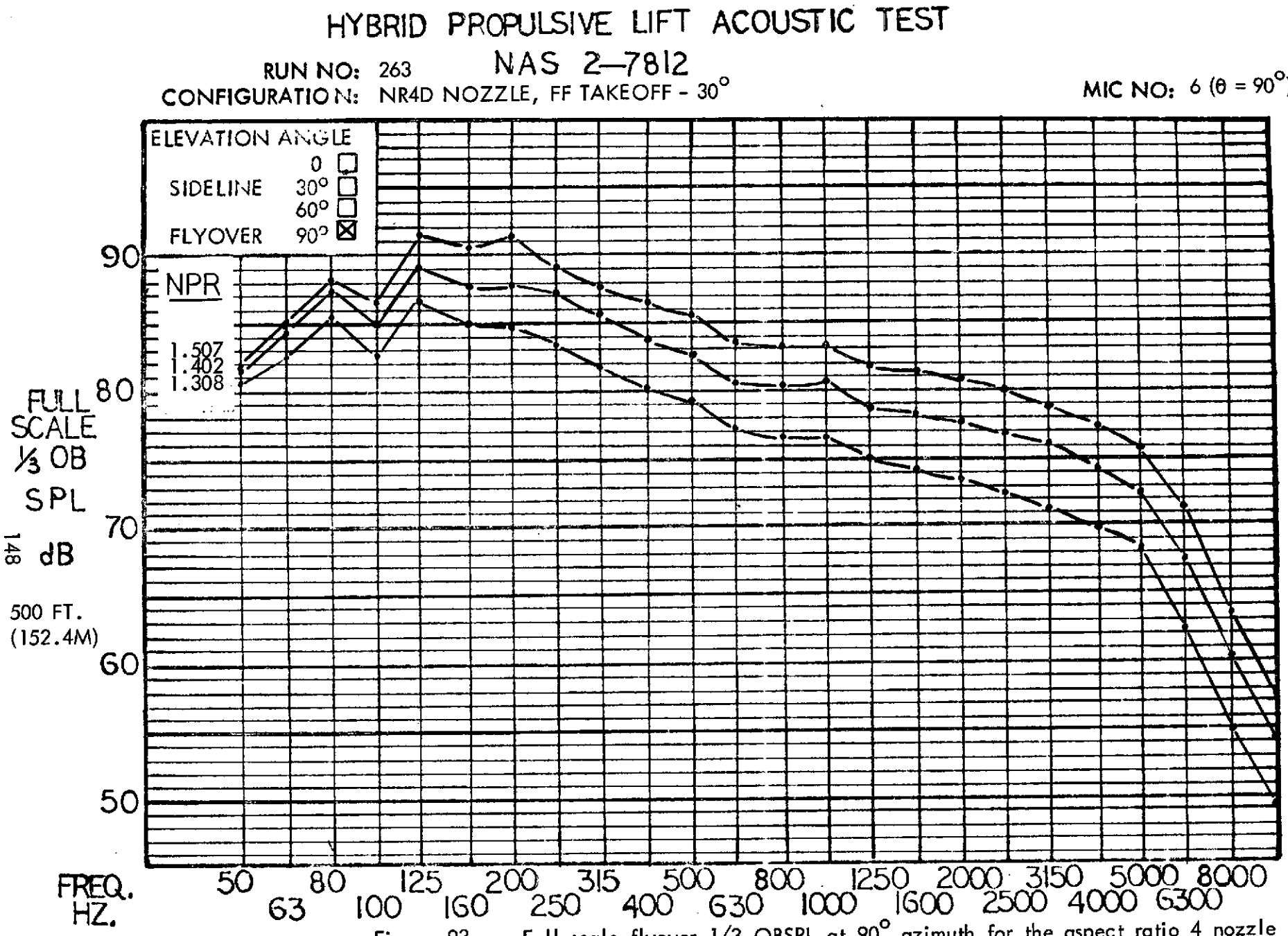

Figure 93 Full scale flyover 1/3 OBSPL at 90° azimuth for the aspect ratio 4 nozzle with deflector and Flex Flap with upper TE blowing; 30° flap angle.

HYBRID PROPULSIVE LIFT
ACOUSTIC TEST
NAS 2-7812

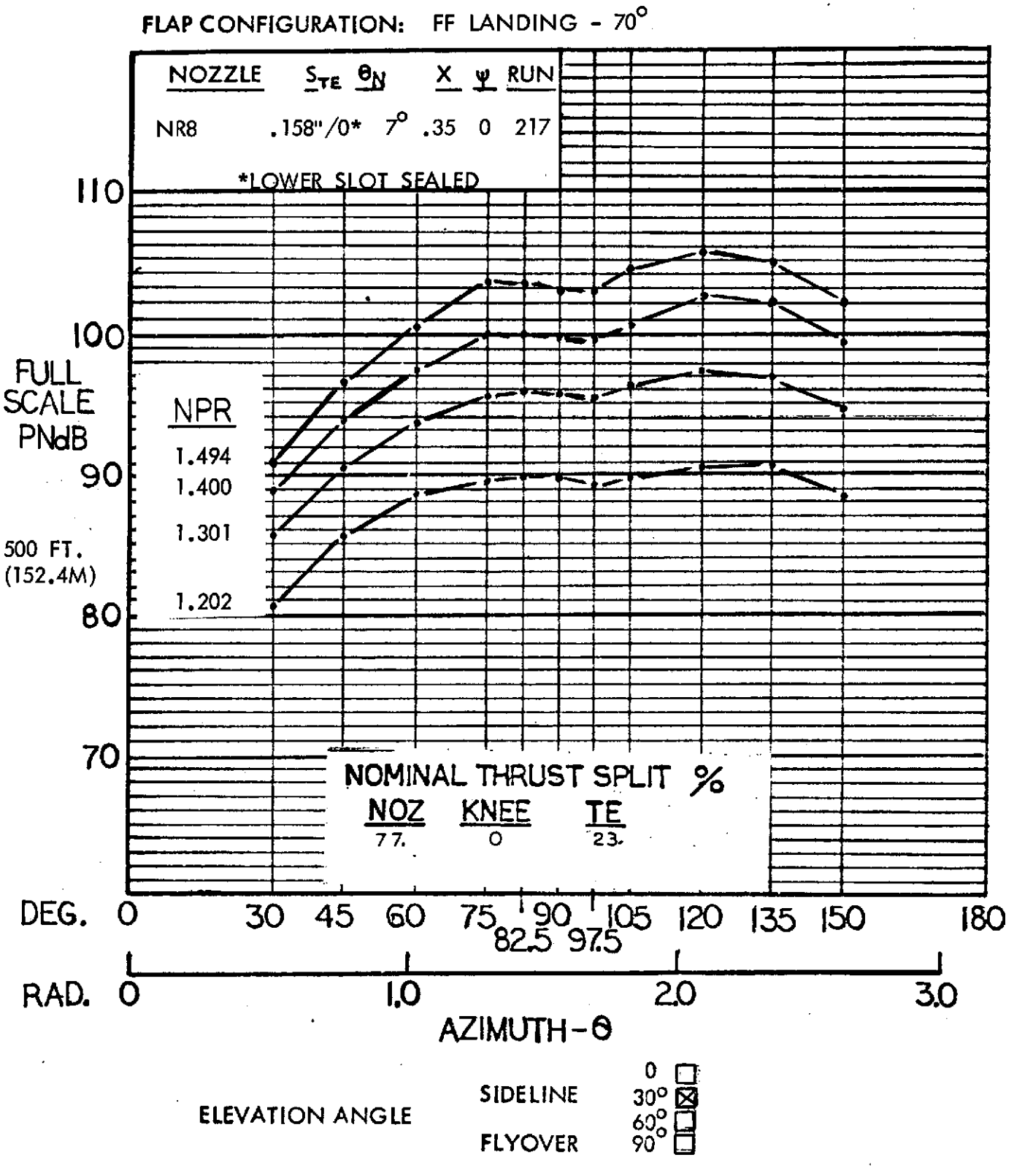

Figure 94 Full scale sideline PNL for the aspect ratio 8 nozzle and Flex Flap with upper TE blowing; 70° flap angle.

HYBRID PROPULSIVE LIFT
ACOUSTIC TEST
NAS 2-7812

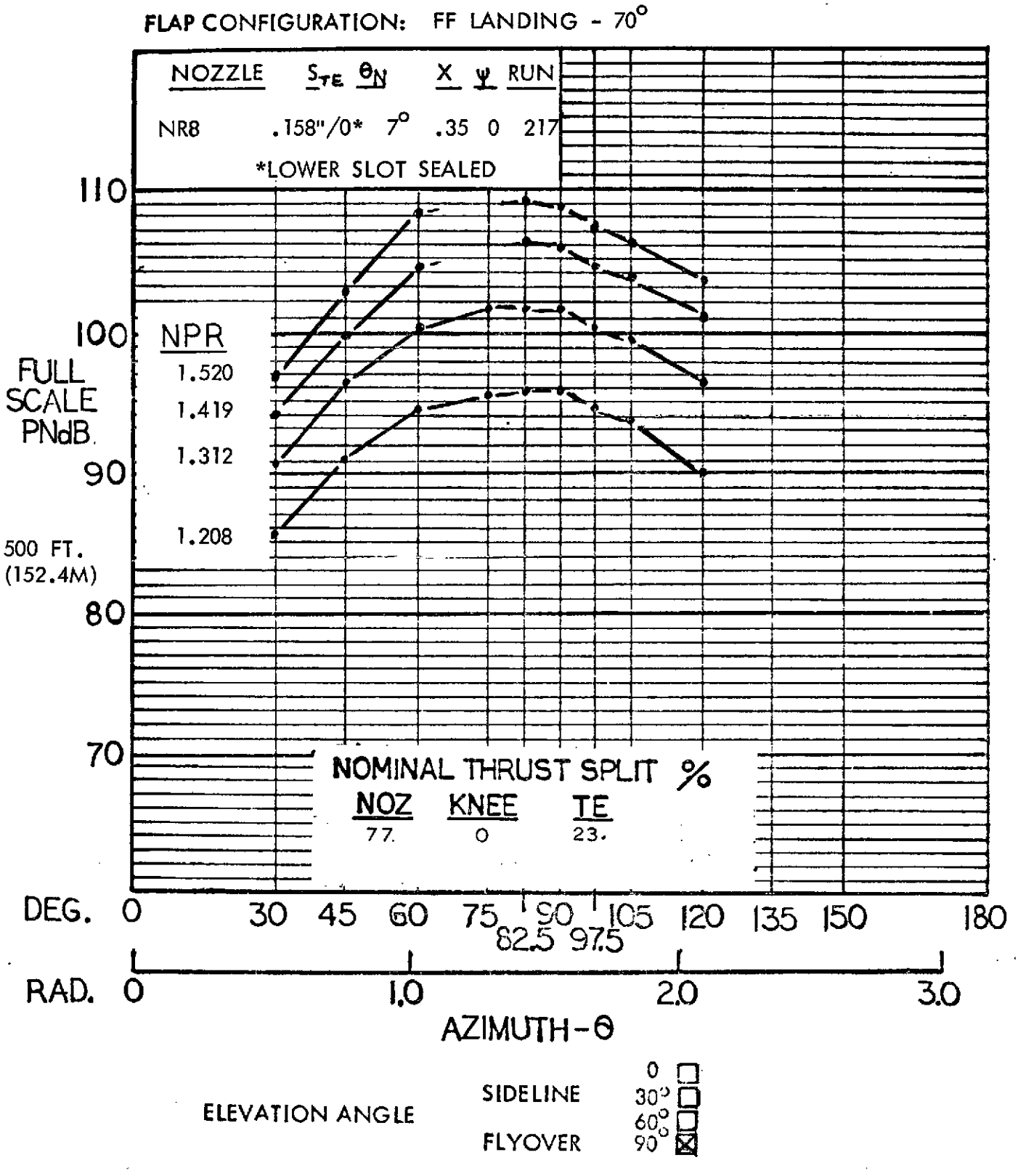

Figure 95 Full scale flyover PNL for the aspect ratio 8 nozzle and Flex Flap with upper TE blowing; 70° flap angle.

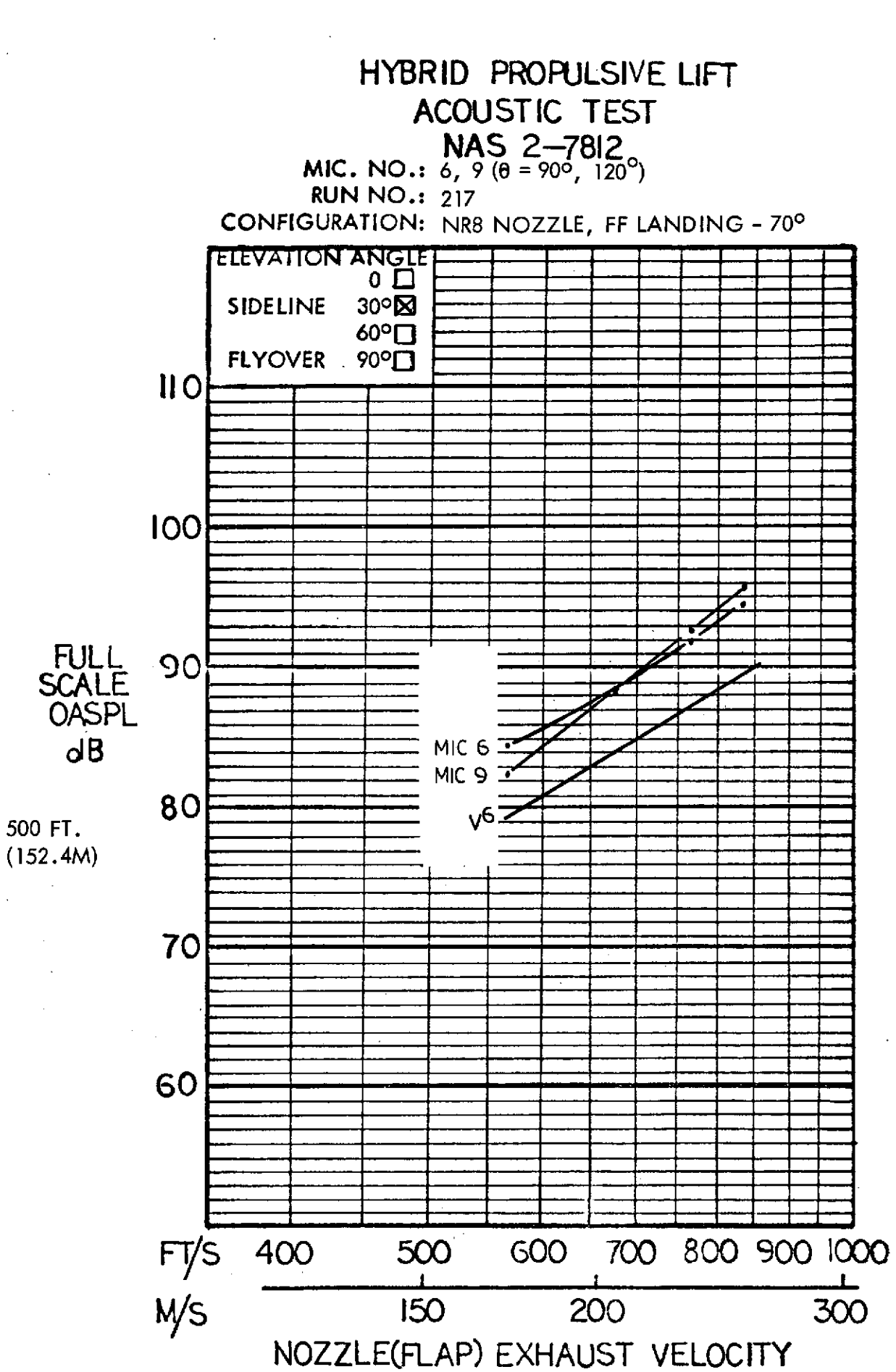

Figure 96 Full scale sideline OASPL at 90° and 120° azimuth for the aspect ratio 8 nozzle and flex flap with upper TE blowing; 70° flap angle.

HYBRID PROPULSIVE LIFT ACOUSTIC TEST

NAS 2—7812

RUN NO: 217

CONFIGURATION: NR8 NOZZLE, FF LANDING - 70°

MIC NO: 6, 9 (θ = 90°, 120°)

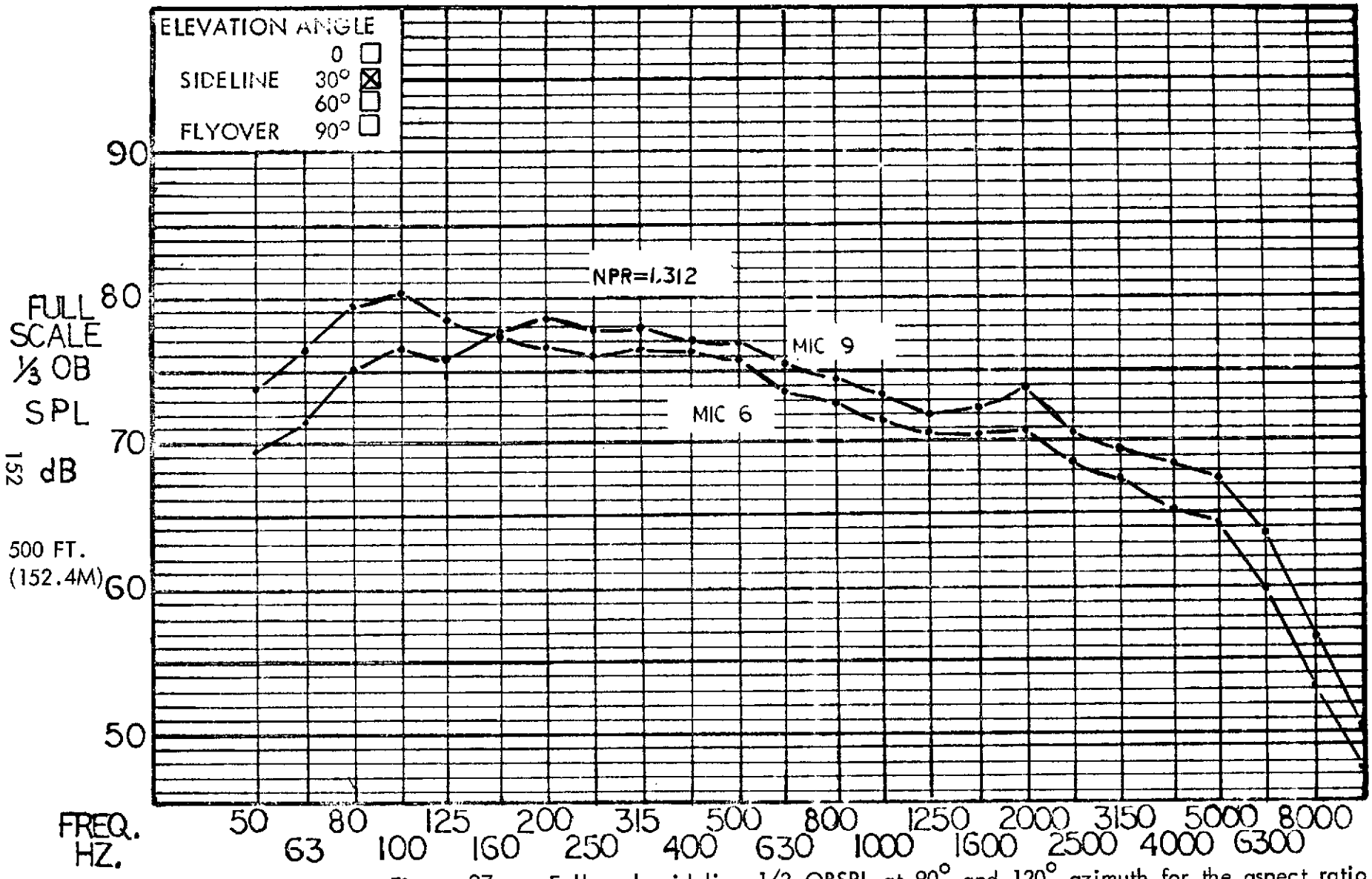

Figure 97 Full scale sideline 1/3 OBSPL at 90° and 120° azimuth for the aspect ratio 8 nozzle and Flex Flap with upper TE blowing; 70° flap angle.

HYBRID PROPULSIVE LIFT
ACOUSTIC TEST
NAS 2-7812

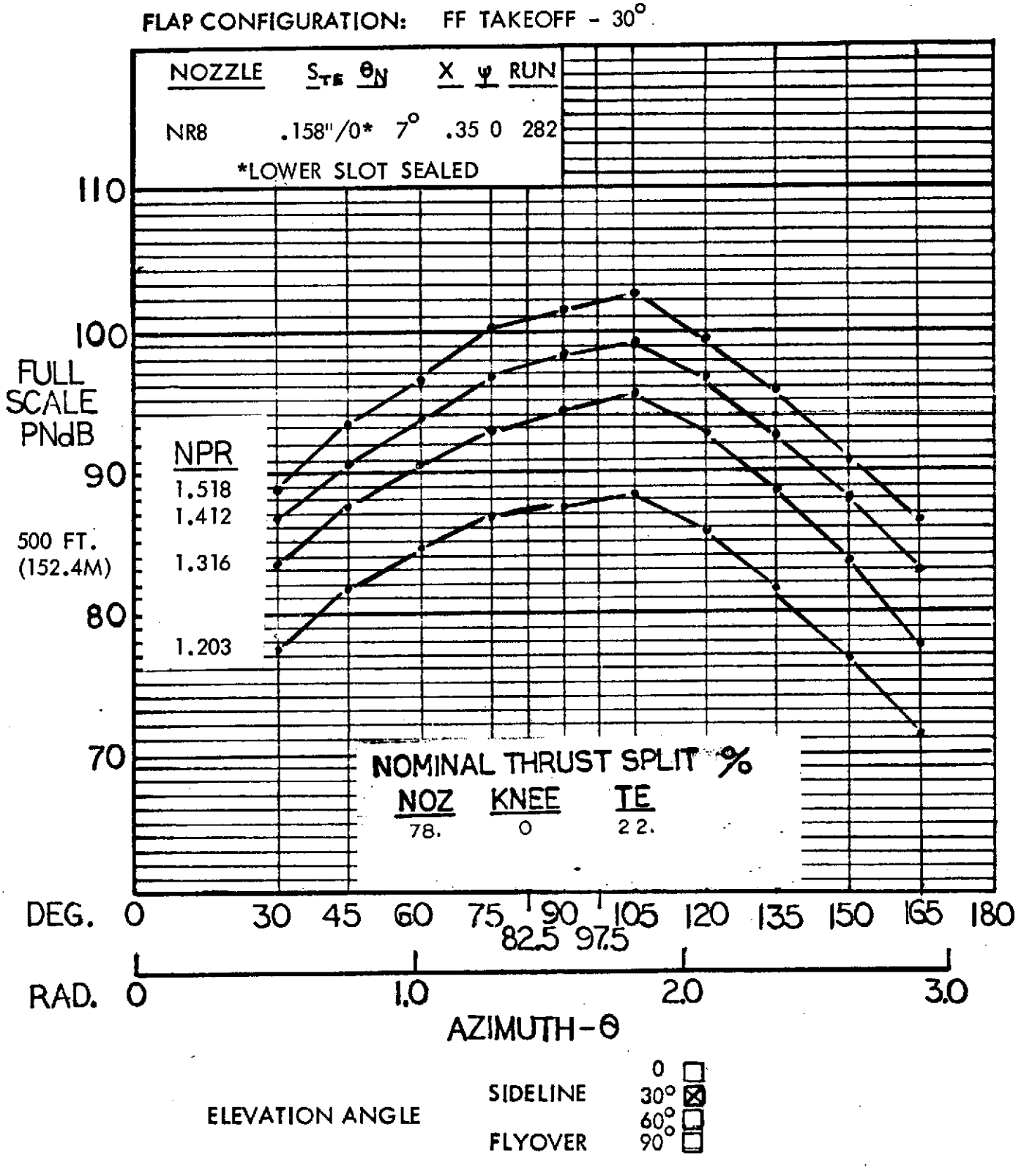

Figure 98 Full scale sideline PNL for the aspect ratio 8 nozzle and Flex Flap with upper TE blowing; 30° flap angle.

HYBRID PROPULSIVE LIFT
ACOUSTIC TEST
NAS 2-7812

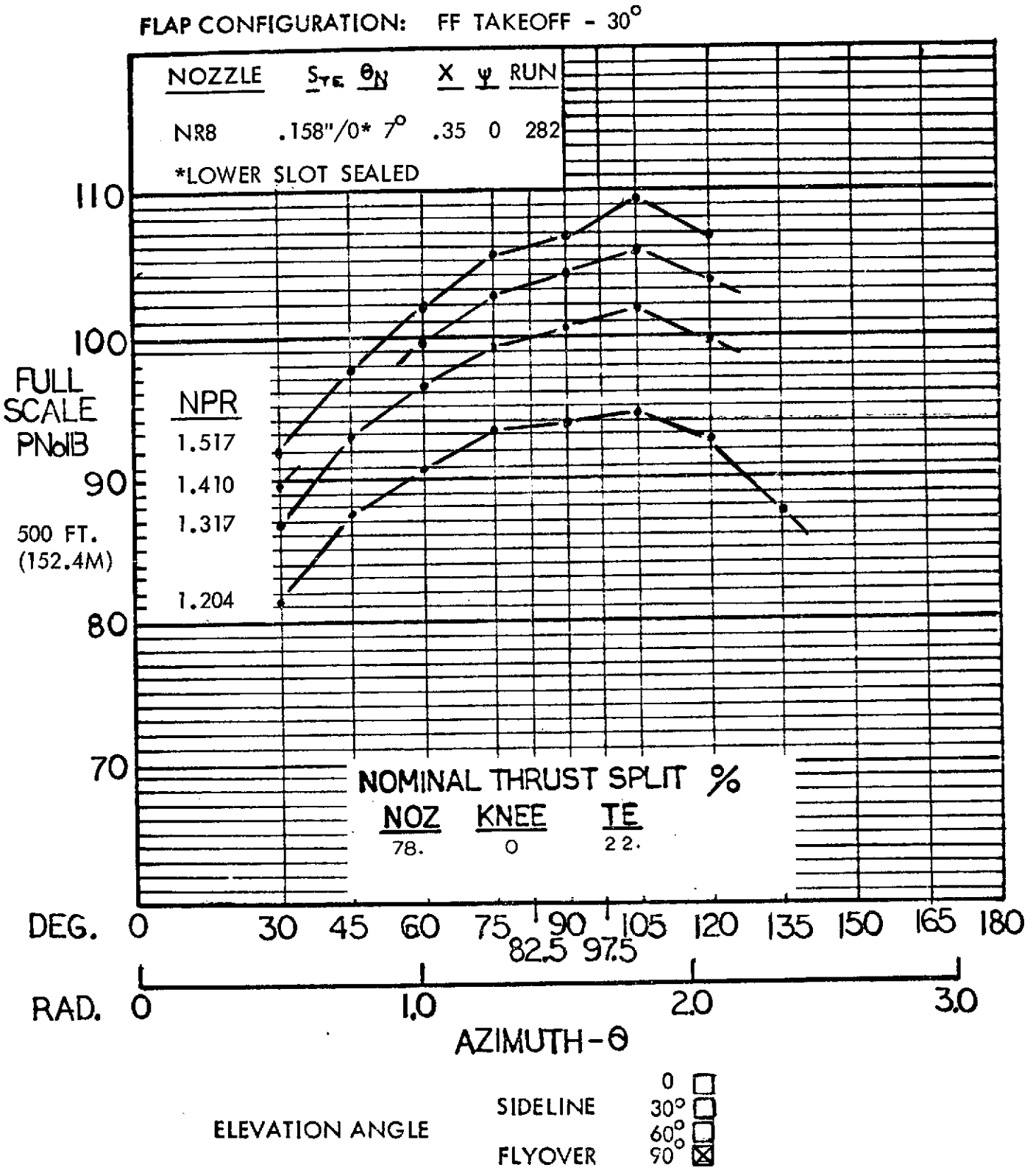

Figure 99 Full scale flyover PNL for the aspect ratio 8 nozzle and Flex Flap with upper TE blowing; 30° flap angle.

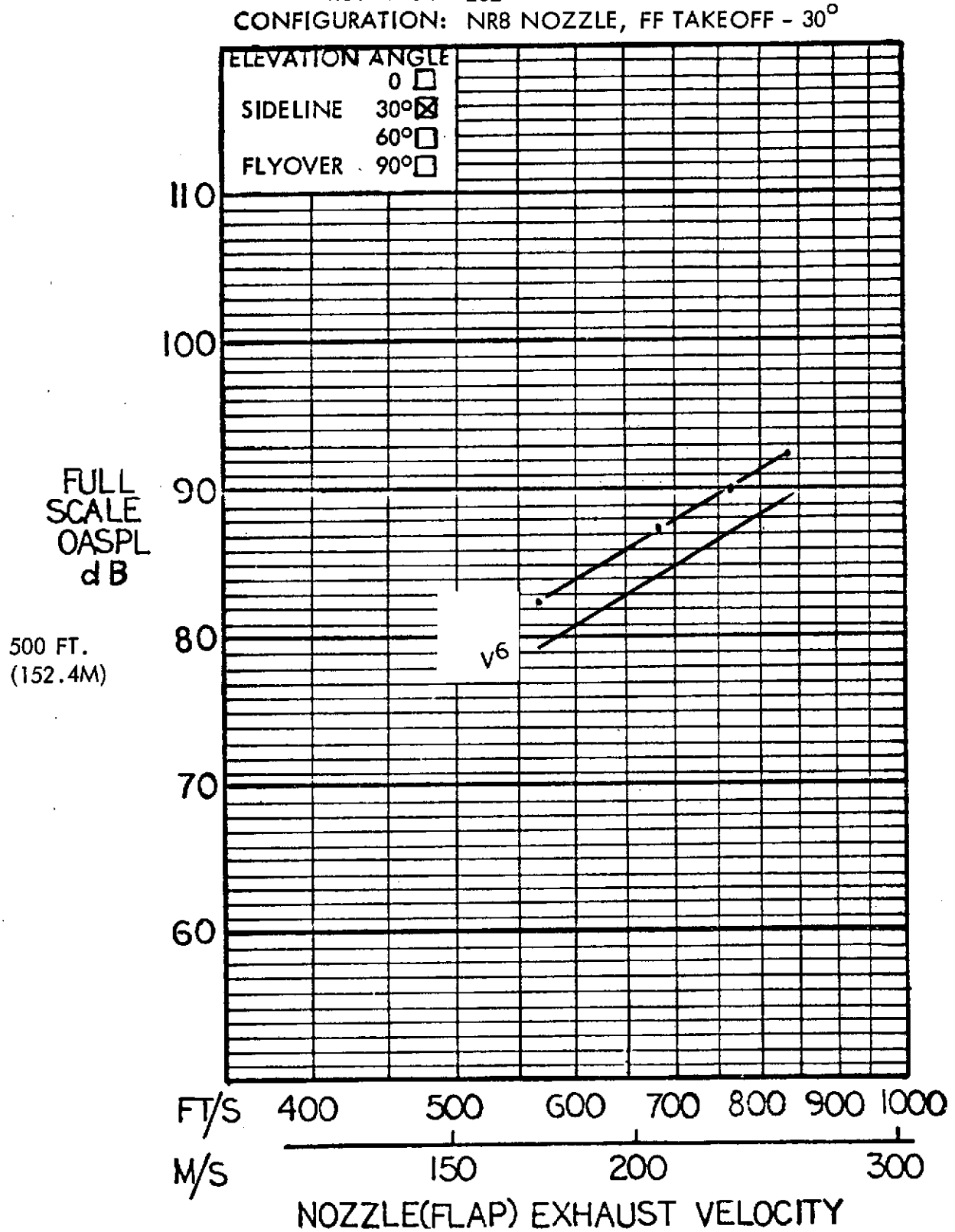

Figure 100 Full scale sideline OASPL at 90° azimuth for the aspect ratio 8 nozzle and Flex Flap with upper TE blowing; 30° flap angle.

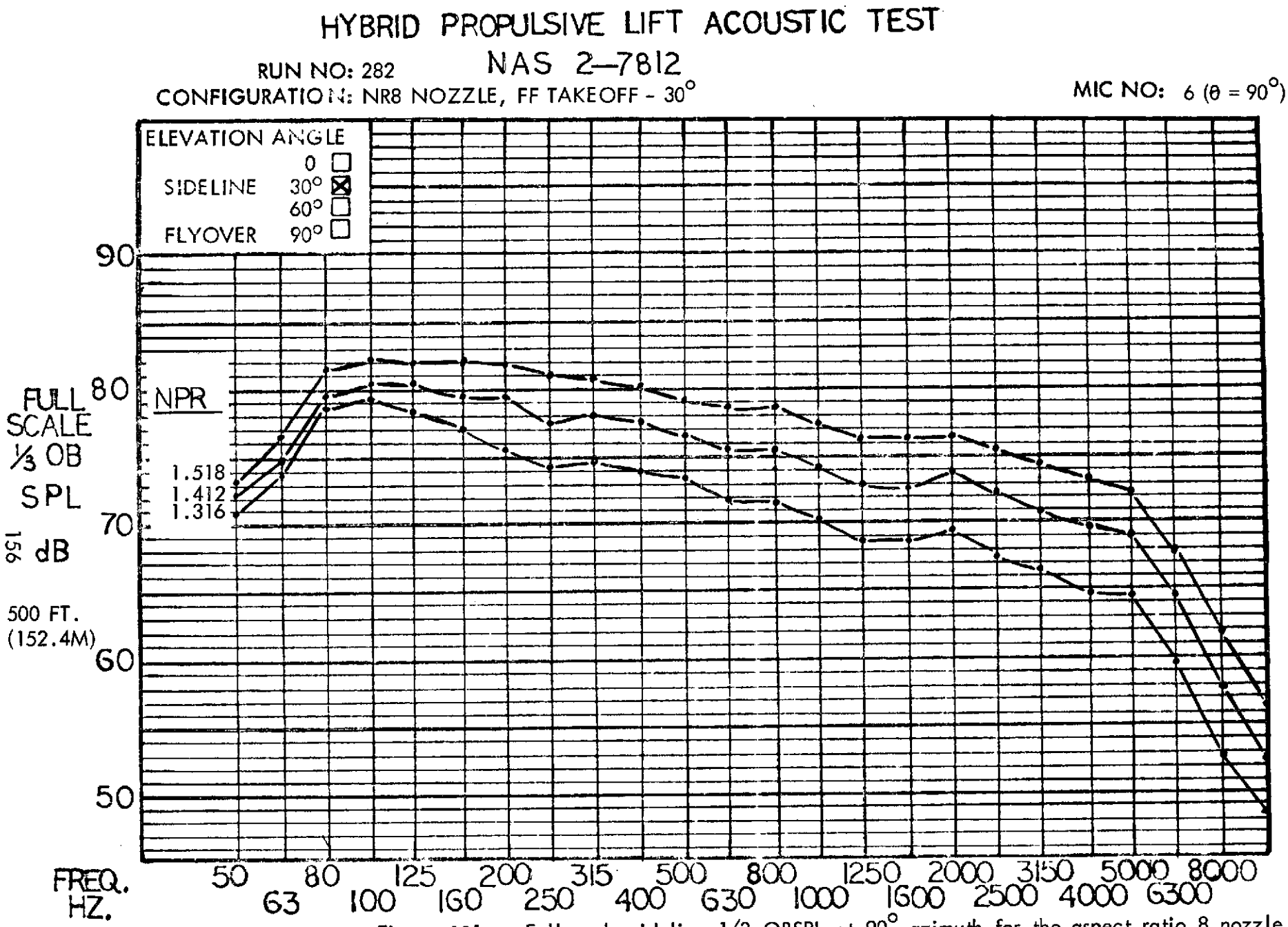

Figure 101 Full scale sideline 1/3 OBSPL at 90° azimuth for the aspect ratio 8 nozzle and Flex Flap with upper TE blowing; 30° flap angle.

HYBRID PROPULSIVE LIFT
ACOUSTIC TEST
NAS 2-7812

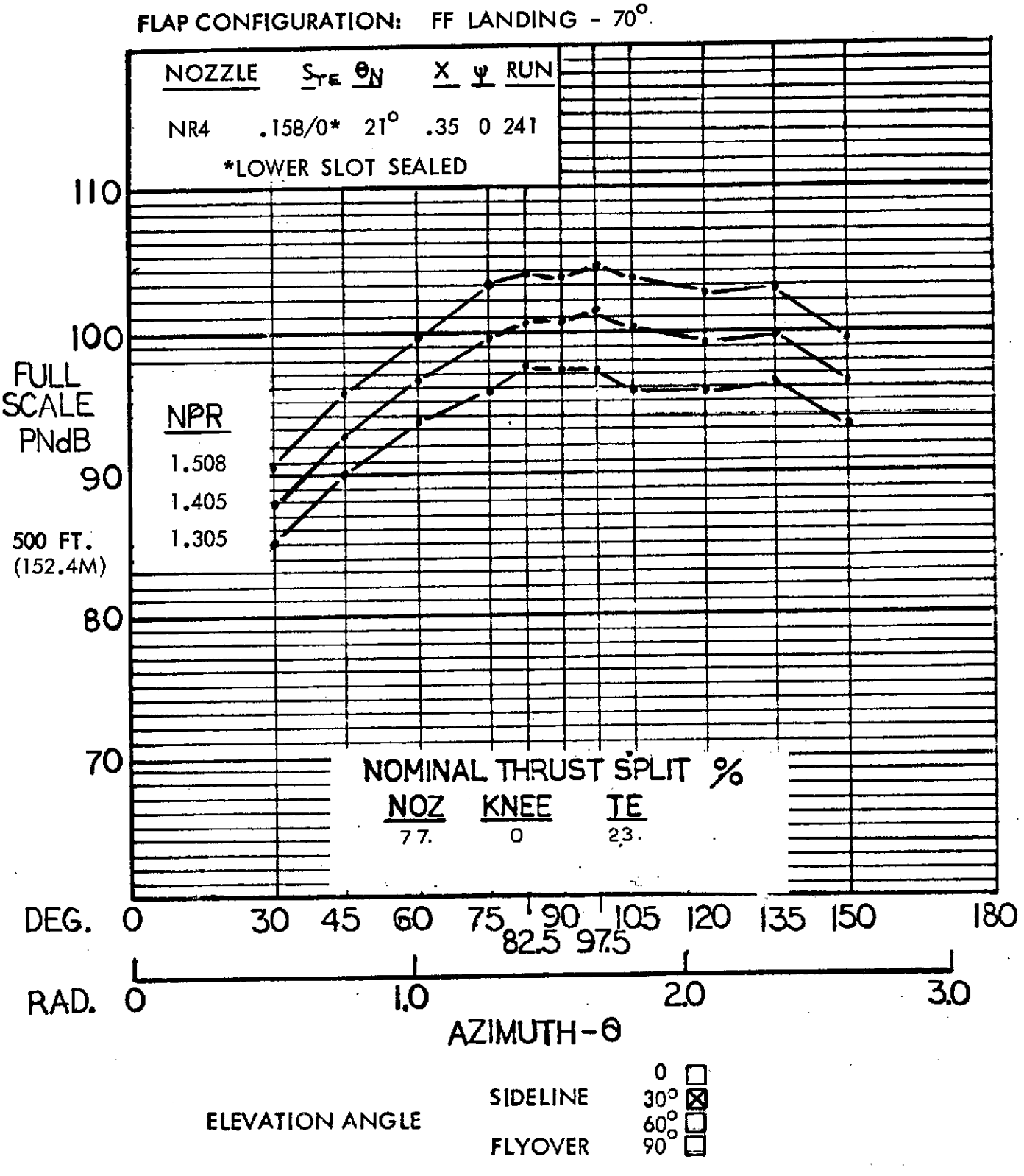

Figure 102 Full scale sideline PNL for the aspect ratio 4 nozzle and Flex Flap with upper TE blowing; 70° flap angle.

HYBRID PROPULSIVE LIFT
ACOUSTIC TEST
NAS 2-7812

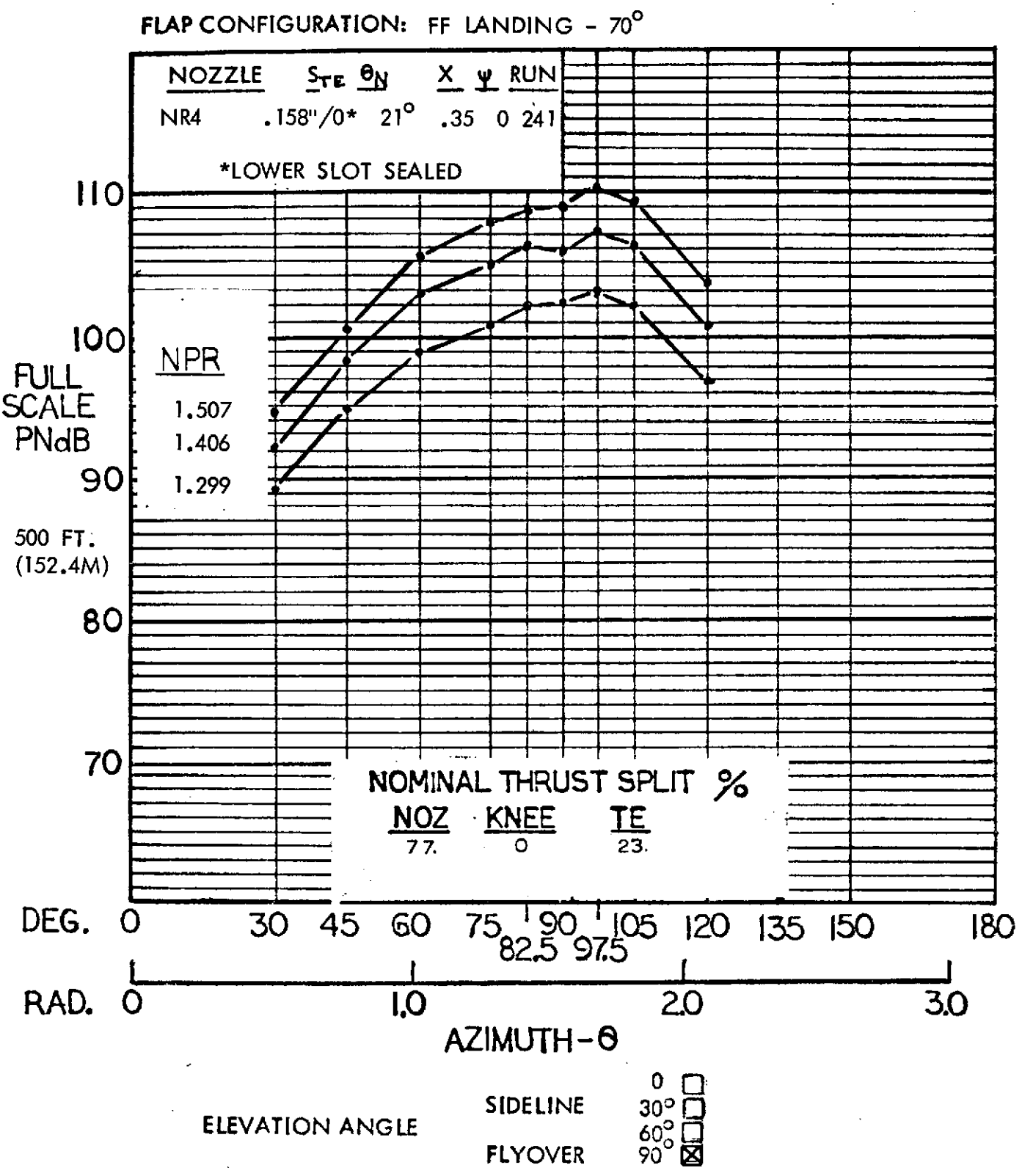

Figure 103 Full scale flyover PNL for the aspect ratio 4 nozzle and Flex Flap with upper TE blowing; 70° flap angle.

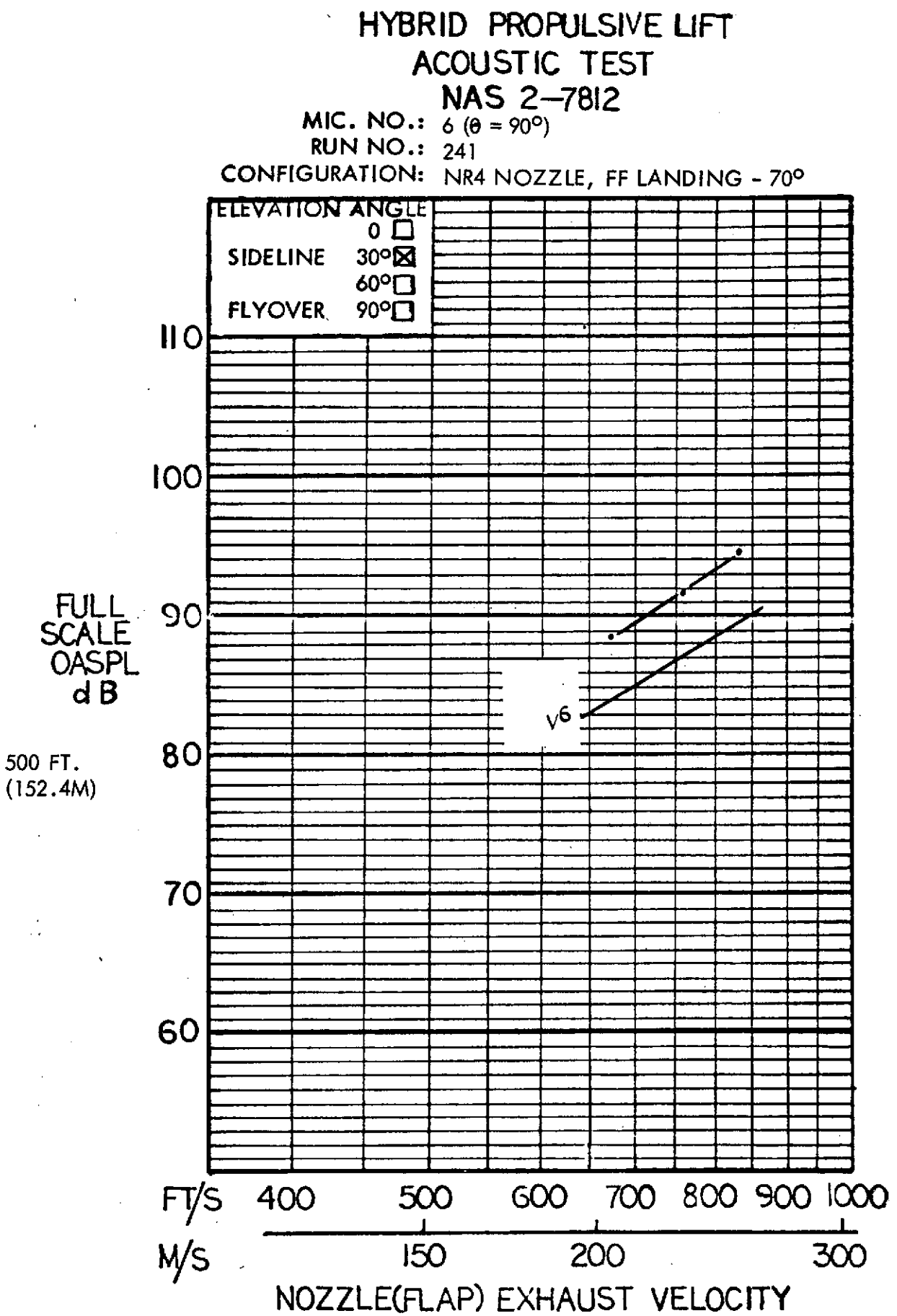

Figure 104 Full scale sideline OASPL at 90° Azimuth for the aspect ratio 4 nozzle and Flex Flap with upper TE blowing; 70° flap angle.

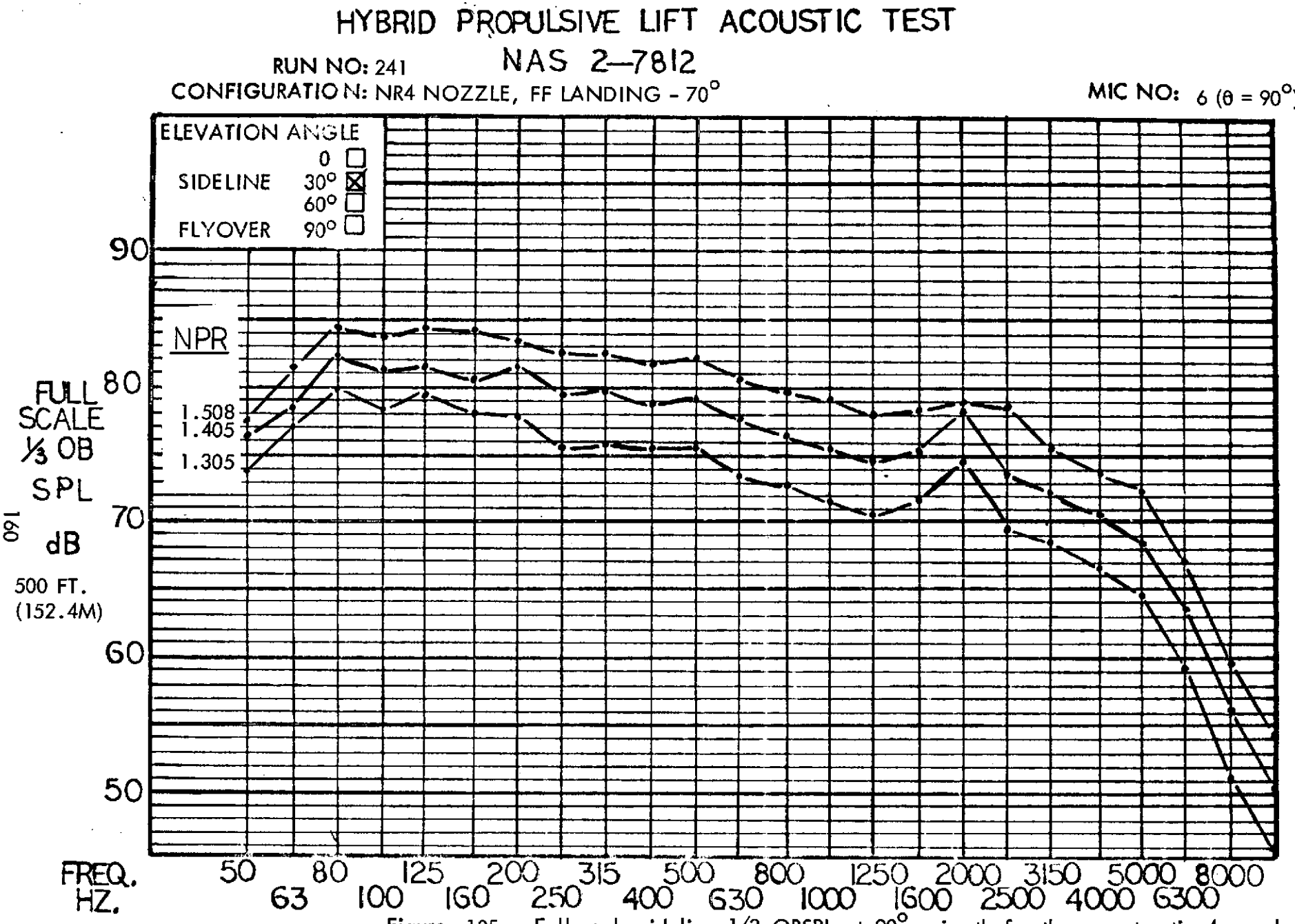

Figure 105 Full scale sideline 1/3 OBSPL at 90° azimuth for the aspect ratio 4 nozzle and Flex Flap with upper TE blowing; 70° flap angle.

HYBRID PROPULSIVE LIFT
ACOUSTIC TEST
NAS 2-7812

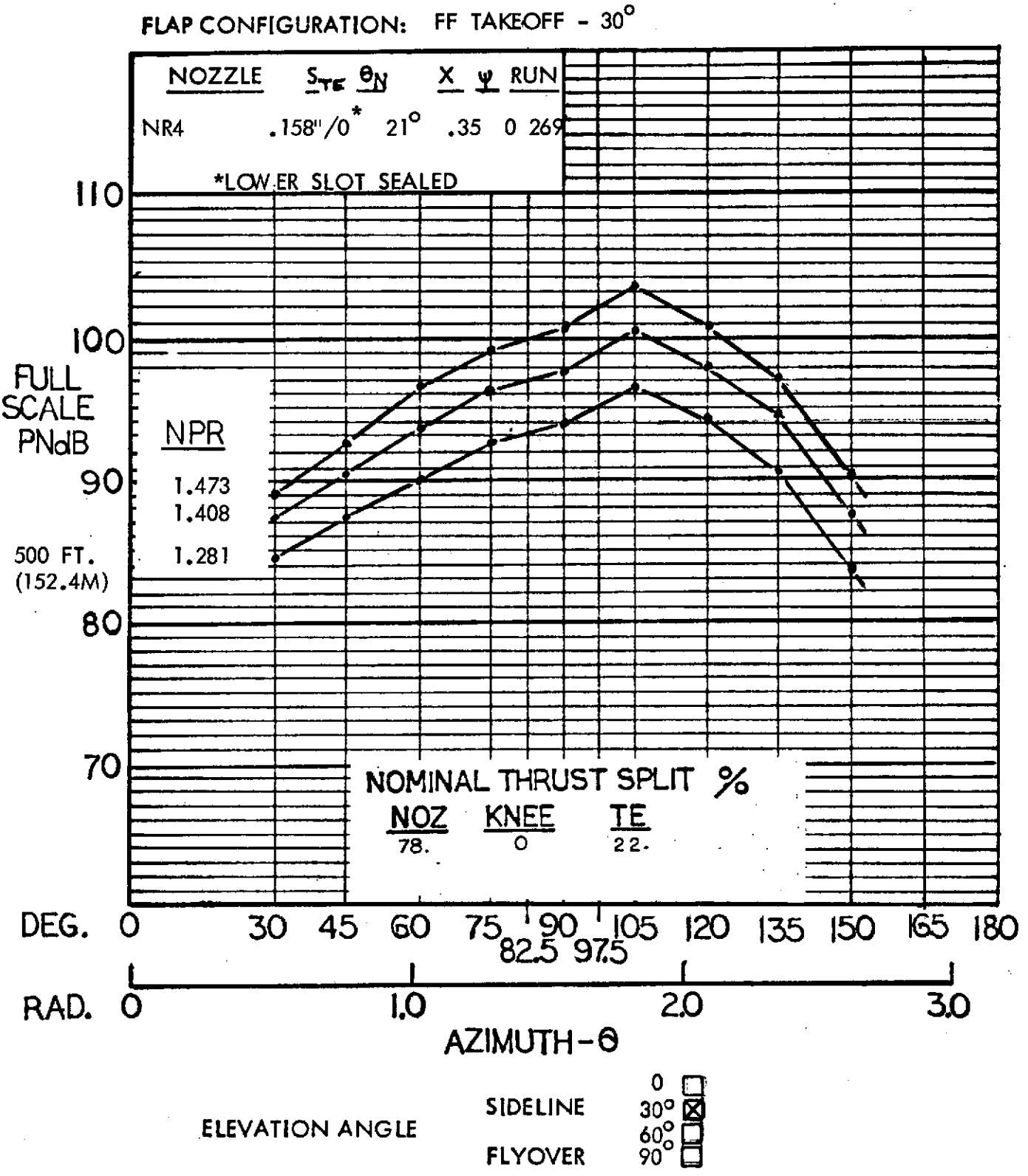

Figure 106 Full scale sideline PNL for the aspect ratio 4 nozzle and Flex Flap with upper TE blowing; 30° flap angle.

HYBRID PROPULSIVE LIFT
ACOUSTIC TEST
NAS 2-7812

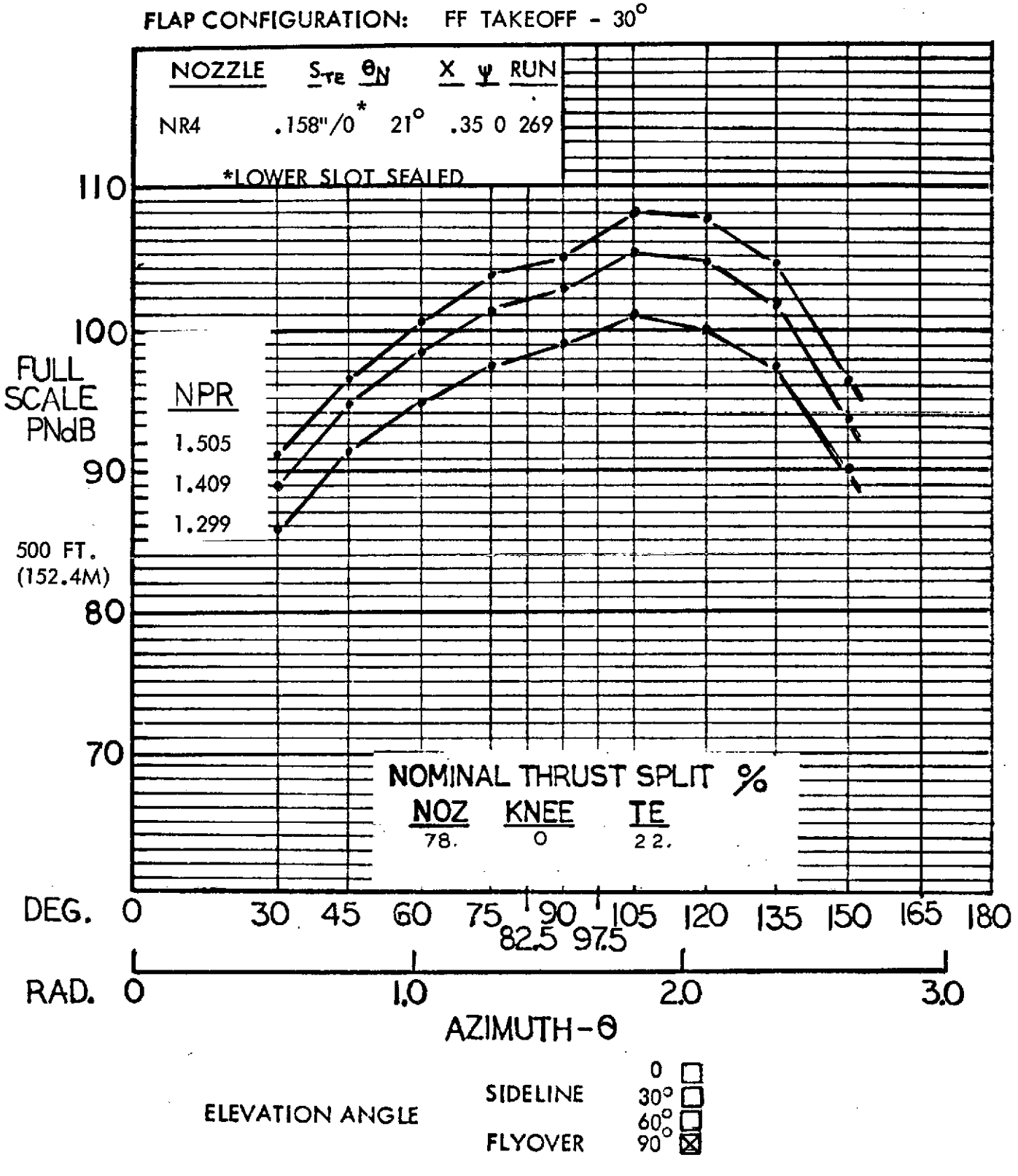

Figure 107 Full scale flyover PNL for the aspect ratio 4 nozzle and Flex Flap with upper TE blowing; 30° flap angle

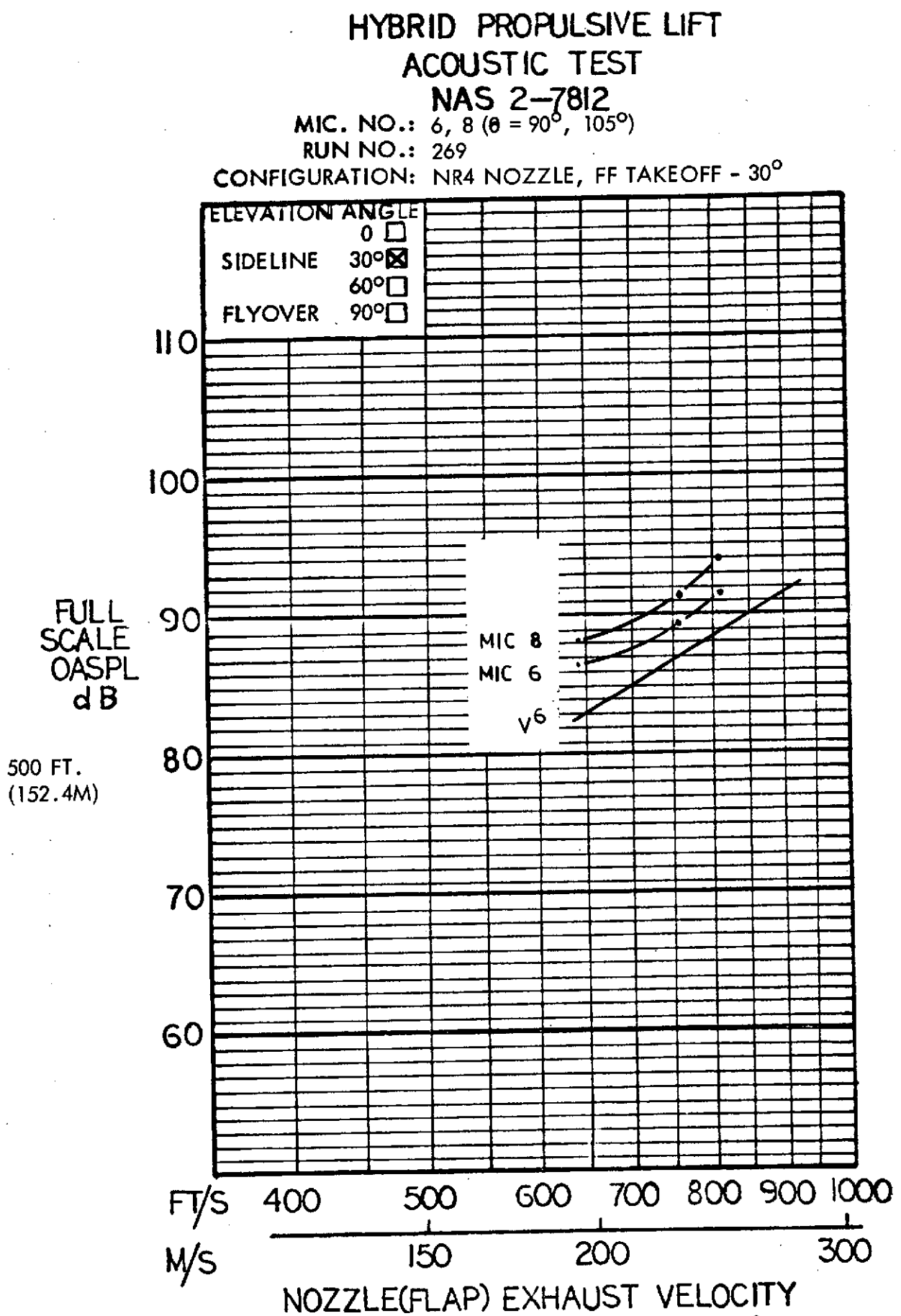

Figure 108 Full scale sideline OASPL at 90° and 105° azimuth for the aspect ratio 4 nozzle and Flex Flap with upper TE blowing; 30° flap angle.

HYBRID PROPULSIVE LIFT ACOUSTIC TEST

NAS 2—7812

RUN NO: 269

CONFIGURATION: NR4 NOZZLE, FF TAKEOFF - 30°

MIC NO: 8 (θ = 105°)

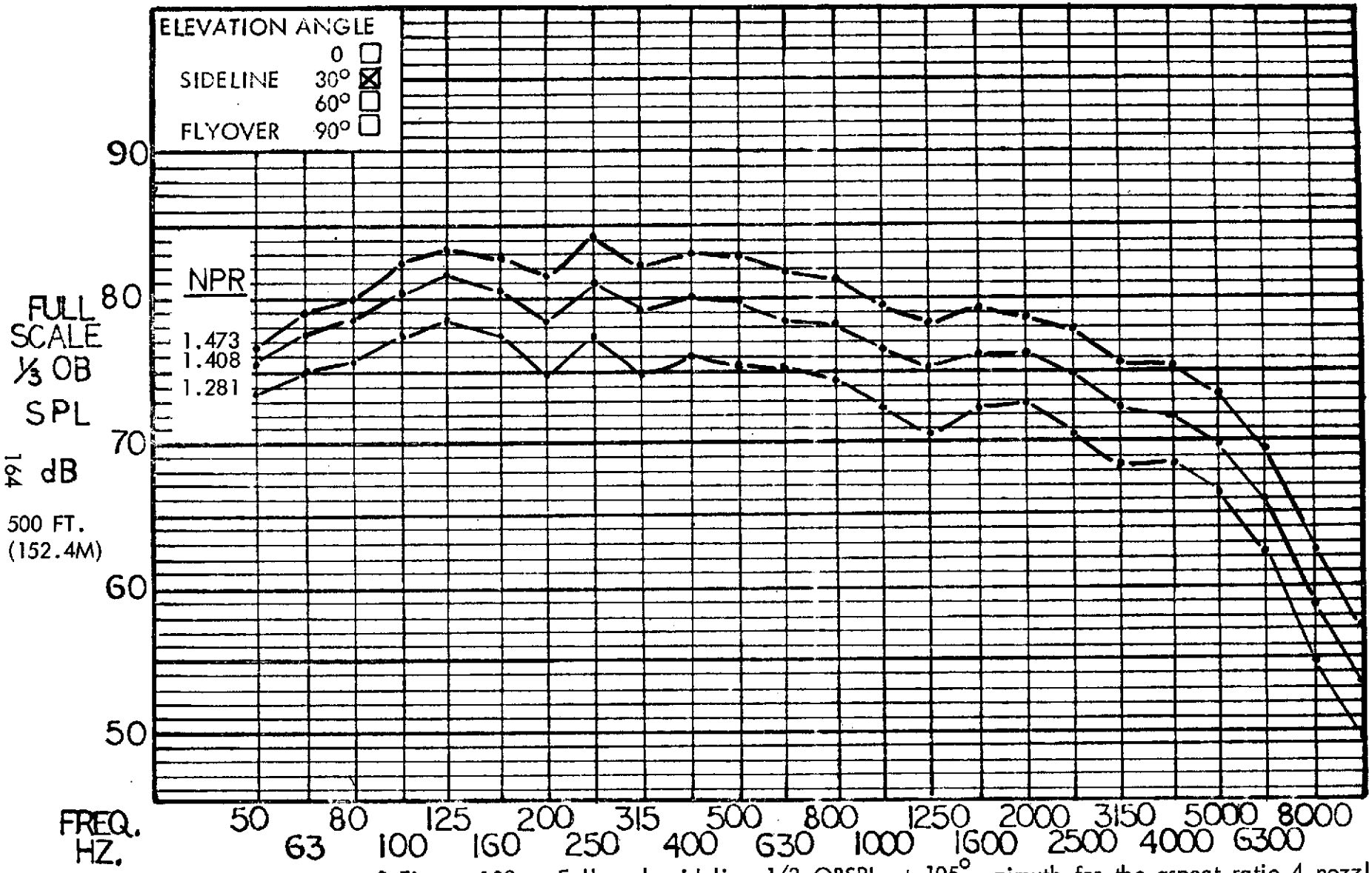

* Figure 109 Full scale sideline 1/3 OBSPL at 105° azimuth for the aspect ratio 4 nozzle and Flex Flap with upper TE blowing; 30° flap angle.

HYBRID PROPULSIVE LIFT
ACOUSTIC TEST
NAS 2-7812

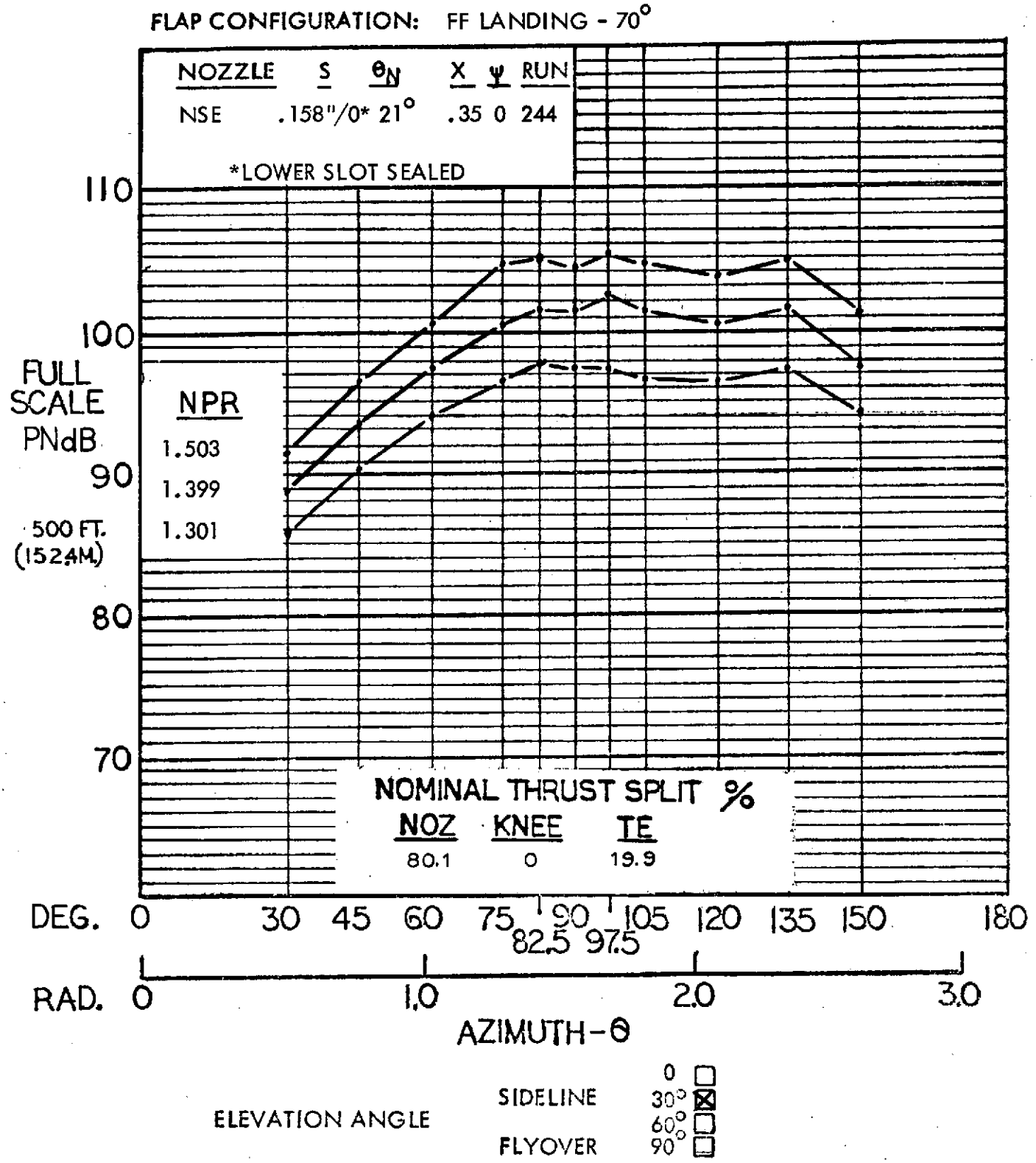

Figure 110 Full scale sideline PNL for the simulated engine nozzle and Flex Flap with upper TE blowing; 70° flap angle.

HYBRID PROPULSIVE LIFT
ACOUSTIC TEST
NAS 2-7812

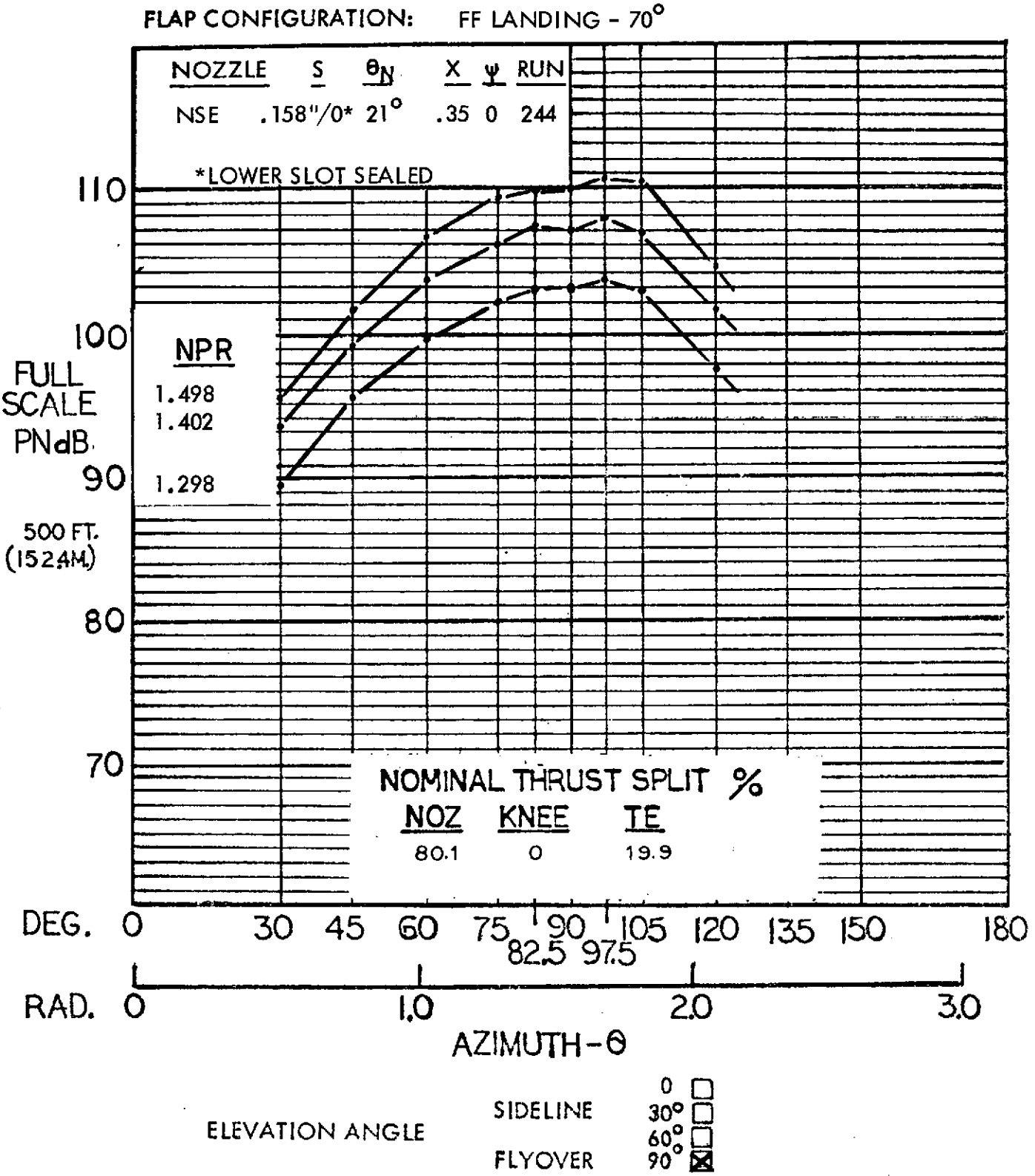

Figure 111 Full scale flyover PNL for the simulated engine nozzle and Flex Flap with upper TE blowing; 70° flap angle.

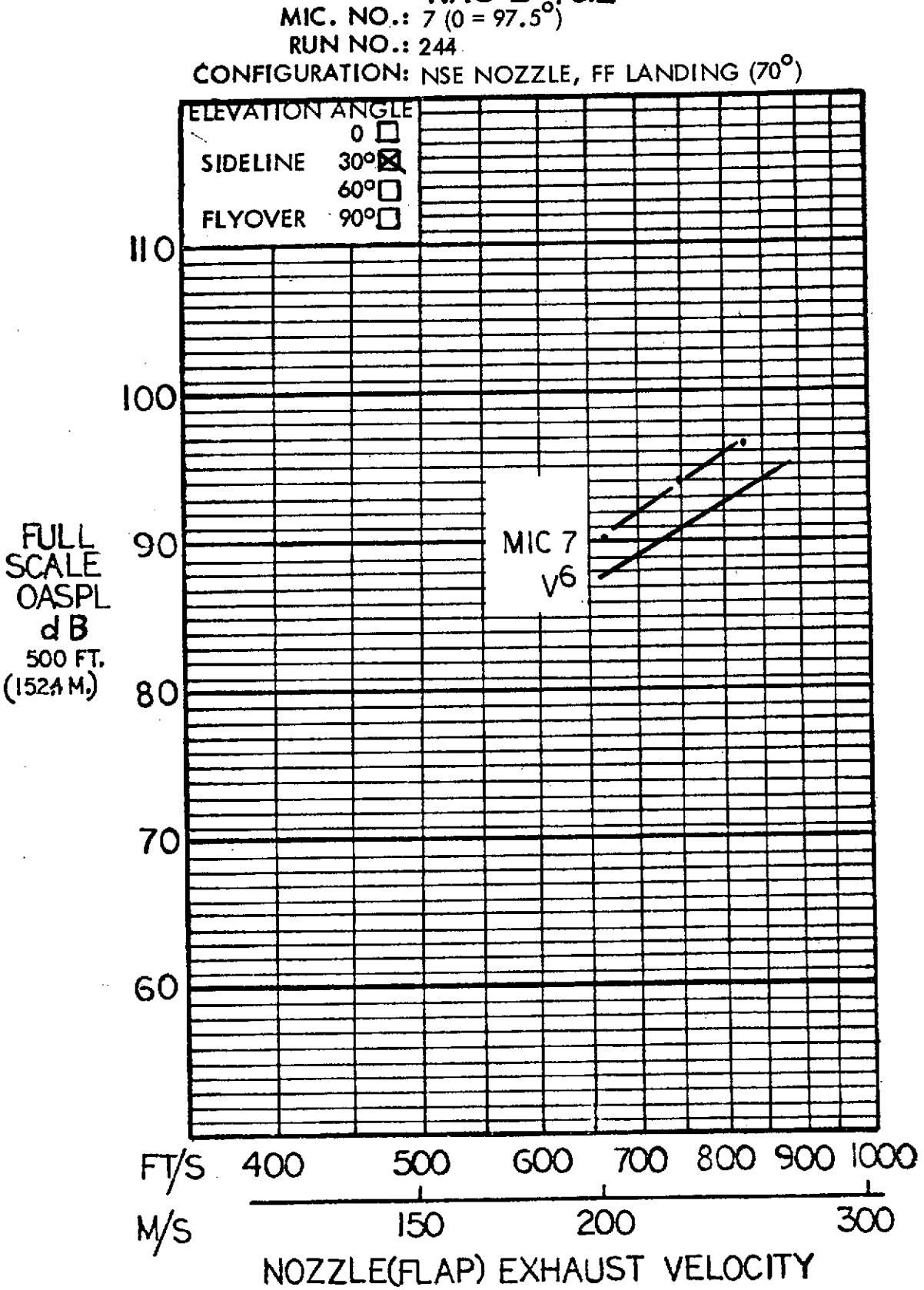

Figure 112 Full scale sideline OASPL at 97.5° azimuth for the simulated engine nozzle and Flex Flap with upper TE blowing; 70° flap angle.

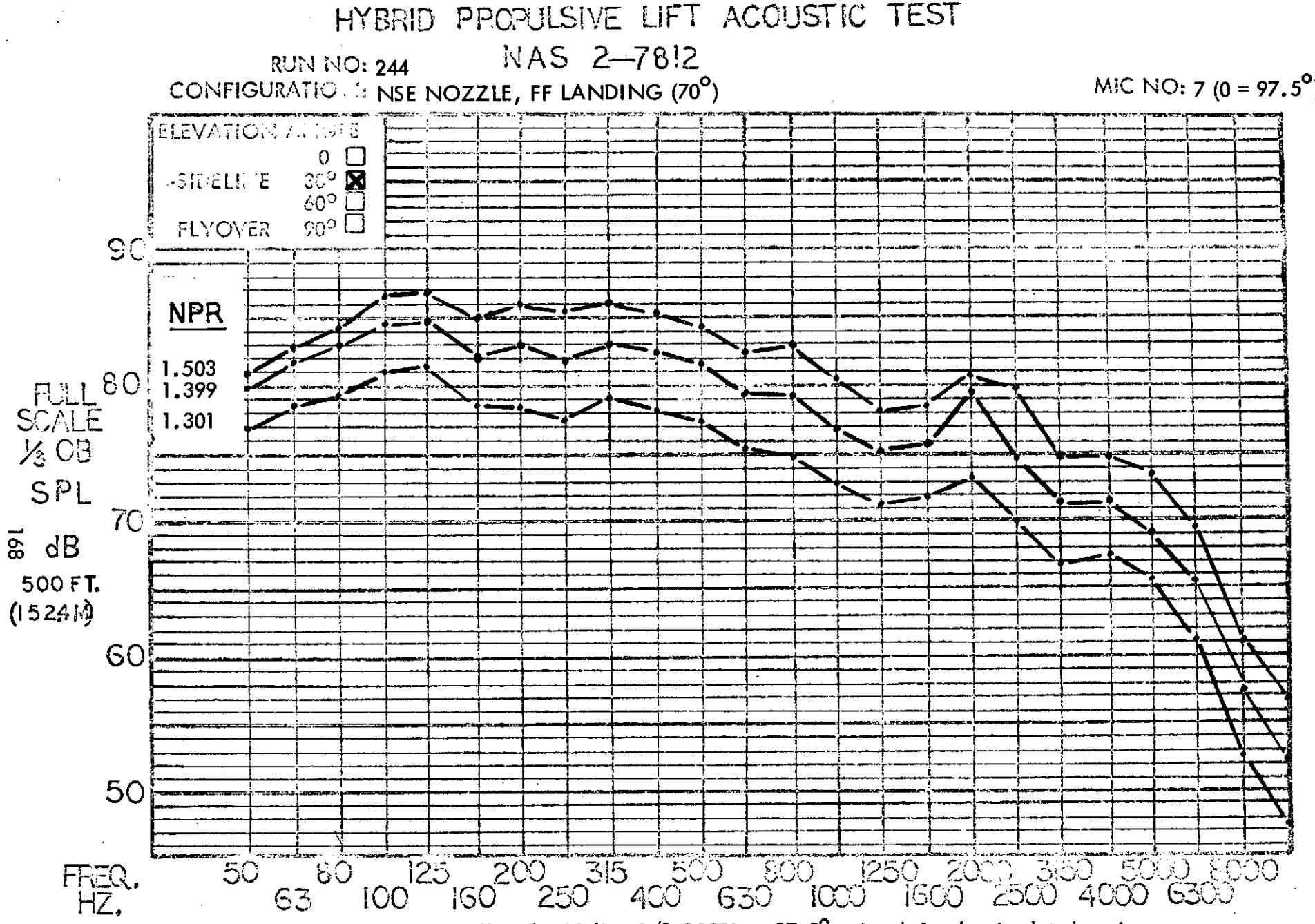

Figure 113 Full scale sideline 1/3 OBSPL at 97.5° azimuth for the simulated engine nozzle and Flex Flap with upper TE blowing; 70° flap angle.

HYBRID PROPULSIVE LIFT
ACOUSTIC TEST
NAS 2-7812

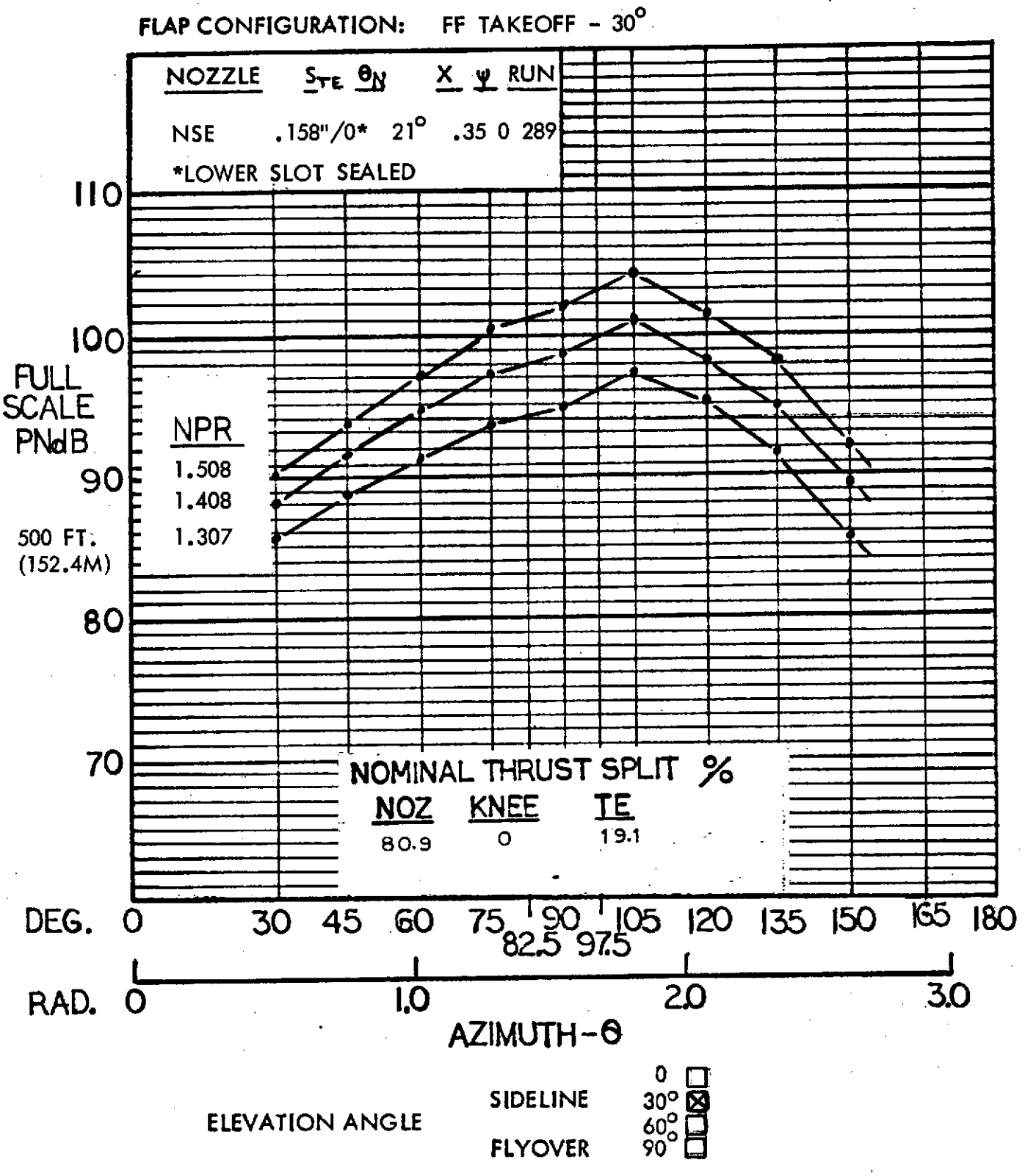

Figure 114 Full scale sideline PNL for the simulated engine nozzle and Flex Flap with upper TE blowing; 30° flap angle.

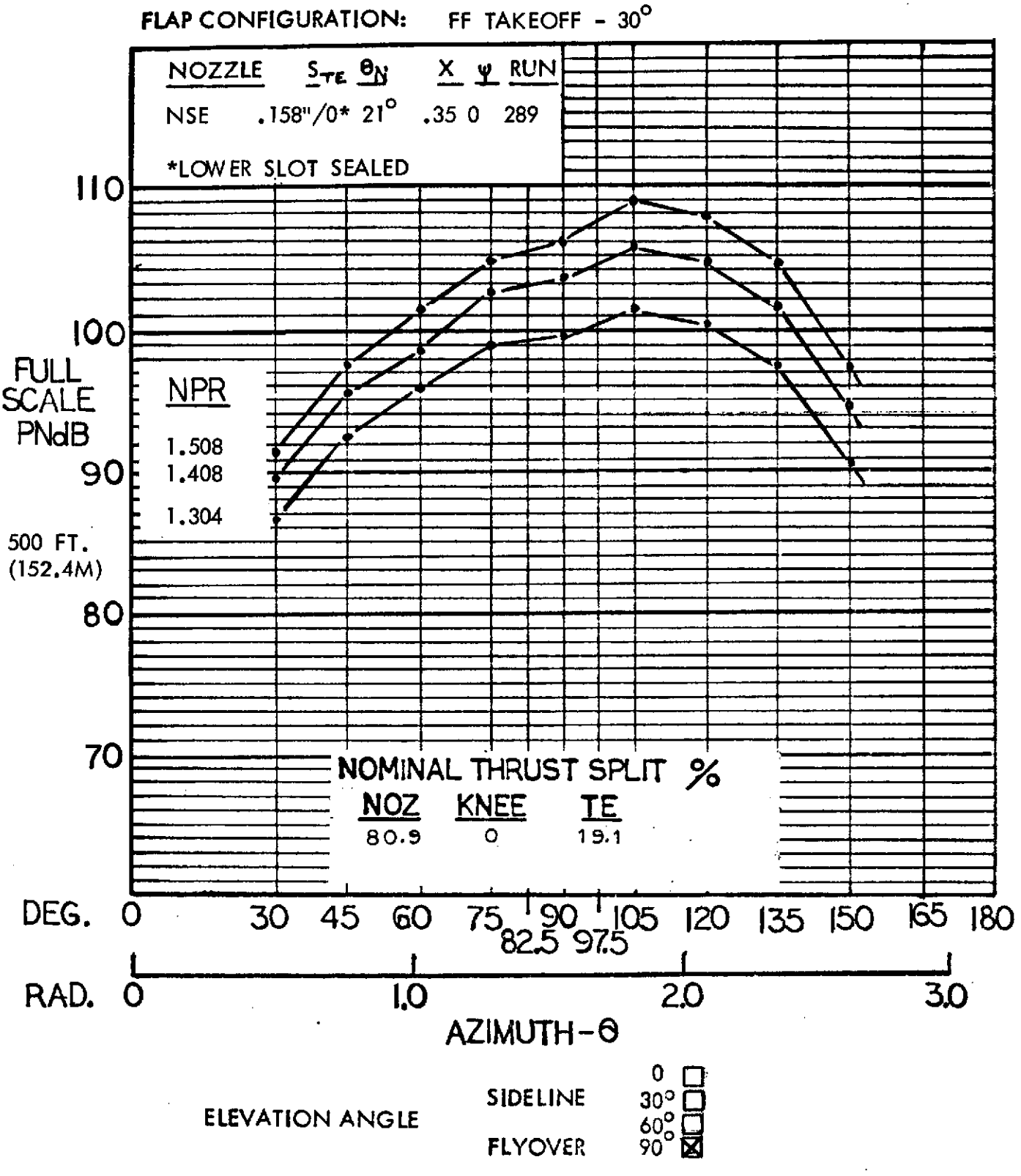

Figure 115 Full scale flyover PNL for the simulated engine nozzle and Flex Flap with upper TE blowing; 30° flap angle

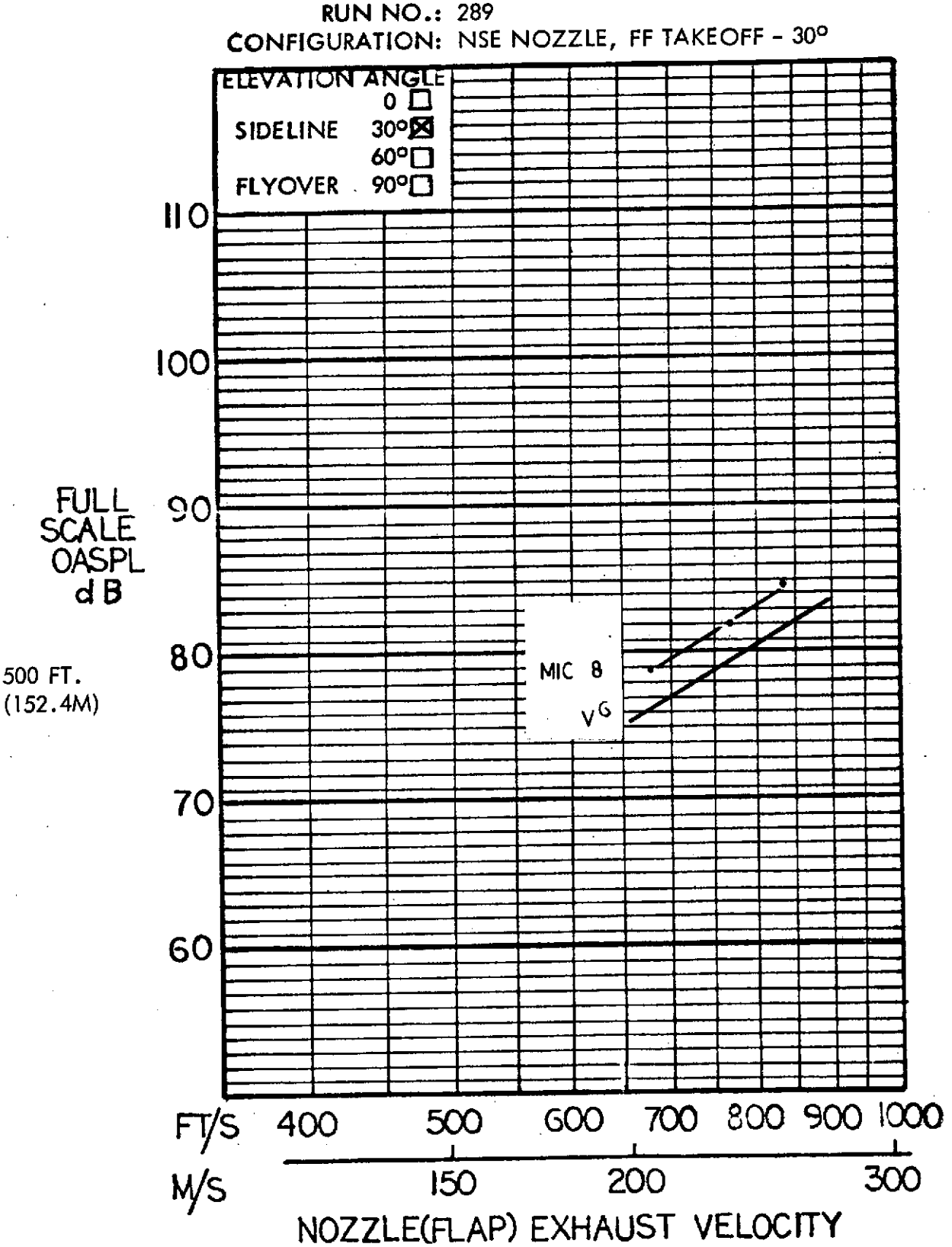

Figure 116 Full scale sideline OASPL at 105° azimuth for the simulated engine nozzle and Flex Flap with upper TE blowing; 30° flap angle.

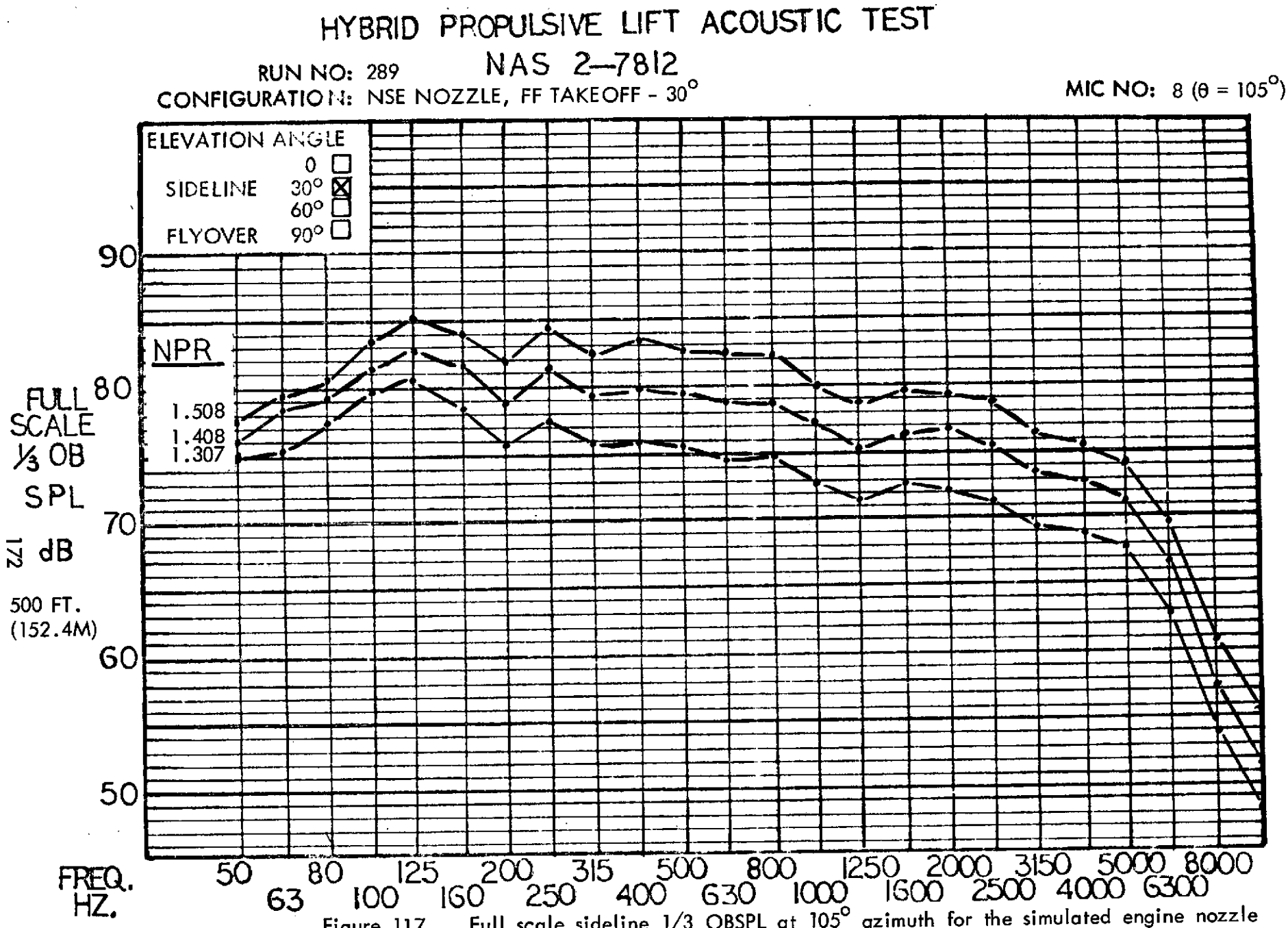

Figure 117 Full scale sideline 1/3 OBSPL at 105° azimuth for the simulated engine nozzle and Flex Flap with upper TE blowing; 30° flap angle

HYBRID PROPULSIVE LIFT
ACOUSTIC TEST
NAS 2-7812

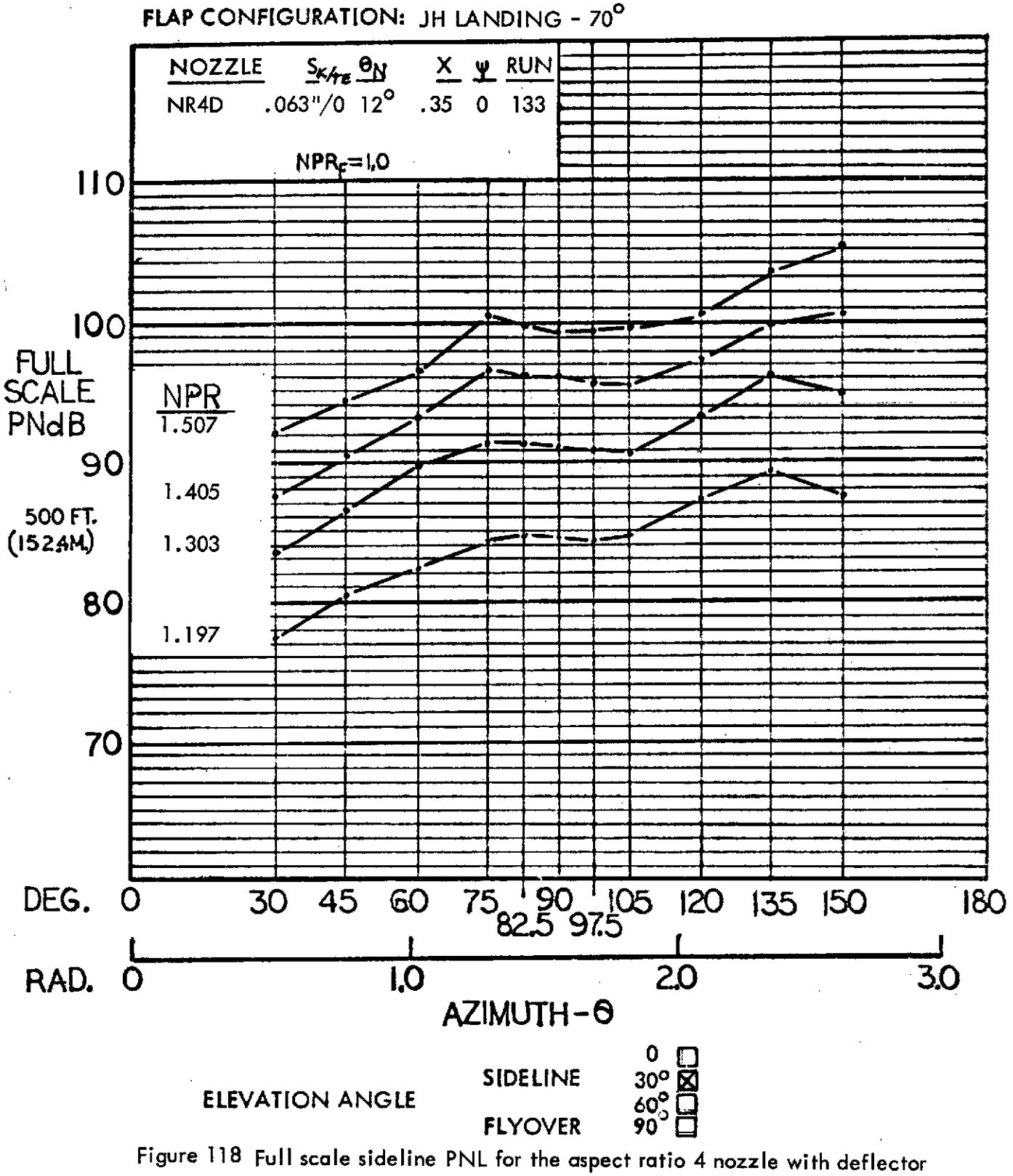

Figure 118 Full scale sideline PNL for the aspect ratio 4 nozzle with deflector and JH flap, USB only; 70° flap angle.

HYBRID PROPULSIVE LIFT
ACOUSTIC TEST
NAS 2-7812

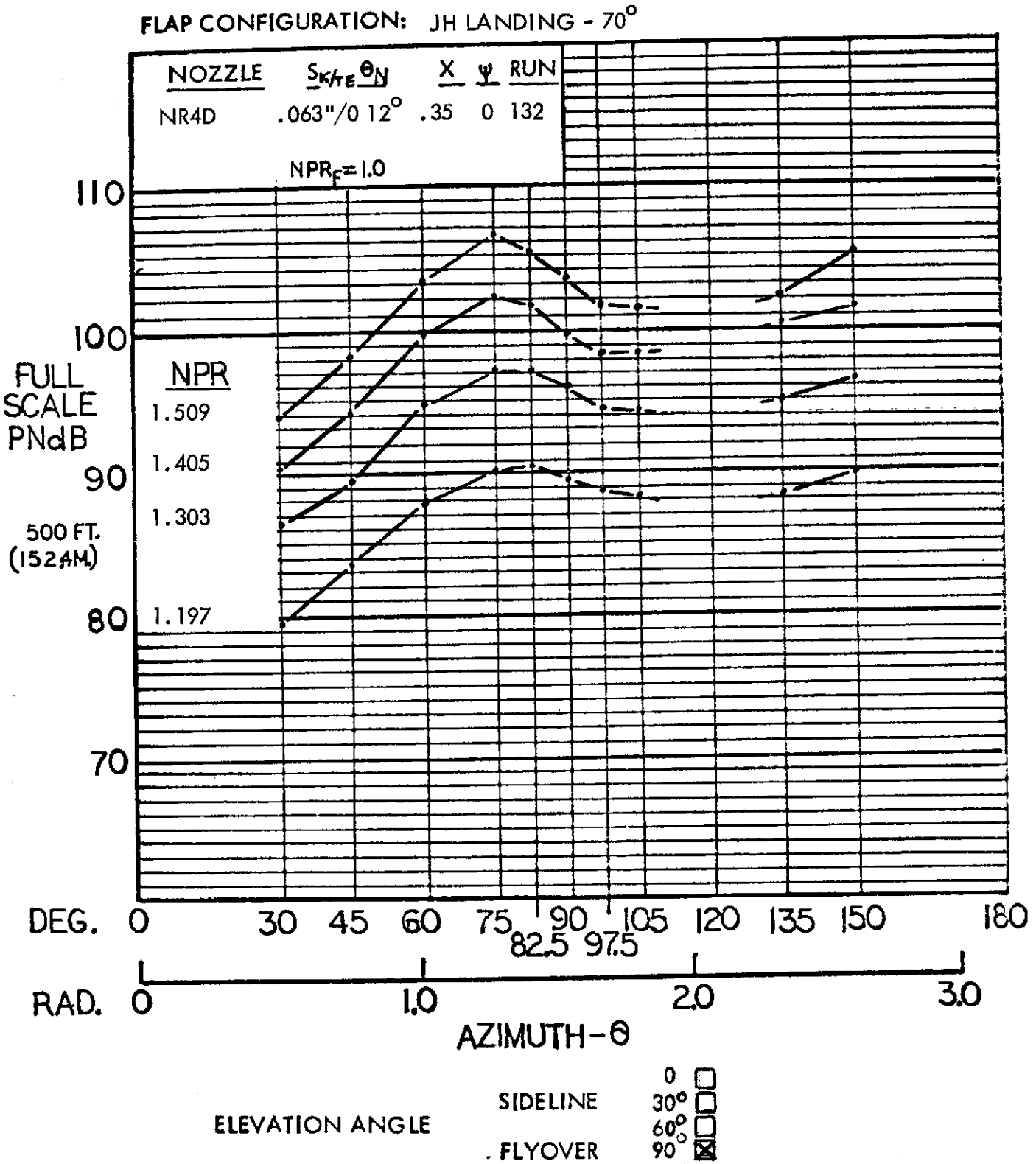

Figure 119 Full scale flyover PNL for the aspect ratio 4 nozzle with deflector and JH flap, USB only; 70° flap angle.

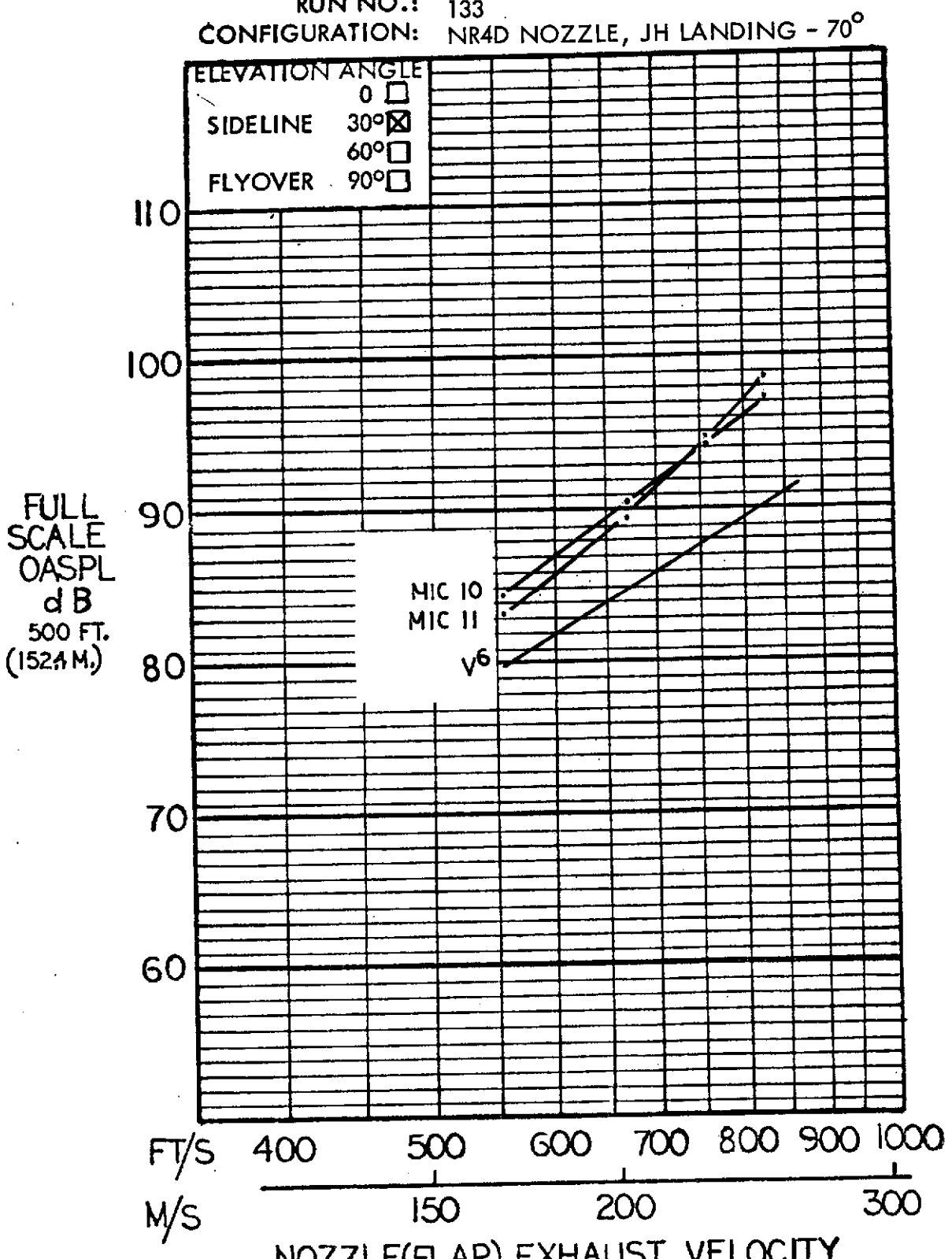

Figure 120 Full scale sideline OASPL at 135° and 150° azimuth for the aspect ratio 4 nozzle with deflector and JH flap, USB only; 70° flap angle.

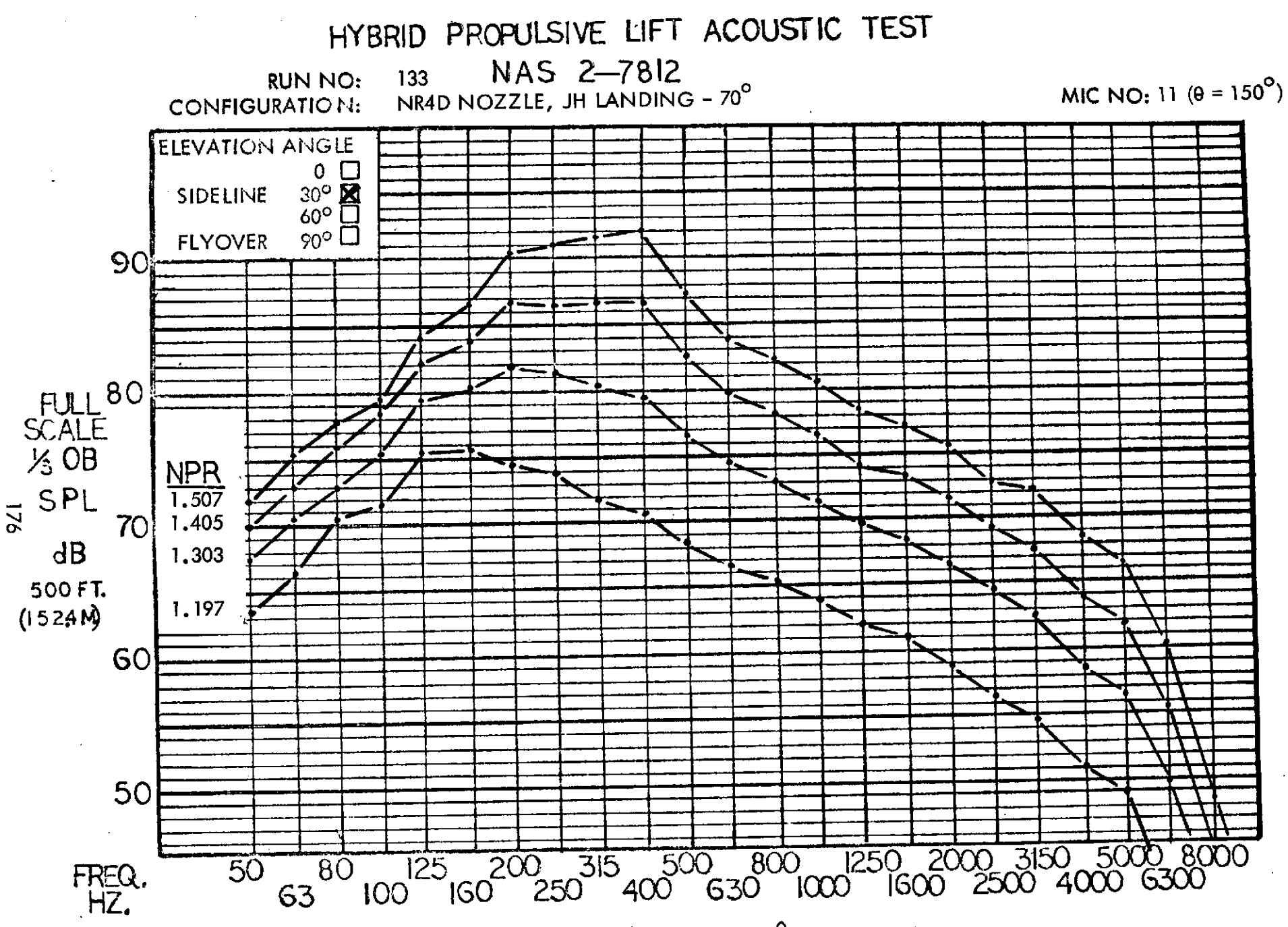

Figure 121 - Full scale sideline 1/3 OBSPL at 150° azimuth for the aspect ratio 4 nozzle with deflector and JH flap, USB only, 70° flap angle.

HYBRID PROPULSIVE LIFT
ACOUSTIC TEST
NAS 2-7812

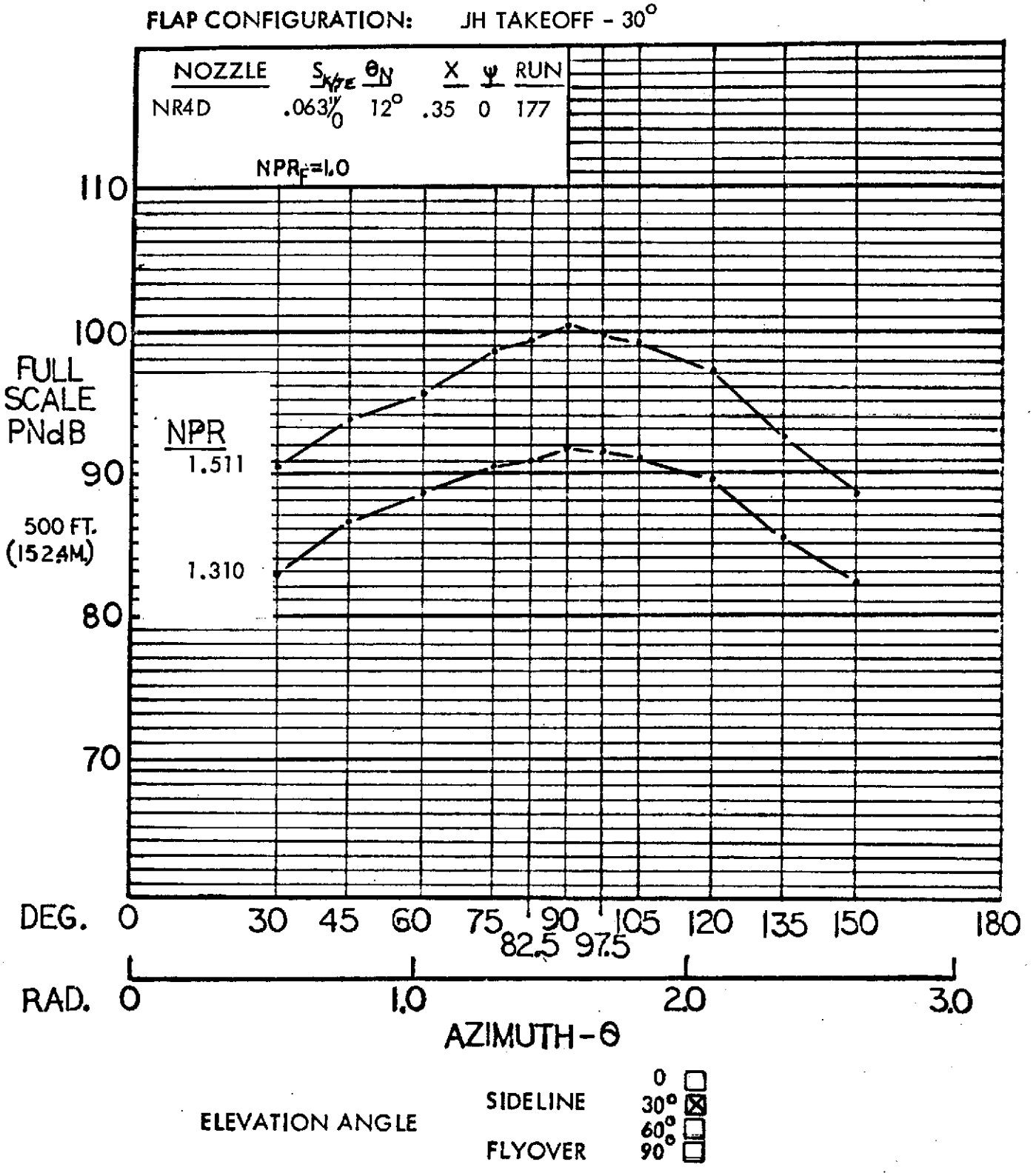

Figure 122 - Full scale sideline PNL for the aspect ratio 4 nozzle with deflector and JH flap, USB only; 30° flap angle.

HYBRID PROPULSIVE LIFT
ACOUSTIC TEST
NAS 2-7812

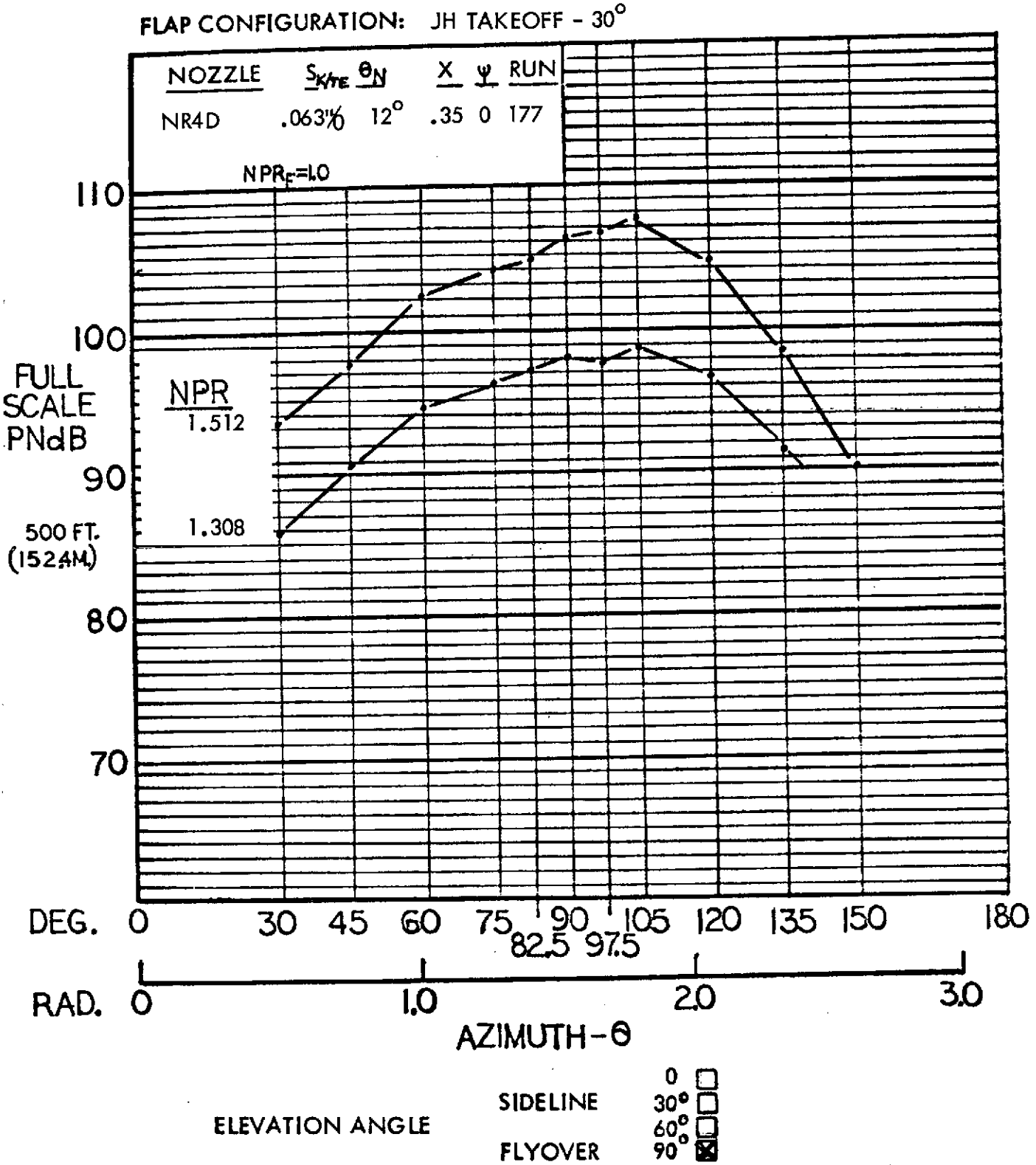

Figure 123 - Full scale flyover PNL for the aspect ratio 4 nozzle with deflector and JH flap, USB only; 30° flap angle.

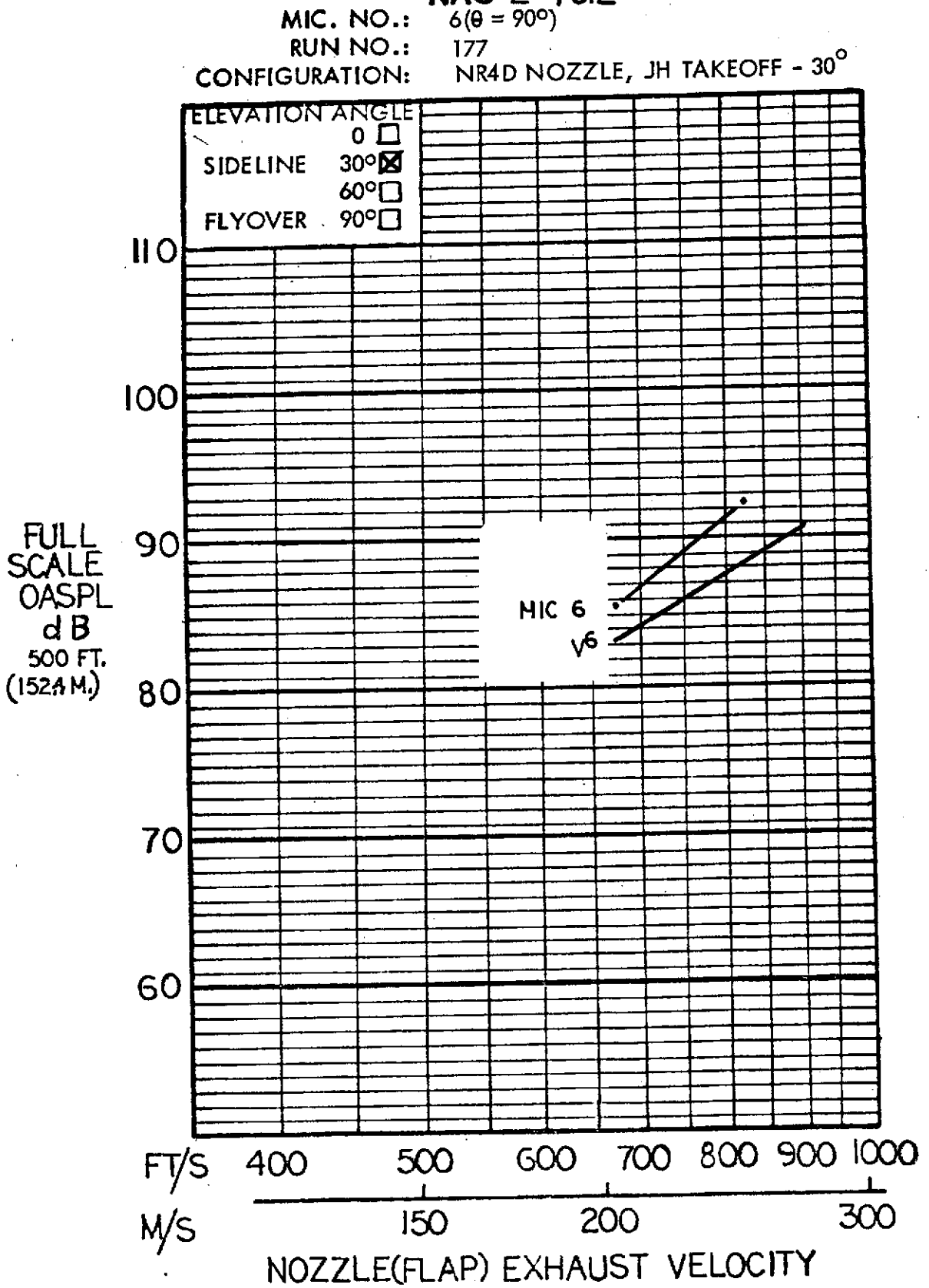

Figure 124 - Full scale sideline OASPL at 90° azimuth for the aspect ratio 4 nozzle with deflector and JH flap, USB only, 30° flap angle.

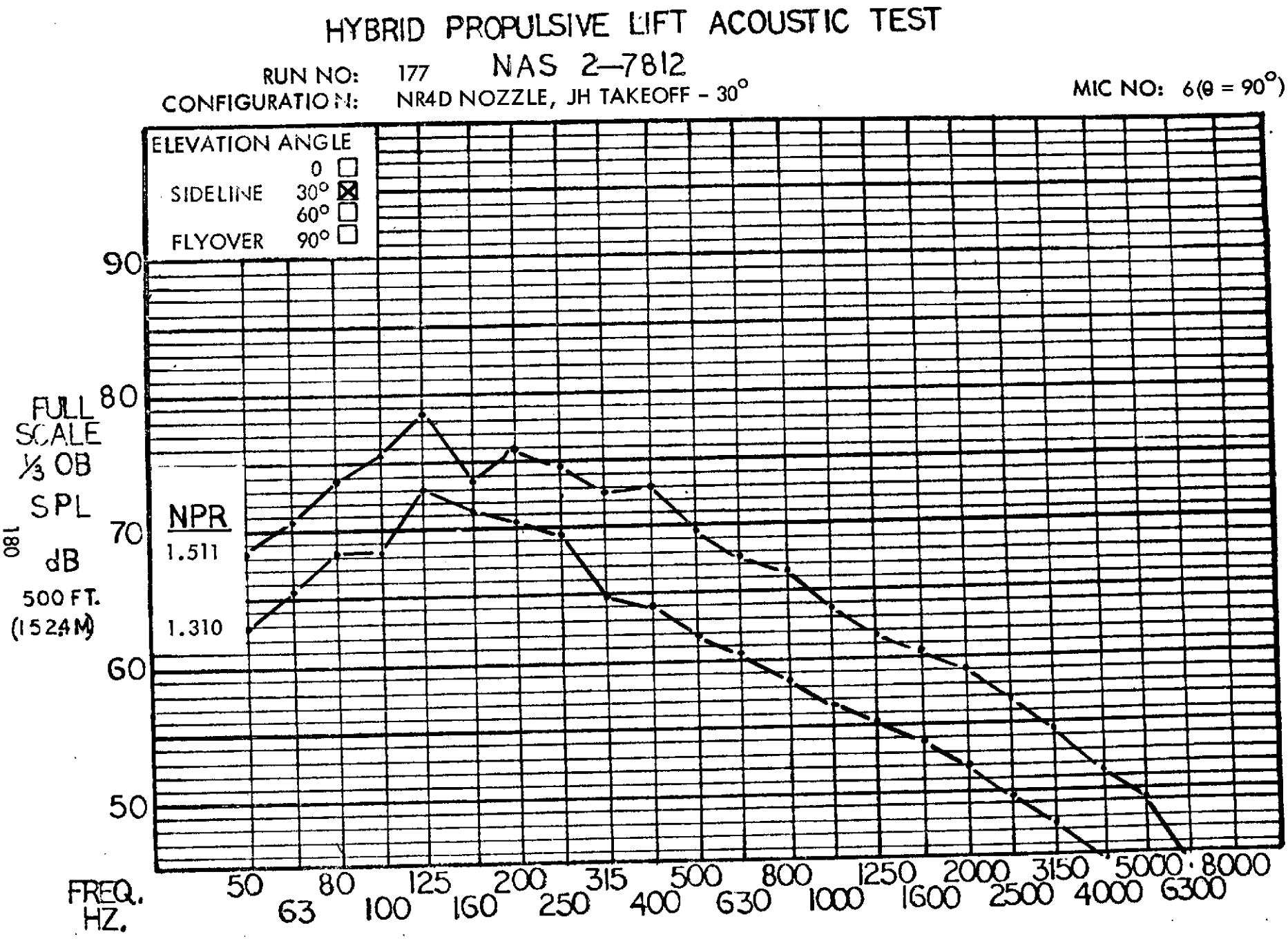

Figure 125 - Full scale sideline 1/3 OBSPL at 90° azimuth for the aspect ratio 4 nozzle with deflector and JH flap, USB only; 30° flap angle.

HYBRID PROPULSIVE LIFT
ACOUSTIC TEST
NAS 2-7812

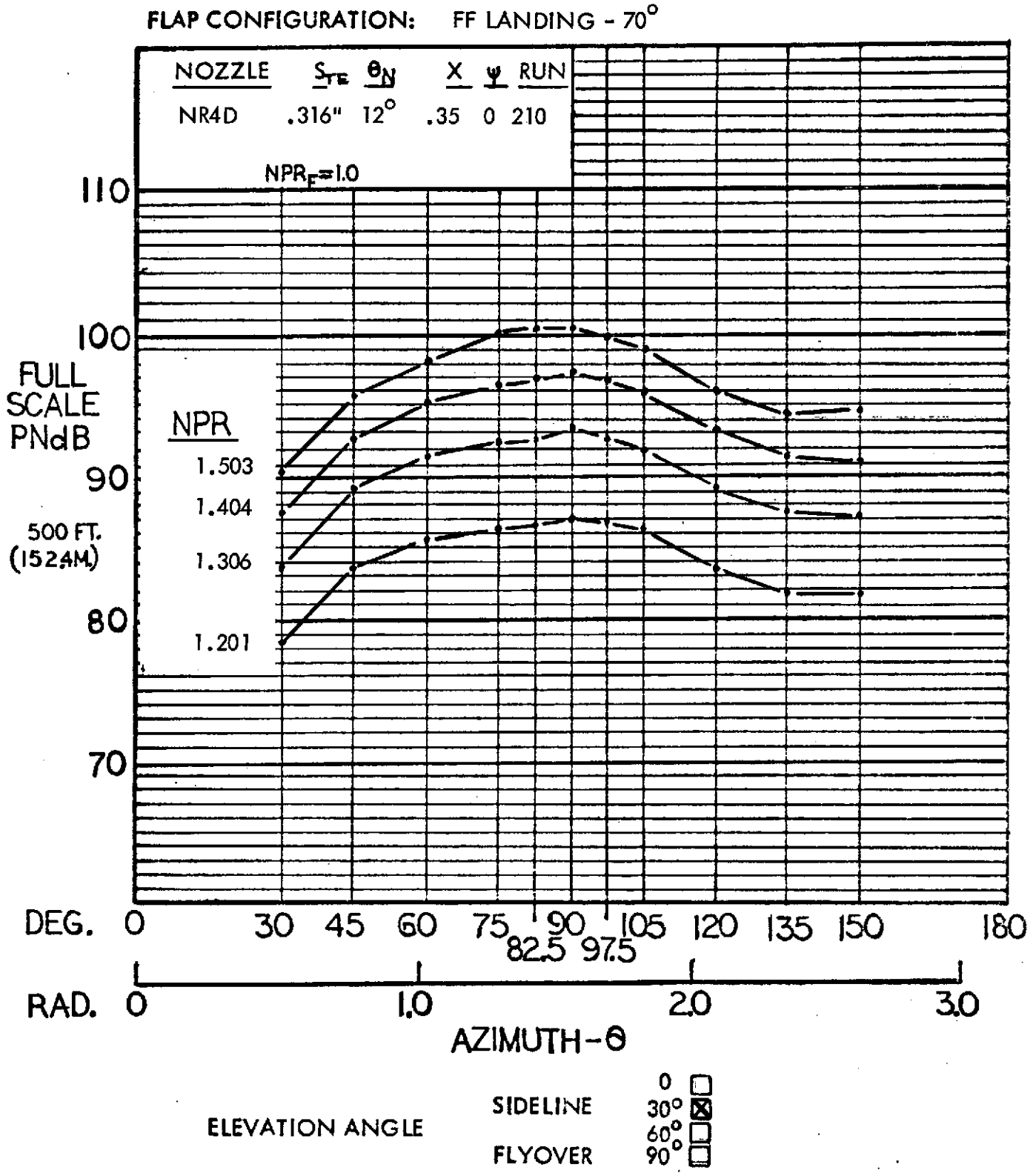

Figure 126 - Full scale sideline PNL for the aspect ratio 4 nozzle with deflector and Flex Flap, USB only; 70° flap angle.

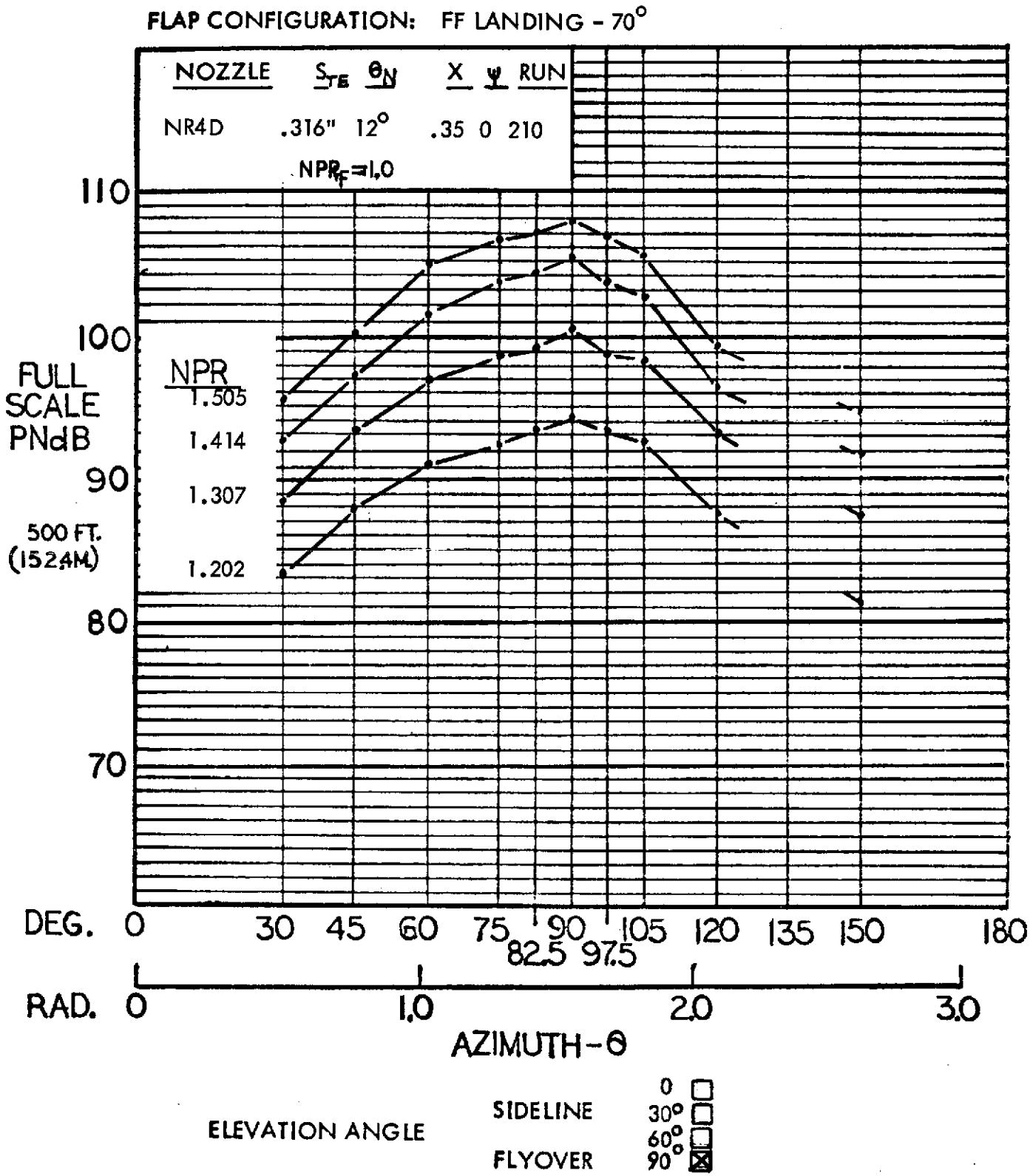

Figure 127 - Full scale flyover PNL for the aspect ratio 4 nozzle with deflector and Flex Flap, USB only; 70° flap angle.

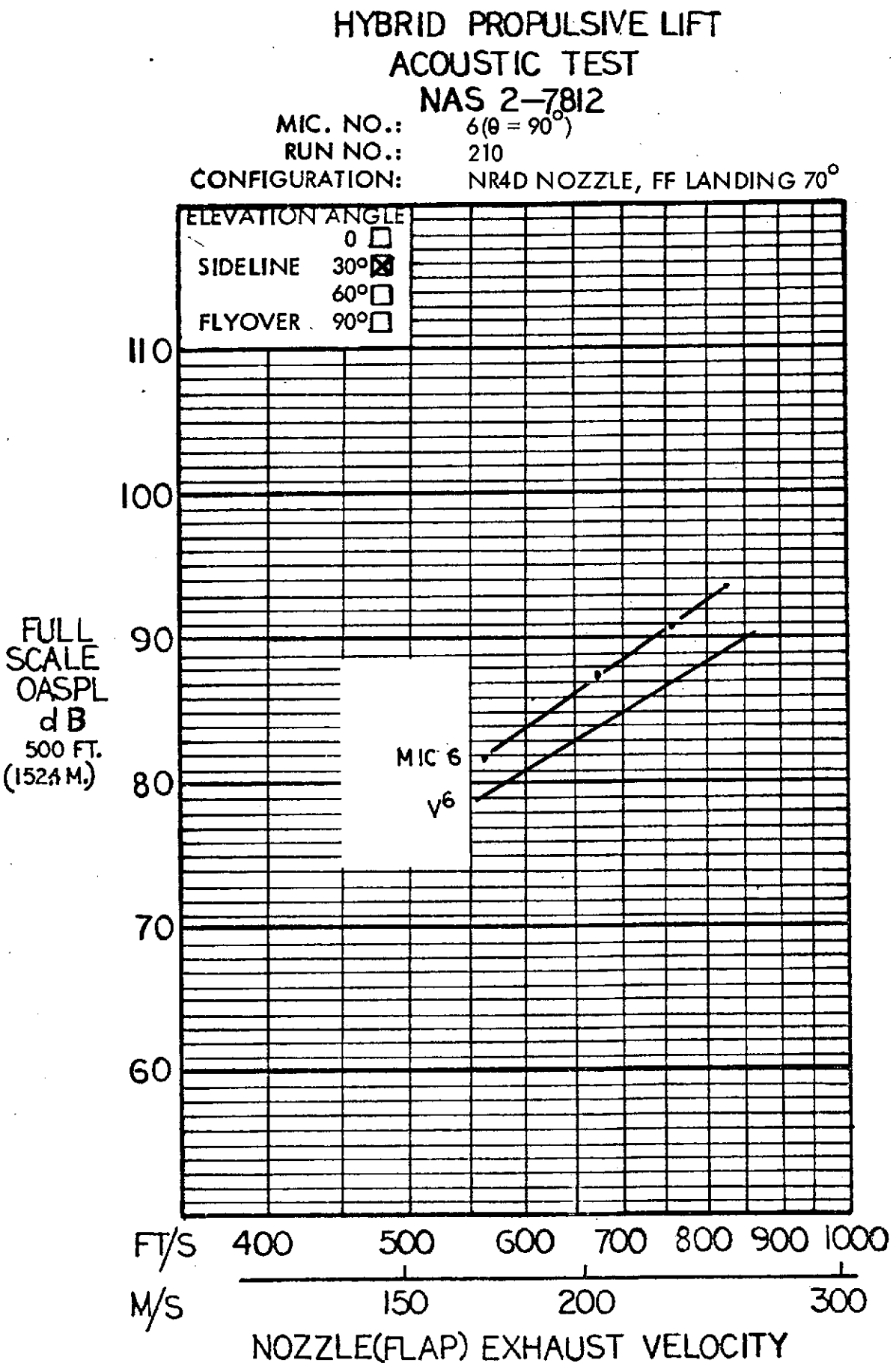

Figure 128 - Full scale sideline OASPL at 90° azimuth for the aspect ratio 4 nozzle with deflector and Flex Flap, USB only, 70° flap angle.

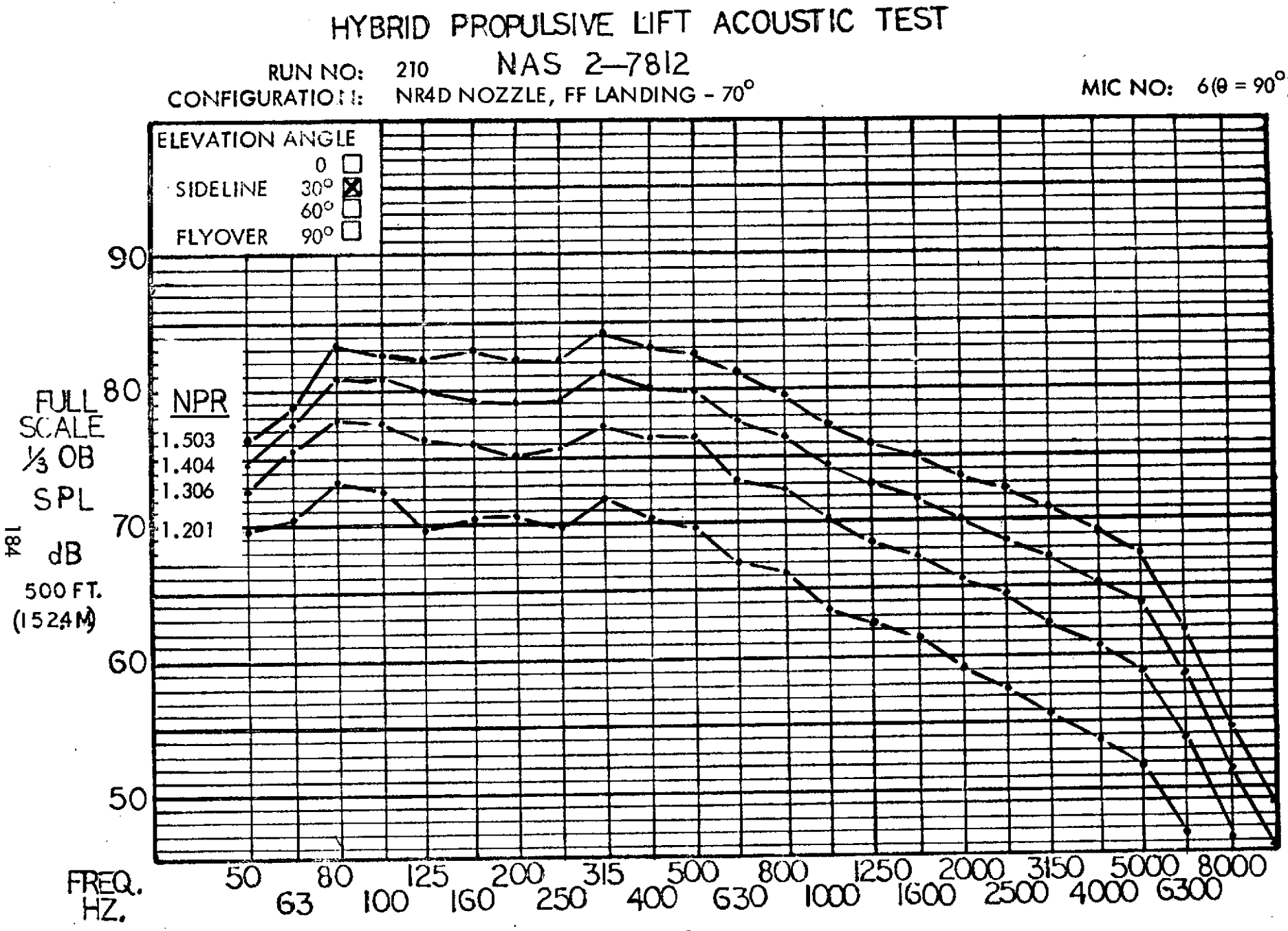

Figure 129 - Full scale sideline 1/3 OBSPL at 90° azimuth for the aspect ratio 4 nozzle with deflector and Flex Flap, USB only, 70° flap angle.

HYBRID PROPULSIVE LIFT
ACOUSTIC TEST
NAS 2-7812

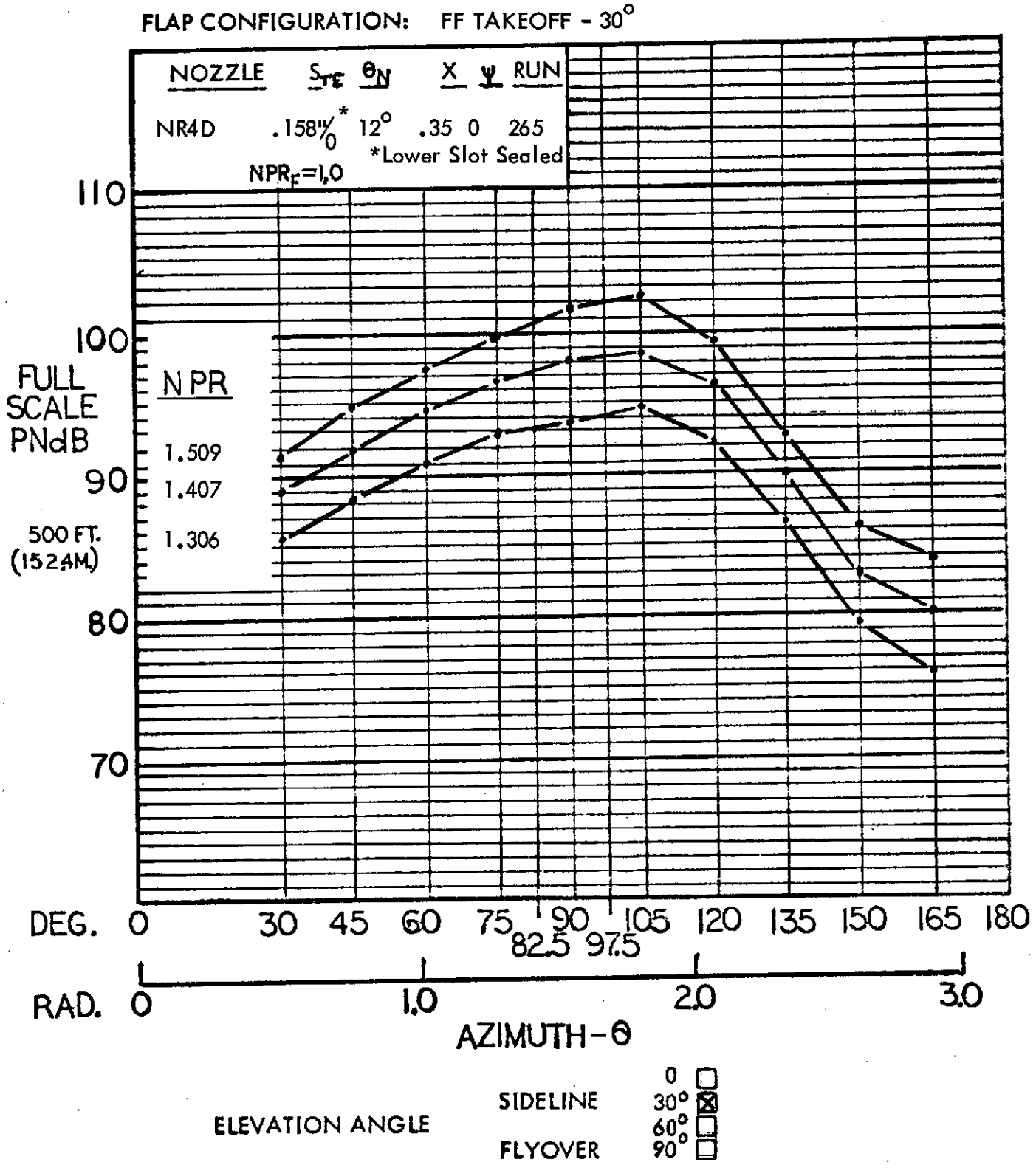

Figure 130 - Full scale sideline PNL for the aspect ratio 4 nozzle with deflector and Flex Flap, USB only, 30° flap angle.

HYBRID PROPULSIVE LIFT
ACOUSTIC TEST
NAS 2-7812

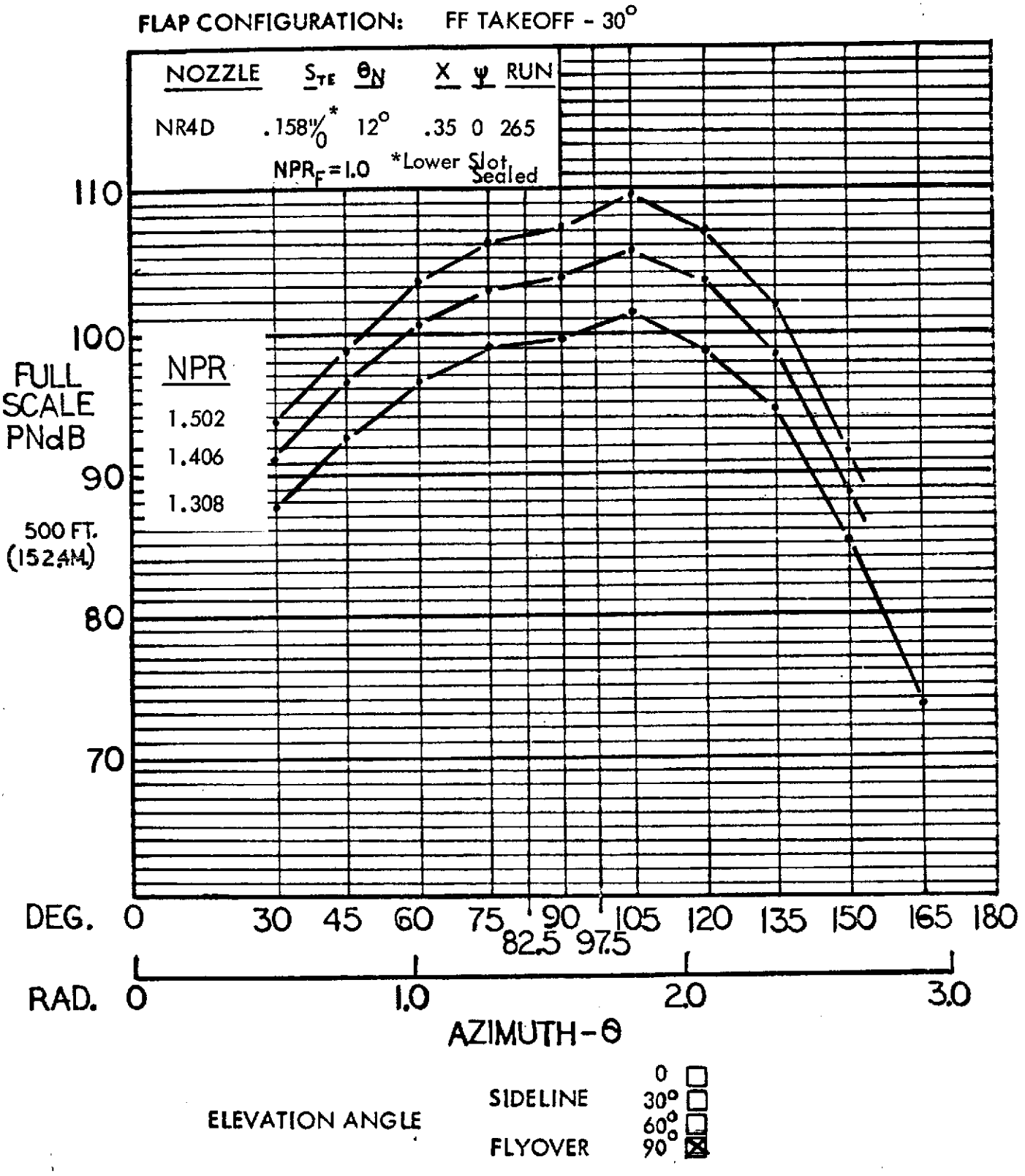

Figure 131 - Full scale flyover PNL for the aspect ratio 4 nozzle with deflector and Flex Flap, USB only, 30° flap angle.

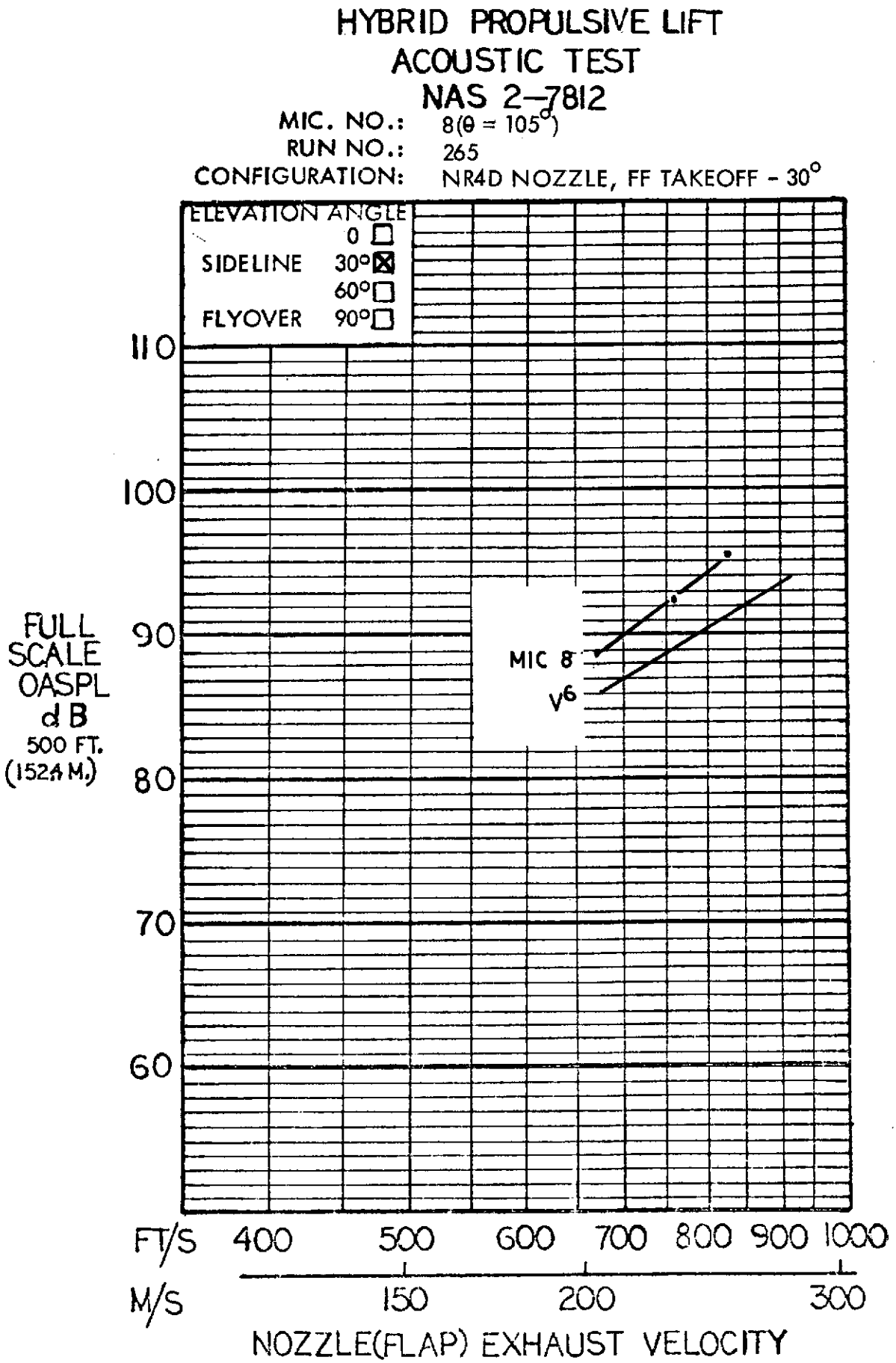

Figure 132 - Full scale sideline OASPL at 105° azimuth for the aspect ratio 4 nozzle with deflector and Flex Flap, USB only, 30° flap angle.

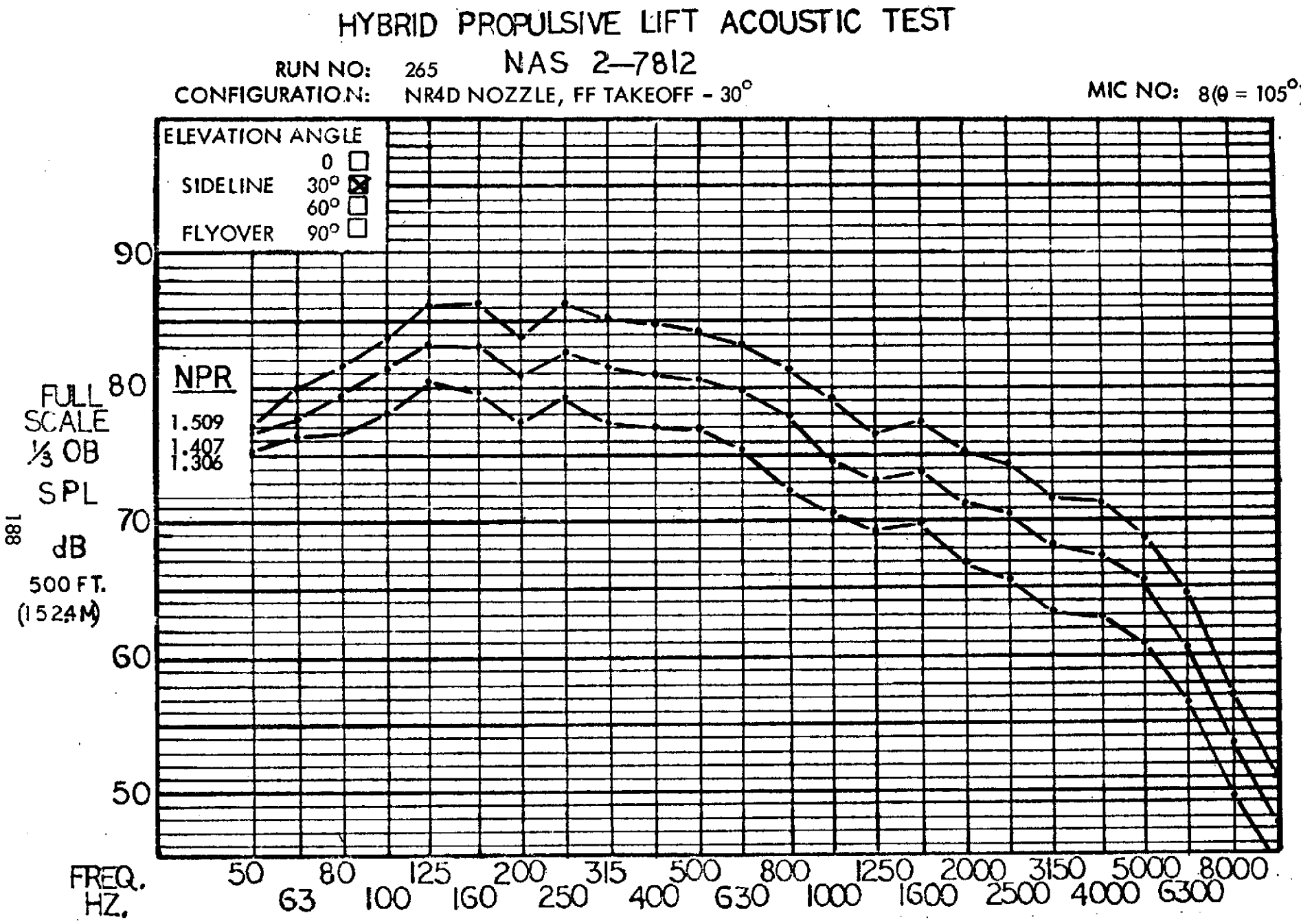

Figure 133 - Full scale sideline 1/3 OBSPL at 105° azimuth for the aspect ratio 4 nozzle with deflector and Flex Flap, USB only; 30° flap angle.

HYBRID PROPULSIVE LIFT
ACOUSTIC TEST
NAS 2-7812

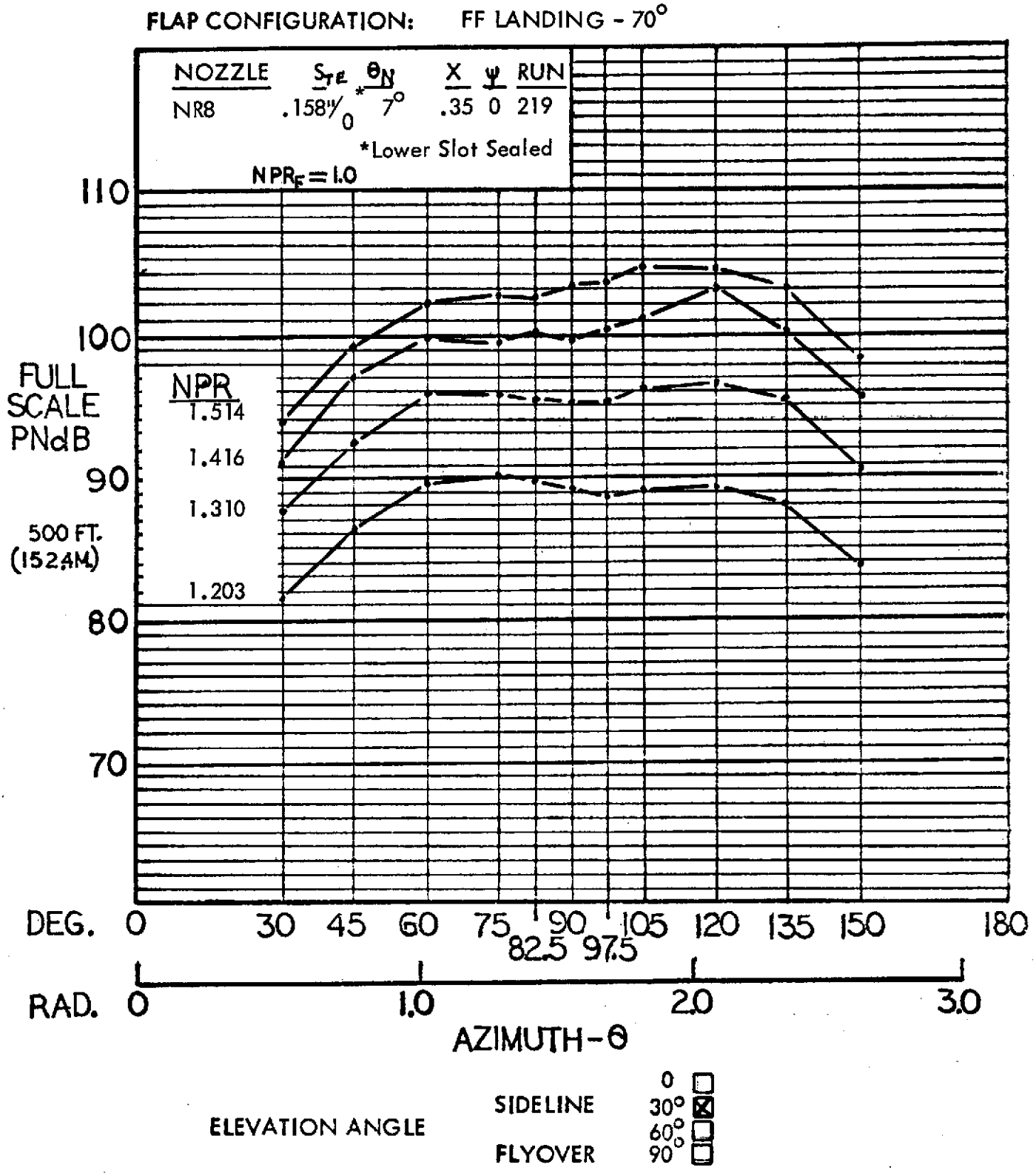

Figure 134 - Full scale sideline PNL for the aspect ratio 8 nozzle and Flex Flap, USB only; 70° flap angle.

HYBRID PROPULSIVE LIFT
ACOUSTIC TEST
NAS 2-7812

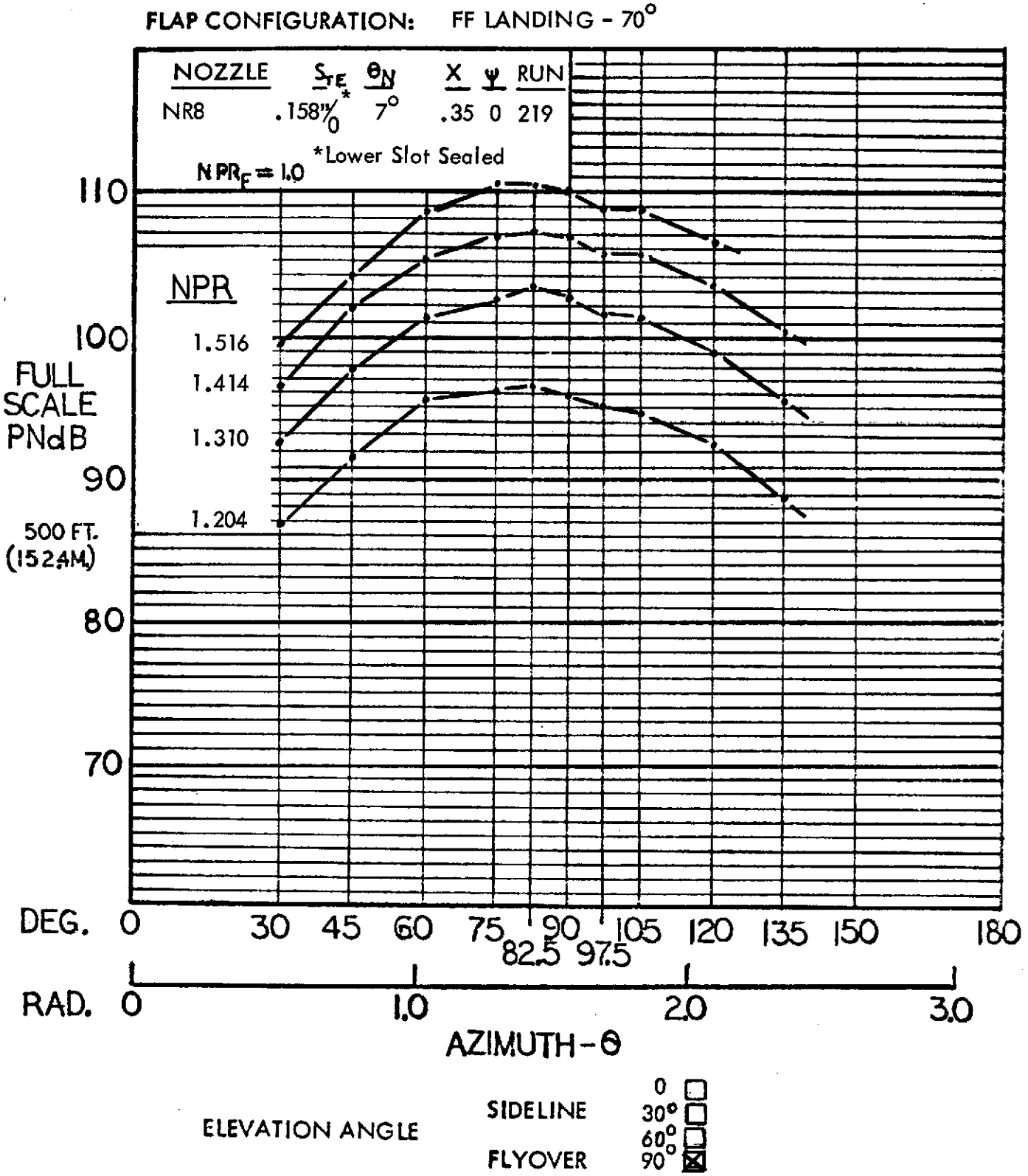

Figure 135 - Full scale flyover PNL for the aspect ratio 8 nozzle and Flex Flap, USB only; 70° flap angle.

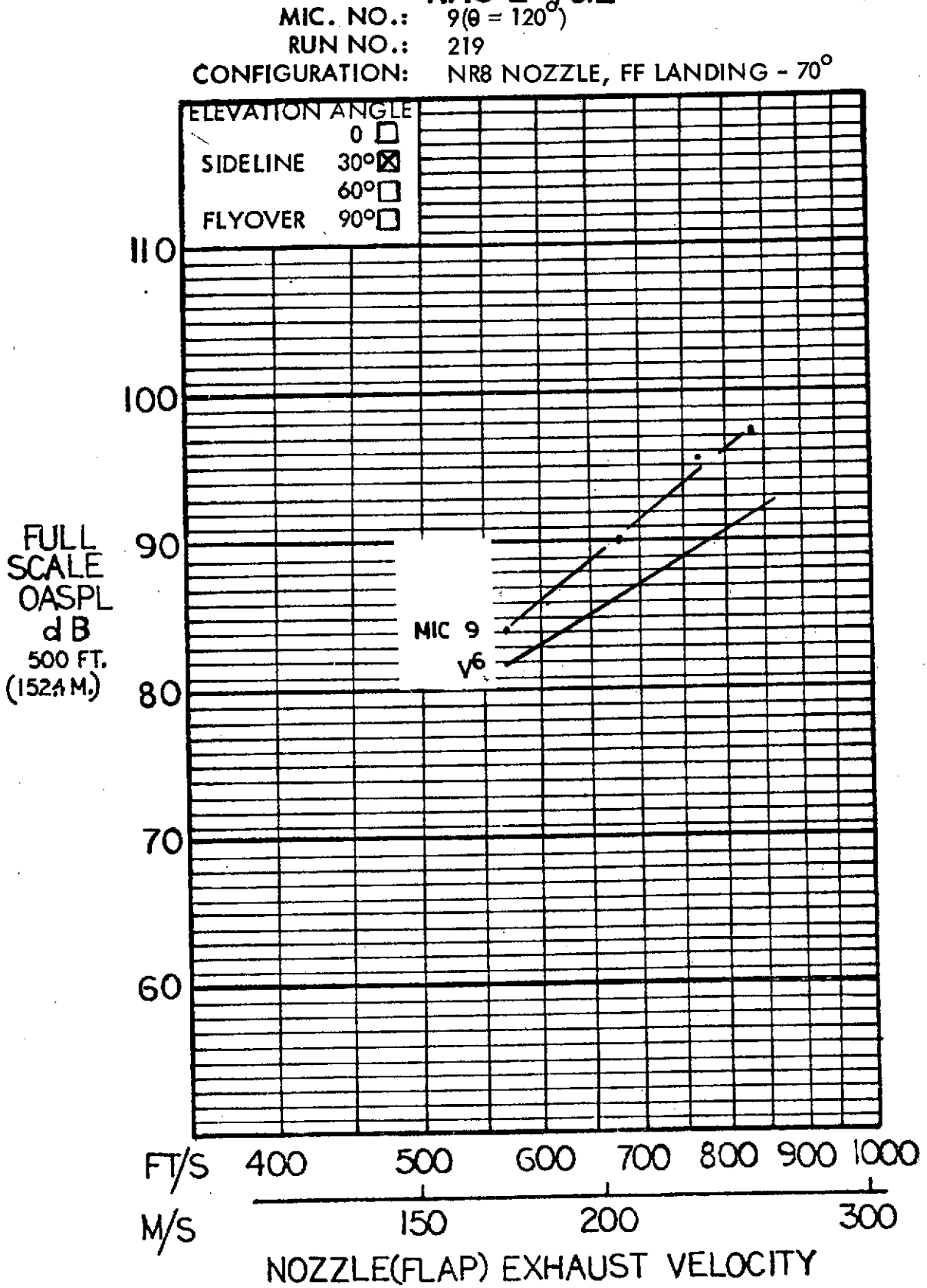

Figure 136 - Full scale sideline OASPL at 120° azimuth for the aspect ratio 8 nozzle and Flex Flap; USB only, 70° flap angle.

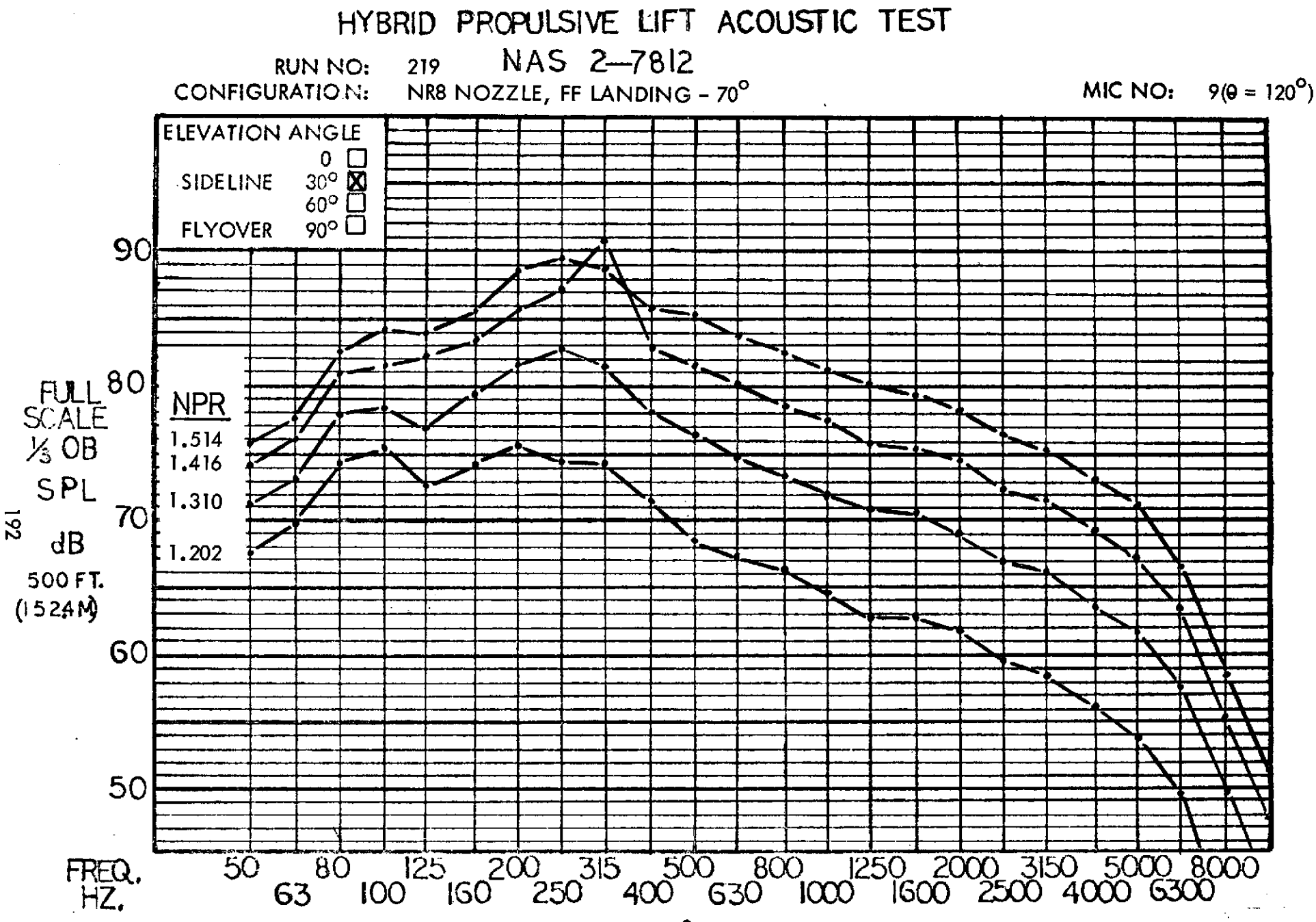

Figure 137 - Full scale sideline 1/3 OBSPL at 120° azimuth for the aspect ratio 8 nozzle and Flex Flap, USB only; 70° flap angle.

HYBRID PROPULSIVE LIFT
ACOUSTIC TEST
NAS 2-7812

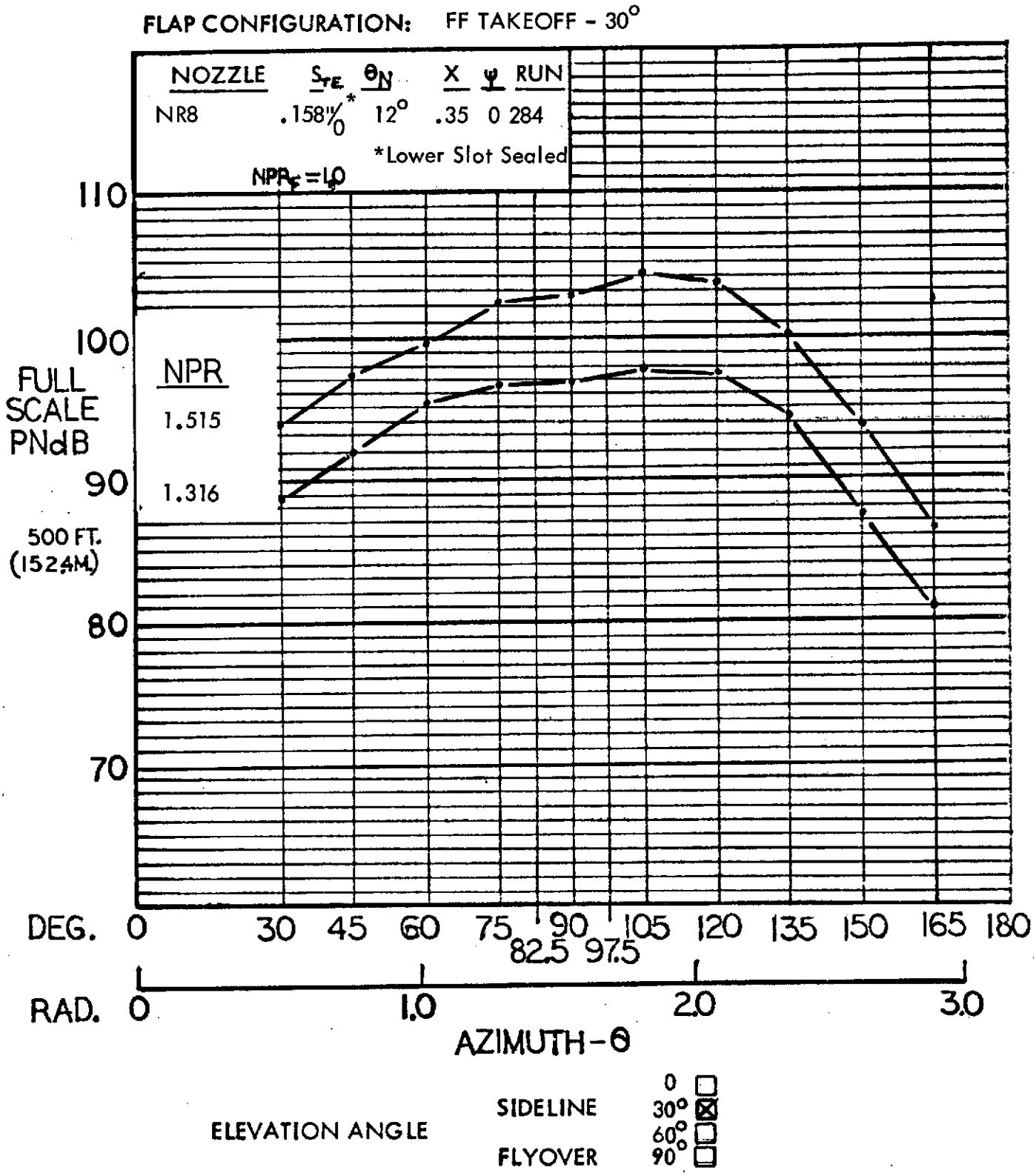

Figure 138 - Full scale sideline PNL for the aspect ratio 8 nozzle and Flex Flap, USB only, 30° flap angle.

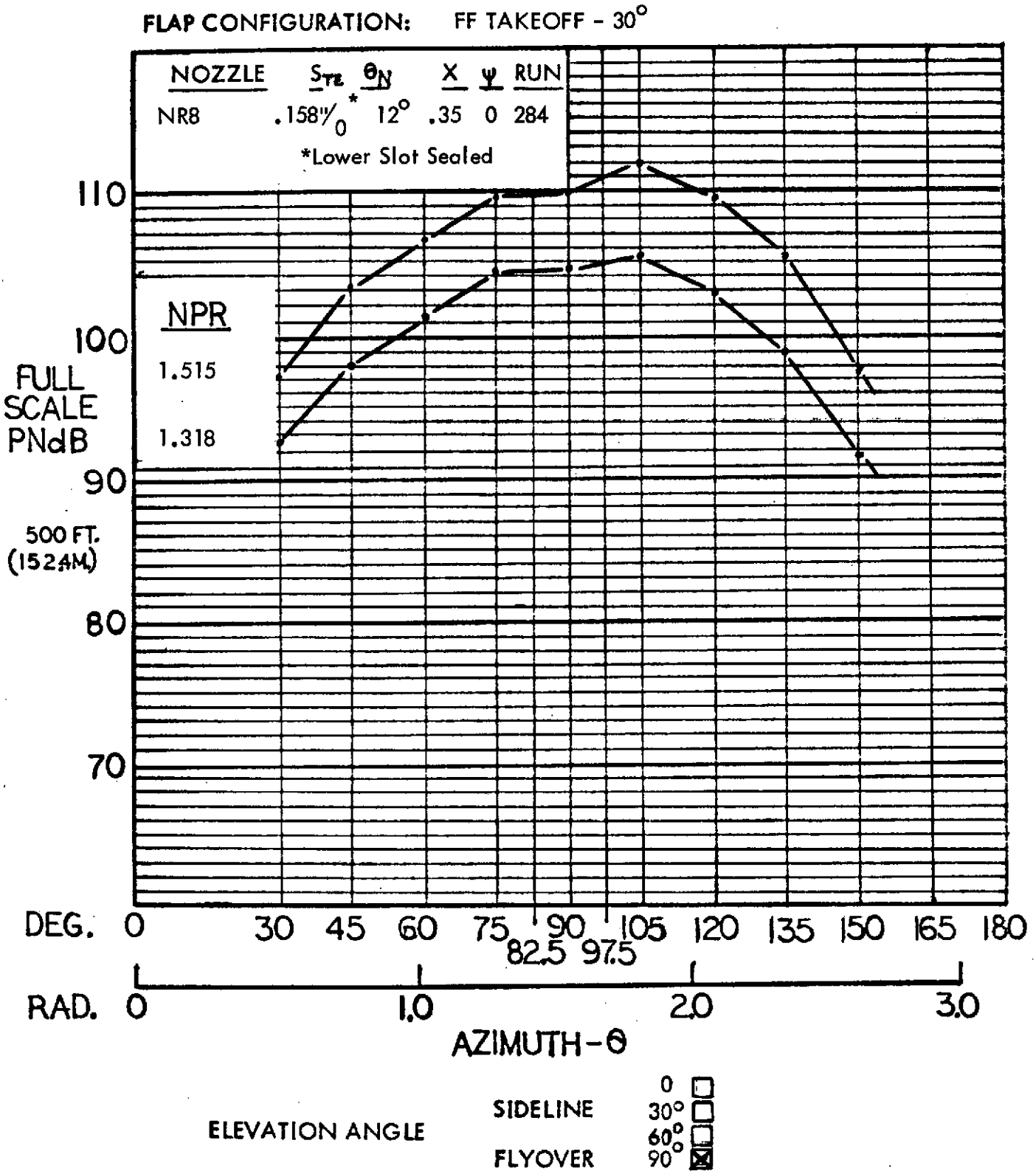

Figure 139 - Full scale flyover PNL for the aspect ratio 8 nozzle and Flex Flap, USB only, 30° flap angle.

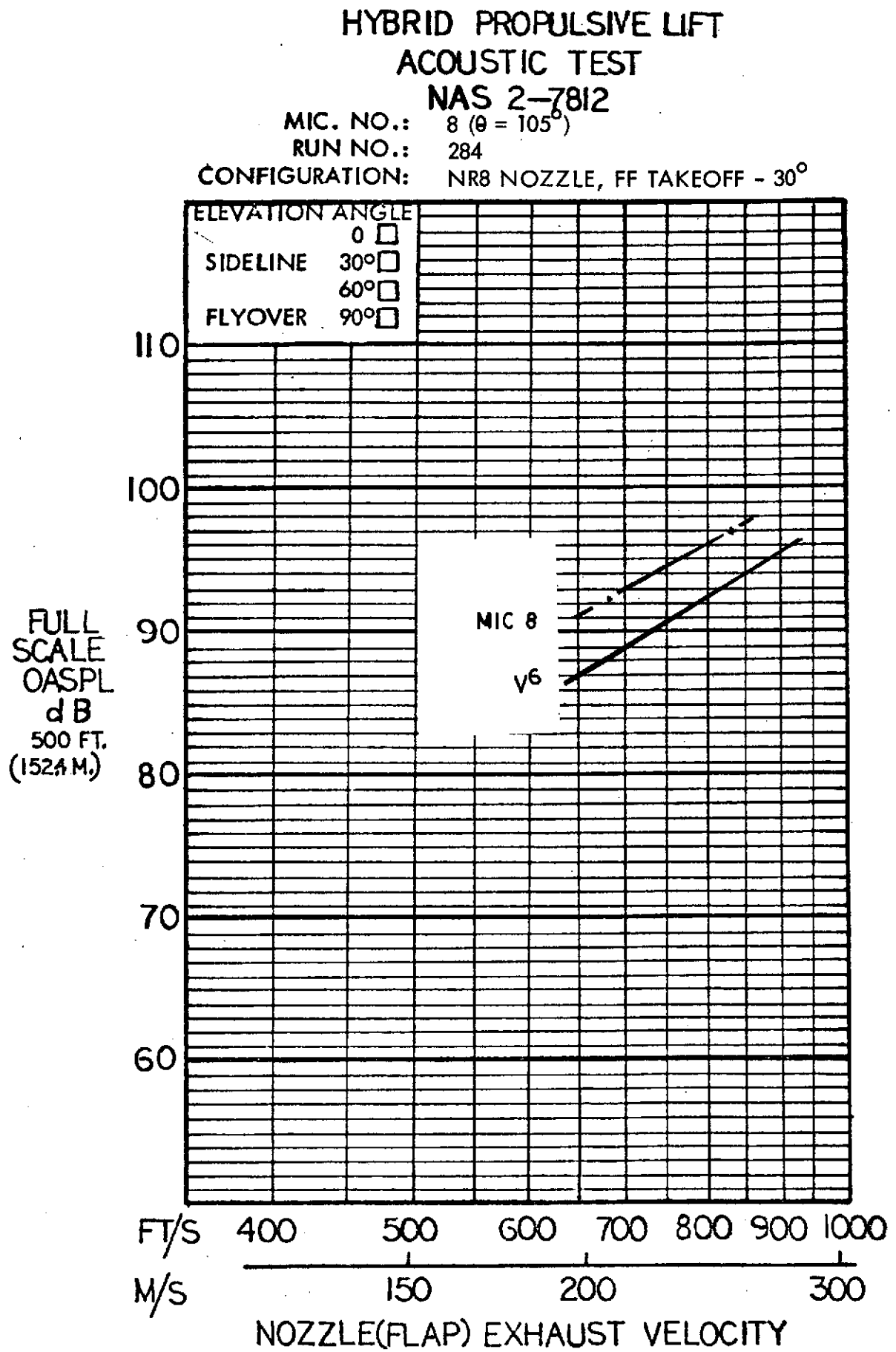

Figure 140 - Full scale sideline OASPL at 105° azimuth for the aspect ratio 8 nozzle and Flex Flap, USB only; 30° flap angle.

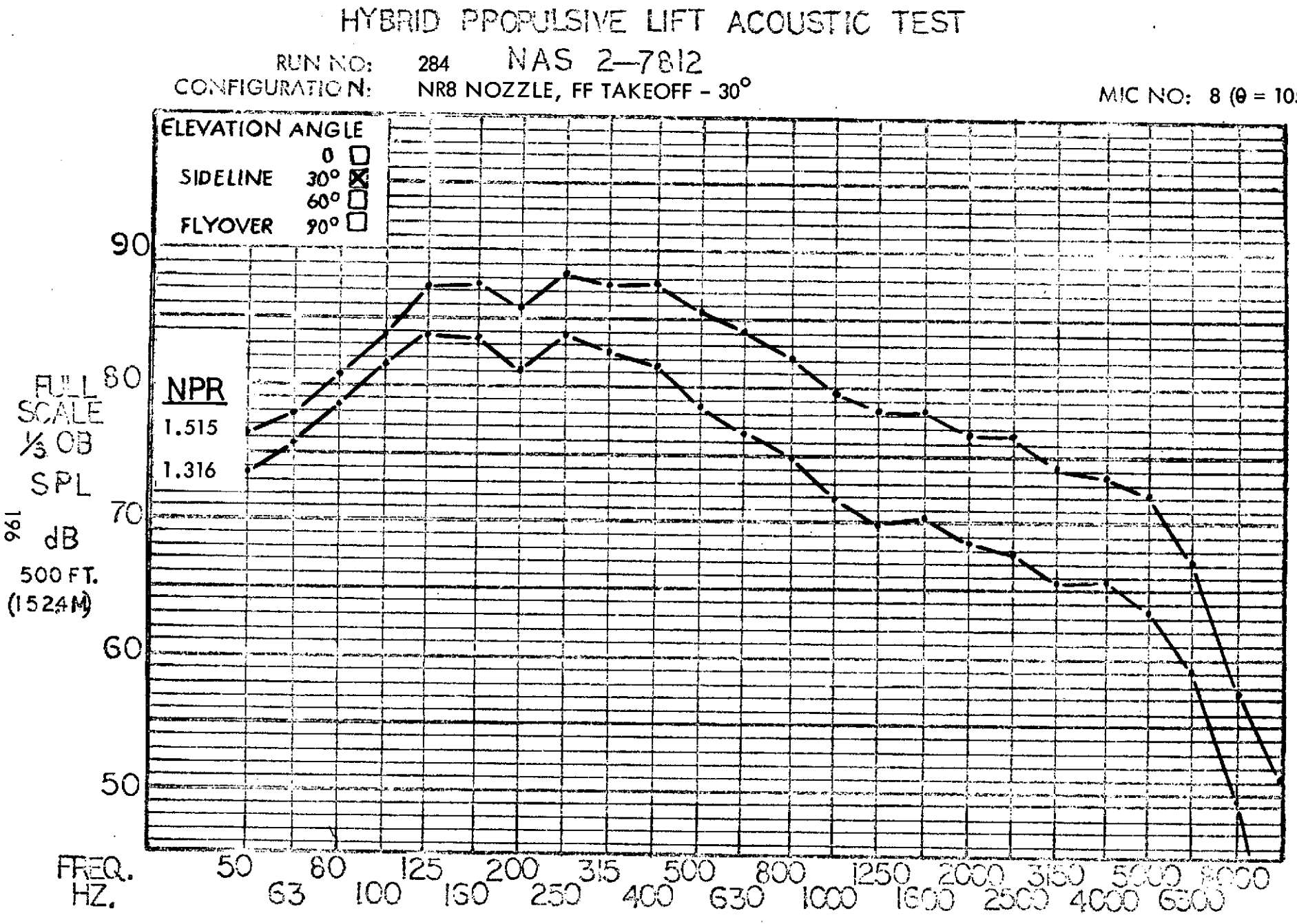

Figure 141 – Full scale sideline 1/3 OBSPL at 105° azimuth for the aspect ratio 8 nozzle and Flex Flap, USB only; 70° flap only.

HYBRID PROPULSIVE LIFT
ACOUSTIC TEST
NAS 2-7812

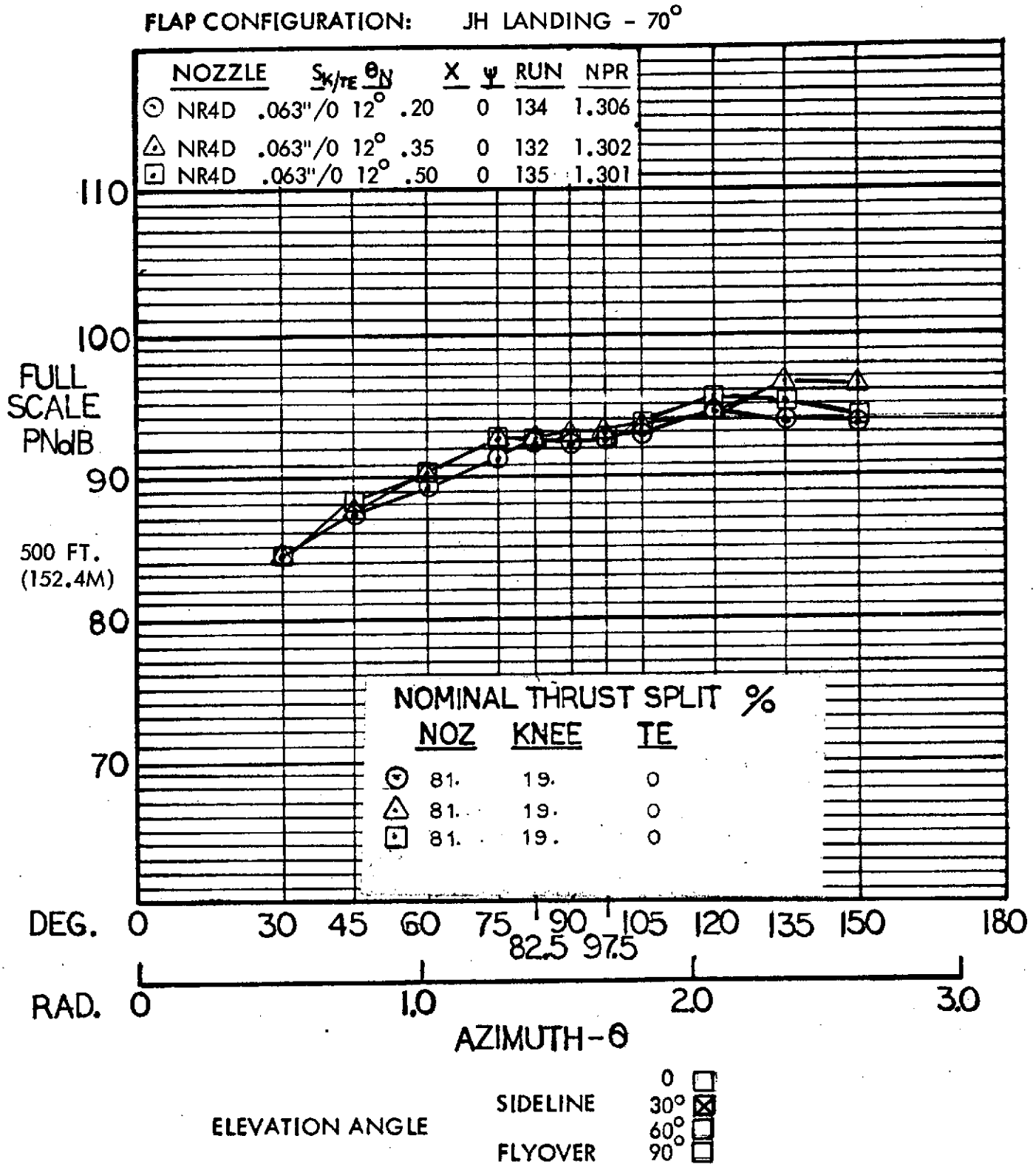

Figure 142 Full scale sideline PNL; comparison of three nozzle longitudinal positions, aspect ratio 4 nozzle with deflector and JH flap with knee blowing, 70° flap angle.

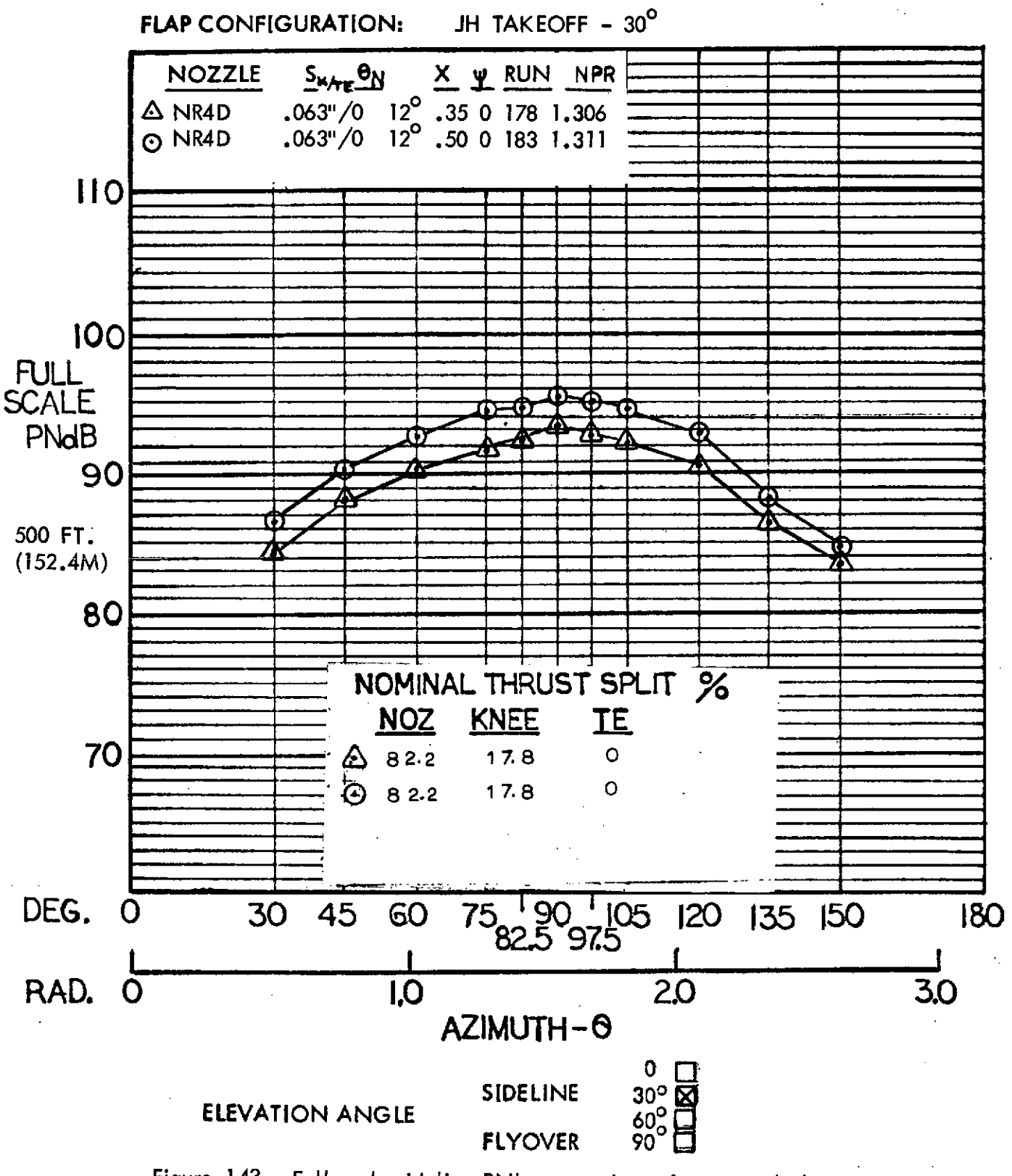

Figure 143 Full scale sideline PNL; comparison of two nozzle longitudinal positions, aspect ratio 4 nozzle with deflector and JH flap with knee blowing, 30° flap angle.

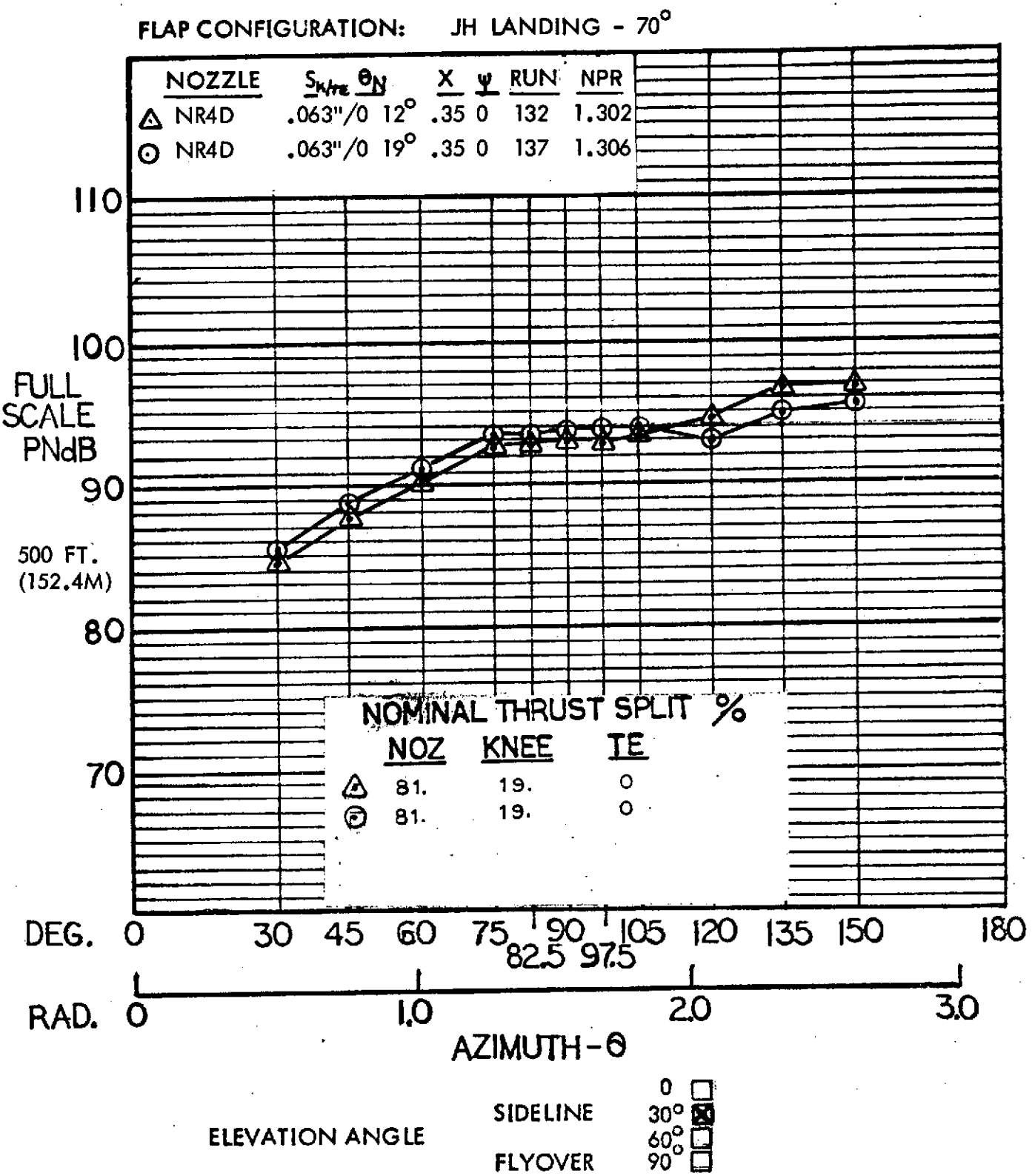

Figure 144 Full scale sideline PNL; comparison of two nozzle impingement angles, aspect ratio 4 nozzle with deflector, JH flap with knee blowing, 70° flap angle.

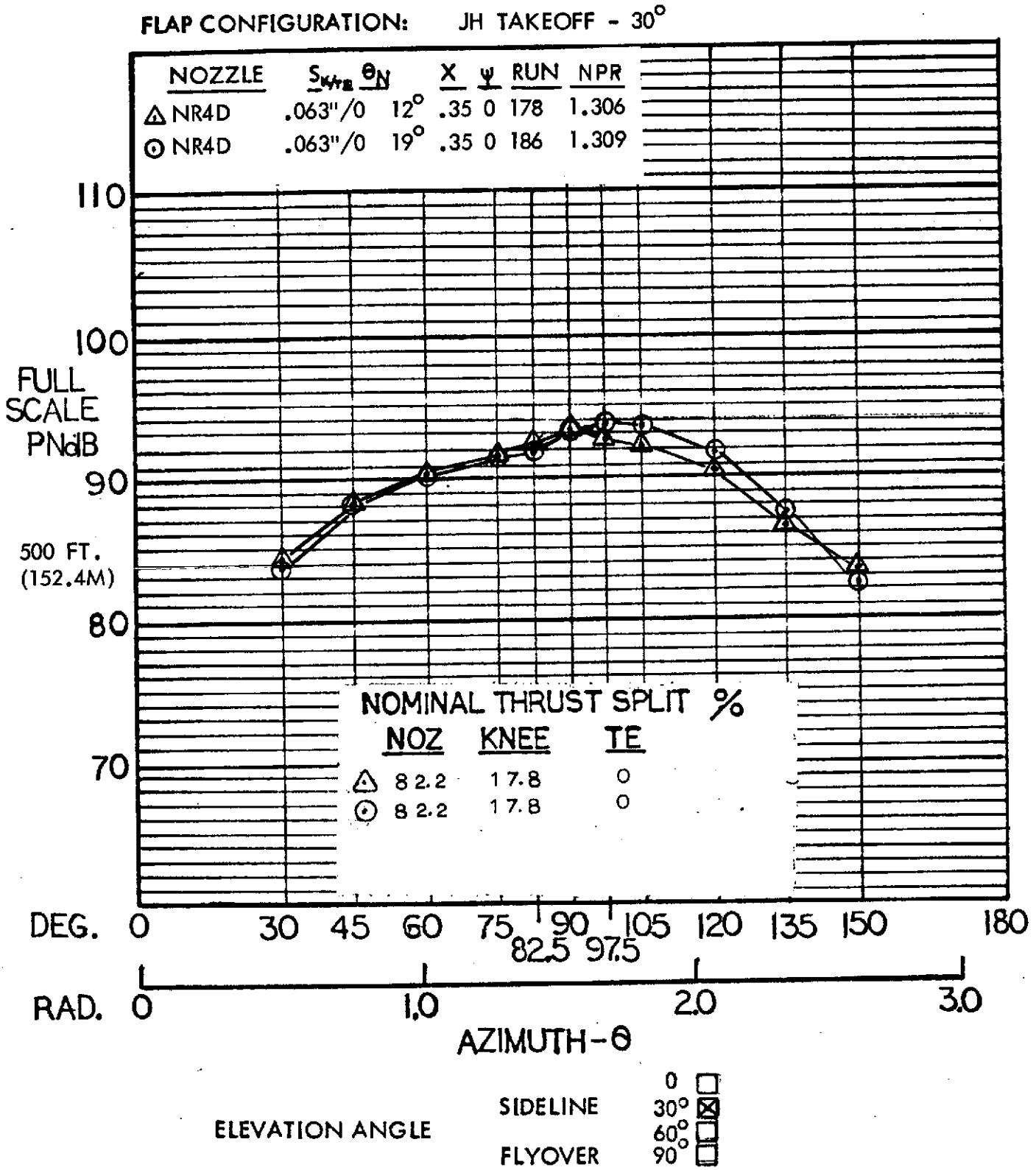

Figure 145 Full scale sideline PNL; comparison of two nozzle impingement angles, aspect ratio 4 nozzle with deflector, JH flap with knee blowing, 30° flap angle.

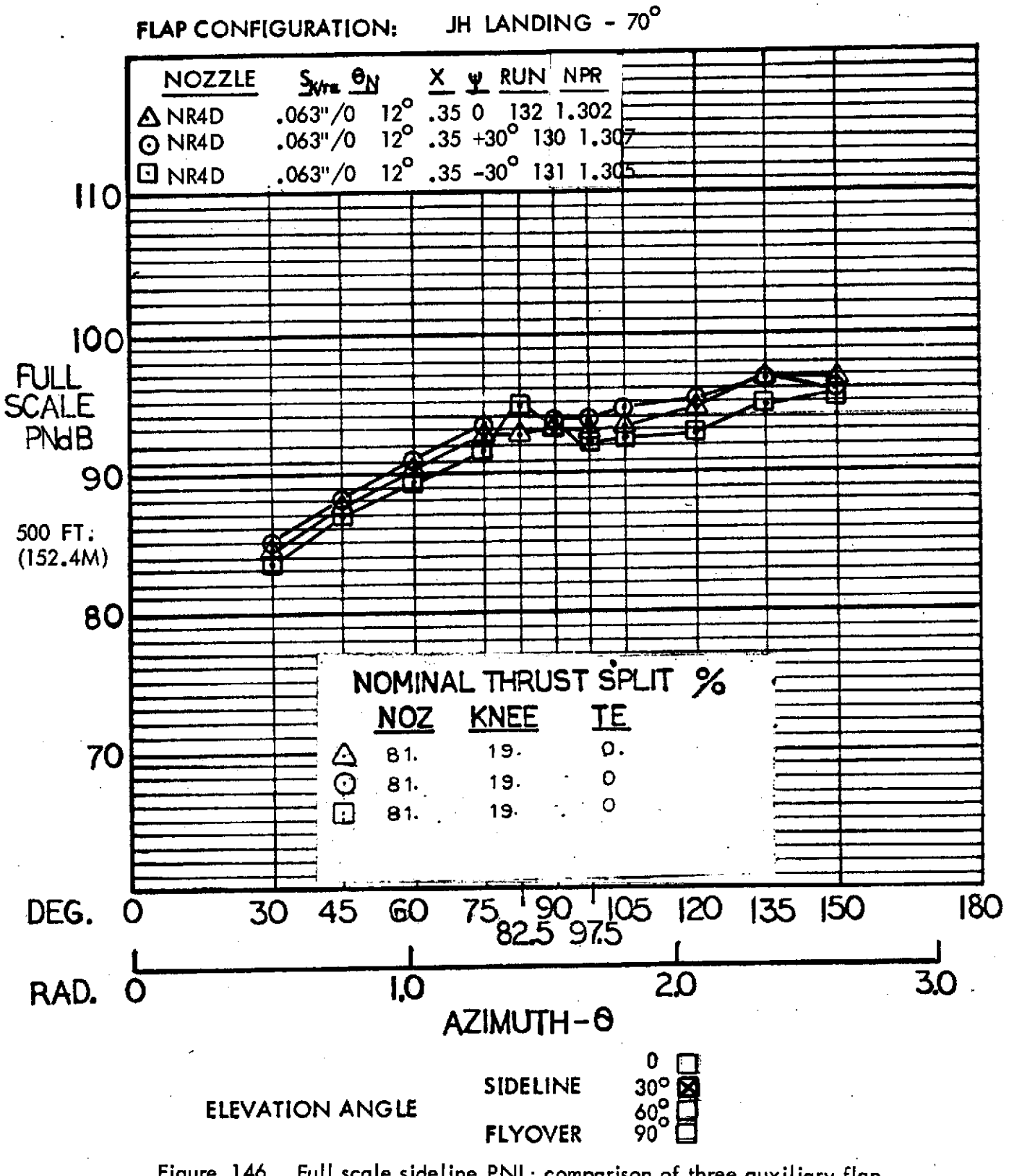

Figure 146 Full scale sideline PNL; comparison of three auxiliary flap angles, aspect ratio 4 nozzle with deflector, JH flap with knee blowing, 70° flap angle.

HYBRID PROPULSIVE LIFT
ACOUSTIC TEST
NAS 2-7812

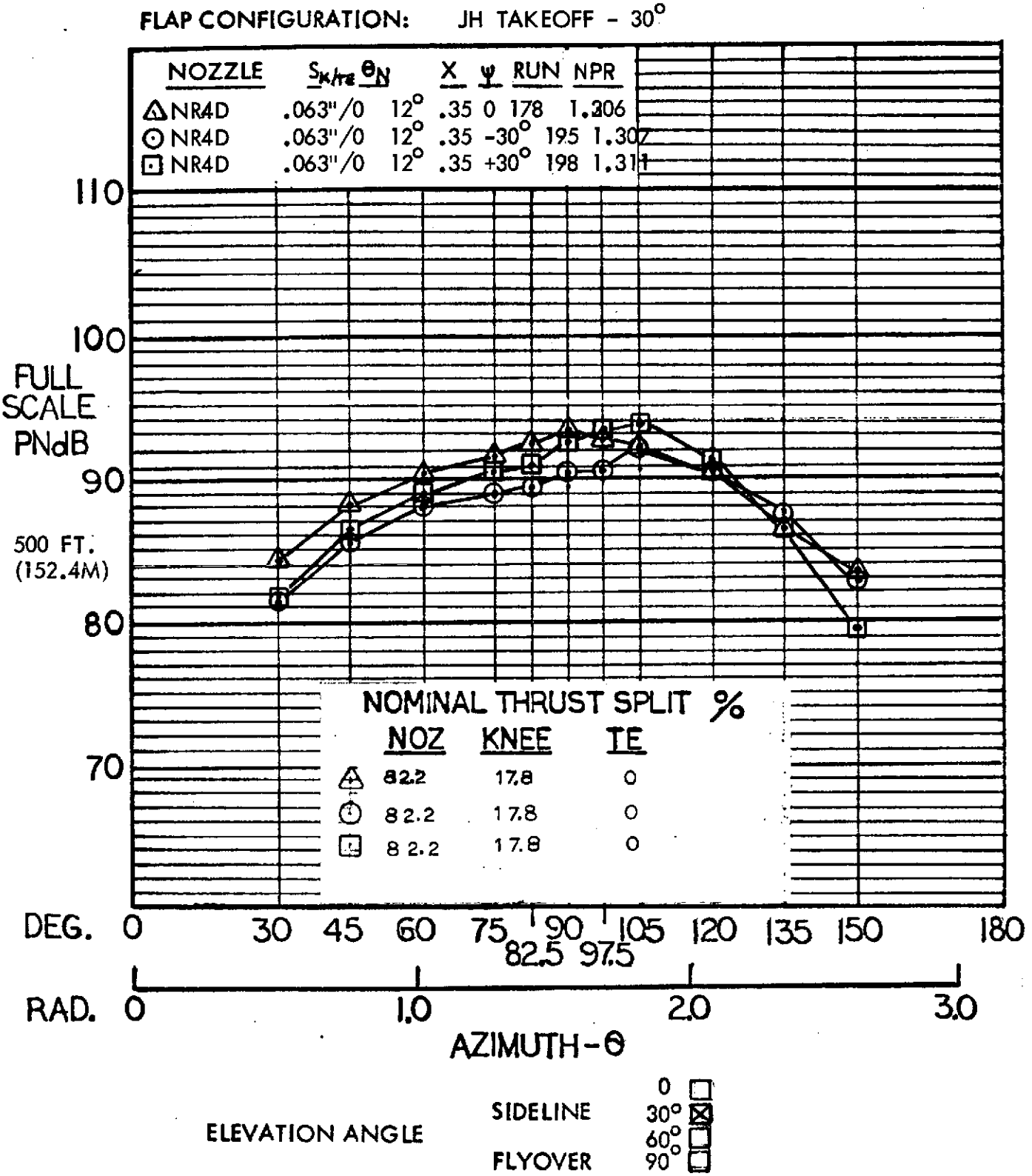

Figure 147 Full scale sideline PNL; comparison of three auxiliary flap angles, aspect ratio 4 nozzle with deflector, JH flap with knee blowing, 30° flap angle.

HYBRID PROPULSIVE LIFT
ACOUSTIC TEST
NAS 2-7812

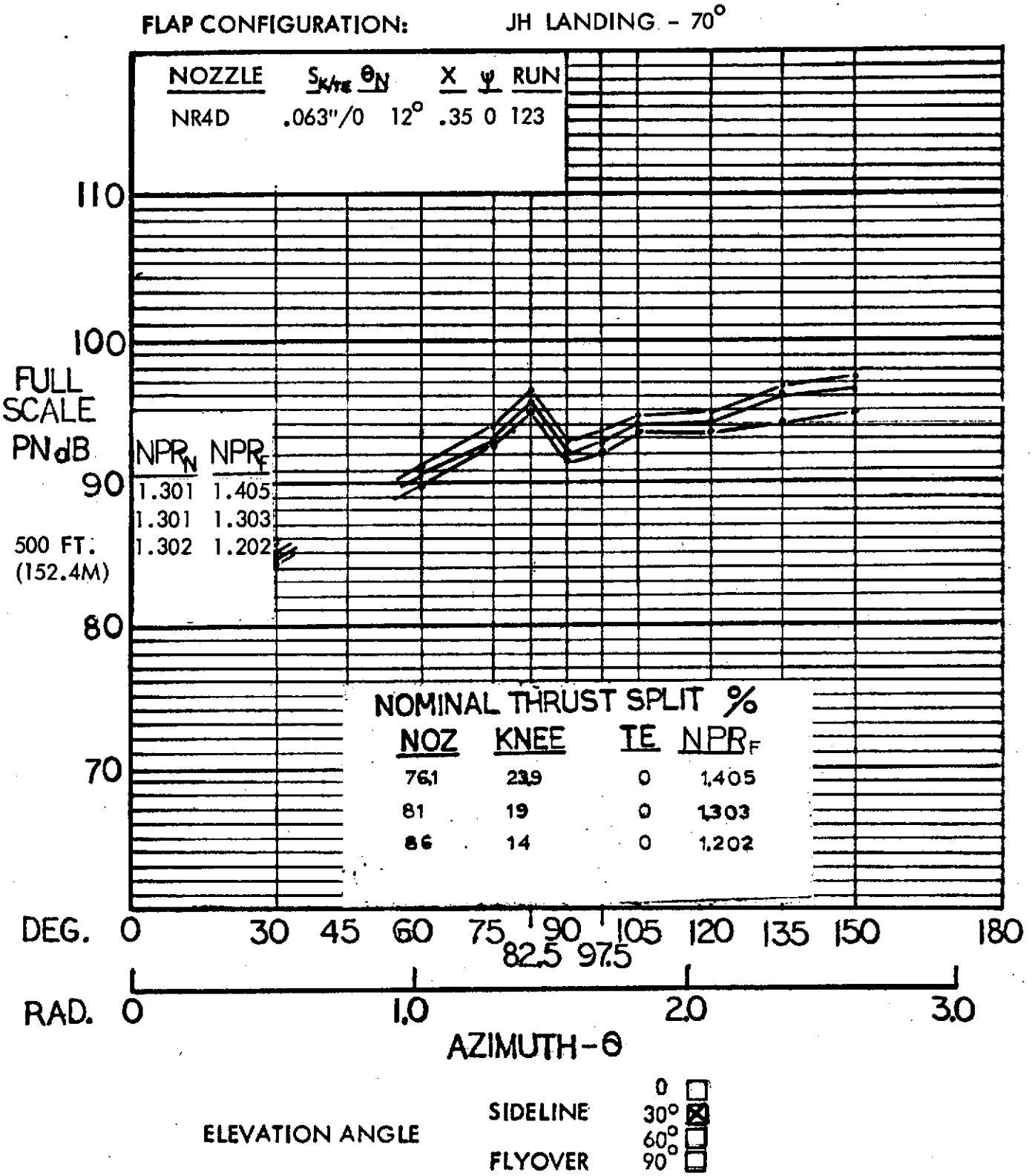

Figure 148 Full scale sideline PNL; variation of flap pressure ratio with constant nozzle pressure ratio, aspect ratio 4 nozzle with deflector, JH flap with knee blowing, 70° flap angle.

HYBRID PROPULSIVE LIFT
ACOUSTIC TEST
NAS 2-7812

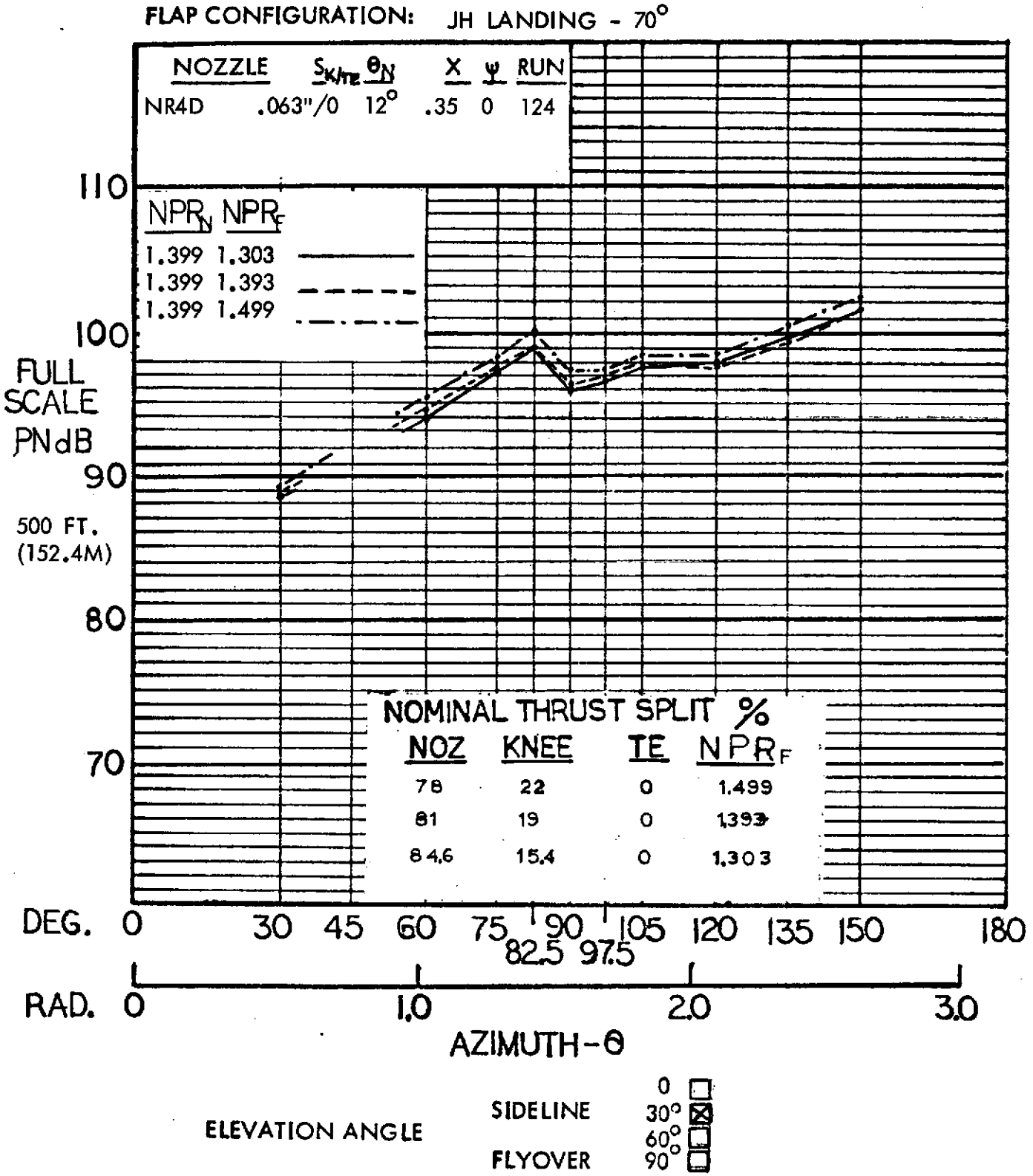

Figure 149 Full scale sideline PNL; variation of flap pressure ratio with constant nozzle pressure ratio, aspect ratio 4 nozzle with deflector, JH flap with knee blowing, 70° flap angle.

HYBRID PROPULSIVE LIFT
ACOUSTIC TEST
NAS 2-7812

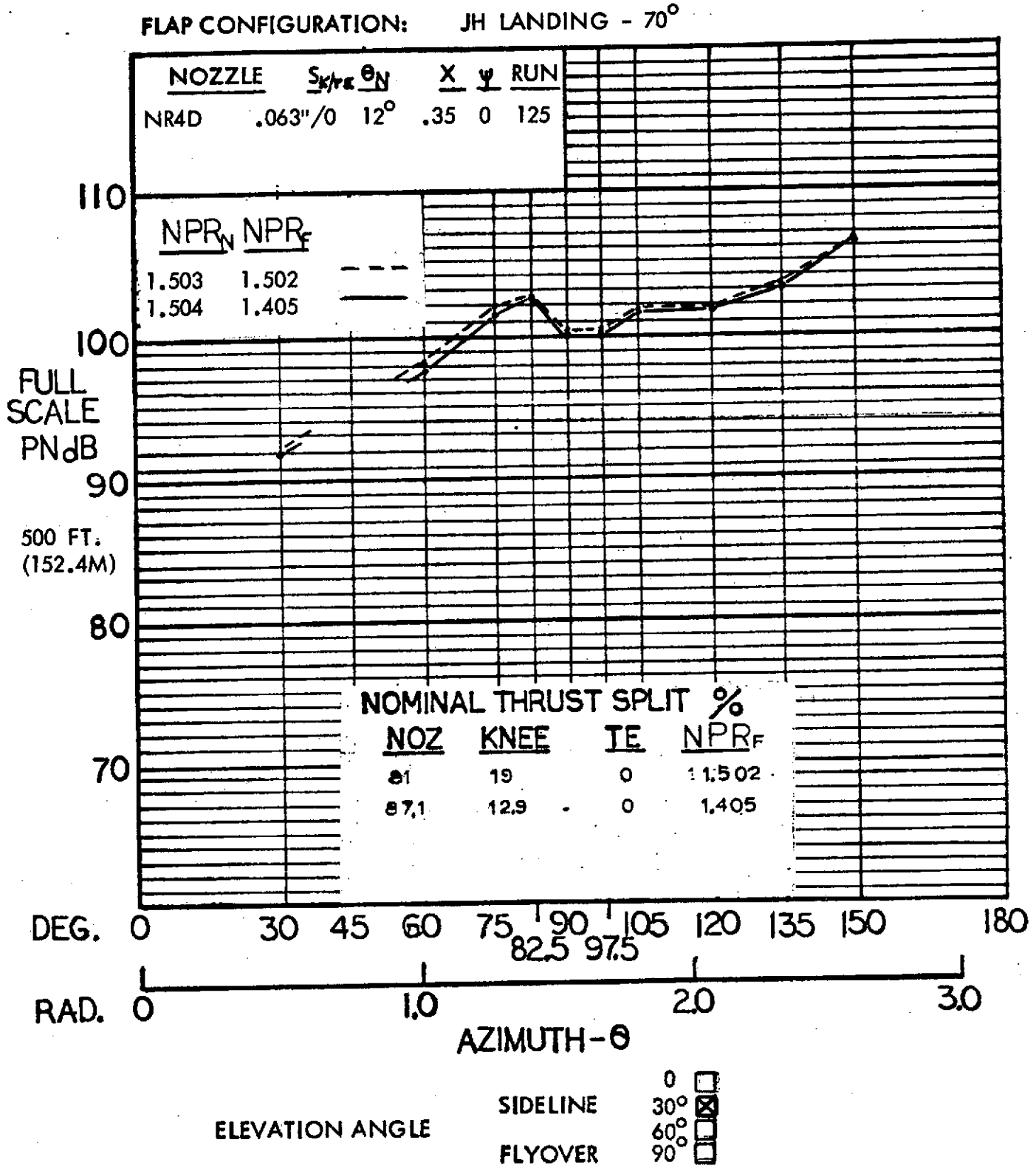

Figure 150 Full scale sideline PNL; variation of flap pressure ratio with constant nozzle pressure ratio, aspect ratio 4 nozzle with deflector, JH flap with knee blowing, 70° flap angle.

HYBRID PROPULSIVE LIFT
ACOUSTIC TEST
NAS 2-7812

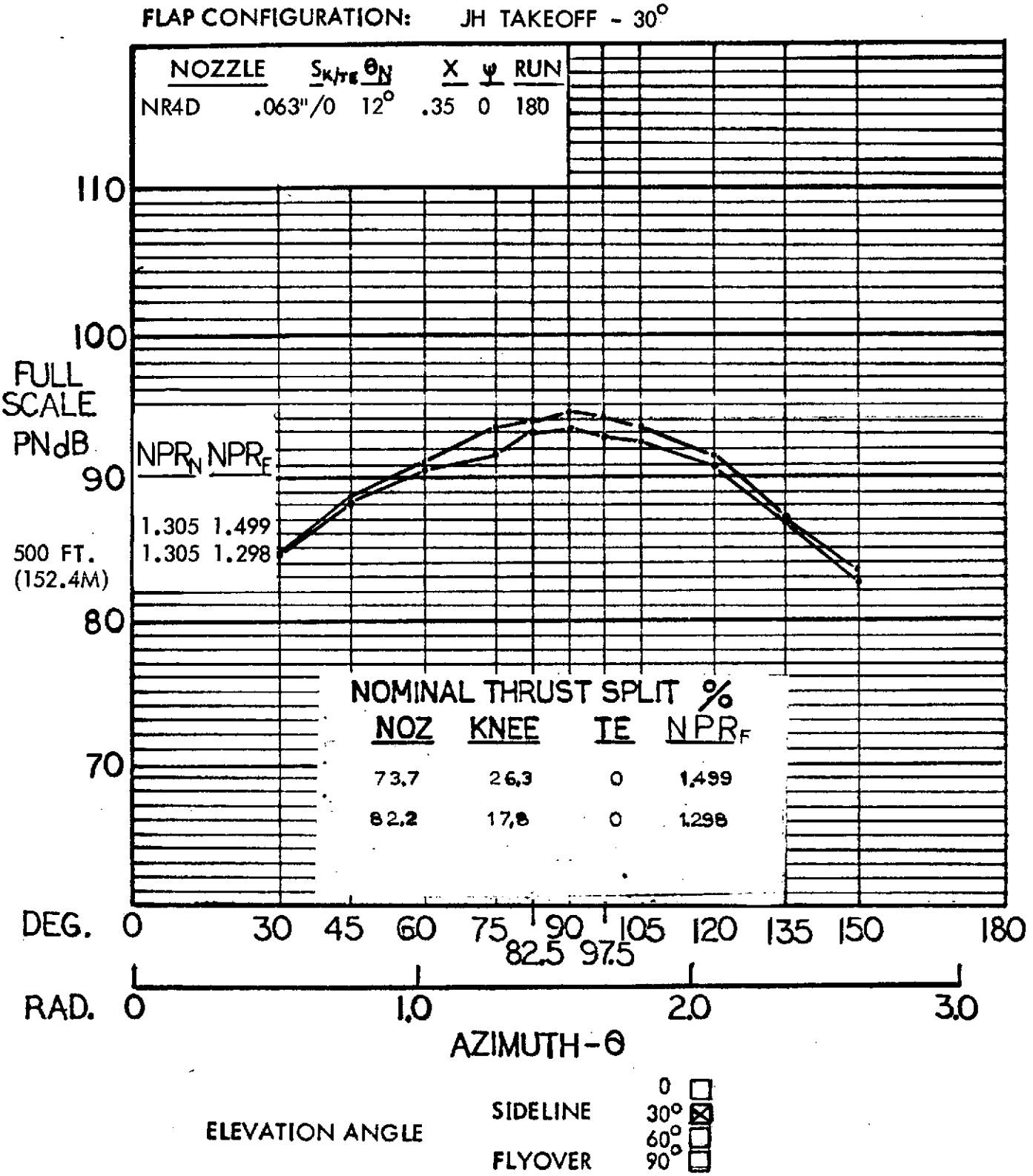

Figure 151 Full scale sideline PNL; variation of flap pressure ratio with constant nozzle pressure ratio, aspect ratio 4 nozzle with deflector, JH flap with knee blowing, 30° flap angle.

HYBRID PROPULSIVE LIFT
ACOUSTIC TEST
NAS 2-7812

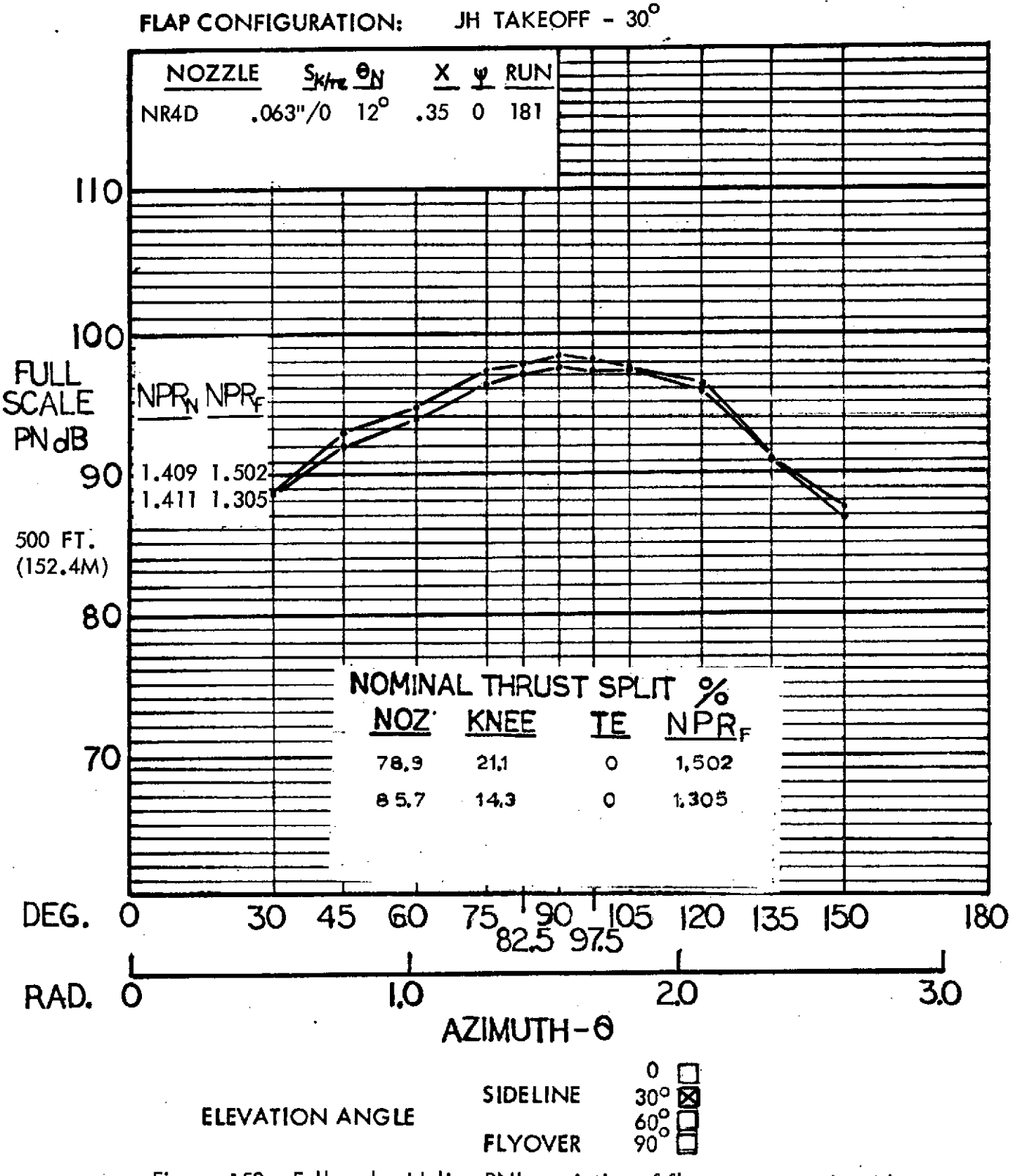

Figure 152 Full scale sideline PNL; variation of flap pressure ratio with constant nozzle pressure ratio, aspect ratio 4 nozzle with deflector, JH flap with knee blowing, 30° flap angle.

HYBRID PROPULSIVE LIFT
ACOUSTIC TEST
NAS 2-7812

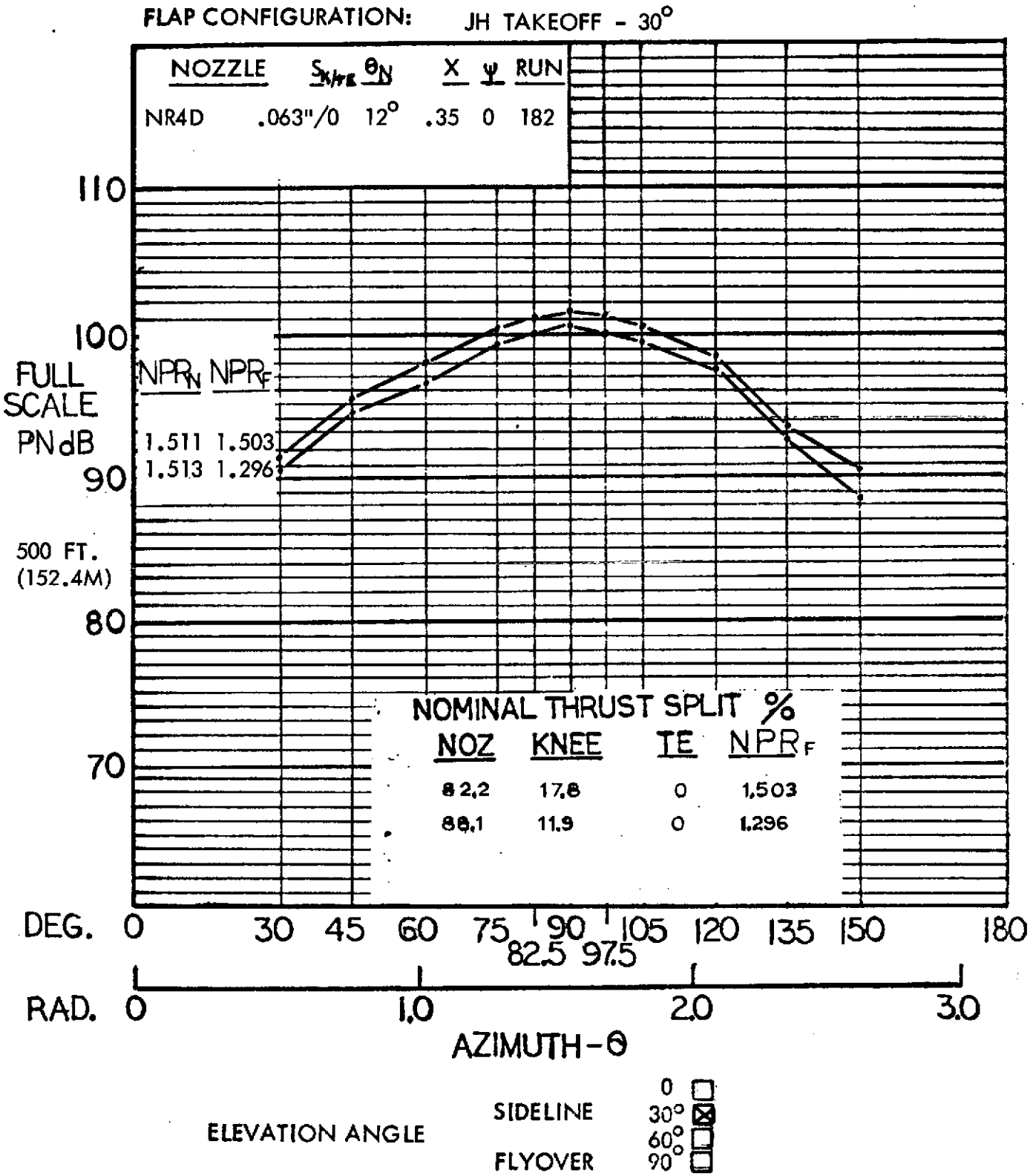

Figure 153 Full scale sideline PNL; variation of flap pressure ratio with constant nozzle pressure ratio, aspect ratio 4 nozzle with deflector, JH flap with knee blowing, 30° flap angle.

HYBRID PROPULSIVE LIFT
ACOUSTIC TEST
NAS 2-7812

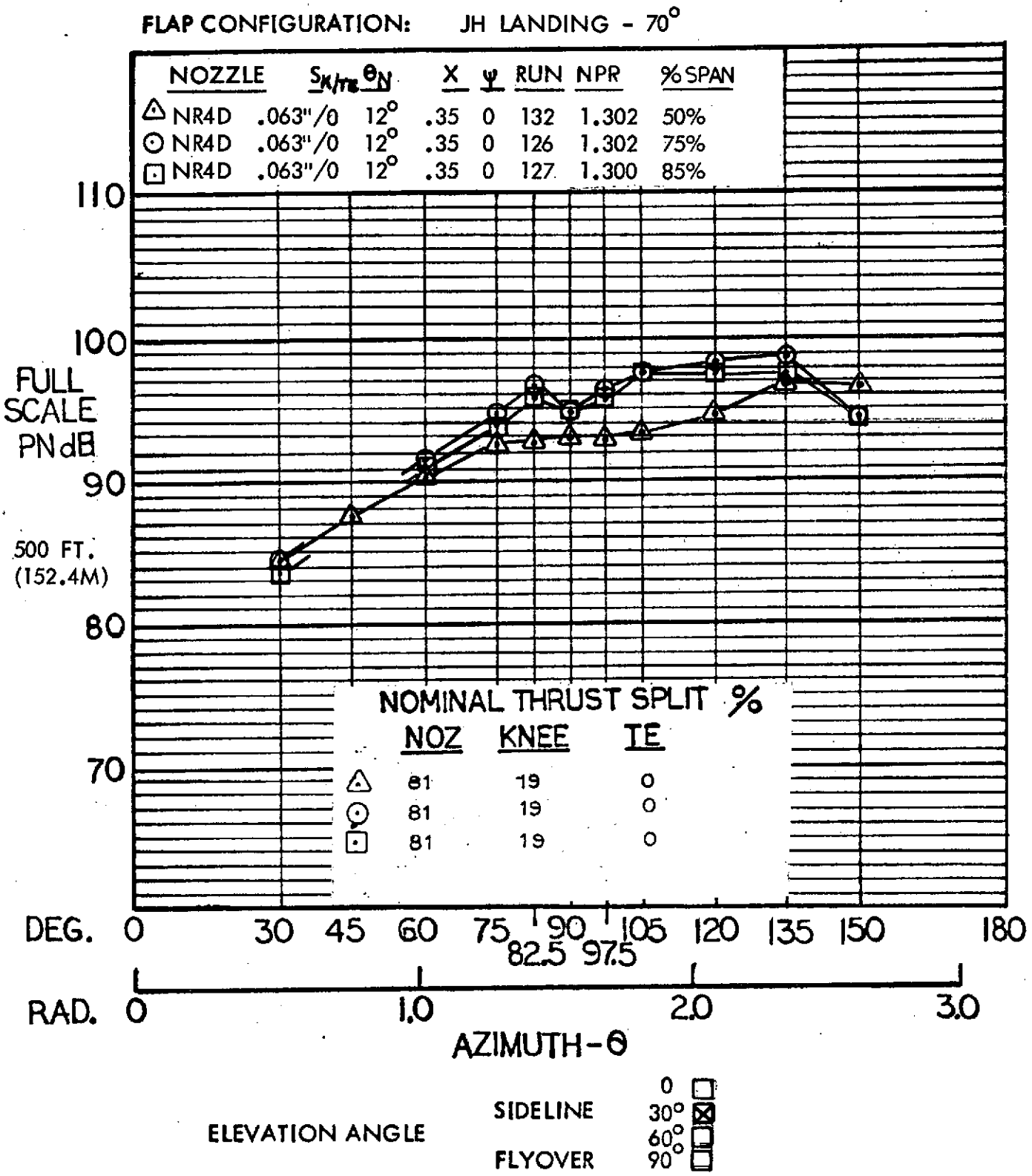

Figure 154 Full scale sideline PNL; comparison of three nozzle spanwise positions, aspect ratio 4 nozzle with deflector, JH flap with knee blowing, 70° flap angle.

HYBRID PROPULSIVE LIFT
ACOUSTIC TEST
NAS 2-7812

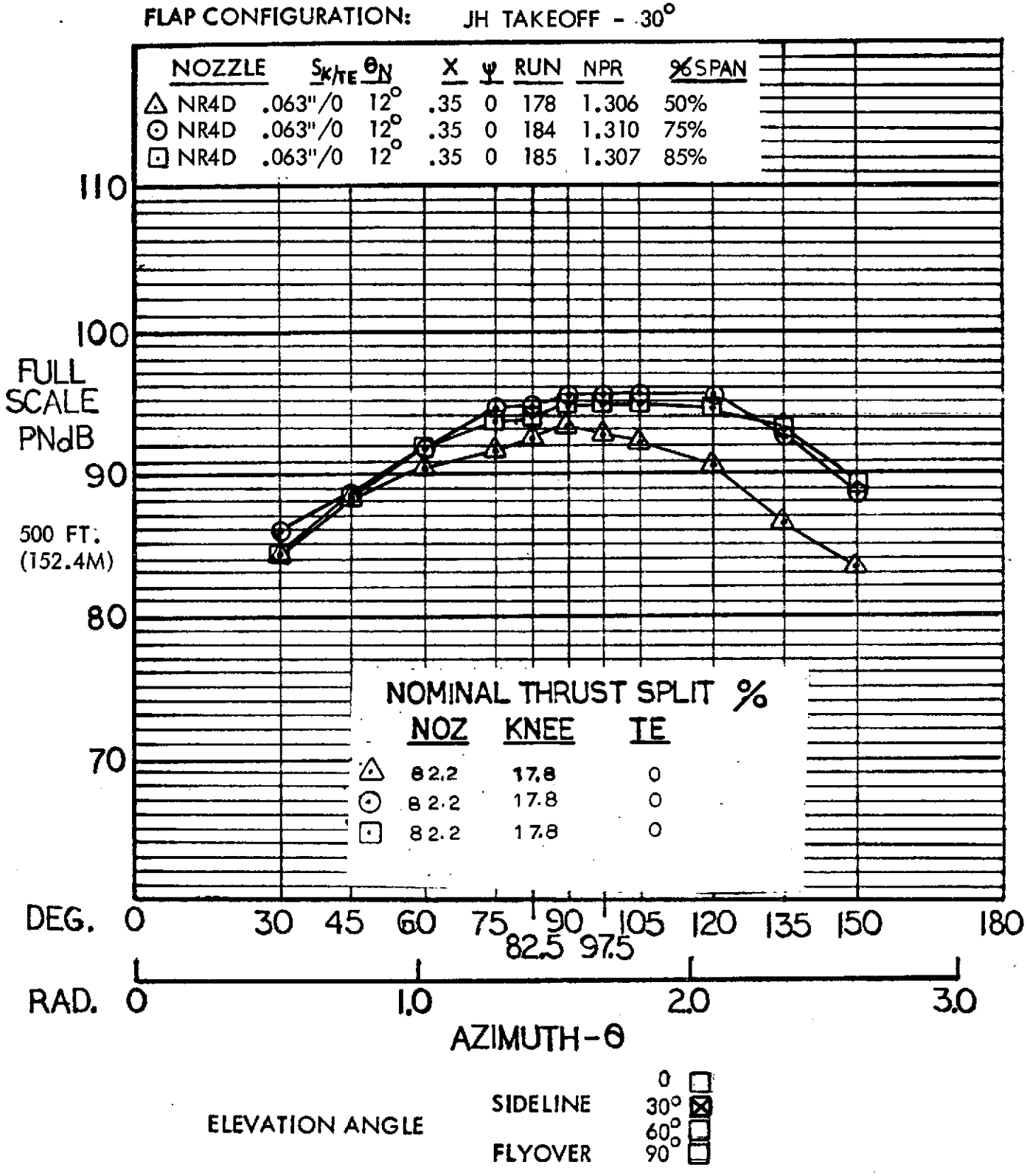

Figure 155 Full scale sideline PNL; comparison of three nozzle spanwise positions, aspect ratio 4 nozzle with deflector, JH flap with knee blowing, 30° flap angle.

HYBRID PROPULSIVE LIFT
ACOUSTIC TEST
NAS 2-7812

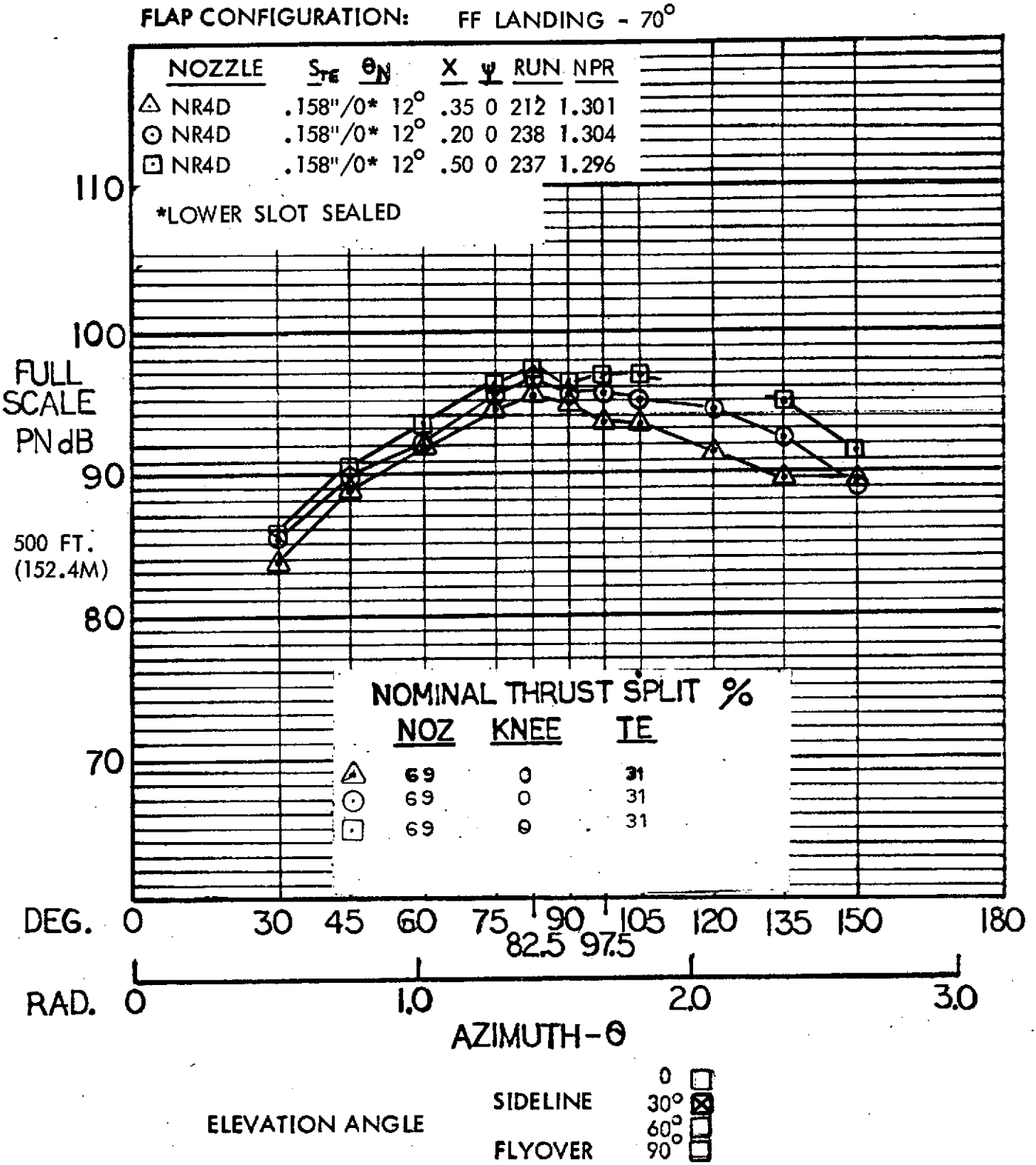

Figure 156 Full scale sideline PNL; comparison of three nozzle longitudinal positions, aspect ratio 4 nozzle with deflector, Flex Flap with upper TE blowing, 70° flap angle.

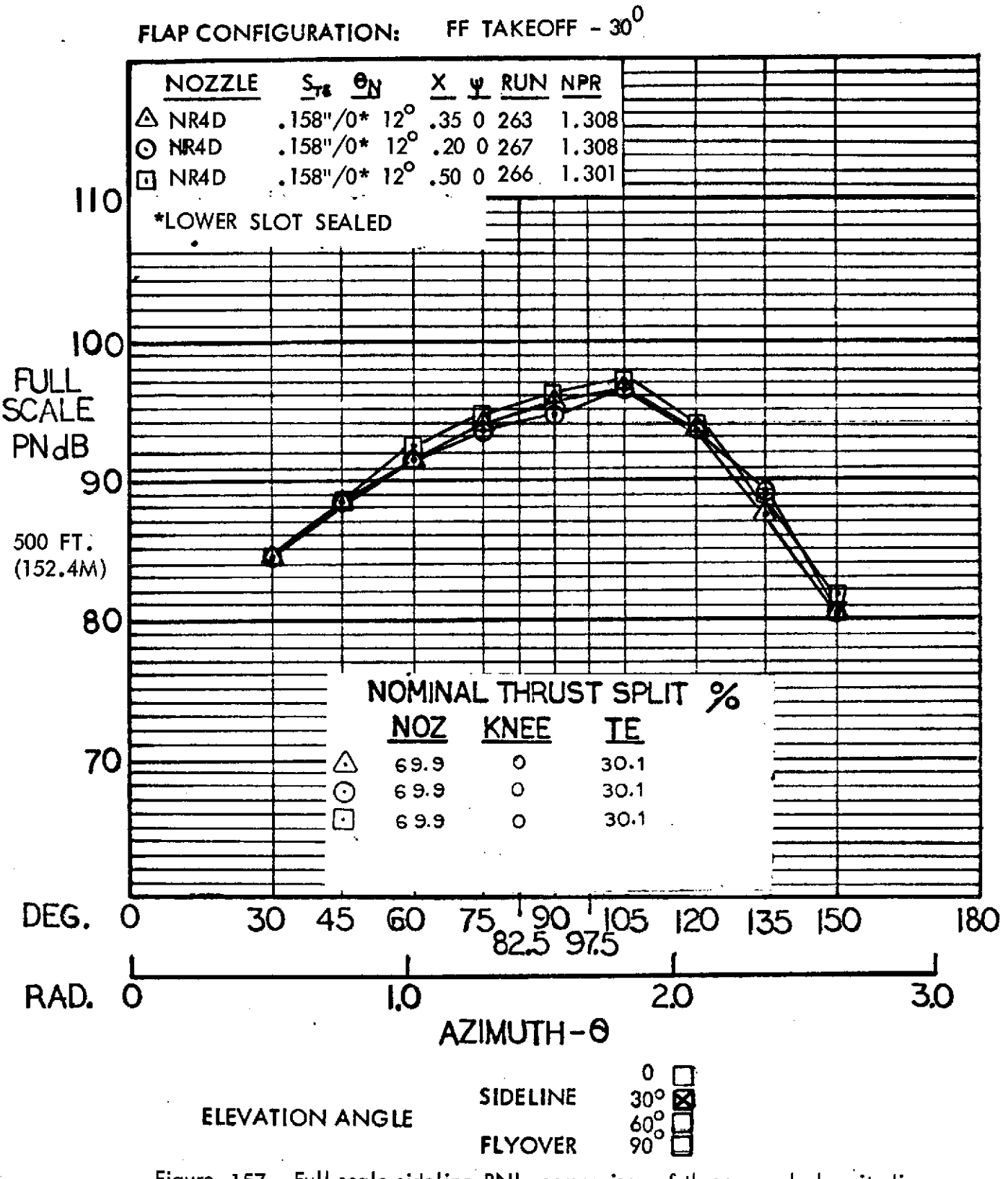

Figure 157 Full scale sideline PNL; comparison of three nozzle longitudinal positions, aspect ratio 4 nozzle with deflector, Flex Flap with upper TE blowing, 30° flap angle.

HYBRID PROPULSIVE LIFT
ACOUSTIC TEST
NAS 2-7812

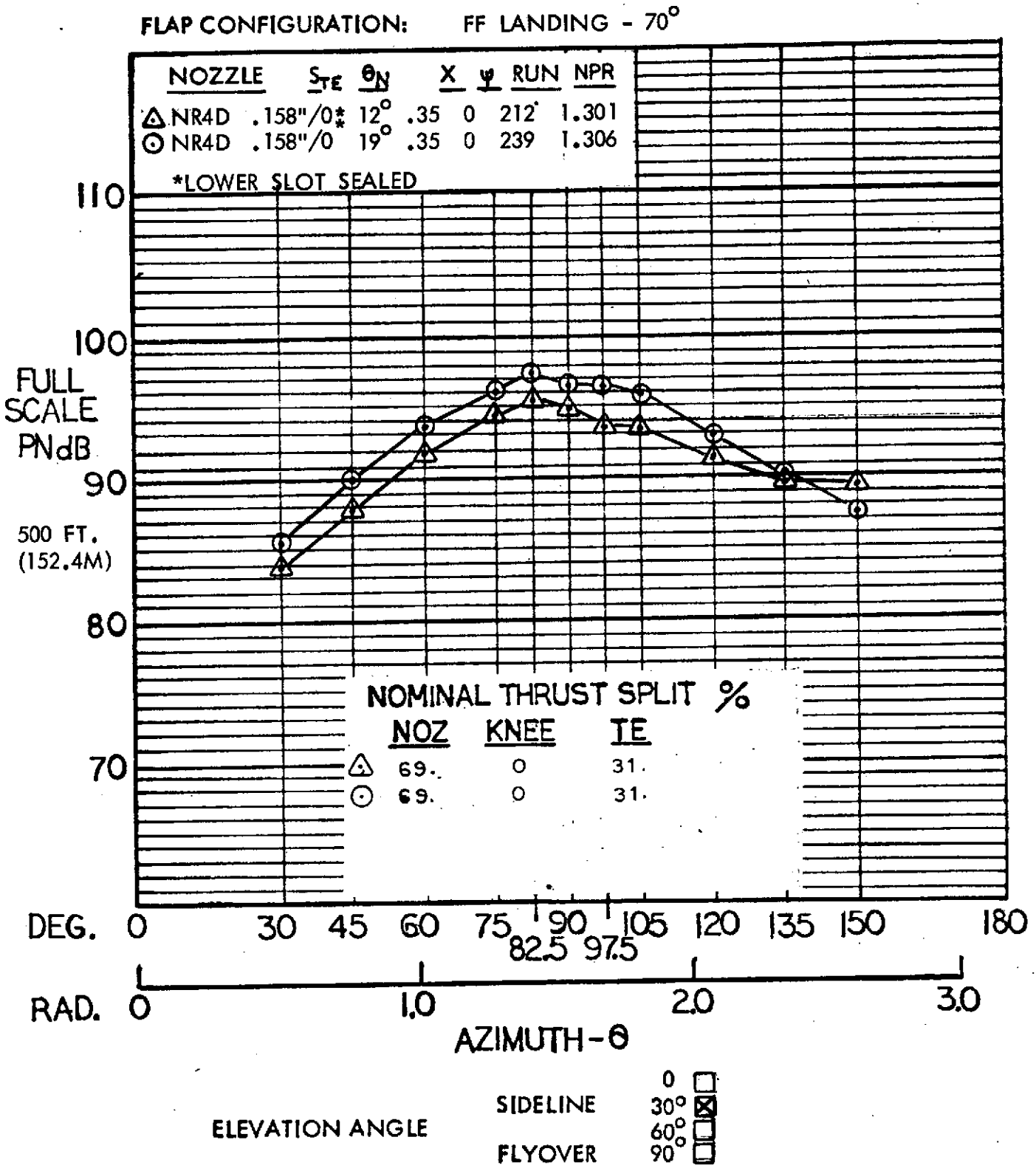

Figure 158 Full scale sideline PNL; comparison of two nozzle impingement angles, aspect ratio 4 nozzle with deflector, Flex Flap with upper TE blowing, 70° flap angle.

HYBRID PROPULSIVE LIFT
ACOUSTIC TEST
NAS 2-7812

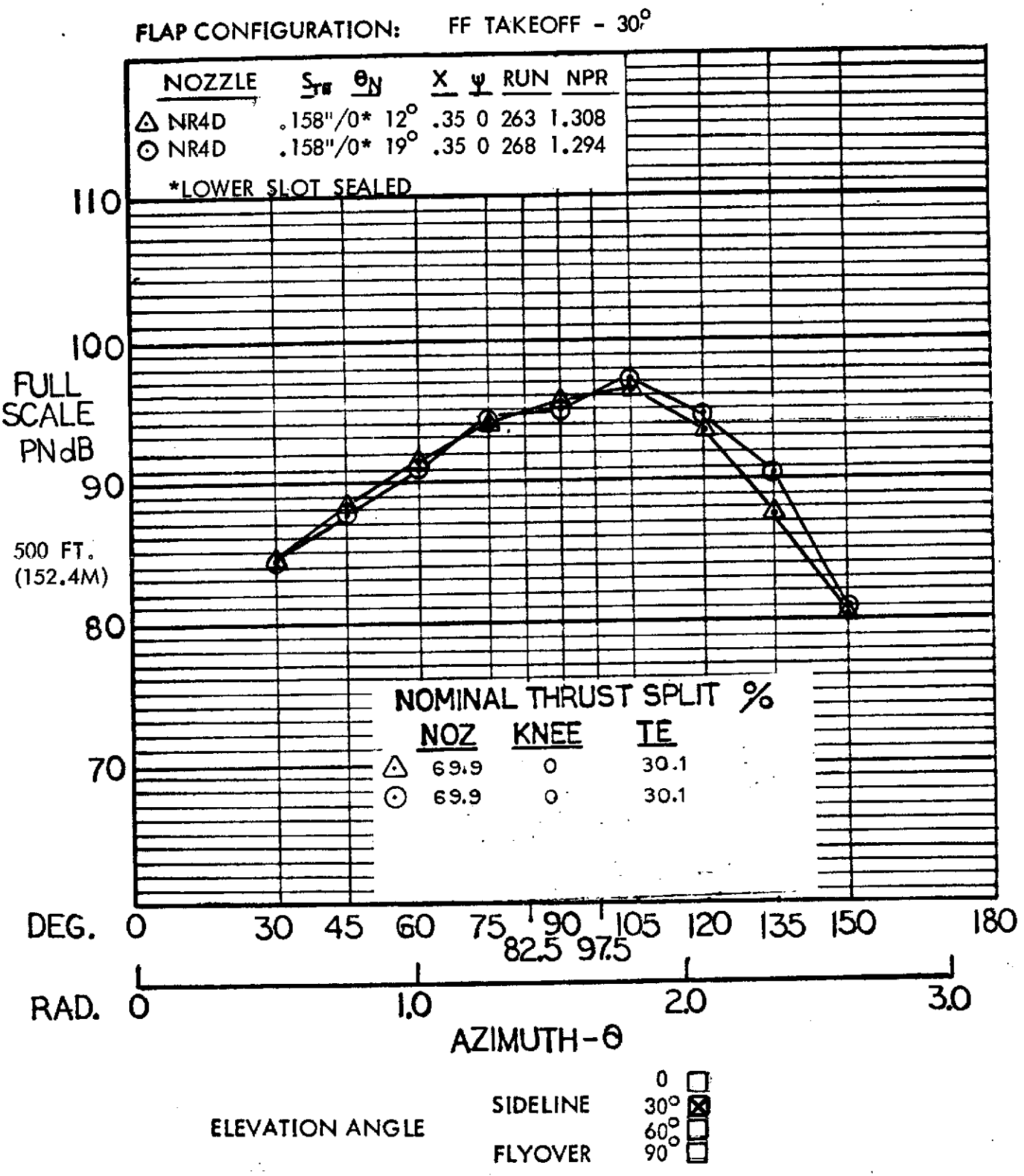

Figure 159 Full scale sideline PNL; comparison of two nozzle impingement angles, aspect ratio 4 nozzle with deflector, Flex Flap with upper TE blowing, 30° flap angle.

HYBRID PROPULSIVE LIFT
ACOUSTIC TEST
NAS 2-7812

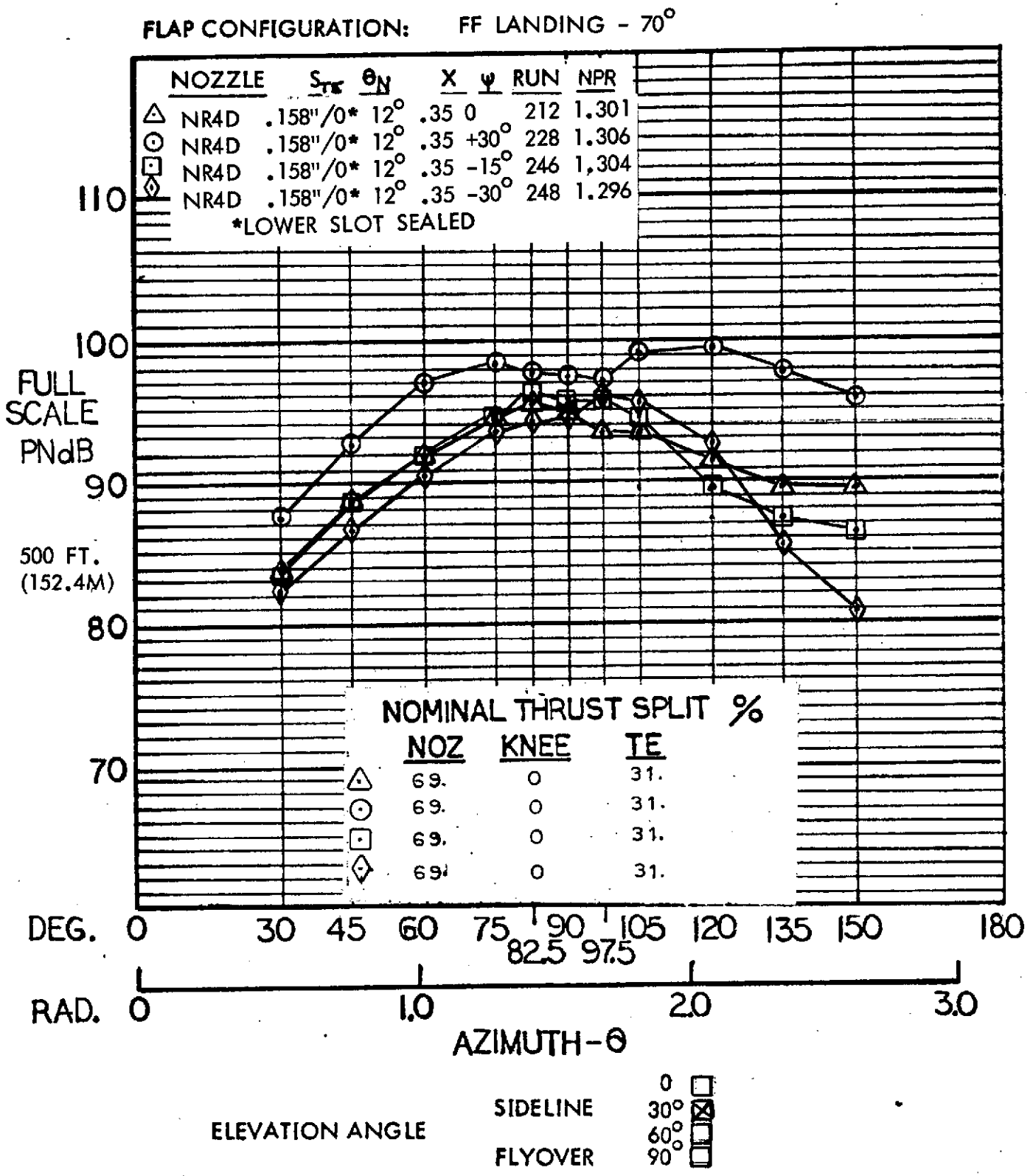

Figure 160 Full scale sideline PNL; comparison of four auxiliary flap angles, aspect ratio 4 nozzle with deflector, Flex Flap with upper TE blowing, 70° flap angle.

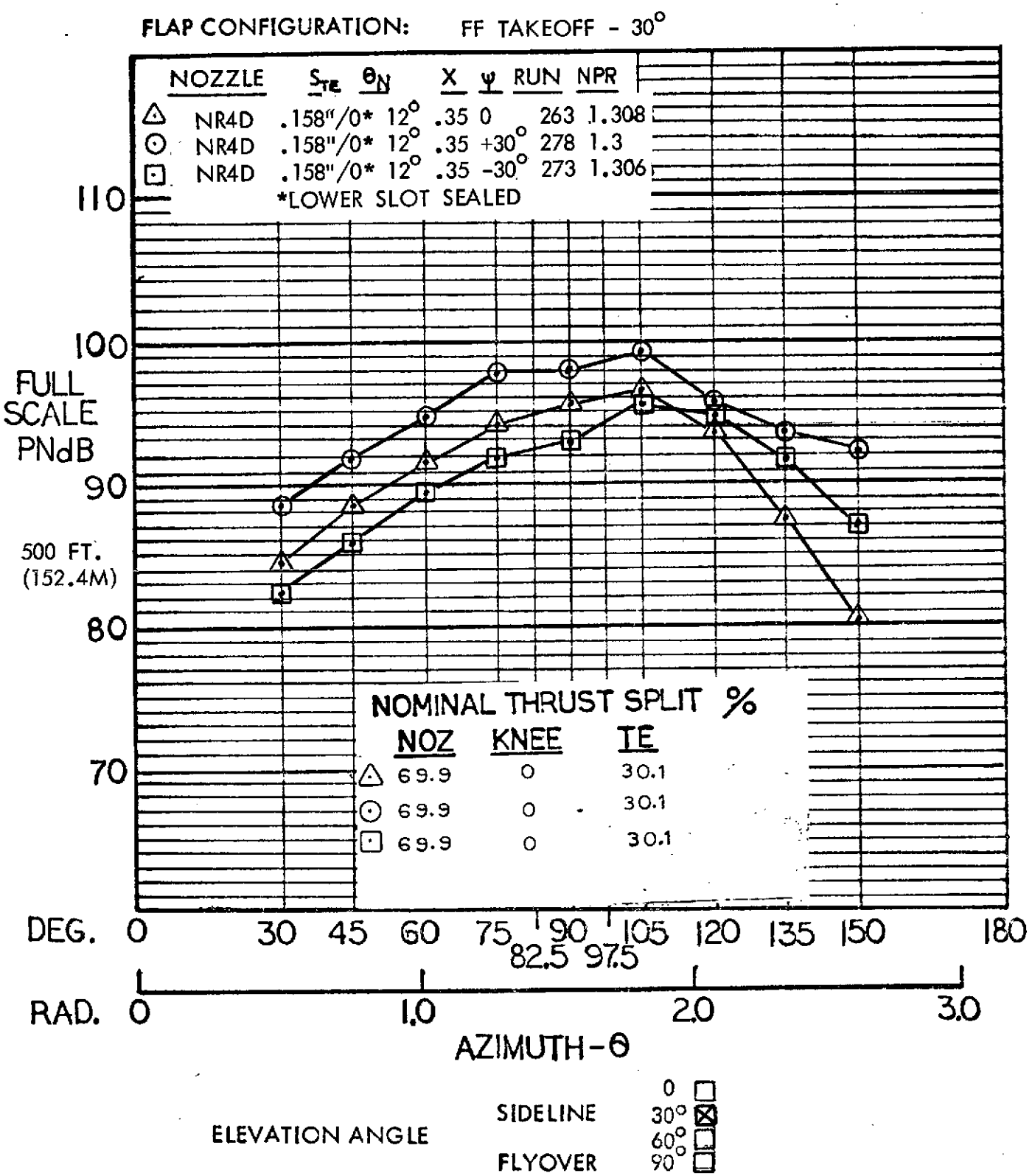

Figure 161 Full scale sideline PNL; comparison of four auxiliary flap angles, aspect ratio 4 nozzle with deflector, Flex Flap with upper TE blowing, 30° flap angle.

HYBRID PROPULSIVE LIFT
ACOUSTIC TEST
NAS 2-7812

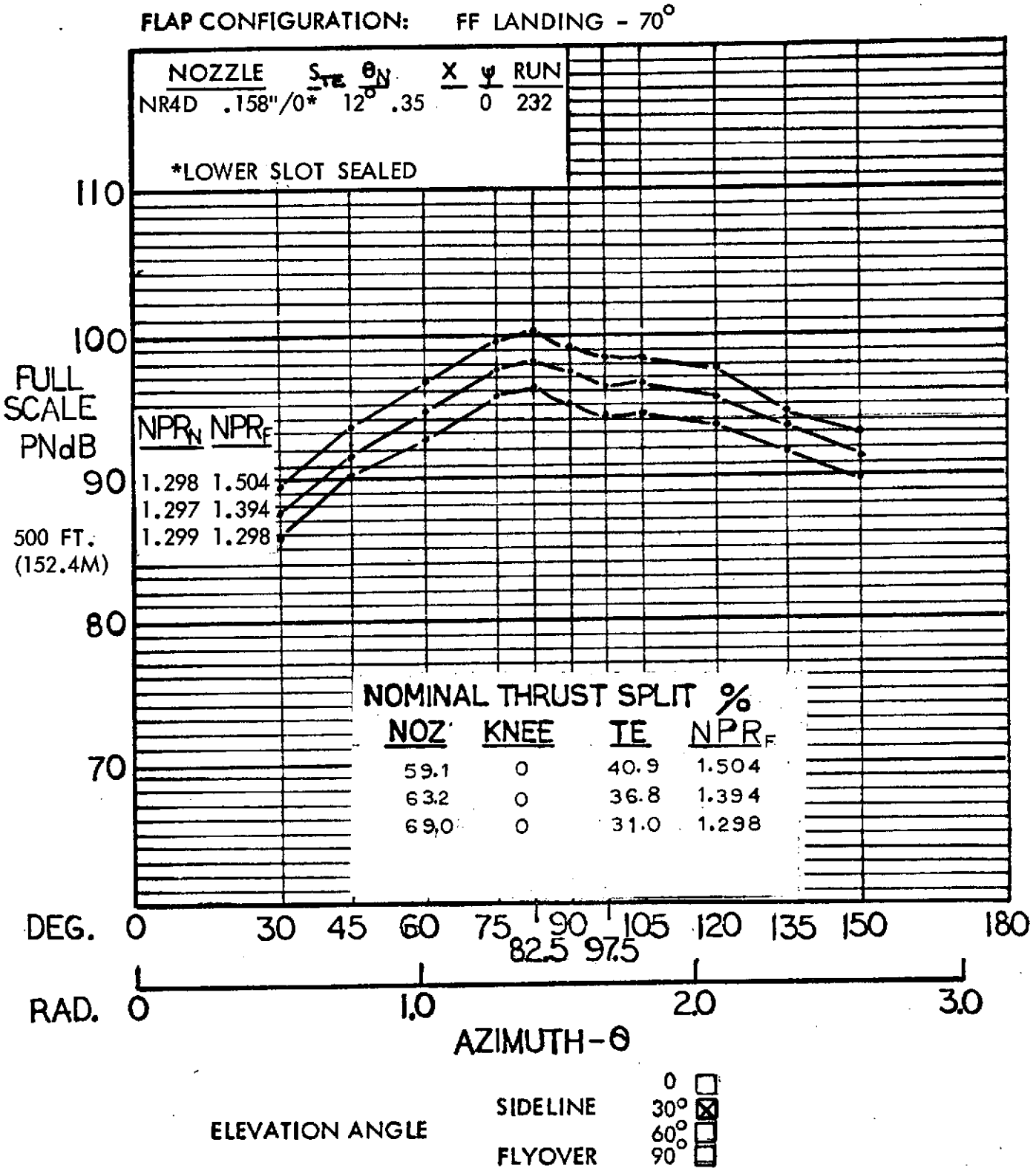

Figure 162 Full scale sideline PNL; variation of flap pressure ratio with constant nozzle pressure ratio, aspect ratio 4 nozzle with deflector, Flex Flap with upper TE blowing, 70° flap angle.

HYBRID PROPULSIVE LIFT
ACOUSTIC TEST
NAS 2-7812

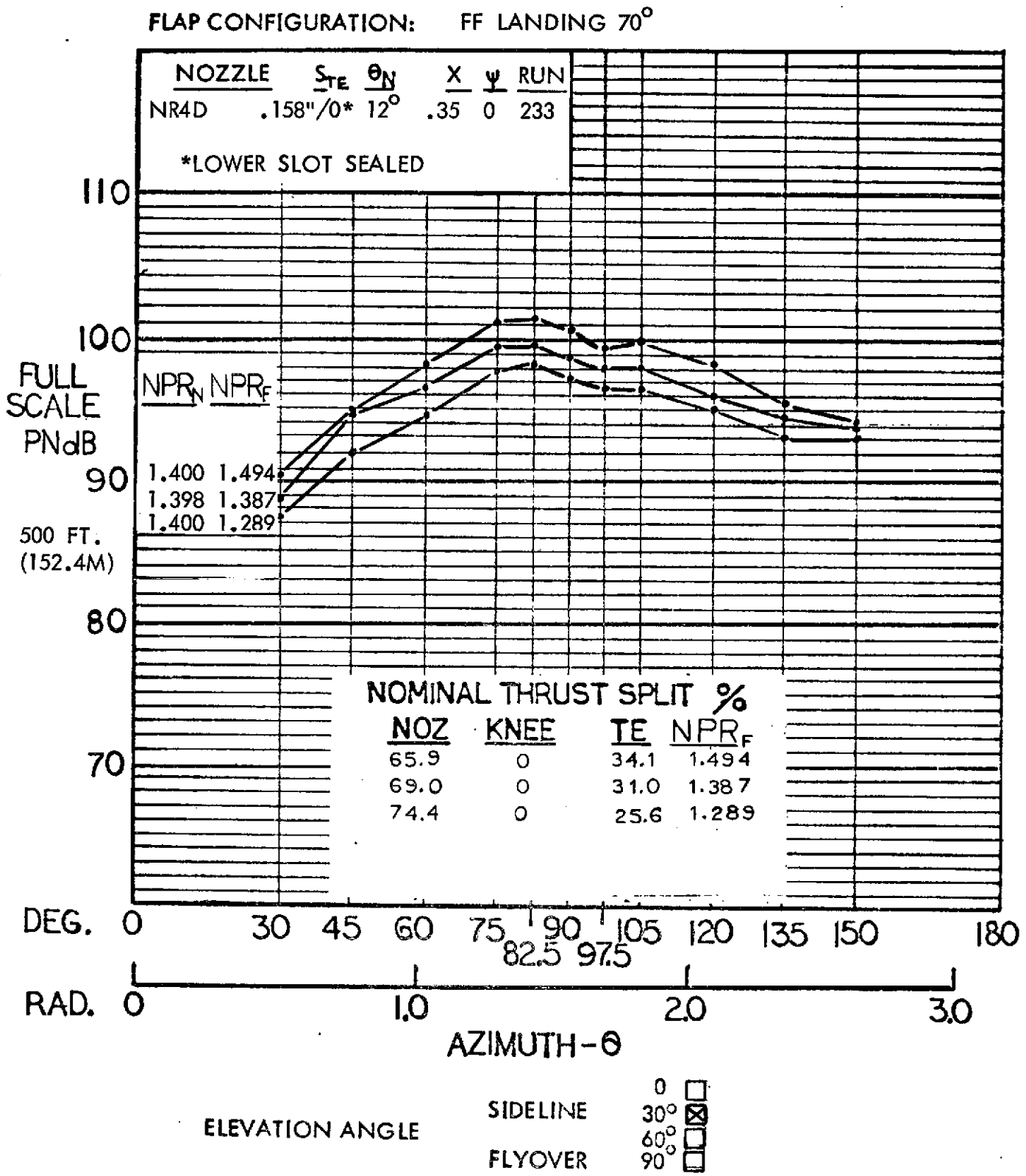

Figure 163 Full scale sideline PNL; variation of flap pressure ratio with constant nozzle pressure ratio, aspect ratio 4 nozzle with deflector, Flex Flap with upper TE blowing, 70° flap angle.

HYBRID PROPULSIVE LIFT
ACOUSTIC TEST
NAS 2-7812

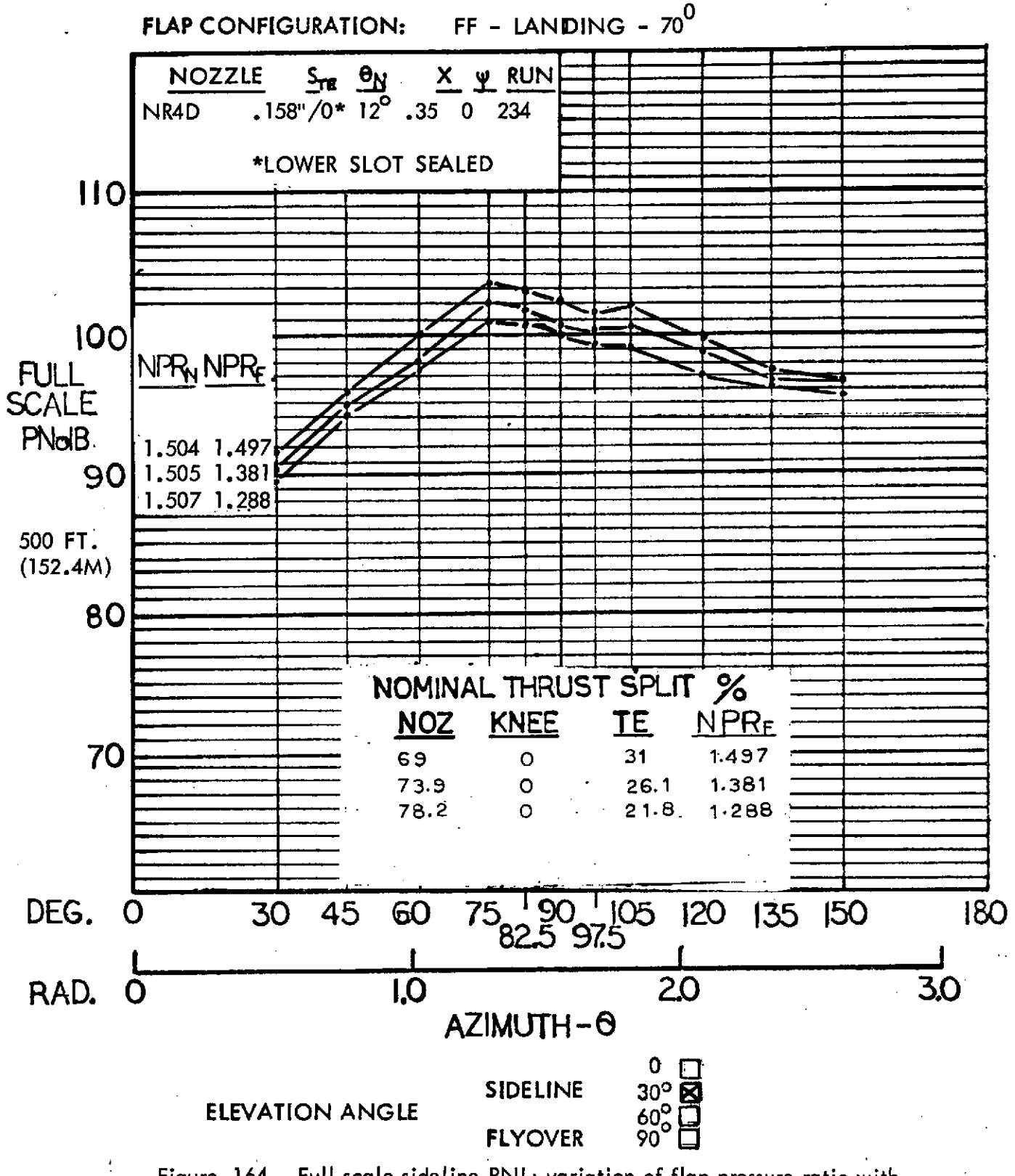

Figure 164 Full scale sideline PNL; variation of flap pressure ratio with constant nozzle pressure ratio, aspect ratio 4 nozzle with deflector, Flex Flap with upper TE blowing, 70° flap angle.

HYBRID PROPULSIVE LIFT
ACOUSTIC TEST
NAS 2-7812

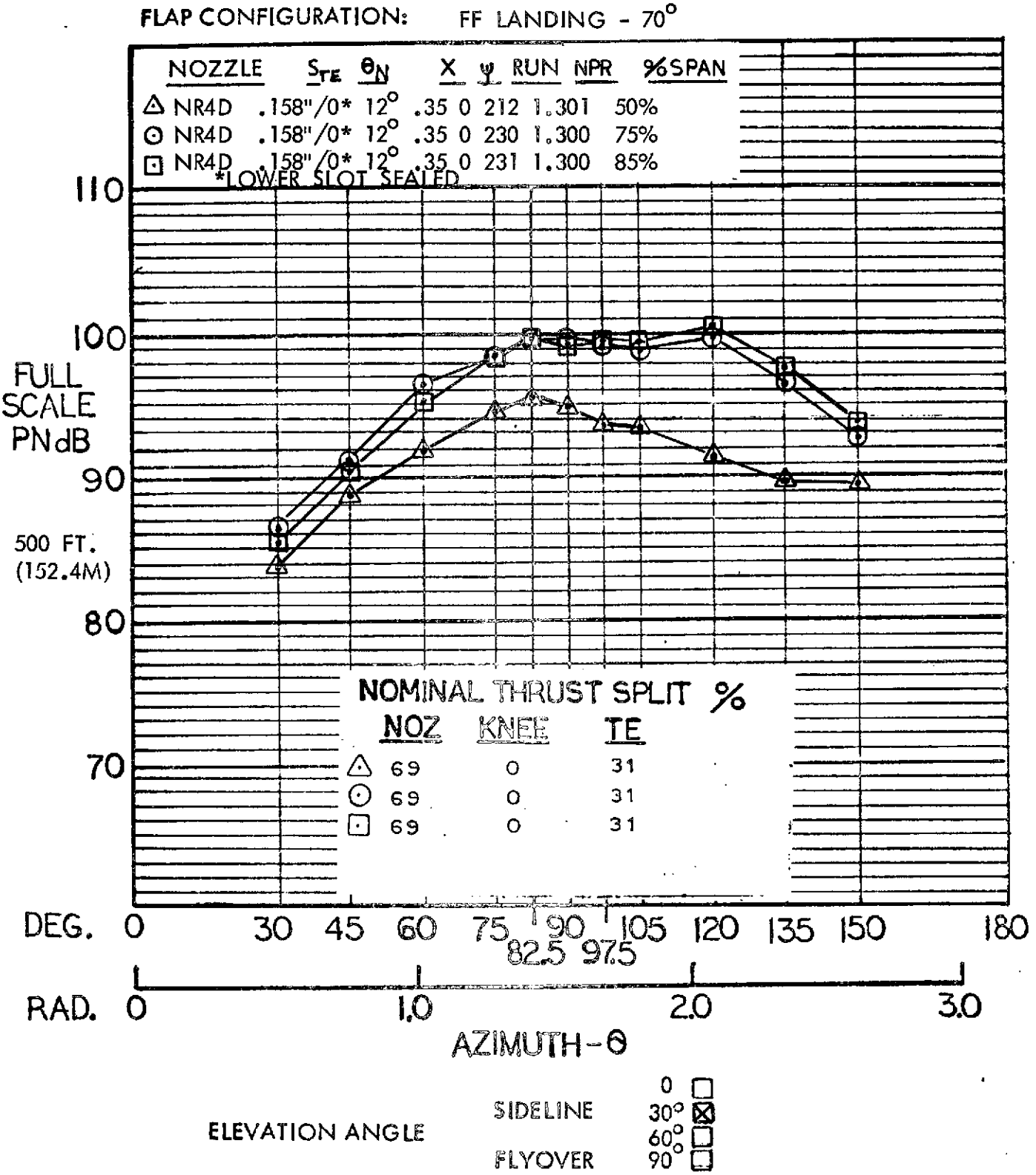

Figure 165 Full scale sideline PNL; comparison of three nozzle spanwise positions, aspect ratio 4 nozzle with deflector, Flex Flap with upper TE blowing, 70° flap angle.

ADDENDUM

SUPPLEMENTARY TESTS

Addendum Contents

	Page
Addendum Contents	A-1
Summary of Figures	A-2
Introduction	A-3
Test Apparatus	A-3 - A-4
Instrumentation	A-4
Aerodynamic Results	A-5 - A-6
Acoustics	A-6 - A-9
Conclusions	A-10
Figures	A-11 - A-56

Summary Of Figures

Figure	Description	Page
A-1 - A-5	Spoiler installation and acoustic modifications.	A-11 - A-15
	Aerodynamic and Propulsion Data	
A-6 - A-9	Surface pressure data.	A-16 - A-21
A-10 - A-14	Flow visualization data.	A-22 - A-31
A-15	Flap trailing edge wake survey.	A-32 - A-33
	Spoiler Acoustic Data	
A-16 - A-19	Baseline; NR4D nozzle, JH flap, 70° flap angle, 20° segmented spoiler.	A-34 - A-37
A-20 - A-23	Comparison; NR4D nozzle, JH flap, 70° and 50° flap angle, spoiler at 0° and 20°, no flap blowing.	A-38 - A-41
A-24 - A-26	Comparison; NR4D nozzle, JH flap, 70° flap angle, spoiler at 0° and 20°, knee blowing.	A-42 - A-44
A-27	Comparison; NR4D nozzle, JH flap, 50° flap angle, spoiler at 20° with three modifications.	A-45
A-28 - A-30	Comparison; NR4D nozzle, JH flap, 50° flap angle, spoiler at 0°, 20° and 20° with mesh.	A-46 - A-48
	Aft Directivity Acoustic Data	
A-31 - A-32	Radial PNL; NR4D nozzle, JH and Flex Flap.	A-49 - A-50
A-33	Spectra; NR4D nozzle, JH flap, 30°, 50°, and 70° flap angle.	A-51
A-34 - A-38	Spectra; NR4D nozzle, JH flap, 70° flap angle.	A-52 - A-55

ADDENDUM

SUPPLEMENTARY TESTS

Introduction

A short supplementary test program was performed in May, 1974 to secure additional data on the effects of spoilers and to provide insight into the aft directivity phenomena of the JH landing flap. This addendum contains additional test data as well as appropriate data from the basic test program required for the directivity discussion.

Test Apparatus

The test apparatus used for this supplemental test program consisted of the same basic equipment used for the original tests plus a limited amount of additional instrumentation and model modification.

All of the additional tests were run using the NR4D nozzle positioned at flap mid-span on the 35 percent wing chord position and at a jet impingement angle of 12 degrees. The JH flap was used with the wing tip installed for all tests. Flap angles of both 70° (landing) and 50° (an intermediate position not previously used) were tested. The trailing edge slots were sealed for all tests. The knee slot gap was set at 0.063 inches for all tests which produced a nominal thrust split of 81% of the total thrust from the nozzle and 19% from the knee slot.

A segmented 20 degree spoiler was fabricated for the additional tests. This spoiler is simply a flat plate with trailing edge tabs bent upward 20°. Each tab and gap is 2.4 inches (10% chord) square (except the two end tabs which

were cut off even with the ends of the flap), the center tab being positioned at the nozzle centerline. The spoiler was positioned such that the end of the tabs (before bending) coincides with the knee slot. Figure A-1 shows the spoiler installed.

Four different modifications of the basic segmented spoiler described above were tested in an effort to reduce the noise associated with it. These are:

(1) A porous metal cover over the spoiler upper surface. Figure A-2.

(2) A solid, non-segmented plate spoiler. Figure A-3.

(3) A segmented rubber cover for the spoiler upper surface. Figure A-4.

(4) A fine mesh wire screen which covered the segmented spoiler upper surface and gaps behind the nozzle. Figure A-5.

Instrumentation

Instrumentation for the additional tests was the same as for the original tests except for provisions for upper flap surface pressure measurements. Ten static pressure measurements were obtained by installing plastic tubing along the flap upper surface in a chordwise direction. Figure A-1 shows the surface pressure tubing installation used for this test. The tubing was installed slightly offset from the nozzle centerline to avoid interfering with the flap trailing edge wake survey rake. Total pressure readings were taken also along the flap upper surface adjacent to the surface pressure tubing in a chordwise direction with a hand-held pressure probe. An attempt was made to hold the probe about 1/2 to 3/4 inch above the flap surface, but the pressure data from this probe are subject to errors caused by misalignment and mislocation relative to the surface.

Aerodynamic Results

General - Previously it had been theorized that some of the unusual acoustic properties of the JH 70° flap could be caused by: (1) flow through the pie-shaped segment between the deflected flap and the undeflected trailing edge of the wing tip; (2) the noise associated with a possible separation bubble at the flap knee; or (3) the velocity of the flow around the flap knee relative to the nozzle exit velocity varying with nozzle pressure ratio, i.e., a non-constant velocity ratio at a given flap chordwise position. The first theory was virtually eliminated during the basic tests by testing with the tip on and off and by closing the flap-to-tip gap with a flat plate. The supplemental tests utilized flow visualization and surface pressure measurements which rule out the second theory. Data obtained using the hand-held probe to check the third theory are inconclusive.

Surface Pressures - Results of the surface pressure survey are presented in Figures A-6 through A-9. Static pressure coefficient profiles are shown in Figure A-6 for the JH 70° flap both with and without spoiler and with and without knee blowing. Figure A-7 shows comparable data for the JH 50° flap without knee blowing. Similar data with knee blowing were not obtained because of a model problem on the first assembly of the 50° flap position. Comparable plots for the same configurations are shown in Figures A-8 and A-9 in the form of local dynamic pressure divided by nozzle dynamic pressure as a function of surface distance. The bumps in Figures A-6 through A-9 at about 0.34 s/C are caused by a surface discontinuity at the leading edge of the aft flap. This abrupt contour change resulted from installation of rubber strips which were used to seal the trailing edge slots.

Note that only the 50° flap data on Figure A-9b show the trend of increasing q_s/q_n with increasing nozzle pressure ratio which had been suspected for the

70° flap position. If any trend is present for the 70° flap position, it is in the opposite direction.

Flow Visualization - Representative photographs from the flow visualization study are presented in Figures A-10 through A-14. Nothing of an unusual nature can be discerned from the "no spoiler" flow patterns. Perhaps the most noteworthy effect visible on all the photographs is how the flow spreads quickly from the USB nozzle exit to cover the entire flap and corner of the wing tip.

Knee blowing produces very little effect on the visible flow pattern. Some difference is noted near the flap ends where, with knee blowing, the pattern is more nearly parallel to the flap edge.

Spoiler-on flow patterns are quite interesting with visual indication of the desired flow separation behind some of the tabs and reattachment on the flap further downstream.

Trailing Edge Surveys - Comparisons of flap trailing edge pressure distributions made during the supplemental tests are presented in Figure A-15. Figure A-15a shows the effect of changing the flap deflection angle from 70 to 50 degrees. Figure A-15b shows the effect of the segmented 20° spoiler, both with and without knee blowing, on the JH 70° flap.

Acoustics

General - Acoustic measurements were obtained for the JH flap with and without knee blowing, with and without the segmented spoiler, and at 50° and 70° flap angles. Further comparative data using four modified spoilers were obtained at

the 50° flap angle to determine the feasibility of reducing spoiler-generated noise. One of these modifications was successful.

The 70° JH flap was run without modification in order to provide an additional check of repeatability of the acoustic test data. Acoustic measurements have been obtained on four separate occasions with this configuration which does not provide a conventional statistical sample. However, Run 132 was selected as a baseline and a difference was obtained for each microphone and repeat runs. This provided 280 differences,and, assuming a normal distribution, a mean of +.15 PNdB and standard error of 1.02 PNdB was calculated. This indicates that if any particular microphone measurement is chosen as a reference, about 70 percent of the subsequent repetitions should be within ±1 PNdB. A major source of this error is probably due to the use of nominal pressure ratio as the controlling parameter when establishing the test point.

Spoiler Test Data - Figures A-16 through A-19 show baseline 70° flap data with the 20° segmented spoiler installed. These full-scale data incorporate a model scale of 0.2, as in the body of this report. Figures A-20 and A-21 show 50° flap sideline and flyover data for 0° (no spoiler) and 20° spoiler angle without knee blowing. Figures A-22 and A-23 show similar 70° flap angle data, while Figures A-24, A-25, and A-26 show 70° flap results with knee blowing. The segmented spoiler increases peak flyover noise by 1 to 2 PNdB and peak sideline noise by 2 to 4 PNdB.

Modified spoilers were tested at the 50° flap angle to evaluate methods of reducing the spoiler-induced noise. Figure A-27 summarizes the sideline noise levels for the basic spoiler and three unsuccessful modifications. These modifications included a metal plate of about 30 percent porosity which covered the spoiler upper surface, a solid, unsegmented spoiler, and a segmented rubber cover for the spoiler upper surface.

A significant reduction in noise levels was achieved with a fine mesh wire screen which covered the spoiler upper surface and the segment gaps behind the nozzle, as depicted in Figure A-5. The screen was ordinary household aluminum windown screen with frayed trailing edges. Figures A-28 through A-30 provide a comparison of the no-spoiler, 20°-segmented spoiler, and screened 20°-segmented spoiler configurations. Peak sideline noise levels were reduced 3 PNdB by the addition of the screen, which results in 1 PNdB lower noise than the no-spoiler case. Similarly, the screened spoiler peak flyover levels were 2 to 3 PNdB lower than the unscreened configuration.

JH Landing Flap Aft Directivity - Initial testing of the JH flap at the landing flap angle of 70° revealed that peak noise levels occur aft of the wing at the 150° azimuth position. This aft directivity is illustrated by the radial noise levels shown on Figure A-31. At the takeoff flap angle, the noise levels in the 100°-150° azimuth arc decrease in contrast to the landing case. This may not indicate conclusively that the two flap positions have dissimilar noise radiation patterns as the existing microphone array would not detect the possible rotation of the noise peak with the flap. Figure A-32 shows the radial noise levels obtained with the Flex Flap and it is apparent that the landing position noise directivity does not resemble the comparable JH flap pattern.

The aft noise frequency characteristics may be evaluated by referring to Figures A-33 through A-36. Figures A-33, A-34, and A-35 illustrate 1/3 octave band sound pressure levels at three flap angles, three azimuth positions, and four nozzle pressure ratios, respectively. The predominant noise occurs in a frequency band from 100 Hz to 400 Hz and becomes less pronounced as the flap angle decreases and as the observer moves forward. Significant changes in both amplitude and spectral characteristics occur with increasing nozzle pressure ratio, as energy increases in the 315 Hz and 400 Hz one-third octave band (full scale).

The NR4D nozzle assembly included a lower plate which was installed to hold a fixed nozzle area from run to run. (This plate simply simulated a portion of the wing upper surface.) Removing the bottom plate, which increases the mass flow, shifts this peak to the 250 Hz one-third octave band, as shown on Figure A-35.

A digital narrow band analysis using a Fast Fourier Transform program was used to define the spectral changes that occur as the nozzle pressure ratio increases. Figure A-36 shows these narrow band spectra for three pressure ratios. The sharp amplitude increase at the 1.511 nozzle pressure ratio is shown to be generated by a discrete frequency component at about 350 Hz.

The source of this energy was initially thought to be associated with flow through the flap-wing tip slot between the deflected flap and undeflected chord section of the wing tip. This premise was investigated both by removing the wing tip and by closing the slot with a flat plate. Figure A-37 shows that the basic spectrum was not significantly affected by these two changes.

One other possible source that could create this pattern is the noise associated with the accelerated flow around the knee of the flap. In the extreme case, i.e., the highest nozzle pressure ratio, local flow separation at the knee was considered to be a probable source of narrow band energy. Results from the flow visualization studies and pressure surveys do not substantiate the separation theory, however.

One other narrow band noise source with the JH flap produces a peak in the 5000 Hz - 6300 Hz 1/3 octave bands. Figure A-38 indicates that flow through the knee slot is responsible. This peak can increase the perceived noise levels by 1-2 PNdB at the mid-azimuth positions and is most noticeable at low nozzle pressure ratios.

Conclusions

The supplementary test program on the JH flap, aspect ratio four nozzle with deflector at the 35 percent chord and mid-span position at 12° impingement angle disclosed the following:

1. The noise peak at the 150° azimuth position produced by the JH landing flap occurs in the 100 Hz - 400 Hz (full scale) frequency band. At high pressure ratios, a discrete frequency forms at approximately 350 Hz.
2. No evidence of flow separation was disclosed by flow visualization or surface pressure measurements.
3. The JH knee slot produces narrow band noise at 5000 Hz - 6300 Hz (full scale) which can increase perceived noise levels 1-2 PNdB at the mid-azimuth positions and lower pressure ratios.
4. Peak perceived noise levels are increased by the segmented spoiler at a 20° angle: 1-2 PNdB at flyover, and 2-4 PNdB on the sideline.
5. A fine mesh wire screen reduces the 20° spoiler-induced noise to a level about 1 PNdB below the no-spoiler level.

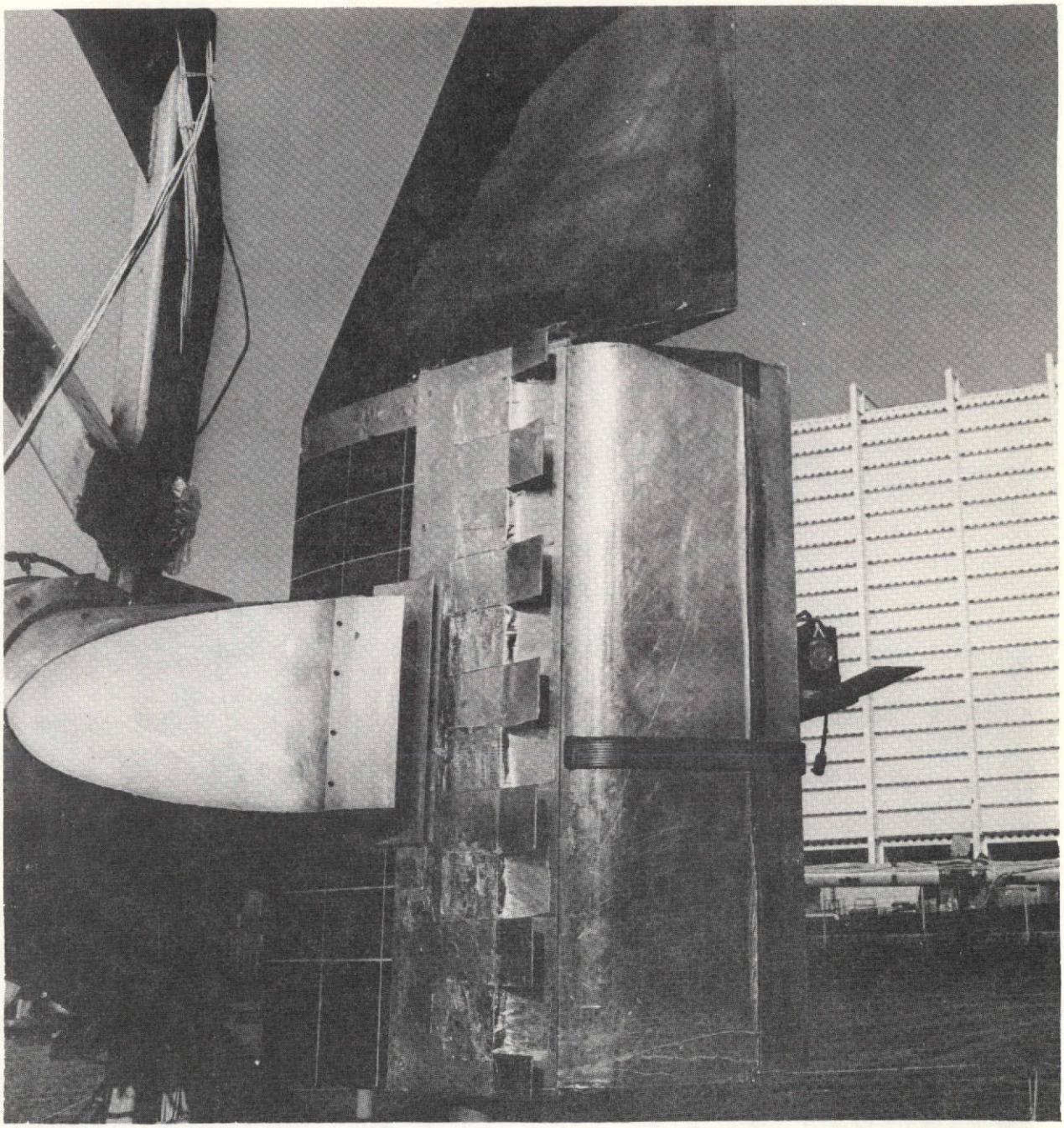

Figure A-1 Model view with 20 degree segmented spoiler, flap surface pressure tubing installed, and pressure rake installed.

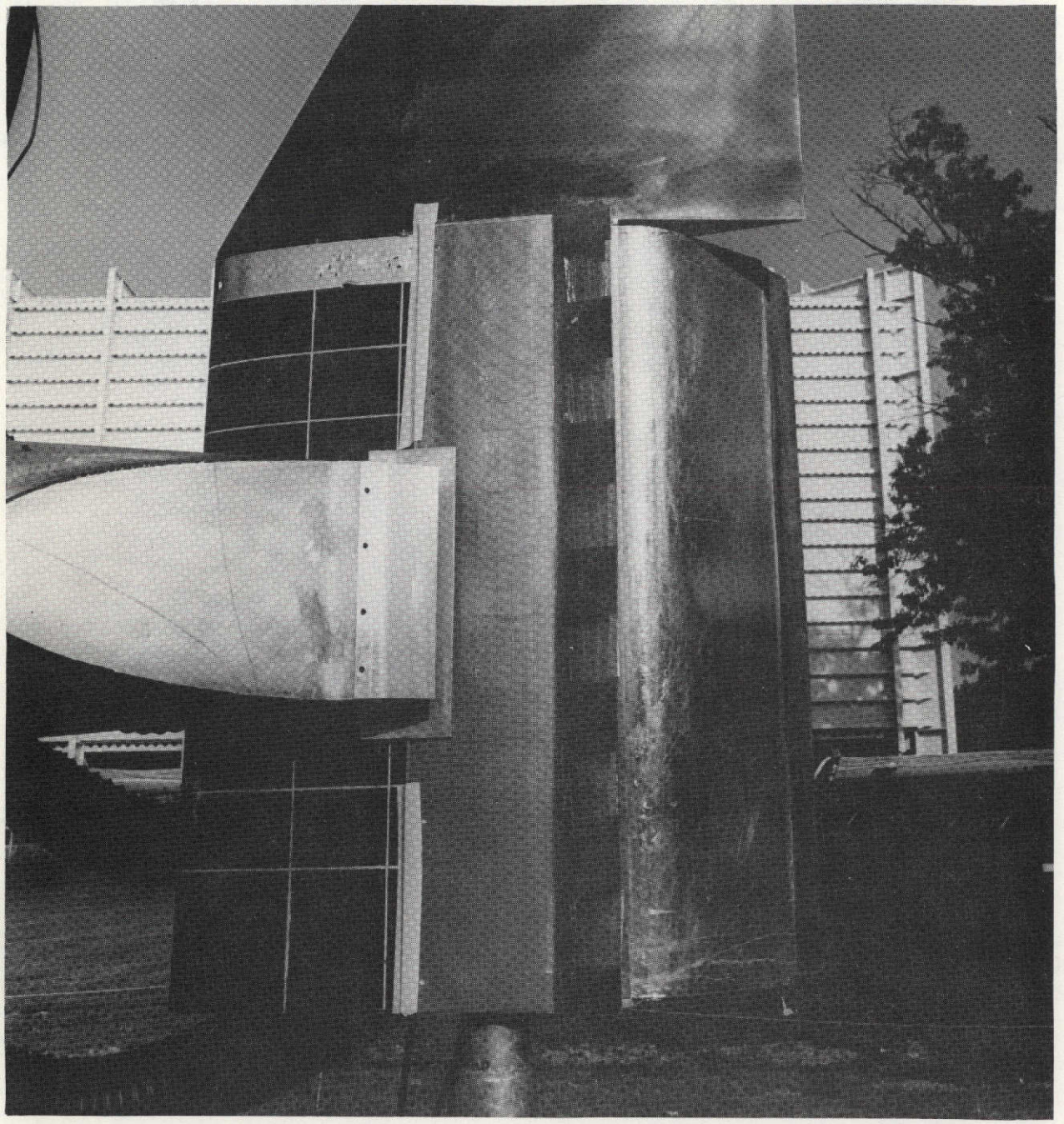

Figure A-2 Model view with porous metal cover over spoiler upper surface.

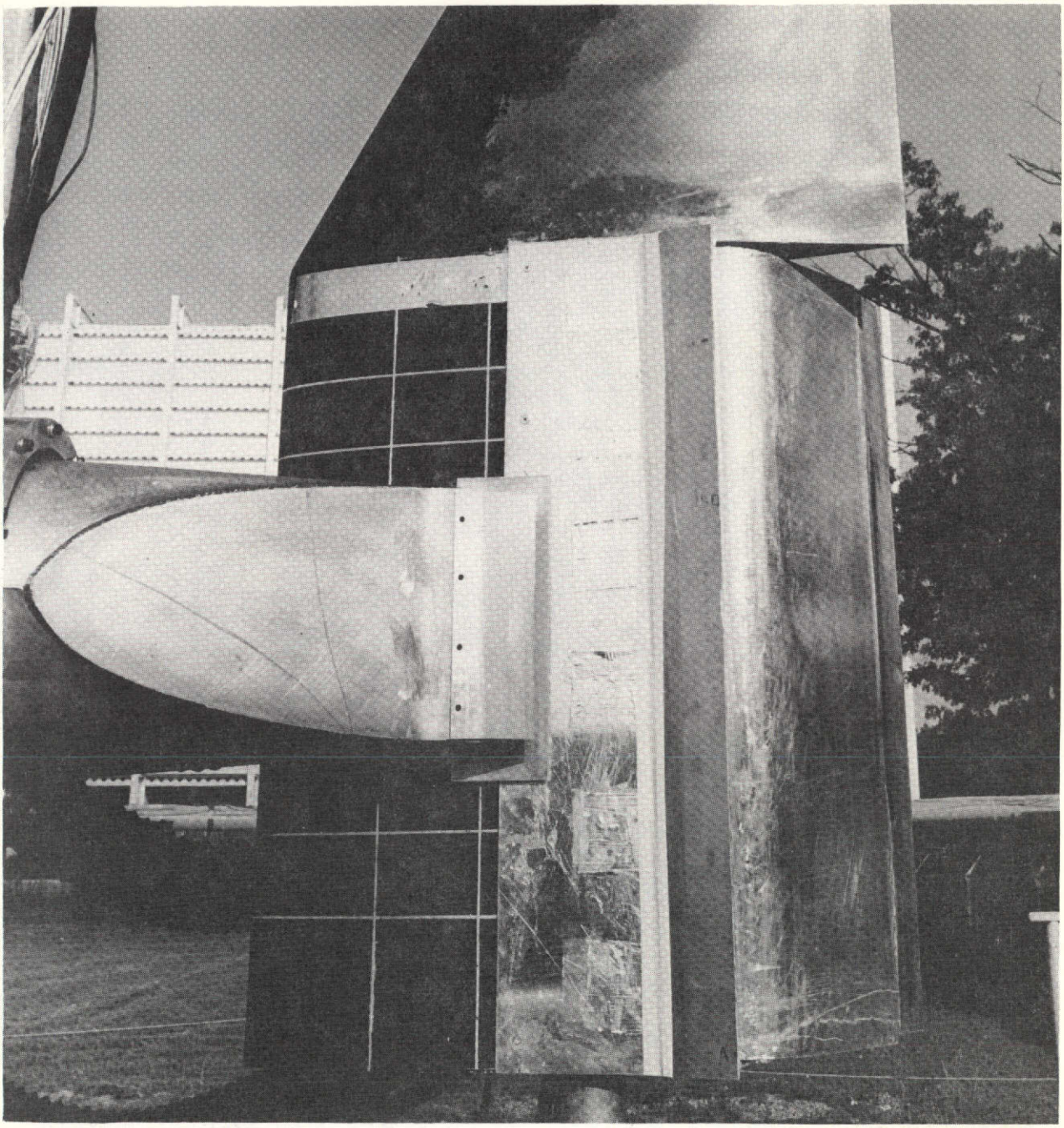

Figure A-3 Model view showing solid, non-segmented plate spoiler.

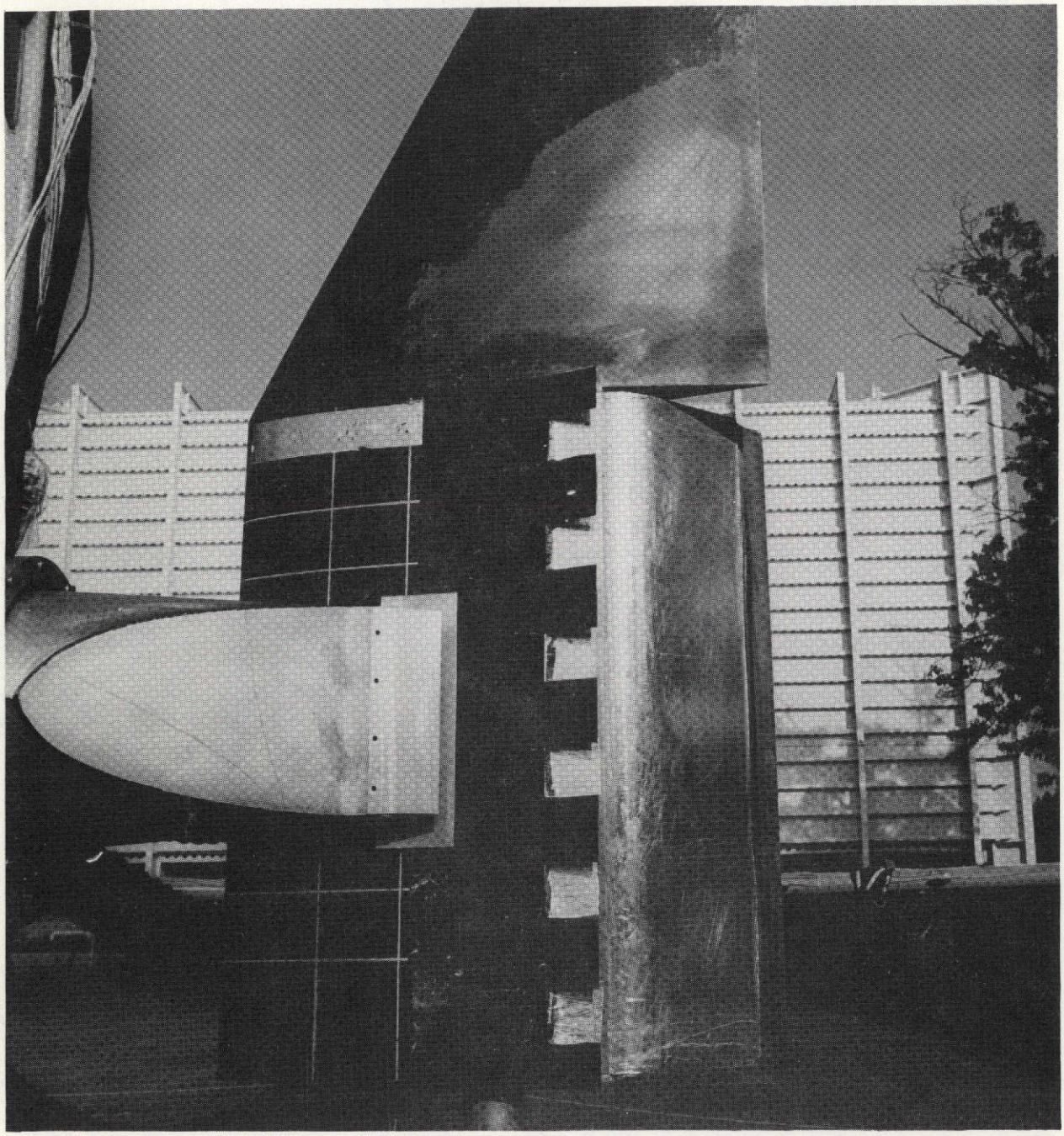

Figure A-4 Model view showing spoiler with segmented rubber cover.

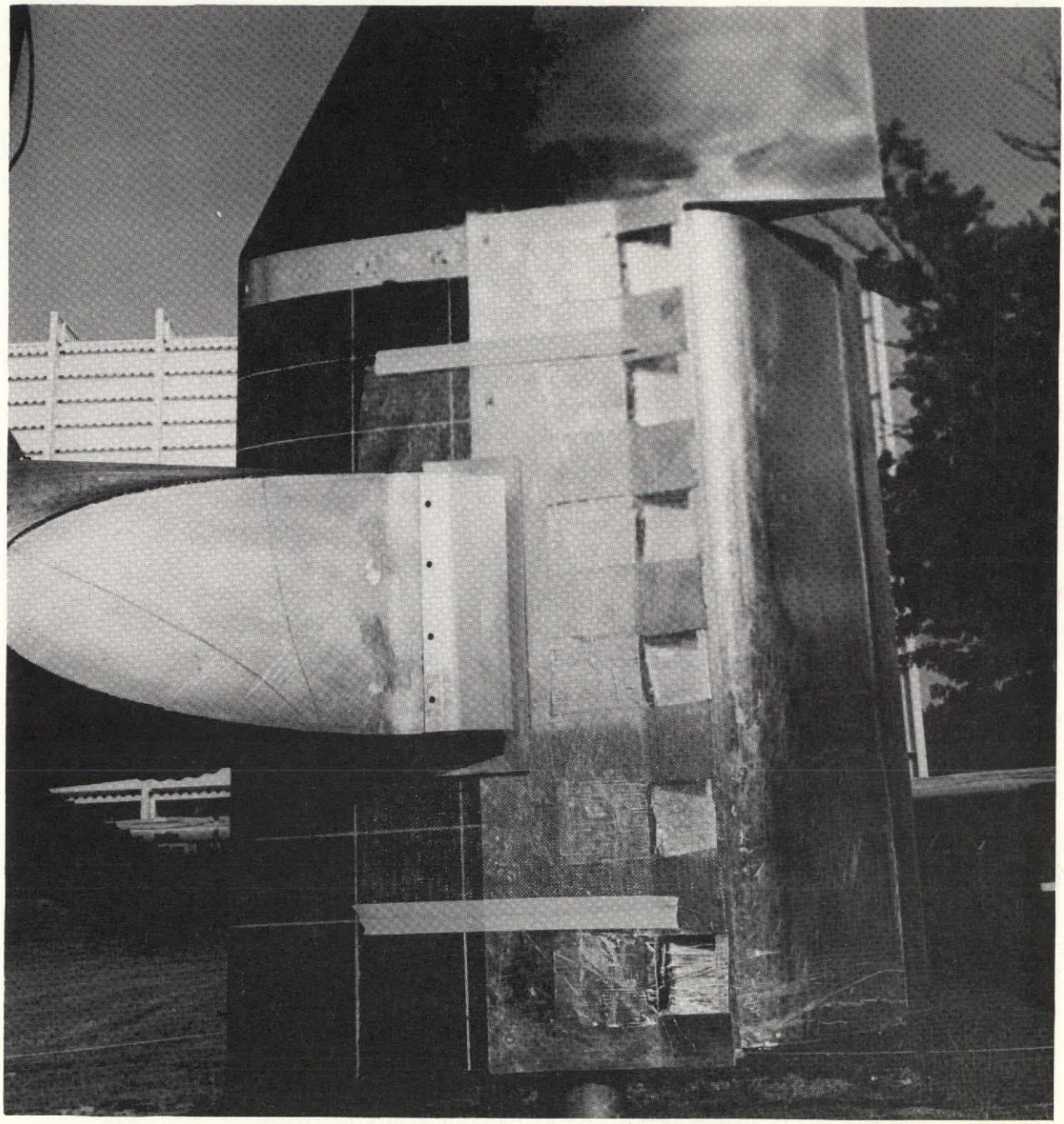

Figure A-5 Model view showing fine wire mesh screen over spoiler upper surface.

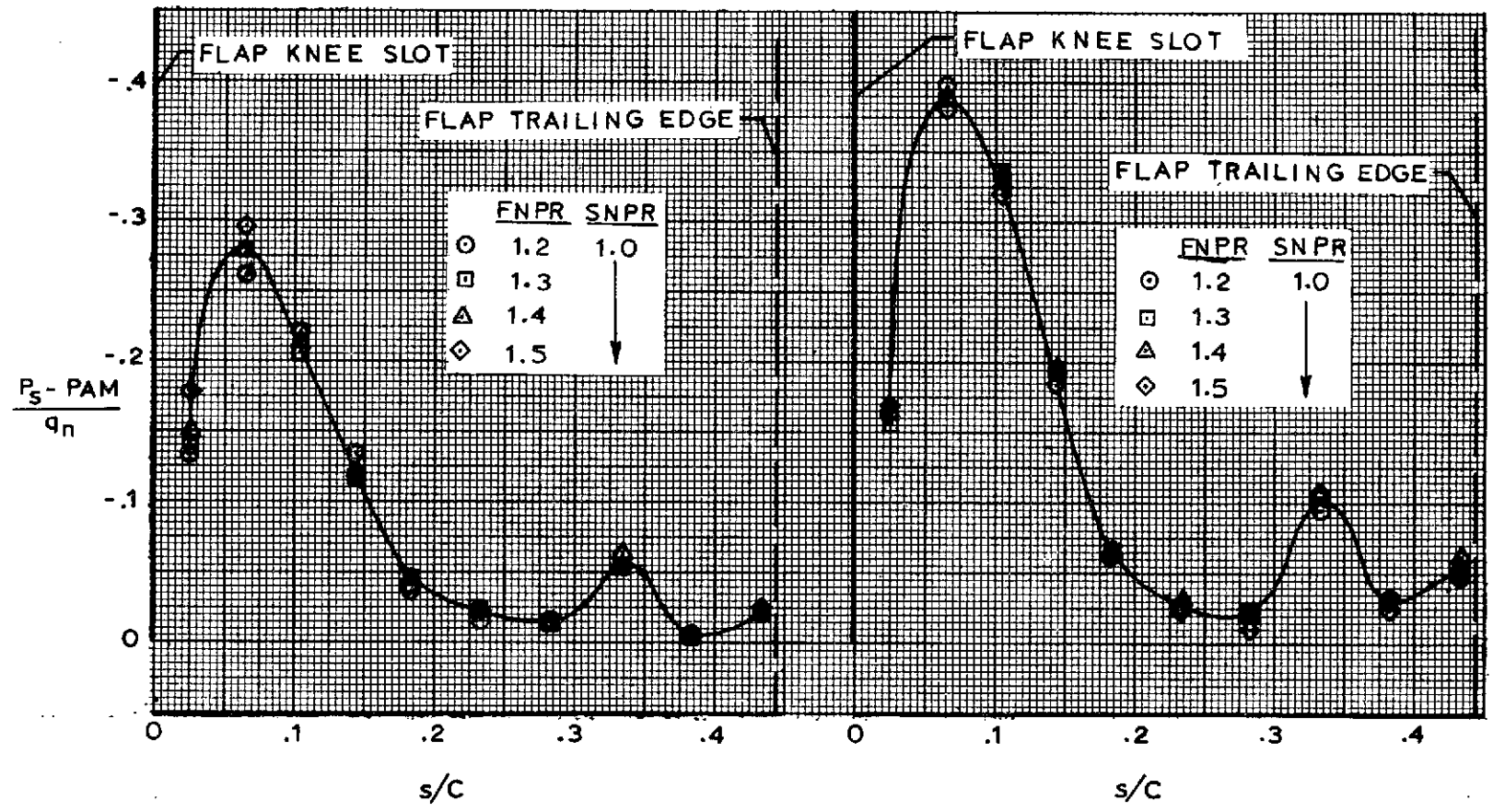

(a) With 20 degree spoiler.
Without knee blowing.

(b) Without spoiler.
Without knee blowing.

Figure A-6 Static pressure coefficient profile over flap upper surface.
JH 70°flap.

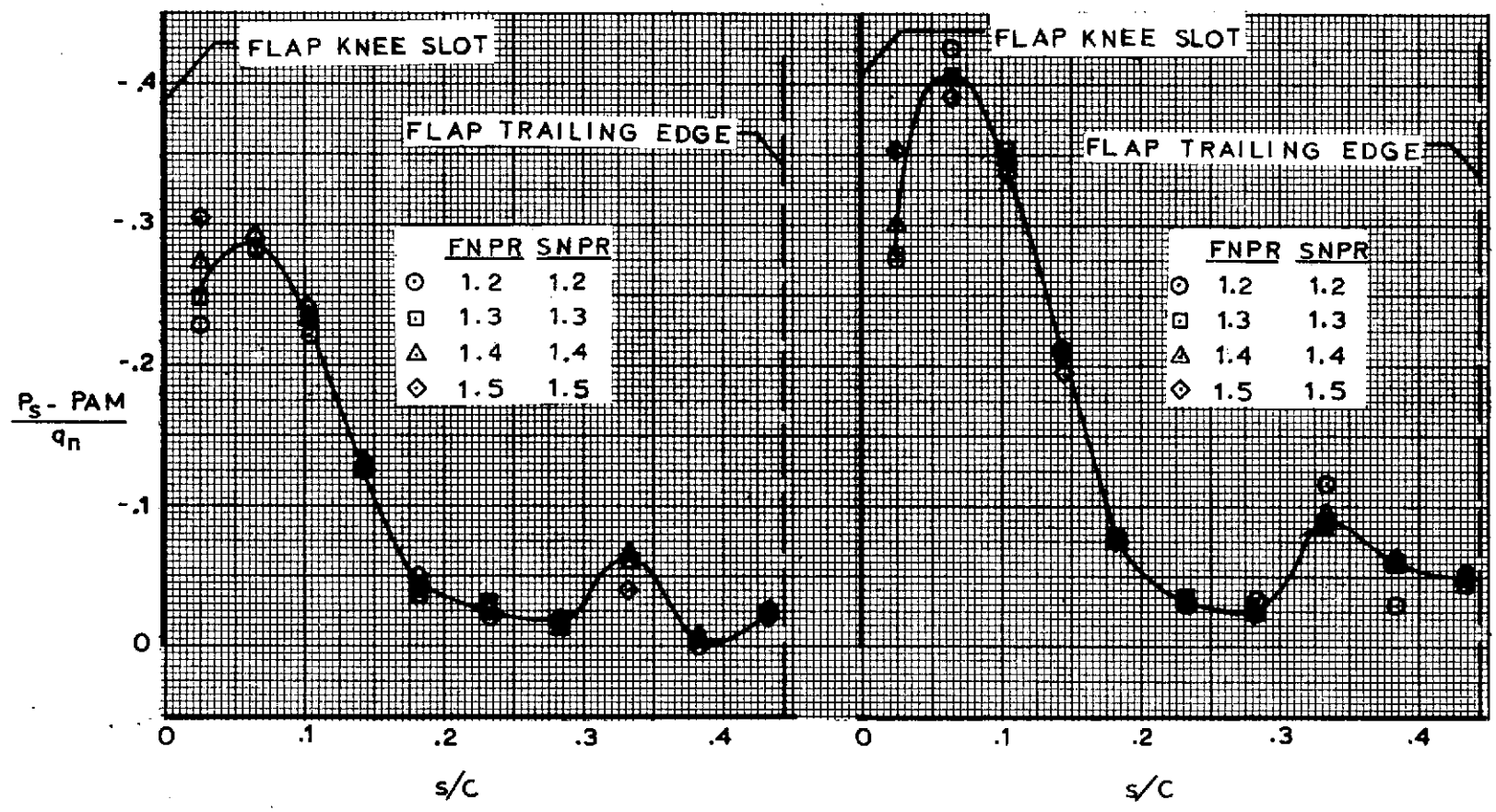

(c) With 20 degree spoiler.
With knee blowing.

(d) Without spoiler.
With knee blowing.

Figure A-6 Concluded.

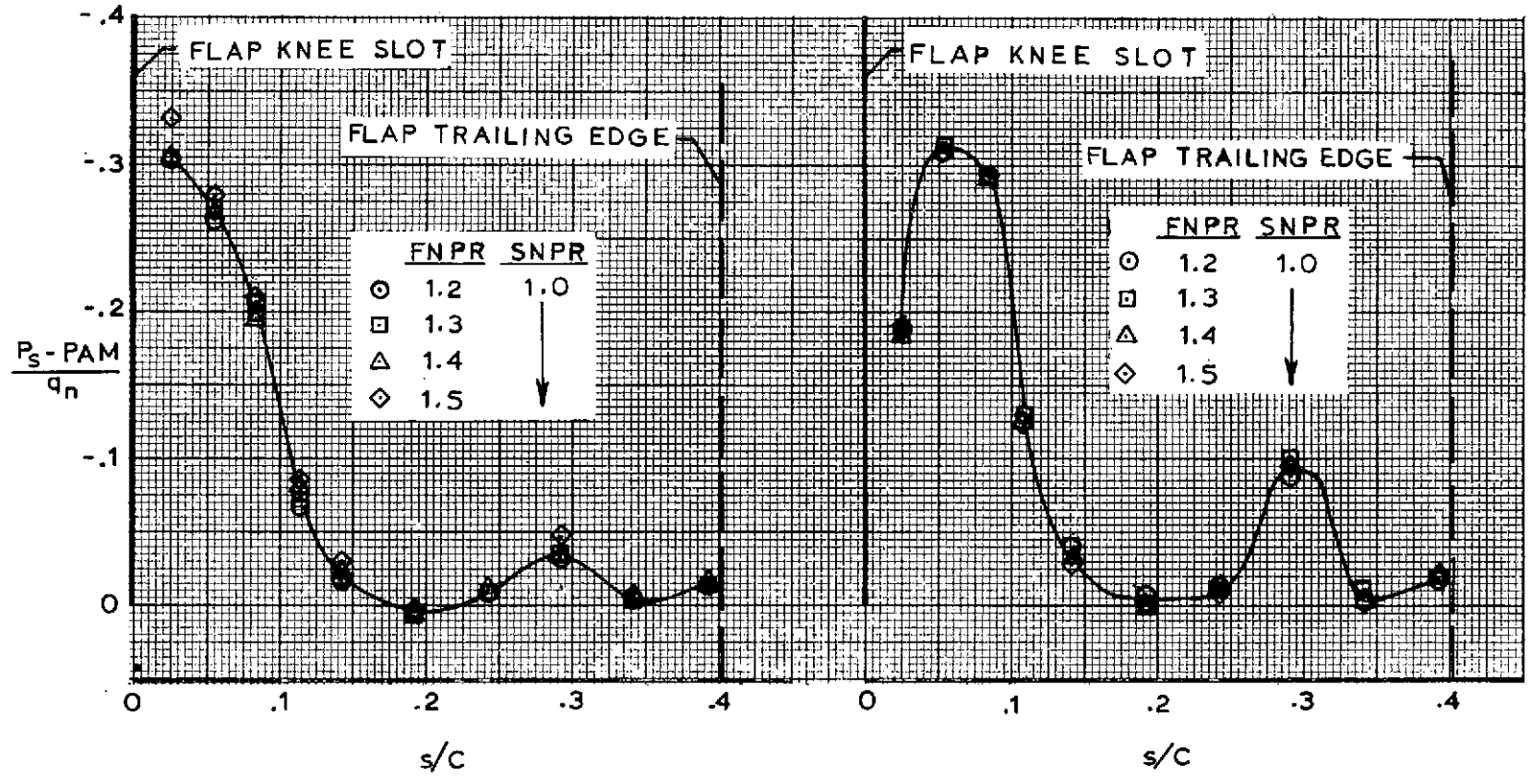

(a) With 20 degree spoiler.
Without knee blowing.

(b) Without spoiler.
Without knee blowing.

Figure A-7 Static pressure coefficient profile over flap upper surface.
JH 50°flap.

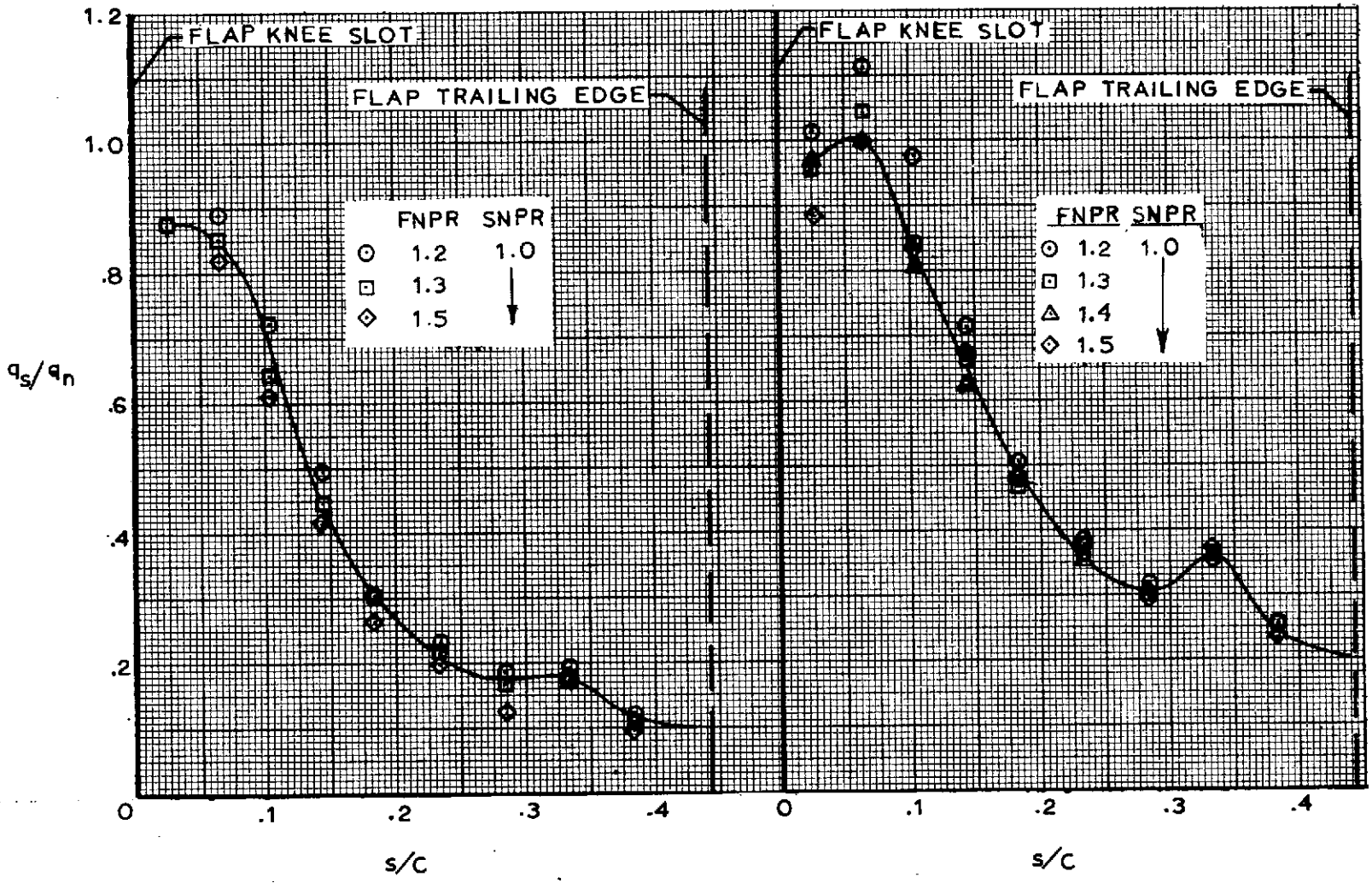

(a) With 20 degree spoiler. Without knee blowing.

(b) Without spoiler. Without knee blowing.

Figure A-8 Flow decay profile over flap upper surface. JH 70° flap.

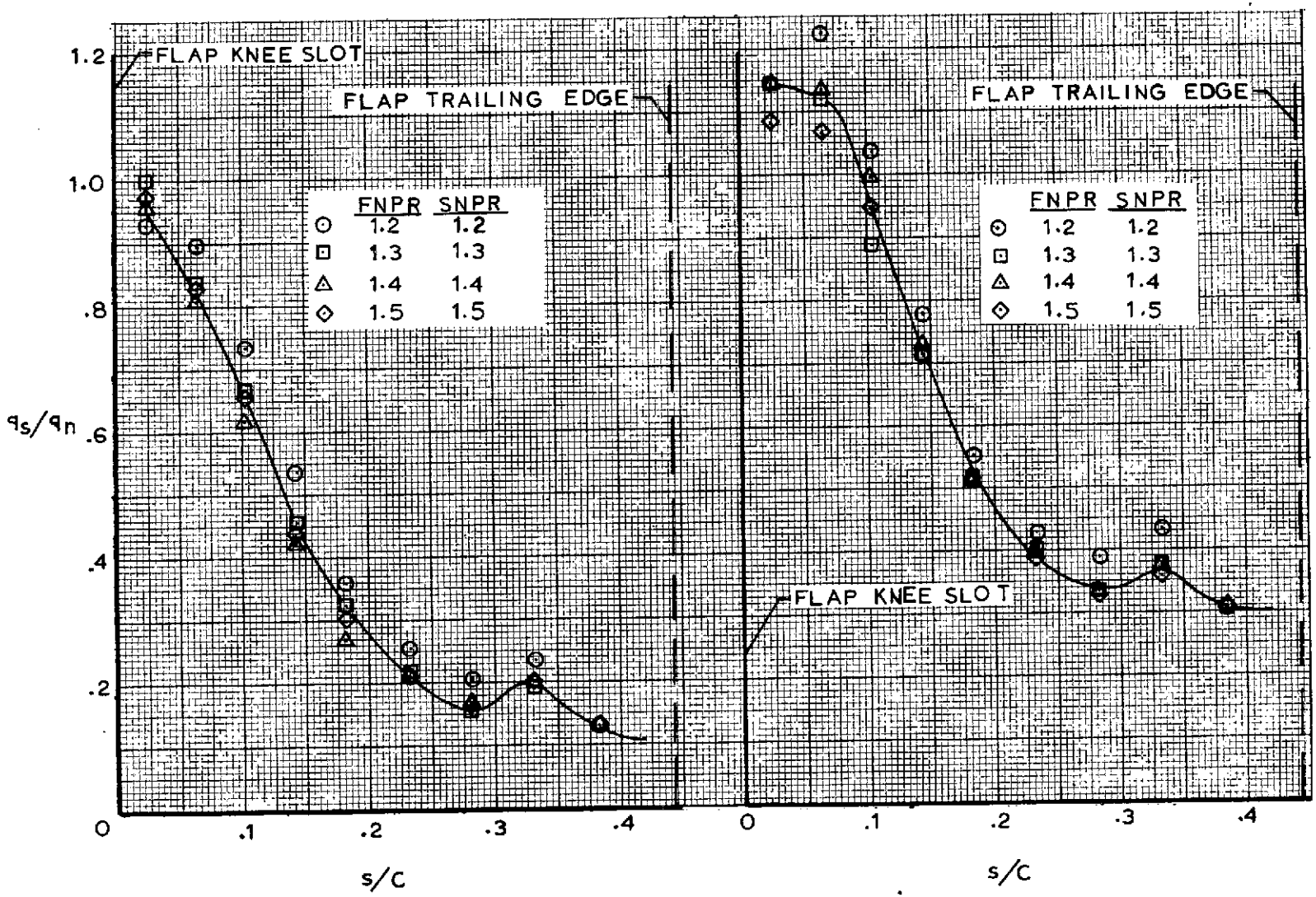

(c) With 20 degree spoiler
With knee blowing.

(d) Without spoiler.
With knee blowing

Figure A-8 Concluded.

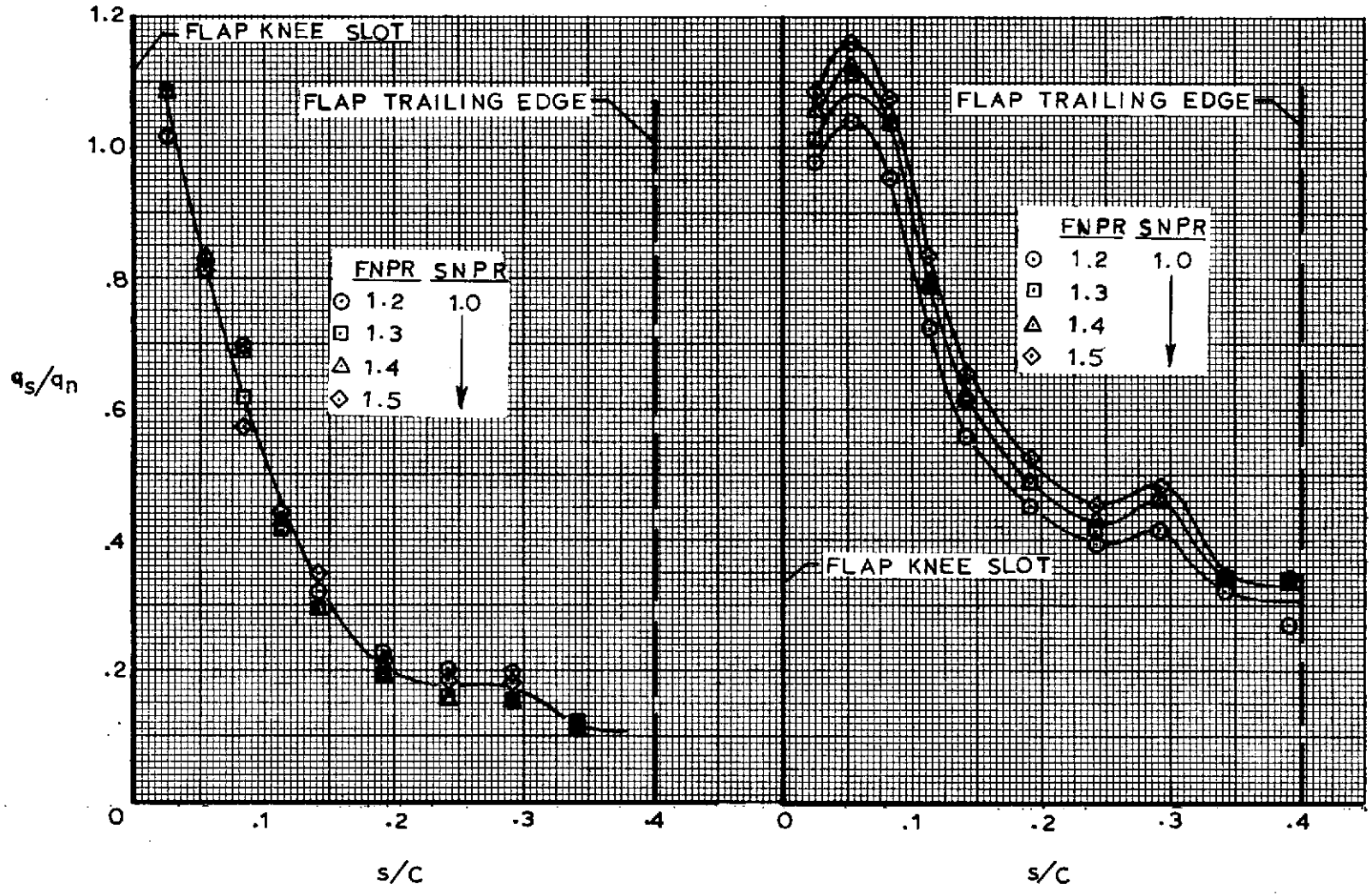

(a) With 20 degrees spoiler. Without knee blowing.

(b) Without spoiler. Without knee blowing.

Figure A-9 Flow decay profile over flap upper surface. JH 50°flap.

(a) FNPR = 1.2

Figure A-10 Flow visualization study. Jacobs-Hurkamp 70 flap. Without knee blowing.

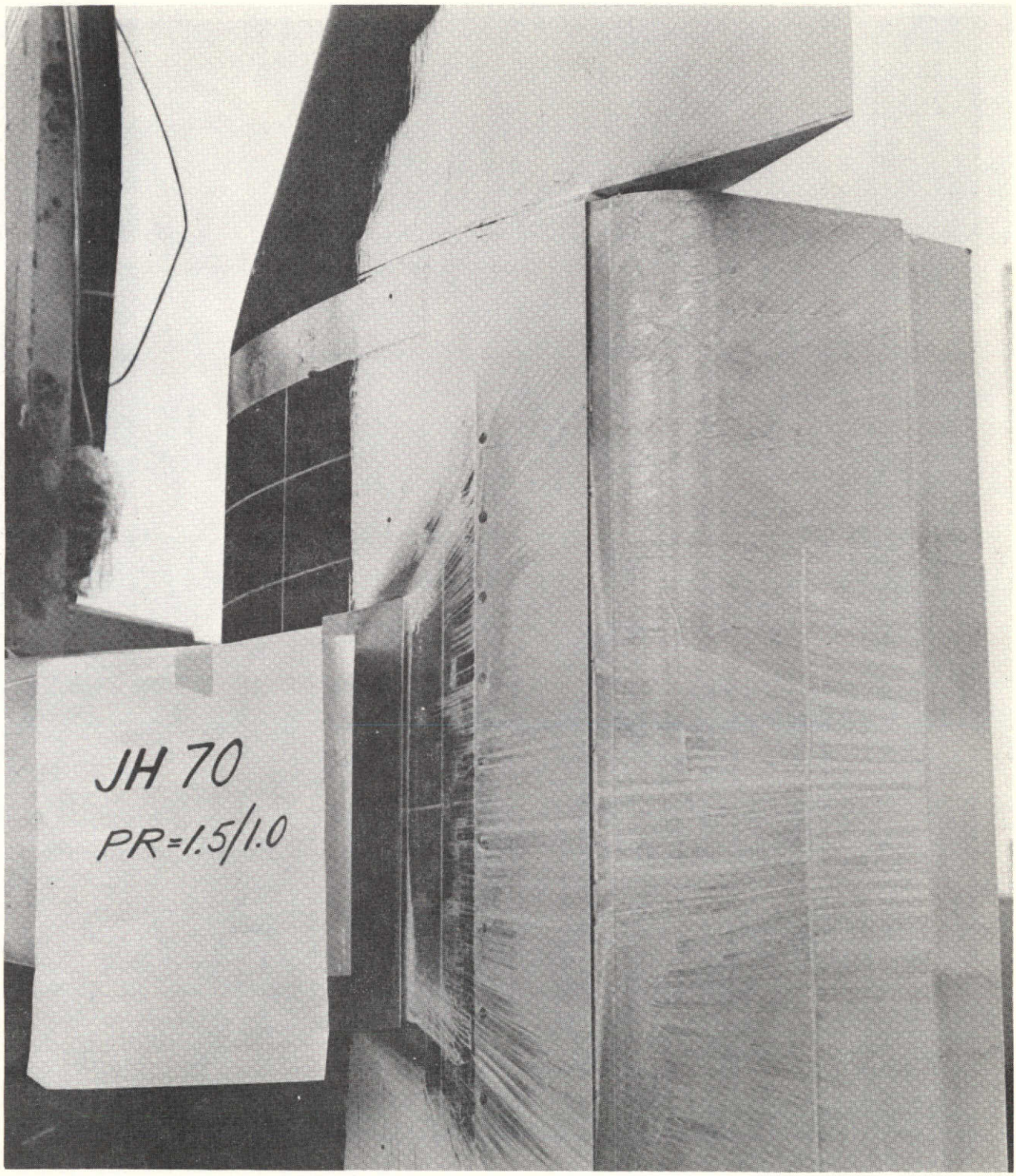

(b) FNPR = 1.5. Overall view.

Figure A-10 Continued.

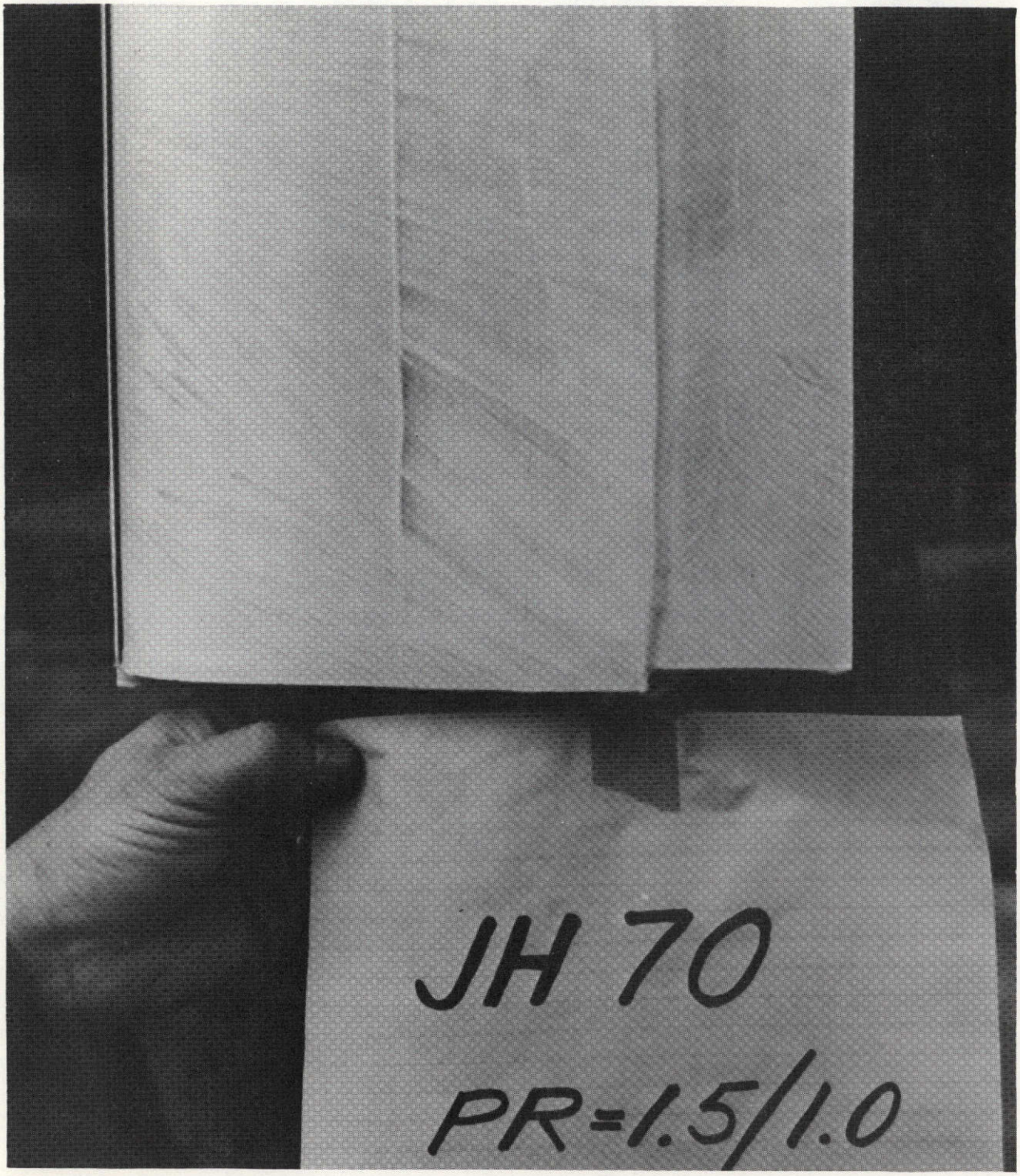

(c) FNPR = 1.5. Closeup view.

Figure A-10 Concluded.

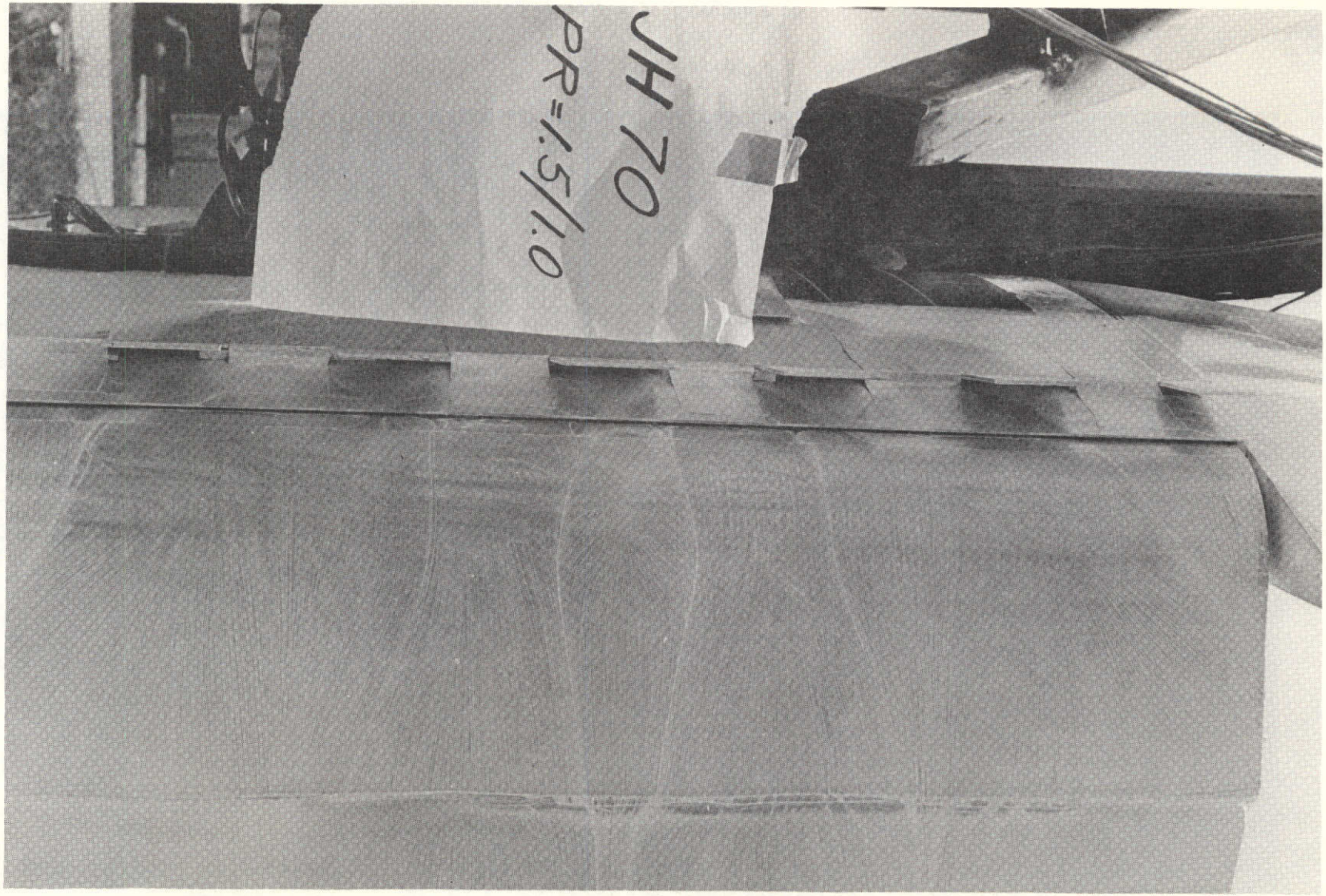

(a) Overall view.

Figure A-11 Flow visualization study. Jacobs-Hurkamp 70 flap with 20 degree segmented spoiler. Without knee blowing. FNPR = 1.5.

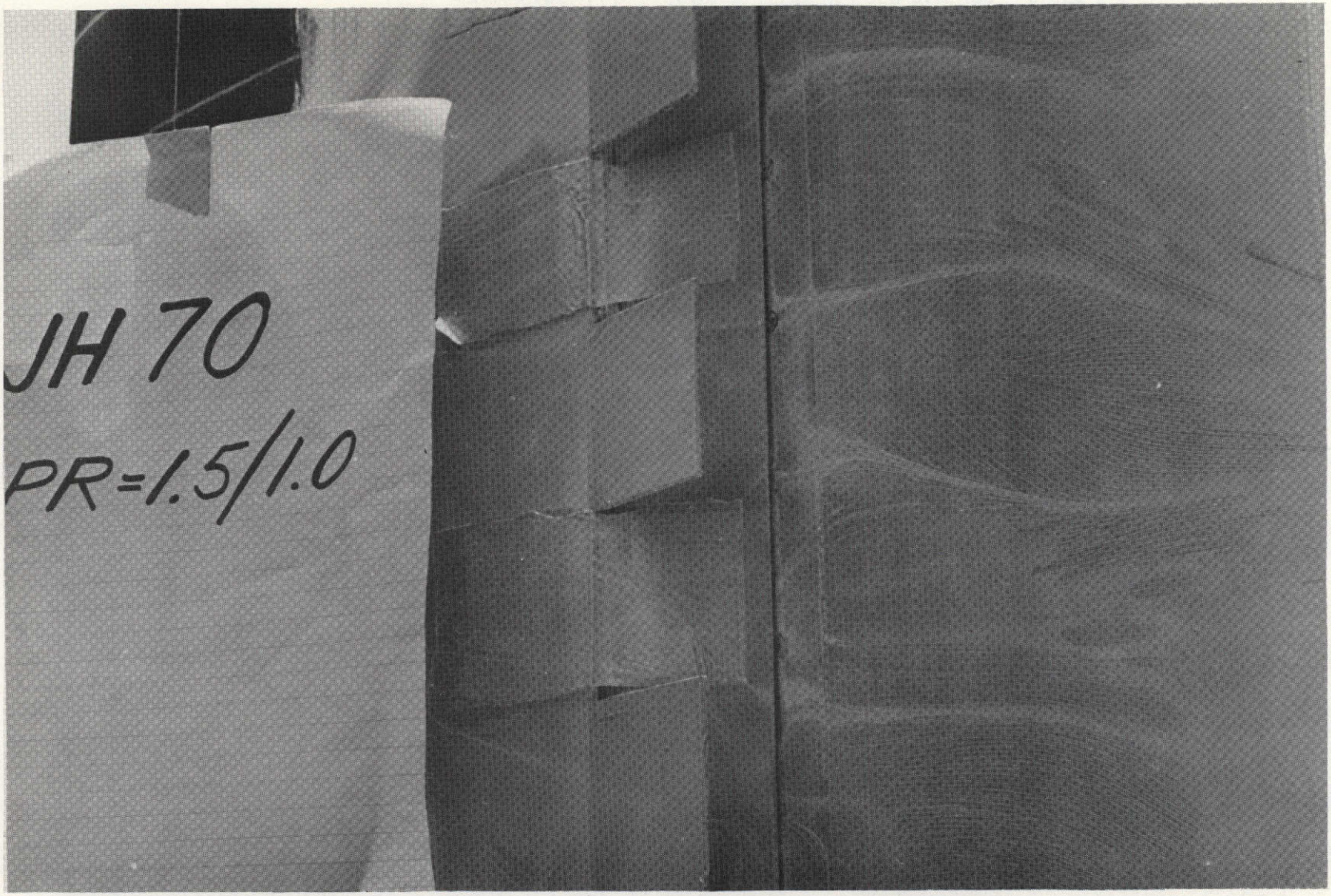

(b) Closeup view.

Figure A-11 Concluded.

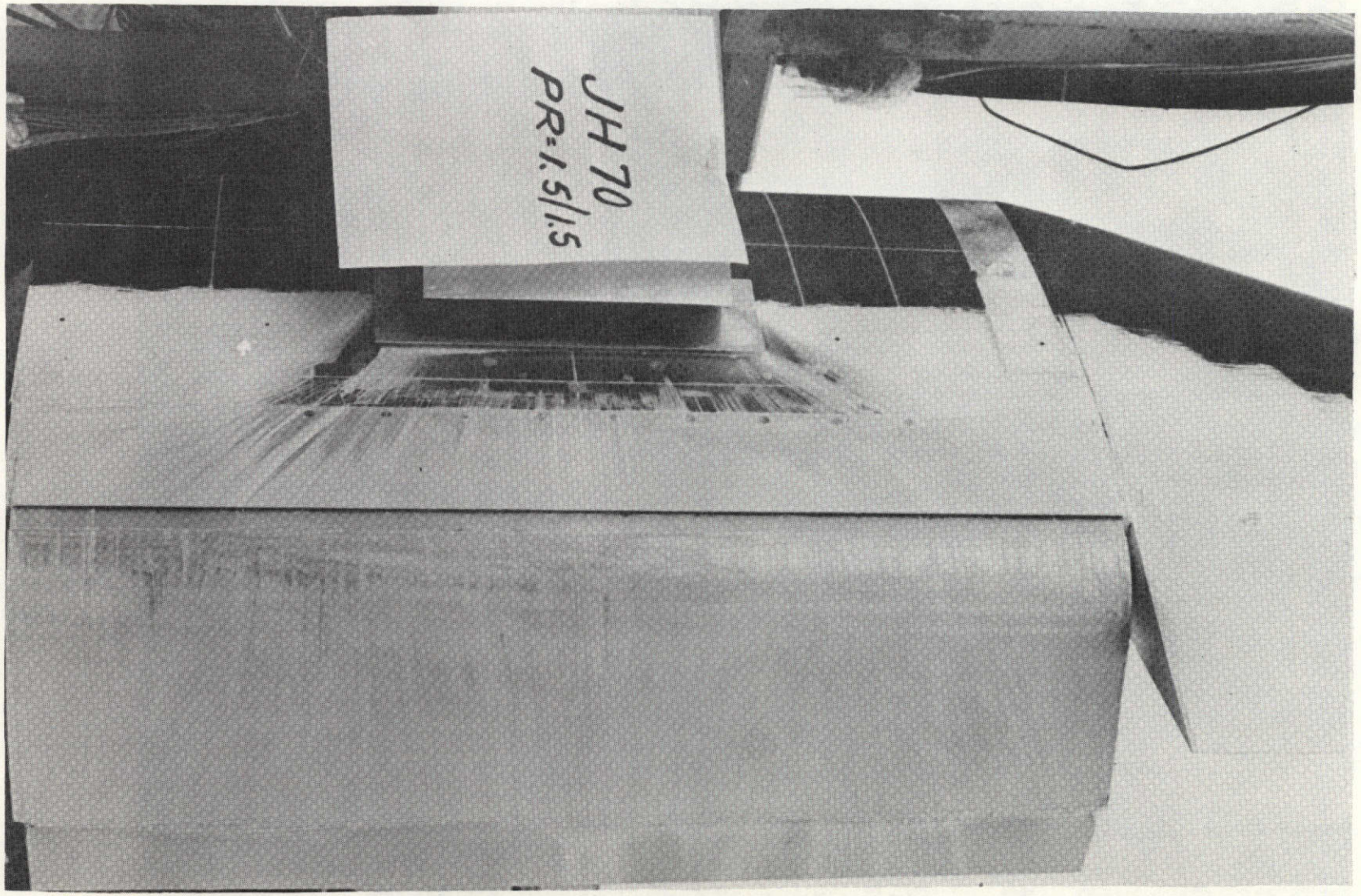

(a) Overall view.

Figure A-12 Flow visualization study. Jacobs-Hurkamp 70 degree flap. With knee blowing. FNPR = 1.5, SNPR = 1.5.

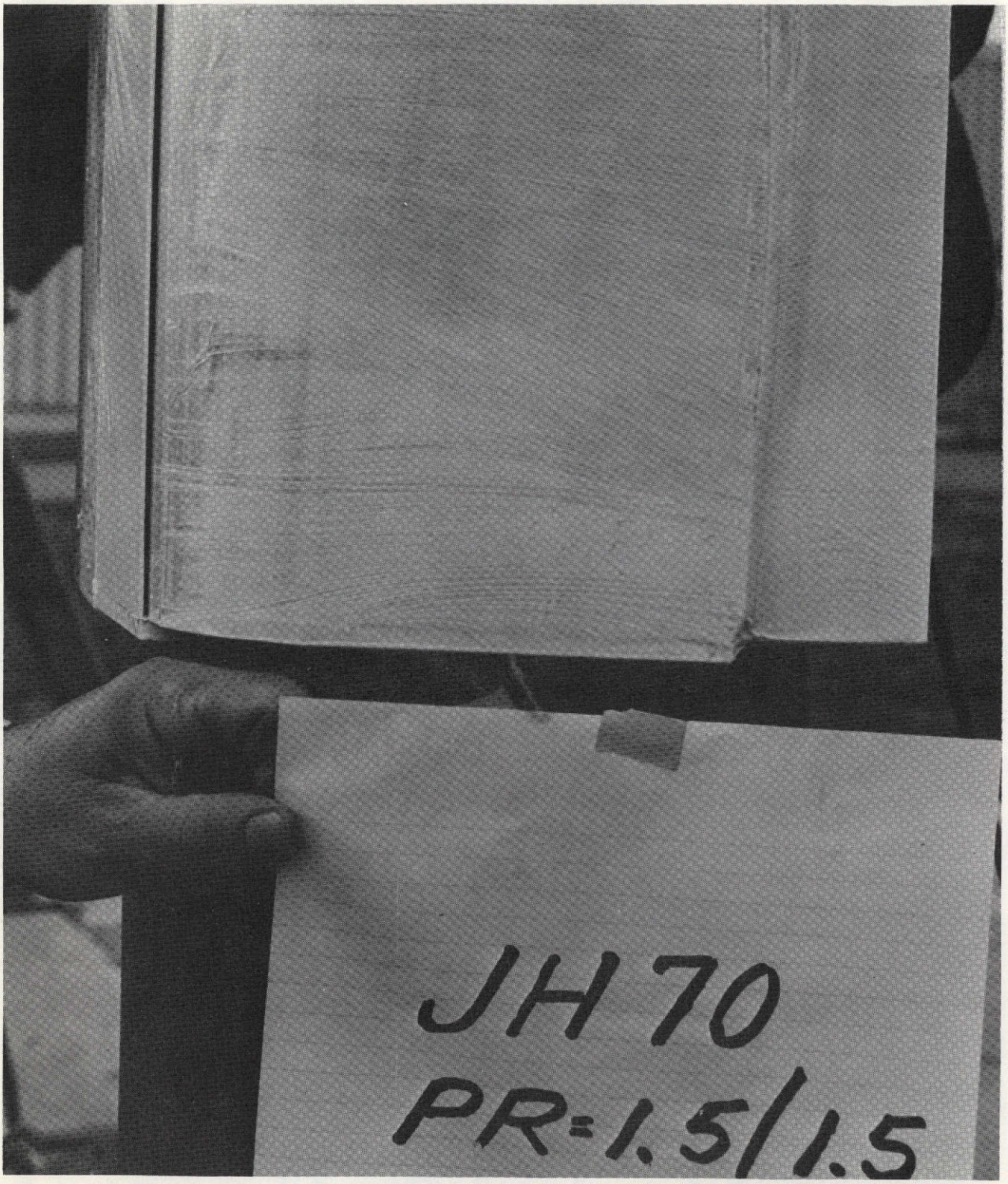

(b) Closeup view.

Figure A-12 Concluded.

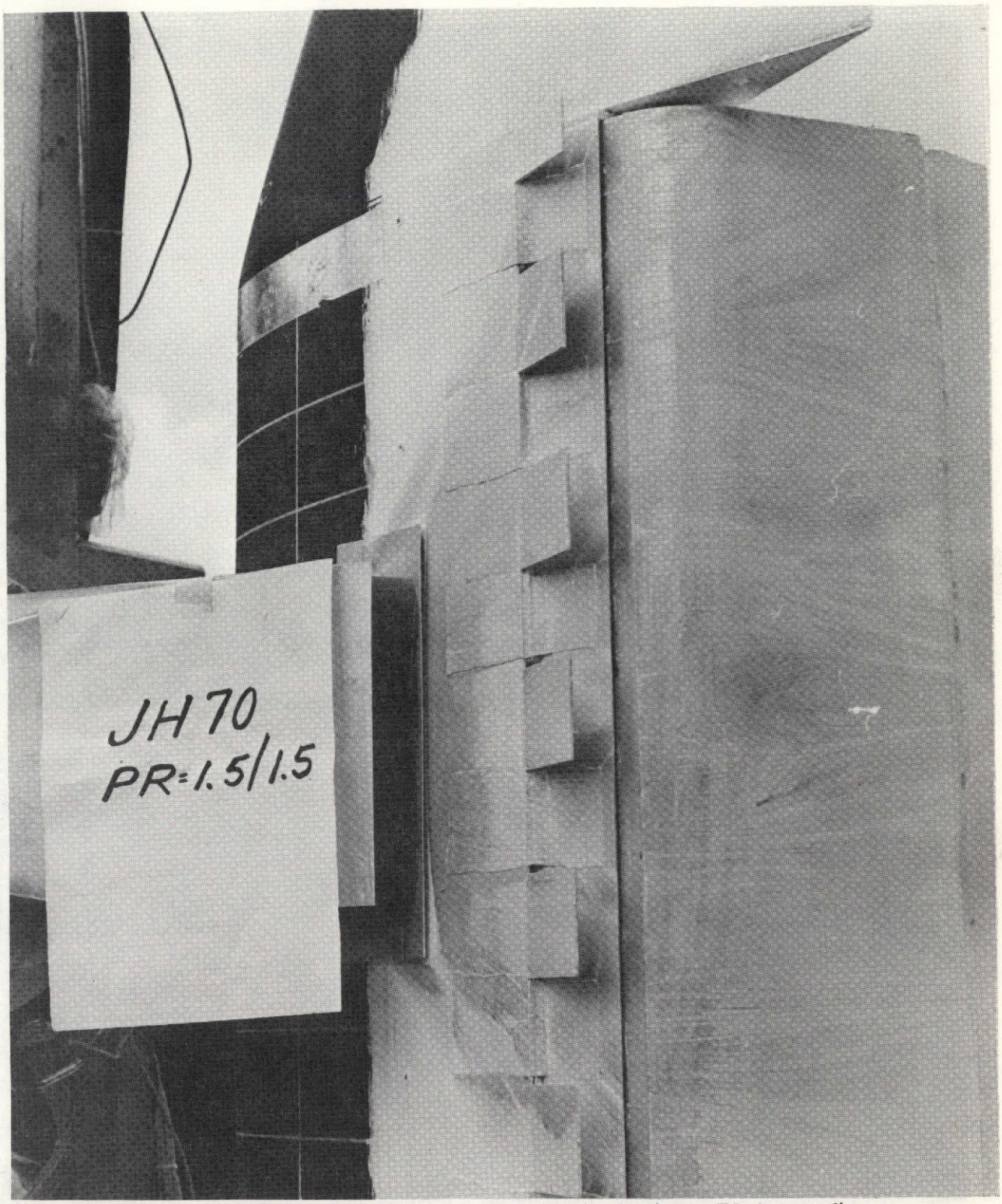

Figure A-13 Flow visualization study. Jacobs-Hurkamp 70 degree flap with 20 degree segmented spoiler. With knee blowing. FNPR = 1.5, SNPR = 1.5.

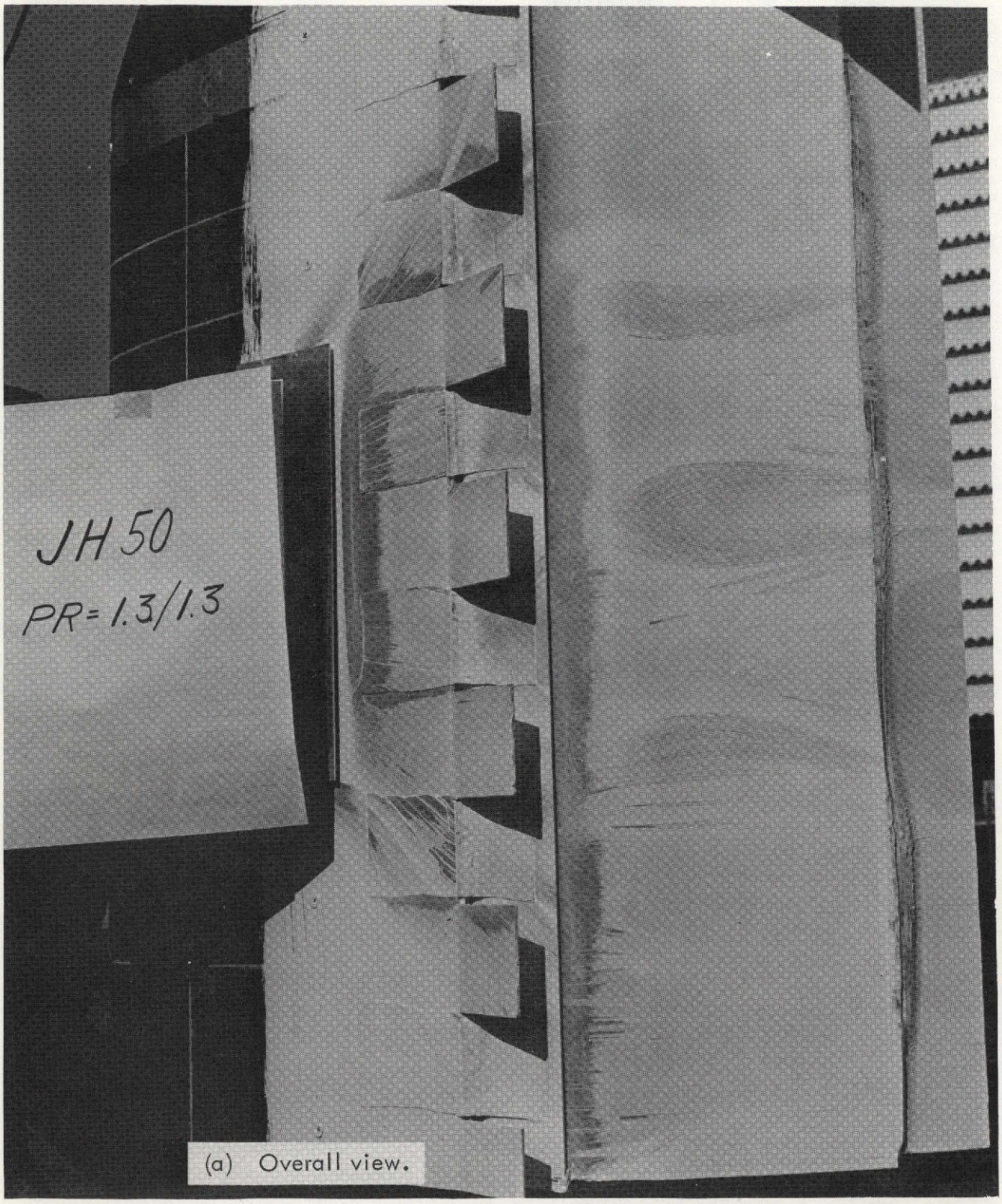

Figure A-14 Flow visualization study. Jacobs-Hurkamp 50 degree flap with 20 degree segmented spoilers. With knee blowing. FNPR = 1.3, SNPR = 1.3.

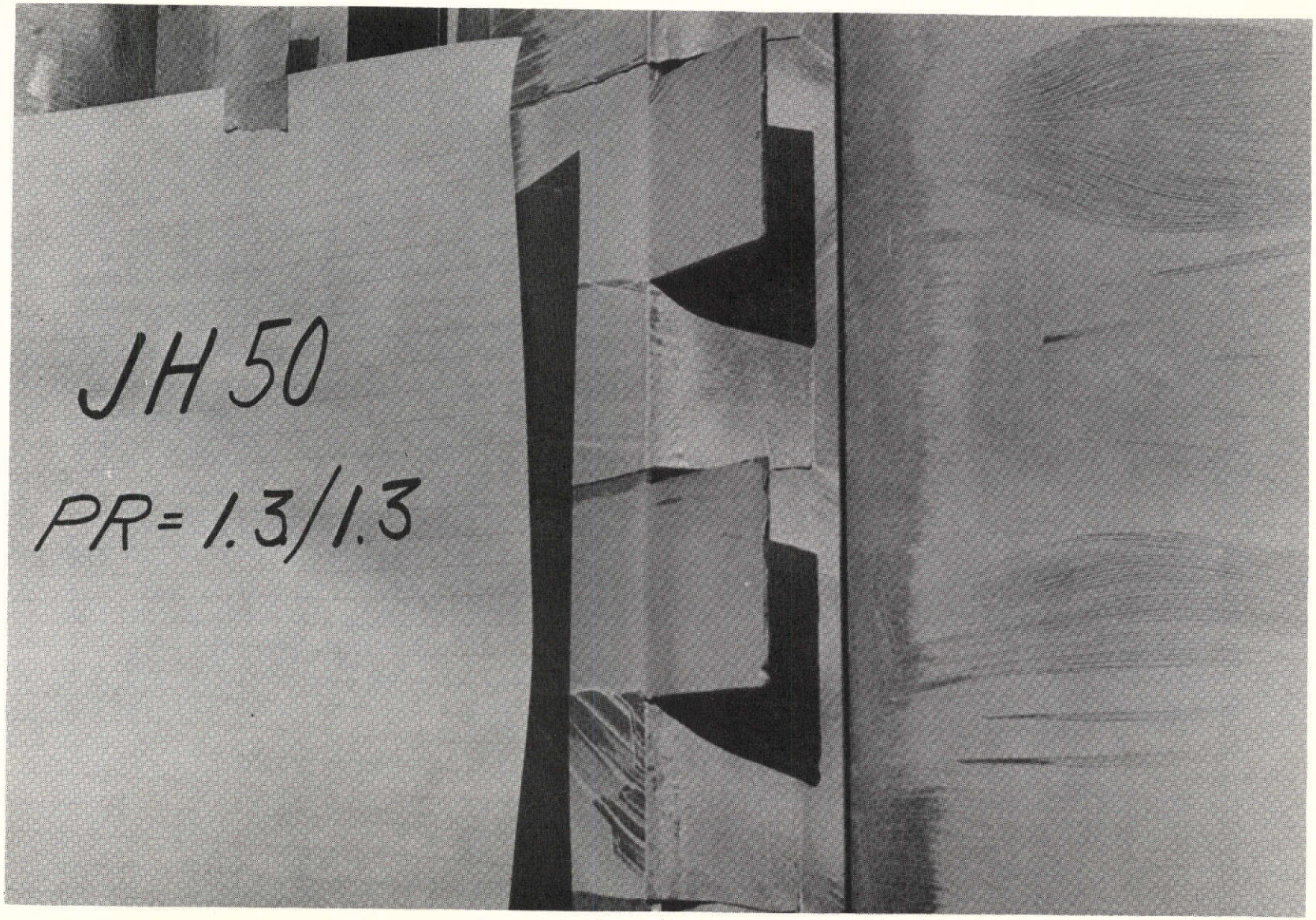

(b) Closeup view.

Figure A-14 Concluded.

CURVE	NOZZLE	FLAP	FD	AK/ANT	ATE/ANT	X/C	ETA/B	THETA	FNPR	SNPR
1	NR4D	JH	0.87 (50°)	.05	0	.35	.50	.21 (12°)	1.5	1.0
2	↓	↓	1.22 (70°)	↓	↓	↓	↓	↓	↓	↓

TOTAL PRESSURE RAKE AT FLAP MIDSPAN NORMAL TO TRAILING EDGE

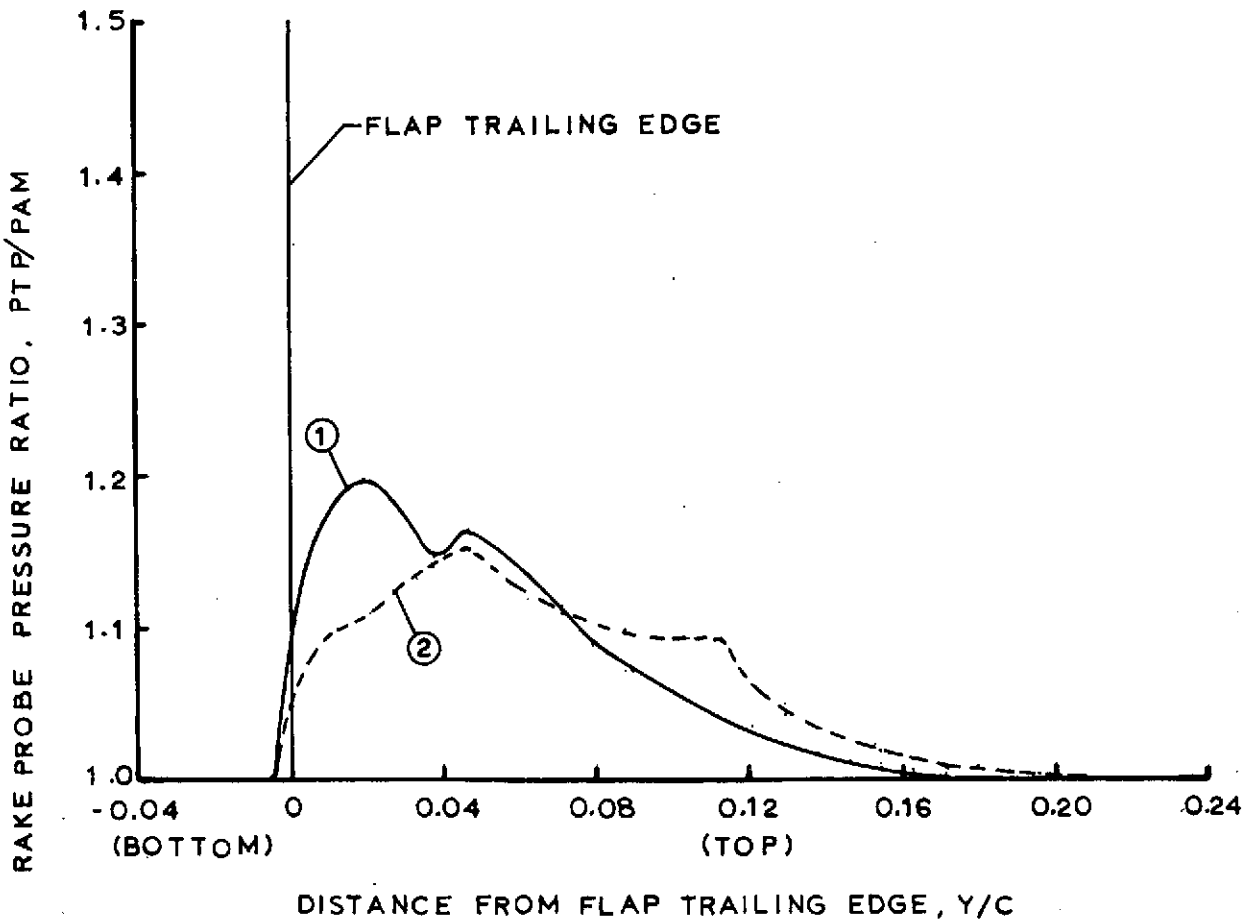

(a) Comparison of flap deflection angle on pressure distribution at the flap trailing edge.

Figure A-15 Flap trailing edge wake survey.

CURVE	NOZZLE	FLAP	FD	AK/ANT	ATE/ANT	X/C	ETA/B	THETA	FNPR	SNPR	SPOILER
1	NR4D	JH	1.22 (70°)	.05	0	.35	.50	.21 (12°)	1.5	1.0	YES
2										1.5	YES
3										1.0	NO
4										1.5	NO

TOTAL PRESSURE RAKE AT FLAP MIDSPAN NORMAL TO TRAILING EDGE

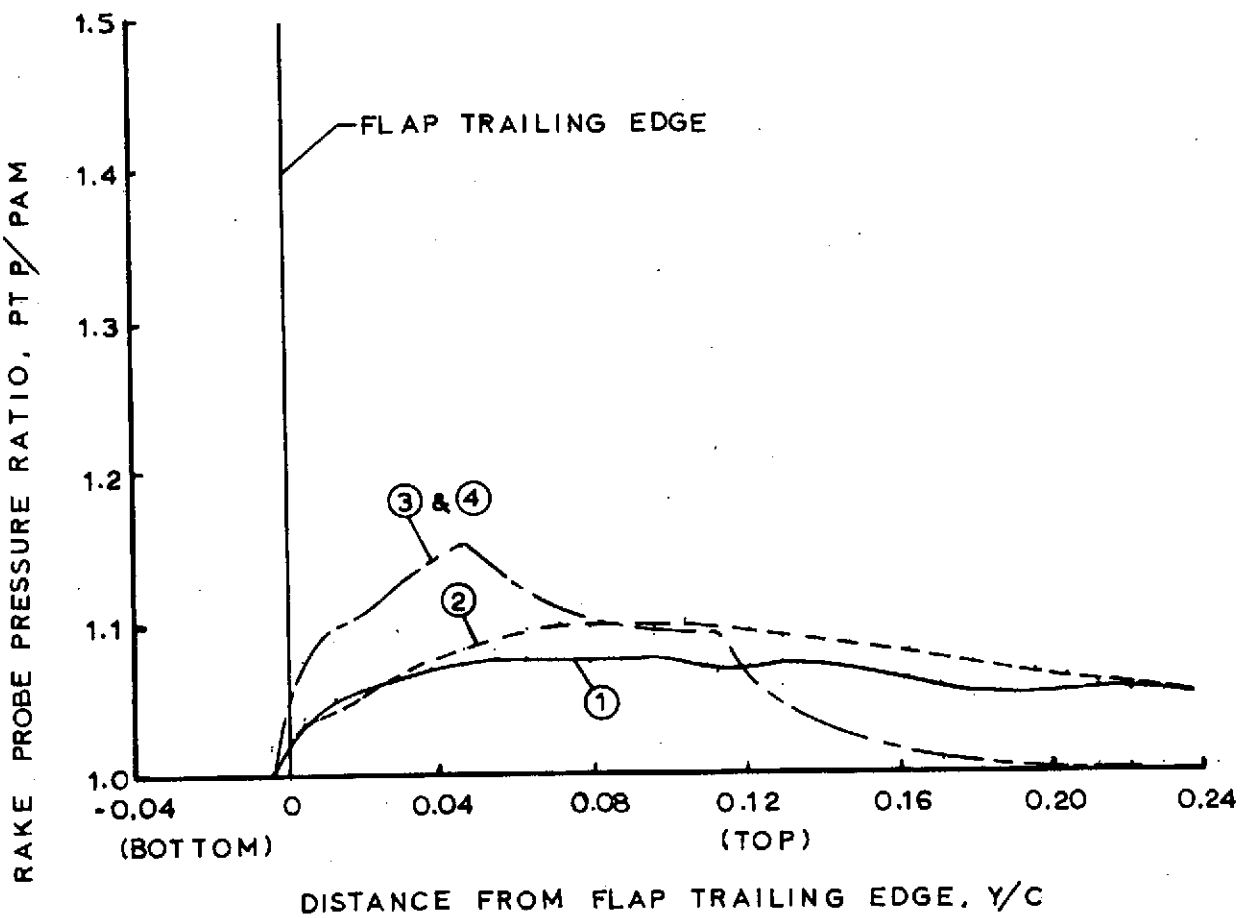

(b) Comparison of 20 degree spoiler effect on pressure distributions at the flap trailing edge.

Figure A-15 Concluded.

HYBRID PROPULSIVE LIFT
ACOUSTIC TEST
NAS 2-7812

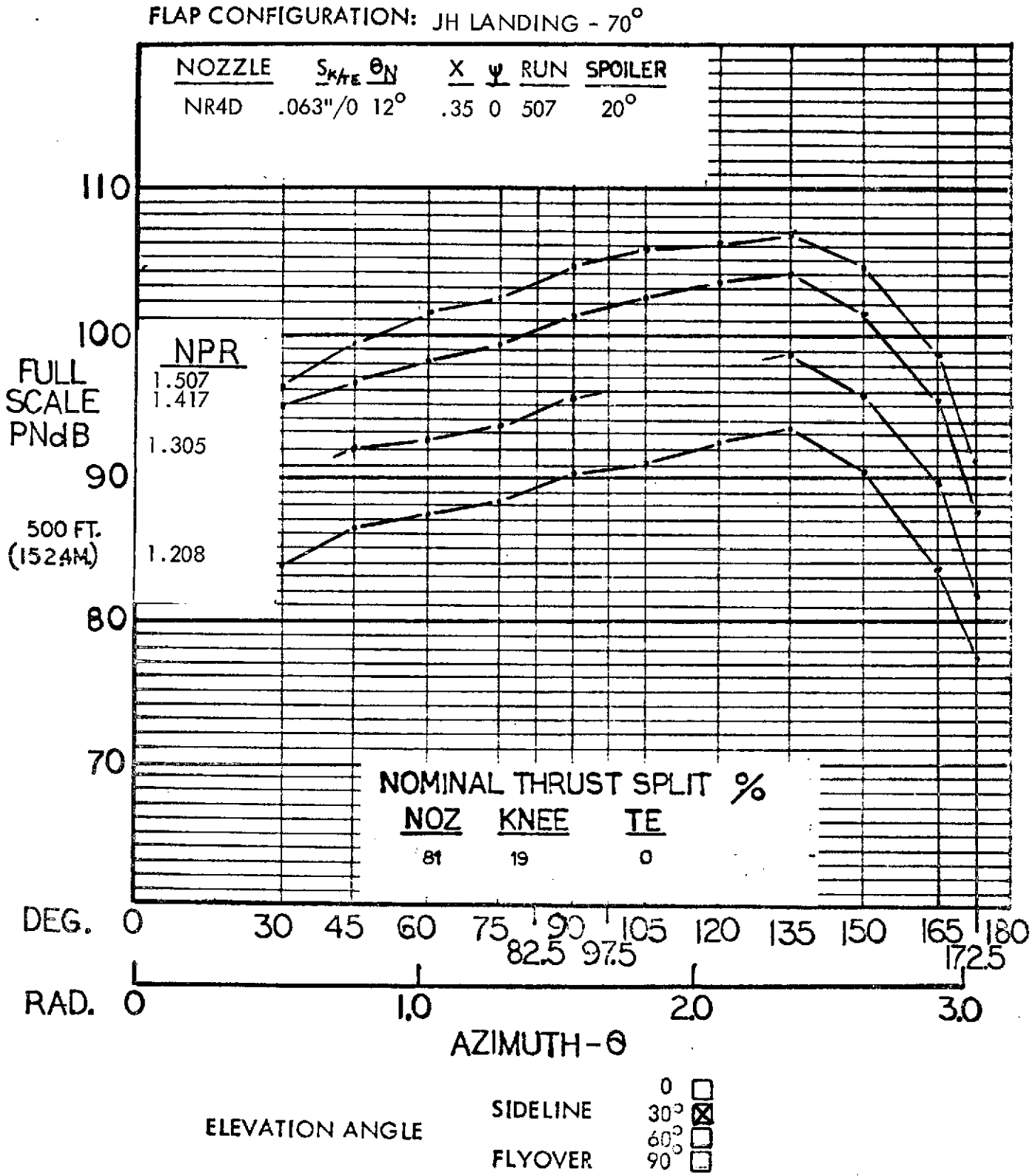

Figure A-16 Full scale sideline PNL for the aspect ratio 4 nozzle with deflector and JH flap with knee blowing; 70° flap angle, segmented spoiler at 20°.

HYBRID PROPULSIVE LIFT
ACOUSTIC TEST
NAS 2-7812

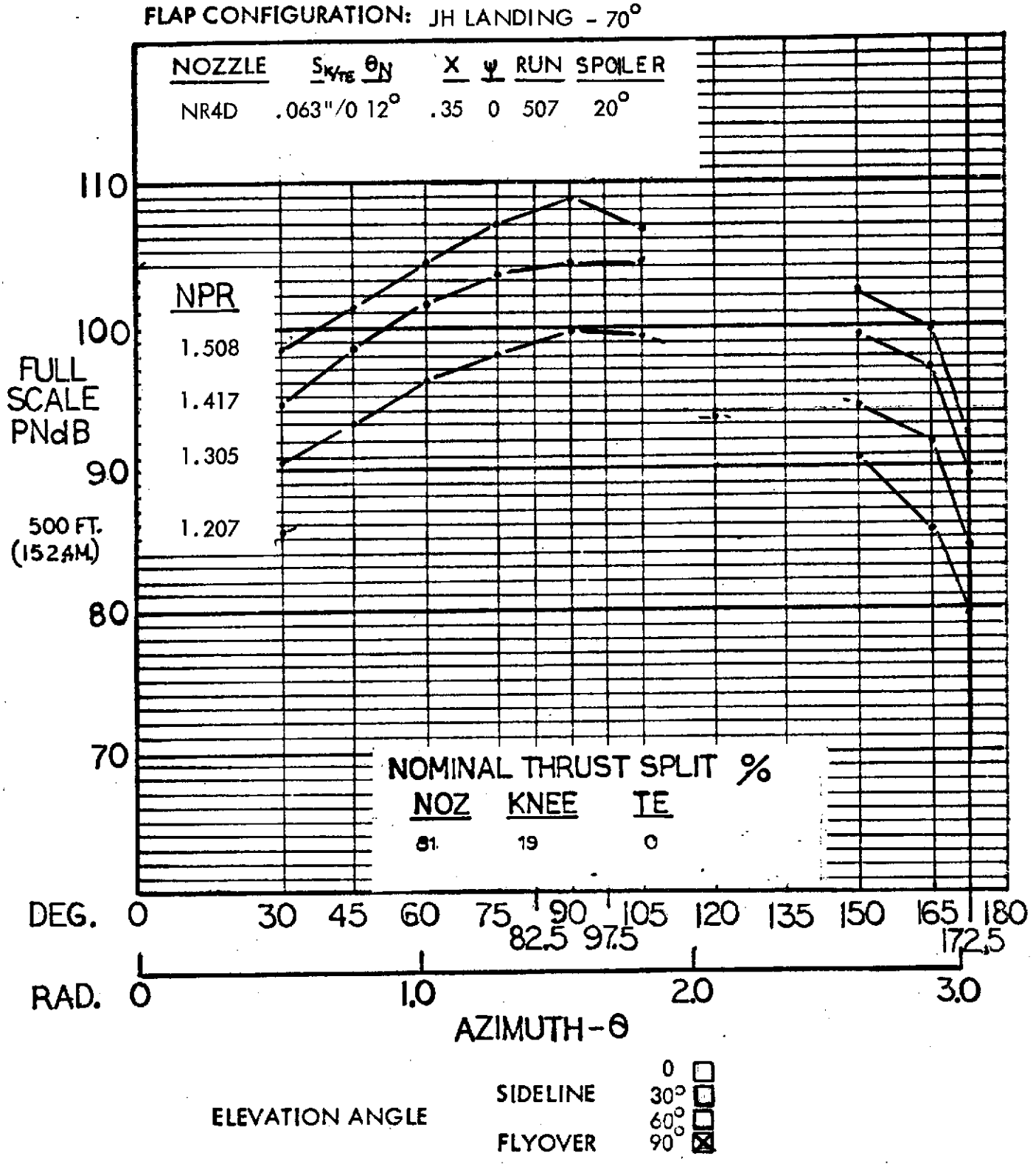

Figure A-17 Full scale flyover PNL for the aspect ratio 4 nozzle with deflector and JH flap with knee blowing; 70° flap angle, segmented spoiler at 20°.

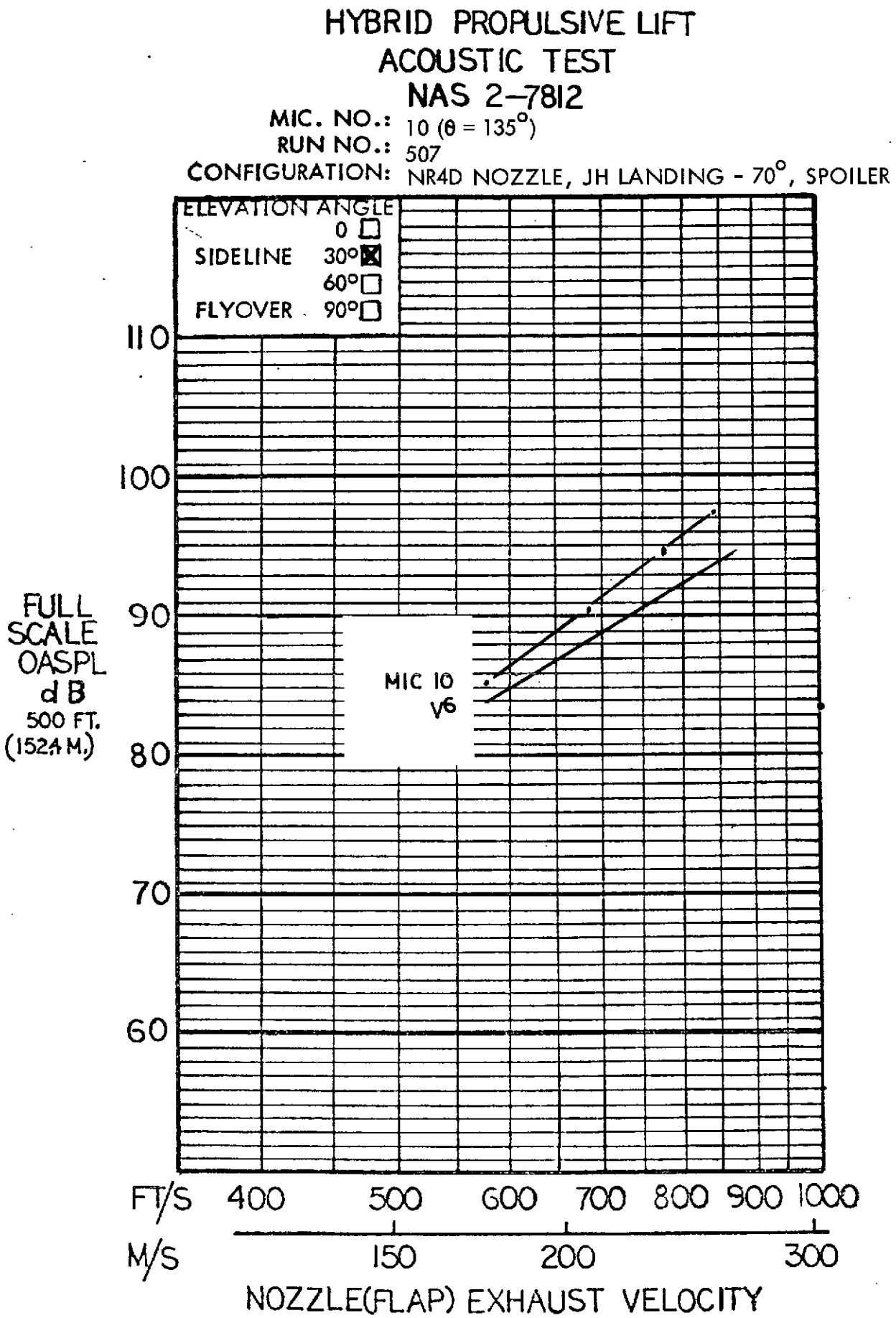

Figure A-18 Full scale sideline OASPL at 135° azimuth for the aspect ratio 4 nozzle with deflector and JH flap with knee blowing; 70° flap angle, segmented spoiler at 20°.

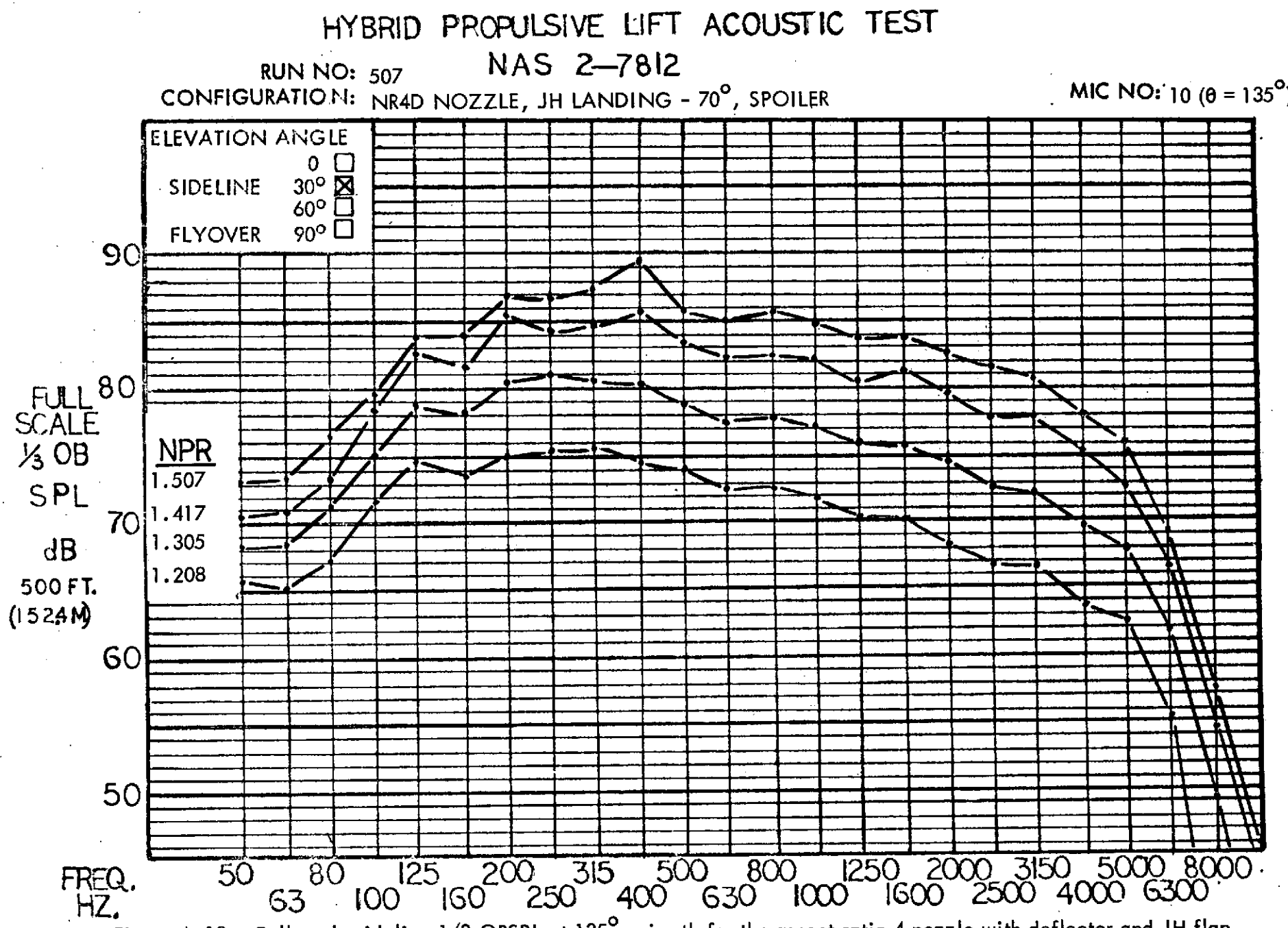

Figure A-19 Full scale sideline 1/3 OBSPL at 135° azimuth for the aspect ratio 4 nozzle with deflector and JH flap with knee blowing; 70° flap angle, segmented spoiler at 20°.

HYBRID PROPULSIVE LIFT
ACOUSTIC TEST
NAS 2-7812

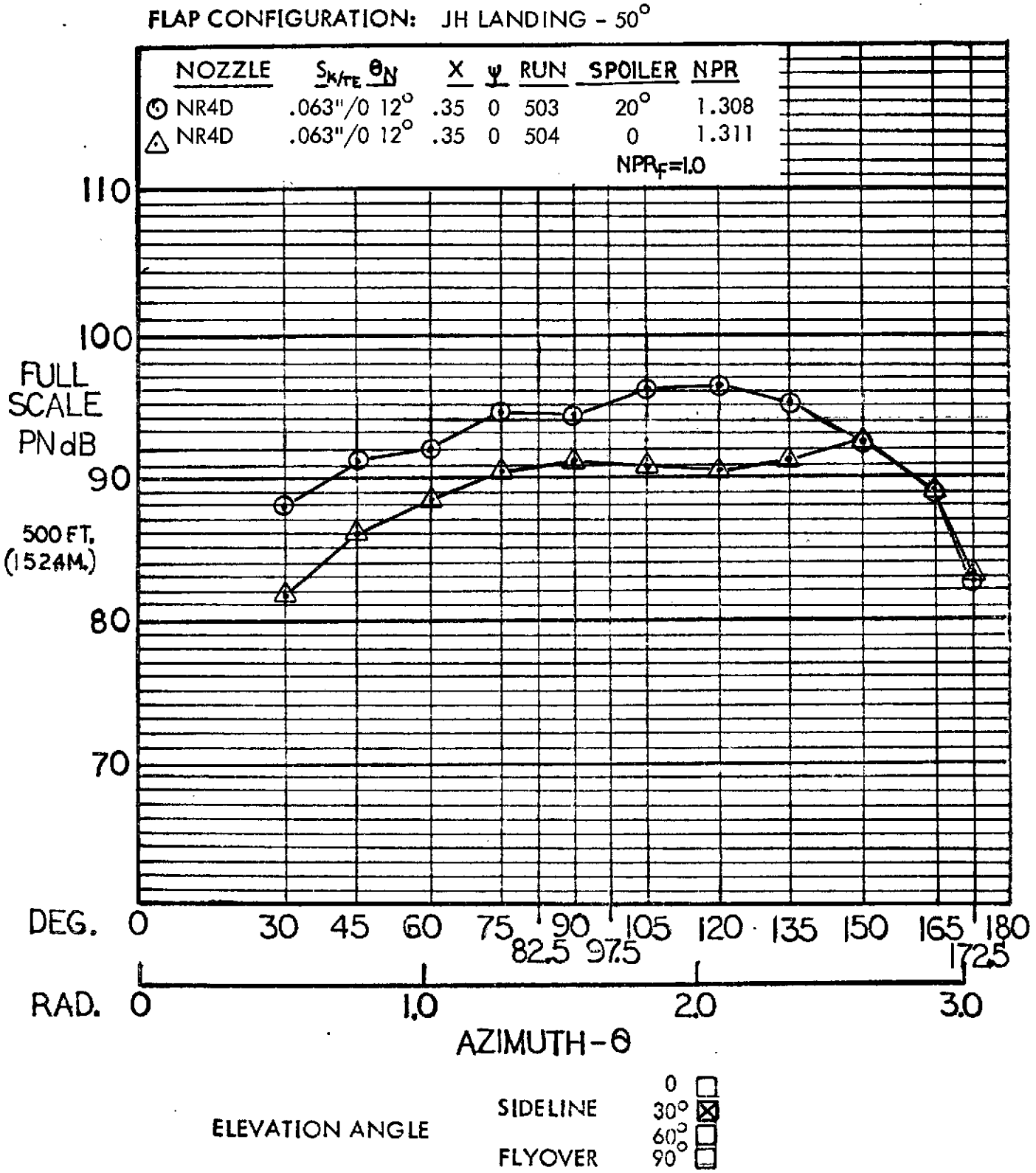

Figure A-20 Comparison of full scale sideline PNL for spoiler angles of 0° and 20°; JH flap at 50° flap angle, NR4D nozzle, no flap blowing.

HYBRID PROPULSIVE LIFT
ACOUSTIC TEST
NAS 2-7812

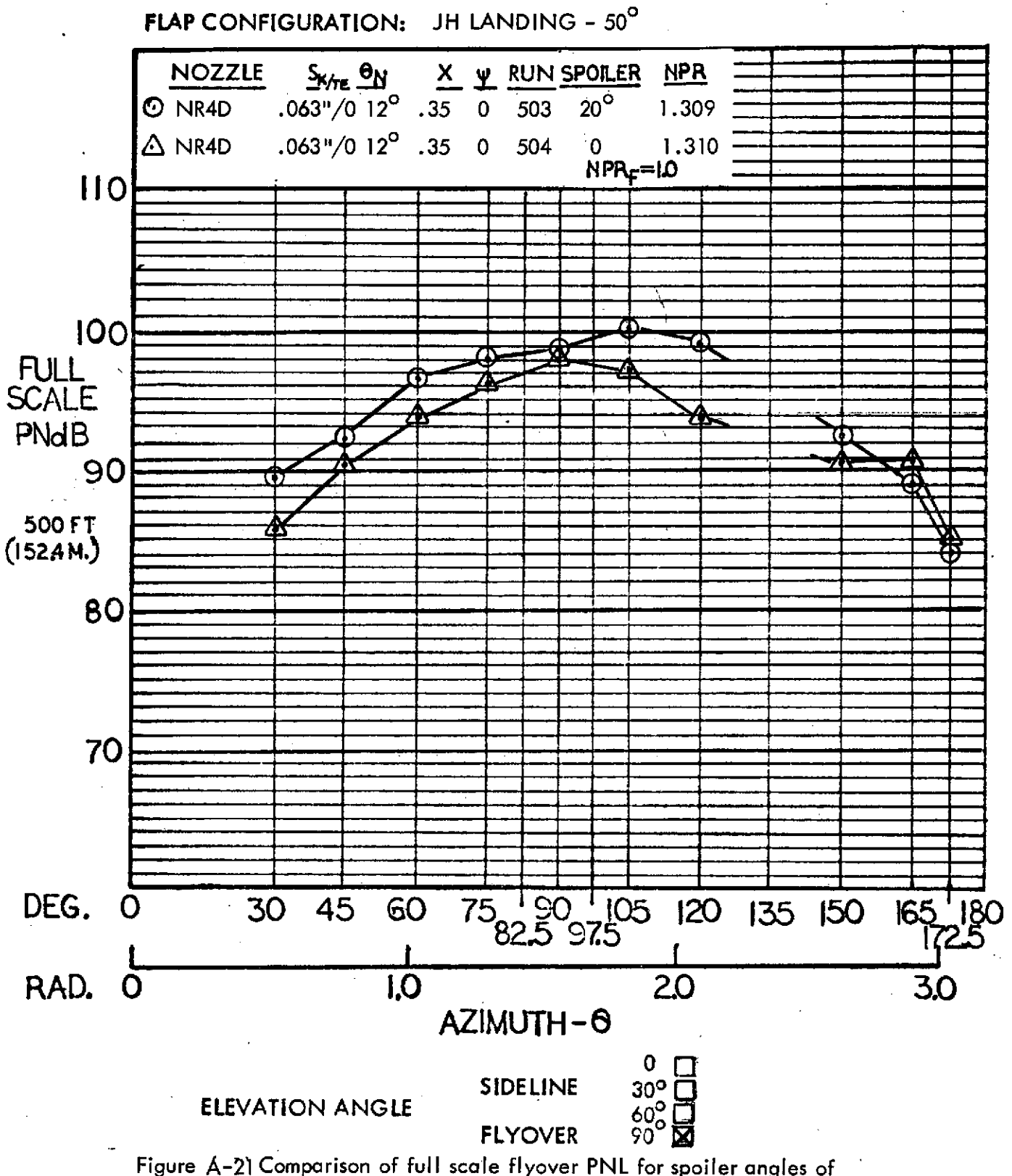

Figure A-21 Comparison of full scale flyover PNL for spoiler angles of 0° and 20°; JH flap, 50° flap angle, NR4D nozzle, no flap blowing.

HYBRID PROPULSIVE LIFT
ACOUSTIC TEST
NAS 2-7812

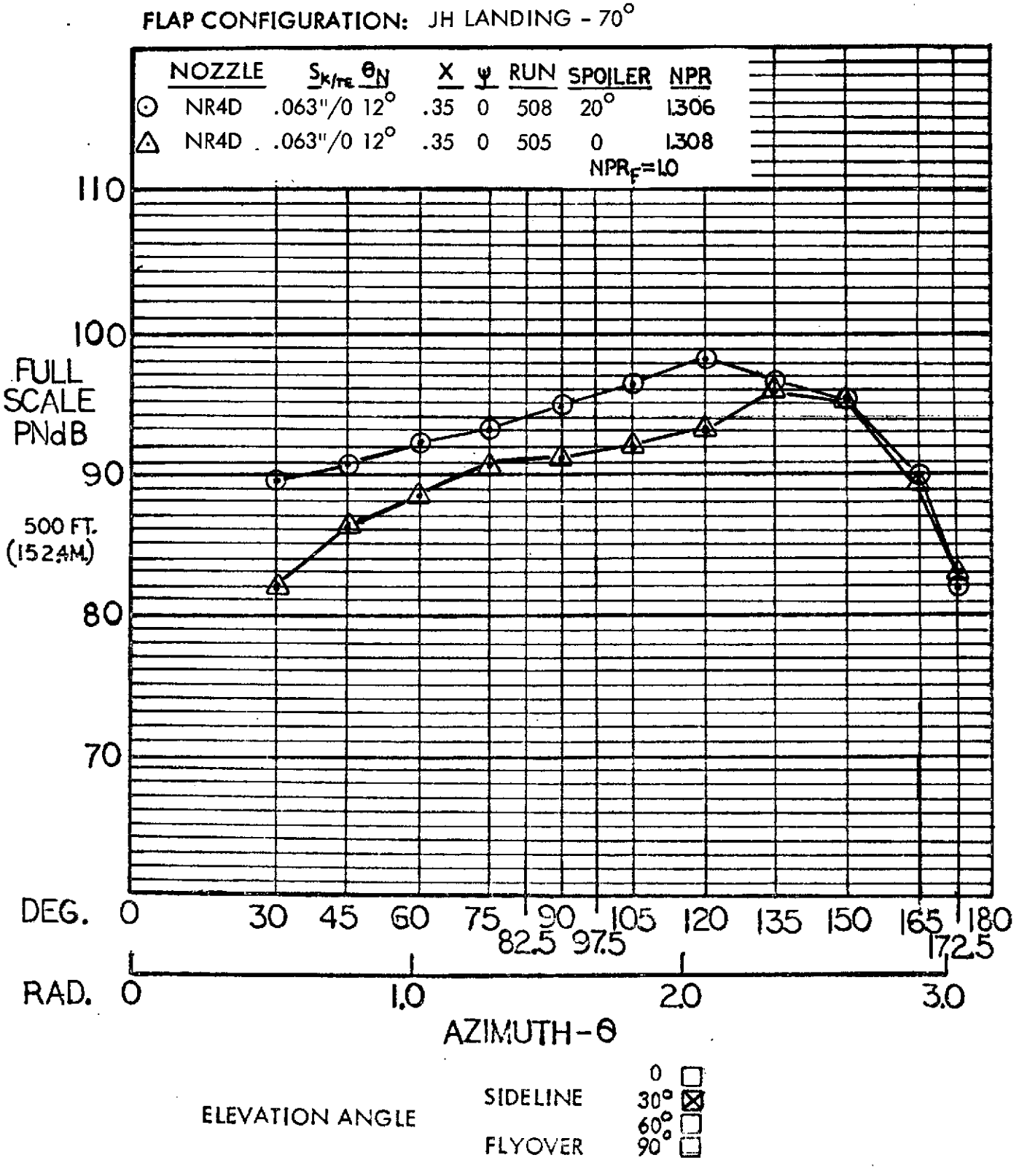

Figure A-22 Comparison of full scale sideline PNL for spoiler angles of 0° and 20°, JH flap, 70° flap angle, NR4D nozzle, no flap blowing.

HYBRID PROPULSIVE LIFT
ACOUSTIC TEST
NAS 2-7812

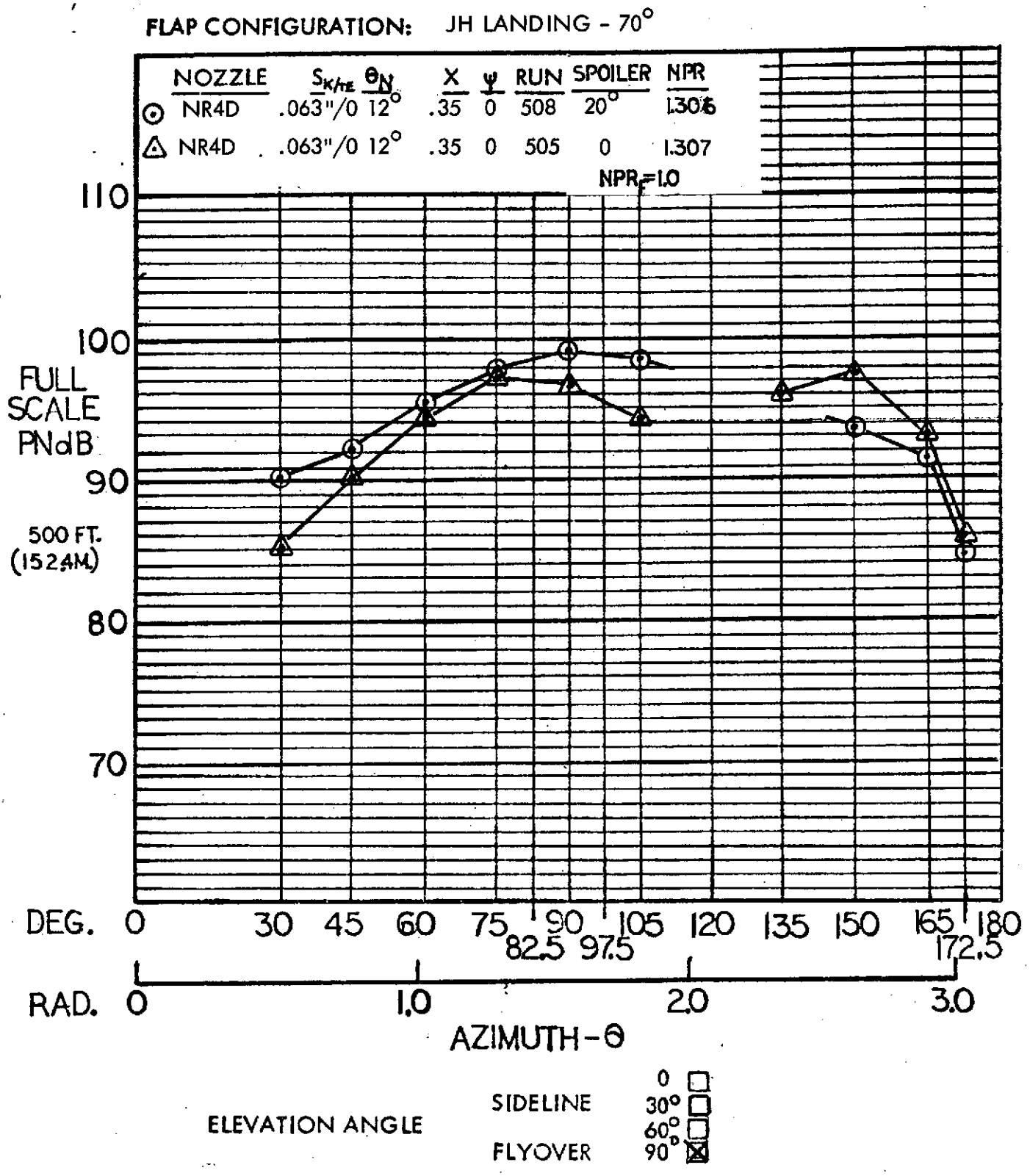

Figure A-23 Comparison of full scale flyover PNL for spoiler angles of 0° and 20°, JH flap, 70° flap angle, NR4D nozzle, no flap blowing.

HYBRID PROPULSIVE LIFT
ACOUSTIC TEST
NAS 2-7812

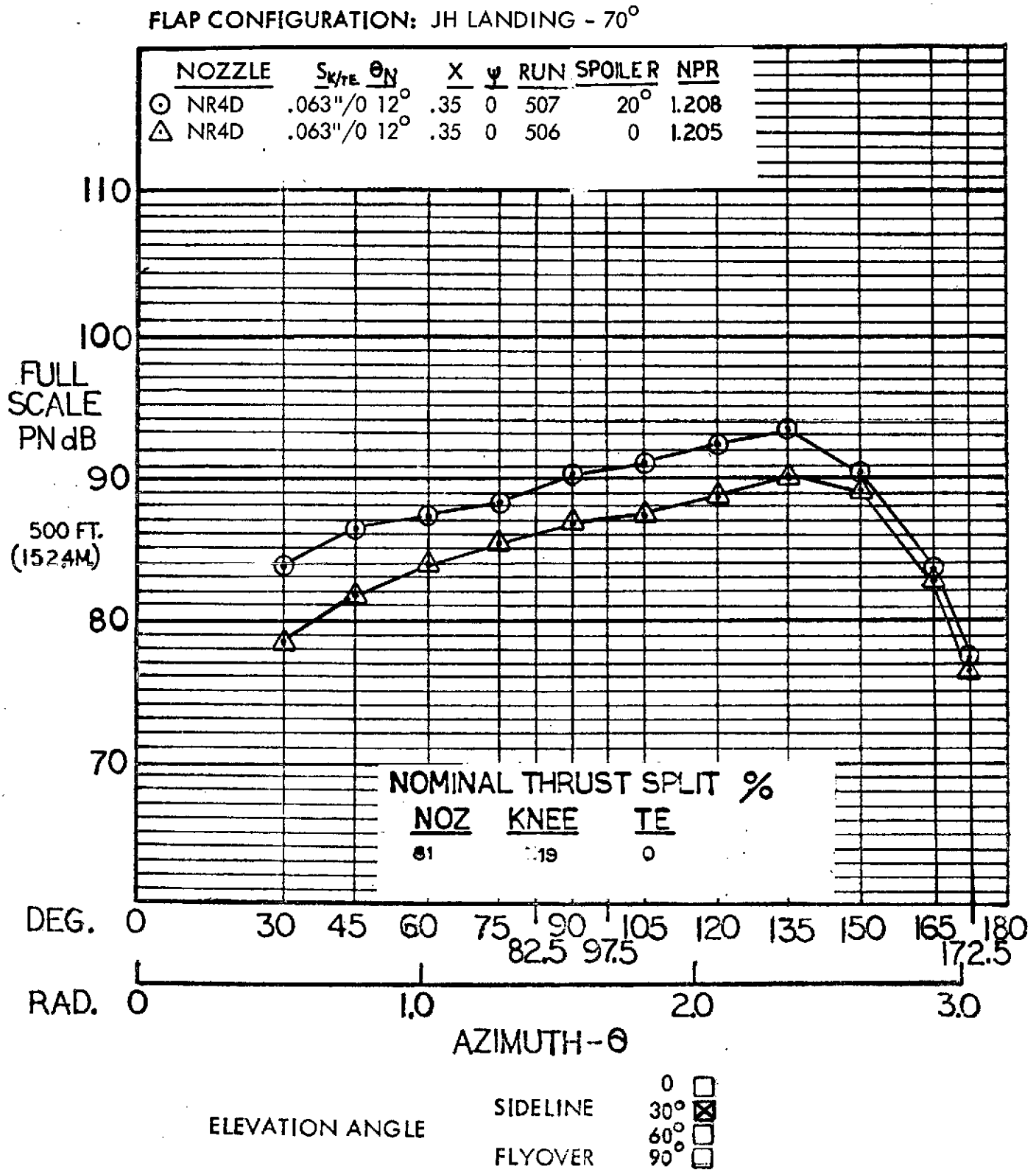

Figure A-24 Comparison of full scale sideline PNL for spoiler angles of 0° and 20°, JH flap, 70° flap angle, NR4D nozzle, knee blowing.

HYBRID PROPULSIVE LIFT
ACOUSTIC TEST
NAS 2-7812

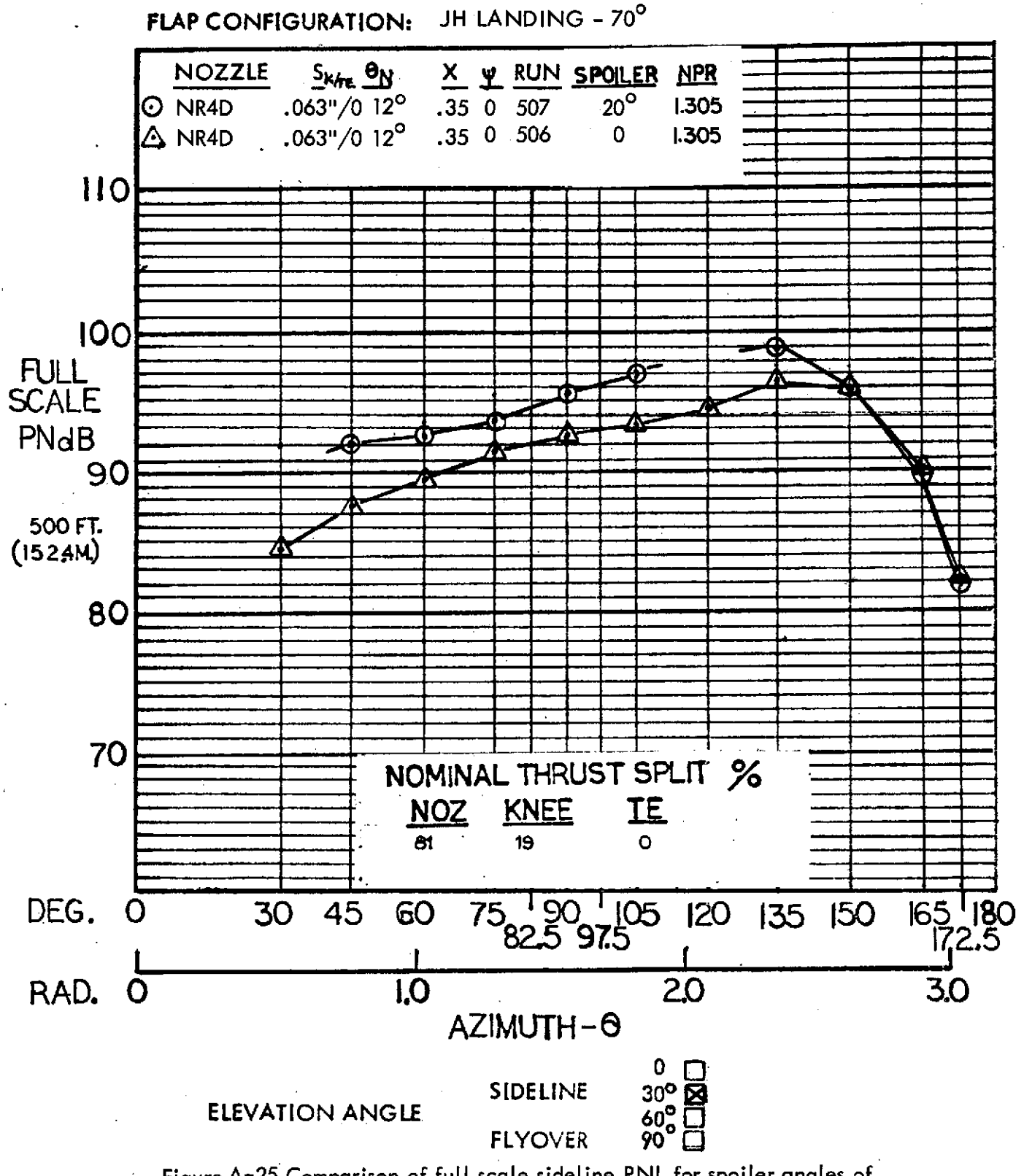

Figure A-25 Comparison of full scale sideline PNL for spoiler angles of 0° and 20°, JH flap, 70° flap angle, NR4D nozzle, knee blowing.

HYBRID PROPULSIVE LIFT
ACOUSTIC TEST
NAS 2-7812

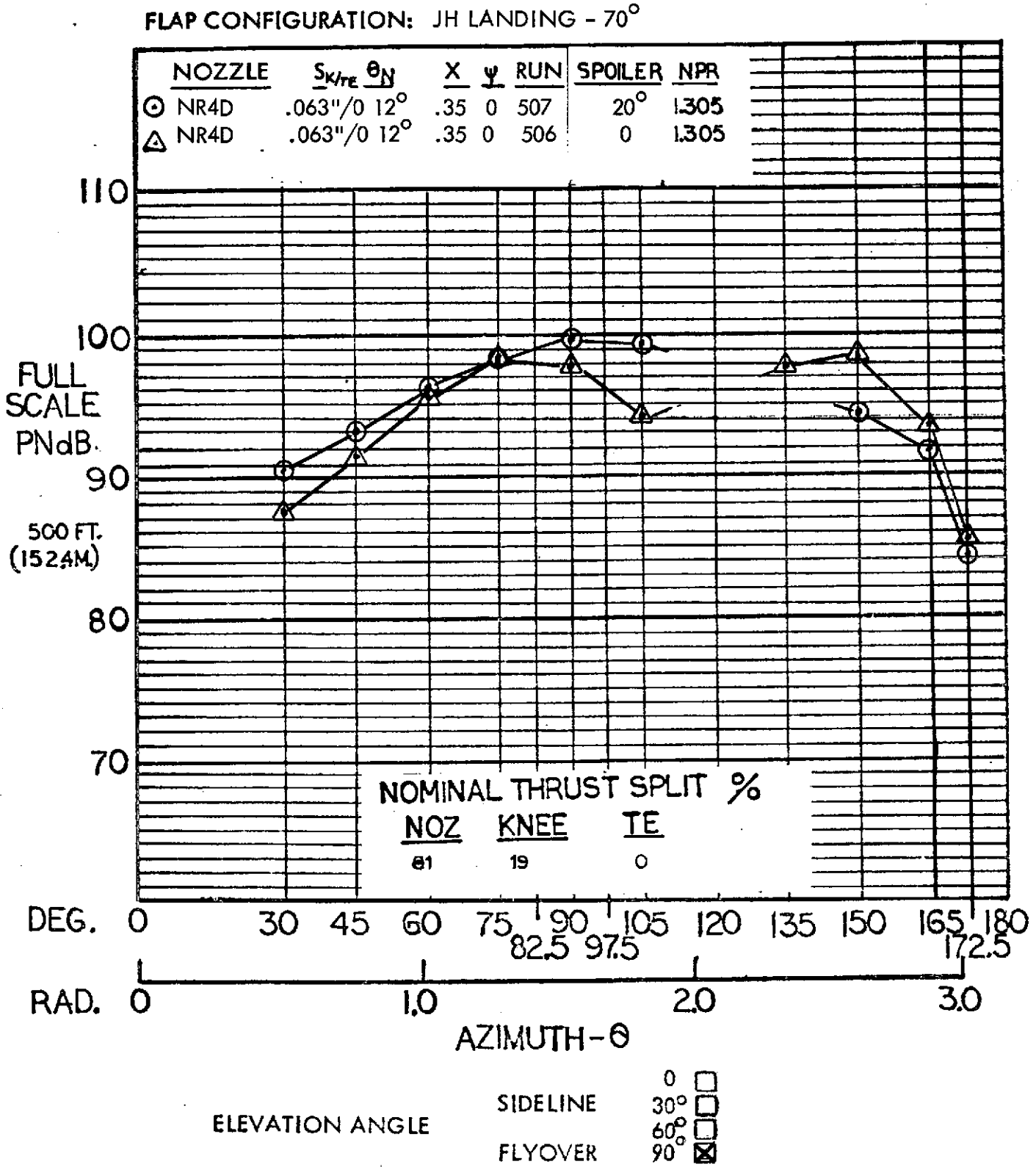

Figure A-26 Comparison of full scale flyover PNL for spoiler angles of 0° and 20°, JH flap, 70° flap angle, NR4D nozzle, knee blowing.

HYBRID PROPULSIVE LIFT
ACOUSTIC TEST
NAS 2-7812

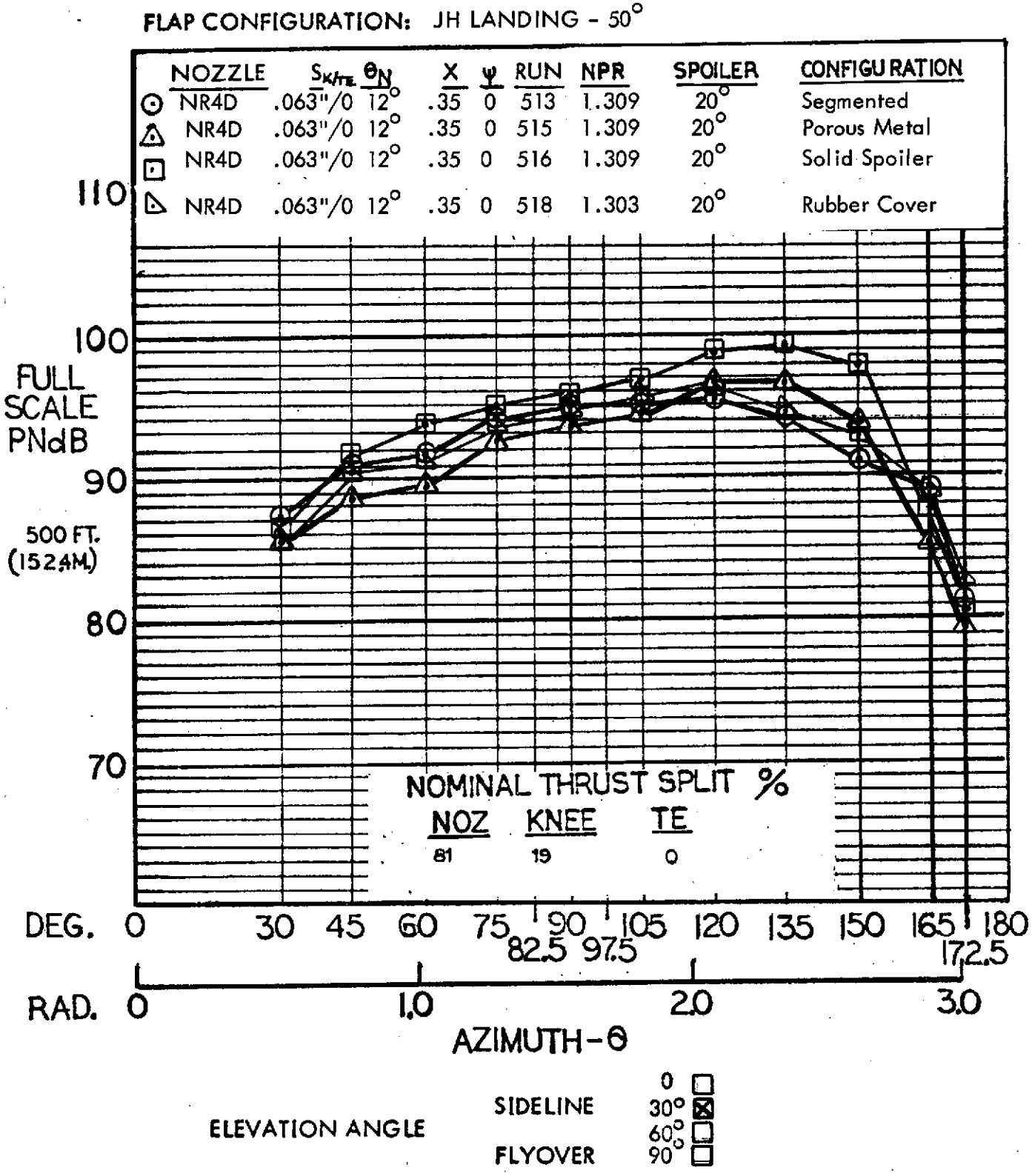

Figure A-27 Full scale sideline PNL for JH flap, 50° flap angle, NR4D nozzle, knee blowing; segmented spoiler and acoustic modifications.

HYBRID PROPULSIVE LIFT
ACOUSTIC TEST
NAS 2-7812

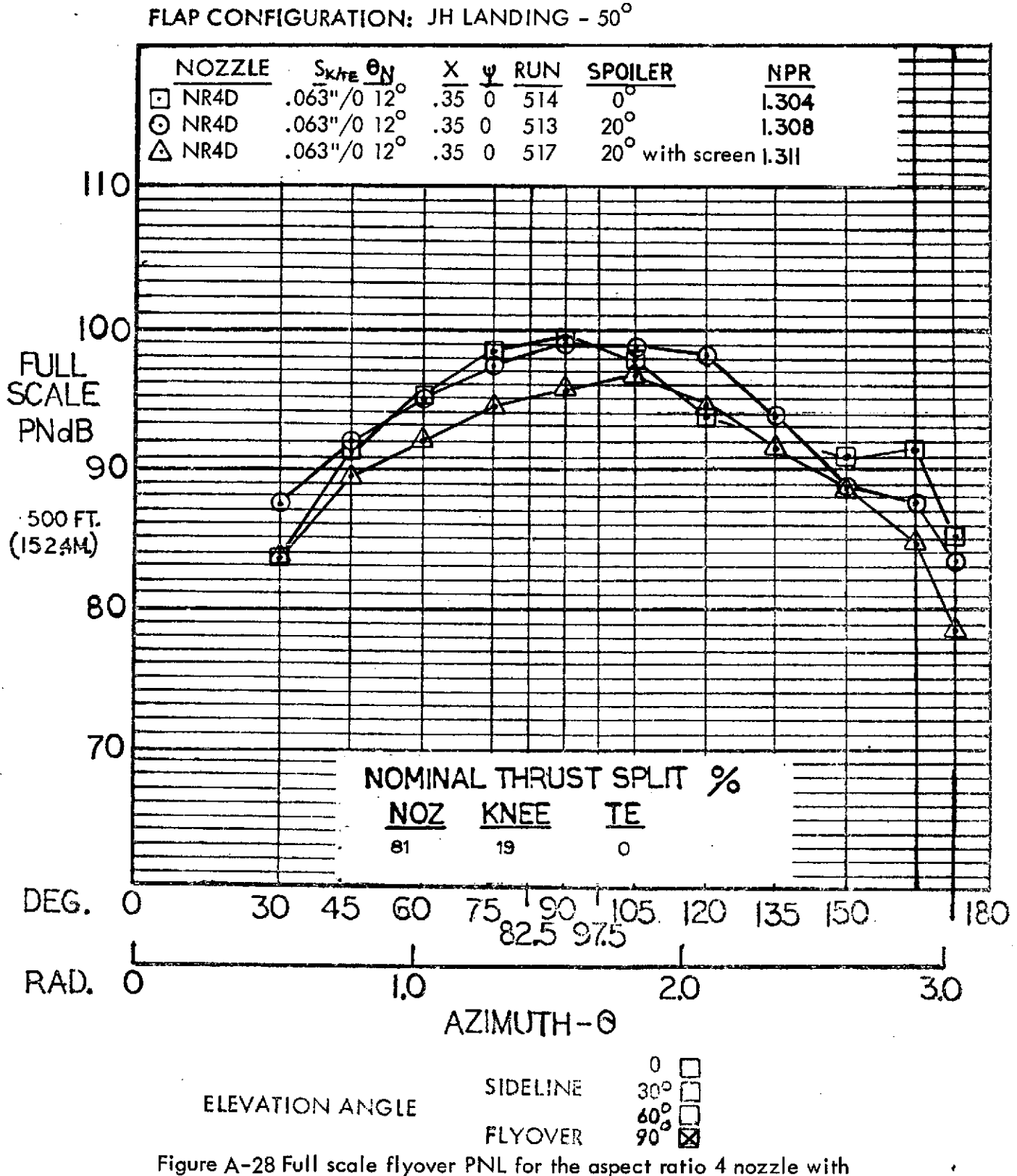

Figure A-28 Full scale flyover PNL for the aspect ratio 4 nozzle with deflector, JH flap with knee blowing, 50° flap angle, segmented spoiler at 0°, 20°, and 20° with screen.

HYBRID PROPULSIVE LIFT
ACOUSTIC TEST
NAS 2-7812

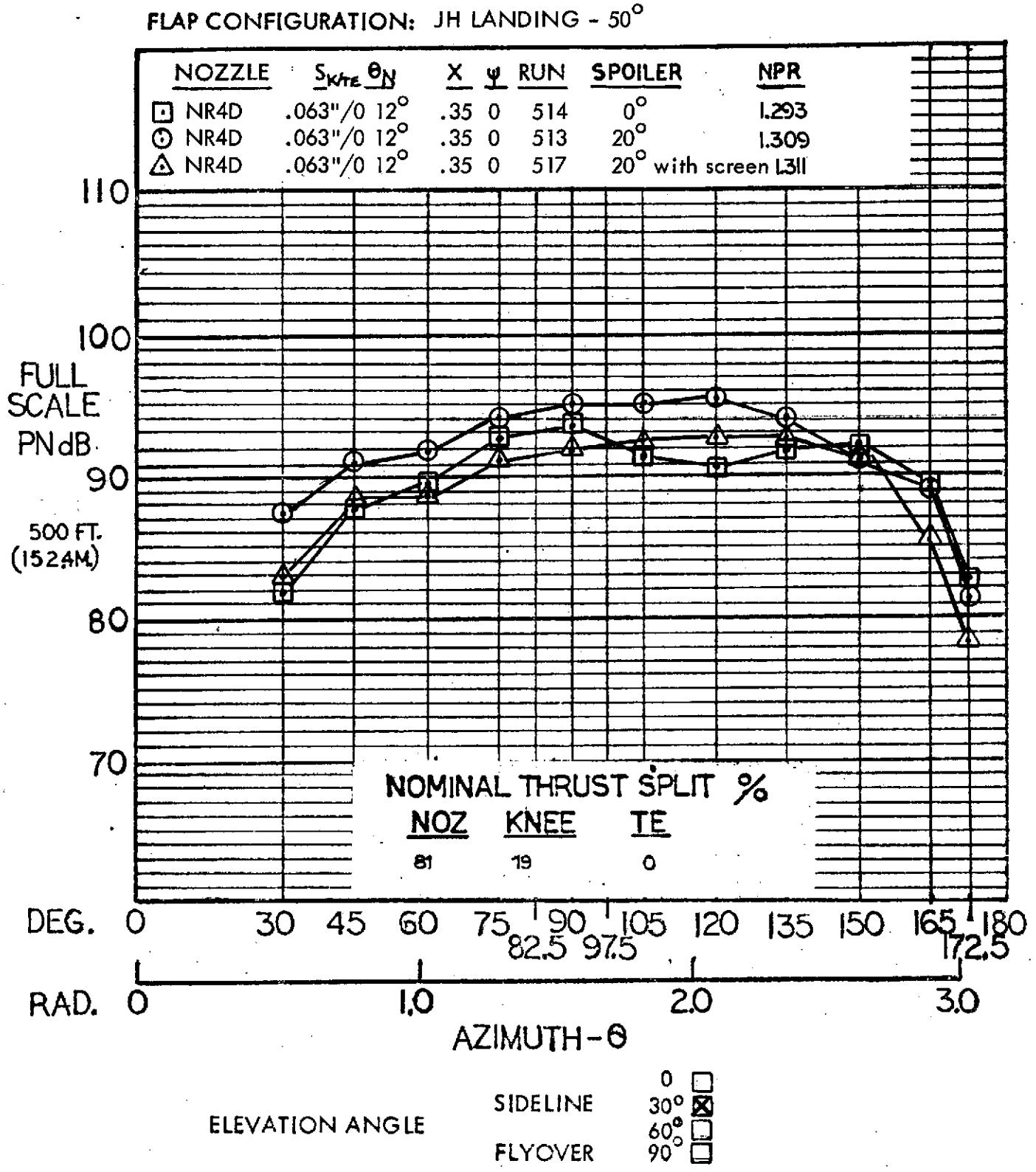

Figure A-29 Full scale sideline PNL for the aspect ratio 4 nozzle with deflector, JH flap with knee blowing, 50° flap angle, segmented spoiler at 0°, 20°, and 20° with screen.

HYBRID PROPULSIVE LIFT ACOUSTIC TEST

RUN NO: 513, 517, 514 NAS 2—7812

CONFIGURATION: NR4D NOZZLE, JH LANDING - 50° WITH SEGMENTED SPOILER

MIC NO: 6, 9 (θ=90°, 120°)

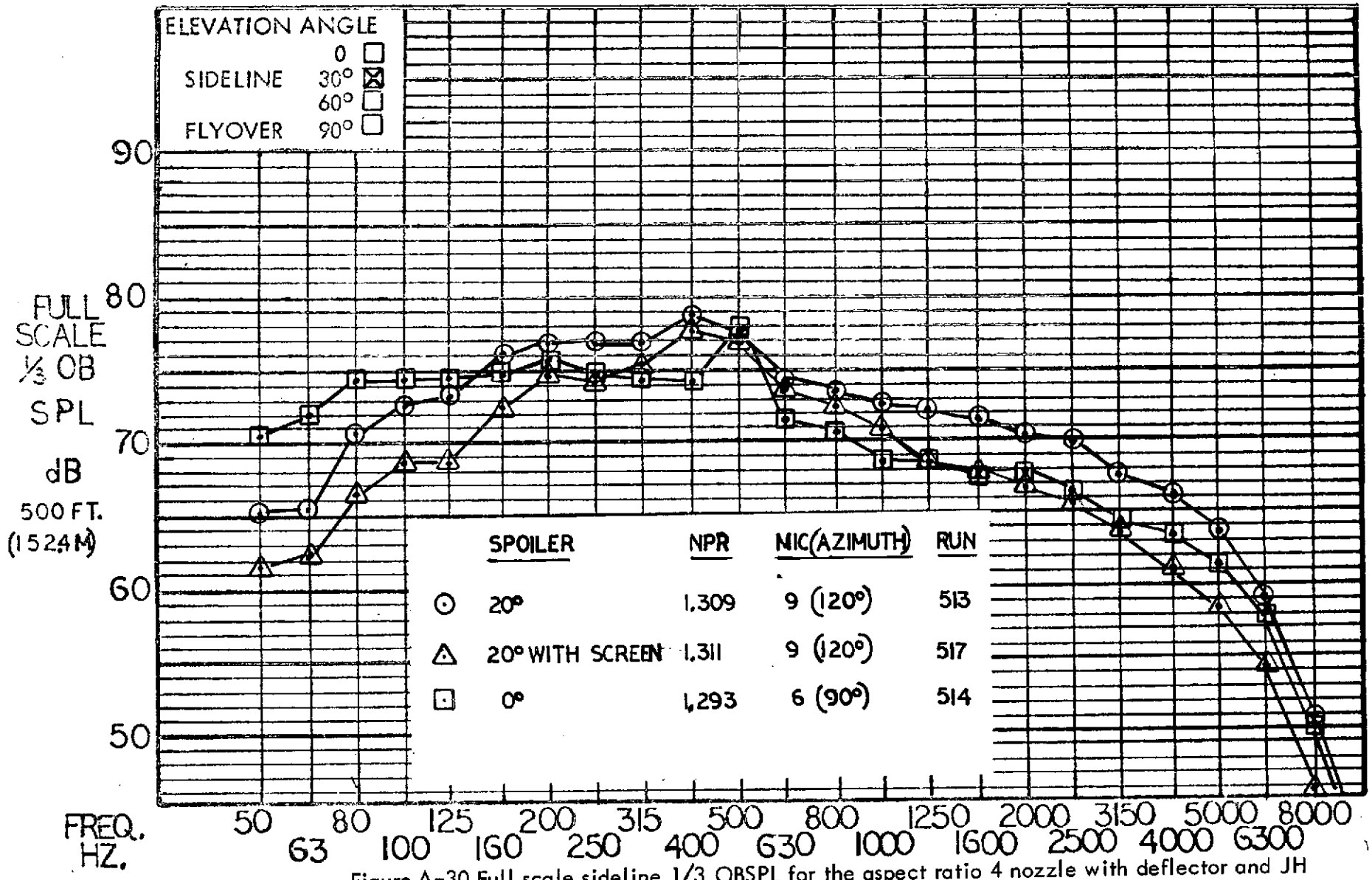

Figure A-30 Full scale sideline 1/3 OBSPL for the aspect ratio 4 nozzle with deflector and JH flap with knee blowing and segmented spoiler; 50° flap angle.

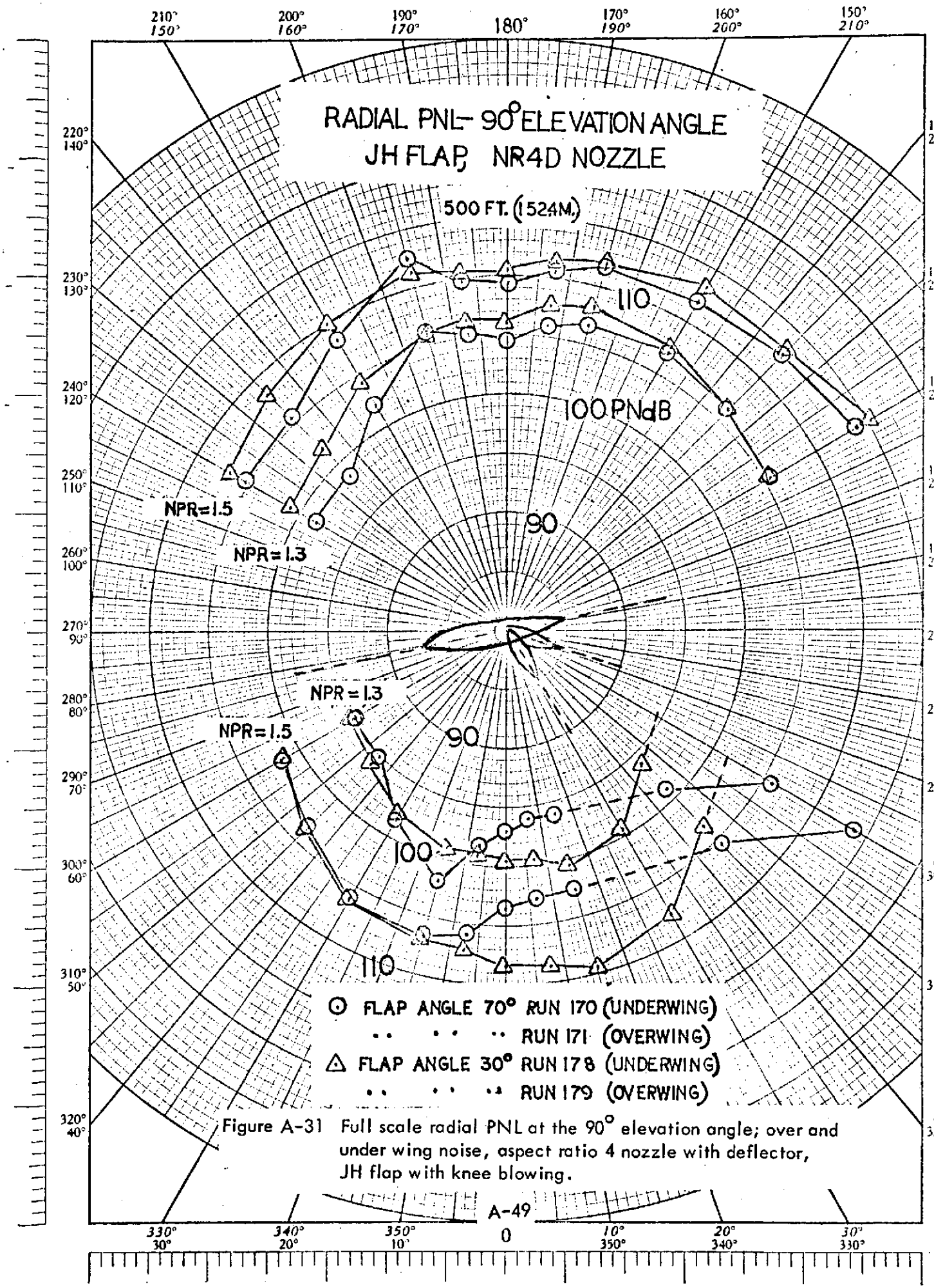

Figure A-31 Full scale radial PNL at the 90° elevation angle; over and under wing noise, aspect ratio 4 nozzle with deflector, JH flap with knee blowing.

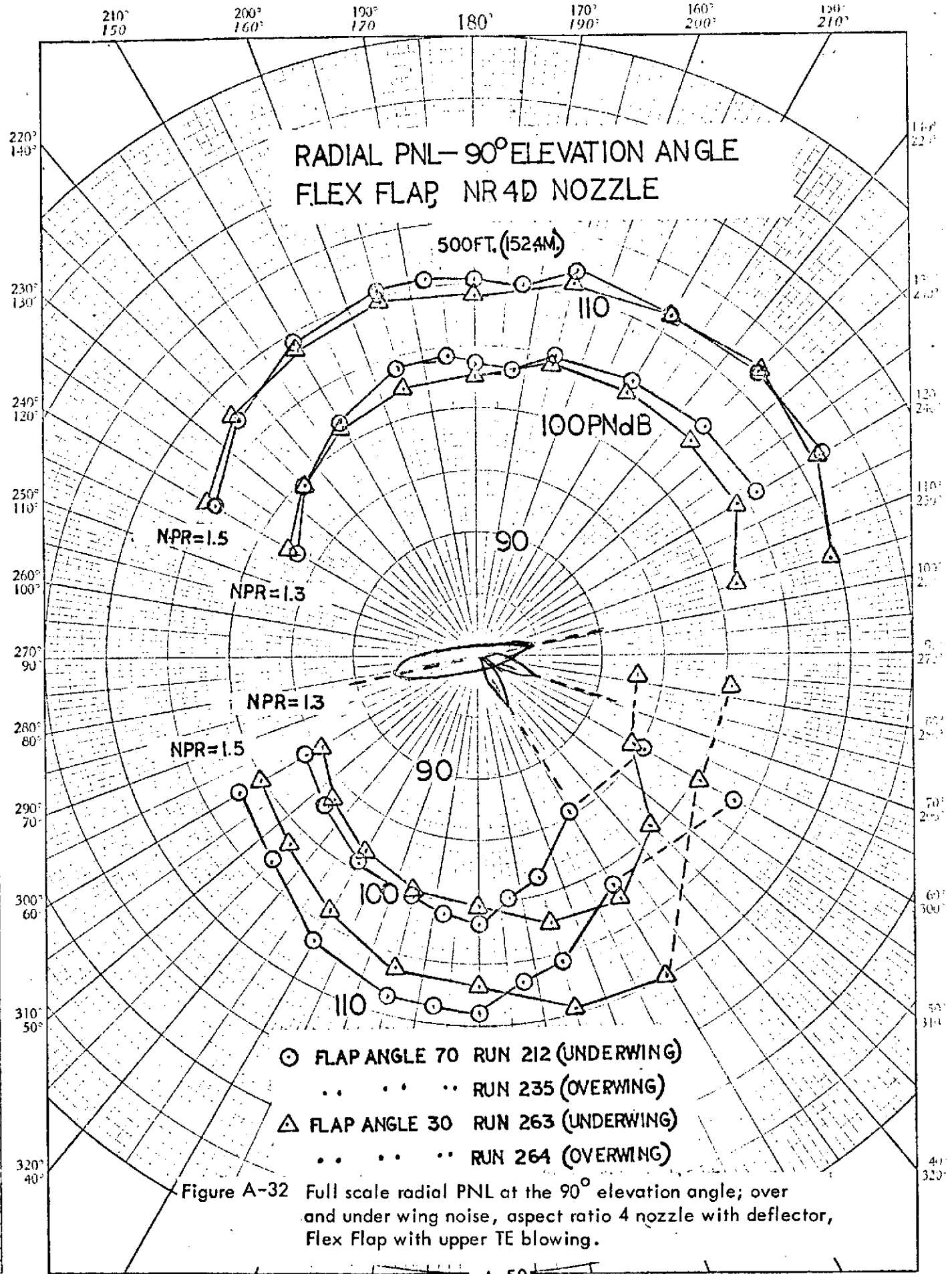

Figure A-32 Full scale radial PNL at the 90° elevation angle; over and under wing noise, aspect ratio 4 nozzle with deflector, Flex Flap with upper TE blowing.

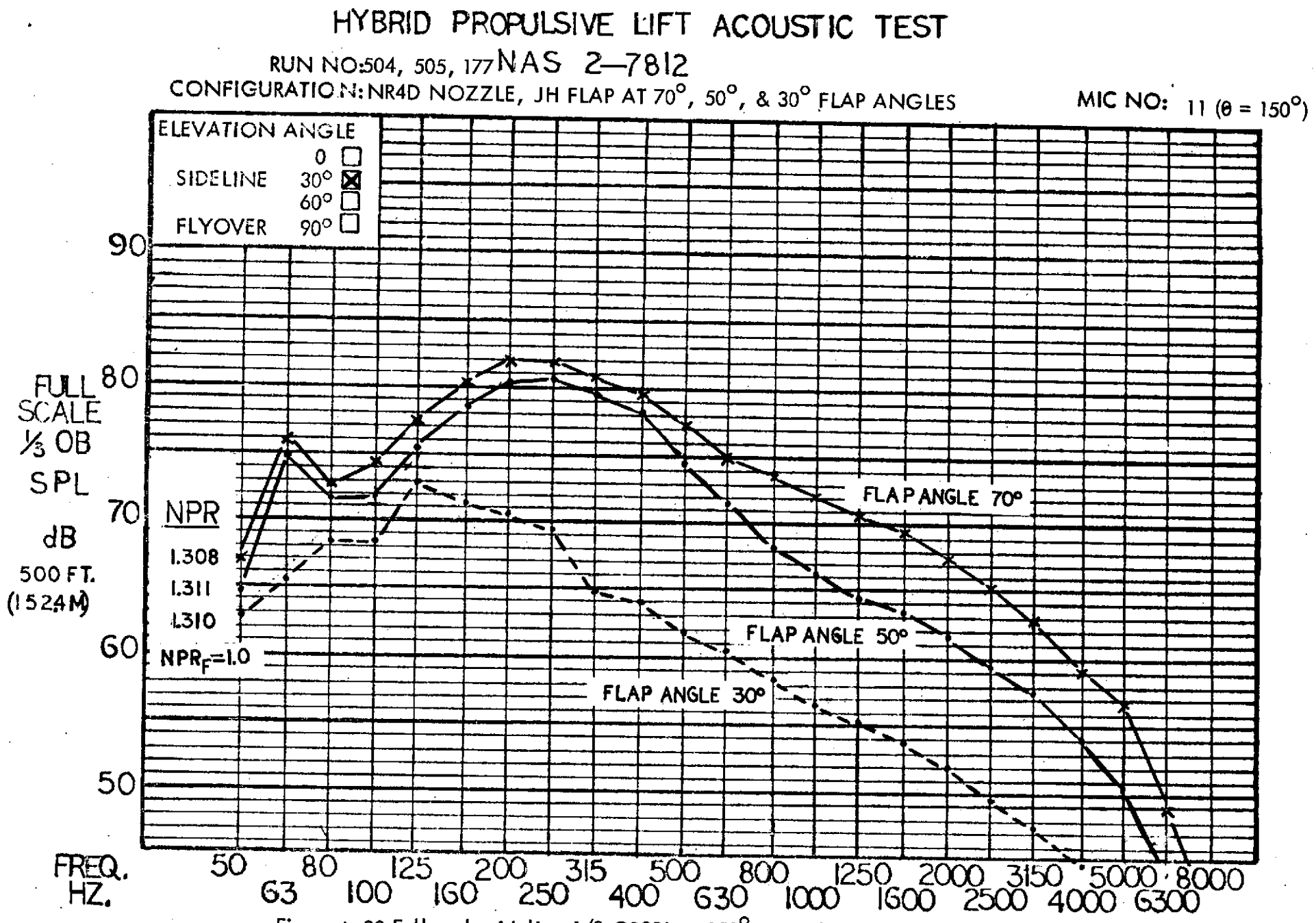

Figure A-33 Full scale sideline 1/3 OBSPL at 150° azimuth for aspect ratio 4 nozzle with deflector and JH flap, no flap blowing, flap angles of 70°, 50°, and 30°.

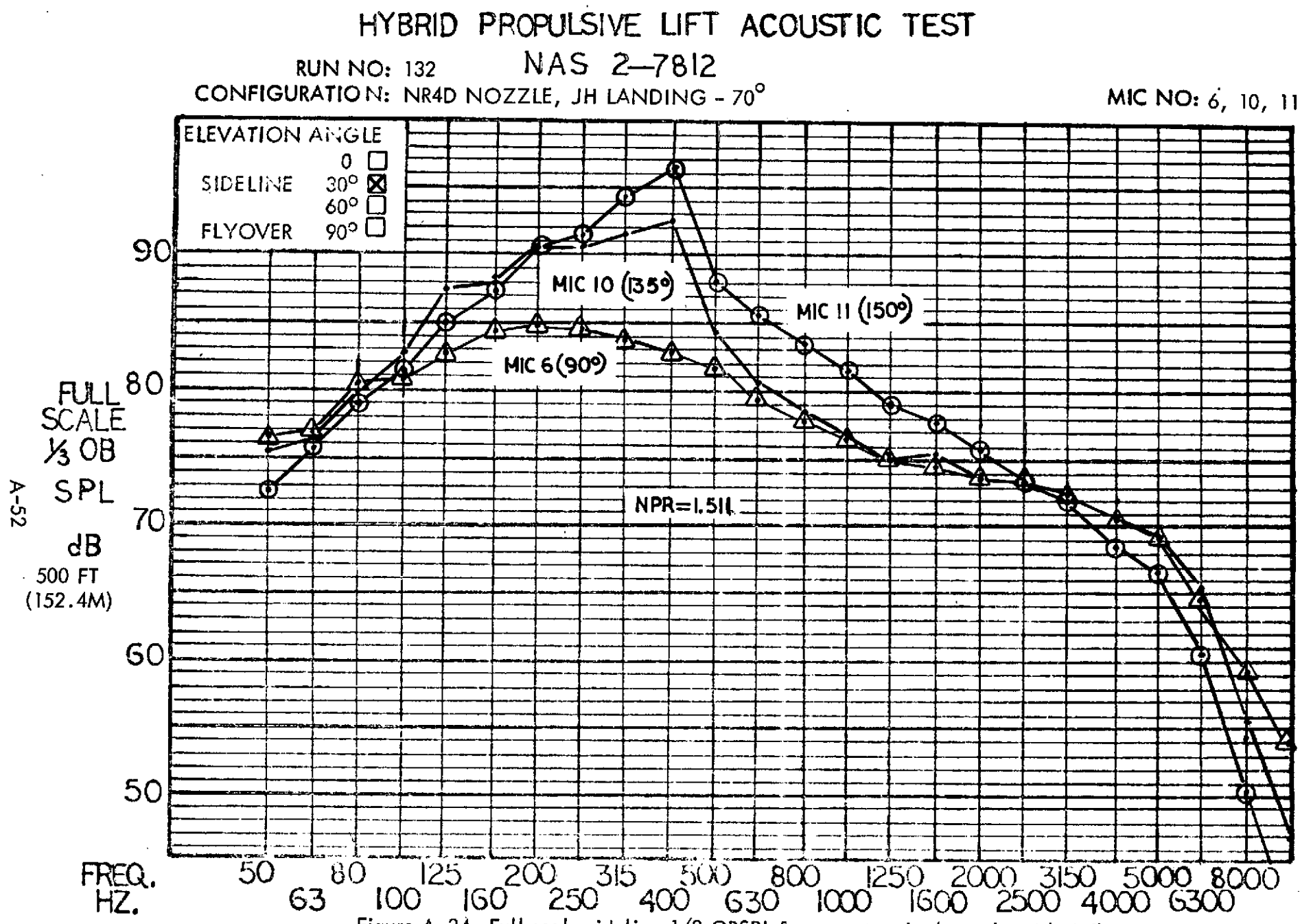

Figure A-34 Full scale sideline 1/3 OBSPL for aspect ratio 4 nozzle with deflector, 90°, 135°, and 150° azimuth position.

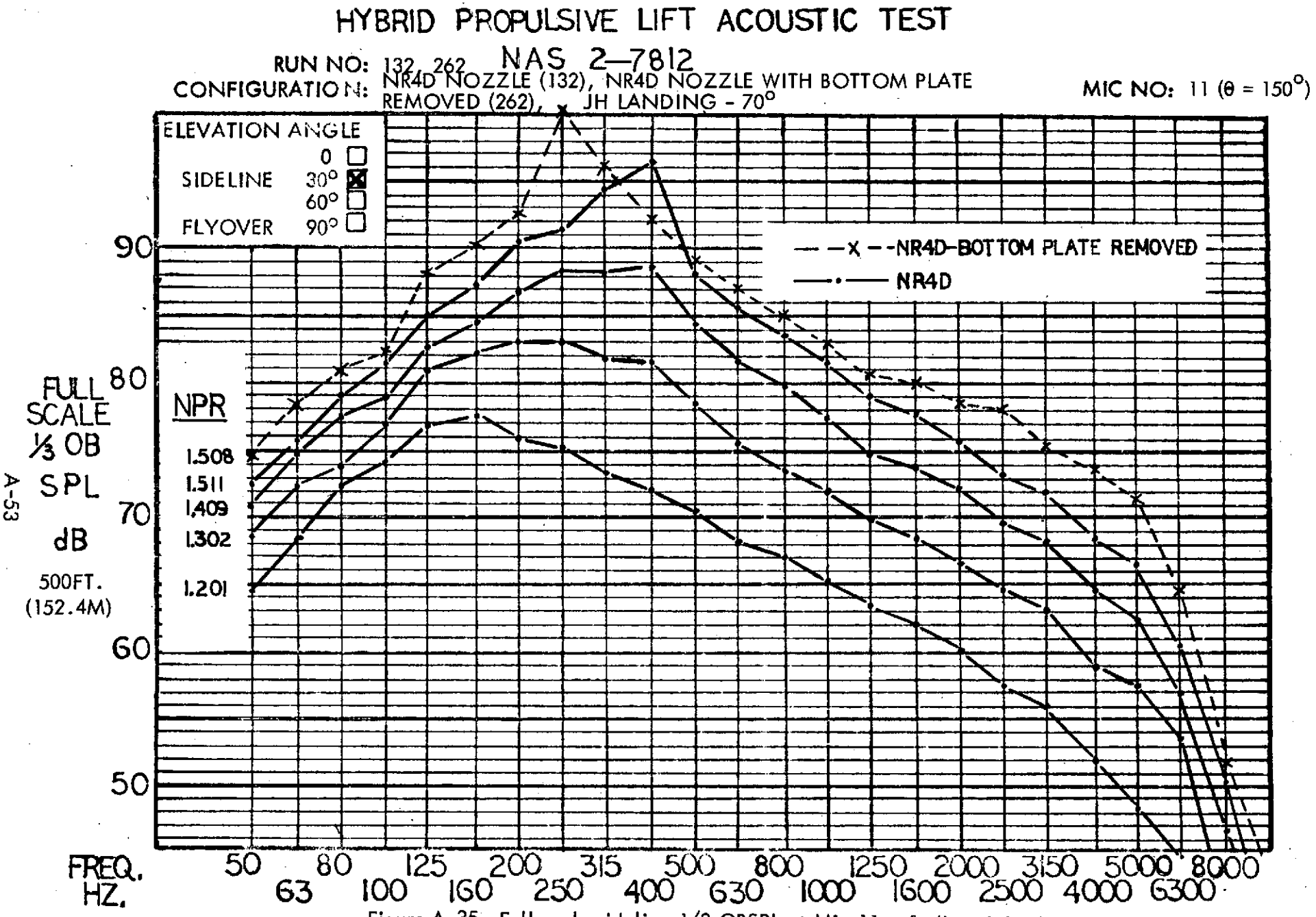

Figure A-35 Full scale sideline 1/3 OBSPL at Mic 11, aft directivity increase with nozzle pressure ratio, JH landing flap.

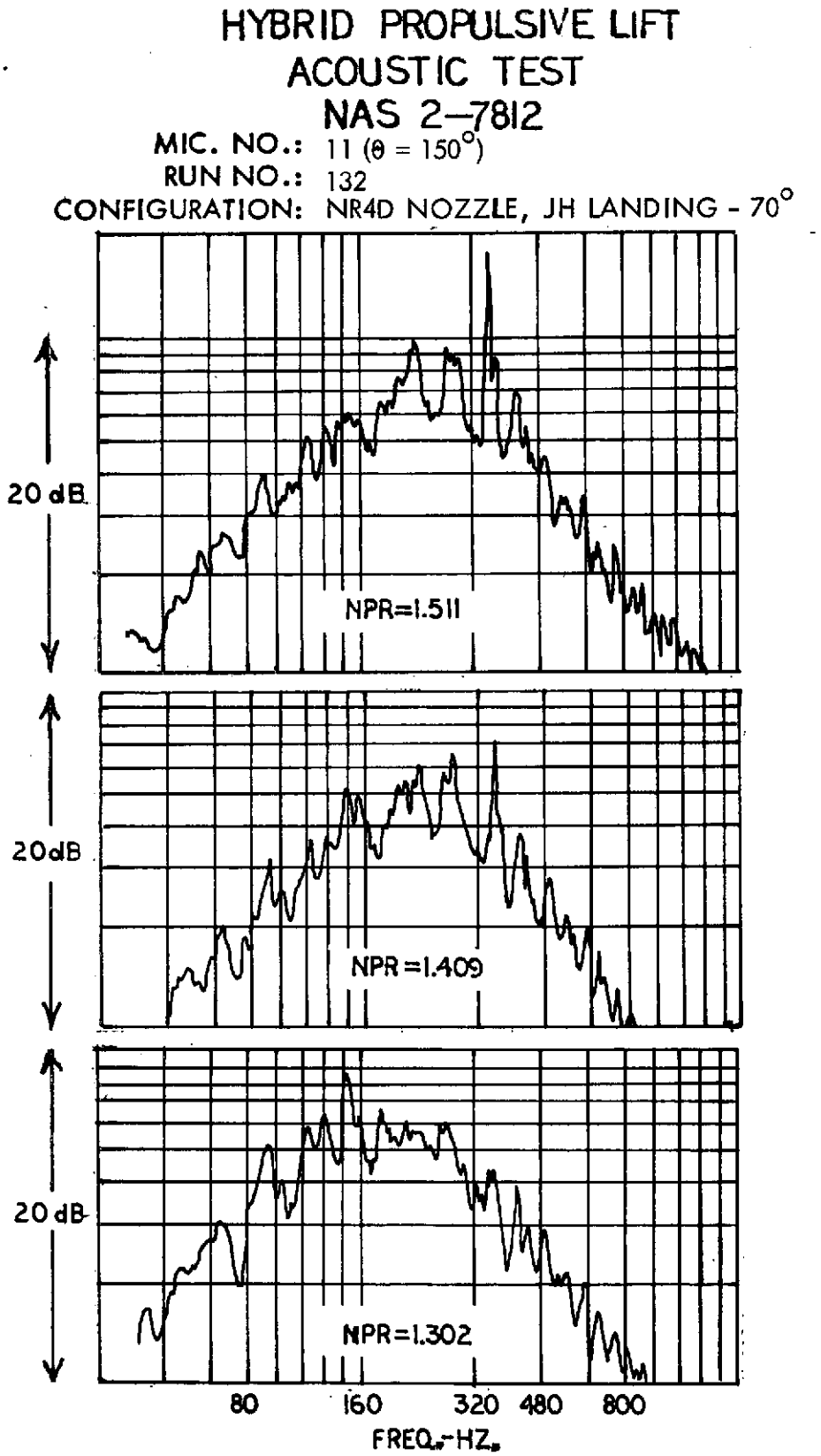

Figure A-36 Full scale 30° sideline narrow band noise (effective analysis bandwidth = 2.56 Hz) at 150° azimuth for the aspect ratio 4 nozzle with deflection and JH flap with knee blowing; 70° flap angle.

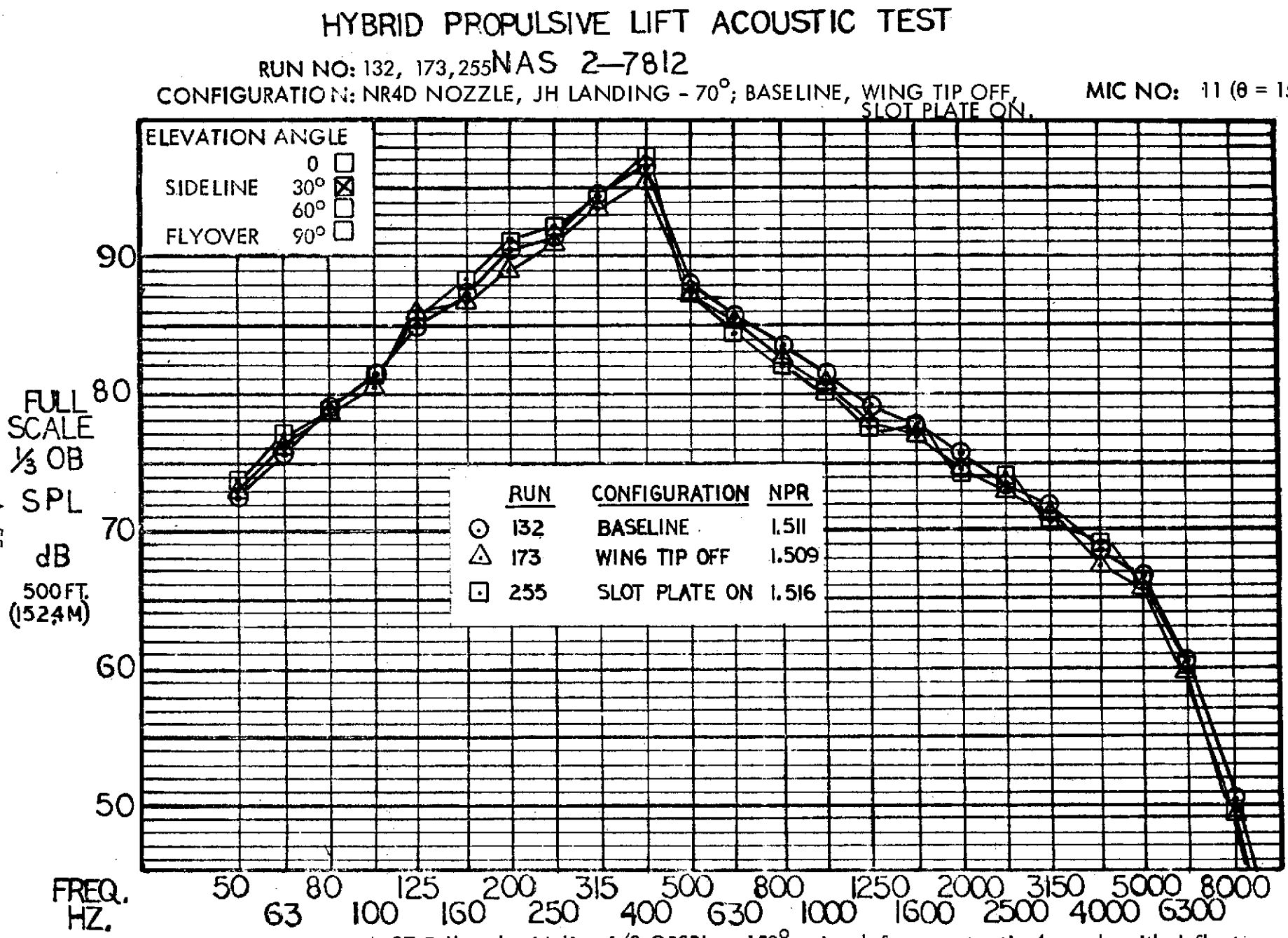

Figure A-37 Full scale sideline 1/3 OBSPL at 150° azimuth for aspect ratio 4 nozzle with deflector and JH flap at 70° flap angle; comparison of baseline, wing tip off, slot plate on.

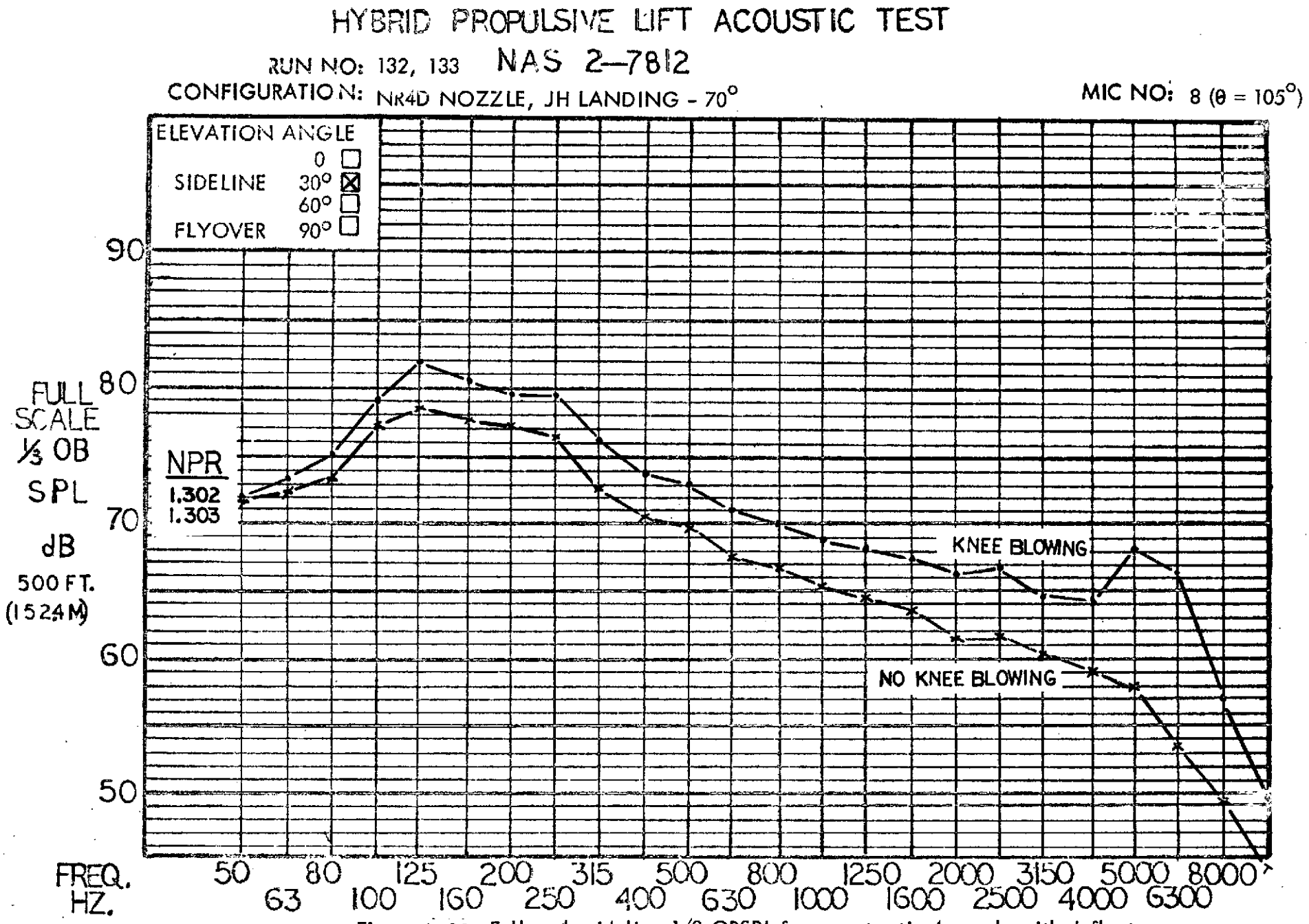

Figure A-38 Full scale sideline 1/3 OBSPL for aspect ratio 4 nozzle with deflector and JH flap, with and without knee blowing, 70° flap angle.